

VED SRIVASTAVA, ANDREI YUDIN, AND MICHAL LEBL

Peptides 2015

PROCEEDINGS OF THE TWENTY-FOURTH AMERICAN
PEPTIDE SYMPOSIUM



JUNE 20-25, 2015

ORLANDO, FLORIDA

Peptides 2015

Proceedings of the Twenty-Fourth American
Peptide Symposium

June 20-25, 2015, Orlando, FL, U.S.A.

Edited by

Ved Srivastava

Department of Chemistry

GlaxoSmithKline

Andrei Yudin

Department of Bioorganic Chemistry

The University of Toronto

Michal Lebl

Prompt Scientific Publishing

San Diego, CA

michallebl@gmail.com

American Peptide Society

Sold and distributed by www.promptpublishing.com

ISBN 978-0-9839741-5-4

Copyright ©2015 American Peptide Society

All rights reserved. No part of the material protected by this copyright notice may be reproduced or utilized in any form or by any means, electronic or mechanical, including photocopying, recording or by any information storage and retrieval system, without written permission from the copyright owner. Produced by Prompt Scientific Publishing, San Diego, U.S.A.

www.promptpublishing.com

Introduction

It was our pleasure and honor to host the peptide community for 6 days of stimulating science of peptide chemistry, biochemistry, and biology. The meeting theme - ***Enabling Peptide Research from Basic Science to Drug Discovery*** - embraces the spirit of the scientific and social programs we have assembled for you.

Recently, the use of peptides as drugs has been increasing exponentially, especially in metabolic diseases and in exploring intracellular targets. A 'pre-Symposium,' with a theme of peptides in metabolic diseases, was planned with an emphasis on basic pharmacology and peptide targets. This is followed by a number of regular scientific sessions, which focus on topics as diverse as macrocycles, synthetic peptides, medicinal chemistry and peptide therapeutics, all representing emerging peptide technologies.

The scientific program for 2015 opened with distinguished lecture by Dr. Richard A. Lerner of The Scripps Research Institute and the symposium was concluded with a lecture by Dr. Jeffrey Friedman of the Rockefeller Institute.

Unlike previous events, two workshops were conducted at this meeting: (1) workshop on peptide Chemistry Manufacturing and Controls (CMC) and regulatory challenges; and (2) workshop on career development, job search strategy and interview preparation. The lectures from awards winners, including the Merrifield, Vincent du Vigneaud, Makineni, and Goodman Awards were spread out over the six days of the symposium.

We are very grateful to a number of people who made the planning of this conference significantly easier. We are thankful to Judy Warner, Symposium Manager, Lars Sahl, Webmaster, Becci Totzke, Society Manager, the APS Council, Scientific Advisory Committee, Travel Award Committee, Student Affairs Committee, Sponsorship Committee, Orlando Local Organizing Committee, those who submitted abstracts, and to all the symposium attendees.

We highly appreciate and thank all the sponsors and exhibitors. Without their generous support we would not be able to put together an outstanding scientific program and delightful food, conversation and fun.



Ved Srivastava, Co-Chair



Andrei Yudin, Co-Chair

Editor's Remarks

The American Peptide Society used the same production team (scientific and technical editor, ML and PS) as in the last several symposia. Manuscripts were accepted through the internet page, entered into the database which allowed creating indexes on the fly and simplified communication with authors. Processed manuscripts were available for proofing eight weeks after the symposium ended – helping us to correct errors made by us and authors in the rush to deliver the book as soon as possible. The finalized book was available on the website for free downloading and the hard copy is available from “just in time” printing process at www.lulu.com. Due to the fact that the American Peptide Society is a nonprofit organization, there is no margin charged for the book, and all members can order it for production cost. Our thanks go to all authors who delivered manuscripts of a high technical quality before the deadline.

We believe that the quality of the figures and schemes is an important part of the presentation skills of the authors and, as in the last symposia, we let them show it. In the past we were insisting on the delivery of only monochromatic graphics with large enough details (fonts). Since only less than 2% of all distributed books were produced in paper form (98% of proceeding books from the last symposium were downloaded free by the public as a pdf file), we have accepted color graphics as well, which, of course, only shows in the pdf version of the book.

However, this year was very different. Our survey has shown that an overwhelming majority of you wish that everything presented at the symposium should be available to the participants electronically. Actually only 4.6% of the responders did not want everything to be available. We tried to find out the reasons and the answers puzzled us – either the authors did not want to be plagiarized (why did they present anything at the symposium is beyond us), or they claimed that the results were not published yet (well, isn't it a reason to show your newest results to come to the conference and share it with participants). We asked the presenters whether they want to send us their posters and/or lecture slides and actually some of the scientists did send us their material. We took the job of photographing every displayed poster and combine the pictures with electronic submissions into “The compilation of posters and lectures from 24th American Peptide Symposium” which was distributed to all participants of the symposium in a private email. Requests from a few scientists that their contribution be kept out of view were honored and the content of their poster was deleted. Only eight scientists had this request and surprisingly we then received the manuscripts describing the same material.

Some statistics: 78 lectures (8 slide sets were submitted for compilation), 364 posters were registered at the symposium (13 were withdrawn and 45 were not presented) – we have received 53 in electronic form – and all 301 posters presented are included in our compilation. If you wish to receive a link to the compilation, let us know. From the total of 379 potential contributions to the proceedings book we received only 105 manuscripts (28%), making it less than representative sample of the symposium.

Comparing materials coming into the proceedings book with what was available on the posters, we would strongly recommend abandoning the form of a proceedings book and replacing it with a collection of poster and lecture materials. It could be registered as an electronic book and have its own doi identifiers for secondary literature searching. It could continue to be called “Proceedings”. The main reasons for suggestion this change are: (i) only eight books of the last proceeding were produced in printed form; (ii) posters contain more data than the proceedings manuscripts; (iii) only a small fraction of material presented at the conference ends up in a proceedings book; and (iv) authors would not have to do anything in addition to preparation of their posters or lectures.

Roseann Story-Lebl
Technical Editor
rpstory@gmail.com

Michal Lebl
Scientific Editor
michallebl@gmail.com

A Message from the President of the American Peptide Society

President's address of welcome, June 20, 2015



On behalf of the American Peptide Society, welcome to the Society's 24th Peptide Symposium.

You made a good decision to come. In addition to the academic riches offered by the program, the attention paid to the potential for practical applications alone would justify anyone's time and effort to be here. It was not so long ago that much of Pharma still held to the dogma that no drug shall be above 500 Da in general and that the peptide bond in particular is an invention of Satan. We, on the other hand, know that the proportion of licensed drugs that are based on peptides and proteins constantly grows and that such drugs have an easier, faster, and safer passage through development than do small molecules. It is easy to demonstrate that hits selected from large libraries of individual organic compounds have an intrinsically higher probability than peptides of leading to drugs with severe unsuspected side effects.

The APS is 25 this year. It was set up to take over the organization of these Symposia, to help further the careers of young investigators, to create a Journal, and to join others, particularly FASEB, in advocacy for science in general and our corner of science in particular.

As a non-American, it is easier for me to assert without arrogance that the American Peptide Society constitutes a significant international community of scientists, and I am glad that the great majority of you have accepted our offer of membership. If you are still wondering why you did so, I have listed some of the member benefits in the introduction to the Program book.

Our decision to abolish membership dues was a new departure. We thank Wiley for helping us to implement it by agreeing that a paid personal subscription to our Journal, *Peptide Science*, shall no longer be an obligation of membership but an optional advantage for members.

We are proud of *Peptide Science*. It has consistently had the best impact factor in the peptide field and your original articles and reviews on all aspects of peptide science will be warmly welcomed.

Among other changes that you may notice is that the APS no longer organizes large invitation-only celebratory events. The Speakers' Dinner is now a buffet 'Meet the Speakers' reception freely open to all. The event to honor the Merrifield Awardee is now a Buffet Reception for which tickets are available at Registration. On the other hand, events organized by Sponsors or Exhibitors obviously have to be limited in numbers, but please understand that if you are an invited guest (or, maybe worse, not an invited guest) at a closed event, it isn't being paid for by the APS.

Speaking of young investigators, I am proud that for many years now APS Symposia co-Chairs always reserve a number of oral presentation slots for them. Watch out for them. The possession of more hair and/or fewer wrinkles might serve to identify some of them, but as to the science, I promise you that you will not detect any difference!

When Symposia start off in the mornings, speeches like this one serve the very useful purpose of allowing everybody 15 minutes extra in bed. As today we have an evening start, I will now stop. I thank all involved in planning, organizing, and providing support for the Symposium and all those who are making scientific contributions and providing exhibits. Others will elaborate on those thanks at the appropriate times during the Symposium.

Our co-Chairs' vision, hard work and dedication promise to make this a very stimulating and rewarding week. I truly hope that everyone enjoys the meeting!

Robin Offord

APS President, 2013-2015

24th AMERICAN PEPTIDE SYMPOSIUM
*Enabling Peptide Research
from Basic Science to Drug Discovery*

June 20-25, 2015
Orlando, Florida

Co-Chairs

Ved Srivastava
Department of Chemistry
GlaxoSmithKline

Andrei Yudin
Department of Bioorganic Chemistry
The University of Toronto

Student Travel Award Committee

Bradley Nilsson, University of Rochester, Rochester

Student Activities Committee

Co-Chairs:

Audrey Kelleman, Grace Materials Technologies, Albany

Wendy Hartsock, Biotage, Charlotte, NC

Students team members:

Diego Diaz, Melody Fulton, Solomon Gisemba, Laura Hanold, Amber Lynn Koenig

List of 24th American Peptide Symposium Sponsors

The 24th American Peptide Symposium was made possible through the generous support of the following organizations:

GOLD SPONSORS

IPSEN

PolyPeptide Group

Protein Technologies, Inc.

SILVER SPONSORS

aapptec

GlaxoSmith Kline

Bachem

GlyTech, Inc.

CEM Corporation

Sanofi

Ferring Pharmaceuticals

BRONZE SPONSORS

Bachem

Biotage

Novo Nordisk

Daiso FineChemUSA Inc.

MedImmune

Merck

Pfizer

ORANGE SPONSORS

Advanced ChemTech

CSBio Co.

Sigma-Aldrich

Biopeptek

EMD Millipore

Zoetis

Bristol-Myers Squibb

Peptides&Elephants

ChemPep

Peptides International

TRAVEL AWARD SPONSORS

New England Biolabs

Phylogica

RaPharma

Organic & Biomolecular Chemistry

Chemical Science

List of 24th American Peptide Symposium Exhibitors

aapptec
Advanced ChemTech
Advion
American Peptide Society
AnaSpec
Bachem Americas, Inc.
BCN Peptides S.A.
Biotage
C.A.T. GmbH&Co
CBL Biopharma
CEM Corporation
CordenPharma
CPC Scientific Inc.
CS Bio Co.
DAISO Fine Chem USA, Inc.
EMD Millipore
GL Biochem (Shanghai) Ltd.
Intavis, Inc.
Interchin Inc.
IRIS Biotech GmbH
LMS Co. Ltd.
NeoScientific
PCAS Biomatrix Inc.
Peptide International, Inc.
Peptide Institute
Peptide Machines, Inc.
Peptides and Elephants
PolyPeptide Group
Protein Technologies, Inc.
Rapp Polymere GmbH
Sunresin New Materials Co. Ltd.
Sussex Research
Tianjin Nankai Hecheng Science & Technology Co. Ltd.
USV Limited
Wiley
Zhejiang Ontores Biotechnologies Co. Ltd.

The American Peptide Society

The American Peptide Society (APS), a nonprofit scientific and educational organization founded in 1990, provides a forum for advancing and promoting knowledge of the chemistry and biology of peptides. More than 500 members of the Society come from North America and from more than thirty other countries throughout the world. Establishment of the American Peptide Society was a result of the rapid worldwide growth that has occurred in peptide-related research, and of the increasing interaction of peptide scientists with virtually all fields of science. A major function of the Society is the biennial American Peptide Symposium. The Society recommends awards to outstanding peptide scientists, works to foster the professional development of its student members, interacts and coordinates activities with other national and international scientific societies, sponsors travel awards to the American Peptide Symposium, and maintains a website at www.AmPepSoc.org.

The American Peptide Society is administered by Officers and Councilors who are nominated and elected by members of the Society. The Officers are: President: Philip Dawson, Scripps Research Institute, President Elect: Marcey Waters, University of North Carolina at Chapel Hill, Secretary: Juan Del Valle, University of South Florida, Treasurer: Pravin T.P. Kaumaya, The Ohio State University, Past President: Robin E. Offord, Mintaka Foundation for Medical Research. The councilors are: Jung-Mo Ahn, University of Texas at Dallas, Michael Carrasco, Santa Clara University, Waleed Danho, Retired, David Craik, University of Queensland, Mark Distefano, University of Minnesota, Emanuel Escher, Institute de Pharmacology, University of Sherbrooke, Robert P. Hammer, New England Peptide, Carrie Haskell-Luevano, University of Minnesota, Joshua Kritzer, Tufts University, David Lawrence, University of North Carolina at Chapel Hill, Laszlo Otvos, Temple University, Michael Pennington, Peptides International, Andrei Yudin, University of Toronto, Neal Zondlo, University of Delaware.

Membership in the American Peptide Society is open to scientists throughout the world who are engaged or interested in the chemistry or biology of peptides and small proteins. For further information on the American Peptide Society, please visit the Society web site at www.americanpeptidesociety.org or contact Becci Totzke, Association Manager, P. O. Box 13796, Albuquerque, NM 87192, U.S.A., tel (505) 459-4808; fax (775) 667-5332; e-mail apsmanager14@gmail.com. Contact Info: <http://www.americanpeptidesociety.org/pages/contact.asp>

American Peptide Symposia

1st	1968	Saul Lande & Boris Weinstein	New Haven	CT
2nd	1970	F. Merlin Bumpus	Cleveland	OH
3rd	1972	Johannes Meienhofer	Boston	MA
4th	1975	Roderich Walter	New York	NY
5th	1977	Murray Goodman	San Diego	CA
6th	1979	Erhard Gross	Washington	DC
7th	1981	Daniel H. Rich	Madison	WI
8th	1983	Victor J. Hruby	Tucson	AZ
9th	1985	Kenneth D. Kopple & Charles M. Deber	Ontario	Canada
10th	1987	Garland R. Marshall	St. Louis	MO
11th	1989	Jean E. Rivier	San Diego	CA
12th	1991	John A. Smith	Cambridge	MA
13th	1993	Robert S. Hodges	Alberta	Canada
14th	1995	Pravin T.P. Kaumaya	Columbus	OH
15th	1997	James P. Tam	Nashville	TN
16th	1999	George Barany & Gregg B. Fields	Minneapolis	MN
17th	2001	Richard A. Houghten & Michal Lebl	San Diego	CA
18th	2003	Michael Chorev & Tomi K. Sawyer	Boston	MA
19th	2005	Jeffery W. Kelly & Tom W. Muir	San Diego	CA
20th	2007	Emanuel Escher & William D. Lubell	Quebec	Canada
21st	2009	Richard DiMarchi & Hank Mosberg	Bloomington	IN
22nd	2011	Philip Dawson & Joel Schneider	San Diego	CA
23rd	2013	David Lawrence & Marcey Waters	Waikoloa	HI
24th	2015	Ved Srivastava & Andrei Yudin	Orlando	FL

2015 R. Bruce Merrifield Award

(Previously the Alan E. Pierce Award) The Merrifield Award was endowed by Dr. Rao Makineni in 1997, in honor of R. Bruce Merrifield (1984 Nobel Prize in Chemistry), inventor of solid phase peptide synthesis. Previously, it was called the Alan E. Pierce Award and was sponsored by the Pierce Chemical Company from 1977-1995.

Horst Kessler



Professor Horst Kessler's main field is medicinal chemistry in peptides and peptidomimetics using conformational design. In addition he has developed many novel NMR techniques to investigate structure, dynamics and function of peptides and biologically important proteins such as p53, Hsp90, spider silk. Kessler has pioneered conformational analysis of (cyclic) peptides in solution in combination with Molecular Dynamics calculations, the use of D-amino acids in cyclic peptides for conformational control and the design of constrained peptides. He discovered and developed sugar amino acids for their use as mimetics and improved the synthesis of Aza-analogues and N-methylated peptides. One of Kessler's present interests is in the use of multiple

N-methylation of peptides for achieving super-activities, receptor subtype selectivities and oral availabilities of cyclic peptides.

By systematic incorporation of the RGD tripeptide sequence in cyclic peptides and development of nonpeptidic mimetics, Professor Kessler could develop very active ligands to bind and discriminate the different integrin subtypes $\alpha\beta3$, $\alpha\beta5$, $\alpha\beta6$, $\alpha5\beta1$ and $\alpha11\beta3$. They have been modified and optimised for their use in Molecular Imaging in animals and humans, for improvement of biomaterials via coating and for biophysical studies.

Kessler studied chemistry in Leipzig and Tübingen (Germany) and in 1971, he was appointed as full professor of Organic Chemistry at the age of 31 at the Goethe University in Frankfurt. In 1989 he moved to the Technische Universität München, TUM. After Kessler's retirement he became Emeritus of Excellence and Carl von Linde Professor at the Institute for Advanced Study at TUM, which allowed him to continue to do research with a small group.

Kessler has published more than 700 papers (highly cited, h-factor 88) and 21 of his former co-workers are professors all around the world.

Design, Structure and Dynamics of Small Molecules, Peptides and Proteins

Horst Kessler

IAS TU Munchen, Germany

Nowadays it is evident that the biological function of peptides is controlled by their 3D structure. Solely one out of numerous conformations of a highly flexible linear peptide shows bioactivity. Thus, restraining the conformational space e.g. by backbone cyclization and thereby excluding the undesired conformations, binding affinity and receptor selectivity of peptidic ligands can be increased. A number of novel NMR methods have been developed to investigate the structure and dynamics of conformationally restraint peptides. Additionally, incorporation of D-amino acids of N-methylated amino acids allows a spatial screening to optimize peptides according to their biological activity or bioavailability. Using these techniques, we developed superactive small cyclic peptides as antagonists for the RGD-binding subfamily of integrins, a prominent class of cell adhesion receptors. By means of rational design and SAR studies, we were able to develop integrin subtype selective peptidomimetics that bind either the $\alpha\beta3$ or $\alpha5\beta1$ subtype and show even higher selectivities and activities. Functionalization of these targeting molecules allows, e.g. selective molecular imaging of cancer and myocardial infarctions in animals and man. The characterization of integrin expression in different cancers will enable a personalized treatment in the future. Moreover, functionalized integrin ligands have also been coated on surfaces of biomaterials (hip implants or stents) to stimulate osseointegration. On nanostructured surfaces the biophysical behaviour of cells binding different integrin ligands has also been investigated.

R. Bruce Merrifield Award Winners

2015 - Horst Kessler, IAS TU, Munchen, Germany
2013 - James P. Tam, Nanyang Technical University, Singapore
2011 - Richard DiMarchi, Indiana University
2009 - Stephen Kent, University of Chicago
2007 - Isabella Karle, Naval Research Laboratory, D.C.
2005 - Richard A. Houghten, Torrey Pines Institute for Molecular Studies
2003 - William F. DeGrado, University of Pennsylvania
2001 - Garland R. Marshall, Washington University Medical School
1999 - Daniel H. Rich, University of Wisconsin-Madison
1997 - Shumpei Sakakibara, Peptide Institute, Inc.
1995 - John M. Stewart, University of Colorado-Denver
1993 - Victor J. Hruby, University of Arizona
1991 - Daniel F. Veber, Merck Sharp & Dohme
1989 - Murray Goodman, University of California-San Diego
1987 - Choh Hao Li, University of California-San Francisco
1985 - Robert Schwyzler, Swiss Federal Institute of Technology
1983 - Ralph F. Hirschmann, Merck Sharp & Dohme
1981 - Klaus Hofmann, University of Pittsburgh, School of Medicine
1979 - Bruce Merrifield, The Rockefeller University
1977 - Miklos Bodansky, Case Western Reserve University

2015 Vincent du Vigneaud Award

Sponsored by BACHEM Inc.

Jean Chmielewski



Jean Chmielewski is the AW Kramer Distinguished Professor of Chemistry at Purdue University and a faculty member in the Weldon School of Biomedical Engineering. Jean obtained her undergraduate B.S. degree in chemistry in 1983 from St. Joseph's University where she worked on prostaglandin oligomerization with George Nelson. She moved to Columbia University for graduate school and completed her Ph.D. in 1988 in the area of bioorganic and biomimetic chemistry with Ronald Breslow. Jean joined the labs of E. T. Kaiser of Rockefeller University as an NIH postdoctoral fellow and, subsequently, Peter Schultz of the University of California, Berkeley where she investigated peptide fragment coupling, covalent methods to stabilize peptide conformations and DNA binding antibodies. After her postdoctoral appointments, she was recruited to the faculty in the Chemistry Department of Purdue University.

Jean has investigated the structure and function of many unique peptide systems over the past two decades, including the design of crosslinked peptide fragments to disrupt protein-protein interactions within HIV enzymes, and the introduction of environmental control into self replicating peptides. More recently her peptide research has been focused on peptide shuttles for cellular delivery of therapeutic agents, non-lytic antimicrobial peptides that target intracellular pathogens, and the hierarchical assembly of peptides into highly varied biomaterials for drug delivery and regenerative medicine.

Jean has won numerous awards for her research, including the Arthur C. Cope Scholar Award and the Edward Leete Award, both from the American Chemical Society, and the Agnes Fay Morgan Research Award from Iota Sigma Pi. She has also been honored many times for her teaching and mentoring of students, including the Charles R. Murphy Award- the highest teaching award of Purdue University. She is a fellow of the American Association for the Advancement of Science

Targeting Intracellular Pathogenic Bacteria with Unnatural Proline-Rich Peptides: Coupling Antibacterial Activity with Macrophage Penetration

Jean Chmielewski

*Department of Chemistry, 560 Oval Drive, Purdue
University, West Lafayette, IN 47907, USA*

A significant challenge in the development of effective antibacterial agents arises from bacterial pathogens that have evolved to inhabit mammalian cells, such as phagocytic macrophages. Within these intracellular safe havens the bacteria reproduce and form a repository, and are able to evade the host immune response as well as a number of antibiotic drugs. Therefore, there is a great need to develop antibiotics with the ability to enter mammalian cells and target intracellular pathogens at their specific sub-cellular site. We have developed a class of molecules, cationic amphiphilic polyproline helices (CAPHs) that enter mammalian cells through both direct transport and endocytosis. We have determined that CAPHs also have potent antibacterial activity *in vitro* with a non-lytic mechanism of action. This dual mode of action, non-lytic antibacterial activity with the ability to localize within mammalian cells, provided us with agents with a pronounced ability to target and kill pathogenic intracellular bacteria, including *Salmonella* and *Brucella*, within human macrophages.¹

1 J. Kuriakose, V. Hernandez, M. Nepal, A. Brezden, V. Pozzi, M. Seleem, J. Chmielewski, *Ang. Chem.*, **2013**, 52, 9644-9667.

2015 Vincent du Vigneaud Award

Sponsored by BACHEM Inc.

David Craik



David Craik is a Professor at the Institute for Molecular Bioscience, The University of Queensland. He obtained his PhD in organic chemistry from La Trobe University in Melbourne, Australia (1981) and undertook postdoctoral studies at Florida State and Syracuse Universities before taking up a lectureship at the Victorian College of Pharmacy in 1983. He was appointed Professor of Medicinal Chemistry and head of School in 1988. He moved to University of Queensland in 1995 to set up a new biomolecular NMR laboratory. His research focuses on peptides in drug design, and on toxins, including conotoxins. His group has a particular focus on structural studies of disulfide-rich proteins, and on the discovery and applications of cyclic peptides and novel peptide topologies. He has trained 60 PhD students and is the author of more than 550 scientific publications.

Discovery of Cyclic Peptides in Plants and Their Applications in Drug Design and Agriculture

David Craik

Institute for Molecular Bioscience, The University of
Queensland, Brisbane, QLD 4072, Australia

More than 300 examples of ribosomally synthesized head-to-tail cyclised proteins have been discovered in bacteria, plants and animals over the last decade¹. The cyclotides² are the largest family of these circular proteins and have applications in drug design³ and agriculture⁴. They occur in plants from the Violaceae (violet), Rubiaceae (coffee), Fabaceae (legume), Solanaceae (potato) and Cucurbitaceae (cucurbit) families and have a diverse range of biological activities, including uterotonic, anti-HIV, and insecticidal activities, the latter suggesting that their natural function is in plant defense. Individual plants express suites of 10-100 cyclotides. Cyclotides typically comprise ~30 amino acids, and incorporate three disulfide bonds arranged in a cystine knot topology. The combination of this knotted structure with a circular backbone renders the cyclotides impervious to enzymatic breakdown and makes them exceptionally stable. This presentation will describe the discovery of cyclotides in plants, their structural characterization, evolutionary relationships and their applications in drug design. Their stability and compact structure makes them an attractive protein framework onto which bioactive peptide epitopes can be grafted to stabilize them. Cyclotides have the ability to penetrate cells and thus they are a promising framework for the delivery of bioactive epitopes to intracellular targets.

1 Craik D J: *Science*, **2006**, 311, 1561

2 Gruber C W et al: *The Plant Cell*, **2008**, 20, 2471- 2483.

3 Henriques S T, Craik D J: Cyclotides as templates in drug design. *Drug Discovery Today*, **2010**, 15, 57-64.

4 Craik D J: *Toxins* **2012**, 4, 139-156

Vincent du Vigneaud Award Winners

2015 - Jean Chmieliewski, Purdue University, West Lafayette
2015 - David Craik, The University of Queensland, Australia
2013 - Kit Lam, University of California, Davis
2013 - Michael Chorev, University of Colorado Denver
2011 - Fernando Albericio, University of Barcelona
2011 - Morten Meldal, Carlsberg Laboratory, Copenhagen
2010 - Phil Dawson, Scripps Research Institute
2010 - Reza Ghadiri, Scripps Research Institute
2008 - Jeffery W. Kelly, Scripps Research Institute
2008 - Tom W. Muir, Rockefeller University
2006 - Samuel H. Gellman, University of Wisconsin
2006 - Barbara Imperiali, Massachusetts Institute of Technology
2004 - Stephen B. H. Kent, University of Chicago
2004 - Dieter Seebach, Swiss Federal Institute of Technology, Zurich
2002 - Horst Kessler, Technical University of Munich
2002 - Robert Hodges, School of Medicine, University of Colorado
2000 - Charles M. Deber, University of Toronto
2000 - Richard A. Houghten, Torrey Pines Institute for Molecular Studies
1998 - Peter W. Schiller, Clinical Research Institute of Montreal
1998 - James A. Wells, Genentech, Inc.
1996 - Arthur M. Felix, Hoffmann-La Roche, Inc.
1996 - Richard G. Hiskey, University of North Carolina
1994 - George Barany, University of Minnesota, Minneapolis
1994 - Garland R. Marshall, Washington University Medical School, St. Louis
1992 - Isabella L. Karle, Naval Research Laboratory
1992 - Wylie W. Vale, The Salk Institute for Biological Studies
1990 - Daniel H. Rich, University of Wisconsin-Madison
1990 - Jean E. Rivier, The Salk Institute for Biological Studies
1988 - William F. De Grado, DuPont Central Research
1988 - Tomi K. Sawyer, The Upjohn Company
1986 - Roger M. Freidinger, Merck Sharpe & Dohme
1986 - Michael Rosenblatt, Massachusetts General Hospital
1986 - James P. Tam, The Rockefeller University
1984 - Betty Sue Eipper, The Johns Hopkins University
1984 - Lila M. Gierasch, University of Delaware
1984 - Richard E. Mains, The Johns Hopkins University

The 2015 Rao Makineni Lectureship

Endowed by PolyPeptide Laboratories and Murray and Zelda Goodman (2003)

Paramjit S. Arora



Paramjit Arora is a Professor of Chemistry at New York University. He obtained his B.S. in Chemistry from UC Berkeley and received his Ph.D. degree in Chemistry from UC Irvine. He then pursued an American Cancer Society postdoctoral fellowship at the California Institute of Technology before joining the faculty of New York University in 2002. His research efforts are aimed at evaluating synthetic strategies for modulating protein- protein interactions. Proteins often utilize small folded domains for recognition of other biomolecules. The basic hypothesis guiding research efforts in the Arora Group is that mimicry of these folded peptide domains with metabolically stable synthetic molecules would lead to modulators of the desired interaction. The group has made significant progress in developing strategies that provide conformationally defined peptide and peptidomimetic foldamers. These efforts have led to the Hydrogen-Bond Surrogate α -helices and the Oxopiperazine Helix Mimetics. Both compound classes have been shown to interfere with chosen protein- protein interactions in cell-free, cell culture and animal models. The group has also described computational strategies to approach the critical question of how to identify the subset of protein-protein interactions that are amenable to disruption by synthetic ligands.

The Rao Makineni Lectureship Winners

- 2015 - Paramjit S. Arora, New York University, New York
- 2013 - Sam Gellman, University of Wisconsin, Madison
- 2011 - Jeffery W. Kelly, The Scripps Research Institute
- 2009 - William DeGrado, University of Pennsylvania
- 2007 - Ronald T. Raines, University of Wisconsin - Madison
- 2005 - Robin E. Offord, Centre Medical Universitaire, Switzerland
- 2003 - James P. Tam, Vanderbilt University

The 2015 Murray Goodman Scientific Excellence & Mentorship Award

The Goodman Award recognizes an individual who has demonstrated career-long research excellence in the field of peptide science. In addition, the selected individual should have been responsible for significant mentorship and training of students, post-doctoral fellows, and/or other co-workers. The Awards Committee may also take into account any important contributions to the peptide science community made by the candidate, for example through leadership in the American Peptide Society and/or its journals. Endowed by Zelda Goodman (2007).

George Barany



George has been a professor in the Department of Chemistry at the University of Minnesota since 1980 and is currently a Distinguished McKnight University Professor. He was born in Hungary in 1955 and immigrated with his family to the United States in 1960. He attended Stuyvesant High School in New York City, and continued directly to The Rockefeller University where he started his graduate studies in 1971 with Professor Bruce Merrifield. He published his first paper in 1973 on the synthesis of an ATP-binding peptide and earned his doctorate in 1977 for development of the dithiasuccinoyl (Dts) protecting group.

Dr. Barany is internationally recognized for his pioneering development of mild methods for solid-phase synthesis of peptides, the co-invention of DNA-on-a-chip technology, and the introduction of the concept of orthogonality into organic chemistry and chemical biology. His research interests encompass peptide synthesis, protecting groups for organic functionalities, the chemistry of thiols, disulfides, and polysulfanes, functionalization of soluble and insoluble polymers, methods for preparation of chemical combinatorial libraries, and the mechanisms of protein folding including the design and synthesis of constructs that autonomously fold in aqueous media.

Professor Barany's ground-breaking research is described in nearly 370 scientific publications, including a number of seminal review articles, and numerous patents which span the fields of peptide synthesis resin supports (PEG-PS, CLEAR), peptide synthesis reagents and protecting groups (PAL, HAL, XAL, BAL, Clear-OX), technologies for the synthesis of antisense (phosphorothioate) DNA and RNA, and universal DNA arrays for detection of genetic diseases. His inventions have netted nearly 91.4 million in royalties and licensing fees to the University of Minnesota. Interestingly, Dr. Barany synthesized the active ingredient of garlic, and collaborated to show its chemopreventive properties.

While at Minnesota, Professor Barany has mentored approximately 60 graduate and post-doctoral students, and over 100 undergraduates. Many of his protégés have gone on to prominence as independent scientists in academia, industry, biotechnology, and government, and several of them have received prestigious awards of their own.

George Barany received the Vincent du Vigneaud Award for outstanding achievements in peptide research in 1994, and the Ralph F. Hirschmann Award in peptide Chemistry from the American Chemical Society in 2006. He served a six-year term on the Council of the American Peptide Society, and in 1999 was co-chair of the Sixteenth American peptide Symposium held in Minneapolis.

Murray Goodman Scientific Excellence & Mentorship Award Winners

2015 - George Barany, University of Minnesota, Minneapolis

2013 - Robert Hodges, University of Colorado, Denver

2011 - Victor J. Hruby, University of Arizona

2009 - Charles M. Deber, University of Toronto, Hospital for Sick Children

Young Investigators' Competition

Oral Presentation Winners

1st	Timothy Siegert	Tufts University	<i>Cyclic Peptides that Bind a Vesicle Trafficking Protein: A Concerted Computational and Synthetic Approach</i>
2nd	Michael Ferracane	University of Florida	<i>Opioid Ligand Binding to Opioid Receptors: Insight and Implications for Peptide Design</i>
3rd	Sylvia Els-Heindl	University of Leipzig	<i>High Metabolic in vivo Stability and Bioavailability of a Palmitoylated Ghrelin Receptor Ligand Assessed by Mass Spectrometry</i>

Poster Competition Winners

Margherita Di Pisa	Université Pierre et Marie Curie	<i>Short cationic cell penetrating lipopeptides: design, synthesis, evaluation of the internalization properties and intracellular localization</i>
Ziqing Qian	The Ohio State University	<i>Intracellular Delivery of Peptidyl Ligands by Reversible Cyclization: Discovery of a PDZ Domain Inhibitor that Rescues CFTR Activity</i>
Valle Palomo	The Scripps Research Institute	<i>Quantum-dot/Dopa-peptide bioconjugates function as tools for in vitro exopeptidase sensing</i>
Daniel Nielsen	University of Queensland	<i>Flexibility and Rigidity in Orally Bioavailable Cyclic Peptides</i>
Saghar Mowlazadeh Haghighi	University of Arizona	<i>Conformationally Constrained Ac-His-D-Nal(2)-Nle-Trp-NH₂ Analogues Leads to Selective Melanotropins</i>
Naila Assem	The Scripps Research Institute	<i>A convergent approach for peptide macrocyclization and labeling</i>

Contents

Introduction	vii
Editor's remarks	viii
Message from the president of the American Peptide Society	ix
Symposium Sponsors and Exhibitors	xii
American Peptide Society	xiv
American Peptida Symposia	xv
The Merrifield Award	xvi
The Vincent Du Vigneaud Awards	xviii
The Makineni Lecture	xxi
The Murray Goodman Award	xxii
Yound Investigator's Competition	xxiii
Contents	xxiv
 Orthogonal Solid-Phase Peptide Synthesis	 1
<i>George Barany</i>	
Total Synthesis, Functional Analysis and Biological Evaluation of Antibiotic Peptide Natural Products	9
<i>Masayuki Inoue, Takuya Kaji, Motoki Murai, Takefumi Kuranaga, Hiroshi Hamamoto, Kazuhisa Sekimizu</i>	
The Nature of Peptidomimetics: Synthetic Peptide Macrocycles as Potential Therapeutics and Artificial Peptide Helices	12
<i>Danielle A. Guarracino, John J. Ferrie, Jessica J. Gruskos, Ari L. Goldwaser, Megan E. Decker, Anginelle M. Alabanza, Camille T. Robertson, Sanjna S. Sanghvi, Susan Knox, Dylan H. Nguyen, Kayla Gentile, Maria Minor</i>	
Downsizing Proteins Without Losing Potency or Function	16
<i>David P. Fairlie, Mei-Kwan Yau, Johan K. Hamidon, Rane Singh, Junxian Lim, Jacky Y. Suen, Jessica A. Rowley, Rink-Jan Lohman, Martin J. Stoermer, Abishek Iyer, Robert C. Reid</i>	
The Main-Chain Oxygen: Unappreciated Effects on Peptide and Protein Structure	20
<i>Robert W. Newberry, Ronald T. Raines</i>	
Opioid Ligand Binding to Opioid Receptors: Insight and Implications for Peptide Design	22
<i>Michael J. Ferracane, Jane V. Aldrich</i>	
Designing Enzyme-Like Catalysts: A Rhodium(II) Metallopeptide Case Study	24
<i>Farrukh Vohidov, Brian V. Popp, Zachary T. Ball</i>	
Butelase 1: A Versatile and Multi-Purpose Ligase	27
<i>James P. Tam, Giang K.T. Nguyen, Xinya Hemu</i>	

Novel Agents that Prevent Atherosclerosis: Multivalent Peptide Constructs and Self-Assembling Cyclic DL- α -Peptides	30
<i>Bruce E. Maryanoff, Luke J. Leman, Yannan Zhao, Tomohiro Imura, Audrey S. Black, David J. Bonnet, Linda K. Curtiss, M. Reza Ghadiri</i>	
Rippled β -Sheet Fibrils from Coassembled Enantiomeric Amphipathic Peptides as Potential Microbicide Biomaterials	33
<i>Bradley L. Nilsson, Danielle M. Raymond, Jade J. Welch</i>	
Antibody Cross-Reactivity to Hemagglutinin Protein Antigens Demonstrates Feasibility for Development of a “Universal” Influenza A Synthetic Peptide Vaccine	36
<i>Ziqing Jiang, Lajos Gera, Colin T. Mant, Robert S. Hodges</i>	
Solid-Phase Synthesis of Azasulfurylphenylalanine4-GHRP-6	40
<i>Stéphane Turcotte, William D. Lubell</i>	
Design of Multivalent Ligands that Cross the Blood Brain Barrier for the Treatment of Neuropathic Pain Without Toxicities	43
<i>Victor J. Hruby, Takashi Yamamoto, Aswini Giri, Davis S. Herman, Tally Largent-Milnes, Todd Vanderah, Frank Porreca</i>	
Isolation, Characterization and Structure-Activity Studies of Novel Brevinin-1 Peptides from the Skin of the Frog <i>Clinotarsus curtipes</i>	45
<i>Parvin Abraham, K. Santhosh Kumar</i>	
Design and Synthesis of Lasso-Inspired Peptides with Antibacterial Activity	47
<i>François Bédard, Riadh Hammami, Ahmed Gomaa, Muriel Subirade, Ismail Fliss, Eric Biron</i>	
Non-Natural D-Amino Acids to Control Bacterial Virulence	51
<i>Michael A. Bertucci, Kareem March</i>	
Angiotensin I-Converting Enzyme Inhibitory Activity of Enzymatic Hydrolysates of Whey Milk, Casein and Egg Albumin by Microbial Enzymes and a Commercial Enzyme	54
<i>Y.A.A. Hamin-Neto, H. Cabral</i>	
Fluorescent Delta Selective Opioid Peptides from a Cyclic Peptide Combinatorial Library	57
<i>M. Cazares, A. Gioseffi, A. Bunnell, Y. Li, C.T. Dooley</i>	
Mechanistic Proposal for Restricted Peptides Action on Parasite Membrane	61
<i>Marcelo D.T. Torres, Adriana F. Silva, Flávio L. Alves, Antonio Miranda, Margareth L. Capurro, Rodrigo M. Cordeiro, Vani X. Oliveira Jr.</i>	
Linear Peptides Related to Angiotensin II with Antiplasmodial Activity	64
<i>Adriana F. Silva, Marcelo D.T. Torres, Leandro S. Silva, Flávio L. Alves, Ana A.S. Pinheiro, Antonio Miranda, Margareth L. Capurro, Vani X. Oliveira Jr.</i>	
Antiplasmodial Activity of Angiotensin II Analogs	67
<i>Danieli Melo de Freitas, Vani Xavier Oliveira Jr.</i>	

Effects of Methyl and Halogens in Analgesic Peptide Molecules for Their Potent Agonist Activities at MOR/DOR and Antagonist Activity at NK1R	69
<i>Aswini Kumar Giri, C.R. Apostol, P. Davis, D. Rankin, G. Molnar, T.W. Vanderah, F. Porreca, V.J. Hruby</i>	
Structure Activity Relationship of Stable Dynorphin A-(2-13) Analogues Interacting at the Bradykinin-2 Receptor	71
<i>Sara M. Hall, Yeon Sun Lee, Cyf Nadine Ramos Colón, Frank Porreca, Josephine Lai, Victor J. Hruby</i>	
Structure-Activity Relationships of Constrained Dermorphin Analogues Containing an α -Alkyl- β -Substituted Alanines	73
<i>Anika Lasota, Oliwia Fraczak, Adriana Muchowska, Aleksandra Misicka, Michal Nowakowski, Maciej Maciejczyk, Andrzej Ejchart, Aleksandra Olma</i>	
Dimeric Dermorphin Analogues Containing β 3-Homo-Amino Acids: Synthesis, Binding Affinities and Metabolic Stability	77
<i>Oliwia Fraczak, Anika Lasota, Adriana Muchowska, Piotr Kosson, Dagmara Tymecka, Aleksandra Misicka, Aleksandra Olma</i>	
Amphipathic Non-opioid Dynorphin A Analogs to Inhibit Neuroexcitatory Effects at Central Bradykinin Receptors	80
<i>Yeon Sun Lee, Sara M. Hall, Cyf Ramos-Colon, Michael Remesic, Alexander Kuzmin, David Rankin, Todd W. Vanderah, Frank Porreca, Josephine Lai, Victor J. Hruby</i>	
Bauhinia Bauhinioides Kallikrein Inhibitor Fragments with Bradykinin-Like Activities	82
<i>Flavio A. Lopes, Jones M. Silva, Maria Luiza V. Oliva, Antonio Miranda</i>	
Active Leptin Fragments Resistant to Proteolytic Enzymes Present in Human Plasma	84
<i>Paula Y. Tokuyama, Edgar J. Paredes-Gamero, Antonio Miranda</i>	
Leptin Fragment Increase Hematopoietic Stem Cell Population and Improve Its Engraftment Ability	86
<i>Carolina C. Dias, Amanda Nogueira-Pedro, Edgar J. Paredes-Gamero, Antonio Miranda</i>	
Biological Studies of Angiotensin II Analogs Using Nanostructured Micelles	88
<i>Cibele Nicolaski Pedron, Daniele Ribeiro Araújo, Vani Xavier Oliveira Jr.</i>	
Cyclotides from Pombalia, Noisettia and Viola Genus: Discovery and Inhibitors of Cellular Migration	91
<i>Meri Emili F. Pinto, Jenny Najas Z. Garavito, Luma G. Magalhães, Adriano D. Andricopulo, Christian W. Gruber, Eduardo M. Cilli, Angelo C. Pinto, Vanderlan S. Bolzani</i>	
Mitsunobu Reaction on Solid Support for Peptide N-terminal Farnesylation	94
<i>Julien Poupart, William D. Lubell</i>	
Structure-Activity Relationship Studies of Dynorphin A Analogs at the Kappa Opioid Receptor	96
<i>Cyf N. Ramos Colon, Yeon Sun Lee, Sara M. Hall, Josephine Lai, Frank Porreca, Victor J. Hruby</i>	

Design and Synthesis of a Novel Tetrapeptide with Improved Selectivity Towards the hMC1R	98
<i>Jonathon R. Sawyer, Saghar Mowlazadeh Haghighi, Yang Zhou, Kaitlyn McLeod, Victor J. Hruby, Minying Cai</i>	
Alcohol Abrogates Intracellular Ca ²⁺ Elevation by Angiotensin II and ATP in Cultured Rat Astrocytes	101
<i>Steve Wu, Zhiqian Wu, Desuo Wang</i>	
Designing AMPed: The Practical Antimicrobial Peptide Editable Database	105
<i>Tripti Garg, George Konstantinidis, Joan Peckham, Admir Monteiro, Roxanne LaCroix, Lenore M. Martin</i>	
Comparing Structures of Two Antimicrobial Peptides Using a Self-Organized Mapping Approach	109
<i>Faramarz Joodaki, Preston Steele, Lenore M. Martin, Michael L. Greenfield</i>	
Multi-Variable Individual Heating Conditions Tested in Parallel Provide Rapid Process Optimization on the Prelude® X	112
<i>Daniel Martinez, James P. Cain, Elizabeth Restituyo-Rosario, Katya Karankevich, Peter Bergwall, Nathaniel Cosper</i>	
Labeling and Expression of Opioid Receptors Using N-terminal Fusion of Fluorescent Proteins	113
<i>C.T. Dooley, A. Gioseffi, Y. Li</i>	
B7H6: A Bio-Marker for the Development of Cancer-Targeted Immunotherapy Applications	117
<i>Mariana Phillips, Constantine Bitsaktsis, David Sabatino</i>	
Structural Determinants of Furin Inhibitors Derived from Influenza Hemagglutinin	119
<i>Monika Lewandowska-Goch, Anna Kwiatkowska, Teresa Lepek, Adam Prahl, Robert Day</i>	
A Dual Photochemical Ring-Opening/Cleavage Approach for the Synthesis and Decoding of One-Bead-One-Compound Cyclic Peptide Libraries	122
<i>Xinxia Liang, Simon Vézina-Dawod, François Bédard, Eric Biron</i>	
Optimized Method to Generate Synthetically Challenging Macrocyclic Tetrapeptides that do not have a Turn Inducer	125
<i>Sanjeewa N. Senadheera, Jane V. Aldrich</i>	
Towards the Development of Cell Permeable Macrocyclic Scaffolds: Probing the Structural Requirements for Enhancing Cellular Uptake	127
<i>Simon Vézina-Dawod, Sophie Fortin, Marie Perrin, Louis-Jean Bordeleau, Stéphane Gobeil, Eric Biron</i>	
Stability Evaluation of Immobilized Peptides Towards Proteases by Mass Spectrometry	131
<i>Silvana L. Giudicessi, María L. Salum, María C. Martínez-Ceron, Osvaldo Cascone, Rosa Erra-Balsells, Silvia A. Camperi</i>	
Multicomponent Dipeptide Supramolecular Hydrogels as Fibronectin-Mimetic Biomaterials	134
<i>Wathsala Liyanage, Bradley L. Nilsson</i>	

One-Bead-One-Peptide Library to Purify <i>Crotalus durissus terrificus</i> Phospholipase A2	137
<i>María C. Martínez-Ceron, Soledad L. Saavedra, Lucía Ávila, Silvana L. Giudicessi, Fernando Albericio, Silvia A. Camperi, Osvaldo Cascone</i>	
Detection of Protease Activity by Concentration Quenching-Based Substrates	139
<i>Daisuke Sato, Wu Zhe, Tamaki Kato</i>	
A New Concept: A Peptide Monolayer for Accurate Positioning of Electroactive Probes at Close Distance from a Gold Surface	141
<i>M. Caruso, E. Gatto, A. Palleschi, M. De Crescenzi, K. Wright, E. Longo, M. De Zotti, F. Formaggio, C. Toniolo, M. Venanzi</i>	
Comparison of the Effects of Myristoylated and Transactivating Peptide (TAT) Conjugated Mitochondrial Fission Peptide Inhibitor (P110) in Myocardial Ischemia/Reperfusion (I/R) Injury	143
<i>Israel Benjamin, Jonathan Vu, Christina Lipscombe, Devon Stutzman, Carly Schmidgall, Harsh Patel, Samir Patel, Qian Chen, Cathy J. Hatcher, Robert Barsotti, Lindon H. Young</i>	
Myristoylated PKC β II Peptide Inhibitor Exerts Dose-Dependent Inhibition of N-Formyl-L-Methionyl-L-Leucyl-L-Phenylalanine (fMLP) Induced Leukocyte Superoxide Release	147
<i>Chinyere B. Ebo, Carly Schmidgall, Christina Lipscombe, Harsh Patel, Qian Chen, Robert Barsotti, Lindon H. Young</i>	
Comparing the Effectiveness of TAT and Myristoylation of gp91ds on Leukocyte Superoxide (SO) Release	150
<i>Harsh Patel, Kyle Bartol, Amelie Bottex, Ryan Remarcke, William Chau, Sydney Walker, Qian Chen, Robert Barsotti, Lindon H. Young</i>	
Pancreatic β -Cell Imaging with High Affinity Peptide Ligands to the GLP-1 Receptor	154
<i>Bikash Manandhar, William Silvers, Amit Kumar, Su-Tang Lo, Xiankai Sun, Jung-Mo Ahn</i>	
Development of a Troponin-Specific Probe for Early Detection of Cardiac Injuries	156
<i>Lara Pes, Young Kim, Ching-Hsuan Tung</i>	
Effects of Mitochondrial-Targeted Antioxidants on Real-Time Blood Nitric Oxide and Hydrogen Peroxide Release in Acute Hyperglycemic Rats	158
<i>Matthew L. Bertolet, Michael Minni, Tyler Galbreath, Robert Barsotti, Lindon H. Young, Qian Chen</i>	
Investigating Metabolic Gender Differences with Melanocortin Antagonist SKY 2-23-7	162
<i>Cody J. Lensing, Skye R. Doering, Danielle N. Adank, Carrie Haskell-Luevano</i>	
Protein Kinase C Beta II (PKC β II) Peptide Inhibitor Exerts Cardioprotective Effects in Myocardial Ischemia/Reperfusion Injury	165
<i>Christina Lipscombe, Israel Benjamin, Devon Stutzman, Amelie Bottex, Chinyere Ebo, William Chau, Harsh Patel, Qian Chen, Cathy J. Hatcher, Robert Barsotti, Lindon H. Young</i>	
Reduced Cycle Times & Solvent Consumption for the Synthesis of (65-74)ACP on the Symphony X®	169
<i>Daniel Martinez, James P. Cain, Elizabeth Restituyo-Rosario, Katya Karankevich, Peter Bergwall, Nathaniel Cosper</i>	

Tris-Benzamide Analogs for Inhibiting Bcl-2 Proteins in Prostate Cancer	170
<i>Joongsoo Kim, Rakesh Kumar, Jung-Mo Ahn</i>	
Peptide Coupling Challenges to Aza-Pipicolyl Smac Mimetic	172
<i>Ramesh Chingle, William D. Lubell</i>	
Structure-Based Design, Synthesis and Evaluation of Novel Peptidic Inhibitors of Thrombin-Induced Activation of Platelets Aggregation	174
<i>Janet Gonzalez, Anna Babinska, Ebenezer L.V. Ewul, Edem Timpo, Alhassan Jallow, Zhiyong Qiu, Radoslaw Bednarek, Maria Swiatkowska, Moro O. Salifu, Manfred Philipp, Cristina C. Clement</i>	
Peptide Ring Closing Metathesis: Minimizing Side Reactions in Aroclor Analogs	177
<i>Solomon A. Gisement, Jane V. Aldrich</i>	
Design and Construction of a Selection Peptide Library Based on the Human Thymic Hormone Thymopoietin Domain	179
<i>Chunjie Gong, Jianhao Xu, Ling Li, Qianhui Li, Huiling Guo, Li Zheng, Honghao Sun, Zhengding Su</i>	
Antimicrobial and Hemolytic Activity of Cysteine-Deleted Tachyplesin (CDT) Analogues in the Pursuit of Therapeutic Selectivity	181
<i>Deborah Heyl, Yeji Park, Jennifer Garvey, Rebecca Newman, Yllka Vladaj</i>	
Synthesis of N-Methyl and Azasulfuryl Urotensin-II(4-11) Derivatives	184
<i>Francesco Merlino, Ali M. Yousif, Salvatore Di Maro, Stéphane Turcotte, Julien Dufour-Gallant, David Chatenet, Paolo Santicioli, Ettore Novellino, Paolo Grieco, William D. Lubell</i>	
Synthesis and Evaluation of Azapeptide Prostaglandin F _{2α} Receptor Modulators in Pursuit of Inhibitors of Preterm Labor	187
<i>Fatemeh Mohammadpour, Sylvain Chemtob, Xin Hou, William D. Lubell</i>	
Conformationally Constrained Ac-His-D-Nal(2')-Nle-Trp-NH ₂ Analogues Leads to Selective Melanotropins	189
<i>Saghar Mowlazadeh Haghighi, Mingying Cai, Yang Zhou, Bailey Lahtinen, Victor J. Hruby</i>	
Solid-Phase Peptide Synthesis and Structural Analyses by Circular Dichroism Spectroscopy of the Cytotoxic D-(KLAKLAK) ₂ Sequence	191
<i>Niki Rana, David Sabatino</i>	
Lasso Peptides and Murein Peptide Ligase Inhibitors as Novel Anti-Mycobacterial Agents	193
<i>Francesca Scotti, Sanjib Bhakta, John P. Malkinson</i>	
Discovery of Novel, Potent and Long Acting CCK Analogs	195
<i>Robert Hunter, Andrew Carpenter, Erin Swiger, Makda Mebrahtu, Robert Wiard, Andrea Acker, Shane Roller, Mark Paulik, Ved Srivastava</i>	
Discovery of Novel and Long Acting GLP-1 Analogs	197
<i>Robert Hunter, Andrew Carpenter, Erin Swiger, Makda Mebrahtu, Robert Wiard, Andrea Acker, Shane Roller, Mark Paulik, Ved Srivastava</i>	

Mono and Bis-Triazoles Incorporated into Chimeric AGRP-Melanocortin Peptide Template as Disulfide-Bridge Mimetics	200
<i>Srinivasa R. Tala, Anamika Singh, Sathya M. Schnell, Katie Freeman, Carrie Haskell-Luevano</i>	
Solid-Phase Synthesis of Aza-Lysine Peptide Analogue of Trypsin Substrate	202
<i>Mariam Traore, William D. Lubell</i>	
<i>In Vitro</i> Evaluation of New, Potent and Selective V2 Receptor Agonists	204
<i>Kazimierz Wisniewski, Hiroe Tariga, Glenn Croston, Diane M. Hargrove, Pierre J-M. Rivière, Gebhard Neyer, Claudio D. Schteingart</i>	
Novel Macrocyclic Peptides Active at Human Melanocortin Receptors: A Preliminary SAR Study	207
<i>A.M. Yousif, M. Cai, F. Merlino, P. Grieco, V.J. Hruby</i>	
A Study on the Structural Stability of the Peptide 2.0(5)-Helix by Infrared Absorption Spectroscopy	210
<i>M. De Zotti, B. Di Napoli, C. Mazzuca, A. Palleschi, G.M.L. Messina, G. Marletta, F. Formaggio</i>	
Mimicking the Binding Sites of Wnt Proteins: Rational Design of Wnt/Fzd-Signaling Modulators	212
<i>Ana I. Fernández-Llamazares, Kevin C.M. Hermans, Peter Timmerman, W. Matthijs Blankesteijn</i>	
Structural Requirement of Fibrogenic Peptide AG97 (SAKVDAIGLEIV) and B160 (VILQSSAADIAR) for Amyloid-Like Fibril Formation and Cellular Activity	215
<i>Fumihiko Katagiri, Kazuki Takeyama, Nobuko Yamada, Atsushi Naito, Satomi Yamada, Kentaro Hozumi, Yamato Kikkawa, Motoyoshi Nomizu</i>	
Misfolding and Oligomerization of Amyloid β (1-40)	217
<i>Sándor Lovas, Charles R. Watts</i>	
Structure Stabilizing Role of Aromatic Interactions is Decided by Spatial Arrangement of Aromatic Pairs: A Case Study with Designed Peptide β -Hairpins	220
<i>Kamlesh Madhusudan Makwana, Radhakrishnan Mahalakshmi</i>	
Differential Potencies for Endogenous Dynorphins Indicate Functional Selectivity at the Delta Opioid Receptor	223
<i>Keith M. Olson, Justin Lavigne, John Streicher, Frank Porreca, Victor J. Hruby</i>	
Probing Peptide-Membrane Interaction by Neutron Scattering	225
<i>Shuo Qian</i>	
Investigating the Effects of Aromatic Amino Acids on Amphipathic Peptide Self-Assembly and Emergent Hydrogel Viscoelasticity	228
<i>Annada Rajbhandary, Bradley L. Nilsson</i>	
Peptide-Guided Design of Mdm2/MdmX Inhibitors with Anticancer Activity	232
<i>Lingyun Qin, Yao Chen, Rong Chen, Jinjin Zhou, Fei Yang, Zhengding Su</i>	

Structural Characterization of PPII helical Oligoproline	234
<i>Patrick Wilhelm, Bartosz Lewandowski, Helma Wennemers</i>	
Development Oral Available Melanotropins Based on the Cyclic Peptide Framework of Sunflower Trypsin Inhibitor-1	236
<i>Minying Cai, David Craik, Horst Kessler, Victor J. Hruby</i>	
Kv1.3 Selective Peptides Based Upon N-Terminal Extension and Internal Substitutions of ShK Toxin	238
<i>Rosendo Estrada, Redwan Huq, Rajeev Tajhya, Satendra Chauhan, Christine Beeton, Michael W. Pennington</i>	
Development of Novel Broad Spectrum Anticancer Small Molecule Peptidomimetics with Nanomolar Activity	241
<i>Lajos Gera, John Tentler, S. Gail Eckhardt, Ziqing Jiang, Angelo D'Alessandro, Robert S. Hodges</i>	
Design of New Antimicrobial Peptides (AMPs) with “Specificity Determinants” that Encode Selectivity for Gram Negative Pathogens and Remove Both Gram-Positive Activity and Hemolytic Activity from Broad-spectrum AMPs	245
<i>Ziqing Jiang, Lajos Gera, Colin T. Mant, Robert S. Hodges</i>	
Structure-Based Optimization of a Potent PACE4 Inhibitor Containing a Decarboxylated P1 Arginine Mimetic	249
<i>Anna Kwiatkowska, Christine Levesque, Frédéric Couture, Kévin Ly, Frédéric Dufour, Robert Day</i>	
From Bench to Clinical Using a Combinatorial Screenings of Phage-Displayed Peptide Libraries	252
<i>Nelson Santiago Vispo, Hortensia Rodríguez Cabrera</i>	
Design, Synthesis and Test of Novel Lipidated Cysteine Analogs as Efficient TLR2/6 Agonists	255
<i>Yang Zhou, Abid H. Banday, Minying Cai, Victor Hruby</i>	
An Auxiliary-Mediated Approach for the Chemoenzymatic Synthesis of Homogenous Glycopeptides	257
<i>Claudia Bello, Christian F.W. Becker</i>	
High-Throughput Process Optimization and Difficult Peptide Synthesis on the Symphony® X	259
<i>Daniel Martinez, James P. Cain, Elizabeth Restituyo-Rosario, Katya Karankevich, Peter Bergwall, Nathaniel Cosper</i>	
A Comparison of Heating Protocols for the Cyclization of Melanotan II on the Prelude® X	260
<i>Daniel Martinez, James P. Cain, Elizabeth Restituyo-Rosario, Katya Karankevich, Peter Bergwall, Nathaniel Cosper</i>	
Identifying Immunogenic CD4+ T-Cell Epitopes of Myeloid Cell Leukemia 1 Using Overlapping 20-mer Peptides Spanning the Whole Protein	262
<i>Joshua S. Woodworth, Else M. Agger, Paul R. Hansen</i>	

Fmoc Solid-Phase Peptide Synthesis of Human α -Calcitonin Gene-Related Peptide and Two Fluorescent Analogs	264
<i>M. Fuente-Moreno, A. Oddo, M. Sheykhzade, D.S. Pickering, P.R. Hansen</i>	
Mechanistic Insights into the Zumbach-Weiss-Kühle Synthesis of Dithiasuccinoyl (Dts)-Protected Amines	266
<i>Matthew J. Henley, Michael J. Barany, Lin Chen, Robert P. Hammer, Alex M. Schrader, Victor G. Young, Jr., George Barany</i>	
Peptide Ligation via Suzuki-Miyaura Cross-Coupling Reaction	268
<i>Tae-Kyung Lee, Bikashy Manandhar, Jung-Mo Ahn</i>	
Multiple Labeling of Peptides via Orthogonal Coupling Reactions and Its Applications	270
<i>Bikash Manandhar, Tae-Kyung Lee, Jung-Mo Ahn</i>	
4,5-Disubstituted N-aminoimidazol-2-One Mimics of Peptide Turn Backbone and Side Chain Conformation	272
<i>Julien Poupart, Duc Doan-Ngoc, William D. Lubell</i>	
Trends to Acid-Labile Cys Protecting Groups: Thp as an Efficient and Non-Aromatic Cys Protecting Group for Fmoc Chemistry	274
<i>Iván Ramos-Tomillero, Hortensia Rodríguez, Fernando Albericio</i>	
Development of Chemistry-Based Protocol for Sequence-Dependent Thioesterification	278
<i>Yusuke Tsuda, Akira Shigenaga, Kohei Tsuji, Masaya Denda, Kohei Sato, Keisuke Kitakaze, Tsubasa Inokuma, Kohji Itoh, Akira Otake</i>	
N-Substituted Arylsulfonamides as Alternative Building Blocks in Peptoid and Peptide Synthesis	280
<i>Simon Vézina-Dawod, Steve Jobin, Antoine Derson, Claire Herby, Eric Biron</i>	
Optimizing a Larger Scale Synthesis of Zyklophin, a Highly Selective Peptide Kappa Opioid Receptor Antagonist	283
<i>Tatyana V. Yakovleva, Jane V. Aldrich</i>	
Application of the DoE Concept for Peptide API Process Development at Bachem	286
<i>Daniel Samson, Wolfgang Seufert, Matteo Villain, Alex Fässler</i>	
Author Index	289

Orthogonal Solid-Phase Peptide Synthesis

George Barany

Department of Chemistry, University of Minnesota, Minneapolis, MN, 55455, USA

Introduction

I am deeply honored to receive the Murray Goodman Scientific Excellence & Mentoring Award, and to join the distinguished company of its past recipients. It was a privilege to know Professor Goodman, whose exceptional combination of scientific innovation and mentorship offers a model we can all hope to emulate.

Our theme is *orthogonality*, a concept I introduced to peptide chemistry during my doctoral studies with Bruce Merrifield at The Rockefeller University [1, 2], and which has been a centerpiece of my independent career on the University of Minnesota chemistry faculty.

Orthogonality

In mathematics, “orthogonality” means intersecting at right angles. In law, it refers to multiple issues that are irrelevant to each other, a point that recently came up in arguments at the U.S. Supreme Court, much to the delight of Justices Roberts and Scalia [3]. In crossword puzzles [4], orthogonal clues can hide the theme. For example, if I asked you “Boston airport” (five letters: answer LOGAN), and “Ball girl?” (three letters: answer DEB), you would get an extra “aha” once you realized that the puzzle was about the wedding of my daughter Deb to my new son-in-law Logan that took place the weekend just preceding the award lecture.

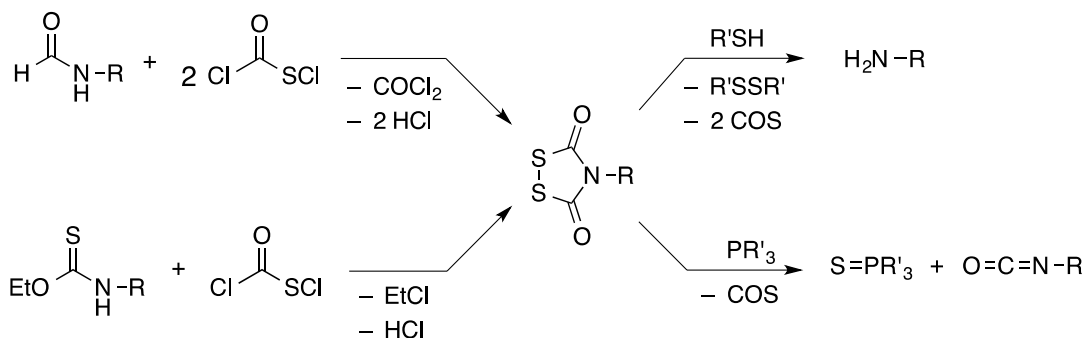
The term “orthogonal” was brought to chemistry in a 1977 *J. Am. Chem. Soc.* communication [1] where we defined an orthogonal system as a set of completely independent protecting groups in which different chemical mechanisms are used to remove each set. Ever since, this word has proven highly useful to succinctly describe a concept of chemoselectivity that chemists and biologists have grasped, at least intuitively, for much longer. Think Emil Fischer’s concept of an enzyme lock and a substrate key [5, 6], or E. J. Corey’s multi-level protecting group combinations for the total syntheses of complex poly-ols [7].

To illustrate, note that for the classic Merrifield scheme, the “temporary” *N*^α-amino Boc protecting group is removed at each cycle by treatment with trifluoroacetic acid (TFA), while all of the “permanent” side-chain protecting groups and the anchor to the support are required to be stable. This makes it necessary to use a much stronger acid, namely anhydrous HF, to achieve the final cleavage, a direct consequence of the fact that the same chemical mechanism is used to cleave both classes [2, 8]. In contrast, a two-dimensional orthogonal scheme can be developed, using the dithiasuccinoyl (Dts) protecting group on the *N*^α-amino group. Dts is very acid stable, but removable under mild conditions by thiolysis—hence fitting our definition of orthogonality. This now allows the Boc (and related) groups previously used for “temporary” protection to be applied to the side-chains, and taken with Wang’s *p*-alkoxybenzyl ester support [an electron-donating oxygen substituent on the ring makes the ester more acid-labile; see ref. 9], the entire protection scheme is “frame-shifted” to allow for the relatively milder cleavage by TFA. A third dimension of orthogonality can be added by adopting an acid-stable, non-thiolysable but photolabile *ortho*-nitrobenzyl ester, as first introduced into solid-phase peptide synthesis by Dan Rich [10], to provide anchoring to the support—this all was experimentally implemented with Fernando Albericio, as described in our 1985 *J. Am. Chem. Soc.* full paper [11].

Many others, including James Tam [12], Carolyn Bertozzi [13], Barry Sharpless [14], and Steve Zimmerman [15], have developed the idea in different directions, including to describe specific bond-making chemistries, like ligations, “clicks,” “stapling,” chemical modifications of proteins, PEGylation’s, and so forth [citations to this sentence are highly selective, and many more can be found with minimal effort]. In collaborative work with my former student Bob Hammer and my brother Francis, we exploited orthogonality to create universal “zip-code” arrays for highly specific “DNA-on-a-chip” detection of mutations in genetic diseases and cancer [16].

Dithiasuccinoyl (Dts) Chemistry

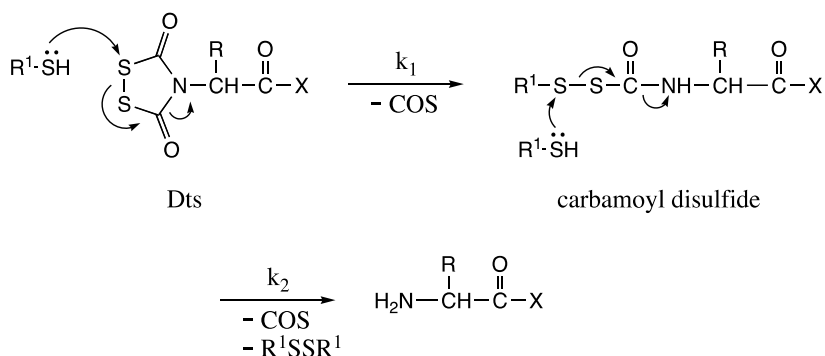
I found the 1,2,4-dithiazolidine-3,5-dione heterocycle in the German patent literature – credit goes to Zumach, Weiss, and Kühle) [17] – and saw how it could be adapted for amino group protection. Groups that cover both free valences of nitrogen are relatively rare. Viewed as a nitrogen atom linked to two molecules of carbonyl sulfide (COS), the analogy to a succinoyl group, but with two sulfurs, led me to coin the dithiasuccinoyl (Dts) moniker. Several multi-step routes to elaborate the Dts heterocycle had been proposed previously, and over the years we adapted and improved the original methods (Scheme 1).



Scheme 1. Preparation and transformations of dithiasuccinoyl (Dts)-amines

In terms of removal, I reasoned that any reductive procedure that cleaved the disulfide would eventually result in the reducing hydrogens ending on the nitrogen. In the process, two COS molecules would be lost, via thiocarbamate intermediates. Later, we realized that reagents like trivalent phosphines, that can “pluck out” a sulfur, make it possible to consider Dts-amines as “masked” isocyanates.

Early on, we established the kinetic and mechanistic details of the thiolytic removal of the Dts group [18, 19], which involved identification of so-called carbamoyl disulfide intermediates (Scheme 2). Although the two steps with rates k_1 and k_2 both involve disulfide cleavage and would nominally appear to be similar, they have rather different features and driving forces ... knowledge we would later be able to use in productive ways.

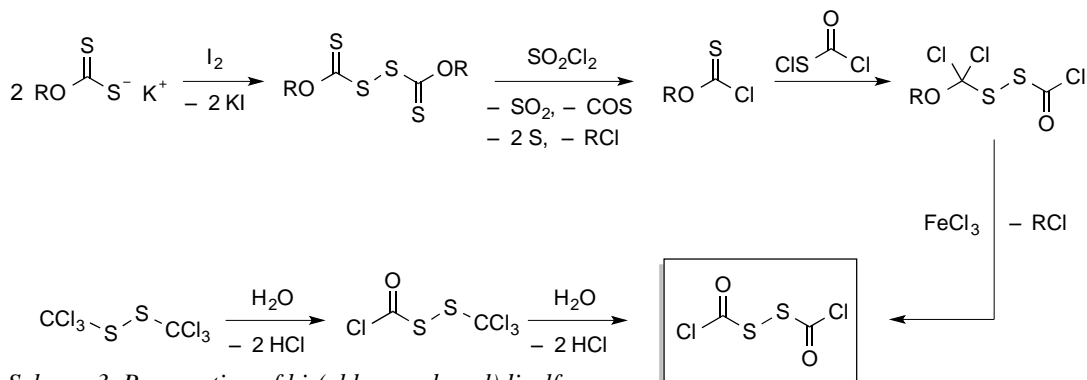


Scheme 2. Thiolytic removal of the dithiasuccinoyl (Dts)-amino protecting group

If we think of Dts as a cyclic carbamoyl disulfide, a myriad of interesting applications have emerged for this family of compounds:

- Primary amino groups that can be protected by Dts include not only the N^α -amino group of α -amino acids [1, 20, 21], but also the building blocks for peptide nucleic acids (PNA) [22] and the side-chains of amino sugar building blocks for certain glycopeptides [23].
- Obviously, Dts cannot be used to protect the N^α -imino group of proline, but fortunately we were able to optimize open-chain carbamoyl disulfide protection for this residue [24].
- We can “invert” the fundamental mechanism of thiolytic deprotection to develop protecting groups for the sulfhydryl side-chain of cysteine, and for “directed” syntheses of inter- and intramolecular disulfides [25, 26].
- The fact that Dts derivatives are “masked” isocyanates [21] can be very important, given all the difficulties and complications of working directly with isocyanates. Moreover, Dts-amino acids are desulfurized to N -carboxyanhydrides (NCA's), and Dts-dipeptides give rise to hydantoins, all under unusually mild conditions [20, 21].
- Focusing on the trivalent phosphorus that can act to desulfurize Dts (and a related compound we call “EDITH”), this chemistry serves as an excellent entry to phosphorothioate DNA and RNA for “anti-sense” applications [27, 28].
- Lastly, Dts chemistry makes it possible to come up with a vastly milder variation to the classic Gabriel synthesis that converts alkyl halides to the corresponding amines – I particularly want to call attention to Mark Wood and collaborators for independent results in this direction [29].

Turning to the preparation of Dts-amines, it was obvious almost from the start that there had to be some way that was more straightforward than what was in the literature. I found a 1973 paper by Kobayashi *et al.* [30] that described a rather roundabout route to bis(chlorocarbonyl)disulfane, the reagent in the box. But look at the structure: it has all of the non-nitrogen atoms that make up Dts, plus two leaving groups – surely this would be a winner. But first, Alayne Schroll, Andy Mott, and David Halsrud in my Minnesota lab had to put in an enormous amount of meticulous work [31] to develop a robust and reproducible route to the desired reagent (Scheme 3).



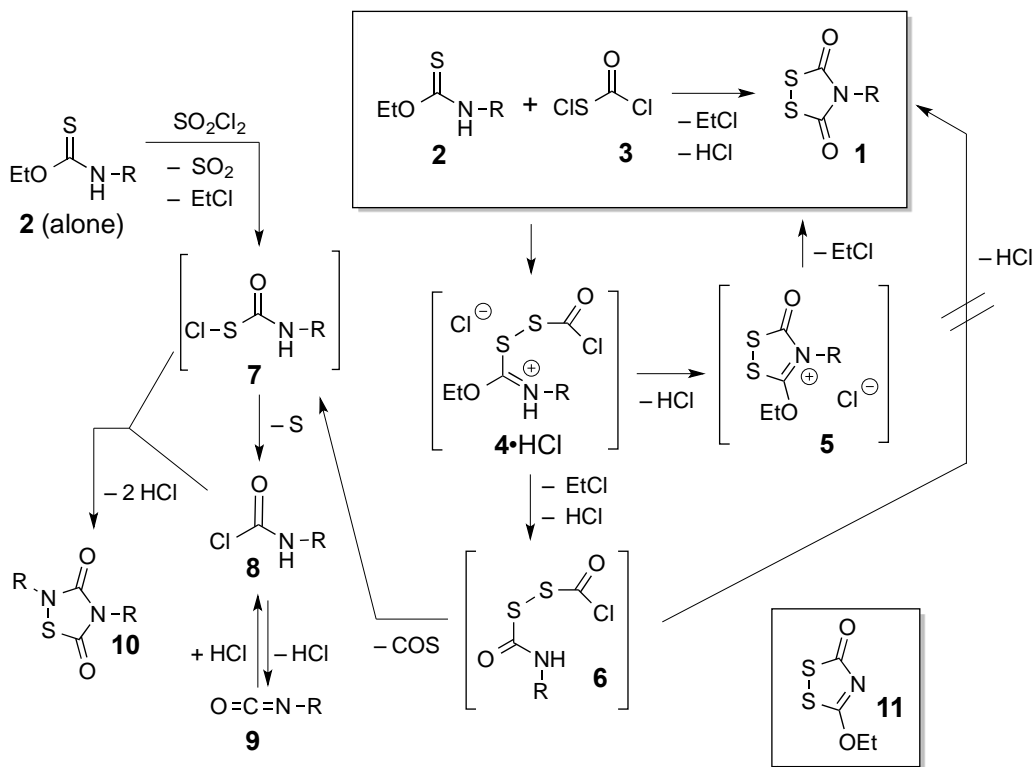
Scheme 3. Preparation of bis(chlorocarbonyl)disulfane

After successfully producing the hard-won reagent, we tried our best to react it with primary amines or amino acids, but none of these experiments gave even the slightest trace of the desired Dts heterocycle. Instead, the products were either isocyanates directly, or derivatives thereof. Therefore, we next investigated additional ways to access the required (chlorocarbonyl)(carbamoyl)disulfane intermediate – which had been postulated by Zumach, Weiss, and Kühle [17] to be an obligatory intermediate in the mechanism for Dts formation – but again, none of these approaches gave Dts.

We had more or less reconciled ourselves to the fact that using bis(chlorocarbonyl)disulfane as a reagent for a single-step synthesis of the Dts heterocycle was not meant to be, when my son Michael joined my lab for a summer while he was still in high school. I remembered a discussion years earlier with Bob Hammer, where he suggested that some of our problems might be due to the fact that our

“leaving group” was HCl, and that maybe they could be circumvented by changing the leaving group to TMS-Cl. In other words, the idea was to use trimethylsilyl (TMS) groups as “big protons” ... and it worked, as communicated to the *J. Am. Chem. Soc.* in 2005 [32]. Since the seeds of this work had been planted while I was still in graduate school, I asked my mentor Bruce Merrifield to be a coauthor, and in fact, this is the last publication of Bruce’s amazing career.

For a further example of how an initially disappointing result could bear fruit, we were long aware of the classic Nefkens Reagent [33] that allows a one-pot method, in aqueous basic solution, to create phthaloyl amino acids, but were repeatedly unsuccessful in creating its Dts analogue, let alone using such a reagent to create Dts-amino acids. In trouble-shooting the chemistry, we found that the Zumach-Weiss-Kühle-type reaction that for other substrates is essentially instantaneous under normal conditions, now slowed down enough to allow us to isolate, characterize, and/or trap relevant intermediates. As revealed at this meeting [34], we found four structures, all of which could be solved at the atomic level by x-ray crystallography, and all of which model stages in the classic Zumach-Weiss-Kühle mechanism towards Dts-amines. In particular, we believe that delving into the molecular geometries will explain why bis(chlorocarbonyl)disulfane fails to give Dts when reacted with primary amines, but successfully gives Dts when reacted with bis(TMS)-amines.



Scheme 4. A full picture of the Zumach-Weiss-Kühle reaction mechanism

Our best current understanding (Scheme 4) is as follows: thiocarbamates **2** react with (chlorocarbonyl)sulfonyl chloride (**3**) to generate an initial adduct **4**, which can cyclize to **5** first, and then lose EtCl, to give Dts (**1**). If however EtCl is lost first, the (chlorocarbonyl)(carbamoyl)disulfane intermediate **6** is surprisingly stable, but does not go to Dts. We also understand the formation of other by-products, such as 1,2,4-thiadiazolidine-3,5-dione (Tda) (**10**), and the outcomes under specialized conditions [like 3-ethoxy-1,2,4-dithiazolin-5-one (EDITH)]

(11), formed when R = H]. Thus, we are finally on the verge of a complete understanding of the Zumach-Weiss-Kühle reaction ... and it took less than 40 years.

Orthogonal Solid-Phase Peptide Synthesis

All along, these investigations into fundamental organosulfur chemistry have informed significant developments in orthogonal solid-phase peptide synthesis. In particular:

- Tracking down a low-level but nonetheless troublesome side reaction in the preparation of Dts-amino acid building blocks, Samuel Zalipsky was compelled to prepare any number of novel polyethylene glycol (PEG) derivatives [20]. A mechanistic control experiment led to the isolation of a PEG-amino acid, and that was used, in turn, to create the first PEG-PS resin [35]. Later work with Fernando Albericio, Jane Chang, Derek Hudson, and Nuria Solé led to more practical formulations, suitable for commercial production [36]. Once peptide chemists realized that their more challenging synthetic targets required support materials that were compatible with both organic solvents and with aqueous media, PEG-PS became the resin support of choice for many experiments, including combinatorial chemistry designs that culminate in biological testing.
- Later, lightning hit a second time, when Maria Kempe parlayed her experience and insights in the field of molecular imprinting to develop the highly counter-intuitive, but very effective, CLEAR family of supports for SPPS [37].
- The signature step of solid-phase synthesis is the anchor to the support, and many of my co-workers, including Fernando Albericio, Jordi Alsina, Yongxin Han, Knud Jensen, Nancy Kneib-Cordonier, Michael Songster, Josef Vágner, and Scott Yokum, made significant contributions to a veritable alphabet soup (or rhyme scheme) of handles (or linkers), like PAL, HAL, XAL, and BAL [38–41].
- I have already alluded to the underlying motivation for orthogonal peptide synthesis – development of milder reaction conditions for the key steps, so that the overall scheme would be conducive to the preparation of the sort of labile constructs needed to solve important biological problems. While our initial focus was to apply Dts chemistry, it later turned out that many of our ideas could be implemented with Carpino’s Fmoc group instead [42]. In this regard, I want to call attention to the important work of Meienhofer’s group at Hoffmann-LaRoche [43] and the Cambridge group of Bob Sheppard and Eric Atherton [44] in expediting the transition from Boc to Fmoc in a sizeable portion of the peptide synthesis laboratories in academia and in the private sector worldwide. In my lab, many students contributed, especially Liz Ottinger who was the first to create phosphopeptides by Fmoc chemistry in the mid ‘90’s [45].
- A central interest of ours has been the management of cysteine residues, including the development of new protecting groups and the regioselective creation of disulfide bridges both in solution and on-resin [the latter exploiting Steve Mazur’s concept, as per ref. 46, of *pseudo-dilution*. Starting with Ioana Annis and Lin Chen, and continuing in collaboration with Arno Spatola, Deanna Long, and Krys Darlak then all at Peptide International, we developed a polymer-supported Ellman’s reagent for oxidation of cysteine-containing peptides under extraordinarily mild conditions, in essence an artificial “chaperone.”
- Lin Chen, Bob Hammer, and others helped to homologate our chemistry to create peptide trisulfides [47], a class of compounds that were speculative novelties when we started, but have since appeared in Nature in surprising ways.
- A productive collaboration with Clare Woodward provided numerous insights into fundamental questions in protein folding research, particularly on the role of disulfide bridges. Using the 58-residue three-disulfide small protein bovine pancreatic trypsin inhibitor (BPTI) as a model, Marc Ferrer, Elisar Barbar, Chris Gross, Hong Pan, Judit Tulla-Puche, Irina Getun, and Natàlia Carulla synthesized and characterized the parent structure along with numerous analogues that were made more flexible by replacing cysteine moieties by pairwise α -amino-*n*-butyric acid (Abu) residues [48–53]. Most dramatically, we designed, synthesized, and characterized BetaCore, the first four-stranded antiparallel β -sheet that folds in water [54]. The synthetic chemistry required orthogonal oxime ligation chemistry that we developed and optimized [55].

Conclusions

In this contribution, I have shared with you a number of scientific stories with the common denominator of “orthogonality.” What started as a simple word – to express and clarify an idea that chemists have implicitly known for much longer – has blossomed significantly in the 21st century as a critical design consideration when carving out new directions in chemical biology. It is particularly appropriate to note that in the last lecture that I heard Murray Goodman give, at a 2001 symposium honoring Bruce Merrifield’s 80th birthday, he spoke about ways that orthogonality had formed his own research.

Acknowledgments

Throughout my scientific career, I have been fortunate to have mentors and role models who cared about me and influenced my development. I made my first professional scientific presentations at age 17, at a Federation meeting in Atlantic City and, a few months later, at a Cold Spring Harbor Symposium [56]. I want to pay tribute to my parents, Michael and Kate Bárány, who guided me into the family business, and Bruce Merrifield, who patiently accepted me into his laboratory when I was still very green. In 1999, it was my privilege to co-Chair the 16th American Peptide Symposium, and welcome a “who’s who in peptide science” (Figure 1) to offer their



perspectives for the new millennium [57]. Jed Fisher has been a good friend from the time we met in 1980 through the present day.

Fig. 1. From left to right: Victor Hruby, Charles Deber, Tom Muir, Robert Hodges, Bruce Merrifield, Robin Offord, Murray Goodman, Arno Spatola, Daniel Veber, and George Barany

Over the years, I’ve mentored about two dozen Ph.D. students, over 30 postdoctoral fellows, and over 100 undergraduates. Beyond what they achieved in my laboratory, almost all of them have gone on to productive independent careers in academia, industry, biotechnology, and government. A full listing appears on my

webpage [58], but I want to single out Alayne Schroll and Bob Hammer, wonderful friends ... and we're still writing papers together. Several of my mentees have achieved recognition of their own, for example, my long-time friend and collaborator, Fernando Albericio, was recognized two years ago with the Vincent du Vigneaud award of the American Peptide Society, and Simon Shannon, the first member of his family to attend college, let alone earn a Ph.D., received a major national achievement award from TRIO in November 2014. Matt Henley, some of whose organosulfur research discoveries were reported at this, his first American Peptide Symposium, won two prizes for undergraduate research this past spring at a local symposium [I also thank Matt for his help in preparing this manuscript].

I view mentoring as a life-long commitment, and my students are my extended family. I thank all of them for what they contributed that has led to my Goodman Award.

References

- Barany, G.; Merrifield, R.B. *J. Am. Chem. Soc.* **99**, 7363-7365 (1977), <http://dx.doi.org/10.1021/ja00464a050>
- Barany, G.; Merrifield, R. B. *The Peptides* (Gross, E., Meienhofer, J., Eds.), Volume 2, Academic Press, New York, 1979, p. 1-284
- <http://www.washingtonpost.com/wp-dyn/content/article/2010/01/11/AR2010011103690.html>
- <http://www.chem.umn.edu/groups/baranygp/puzzles/>, especially <http://tinyurl.com/fab15puz>, <http://tinyurl.com/fivesquaredpuz>, and <http://tinyurl.com/14to24>
- Fischer, E. *Ber. Dtsch. Chem.. Ges.* **27**, 2985-2993 (1894)
- Lemieux R. U.; Spohr U. *Advances in Carbohydrate Chemistry and Biochemistry* (Horton, D., Ed.), Volume 50, Academic Press, New York, 1994, p. 1-20, [http://dx.doi.org/10.1016/S0065-2318\(08\)60149-3](http://dx.doi.org/10.1016/S0065-2318(08)60149-3)
- Corey, E. J.; Venkateswarlu, A. *J. Am. Chem. Soc.* **94**, 6190-6191 (1972), <http://dx.doi.org/10.1021/ja00772a043>
- Merrifield, R. B. *Angew. Chem. Int. Ed. Engl.* **24**, 799-810 (1985), <http://dx.doi.org/10.1002/anie.198507993>
- Wang, S. *J. Am. Chem. Soc.* **95**, 1328-1333 (1973), <http://dx.doi.org/10.1021/ja00785a602>
- Rich, D. H.; Gurwara, S. K. *J. Am. Chem. Soc.* **97**, 1575-1579 (1975), <http://dx.doi.org/10.1021/ja00839a052>
- Barany, G.; Albericio, F. *J. Am. Chem. Soc.* **107**, 4936-4942 (1985), <http://dx.doi.org/10.1021/ja00303a019>
- Tam, J. P.; Yu, Q.; Miao, Z. *Pept. Sci.* **51**, 311-332 (1999) [http://dx.doi.org/10.1002/\(SICI\)1097-0282\(1999\)51:5<311::AID-BIP2>3.0.CO;2-A](http://dx.doi.org/10.1002/(SICI)1097-0282(1999)51:5<311::AID-BIP2>3.0.CO;2-A)
- Sletten, E. M.; Bertozzi, C. R. *Angew. Chem. Int. Ed. Engl.* **48**, 6971-6998 (2009), <http://dx.doi.org/10.1002/anie.200900942>
- Kolb, H. C.; Finn, M. G.; Sharpless, K. B. *Angew. Chem. Int. Ed. Engl.* **40**, 2004-2021 (2001), [http://dx.doi.org/10.1002/1521-3773\(20010601\)40:11<2004::AID-ANIE2004>3.0.CO;2-5](http://dx.doi.org/10.1002/1521-3773(20010601)40:11<2004::AID-ANIE2004>3.0.CO;2-5)
- Wong, C.; Zimmerman, S. C. *Chem. Comm.* **49**, 1679-1695 (2013) <http://dx.doi.org/10.1039/C2CC37316E>
- Gerry, N. P.; Witowski, N. E.; Day, J.; Hammer, R. P.; Barany, G.; Barany, F. *J. Mol. Biol.* **292**, 251-262 (1999), <http://dx.doi.org/10.1006/jmbi.1999.3063>
- Review: Zumach, G.; Kühle, E. *Angew. Chem. Int. Ed. Engl.* **9**, 54-63 (1970), <http://dx.doi.org/10.1002/anie.197000541>
- Barany, G. *Anal. Biochem.* **109**, 114-122 (1980), [http://dx.doi.org/10.1016/0003-2697\(80\)90018-4](http://dx.doi.org/10.1016/0003-2697(80)90018-4)
- Barany, G.; Merrifield, R. B. *J. Am. Chem. Soc.* **102**, 3084-3095 (1980), <http://dx.doi.org/10.1021/ja00529a034>
- Zalipsky, S.; Albericio, F.; Slomczynska, U.; Barany, G. *Int. J. Peptide Protein. Res.* **30**, 740-783 (1987), <http://dx.doi.org/10.1111/j.1399-3011.1987.tb03386.x>
- Albericio, F.; Barany, G. *Int. J. Pept. Prot. Res.* **30**, 177-205 (1987), <http://dx.doi.org/10.1111/j.1399-3011.1987.tb03327.x>
- Planas, M.; Bardají, E.; Jensen, K. J.; Barany, G. *J. Org. Chem.* **64**, 7281-7289 (1999), <http://dx.doi.org/10.1021/jo9824394>
- Jensen, K. J.; Hansen, P. R.; Venugopal, D.; Barany, G. *J. Am. Chem. Soc.* **118**, 3148-3155 (1996), <http://dx.doi.org/10.1021/ja953529i>
- Barany, G. *Int. J. Pept. Prot. Res.* **19**, 321-324 (1982), <http://dx.doi.org/10.1111/j.1399-3011.1982.tb03045.x>
- Schroll, A. L.; Barany, G. *J. Org. Chem.* **54**, 244-247 (1989), <http://dx.doi.org/10.1021/jo00262a051>
- Chen, L.; Barany, G. *Lett. Pept. Sci.* **3**, 283-292 (1996), <http://dx.doi.org/10.1007/BF00127662>
- Xu, Q.; Musier-Forsyth, K.; Hammer, R. P.; Barany, G. *Nucleic Acids Res.* **24**, 1602-1607 (1996), <http://dx.doi.org/10.1093/nar/24.9.1602>
- Xu, Q.; Barany, G.; Hammer, R. P.; Musier-Forsyth, K. *Nucleic Acids Res.* **24**, 3643-3644 (1996), <http://dx.doi.org/10.1093/nar/24.18.3643>
- Wood, M. E.; Cane-Honeysett, D. J.; Dowle, M. D.; Coles, S. J.; Hursthouse, M. B. *Org. & Biomol. Chem.* **1**, 3015-3023 (2003), <http://dx.doi.org/10.1039/B305096C>
- Kobayashi, N.; Osawa, A.; Fujisawa, T. *Chem. Lett.*, 1315-1318 (1973), <http://doi.org/10.1246/cl.1973.1315>

31. Barany, G.; Schroll, A. L.; Mott, A. W.; Halsrud, D. A. *J. Org. Chem.* **48**, 4750-4761 (1983), <http://dx.doi.org/10.1021/jo00172a056>
32. Barany, M. J.; Hammer, R. P.; Merrifield, R. B.; Barany, G. *J. Am. Chem. Soc.* **127**, 508-509 (2005), <http://dx.doi.org/10.1021/ja0455446>
33. Nefkens, G. H. L.; Tesser, G. I.; Nivard, R. J. F. *Rec. Trav. Chim. Pays-Bays* **79**, 688-698 (1960), <http://dx.doi.org/10.1002/recl.19600790705>
34. Henley, M. J.; Barany, M. J.; Chen, L.; Hammer, R. P.; Young, V. G.; Barany, G. In Srivastava, V., Yudin, A., and Lebl, M (Eds.) *Proceedings of the 24th American Peptide Symposium*, American Peptide Society, Orlando, 2015; p. 266, <http://dx.doi.org/10.17952/24APS.2015.266>
35. Zalipsky, S.; Chang, J. L.; Albericio, F.; Barany, G. *React. Polym.* **22**, 243-258 (1994), [http://dx.doi.org/10.1016/0923-1137\(94\)90122-8](http://dx.doi.org/10.1016/0923-1137(94)90122-8)
36. Kates, S. A.; McGuinness, B. F.; Blackburn, C.; Griffin, G. W.; Solé, N. A.; Barany, G.; Albericio, F. *Pept. Sci.* **47**, 365-380 (1998), [http://dx.doi.org/10.1002/\(SICI\)1097-0282\(1998\)47:5<365::AID-BIP4>3.0.CO;2-8](http://dx.doi.org/10.1002/(SICI)1097-0282(1998)47:5<365::AID-BIP4>3.0.CO;2-8)
37. Kempe, M.; Barany, G. *J. Am. Chem. Soc.* **118**, 7083-7093 (1996), <http://dx.doi.org/10.1021/ja954196s>
38. Albericio, F.; Kneib-Cordonier, N.; Biancalana, S.; Gera, L.; Masada, R. I.; Hudson, D.; Barany, G. *J. Org. Chem.* **55**, 3730-3743 (1990), <http://dx.doi.org/10.1021/jo00299a011>
39. Albericio, F.; Barany, G. *Tetrahedron Lett.* **32**, 1015-1018 (1991), [http://dx.doi.org/10.1016/S0040-4039\(00\)74475-3](http://dx.doi.org/10.1016/S0040-4039(00)74475-3)
40. Han, Y.; Bontems, S. L.; Hegyes, P.; Munson, M. C.; Minor, C. A.; Kates, S. A.; Albericio, F.; Barany, G. *J. Org. Chem.* **61**, 6326-6339 (1996), <http://dx.doi.org/10.1021/jo960312d>
41. Jensen, K. J.; Alsina, J.; Songster, M. F.; Vágner, J.; Albericio, F.; Barany, G. *J. Am. Chem. Soc.* **120**, 5441-5452 (1998), <http://dx.doi.org/10.1021/ja974116f>
42. Carpino, L. A.; Han, G. Y. *J. Org. Chem.* **37**, 3404-3409 (1972), <http://dx.doi.org/10.1021/jo00795a005>
43. Chang, C. D.; Meienhofer, J. *Int. J. Pept. Protein Res.* **11**, 246 (1978), <http://dx.doi.org/10.1111/j.1399-3011.1978.tb02845.x>
44. Atherton, E.; Sheppard, R. C. *Solid Phase Peptide Synthesis, A Practical Approach*, IRL Press, Oxford 1989
45. Ottinger, E. A.; Shekels, L. L.; Bernlohr, D. A.; Barany, G. *Biochemistry* **32**, 4354-4361, <http://dx.doi.org/10.1021/bi00067a027>
46. Jayalekshmy, P.; Mazur, S. *J. Am. Chem. Soc.* **98**, 6710-6711 (1976), <http://dx.doi.org/10.1021/ja00437a054>
47. Chen, L.; Zouliková, I.; Slaninová, J.; Barany, G. *J. Med. Chem.* **40**, 864-876 (1997), <http://dx.doi.org/10.1021/jm9607156>
48. Ferrer, M.; Woodward, C.; Barany, G. *Int. J. Pept. Prot. Res.* **40**, 194-207 (1992), <http://dx.doi.org/10.1111/j.1399-3011.1992.tb00292.x>
49. Barbar, E.; Barany, G.; Woodward, C. *Biochemistry* **34**, 11423-11434 (1995), <http://dx.doi.org/10.1021/bi00036a015>
50. Pan, H.; Barbar, E.; Barany, G.; Woodward, C. *Biochemistry* **34**, 13974-13981 (1995), <http://dx.doi.org/10.1002%2Fpro.5560060919>
51. Tulla-Puche, J.; Getun, I. V.; Woodward, C.; Barany, G. *Biochemistry* **43**, 1591-1598 (2004), <http://dx.doi.org/10.1021/bi035301a>
52. Gross, C. M.; Lelièvre, D.; Woodward, C.; Barany, G. *J. Pept. Res.* **65**, 395-410 (2005), <http://dx.doi.org/10.1111/j.1399-3011.2005.00241.x>
53. Getun, I. V.; Brown, C. K.; Tulla-Puche, J.; Ohlendorf, D.; Woodward, C.; Barany, G. *J. Molecular Biol.* **375**, 812-823 (2008), <http://dx.doi.org/10.1016/j.jmb.2007.10.084>
54. Carulla, N.; Woodward, C.; Barany, G. *Protein Sci.* **11**, 1539-1551 (2002), <http://dx.doi.org/10.1110%2Fps.4440102>
55. Carulla, N.; Woodward, C.; Barany, G. *Bioconjugate Chem.* **12**, 726-741 (2001), <http://dx.doi.org/10.1021/bc015518m>
56. Barany, G.; Merrifield, R. B. *Cold Spring Harbor Symposium on Quantitative Biology* **37**, 121-125 (1973)
57. Merrifield, R. B.; Barany, G.; Deber, C. M.; Goodman, M.; Hodges, R. S.; Hruby, V. J.; Muir, T. W.; Offord, R.; Spatola, A. F.; Veber, D. F.; Fields, G. B., in Fields, G. B.; Tam, J. P.; Barany, G. (Eds.) *Peptides for the New Millennium (Proceedings of the Sixteenth American Peptide Symposium)*, American Peptide Society, Minneapolis, 1999, p. 797-804, http://dx.doi.org/10.1007%2F0-306-46881-6_318
58. <http://www.chem.umn.edu/groups/baranygp/>

Total Synthesis, Functional Analysis and Biological Evaluation of Antibiotic Peptide Natural Products

Masayuki Inoue*, Takuya Kaji, Motoki Murai, Takefumi Kuranaga,
Hiroshi Hamamoto, and Kazuhisa Sekimizu

Graduate School of Pharmaceutical Sciences, The University of Tokyo, 7-3-1 Hongo, Bunkyo-ku,
Tokyo, 113-0033, Japan

Introduction

Recently, a novel antimicrobial agent lysocin E (**1**, Figure 1a) was isolated from a culture supernatant of a lysobacter species by Sekimizu and co-workers, and was showed to be effective against Gram-positive bacteria including methicillin-resistant *Staphylococcus aureus* (MRSA) [1]. Peptide **1** had potent antibiotic activity in mouse infection model with ED₅₀ value of 0.6 mg/kg. Therefore, this compound is considered as a promising candidate for treatment of multidrug resistant bacterial infection.

The structure of **1** is featured by a 37-membered macrocycle, five D-amino acid residues, N-methylation on peptide main chain, and C7 fatty acid moiety. Peptide **1** was suspected to target menaquinone-4 (Figure 1b), which is an essential component of the electron transport system on bacterial membranes, and to dissipate the membrane structure in *S. aureus*. In order to investigate further mechanism of action of **1**, the total synthesis and structure-function relationship study were performed.

Results and Discussion

The solid-phase synthesis does not necessitate purification of synthetic intermediates, and thus is advantageous over the solution-phase counterpart, especially for rapid construction of **1**. Moreover, high dilution effect on the solid-phase was expected to facilitate the macrocyclization of the 37-membered ring of **1**. Synthetic strategy to **1** is summarized in Figure 2. The side chain of allyl glutamate would be anchored to 2-chloro-2-trityl resin (Barlos resin), and the following peptide elongation would give linear depsipeptide **3**, which was to be cyclized to generate the peptide **2**. Then, all the side chain protecting groups (*t*-Bu, Tr, TBS and Boc) would be removed simultaneously with the cleavage of the peptide **2** from the Barlos resin to produce **1**.

The solid phase peptide synthesis (SPPS) started from allyl glutamate loaded resin **4** (Figure 3). The attachments of the six Fmoc amino acid residues and threonine fragment, which included the fatty acid moiety on its amine group, were realized by using the HBTU/HOBt activation method under the microwave irradiation, leading to **5**. Then, on-resin esterification of the secondary alcohol of **5** with Fmoc-L-Thr(*t*-Bu)OH was performed. To complete the esterification reaction, the coupling with 10 equiv of Fmoc-L-Thr(*t*-Bu)OH, *N,N'*-diisopropylcarbodiimide, and DMAP were used for three cycles to generate **6**. After the subsequent Fmoc cleavage, a microwave-assisted protocol was re-applied for stepwise coupling of the three amino acid residues to furnish acyclic depsipeptide **3**. Removal of the allyl group of **3** with catalytic Pd(PPh₃)₄ and excess amount of morpholine followed by PyBOP-promoted macrolactamization, resulting in formation of resin bound lactam **2**. Finally, cleavage of **2** from Barlos resin with 95% aqueous TFA completed within 1 hour at room temperature, and then the

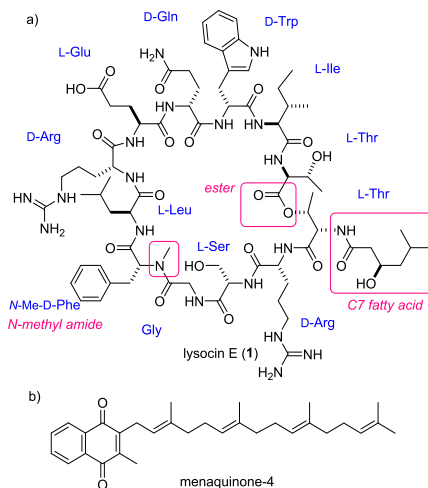


Fig. 1. (a) Structure of Lysocin E (**1**).
(b) Structure of menaquinone-4.

reaction mixture was stirred for additional 2 hours to remove all the protecting groups attached to the side chains. After purification by the reversed-phase HPLC, lysocin E (**1**) was obtained in 4.6% yield from the allyl glutamate loaded resin **4**. The NMR spectra and the retention time in the HPLC of synthetic **1** agreed with those of natural **1**. A comparison of MIC values shows synthesized **1** is in good accordance with that of naturally isolated one [2].

Enantiomer of **1** (*ent*-**1**) was also prepared by the slightly modified conditions from the ones described above. Interestingly, synthesized *ent*-**1** exhibited similar MIC values with that of **1** (Table 1). Retention of antimicrobial activity of *ent*-**1** supported that **1** targets achiral menaquinone-4.

One of the structural features of **1** is the C7 fatty acid attached to the threonine residue. To evaluate the importance of the fatty acid moiety, alternative synthetic route was designed. A series of side chain-modified lysocin analogues would be prepared by the last-step acylation of common amine precursor **7** (Figure 4). Lysocin E amine precursor **7** was synthesized in 25.6% yield by similar synthetic procedure for **1**, and the acylation was successfully proceeded only at the amine group of the threonine residue. Antimicrobial activity of the synthesized analogues were examined and summarized in Table 1. These results suggested that particular length ($n = 7$) of side chain is important to exhibit antimicrobial activity (Table 1, **1**, **8**, **9**, **11** vs. **7**, **10**, **12**). For further investigation of the role of the C7 fatty acid of **1**, the binding affinity of the synthetic analogues to menaquinone-4 are now being explored.

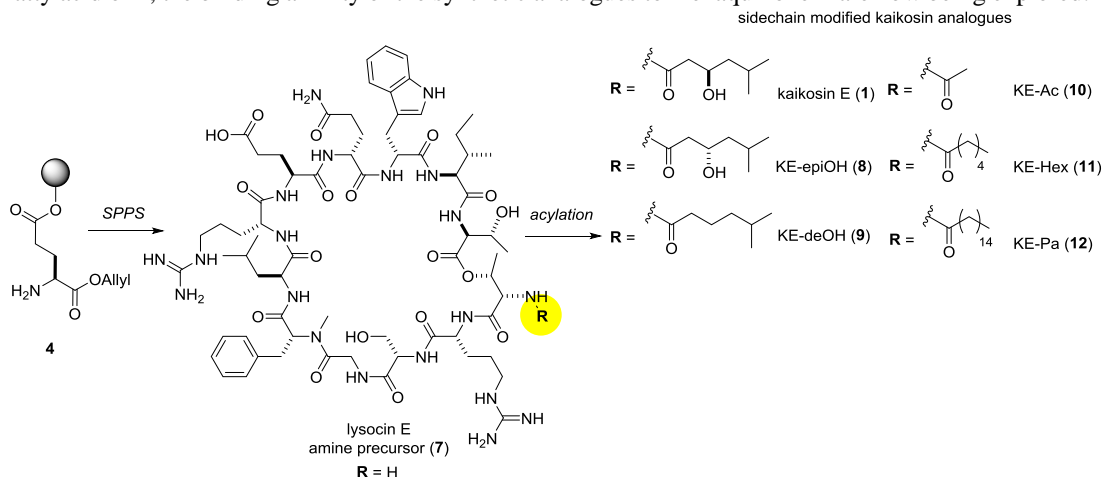


Fig. 4. Synthesis of side chain modified analogues.

The first total synthesis of lysocin E (**1**) and its analogues were achieved via macrocyclization on solid support. To investigate the structure-function relationship of **1**, alternative synthetic route via amine precursor **7** was also established. This work demonstrated that the solid phase approach was effective for rapid production of wide range of lysocin E analogues. MIC values of synthesized lysocin E derivatives implied the importance of the C7 fatty acid moiety of **1** for its antimicrobial activity.

Table 1. Minimal inhibitory concentration of synthetic lysocin derivatives.

Cpd	MIC ($\mu\text{g/mL}$)	Cpd	MIC ($\mu\text{g/mL}$)
1	4	9	8
<i>ent</i> - 1	4	10	128
7	>128	11	8
8	4	12	>128

Acknowledgments

This research was financially supported by the Funding Program for Next Generation World-Leading Researchers (JSPS) to M.I.

References

- Hamamoto, H., et al. *Nat. Chem. Biol.* **11**, 127-133 (2015), <http://dx.doi.org/10.1038/nchembio.1710>
- Murai, M., et al. *Angew. Chem., Int. Ed.* **54**, 1556-1560 (2015), <http://dx.doi.org/10.1002/anie.201410270>

The Nature of Peptidomimetics: Synthetic Peptide Macrocycles as Potential Therapeutics and Artificial Peptide Helices

Danielle A. Guarracino, John J. Ferrie, Jessica J. Gruskos, Ari L. Goldwaser, Megan E. Decker, Anginelle M. Alabanza, Camille T. Robertson, Sanjna S. Sanghvi, Susan Knox, Dylan H. Nguyen, Kayla Gentile, and Maria Minor

The College of New Jersey, Ewing, NJ, 08628, USA

Introduction

Macromolecular structure plays a large role in peptide cellular function. Cyclic peptides comprise a unique class of molecules with much potential in novel drug development. By restricting bond rotation, cyclization can constrain a peptide into a favorable conformation, limiting the degrees of freedom while promoting a larger surface area of interaction with a biological target of interest. Reports on macrocyclic peptide drugs extol their superior characteristics and benefits towards drug oral bioavailability, which includes enhanced intracellular stability as their conformation is less accessible to proteases [1]. Throughout the literature, studies have confirmed that macrocyclization improves drug proteolytic stability, pharmacokinetics and decreased side effects [2]. Given these attributes, further development of cyclic peptide-based therapies is necessary.

Endocrine hormone vasopressin is a small, macrocyclic peptide that controls water balance and

blood pressure by acting on the kidneys [3]. Low concentrations of vasopressin are inherent in the disease Neurogenic Diabetes Insipidus (DI), characterized by extreme dehydration and electrolyte imbalance. Current therapies are limited by the necessity of injection and the structural weaknesses in the backbone of most common drugs. We describe two specific vasopressin designs and one that mimics structurally-related hormone oxytocin (Figure 1a). Our peptides use head-to-tail amide bond cyclization, removing the cysteine-cysteine disulfide connection that could render the peptide linear via exchange in the cell's reducing environment (Figure 1a) [3]. The overall arrangement of amino acids in each design is similar to the parent compounds with the exception of the addition of non-natural diaminopropionic acid (Figure 1a), to emulate the N-terminal region on the hormones, and a glycine

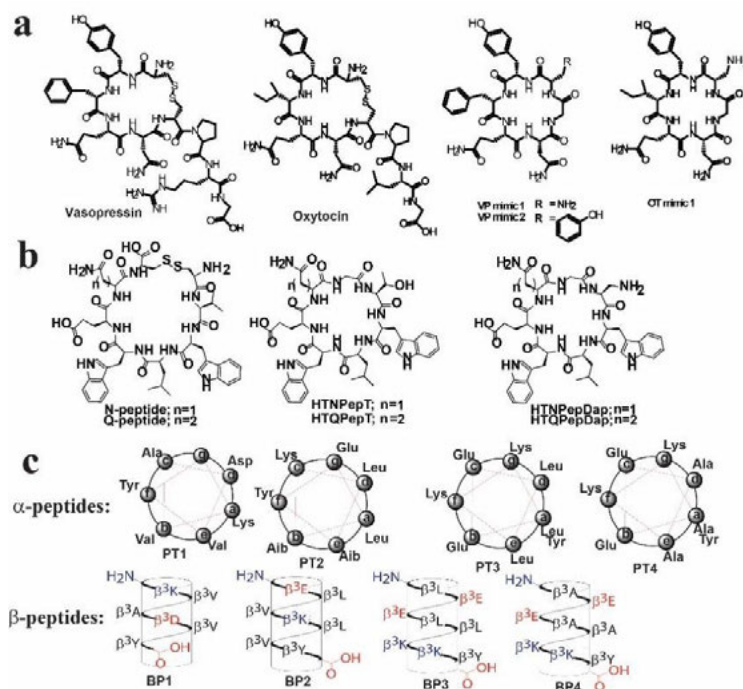


Fig. 1. a) Chemical structures of vasopressin, oxytocin and the vasopressin and oxytocin mimics [3]; b) Chemical structures of literature N- and Q-peptides [6] and the HTN- and Q-pep mimics; c) Sequences for the α -peptides (top) and β -peptides (bottom) described herein with helical wheels and helical net diagrams depicting possible helical arrangement [7].

residue to provide flexibility reminiscent of the disulfide region. The additional tyrosine in VP mimic2 (Figure 1a) was included because studies in the literature show short, linear peptides with three aromatics improved affinity for vasopressin's targets. Each of our designs is smaller, more compact, and retains the residues of utmost importance while removing the 'tail' of three amino acids external to the ring not crucial for binding interactions [3]. On the whole, the mimics remain similar to the parent compounds in structure and design with deliberate differences for improving stability and efficacy. In our study we examined the stability of each compound when treated with a panel of proteases (Figure 2a).

In current research, we employ a similar design strategy developing potential thrombosis inhibitors. Rupturing of atherosclerotic plaques exposes collagen fibrils in arterial vessel walls which creates high shear pathological blood flow [4]. Von Willebrand Factor (vWF) is a multimeric protein essential to the recruitment and adhesion of platelets at these sites of vascular injury [4]. It has distinct domains that bind collagen tightly and bridge platelets through interactions with glycoproteins on the platelet surface [5]. Once an initial layer of platelets are attached, they can accumulate leading to thrombus growth. vWF is intrinsic to both initial platelet tethering and encouraging the growth of the platelet plug. Given the gravity of thrombus formation, and the severe side effects of most anti-platelet medications, there is a significant need for anti-thrombosis pharmaceutical research. Combining the benefits of macrocyclic drugs with the importance of inhibiting vWF in blood clot formation, we designed novel cyclic peptides that target the interface between vWF and collagen, in hopes to prevent nucleation of blood clot formation by inhibiting this initial interaction. There currently exists a literature precedent of cyclic peptides, comprising a region of vWF, found through screening a phage display library that inhibit vWF binding collagen [6]. These compounds displayed IC_{50} values in the moderate mid-micromolar range and were cyclized naturally through disulfide bonds prone to the linearization and enzyme cleavage mentioned above [6]. Starting with these compounds, we developed potential first generation peptide-based therapeutics using our head-to-tail synthesis (Figure 1b). Similar to the vasopressin/oxytocin mimics above, our anti-thrombosis peptides contain a glycine in place of the disulfide bond. Two designs (HTNPepDap and HTQPepDap) utilize diaminopropionic acid to emulate the *N*-terminal region of the parent compounds, however remove the valine residue from the ring, to promote aqueous solubility. Both HTNPepT and HTQPepT replace the valine with a threonine, also to increase solubility. Our ongoing studies include stability assays against the same

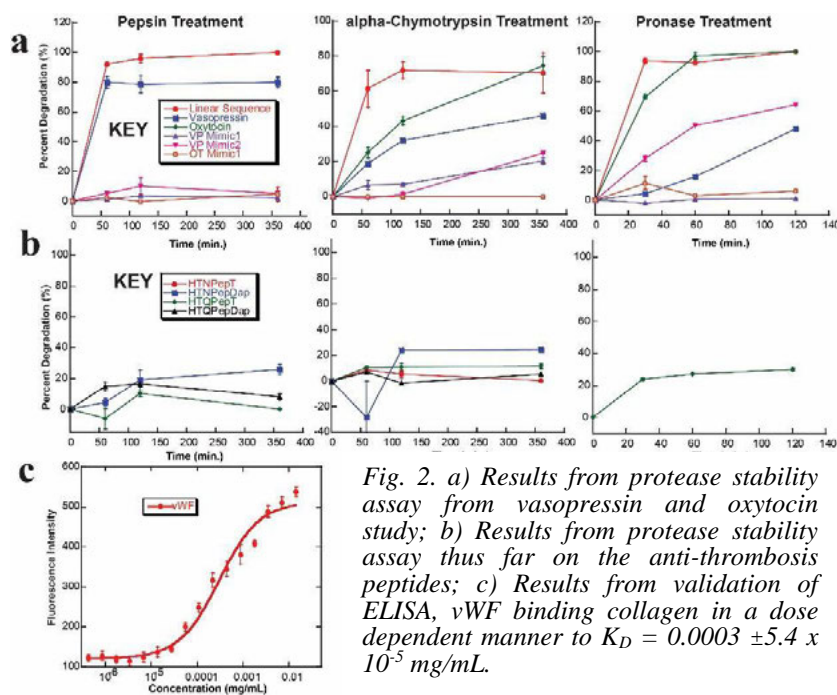


Fig. 2. a) Results from protease stability assay from vasopressin and oxytocin study; b) Results from protease stability assay thus far on the anti-thrombosis peptides; c) Results from validation of ELISA, vWF binding collagen in a dose dependent manner to $K_D = 0.0003 \pm 5.4 \times 10^{-5}$ mg/mL.

protease panel (Figure 2b) as well as competition Enzyme-Linked Immunosorbent Assays to determine whether the cyclic peptides can inhibit vWF binding of collagen.

Frequently, the relationships between proteins are implicated in the disease state and can be traced to interactions between secondary structures of the entities involved. The α -helix comprises the major secondary structure found in natural proteins, playing a functional role in a vast majority of proteins found in the cell [7]. Many

helical interactions have been defined and their mis-regulation implicated in the disease state. In the continuing pursuit of novel peptide-based therapeutics, a better understanding of what dictates α -helical structure is necessary. Additionally, the field of peptidomimetics is rife with examples of non-natural folding oligomers with biological properties. β -peptides, which are oligomers of β -amino acids bearing an extra carbon along the amino acid backbone, can fold into a variety of helices. The 14-helix is most prevalent for peptides comprised of amino acids with substituents in the R3 position, and resembles the native α -helix [7]. There are β -peptides that demonstrate helicity as well as applied biological function, such as inhibiting protein-protein interactions involved in disease. While helical regions in the context of a protein tend to be 10-11 residues, a small subset of two or three amino acids along one side of a helix called “hot spots” contribute most to the binding between proteins [7]. Therefore, an ideal peptidomimetic would be a relatively short peptide of defined structure. To further our understanding of helical control as well as inform the future design of novel short, folded peptides we directly compared the relationship between primary sequence and helicity in 6-8 residue α - and β -peptides using circular dichroism (CD) (Figure 1c). PT2-PT4 are designed to maximize α -helicity, using Aib residues, Leucine zipper or Alanines, respectively [7]. BP1 is designed to maximize 14-helicity, using an established β -peptide model motif, cut down to the smallest possible epitope in 6 residues. PT1 is the “ α -equivalent” of the BP1 design, and BP2-4 are the “ β -equivalent” of the α -peptide designs.

Results and Discussion

The head-to-tail cyclized vasopressin and oxytocin mimics degraded much less and with overall superior stability when compared to vasopressin, oxytocin and a linear control peptide upon treatment with digestive proteases. We used an equation to calculate percent degradation that equates UV absorbance and HPLC peak height to the concentration of peptide in solution. Each solution was treated with the enzyme in the presence of glutathione, a reducing agent often found in the cell which could render the disulfides of the parent compound linear. Pepsin, a stomach enzyme that targets consecutive aromatic residues, degraded the linear control nearly 100% in an hour of treatment, and vasopressin about 80% overall, as expected since all of the compounds contain aromatic residues (Figure 2a) [3]. In comparison, VP mimic2 degraded on average about 5-10%, VP mimic1 about 2.5-4% and OT mimic1 is most stable with only 2-2.5% degradation (Figure 2a) [3]. Alpha-chymotrypsin, an intestinal digestive enzyme which targets aromatic residues, was found to degrade the linear sequence to about 75%, before leveling off, whereas vasopressin and oxytocin were found to degrade to about 50-75%, with vasopressin the more stable of the two parent compounds (Figure 2a) [3]. Each of the hormone mimics demonstrated significantly more stability as compared, with degradation levels at 20% or below [3]. The VP mimics were predictably less stable than the OT mimic, as they contain one or two more aromatics than the OT mimic. Pronase, the most severe test,

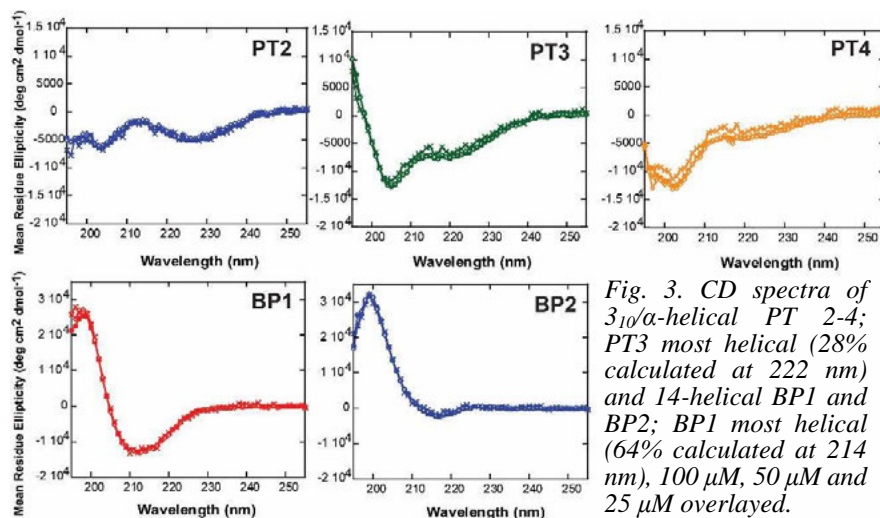


Fig. 3. CD spectra of 3_{10} / α -helical PT 2-4; PT3 most helical (28% calculated at 222 nm) and 14-helical BP1 and BP2; BP1 most helical (64% calculated at 214 nm), 100 μ M, 50 μ M and 25 μ M overlaid.

is actually a mixture of protease enzymes with the ability to cleave nearly every amide bond. As per the other assays, the linear sequence most rapidly degraded over the time course, however in this case oxytocin showed a similar complete degradation after about an hour incubation. Vasopressin had an

unprecedented stability against prolonged pronase treatment with over 50% remaining after 2 hours [3]. Uniquely, VP mimic2 actually showed steady degradation with only about 40% of its original quantity present after 2 hours. VP mimic1 and OT mimic1 were surprisingly unreactive, showing only about 1% and 5-10% degradation, respectively. The sequence of these peptides differ by only one amino acid and this astounding result showed that each peptide had extraordinary stability against the most rigorous protease test. Overall, the three head-to-tail cyclized peptide mimics showed exceptional stability and would make a good prototype for a first generation pharmaceutical.

Continuing work with cyclic peptides as first generation antithrombosis drug leads involved the HTN and Q pep series targeting vWF binding to collagen. These peptides illustrated similar levels of stability when treated with the same panel of proteases. Still in progress, the results from each of the cyclic peptides treated against pepsin, alpha-chymotrypsin and pronase has yielded $\leq 30\%$ degradation for each compound (Figure 2b). Ongoing parallel protease studies on the parent N- and Q-peptides bearing disulfide bonds and a linear vWF peptide will be performed for comparison. The ELISA has been validated using serial dilutions of vWF to achieve a dose dependent response curve that specifies the binding of vWF to collagen (Figure 2c). Plates pre-coated with collagen are incubated with vWF followed by an anti-vWF antibody linked to an assayable horse radish peroxidase enzyme. Upon treatment with a substrate the fluorescent product indicates the presence of vWF. Currently, studies are underway to use this method in conjunction with serial dilutions of cyclic peptide as competitor to view the degree by which fluorescence decreases to indicate the inhibitory effect of the cyclic peptide.

Results from our helical study showed that short 6-8 residue α - and β -peptides can be designed with specific sequences to control the type of secondary structure into which they fold. However, when directly comparing α - and β -peptides we found that primary sequences that control helicity in one type of peptide cannot be substituted into peptides of a different type; optimal designs are generally specific to α - or β -peptides for α - or 14-helical arrangements, respectively. We saw no initiation of cross helicity, and confirmed this by CD spectroscopy (Figure 3). Interestingly, PT2 contained some α -helical structure, whereas BP2, the β -equivalent, had some 14-helical structure, showing that there was some minor overlap in sequence-based control. BP1, the most intensely 14-helical β -peptide, showed a remarkably strong signature considering its short scaffold of only 6 amino acids. This peptidomimetic could be of future use in emulating peptides with biological function. PT3 and, to a lesser extent, PT2 and PT4 showed the possibility of some 3_{10} -helical signature, as well, which is thought to be an intermediate in α -helical folding. Overall, the peptides revealed interesting information about helical control and also paved the way for novel short 3_{10} -/ α -helical peptides as well as 14-helical β -peptides that can be used to probe protein-protein interactions involving short "hot spot" regions.

We conclude that the structure, whether cyclic or helical, of peptides and their peptidomimetics is key in terms of controlling how they fold and function. Our designs move in the direction of novel pharmaceutical design.

Acknowledgments

We thank The College of New Jersey (TCNJ) for start-up funds and continuing support and Bristol-Myers Squibb for summer support in conjunction with the TCNJ Mentored Undergraduate Summer Experience program.

References

1. Marssault, E., Peterson, M.L. *J. Med. Chem.* **54**, 1961-2004 (2011), <http://dx.doi.org/10.1021/jm1012374>
2. Driggers, E.M., Hale, S.P., Lee J., Terrett, N.K. *Nat. Rev. Drug Disc.* **7**, 608-624 (2008), <http://dx.doi.org/10.1038/nrd2590>
3. Ferrie, J.J., Gruskos, J.J., Goldwaser, A.L., Decker, M.E., Guarracino, D.A. *Bioorg. Med. Chem. Lett.* **23**, 989-995 (2013), <http://dx.doi.org/10.1016/j.bmcl.2012.12.041>
4. Ruggeri, Z.M. *Thromb. Res.* **120**, S5-S9 (2007), <http://dx.doi.org/10.1016/j.thromres.2007.03.011>
5. Andrews, R.K., Berndt, M.C. *Thromb. Res.* **114**, 447-453 (2004), <http://dx.doi.org/10.1016/j.thromres.2004.07.020>
6. Depraetere, H., Viaene, A., Deroo, S., Vauterin, S., Deckmyn, H. *Blood* **92**, 4207-4211 (1998).
7. Guarracino, D.A., Alabanza, A.M., Robertson, C.T., Sanghvi, S.S. *J. Biomol. Struct. Dynamics* **33**, 597-605 (2015), <http://dx.doi.org/10.1080/07391102.2014.897260>

Downsizing Proteins Without Losing Potency or Function

David P Fairlie^{1,2,3}, Mei-Kwan Yau^{1,2}, Johan K Hamidon^{1,2}, Rane Singh¹,
 Junxian Lim^{1,2}, Jacky Y Suen^{1,2,3}, Jessica A Rowley^{1,2}, Rink-Jan Lohman^{1,2,3},
 Martin J. Stoermer¹, Abishek Iyer^{1,2,3}, and Robert C Reid^{1,2,3}

¹Division of Chemistry and Structural Biology, Institute for Molecular Bioscience, Brisbane, Queensland, 4072, Australia; ²Australian Research Council Centre of Excellence in Advanced Molecular Imaging, The University of Queensland, Brisbane, Queensland, 4072, Australia; ³Centre for Inflammation and Disease Research, Institute for Molecular Bioscience, Brisbane, Queensland, 4072, Australia

Introduction

Human complement protein C3a (Figure 1) is produced after activation of a complex network of plasma and membrane proteins that constitute the complement system, named for their combined capacity to complement antibody-mediated immune defense [1,2]. C3a itself is an inflammogen, probably best known for its ability to attract (chemotaxis) and degranulate certain immune cells which contain granules that release inflammatory stimuli like histamine, tryptase, heparin and other enzymes most commonly associated with allergies, asthma and acute inflammatory responses [3-8]. We have used this inflammatory protein, which is rapidly degraded in plasma, as a test case to downsize a protein to plasma-stable small molecules that mimic the potent and selective functions of the full length C3a protein. Here we summarize the principle and effectiveness of this idea, which starts with a functionally important amino acid in C3a and rationally grows it into functional surrogates for C3a. We compare activity profiles for the resulting peptidomimetics versus human C3a, all compounds binding to a specific G protein coupled receptor (C3aR) expressed on the plasma membrane surface of human immune and other cell types [9,10].



Fig. 1. Human C3a is 77 amino acids with its GPCR-activating C-terminus boxed.

Results and Discussion

The C-terminal arginine residue of C3a has been reported to be important for binding to and activating human C3aR [11]. Receptor mutagenesis is consistent with C3a interacting through its guanidinium side chain of Arg77 contacting Asp417 while its C-terminal carboxylate contacts Arg161 and Arg340 [12]. Moreover removal of this Arg77 residue from C3a dramatically reduces C3aR binding affinity and agonist efficacy. Our novel approach, inspired by our previous work with ascidiacyclamide and thiazole peptides [13-15], incorporates different dipeptide mimics (Figure 2) into the C-terminal tripeptide segment (Leu-Ala-Arg) of C3a, using a range of heterocycles as conformational constraints (Figure 3). These heterocyclic dipeptide mimics confer potent C3aR agonist or antagonist potencies.

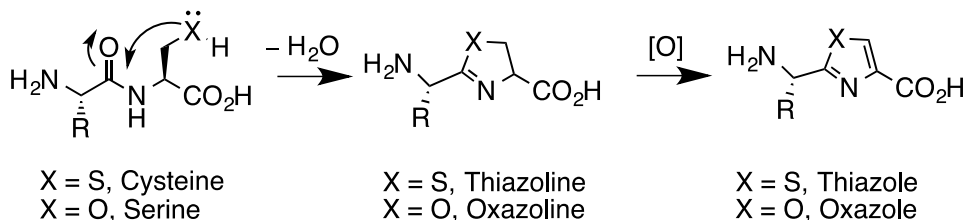


Fig. 2. Heterocyclic dipeptide mimetics derived from dipeptides.

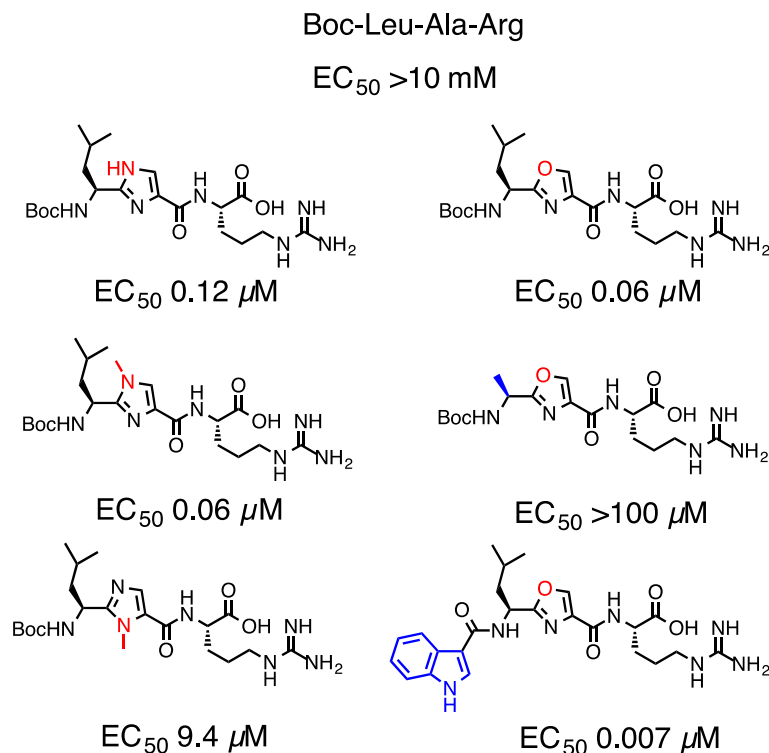


Fig. 3. Agonist potency of peptidomimetics measured by Ca²⁺ release in human monocyte-derived macrophages relative to the tripeptide Boc-Leu-Ala-Arg and hC3a (EC₅₀ 40 nM).

We found that the nature of the heterocycle profoundly affected compound activity. For example, a hydrogen-bond accepting nitrogen conferred agonist activity, with much greater potency for imidazoles and oxazoles (Figure 3) than for oxadiazoles, furans and other heterocycles. Interestingly, there was a linear correlation [9,10] between the C3aR-binding affinity (measured by competition with ¹²⁵I-C3a) and the calculated hydrogen-bond acceptor interaction energy (kcal mol⁻¹) between water and heteroatom of heterocycles compared with the water dimer (determined using *ab initio* methods MP2/6-311++G(3d,3p) and corrected for the basis set superimposition error within Gaussian 09). This enabled us to tune agonist potency by rational variation of the heterocyclic component incorporated into the dipeptide mimetics, coupled with changes to other substituents. All of these compounds were far more stable in rat plasma (unchanged after 2h) than C3a (undetectable after 10 mins), suggesting their use as agonist surrogates for C3a *in vitro* and possibly *in vivo*.

However, the above information only relates to one functional measure of comparable agonist activity for these ligands compared to human C3a. The most potent agonists were therefore further examined for other agonist properties typically exhibited by human C3a. We found that the most potent small molecule agonists also displayed comparable profiles of agonist function and potency to human C3a in other assays such as chemotaxis (migration), ERK phosphorylation, inflammatory gene expression (*TNF*, *IL1β*, *IL8*, *CCL3*, *PTGS2*, *IL6*, *FOSB*, *EGR1*) in human macrophages; mast cell activation and degranulation; and neutrophil migration and activation. These and other activities gave us confidence to examine the agonists in many other *in vitro* and *in vivo* assays to stimulate the C3a receptor and anticipate that the responses would be similar to those of C3a, which is only maintained intact at or near the cell surface where it is formed during complement activation.

However, when a thiazole was incorporated into these peptidomimetics there was an interesting finding of either agonist or antagonist activity, depending upon the location of the sulfur and nitrogen atoms relative to the adjacent amide carbonyl group (Figure 4). When the thiazole nitrogen was adjacent to the carbonyl, agonist activity was observed. When the thiazole sulfur was adjacent to the carbonyl the compound was instead an antagonist. The latter is attributed [16] to orbital interaction between the sulfur and oxygen, indicated by the distance between sulfur and oxygen being less than the sum of the van der Waals radii, and different $\delta^+ \dots \delta^-$ dipole alignments (Figure 4).

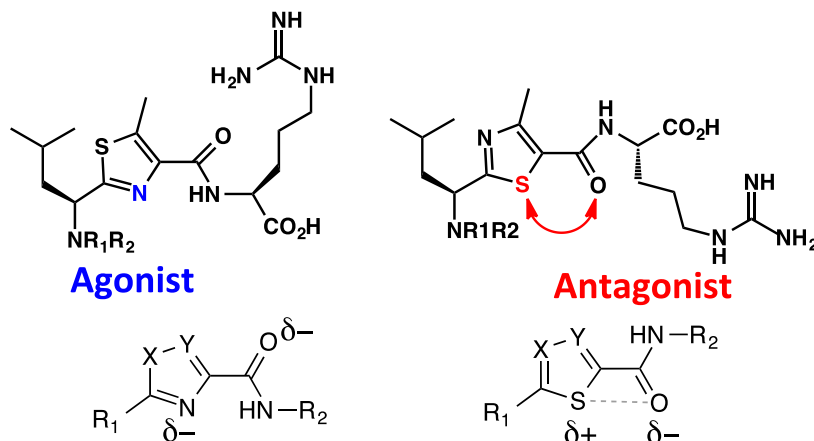


Fig. 4. Heterocycle can control conformation of adjacent amide and hence projection of arginine, dictating agonist versus antagonist action.

As a consequence of these findings, we have been able to gain access to both potent agonists (e.g. Figure 3) and antagonists (e.g. Figure 5) which can be used to probe the effects of modulating the C3a receptor in a range of human and rodent cells and in animal models of C3aR-mediated inflammation and disease. Indications alluded to in the seminar are that antagonists are far more potent than the known feeble antagonist SB290157 [17], in macrophages, mast cells and neutrophils and in animal models such as the rat paw oedema induced by small stable C3aR agonists. Oral delivery of C3aR antagonists (5-20 mg/kg doses) to rats prior to intraplantar administration of C3aR agonist (350 μ g/paw) was able to inhibit the resulting acute inflammation manifested by paw swelling, mast cell activation and degranulation at 30 mins, neutrophil infiltration and activation at 6h, and inflammatory gene and protein expression induced by C3aR agonists *in vivo*.

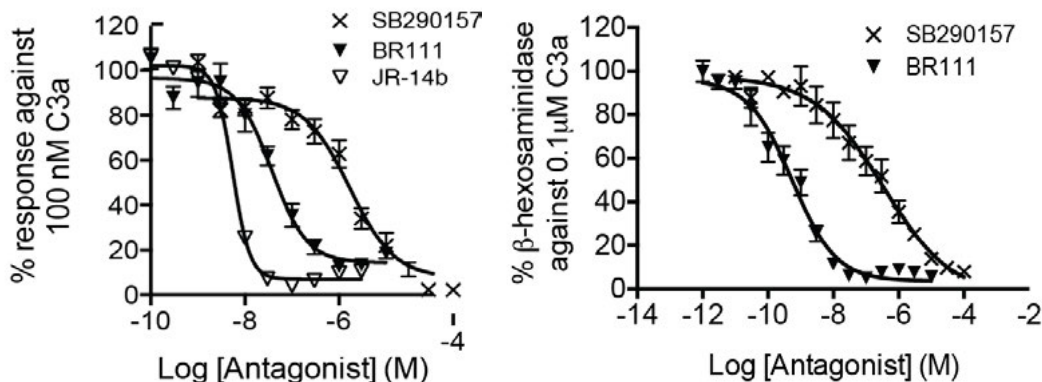


Fig. 5. Antagonism by heterocyclic peptidomimetics of C3a-induced (left): Ca^{2+} release in human monocyte-derived macrophages, (right): β -hexosaminidase release in LAD2 human mast cells.

Acknowledgments

We thank the Australian Research Council for a grant (DP130100629), the Australian National Health and Medical Research Council for grants (1028243, 1030169, 1084018) and for a Senior Principal Research Fellowship to DF (1027369). Enabling support is also gratefully acknowledged from the ARC Centre of Excellence in Advanced Molecular Imaging (CE140100011) and the Queensland State Government (CIF grant).

References

1. Ricklin, D., Hajishengallis, G., Yang, K., et al. *Nature Immunol.* **11**, 785-797 (2010), <http://dx.doi.org/10.1038/ni.1923>
2. Klos, A., Wende, E., Wareham, K.J., Monk, P.N. *Pharmacol. Rev.* **65**, 500-543 (2013), <http://dx.doi.org/10.1124/pr.111.005223>
3. Gerard, N.P., Gerard, C. *Curr. Opin. Immunol.* **14**, 705-708 (2002), [http://dx.doi.org/10.1016/S0952-7915\(02\)00410-7](http://dx.doi.org/10.1016/S0952-7915(02)00410-7)
4. Mizutani, N., Nabe, T., Yoshino, S. *J. Immunol.* **183**, 4039-4046 (2009), <http://dx.doi.org/10.4049/jimmunol.0901468>
5. Zipfel, P.F., Skerka, C. *Nat. Rev. Immunol.* **9**, 729-740 (2009), <http://dx.doi.org/10.1038/nri2620>
6. Hutamekalin, P., Takeda, K., Tani, M., Tsuga, Y., Ogawa, N., Mizutani, N., Yoshino, S. *J. Pharmacol. Sci.* **112**, 56-63 (2010), <http://dx.doi.org/10.1254/jphs.09180FP>
7. Banda, N.K., Hyatt, S., et al. *J. Immunol.* **188**, 1469-1478 (2012), <http://dx.doi.org/10.4049/jimmunol.1102310>
8. Peng, Q., Li, K., Smyth, L.A., Xing, G., Wang, N., Meader, L., Lu, B., Sacks, S.H., Zhou, W. *J. Am. Soc. Nephrol.* **23**, 1474-1485 (2012), <http://dx.doi.org/10.1681/ASN.2011111072>
9. Reid, R.C., Yau, M.K., Singh, R., Hamidon, J.K., Reed, A.N., Chu, P., Suen, J.Y., Stoermer, M.J., Blakeney, J.S., Lim, J., Faber, J.M., Fairlie, D.P. *Nat. Commun.* **4**, 2802 (2013), <http://dx.doi.org/10.1038/ncomms3802>
10. Reid, R.C., Yau, M.K., Singh, R., Hamidon, J.K., Lim, J., Stoermer, M.J., Fairlie, D.P. *J. Med. Chem.* **57**, 8459-8470 (2014), <http://dx.doi.org/10.1021/jm500956p>
11. Wilken, H.C., Gotze, O., Werfel, T., Zwirner, J. *Immunol. Lett.* **67**, 141-145 (1999), [http://dx.doi.org/10.1016/S0165-2478\(99\)00002-4](http://dx.doi.org/10.1016/S0165-2478(99)00002-4)
12. Sun, J., Ember, J.A., Chao, T.H., Fukuoka, Y., Ye, R.D., Hugli, T.E. *Protein Sci.* **8**, 2304-2311 (1999), <http://dx.doi.org/10.1110/ps.8.11.2304>
13. Abbenante, G., Fairlie, D.P., Gahan, L.R., Hanson, G.R., Pierens, G., van den Brenk, A.L. *J. Am. Chem. Soc.* **118**, 10384-10388 (1996), <http://dx.doi.org/10.1021/ja962260f>
14. Sokolenko, N., Abbenante, G., Scanlon, M.J., Jones, A., Gahan, L.R., Hanson, G.R., Fairlie, D.P. *J. Am. Chem. Soc.* **121**, 2603-2604 (1999), <http://dx.doi.org/10.1021/ja983354n>
15. Singh, Y., Stoermer, M.J., Lucke, A., Guthrie, T., Fairlie, D.P. *J. Am. Chem. Soc.* **127**, 6563-6572 (2005), <http://dx.doi.org/10.1021/ja0455300>
16. Reid, R.C., Yau, M., Singh, R., Lim, J., Fairlie, D.P. *J. Am. Chem. Soc.* **136**, 11914-11917 (2014), <http://dx.doi.org/10.1021/ja506518t>
17. Ames, R.S., et al. *J. Immunol.* **166**, 6341-6348 (2001), <http://dx.doi.org/10.4049/jimmunol.166.10.6341>

The Main-Chain Oxygen: Unappreciated Effects on Peptide and Protein Structure

Robert W. Newberry¹ and Ronald T. Raines^{1,2}

¹Dept. of Chemistry, University of Wisconsin-Madison, Madison, WI, 53706; ²Dept. of Biochemistry, University of Wisconsin-Madison, Madison, WI, 53706, USA

Introduction

Current limitations in protein structure prediction and design suggest an incomplete understanding of the forces governing protein folding. As such, noncovalent interactions in proteins, particularly hydrogen bonds, have received great attention [1,2]. In common secondary structure patterns like the α -helix and β -sheet, main-chain N–H hydrogen bond donors approach their carbonyl acceptors approximately along the carbonyl bond axis [3], despite conventional wisdom that hydrogen bond energies are maximized when donors approach at 120° to the carbonyl bond axis [4]. This observation can be rationalized using a modern, quantum-mechanically based model of the carbonyl lone pairs that indicates that the two orbitals differ from the sp^2 -hybridized VSEPR “rabbit ears” assumed commonly. Specifically, one lone pair, approximately sp -hybridized, is oriented along the carbonyl bond axis, while the second, purely p -orbital orients orthogonally (Figure 1).

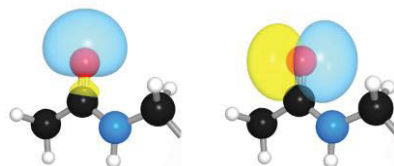


Fig. 1. *s*-Type (left) and *p*-type (right) carbonyl lone pairs.

Canonical hydrogen bonds in protein secondary structure therefore often employ the *s*-rich lone pair; however, the role of the *p*-type lone pair is less clear. We have previously noted that backbone $n \rightarrow \pi^*$ interactions are well poised to exploit this *p*-type lone pair [5]. In an $n \rightarrow \pi^*$ interaction, the filled *p*-type lone pair of a carbonyl oxygen interacts with the empty π^* orbital of an adjacent carbonyl group, and the mixing of these orbitals releases energy. These interactions have energies generally greater than 0.27 kcal/mol each [6], and are ubiquitous in folded proteins [7,8], particularly in the α -helix [9]. Yet, no analogous role for the *p*-type carbonyl lone pair has been identified in β -sheets. We now posit that a previously unappreciated hydrogen bond occurs within the backbone of individual residues in β -sheets.

Results and Discussion

Upon inspection of an idealized β -sheet, we noted close proximity of the *p*-type carbonyl lone pair with the amide N–H group of the same residue (Figure 2) and hypothesized an attraction between them that could be analogous to canonical hydrogen bonds. Compared to traditional hydrogen bonds, these putative interactions are highly distorted, so we first set out to determine if these interactions have the properties typical of other hydrogen bonds.

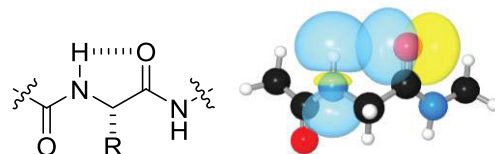


Fig. 2. Putative C5 hydrogen bond in the peptide backbone.

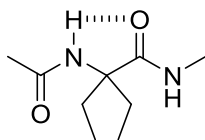


Fig. 3. Diethylglycine scaffold for studying C5 hydrogen bonds.

To probe a single interaction, we preorganized the putative donor and acceptor using a diethylglycine model system (Figure 3); diethylglycines have been shown by computation [10,11], as well as NMR [12–14] and vibrational spectroscopies [12,15], to adopt the “C5” geometry [16], which is an extended conformation that places the carbonyl oxygen in close proximity to the amide proton. Having realized the necessary geometry, we probed the putative interaction by replacing an amide hydrogen bond acceptor with an ester, which is known to attenuate *bona fide* hydrogen bonds. We found that attenuating the putative C5 hydrogen bond caused an increase in the stretching frequency of the donor in the infrared spectrum. In addition, we found that replacement of the amide acceptor with an ester

caused an upfield chemical shift of the donor proton, despite the greater electron-withdrawing character of the ester. Finally, we found that an amide acceptor was much more effective at protecting the donor proton from H/D exchange than was the ester. Together, these data show that these interactions do constitute hydrogen bonding.

To evaluate the relevance of these interactions for proteins, we probed their contributions to the conformational stability of a “tryptophan zipper” model β -hairpin peptide [17]. Upon selective attenuation of the C5 hydrogen bond using an amide-to-ester substitution [18,19], we observed a decrease in global thermostability by CD spectroscopy. Conversely, selective enhancement of a C5 hydrogen bond imparted additional thermostability to this peptide. Together, these results demonstrate that C5 hydrogen bonds are operative in β -sheet structures. Finally, to evaluate their cumulative contributions to conformational stability, we calculated the total energy of C5 hydrogen bonds in the structures of folded proteins and found that they contribute an average of 5 kcal/mol of stabilizing energy to a 100-residue protein.

Our results highlight the importance of a previously unappreciated force in protein folding: the C5 hydrogen bond. The discovery of this interaction explains how proteins make effective use of *both* lone pairs of the main-chain oxygen to stabilize secondary structure. We believe that the integration of these interactions into experimental and computational approaches would advance the understanding of the folding and stability of peptides and proteins.

Acknowledgments

We are grateful to G.J. Bartlett, D.N. Woolfson, and L.L. Kiessling for contributive discussions. We thank W.M. Westler for assistance with NMR spectroscopy, and T. Zhang and M.T. Zanni for assistance with IR spectroscopy. This work was funded by grants R01 AR044276 (NIH) and CHE-1124944 (NSF). This work made use of the National Magnetic Resonance Facility at Madison, which is supported by grant P41 GM103399 (NIH), and the Biophysics Instrumentation Facility at the University of Wisconsin-Madison, which was established by grants BIR-9512577 (NSF) and S10 RR013790 (NIH). High-performance computing was supported by grant CHE-0840494 (NSF). R.W.N. was supported by Biotechnology Training Grant T32 GM008349 (NIH) and by an ACS Division of Organic Chemistry Graduate Fellowship.

References

1. Dill, K.A. *Biochemistry* **29**, 7133-7155 (1990), <http://dx.doi.org/10.1021/bi00483a001>
2. Stickle, D.F., Presta, L.G., Dill, K.A., Rose, G.D. *J. Mol. Biol.* **226**, 1143-1159 (1992), [http://dx.doi.org/10.1016/0022-2836\(92\)91058-W](http://dx.doi.org/10.1016/0022-2836(92)91058-W)
3. Kabsch, W., Sander, C. *Biopolymers* **22**, 2577-2637 (1983), <http://dx.doi.org/10.1002/bip.360221211>
4. Steiner, T. *Angew. Chem. Int. Ed.* **41**, 48-76 (2002), [http://dx.doi.org/10.1002/1521-3773\(20020104\)41:1<48::AID-ANIE48>3.0.CO;2-U](http://dx.doi.org/10.1002/1521-3773(20020104)41:1<48::AID-ANIE48>3.0.CO;2-U)
5. Bretscher, L.E., et al. *J. Am. Chem. Soc.* **123**, 777-778 (2001), <http://dx.doi.org/10.1021/ja005542v>
6. Newberry, R.W., VanVeller, B., Guzei, I.A., Raines, R.T. *J. Am. Chem. Soc.* **135**, 7843-7846 (2013), <http://dx.doi.org/10.1021/ja4033583>
7. Bartlett, G.J., Choudhary, A., Raines, R.T., Woolfson, D.N. *Nat. Chem. Biol.* **6**, 615-620 (2010), <http://dx.doi.org/10.1038/nchembio.406>
8. Newberry, R.W., et al. *Protein Sci.* **23**, 284-288 (2014), <http://dx.doi.org/10.1002/pro.2413>
9. Choudhary, A., Raines, R.T. *Protein Sci.* **20**, 1077-1081 (2011), <http://dx.doi.org/10.1002/pro.627>
10. Benedetti, E., et al. *Biopolymers* **27**, 357-371 (1988), <http://dx.doi.org/10.1002/bip.360270302>
11. Casanovas, J., et al. *J. Phys. Chem. B* **116**, 13297-13307 (2012), <http://dx.doi.org/10.1021/jp3045115>
12. Toniolo, C., et al. *Biopolymers* **27**, 373-379 (1988), <http://dx.doi.org/10.1002/bip.360270303>
13. Bonora, G.M., et al. *J. Am. Chem. Soc.* **106**, 8152-8156 (1984), <http://dx.doi.org/10.1021/ia00338a025>
14. Formaggio, F., et al. *Org. Biomol. Chem.* **10**, 2413-2421 (2012), <http://dx.doi.org/10.1039/C2OB06863J>
15. Maekawa, H., Ballano, G., Toniolo, C., Ge, N.H. *J. Phys. Chem. B* **115**, 5168-5182 (2011), <http://dx.doi.org/10.1021/jp105527n>
16. Toniolo, C., Benedetti, E. *Crit. Rev. Biochem.* **9**, 1-44 (1980), <http://dx.doi.org/10.3109/10409238009105471>
17. Cochran, A.G., Skelton, N.J., Starovasnik, M.A. *Proc. Natl. Acad. Sci. USA* **98**, 5578-5583 (2001), <http://dx.doi.org/10.1073/pnas.091100898>
18. Deechongkit, S., Dawson, P.E., Kelly, J.W. *J. Am. Chem. Soc.* **126**, 16762-16771 (2004), <http://dx.doi.org/10.1021/ja045934s>
19. Deechongkit, S., et. al. *Nature* **430**, 101-105 (2004), <http://dx.doi.org/10.1038/nature02611>

Opioid Ligand Binding to Opioid Receptors: Insight and Implications for Peptide Design

Michael J. Ferracane and Jane V. Aldrich

Department of Medicinal Chemistry, University of Florida, Gainesville, FL, 32610, USA

Introduction

The three opioid receptors (μ , δ , and κ) are important targets for pain management and have also shown promise as targets for treatment of addiction and mood disorders. In the past, research in the field commonly focused on analysis of structure-activity relationships (SAR) and ligands' conformational preferences. Recently, advancements permitted determination of crystal structures for each of the opioid receptors in their antagonist-bound states [1-5]. These structures, combined with computational approaches, permit examination of how opioid ligands may bind to opioid receptors at the atomic level, knowledge that would facilitate the design and development of opioid receptor modulators with greater therapeutic potential.

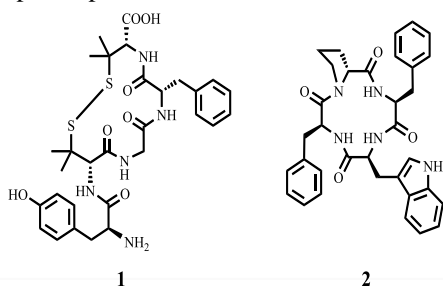


Fig. 1. Structures of DPDPE and CJ-15,208.

[D-Pen²,D-Pen⁵]enkephalin (DPDPE, **1**) (Figure 1) is a selective cyclic peptide agonist at the δ opioid receptor. The SAR and conformational preferences of DPDPE and its analogs were the subject of prior investigation [6-9]. These studies showed that the stereochemistry of the third amino acid has a profound effect on the structure and δ opioid receptor affinity of compounds in the series. This SAR makes DPDPE and its analogs particularly amenable to docking studies, which may help elucidate the active conformation of compounds possessing this scaffold.

The macrocyclic tetrapeptide CJ-15,208 (**2**) and its analogs also have a constrained cyclic structure and bind to opioid receptors [10-12] even though they lack the canonical opioid pharmacophore. While this unusual structure confers many desirable drug-like properties – including oral bioavailability and blood-brain barrier permeability [13-15] – it makes docking studies and rational design of CJ-15,208 analogs particularly challenging.

Herein we utilize docking studies to explore likely binding modes of DPDPE and its analogs, information that can then be used to predict possible binding modes of other opioid ligands, including macrocyclic tetrapeptides such as CJ-15,208.

Results and Discussion

Docking studies with DPDPE and its analogs were performed in four steps. First, a pharmacophore was generated using the atomic coordinates of the phenol (Dmt¹, where Dmt = (S)-2',6'-dimethyltyrosine), N-terminal amine, and phenyl (Phe³) moieties of DIPP-NH₂ (Dmt-Tic-Phe-Phe-NH₂, where Tic = (S)-1,2,3,4-tetrahydro-3-isoquinolinecarboxylic acid) present in the published δ opioid receptor crystal structure [3]. Then, using the coordinates from their crystal structures [6,7], DPDPE, [L-Ala³]DPDPE, and [D-Ala³]DPDPE were subjected to a conformational search to generate a library of conformers for each compound. These conformer libraries underwent virtual screening for binding to a δ opioid receptor model, using the pharmacophore to place conformers into the pocket of the receptor. Finally, the top pose(s) were minimized to obtain final docked pose(s) and docking score(s) were measured.

Using this methodology, only [L-Ala³]DPDPE was capable of aligning all of its essential elements – its phenol (Tyr¹), N-terminal amine, and phenyl (Phe⁴) moieties – with those of DIPP-NH₂. Although the phenol and amine moieties of DPDPE and [D-Ala³]DPDPE overlay with those of DIPP-NH₂, their phenyl groups did not overlap with the important phenyl group of DIPP-NH₂ (Figure 2a). Thus, we propose that the structure of [L-Ala³]DPDPE best resembles the likely bioactive conformation of DPDPE and its analogs, although it is the preferred conformation for only [L-Ala³]DPDPE, and not DPDPE or [D-Ala³]DPDPE, in aqueous solution.

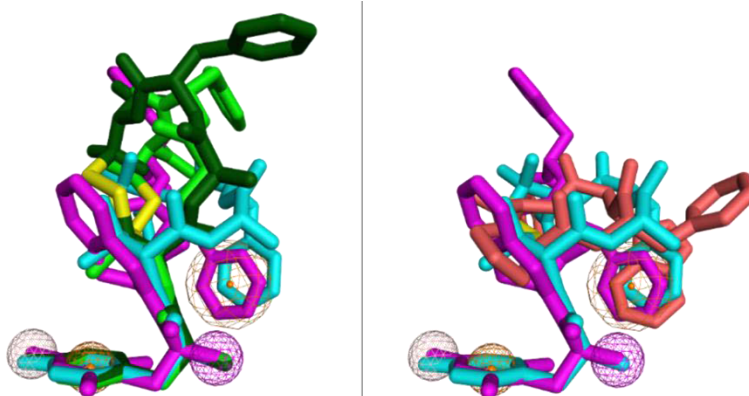


Fig. 2. a) Overlay of DPDPE (light green), [D-Ala³]DPDPE (dark green), and [L-Ala³]DPDPE (cyan) with DIPP-NH₂ (magenta) from the crystal structure of the δ opioid receptor. Only [L-Ala³]DPDPE was capable of overlapping all its pharmacophore elements with those in DIPP-NH₂ (spheres) in the docking studies. b) Overlay of [L-Ala³]DPDPE (cyan), DIPP-NH₂ (magenta), and CJ-15,208 (rose). In this pose, CJ-15,208 achieves overlap with the essential aromatic residue of DIPP-NH₂ and the backbone of [L-Ala³]DPDPE.

Next, docking studies were performed with CJ-15,208. Similar to before, a library of conformers was generated and then docked – using either the phenol or phenyl element from the prior pharmacophore to guide ligand placement – into a κ opioid receptor model. Unfortunately, this process yielded poses that had significant steric clashes between the peptide and the receptor. Therefore, CJ-15,208 was subsequently placed into the κ receptor model manually.

Following manual placement, the essential Trp⁴ aromatic group of CJ-15,208 overlapped with the phenyl group of DIPP-NH₂, and the cyclic backbone of CJ-15,208 achieved significant overlap with the cyclic portion of [L-Ala³]DPDPE in its proposed bioactive conformation at the δ opioid receptor (Figure 2b). While other poses are plausible, the degree of overlap with this pose is encouraging. We are currently using this information to design and synthesize novel CJ-15,208 analogs.

Acknowledgments

This research was supported by R01 DA018832 (National Institute on Drug Abuse) and the University of Florida. Special thanks to the American Peptide Society for an APS Travel Grant for MJF.

References

1. Wu, H., et al. *Nature* **485**, 327-332 (2012), <http://dx.doi.org/10.1038/nature10939>
2. Granier, S., et al. *Nature* **485**, 400-404 (2012), <http://dx.doi.org/10.1038/nature11111>
3. Fenalti, G., et al. *Nat. Struct. Mol. Biol.* **22**, 265-268 (2015), <http://dx.doi.org/10.1038/nsmb.2965>
4. Fenalti, G., et al. *Nature* **506**, 191-196 (2014), <http://dx.doi.org/10.1038/nature12944>
5. Manglik, A., et al. *Nature* **485**, 321-326 (2012), <http://dx.doi.org/10.1038/nature10954>
6. Flippen-Anderson, J.L., et al. *J. Am. Chem. Soc.* **116**, 7523-7531 (1994), <http://dx.doi.org/10.1021/ja00096a008>
7. Collins, N., et al. *J. Am. Chem. Soc.* **118**, 2143-2152 (1996), <http://dx.doi.org/10.1021/ja9531081>
8. Haaseth, R.C., et al. *J. Med. Chem.* **37**, 1572-1577 (1994), <http://dx.doi.org/10.1021/jm00037a007>
9. Haaseth, R.C., et al. *Int. J. Pept. Protein Res.* **36**, 139-146 (1990), <http://dx.doi.org/10.1111/j.1399-3011.1990.tb00957.x>
10. Saito, T., et al. *J. Antibiot.* **55**, 847-854 (2002), <http://doi.org/10.7164/antibiotics.55.847>
11. Aldrich, J.V., et al. *ChemMedChem* **6**, 1739-1745 (2011), <http://dx.doi.org/10.1002/cmdc.201100113>
12. Aldrich, J.V., et al. *Br. J. Pharmacol.* **171**, 3212-3222 (2014), <http://doi.org/10.1111/bph.12664>
13. Aldrich, J.V., et al. *J. Nat. Prod.* **76**, 433-438 (2013), <http://dx.doi.org/10.1021/np300697k>
14. Ross, N.C., et al. *Br. J. Pharmacol.* **165**, 1097-1108 (2012), <http://dx.doi.org/10.1111/j.1476-5381.2011.01544.x>
15. Eans, S.O., et al. *Br. J. Pharmacol.* **169**, 426-436 (2013), <http://dx.doi.org/10.1111/bph.12132>

Designing Enzyme-Like Catalysts: A Rhodium(II) Metallopeptide Case Study

Farrukh Vohidov¹, Brian V. Popp², and Zachary T. Ball^{1*}

¹Rice University, Department of Chemistry, Houston, TX, 77005, USA; ²West Virginia University,
 C. Eugene Bennett Department of Chemistry, Morgantown, WV, 26506, USA

Introduction

Peptides are relatively simple molecules with remarkable capacity for supramolecular assembly and molecular recognition. In this study, harnessing the combined potential of peptide molecular recognition and unique coordination chemistry or catalysis with non-biological transition metals allows the development of new tools for protein chemistry and probe development. While methods for chemical manipulation of recombinant proteins are well established [4,5], natural proteins, which are without engineered sequences or side-chain handles, remain a challenging target for chemical manipulation.

Results and Discussion

We began efforts at selective protein modification with transition-metal catalysts by focusing on rhodium(II) metallopeptides. There was established reactivity of these complexes toward tryptophan side chains [6], and we developed robust, general, and reliable methods for the synthesis and purification of rhodium(II) metallopeptides [7-9]. The metalation of unprotected peptides did not affect folding, and could even be used to enforce helical structure [7].

In orienting experiments, we focused on the modification of helical peptides that self-assemble into heterodimeric coiled coils in the presence of complementary metallopeptides (Figure 1). Treatment with stabilized diazo reagents resulted in clean modification of position “g” on the corresponding substrate helix, immediately flanking the rhodium center. The site of location was established by MS/MS fragmentation methods [1,2] and NMR with isotopically-labeled diazo reagents. Tryptophan was the most reactive side chain. Turnover numbers of up to 50 were obtained at micromolar substrate concentration, and the rate enhancement for complementary substrates relative to an unstructured control reaction was $>10^3$. Even more powerfully, the proximity-driven catalysis enabled modification of many other side chains (Figure 1) that are completely unreactive with simple

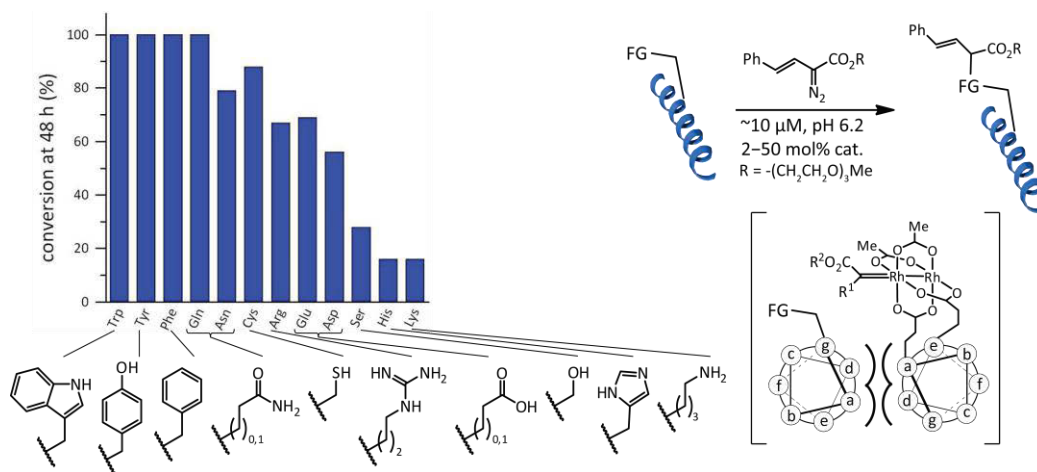


Fig. 1. Site-specific covalent modification of helical peptides catalyzed by rhodium(II) metallopeptides enables remarkably broad and selective amino-acid reactivity. “Conversion” indicates reaction at position “g” of a helix. Site of modification is established by MS/MS fragmentation analysis [1,2].

rhodium catalysts such as $\text{Rh}_2(\text{OAc})_4$. In totality, residues identified as substrates for modification make up >40% of protein amino-acid space. The reactivity demonstrated here enabled a number of studies with similar engineered coils, including design of orthogonally reactive catalyst-substrate [10] pairs and the use of tryptophan-containing coils as tags for proteins expressed in lysate [10,11].

Importantly, these initial studies could be successfully extended from engineered coils to the modification of completely natural protein substrates by employing protein-peptide recognition motifs beyond the coiled coil. We examined modification of SH3 domains in significant detail [3]. The SH3 domain recognized short proline-rich motifs in an extended, PPII-helix conformation. Through proper design of catalyst, it is possible to achieve selective reaction at individual members of members of the Src-family kinase SH3 domains. Even more remarkable, we designed a suites of catalysts that selectively modify different individual amino-acids on the Lck SH3 domain, demonstrating that catalyst control is capable of building ensembles of modified proteins, decorated at different sites near the peptide-binding cleft (Figure 2).

The sensitivity and specificity of the modification methods could be probed by examining human cell lysates from cell lines known to express an individual Src-family kinase. As shown (Figure 3) covalent modification of the Yes kinase was visualized by blotting with a fluorogenic dye specific for the chemical modification. The method identifies Yes, which could also be visualized by a traditional antibody blot technique. The experiment demonstrates that chemical modification succeeds on whole human proteins at natural abundance levels. Because the SH3 domain of a full-length kinase is tied up in intramolecular interactions with a kinase domain loop (see structure, Figure 3), these cell lysate results indicate that catalysis is possible even when the metallopeptide and substrate concentrations lie below the dissociation constant for assembly.

Metallopeptide recognition of SH3 domains is one example of practical rhodium(II) catalysts that employ molecular recognition to achieve selectivity. Small-molecule-rhodium conjugates are also effective in cases where small-molecule ligands for protein-protein interaction sites can be found. In addition, SH2 domains, coiled-coil domains, and other well-known peptide-binding motifs represent suitable targets for catalyst development. Current efforts also include the design and discovery of minimalist catalyst recognition motifs on a protein surface.

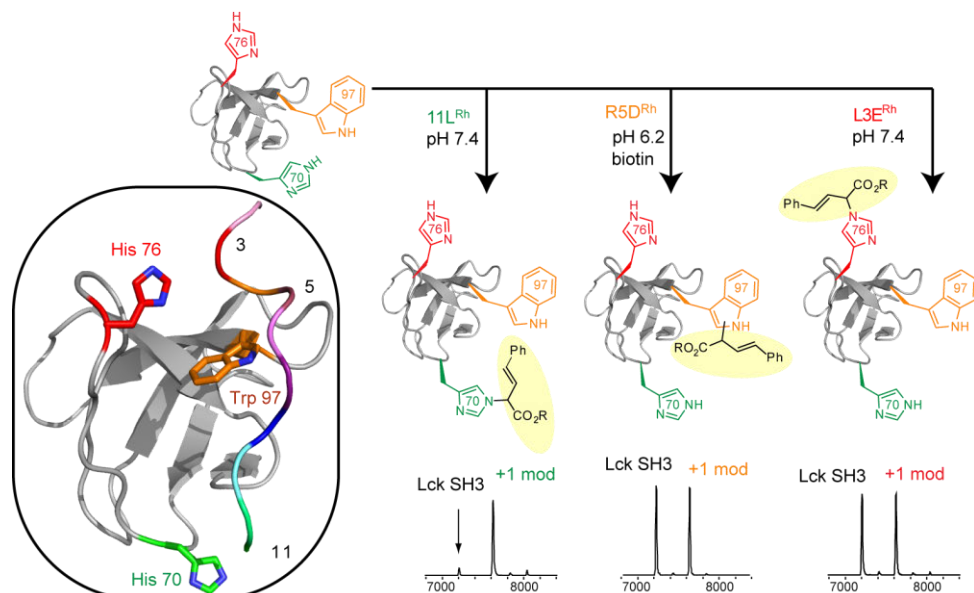


Fig. 2. Site-specific modification different amino-acid sites on the Lck SH3 domain is achieved by catalyst design of rhodium metalloptides at the indicated amino acids (3, 5, or 11) on a proline-rich SH3-binding peptide. Structure-guided catalyst designed enables independent modification of His70, His76, or Trp97 on the Lck SH3 domain [3].

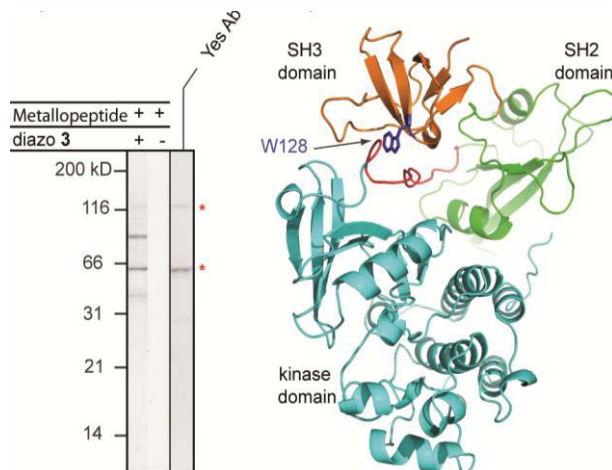


Fig. 3. (left) Gel image demonstrating modification of Yes kinase in human PC-3 cell lysate, with Yes antibody staining at right for comparison. (right) The rest-state structure of Src-family kinases, showing the interaction between the SH3 domain (orange) and a loop region near the kinase domain (cyan), effectively burying the SH3 peptide-binding motif. Shown here for Src (PDB ID: 2SRC).

Acknowledgments

We acknowledge support from the National Institutes of Health under grant number 5R21CA170625, from the Robert A. Welch Foundation Research Grant C-1680, and from the National Science Foundation (CHE-1055569).

References

1. Popp, B.V., Ball, Z.T. *Chem. Sci.* **2**, 690-695 (2011), <http://dx.doi.org/10.1039/c0sc00564a>
2. Popp, B.V., Ball, Z.T. *J. Am. Chem. Soc.* **132**, 6660-6662 (2010), <http://dx.doi.org/10.1021/ja101456c>
3. Vohidov, F., Coughlin, J.M., Ball, Z.T. *Angew. Chem. Int. Ed.* **54**, 4587-4591 (2015), <http://dx.doi.org/10.1002/anie.201411745>
4. Hinner, M.J., Johnsson, K. *Curr. Opin. Biotechnol.* **21**, 766-776 (2010), <http://dx.doi.org/10.1016/j.copbio.2010.09.011>
5. Sletten, E.M., Bertozzi, C.R. *Angew. Chem. Int. Ed.* **48**, 6974-6998 (2009), <http://dx.doi.org/10.1002/anie.200900942>
6. Antos, J.M., Francis, M.B. *J. Am. Chem. Soc.* **126**, 10256-10257 (2004), <http://dx.doi.org/10.1021/ja047272c>
7. Zaykov, A.N., Popp, B.V., Ball, Z.T. *Chem. Eur. J.* **16**, 6651-6659 (2010), <http://dx.doi.org/10.1002/chem.200903092>
8. Zaykov, A.N., MacKenzie, K.R., Ball, Z.T. *Chem. Eur. J.* **15**, 8961-8965 (2009), <http://dx.doi.org/10.1002/chem.200901266>
9. Zaykov, A.N., Ball, Z.T. *Chem. Commun.* **47**, 10927-10929. <http://dx.doi.org/10.1039/c1cc13169a>
10. Chen, Z., Vohidov, F., Coughlin, J.M., Stagg, L.J., Arold, S.T., Ladbury, J.E., Ball, Z.T. *J. Am. Chem. Soc.* **134**, 10138-10145 (2012), <http://dx.doi.org/10.1021/ja302284p>
11. Chen, Z., Popp, B.V., Bovet, C.L., Ball, Z.T. *ACS Chem. Biol.* **6**, 920-925 (2011), <http://dx.doi.org/10.1021/cb2001523>

Butelase 1: A Versatile and Multi-purpose Ligase

James P. Tam, Giang K.T. Nguyen, and Xinya Hemu

School of Biological Sciences, Nanyang Technological University, 60 Nanyang Drive, 637551, Singapore

Introduction

Proteases are ubiquitous and >400,000 putative sequences are found in databases. In contrast, ligases which are peptide-forming enzymes catalyzing the reverse reaction are rare. Thus far only four are identified. Recently, we reported the discovery of butelase 1, a versatile and multi-purpose ligase which is specific for the C-terminal Asn/Asp (Asx) ligation.

Butelase 1, isolated from *Clitoria Ternatea* of the legume family, requires an Asn/Asp (Asx) residue as the recognition site and a sorting signal such as a tripeptide motif Asx-HisVal at the C-terminus of a peptide or protein substrate with HisVal dipeptide as a leaving group (Figure 1) [1]. Butelase 1 accepts most amino acids as a nucleophile to form an Asx-Xaa bond without a trace of the sorting signal. Among the known ligases including sortase A, PATG and PCYC1, butelase 1 is the fastest ligase with catalytic efficiencies as high as $1,300,000 \text{ M}^{-1} \text{ s}^{-1}$. These favorable properties bode well for applications of butelase 1 for ligation, macrocyclization and labeling of peptides, proteins and live cells. Here, we present our recent work of butelase 1 in peptide macrocyclization using sunflower trypsin inhibitor and histatin as examples.

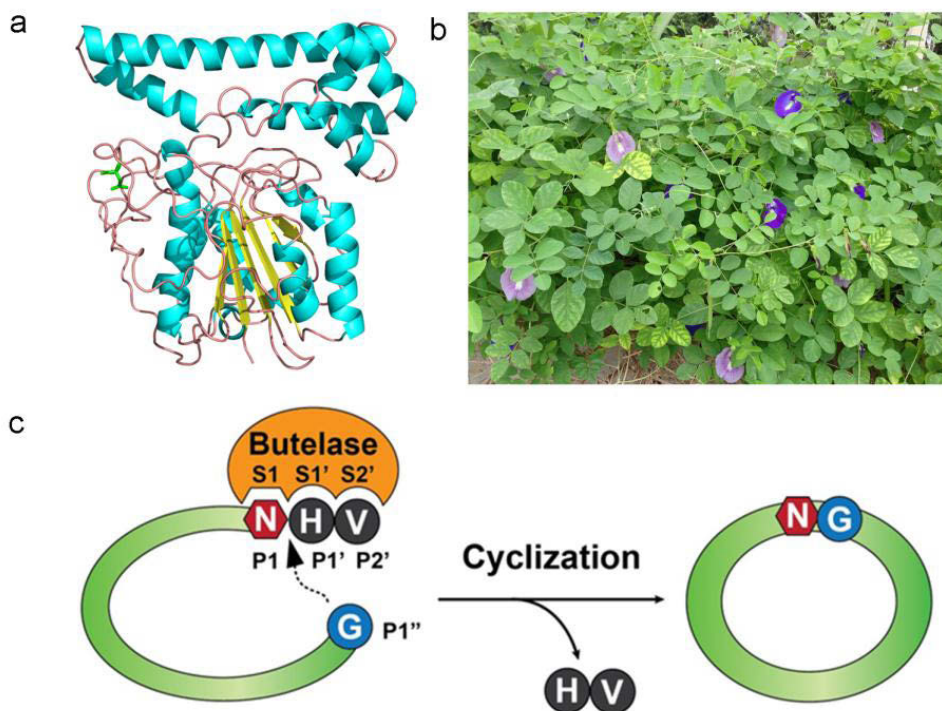


Fig. 1. Schematic illustration of peptide macrocyclization mediated by butelase 1. A. Homology modeling of butelase 1, B. *Clitoria Ternatea*, and C. Macrocyclization mediated by butelase 1 with HV dipeptide as a sorting signal.

Results and Discussion

Sunflower Trypsin Inhibitor and its analog

SFTI-1 is a naturally occurring cyclic peptide from sunflower seeds (*Helianthus annuus*). It consists of 14 amino acids, stabilized by one disulfide bond and is one of the most potent known inhibitor of trypsin [2]. Figure 2 shows that butelase 1 efficiently cyclized SFTI-1 in >95% yield with kinetic parameters of 0.6 s^{-1} for k_{cat} , $51 \text{ }\mu\text{M}$ for K_m and an overall catalytic efficiency of $11,700 \text{ M}^{-1} \text{ s}^{-1}$.

To improve the cyclization efficiency, we synthesized an analog of SFTI-1 with Ile at the P2'' position instead of Arg because most native substrates of butelase 1 have a hydrophobic amino acid (Ile/Leu/Val) at this position. The k_{cat} , K_m , and catalytic efficiency for SFTI analog were found to be 3.80 s^{-1} , $33 \text{ }\mu\text{M}$, and $115,000 \text{ M}^{-1} \text{ s}^{-1}$, respectively. The catalytic efficiency of SFTI analog is approximately 10 times faster than the SFTI-1 (Table 1), confirming the preference for a hydrophobic amino acid of butelase 1 at the P2'' position.

Table 1. Kinetics parameters of SFTI-1 and SFTI analog.

Peptide	Sequence	$k_{cat} \text{ (s}^{-1}\text{)}$	$k_M \text{ (}\mu\text{M)}$	$k_{cat}/k_M \text{ (M}^{-1} \text{s}^{-1}\text{)}$
SFTI-1	GRCTKSIPPICFPNHV	0.6	51	11,700
SFTI _{analog}	GICTKSIPPICFPNHV	3.8	33	115,000

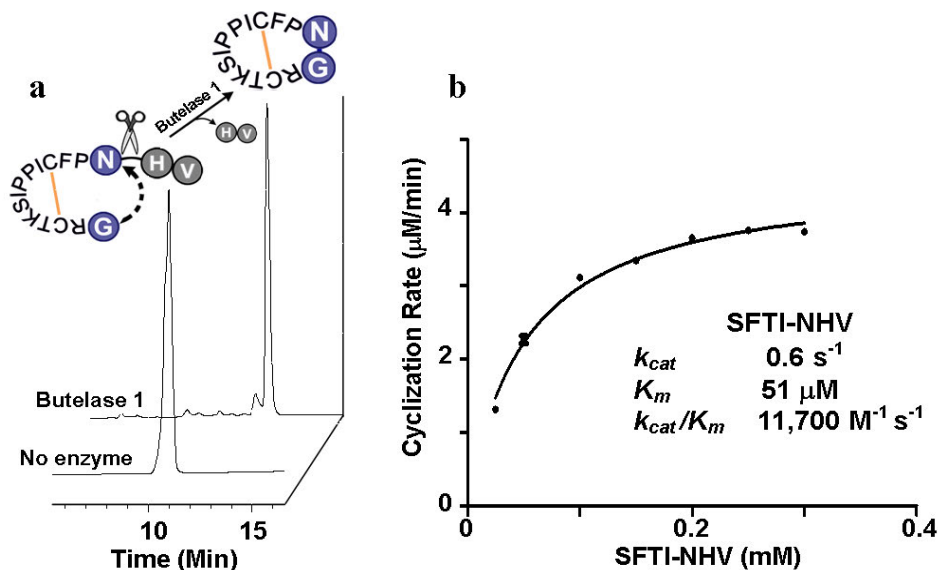


Fig. 2. Butelase mediated cyclization of SFTI-1.

Cyclization of Histatin 1

Histatin is a naturally occurring peptide antimicrobial found in human saliva. Cyclization of histatin has been shown to improve the activity by a 1000 fold [3]. Figure 2 shows the cyclization of histatin-1 was highly efficient with >95% yield in 15 min in the presence of 0.002 molar equivalent of butelase 1. For comparison, histatin cyclization by sortase A required 0.33 molar equivalent and 24 h incubation time to reach 90% yield. Butelase 1 thus cyclizes the histatin peptide 10,000 times faster than sortase A.

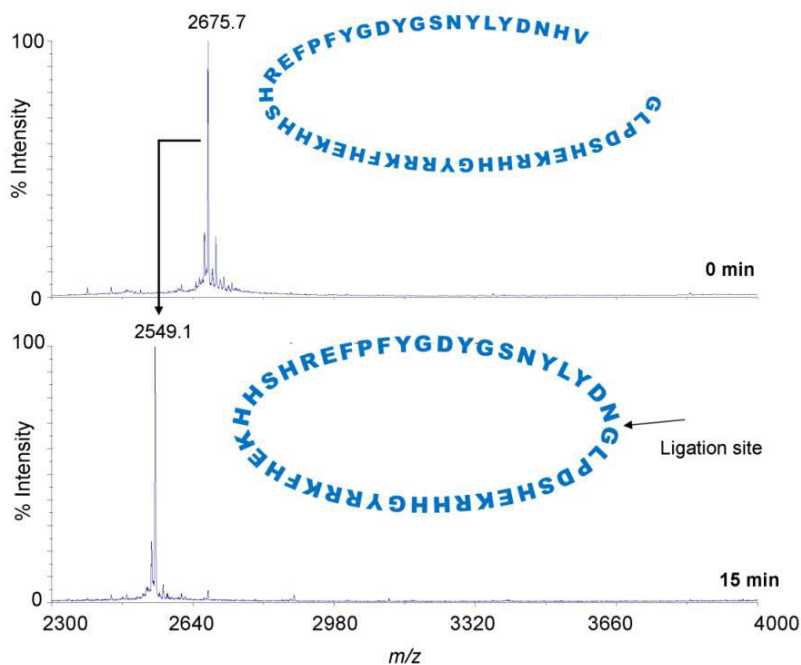


Fig. 3. Butelase-mediated cyclization of histatin-1. The cyclization reaction was performed at 42 °C in the presence of 0.1 μ M butelase 1 and 50 μ M peptide substrate. The reaction was monitored by MS over a time course of 15 min. Peptides shown in the MS profiles carried a net charge of +2.

Conclusion

Currently, there are two orthogonal ligation approaches without the use of a protection group scheme. The first is the *N*-terminal-specific ligation using a bifunctional *N*-terminal amino acid such as Cys, Ser or Thr [4,5]. This popular approach is well developed in the past two decades and can be performed either chemically or by an intein [6]. The second approach is the *C*-terminal-specific ligation. It requires the use of an enzyme, a ligase, to recognize a specific amino acid at or near the *C*-terminus [7]. This approach is highly underdeveloped because naturally occurring ligases are rare and our discovery of butelase 1 as an Asx-specific ligase provides a promising tool to fill this void. An advantage of butelase is its fast kinetic. It generally completes the cyclization (8 to 300+ aa) within minutes. This characteristic of fast kinetics is important not only because of high yield but also because it minimizes the reverse reaction of random cleavage of Asx residues of the products.

Acknowledgments

This work was supported in part by the Singapore National Research Foundation grant NRF-CRP8-2011-05.

References

1. Nguyen, G.K., et al. *Nat. Chem. Biol.* **10**, 732-738 (2014), <http://dx.doi.org/10.1038/nchembio.1586>
2. Luckett, S., et al. *J. Mol. Biol.* **290**, 525-533 (1999), <http://dx.doi.org/10.1006/jmbi.1999.2891>
3. Bolscher, J.G., et al. *FASEB J.* **25**, 2650-2658 (2011), <http://dx.doi.org/10.1096/fi.11-182212>
4. Dawson, P.E., et al. *Science* **266**, 776-779 (1994), <http://dx.doi.org/10.1126/science.7973629>
5. Liu, C.F., J.P. Tam, J.P. *J. Am. Chem. Soc.* **116**, 4149-4153 (1994), <http://dx.doi.org/10.1021/ja00089a001>
6. Xu, M.Q., Evans, T.C. *Methods* **24**, 257-277 (2001), <http://dx.doi.org/10.1006/meth.2001.1187>
7. Mao, H., et al. *J. Am. Chem. Soc.* **126**, 2670-2671 (2004), <http://dx.doi.org/10.1021/ja039915e>

Novel Agents that Prevent Atherosclerosis: Multivalent Peptide Constructs and Self-Assembling Cyclic DL- α -Peptides

Bruce E. Maryanoff¹, Luke J. Leman¹, Yannan Zhao¹, Tomohiro Imura¹,
Audrey S. Black¹, David J. Bonnet², Linda K. Curtiss²,
and M. Reza Ghadiri^{1,3,*}

¹Department of Chemistry; ²Department of Immunology and Microbial Science; ³The Skaggs Institute for Chemical Biology, The Scripps Research Institute, La Jolla, CA, 92037, USA

Introduction

Heart disease is the number one killer worldwide, and is responsible for nearly a third of all deaths in the USA. The principal cause of heart disease is lipid accumulation in the arteries with attendant deposition of atherosclerotic plaque, which is comprised mainly of lipids, cholesterol, calcium salts, cells, and cellular debris. Atherosclerosis can be treated by reducing low-density lipoprotein-cholesterol (LDL-C) via administration of statin drugs. High-density lipoproteins (HDLs) appear to protect against atherosclerosis, such that an increase in their levels and function is desirable. HDL particles, ranging in size from 7-13 nm, are in a constant state of dynamic flux, where the large particles convert into smaller particles, or release free apoA-I. HDL particles accept cholesterol and lipids from peripheral cells and plaques for elimination in the liver (Reverse Cholesterol Transport). The antiatherogenic action of HDL is related to the major structural protein, apolipoprotein A-I (apoA-I), a 243-mer in humans that is comprised of 10 amphiphilic α -helices [1]. ApoA-I mimetic peptides are generally amphiphilic α -helices that can boost levels of cholesterol-mobilizing, HDL-like particles or improve the functional properties of such particles [1]. We have been involved in the design, synthesis, and functional characterization of novel molecules that mimic apoA-I based on the multivalent presentation of 23-mer and 16-mer amphiphilic, α -helical peptides [2]. Some of these derivatives were athero-preventive in a key mouse model on *i.p.* and oral (!) administration [3]. Results from this work led us to explore amphiphilic cyclic DL- α -peptides that could self-assemble into amphiphilic nanotubes.

Results and Discussion

We utilized native chemical ligation [4] to link amphiphilic peptides to small-molecule scaffolds that possessed 2, 3, or 4 reactive arms to obtain two families of monomer, dimer, trimer, and tetramer peptide constructs based on amphiphilic, α -helical subunits containing 23 or 16 amino acids [2]. These multivalent constructs were combined, in a formulation, with (R)-(+)-1,2-dimyristoyl-*sn*-glycero-3-phosphocholine (DMPC) to obtain discoidal nanoparticles in the HDL size range [2]. We systematically studied the formation of lipid nanodiscs and their functional effects in relation to helix multimerization. For *in vitro* functional characterization, we measured the effect of each construct on cholesterol efflux from cholesterol-laden macrophage cells (J774). In both series, the multivalent constructs promoted cholesterol efflux more efficiently than the monomeric peptide. In the 16-mer family, the efficacy was in the order: tetramer-16 > trimer-16 > dimer-16 >> monomer-16. All of the peptide nanoparticles, except for monomer-16, fostered HDL remodeling in human plasma *in vitro*, which constitutes to the increase in small, dense HDL levels within the HDL particle distribution.

When administered *i.p.* to mice, the nanoparticles containing multivalent constructs exhibited superior plasma concentrations and much longer residence times (e.g., 6-8 h for trimer-23 and trimer-16 nanoparticles) compared with nanolipid particles from monomers. The small, dense HDL bands were enhanced from 2-8 h post-injection for dimer-23 and trimer-23, reflecting substantial remodeling of mouse HDLs *in vivo*. We carried out athero-prevention studies in low-density lipoprotein receptor-null (LDLR^{-/-}) mice. At 10 weeks of age, the mice were switched from a normal chow diet to a high-fat diet, and daily 40-mg/kg *i.p.* injections of trimer-23/DMPC nanoparticles were initiated. After two weeks, plasma total cholesterol levels were reduced by 40%, compared to vehicle (phosphate-buffered saline, PBS) controls. The plasma HDLs were also remodeled in favor of smaller HDL particle sizes. In further cholesterol reduction studies, trimer-23/DMPC nanoparticles were administered orally in the drinking water (~50 mg/kg/day). After two weeks, the trimer nanoparticles reduced plasma total

cholesterol levels by 40% compared to PBS control. To establish the effect of the trimer-23/DMPC nanoparticles on atherosclerotic plaque development, groups of LDLr^{-/-} mice were treated with daily i.p. injections (40 mg/kg) or orally (in drinking water, ~50 mg/kg/day) for 10 weeks. Daily i.p. treatment with the trimer-23 nanoparticles reduced aorta lesion areas and heart aortic valve plaque volumes by 55% and 61%, respectively. Surprisingly, oral administration of the trimer-23 nanoparticles for 10 weeks markedly reduced aorta lesion areas and heart aortic valve plaque by 50% and 70%.

These exciting findings inspired us to consider the potential for athero-preventive effects with amphiphilic cyclic DL- α -peptides, a signature molecule of the Ghadiri group, which ought to self-assemble into amphiphilic nanotubes with dimensionality that might mimic apoA-I α -helices (Figures 1 and 2). The synthesis of amphipathic cyclic DL- α -peptides involved efficient assembly of linear precursor peptides and cyclization on a solid support. Certain cyclic peptides promoted cellular cholesterol efflux *in vitro* and HDL remodeling *in vivo*; c[wLwReQeR], **1**, and c[wLwSeQsO], **2**, were prototypes (Figure 2). *N*-Methylation of L and Q in **2**, which will prevent nanotube assembly, markedly attenuated cholesterol efflux activity. Compound **1** was administered orally (in drinking water *ad libitum*) to LDLr^{-/-} mice on a high-fat diet for 10 weeks with two separate dose regimes: 35 and 3.5 mg/kg. At 2 and 10 weeks, **1** (at 35 mg/kg) reduced total plasma cholesterol by 54% and 30%, respectively (vs. PBS control). After 10 weeks, **1** (at 35 mg/kg) was found to reduce aortic lesion area by 26% and aortic valve plaque by 50% (vs. PBS). The dose of 3.5 mg/kg was not effective. Numerous cyclic DL- α -peptides with different side chains were evaluated *in vitro* to find those with promise for oral testing *in vivo* with an endpoint of cholesterol lowering after oral administration for 2 weeks (at 35 mg/kg). Compound **1** exhibited the best activity (-50%), with no activity evident for **1** at one-tenth of the 35-mg/kg dose. Other effective compounds were: c[wLwSeQhK] (-33%) and c[wLwKhShK] (-31%).

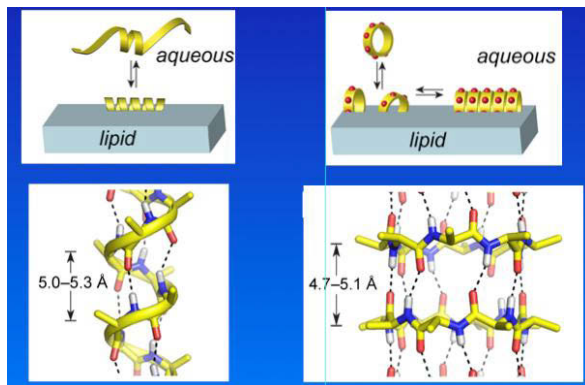


Fig. 1. Comparison of α -helix and DL- α -peptides.

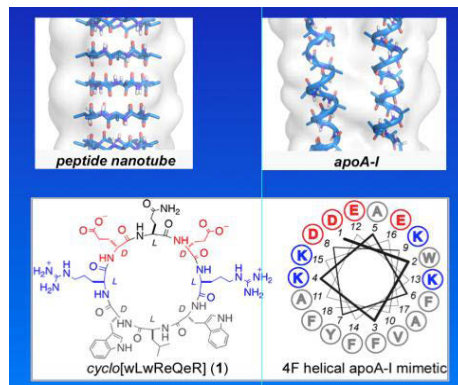


Fig. 2. Formation of nanotubes.

We used DNA sequencing and qPCR of group-specific 16S rRNA gene copies vs. total bacterial 16S rRNA gene copies to probe the mechanistic relevance of the microbiome (Figure 3). Compound **1** modulated the microbiome such that the profile in mice fed a high-fat diet was shifted to one akin to that in mice fed a chow diet (Figure 3). Specifically, c[wLwReQeR] and c[wLwKhShK] decreased the ratio of firmicutes/bacteroidetes by 56% and 35%, respectively (Figure 4). These results suggest that a key factor in the observed oral activity for these cyclic peptides may well be modulation of the mouse microbiome. In conclusion, certain cyclic DL- α -peptides may offer a novel means for treating atherosclerosis.

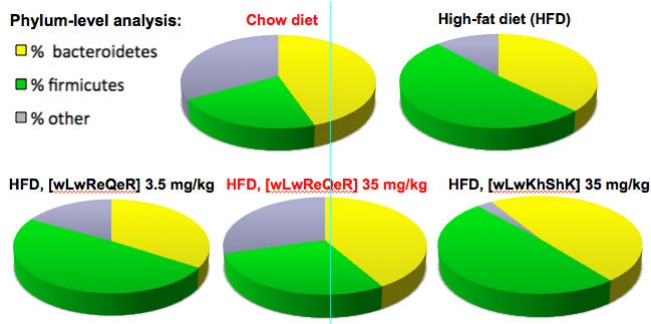


Fig. 3. Microbiome profiles in tested mice.

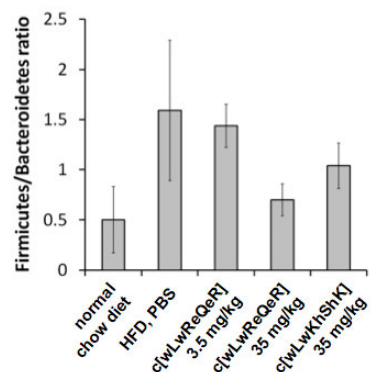


Fig. 4. Ratio of firmicutes/bacteroidetes.

Acknowledgments

We thank the NIH for financial support (NHLBI HL104462), the American Heart Association Western States Affiliate for a postdoctoral fellowship (12POST12040298) to Dr. Y. Zhao, and the National Institute of Advanced Science and Technology (AIST) for a visiting research fellowship to Dr. T. Imura.

References

1. Leman, L.J., Marvanoff, B.E., Ghadiri, M.R. *J. Med. Chem.* **57**, 2169-2196 (2014), <http://dx.doi.org/10.1021/jm4005847>
2. Zhao, Y., Imura, T., Leman, L.J., Marvanoff, B.E., Ghadiri, M.R. *J. Am. Chem. Soc.* **135**, 13414-13424 (2013), <http://dx.doi.org/10.1021/ja404714a>
3. Zhao, Y., Black, A.S., Bonnet, D.J., Marvanoff, B.E., Curtiss, L.K., Leman, L.J., Ghadiri, M.R. *J. Lipid Res.* **55**, 2053-2063 (2014), <http://dx.doi.org/10.1194/jlr.M049262>
4. Dawson, P.E., Muir, T.W., Clark-Lewis, I., Kent, S.B. *Science* **266**, 776-779 (1994).

Rippled β -Sheet Fibrils from Coassembled Enantiomeric Amphipathic Peptides as Potential Microbicide Biomaterials

Bradley L. Nilsson, Danielle M. Raymond, and Jade J. Welch

University of Rochester, Department of Chemistry, Rochester, NY, 14618, USA

Introduction

Amphipathic β -sheet peptides that assemble into cross- β bilayer fibrils have been widely applied as functional biomaterials [1]. We recently discovered that enantiomeric D- and L-Ac-(FKFE)₂-NH₂ peptides readily coassemble into two-component “rippled β -sheet” fibrils (see Figure 1) [2] (as opposed to classical pleated β -sheet materials), consistent with Pauling’s prediction for mixtures of enantiomeric β -sheet peptides [3]. Coassembly was confirmed by isotope-edited IR spectroscopy and FRET-based fluorescence spectroscopy. The preference for coassembly into rippled β -sheets relative to self-sorting into pleated β -sheets is thermodynamically favored. Rippled β -sheet fibrils have unique emergent properties compared to pleated β -sheet fibrils, including enhanced hydrogel elasticity and resistance to protease degradation [4].

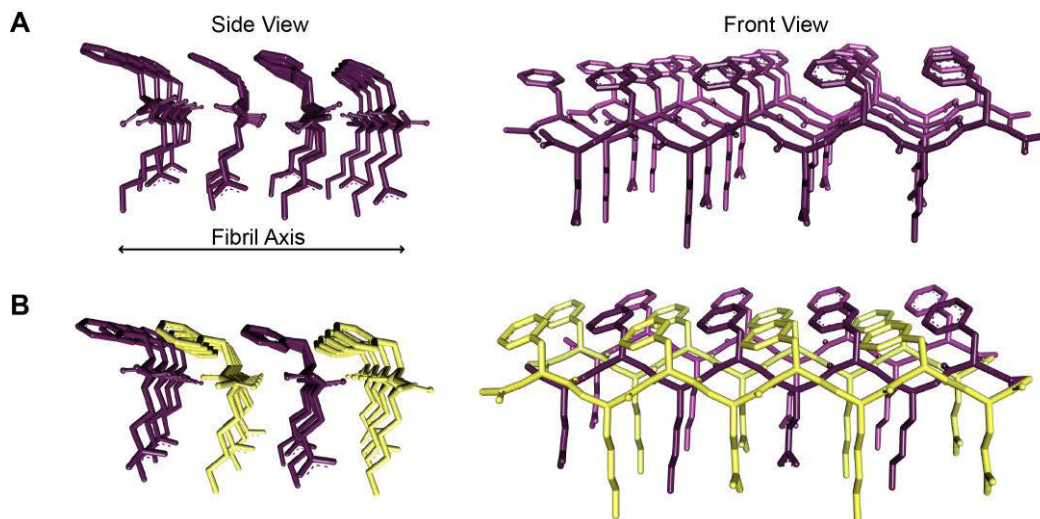


Fig. 1. A. Representative self-assembled pleated β -sheets of L-Ac-(FKFE)₂-NH₂. The fibril axis is parallel to the plane of the page as shown in the left image; the fibril axis is perpendicular to the page in the image to the right. Fibrils of this peptide are composed of the bilayer of the indicated β -sheets. B. Representative pleated β -sheets of coassembled L- and D-Ac-(FKFE)₂-NH₂ peptides. The L-peptide is shown in purple and the D-peptide is shown in yellow.

Engineered rippled β -sheet scaffolds have potential for application as multicomponent noncovalent materials. There is a need for novel hydrogel materials that can be exploited as microbicides to prevent the sexual transmission of HIV. Recent studies indicate that hydrogels commonly used as personal lubricants are irritating to vaginal and rectal mucosa leading to fears that these materials may enhance the spread of HIV and other sexually transmitted diseases [5]. Ideal hydrogel materials for intravaginal or intrarectal application should be non-irritating and non-immunogenic. Nanofibrils of Ac-(FKFE)₂-NH₂ and related amphipathic peptides have been shown to be non-immunogenic, supporting their potential for application as vaginal or rectal microbicides [6]. In addition, ideal microbicides should be deliverable, shear-responsive hydrogels that maintain integrity in vaginal and rectal environments. These materials must also facilitate the multivalent display of functional groups that are accessible to interact with HIV virions or target cells. Finally, microbicides must exhibit stability to proteolytic

degradation. Herein, we discuss the properties of rippled β -sheet derived from amphipathic enantiomeric peptides that suggest the potential of these as hydrogel materials targeted to the prevention of sexually transmitted diseases, including HIV.

Results and Discussion

We recently reported that enantiomeric amphipathic peptides undergo coassembly to form rippled β -sheet structures [2]. Specifically, we discovered that equimolar mixtures of D- and L-Ac-(FKFE)₂-NH₂ peptides selectively coassemble into two-component rippled β -sheets as opposed to assembling into self-sorted, single enantiomer pleated β -sheet fibrils. Coassembly was confirmed by isotope-edited IR spectroscopy and FRET analysis in which the enantiomers were labeled with acceptor and donor fluorophores. The mechanistic basis for preferential coassembly of enantiomers was also explored. We conducted isothermal titration calorimetry experiments using the L-Ac-(FEFE)₂-NH₂ peptide and L- and D-Ac-(FKFK)₂-NH₂ peptides. These cationic and anionic peptides fail to self-assemble due to charge repulsion at neutral pH. However, when peptides of opposite charge are mixed they readily coassemble. Either L- or D-Ac-(FKFK)₂-NH₂ peptides were titrated into L-Ac-(FEFE)₂-NH₂. The L/L mixture provided pleated β -sheets while the L/D mixture provided rippled β -sheets. It was found that rippled β -sheet formation had an ~ 9 kcal mol⁻¹ enthalpic advantage over pleated β -sheet formation.

The structural basis for this energetic advantage for rippled β -sheet formation is not completely understood. One possible explanation lies in differences for β -sheet strand registry between pleated and rippled sheets for the Ac-(FKFE)₂-NH₂ peptide. For pleated β -sheet formation from self-assembly of single enantiomers it has been proposed that the strand alignment requires the *N*-terminal Phe residue to be out of register [7], leaving hydrogen bond donors and acceptors unsatisfied as well as less than optimal pairing of the dangling hydrophobic side chain. In rippled β -sheets formed from enantiomeric Ac-(FKFE)₂-NH₂ peptides, the putative β -sheet alignment is completely in register, resulting in structures with additional stabilizing hydrogen bonds. In addition, the side chain arrangement of rippled β -sheets differs from that observed in pleated β -sheets. In pleated sheets, cross-strand side chain groups exist in an eclipsed-like conformation (Figure 1A) whereas rippled sheets orient the side chain groups in a staggered-like conformation. These differences in cross-strand side chain orientation may also contribute to the significant enthalpic advantage for rippled β -sheets. Additional studies are ongoing to elucidate the precise physicochemical basis for preferential rippled β -sheet formation.

We have also found that rippled β -sheets derived from enantiomeric Ac-(FKFE)₂-NH₂ peptides have protease degradation profiles that make them attractive candidates for microbicide hydrogels. Specifically, we have reported that rippled β -sheets resist degradation from common proteases, including trypsin, chymotrypsin, and proteinase K [4]. We formed hydrogels from L- and D-Ac-(FKFE)₂-NH₂ peptides: pleated β -sheet hydrogels from either L- or D-Ac-(FKFE)₂-NH₂ and rippled β -sheet hydrogels from coassembled L- and D-Ac-(FKFE)₂-NH₂. It was found that pleated β -sheet hydrogels derived from L-Ac-(FKFE)₂-NH₂ were completely degraded by these proteases in hours. In contrast, the rippled β -sheet hydrogels were as resistant to the proteases as the all-D pleated β -sheet fibrils (Figure 2).

Thus, rippled β -sheet hydrogels are exceptionally stable materials that meet several of the criteria necessary for the creation of novel anti-HIV microbicides that prevent sexual transmission of the virus. We have

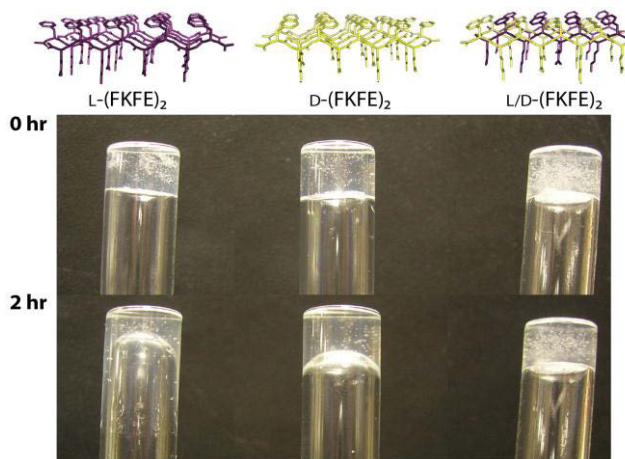


Fig. 2. Digital images of hydrogels incubated with chymotrypsin showing degradation of the L-pleated sheet material after several hours. Rippled β -sheet hydrogels were stable to degradation even after 5 days.

previously shown that pleated β -sheets that display the entry inhibitor aplaviroc also have specific anti-HIV properties [8]. Appropriate modification of rippled β -sheet materials should also result in similar properties that elicit specific protection against HIV. Work is ongoing to establish the immunogenicity of rippled β -sheet materials. While additional development is necessary, rippled β -sheets have great potential as novel, next-generation hydrogel biomaterials for the prevention of sexually transmitted diseases that avoid the problems with existing commercial hydrogels.

Acknowledgments

The National Science Foundation (DMR-1148836) supported this work.

References

1. Bowerman, C.J., Nilsson, B.L. *Biopolymers* **98**, 169-184 (2012), <http://dx.doi.org/10.1002/bip.22058>
2. Swanekamp, R.J., DiMaio, J.T.M., Bowerman, C.J., Nilsson, B.L. *J. Am. Chem. Soc.* **134**, 5556-5559 (2012), <http://dx.doi.org/10.1021/ja301642c>
3. Pauling, L., Corey, R.B. *Proc. Natl. Acad. Sci. USA* **39**, 253-256 (1953).
4. Swanekamp, R.J., Welch, J.J., Nilsson, B.L. *Chem. Commun.* **50**, 10133-10136 (2014), <http://dx.doi.org/10.1039/C4CC04644G>
5. Wolf, L.K. *Chem. & Eng. News* **90**, 46-47 (2012).
6. Rudra, J.S., Sun, T., Bird, K.C., Daniels, M.D., Gasiorowski, J.Z., Chong, A.S., Collier, J.S. *ACS Nano* **6**, 1557-1564 (2012), <http://dx.doi.org/10.1021/nn204530r>
7. Hwang, W., Marini, D.M., Kamm, R.D., Zhang, S. *J. Chem. Phys.* **118**, 389-397 (2003), <http://dx.doi.org/10.1063/1.1524618>
8. DiMaio, J.T.M., Easterhoff, D., Moore, A.M., Dewhurst, S., Nilsson, B.L., in Lebl, M. (Ed.) *Peptides: Peptides Across the Pacific (Proceedings of the 23rd American Peptide Symposium)*, American Peptide Society, San Diego, 2013, pp. 154-155, <http://dx.doi.org/10.17952/23APS.2013.154>

Antibody Cross-Reactivity to Hemagglutinin Protein Antigens Demonstrates Feasibility for Development of a “Universal” Influenza A Synthetic Peptide Vaccine

Ziqing Jiang, Lajos Gera, Colin T. Mant, and Robert S. Hodges

Department of Biochemistry and Molecular Genetics, University of Colorado Denver,
 Anschutz Medical Campus, School of Medicine, Aurora, CO, 80045, USA

Introduction

Influenza A viruses spread rapidly, causing widespread seasonal epidemics of respiratory disease worldwide, which results in more than a billion cases and 500,000 deaths annually [1]. Current influenza vaccines primarily elicit antibodies against the receptor-binding region of the head domain of the hemagglutinin (HA) glycoprotein trimer (Figure 1). This region is hyper-variable and highly mutable, leading to new forms of the virus that can evade neutralizing antibodies. The stem region of HA contains highly conserved α -helical sequences as a result of their functional role in membrane fusion and virus entry. Studies have shown that a few rare neutralizing human monoclonal antibodies can recognize these highly conserved epitopes and neutralize both homotypic and heterotypic influenza strains [2,3]. There are some 18 HA subtypes in influenza A virus that infect humans, animals and birds (Figure 1) [4].

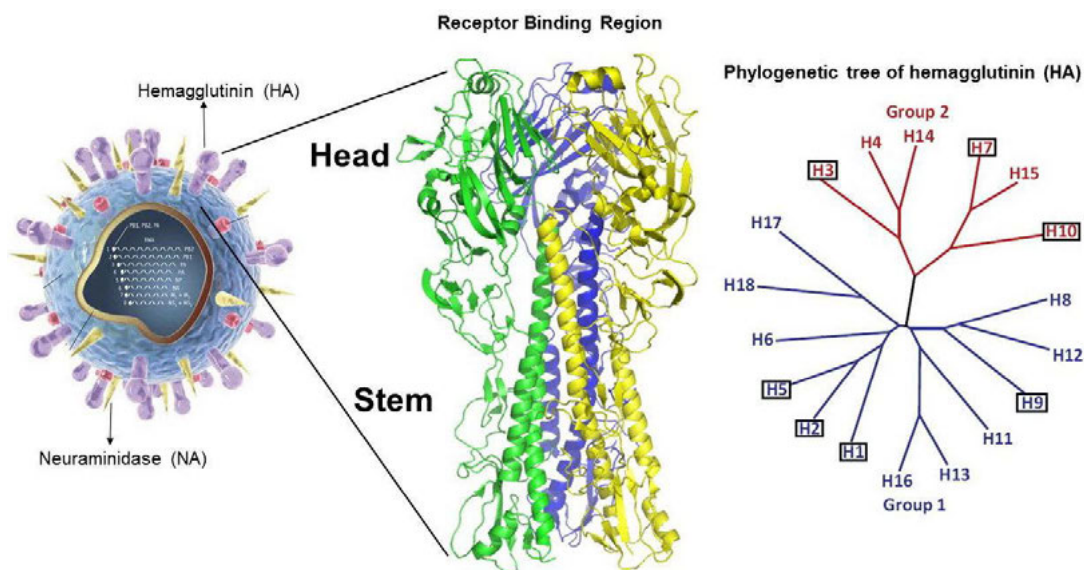


Fig. 1. The influenza virus with surface proteins hemagglutinin (HA) and neuraminidase (NA) is shown in the left panel. The middle panel shows the X-ray structure of the HA trimeric glycoprotein. The right panel shows the phylogenetic tree of HA, group 1 (colored blue) and group 2 (colored red). The subtypes that have been confirmed in humans are boxed.

Subtypes associated with pandemic human influenza are H1, H2 and H3. H1 and H3 subtypes are continually undergoing immune selection (antigenic drift), so that antibody-resistant strains continue to emerge and cause new human pandemics, necessitating formulation of new vaccines every year [5,6]. Subtypes H5, H7 and H9 are recognized by the World Health Organization as “potential pandemic viruses” and humans have no pre-existing immunity to these subtypes [7].

Our strategy is to develop a “Universal” Influenza Synthetic Peptide Vaccine based on highly conserved α -helical epitopes in the stem region of HA. Such a vaccine would not have to be changed annually and would protect against antigenic drift as well as antigenic shift variants. Synthetic peptide vaccines have major advantages over existing vaccine approaches to prevent viral infections when there is a detailed understanding of the mechanism of virus entry into the cell: 1) one can select the target protein and a particular sequence within the target protein; 2) side-effects from unnecessary proteins, other molecules and unnecessary epitopes within the target protein are eliminated; and 3) simplicity, small size, easy to manufacture and the low cost of goods.

Results and Discussion

Our platform technology consists of a disulfide-bridged two-stranded α -helical coiled-coil peptide template of 29 residues per strand where the α -helical epitopes from the HA protein are inserted into the template to display the exposed helical surface of the native protein. The templated B-cell epitopes have five out of every seven residues exposed on the surface of the coiled-coil with the two-stranded

helical conformation stabilized by converting the native buried hydrophobic residues to Ile/Leu residues (Figure 2).

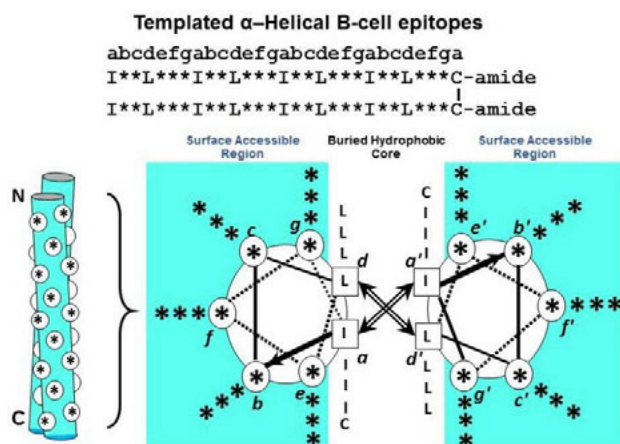


Fig. 2. A two-stranded α -helical coiled-coil template to display α -helical epitopes. In the cross-sectional view, the direction of the α -helices is into the page from the NH_2 to the COOH terminus, with the polypeptide chains parallel and in-register. In a homo-two-stranded coiled-coil two identical α -helical B-cell epitopes are displayed. The template-stabilizing disulfide-bridge is also buried in the hydrophobic core between the two α -helices. Antibodies generated to this immunogen bind the corresponding α -helix in the native HA protein.

Templated Peptide Immunogen with T-cell and B-cell Epitopes

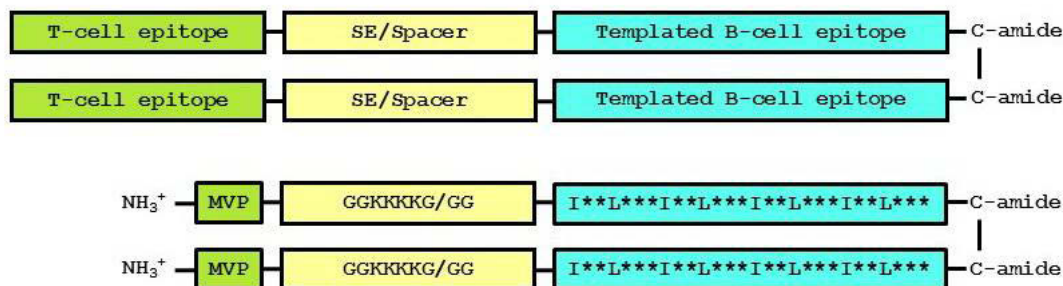


Fig. 3. Templated peptide immunogens where each polypeptide chain contains an eighteen residue T-cell epitope followed by a positively charged solubility enhancer (SE) (if required) or a two-Gly spacer, a 28-residue helical B-cell epitope from the protein of the interest and a C-terminal disulfide-bridge to further stabilize the helical conformation. The T-cell epitope is denoted MVP for a measles virus promiscuous T-cell epitope [8].

The peptide immunogens used in this study are shown in Figure 3. Each immunogen consists of two polypeptide chains containing an *N*-terminal T-cell epitope, a solubility enhancer region or spacer, a 28-residues B-cell epitope and a *C*-terminal disulfide-bridge.

Shown in Figure 4 is the sequence of immunogen 4P1 (residues 401-428). The antibodies to this immunogen were generated in rabbits after three immunizations on days 1, 15 and 44. IgG was purified from the final rabbit sera and used to evaluate antibody cross-reactivity to a series of H1N1 subtypes and seven different HA proteins from subtypes H1N1, H2N2 and H5N1 from group 1 and H3N2, H7N7 and H7N9 from group 2. The results indicate that the antibodies to immunogen 4P1 (401-428) cross-react with all H1N1 subtypes tested (Figure 4, panel A). As shown in the middle panel of Figure 4, the H1N1 sequences from 1934 to present are highly conserved in this 4P1 region which explains the excellent cross-reactivity of 4P1 antibodies to H1N1 subtypes (Figure 4, panel A). Though the 4P1 sequence has the potential to be a vaccine against all H1N1 subtypes, which would be a major advantage over existing vaccines, the antibodies are not significantly cross-reactive with H5N1 and H2N2 from group 1 and group 2 HA antigens H3N2, H7N7 and H7N9 (Figure 4, panel B). In Figure 4 panels A and B the negative control HA protein for ELISA was the Brisbane/59/07 from H1N1. This HA protein contained residues 18-343 and is missing the antibody binding site 401-428 used in our vaccine construct for raising polyclonal antibodies in rabbits. It is very clear why these antibodies do not bind to H2N2, H5N1, H3N2, H7N7 and H7N9. Non-conservative substitutions in these HA proteins are indicated in pink in the middle panel of Figure 4.

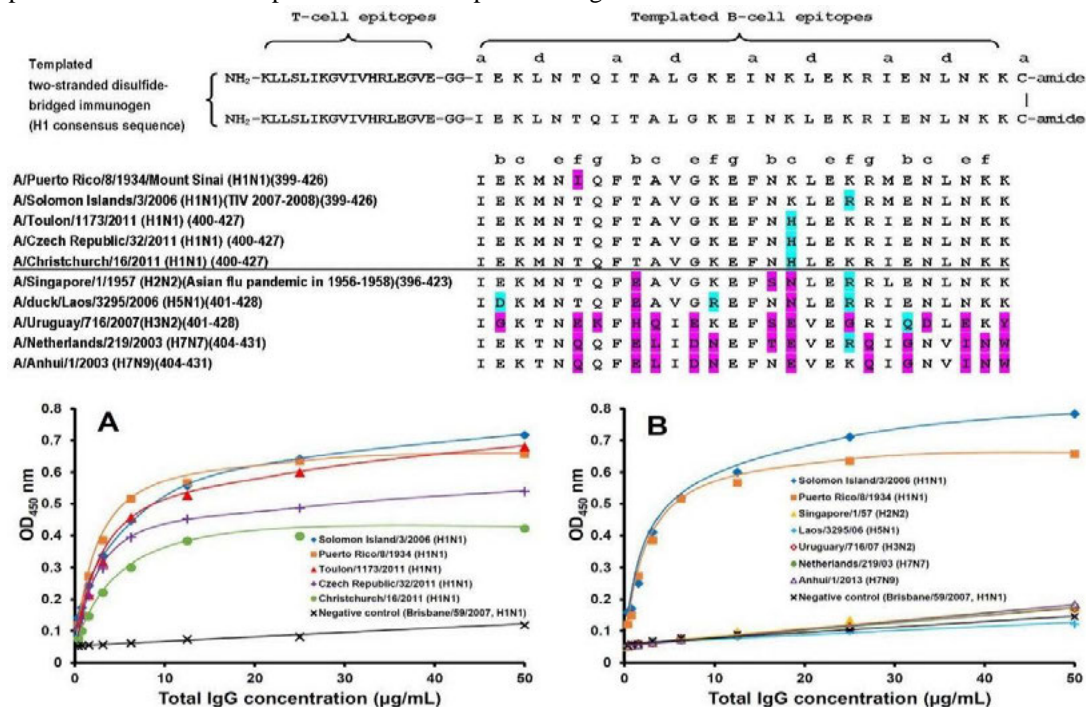


Fig. 4. Top panel shows the sequence of the synthetic peptide vaccine consisting of a H1 consensus sequence, 4P1, inserted into the disulfide-bridged two-stranded α -helical coiled-coil template stabilized by Ile and Leu residues at positions *a* and *d*. The middle panel shows the sequences of five different H1N1 sequences and five representative sequences from H2N2, H5N1, H3N2, H7N7 and H7N9. Conservative substitutions are indicated in blue and non-conservative substitutions are indicated in pink. The lower panel shows the ELISA results of antibody binding to five different HA proteins from H1N1 and the negative control HA protein, Brisbane/59/07 (H1N1), which consists of amino acid residues 18-343 (panel A). Panel B shows the ELISA results of antibody binding to two H1 and five HA proteins from H2N2, H5N1, H3N2, H7N7, H7N9 and the Brisbane negative control HA protein.

To obtain cross-reactive antibodies to group 1 and group 2 HA proteins, work is in progress to use region 5P (421-449). This region was shown by our group to provide cross-reactive antibodies to group 1 and 2 when the synthetic disulfide-bridged two-stranded coiled-coil template was covalently linked to Keyhole Limpet Hemocyanin (KLH) [9].

What is most informative from these results is that an 18-residue promiscuous T-cell epitope from measles virus fusion (F) protein (MVF) can replace the need to conjugate the synthetic peptide immunogen to a carrier protein like keyhole limpet hemocyanin (KLH) as we did previously [9] and still generate an excellent antibody response. The T-cell epitope utilized in this study was first identified in 1990 [8] and first reported in synthetic peptide vaccine constructs in 1995 [10].

In conclusion, we first demonstrated the usefulness of our two-stranded α -helical coiled-coil template technology in our studies to develop a synthetic peptide vaccine against Severe Acute Respiratory Syndrome (SARS) [11,12]. Here we have incorporated a 28-residue α -helical sequence from the stem domain of hemagglutinin from H1N1 and showed that we can generate polyclonal antibodies that cross-react with all H1N1 subtypes in the region 401-428. These results suggest that a synthetic peptide vaccine for H1N1 including this region would not have to be changed annually and would protect against antigenic drift and antigenic shift variants. This technology has general applicability to be used to generate antibodies to any surface exposed α -helical region in any protein.

Acknowledgments

We thank the John Stewart Endowed Chair in Peptide Chemistry to Robert S. Hodges for financial support. We are very grateful for the following reagents obtained through BEI Resources, NIAID, NIH: Hemagglutinin (HA) Proteins from Influenza Virus, Recombinants from Baculovirus, A/Solomon Islands/3/2006 (H1N1), NR-15170; A/Puerto Rico/8/1934 (H1N1), NR-19240; A/Toulon/1173/2011 (H1N1)pdm09, NR-34587; A/Czech Republic/32/2011 (H1N1)pdm09, NR-42486; A/Christchurch/16/2011 (H1N1)pdm09, NR-42487; A/Brisbane/59/2007 (H1N1), NR-13411; A/Singapore/1/1957 (H2N2), NR-2668; A/duck/Laos/3295/2006 (H5N1), NR-13509; A/Uruguay/716/2007 (H3N2), NR-15168; A/Netherlands/219/2003 (H7N7), NR-2633; A/Anhui/1/2013 (H7N9), NR-45118.

References

1. <http://www.who.int/topics/influenza/en/>
2. Sui, J., et al. *Nat. Struct. Mol. Biol.* **16**, 265-273 (2009), <http://dx.doi.org/10.1038/nsmb.1566>
3. Wang T.T., Palese, P. *Nat. Struct. Mol. Biol.* **16**, 233-234 (2009), <http://dx.doi.org/10.1038/nsmb.1574>
4. Wu, Y., Wu, Y., Tefsen, B., Shi, Y., Gao, G.F. *Trends Microbiol.* **4**, 183-191 (2014), <http://dx.doi.org/10.1016/j.tim.2014.01.010>
5. Subbarao, K. et al. *Immunity* **24**, 5-9 (2006), <http://dx.doi.org/10.1016/j.immuni.2005.12.005>
6. Doherty P.C., Kelso A. *J. Clin. Invest.* **118**, 3273-3275 (2008), <http://dx.doi.org/10.1172/JCI37232>
7. Fiore, A.E., Bridges, C.B. and Cox, N.J. (2009) Seasonal Influenza Vaccines. In *Vaccines for Pandemic Influenza*. (Compans, R.W. and Orenstein, W.A., Eds.) (pp. 43-82). Springer Verlag, Berlin Heidelberg.
8. Partidos, C.D., Steward, M.W. *J. Gen. Virol.* **71**, 2099-2105 (1990).
9. Jiang, Z., Gera, L., Hartsock, W.J., Hirsch, B., Mant, C.T., Qian, Z., Holmes, K.V., and Hodges, R.S. In *Peptides: Peptides Across the Pacific (Proceedings of the 23rd American Peptide Symposium and the 6th International Peptide Symposium)*, (Lebl, M. Ed.), American Peptide Society and Prompt Scientific Publishing, San Diego, 2013, p. 132-133, <http://dx.doi.org/10.17952/23APS.2013/132>
10. Lairmore, M.D., DiGeorge, A.M., Conrad, S.F., Trevino, A.V., Lal, R.B., Kaumaya, P.T.P. *J. Virol.* **69**, 6077-6089 (1995).
11. Tripet, B., Kao, D., Jeffers, S., Holmes, K.V., Hodges, R.S. *J. Struct. Biol.* **155**, 176-194 (2006), <http://dx.doi.org/10.1016/j.jsb.2006.03.019>
12. Yan Z., Hartsock W.J., Qian Z., Holmes K.V., and Hodges R.S., In *Small Wonders: Peptides for Disease Control*. (Rajasekaran, K., et al. Eds.) American Chemical Society, Washington, DC, 2012, pp. 93-136, <http://dx.doi.org/10.1021/bk-2012-1095.ch006>

Solid-Phase Synthesis of Azasulfurylphenylalanine⁴-GHRP-6

Stéphane Turcotte and William D. Lubell*

Département de Chimie, Université de Montréal, C.P. 6128, Succursale Centre-Ville,
 Montréal, QC, H3C 3J7, Canada

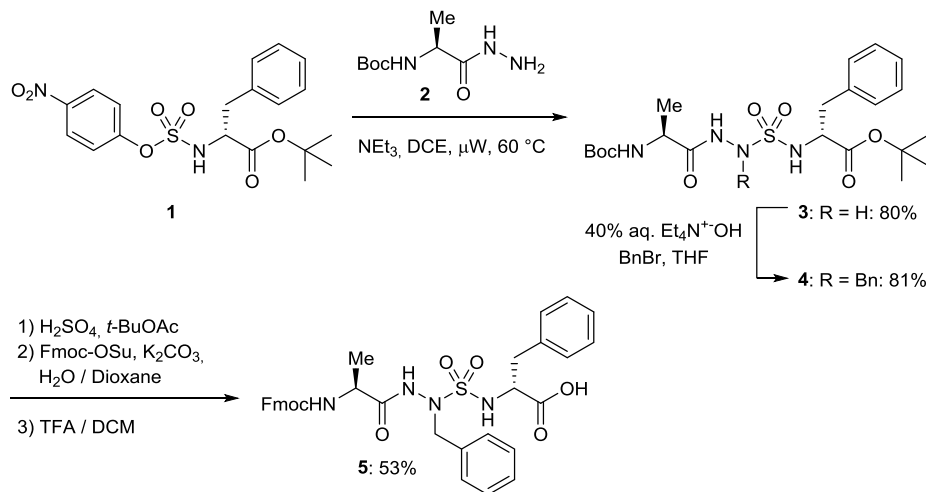
Introduction

Azasulfurylpeptides possess an amino sulfamide as an amino amide surrogate in which the C_αH and carbonyl components are respectively replaced by nitrogen and a sulfonyl group [1-4]. Uniting the properties of azapeptides [5] and sulfonamides [6-7], azasulfurylpeptides have served as transition state mimics of amide bond hydrolysis in a micromolar human immunodeficiency virus-1 (HIV-1) proteinase inhibitor [2]. Azasulfurylpeptides may similarly stabilize γ-turn conformations [8]. Solid-phase chemistry has however yet to be employed for the synthesis of azasulfurylpeptides. Targeting an azasulfurylpeptide analog of growth hormone releasing peptide-6 (GHRP-6, His-D-Trp-Ala-Trp-D-Phe-Lys-NH₂) in the context of our program to develop modulators of the cluster of differentiation-36 [9-11], we report herein a solid-phase approach to prepare azasulfurylphenylalanine⁴ [AsF⁴]-GHRP-6.

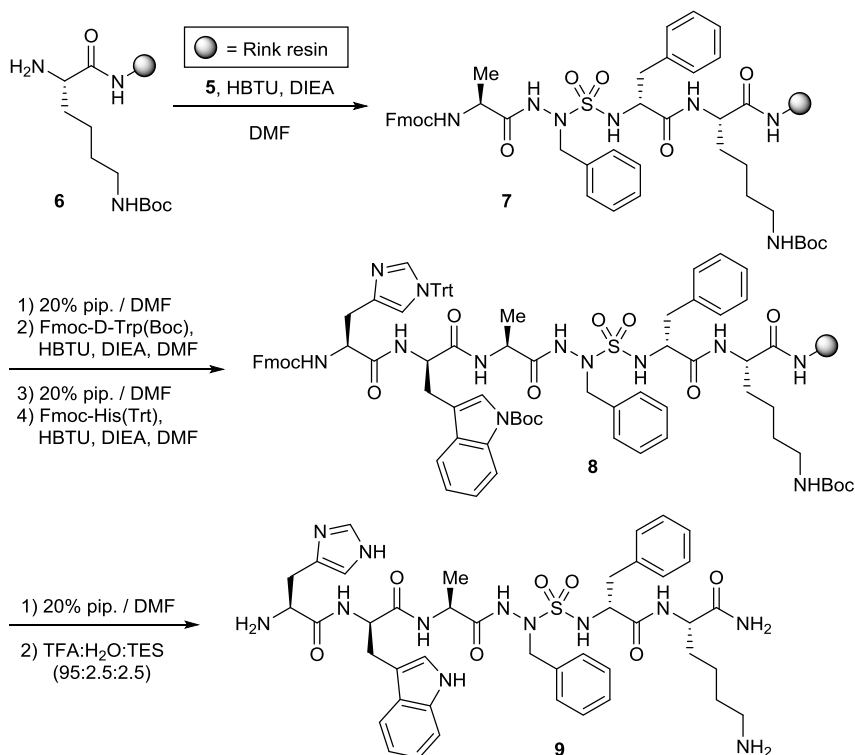
Results and Discussion

A solid-phase synthetic method was developed to make [AsF⁴]-GHRP-6 employing an AsF-tripeptide building block on Rink amide resin. The required AsF-tripeptide building block was synthesized in solution by a route featuring the construction and alkylation of azasulfurylglycine (AsG) tripeptide **3**, which was made without formation of symmetric sulfamide side product by acylation of hydrazide **2** with *p*-nitrophenyl-sulfamate **1** (Scheme 1) [3]. Chemoselective alkylation on the AsG-tripeptide **3** using benzyl bromide and tetraethylammonium hydroxide installed the benzyl side-chain onto the *N*-aminosulfamide residue. Selective cleavage of the Boc protecting group of **4** in the presence of the *tert*-butyl ester was accomplished using 400 mol% of sulfuric acid in *tert*-butyl acetate [12]. Amine protection with the Fmoc group and carboxylate liberation by *tert*-butyl ester cleavage using TFA afforded *N*-Fmoc-alaninyl-azasulfurylphenylalaninyl-D-phenylalanine (**5**) in 53% overall yield starting from **4**.

Scheme 1. Solution-phase syntheses of azasulfuryl tripeptide *N*-(Fmoc)-Ala-AsF-D-Phe (**5**).



Scheme 2. Solid-phase peptide synthesis of [AsF⁴]-GHRP-6 (**9**).



The AsF-tripeptide building block **5** was coupled onto the Lys(Boc) residue bound to Rink amide resin **6** using HBTU and DIEA in DMF (Scheme 2). Employing piperidine in DMF for Fmoc group removals, the peptide was elongated by couplings with Fmoc-D-Trp(Boc), followed by Fmoc-His(Trt) using HBTU and DIEA in DMF. Cleavage of the peptide from the resin using a solution of TFA:H₂O:TES (95:2.5:2.5) in a cold room (4 °C), and purification by HPLC afforded [AsF⁴]-GHRP-6 (**9**) in 12% overall yield from tripeptide **5** (Table 1).

Notably, an alternative strategy failed to provide the *N*-aminosulfamide on resin by the attempted generation of a supported sulfamate on treatment of the peptide resin with *p*-nitrophenyl chlorosulfate, followed by coupling to hydrazide. In solution, activation of valine *iso*-propylamide with *p*-nitrophenyl chlorosulfate gave the desired sulfamate in only 15% yield, presumably because intramolecular cyclization occurred on the *C*-terminal amide nitrogen to form a sulfahydantoin analog (not isolated) [13].

Table 1. Yield and purity of [AsF⁴]-GHRP-6 (**9**).

Peptide	Crude purity ^a	Isolated Purity ^b	Isolated Yield ^c	HRMS	
				<i>m/z</i> (cal)	<i>m/z</i> (obs)
His-D-Trp-Ala-AsF-D-Phe-Lys-NH ₂ (9)	73%	>99%	12%	893.3851	893.3832

^aCrude peptide purity ascertained by LC-MS analysis using 5-80% MeOH (0.1% FA) in H₂O (0.1% FA) as eluent.

^bIsolated peptide purity ascertained by LC-MS analysis in two systems: MeOH (0.1% FA) in H₂O (0.1% FA), and MeCN (0.1% FA) in H₂O (0.1% FA). ^cIsolated yields calculated based on resin loading.

In conclusion, a solid-phase method was developed for the synthesis of [AsF⁴]-GHRP-6 (**9**) featuring the solution-phase synthesis of AsF tripeptide **5** and its application on Rink amide resin. Building on this method for solid-phase synthesis, libraries of azasulfurylpeptides may be generated for studying structure-activity relationships.

Acknowledgments

This research was supported by the Natural Sciences and Engineering Research Council of Canada (NSERC), the Ministère du développement économique de l'innovation et de l'exportation du Québec (#878-2012, Traitement de la dégénérescence maculaire) and Amorchem for support. S.T. would like to thank the FQRNT for graduate student fellowships.

References

1. Cheeseright, T.J., Edwards, A.J., Elmore, D.T., Jones, J.H., Raissi, M., Lewis, E.C. *J. Chem. Soc., Perkin Trans. 1*, 1595-1600 (1994), <http://dx.doi.org/10.1039/P19940001595>
2. Cheeseright, T.J., Daenke, S., Elmore, D.T., Jones, J.H. *J. Chem. Soc., Perkin Trans. 1*, 1953-1955 (1994) <http://dx.doi.org/10.1039/P19940001953>
3. Turcotte, S., Bouavad-Gervais, S.H., Lubell, W.D. *Org. Lett.* **14**, 1318-1321, (2012) <http://dx.doi.org/10.1021/ol3001987>
4. Turcotte, S., Havard, T., Lubell, W.D., In *Proceedings to the 32nd European Peptide Symposium*, Kokotos, G., Constantinou-Kokotou, V., Matsoukas, J., Eds. Athens, Grece, **2012**; pp 140-141.
5. Proulx, C., Sabatino, D., Hopewell, R., Spiegel, J., García Ramos, Y., Lubell, W.D. *Future Med. Chem.* **3**, 1139-1164 (2011), <http://dx.doi.org/10.1021/ol302021n>
6. Baldauf, C., Günther, R., Hofmann, H.J. *J. Mol. Struct.-Theochem.* **675**, 19-28 (2004), <http://dx.doi.org/10.1016/j.theochem.2003.12.029>
7. Bharatam, P.V., Gupta, A., Kaur, D. *Tetrahedron* **58**, 1759-1764 (2002), [http://dx.doi.org/10.1016/S0040-4020\(02\)00061-3](http://dx.doi.org/10.1016/S0040-4020(02)00061-3)
8. Turcotte, S., Lubell, W.D. *Biopolymers (Peptide Sci.)* (2015), Accepted, <http://dx.doi.org/10.1002/bip.22632>
9. Picard, E., Houssier, M., Bujold, K., Sapieha, P., Lubell, W., Dorfman, A., Racine, J., Hardy, P., Febbraio, M., Lachapelle, P. *Aging* **2**, 981 (2010).
10. Sabatino, D., Proulx, C., Pohankova, P., Ong, H., Lubell, W.D. *J. Am. Chem. Soc.* **133**, 12493-12506 (2010), <http://dx.doi.org/10.1021/ja203007u>
11. Proulx, C., Picard, E., Boeglin, D., Pohankova, P., Chemtob, S., Ong, H., Lubell, W.D. *J. Med. Chem.* **55**, 6502-6511 (2012), <http://dx.doi.org/10.1021/jm300557t>
12. Lin, L.S., Thomas, L.J., de Laszlo, S.E., Truong, O., Kamenecka, T., Hagmann, W.K. *Tetrahedron Lett.* **41**, 7013-7016 (2000), [http://dx.doi.org/10.1016/S0040-4039\(00\)01203-X](http://dx.doi.org/10.1016/S0040-4039(00)01203-X)
13. Albericio, F., Bryman, L.M., Garcia, J., Michelotti, E.L., Nicolás, E., Tice, C.M. *J. Comb. Chem.* **3**, 290-300 (2001), <http://dx.doi.org/10.1021/cc000111u>

Design of Multivalent Ligands that Cross the Blood Brain Barrier for the Treatment of Neuropathic Pain Without Toxicities

Victor J. Hruby¹, Takashi Yamamoto¹, Aswini Kumar Giri¹,
Davis S. Herman², Tally Largent-Milnes², Todd Vanderah², and Frank Porreca

¹Dept. of Chemistry and Biochemistry; ²Dept. of Pharmacology, University of Arizona, Tucson, AZ, 85721, USA

Introduction

Pain, especially prolonged and neuropathic, is the most ubiquitous and expensive disease in the U.S. and worldwide and treatments are inadequate or ineffective and often lead to enhanced pain sensitivity, addiction and poor quality of life. New modalities for treatment are urgently needed but are not forthcoming from pharma. We have proposed that a new approach to drug design is needed which takes into account the changes in the expressed genome that accompany these disease states [1]. In particular, in prolonged and neuropathic pain there is up-regulation of neurotransmitters and their receptors in ascending and descending pain pathways that are stimulatory and therefore enhance the pain perception. From these and other findings, we have hypothesized that the design of a multivalent ligand that has agonist activity at the mu and delta opioid receptors (balanced or favoring μ or δ receptors) with antagonist activities at the up-regulated stimulatory receptor (e.g. ligands for neurokinin-1 (NK-1) receptor) all in single ligand, would have potent analgesic activities but without the toxicities of current opioid drugs and without the development of tolerance or addiction.

Results and Discussion

The design of a multivalent ligand with multiple pharmacophores all in a single molecule requires special considerations in drug design. Each pharmacophore for each target requires a unique structure, and each receptor-binding pocket for each pharmacophore has a unique 3D structural requirement. Each unique pharmacophore must be in the designed ligand and they must not interfere with each other when they bind to their respective receptor/acceptor. Therefore, the issues of potential overlapping pharmacophores or separated pharmacophores by appropriate biocompatible linkers must be considered as part of the design process. Though we have had failures, we also have had several successes. Here we will discuss the design and biological properties of trivalent ligands that have mu and delta opioid receptor agonist activity and neurokinin-1 receptor antagonist activity, all in a relatively simple peptidomimetic scaffold that crosses the blood brain barrier.

Our specific design of multivalent ligands is quite simple because there is much that we and others in the literature have done in examining the SAR of mu and delta opioid agonists and NK-1 receptor antagonists. Among the key pharmacophore structural moieties for mu/delta agonists is a free amino terminal group, and the NK-1 receptor antagonists require a specific nonpeptide moiety at the C-terminal. Thus a linear peptide serves both pharmacophores well with an intervening linker or address moiety.

Mu/Delta Ag.--Spacer/Address—NK-1 R. Ant.

Fig. 1. Design of Mu-Delta Opioid Receptor Agonist, NK-1 Receptor Antagonist in a Multivalent Ligand.

In our design we used a linker amino acid that also serves as an address for all three receptors. In Table 1, we provide the structures of three of our lead peptides which serve as the basis for what led us to attain a ligand with all the desired biological properties and none of the toxicities or development of tolerance or addictive behaviors found in current opioid drugs. The results of binding at human delta

Table 1. Structure and selected biological activities of trivalent ligands for treatment of pain.

Structure	K_i (μ) nM	K_i (δ) nM	K_i hNK1 nM	K_i nNK1 nM
1) Tyr-D-Ala-Gly-Phe-Met-Pro-Leu-Trp-3',5'-Bn (OF ₃) ₂	36	2.8	0.080	0.29
2) Tyr-D-Ala-Gly-Phe-Met-Pro-Leu-Trp-NH-3',5'-Bn (OF ₃) ₂	16	0.66	0.006	7.3
3) DMT-D-Ala-Gly-N-MePhe-Pro-Leu-Trp-NH-3',5'-Bn (OF ₃) ₂	0.71	6	2.2	4.8

and mu receptors and at human and rat neurokinin receptors are provided. Note that compounds **1** and **2** are delta opioid receptor selective, while **3** is mu opioid receptor structure selective.

We also have examined second messenger cAMP activities and efficacies, as well as MVD and GP1 tissue assay activities (for **1** and **2** see references [2] and [3] for data). In all cases, the compounds are agonists at opioid receptors and antagonists at neurokinin 1 receptors (for **3**, manuscript in preparation). Extensive *in vivo* studies of analgesic activity in acute and neuropathic pain models have been made. To summarize, our 3 compounds show potent analgesic effects in both acute and neuropathic pain models given *i.p.* or given *i.v.*, and all three compounds cross the blood brain barrier. In addition, we have demonstrated that these ligands have none of the toxicities associated with morphine long term use including: 1) no motor impairment; 2) no development of tolerance after several days of administration of drug; 3) no development of place preference, an assay for addiction potential after several days of administration; and 4) no inhibition of gut transit (constipation) as well as others [3,4,5].

We are very excited about these findings which strongly suggest that this multivalent approach to drug has great potential for the development of novel drugs for the treatment of prolonged pain without toxicities or the development of tolerance, and our approach can find applications to other degenerative diseases.

Acknowledgments

We thank Christine Hiner Kasten for helping in preparing the manuscript. Support by grants from the U.S. Public Health Service, National Institute of Health, NIDA, POI DA 006284 and NIDA R01 DA 13449.

References

1. Hruby, V.J., et.al. *Am. Assoc. Pharm-Sci. J.* **8**, E450-460 (2000), <http://dx.doi.org/10.1208/aapsj080353>
2. Yamamoto, T. Nair, P., et.al. *J. Med. Chem.* **50**, 2779-2786 (2007), <http://dx.doi.org/10.1021/jm061369n>
3. Yamamoto, T., et.al. *J. Med. Chem.* **51**, 6334-6347 (2008), <http://dx.doi.org/10.1021/jm800389v>
4. Largent-Milnes, T.M., Yamamoto, T., Nair, P., Moulton, J.W., Hruby, V.J., Lai, J., Porreca, F., Vanderah T.W. *Brit. J. Pharmacol.* **161**, 986-1001 (2010), <http://dx.doi.org/10.1111/j.1476-5381.2010.00824.x>
5. Largent Milnes, T.M., et.al. *J. Pharma. Exp. Therap.* **347**, 7-19(2013), <http://dx.doi.org/10.1124/jpet.113.205245>

Isolation, Characterization and Structure-Activity Studies of Novel Brevinin-1 Peptides from the Skin of the Frog *Clinotarsus curtipes*

Parvin Abraham and K. Santhosh Kumar

Chemical Biology Laboratory, Rajiv Gandhi Centre for Biotechnology, Thiruvananthapuram, Kerala, India

Introduction

Antimicrobial peptides (AMPs) have attained enormous attention as a substituent of antibiotics recently. The very quick mode of action on microbial targets and the less probability of forming resistance by the bacterial strains against AMPs place these molecules superior to conventional antibiotics. Usually they are small peptides comprising 9-40 amino acid residues, rich in basic amino acids and thus owing a positive charge. They are electrostatically attracted towards the negatively charged membrane.

Of the variable sources of AMPs, amphibian skin is regarded as a major source. They are secreted by the granular glands and released to the skin surface upon different kind of stimuli including any microbial attack or predator attack. Herein, we describe the isolation, characterization and plausible mode of action of brevinin-1CTcu1-5 peptides.

Results and Discussion

Five novel brevinin peptides (Brevinin1 CTcu1-5) were identified from the skin secretion of the frog *Clinotarsus curtipes*, inhabiting in the Western Ghats region of Kerala, India (Figure 1) and their sequences are given in Table 1. They were antibacterial in nature with their MICs ranging from 6.25ug/mL to 100 ug/mL and were hemolytic against RBCs (Table 2). The broad antibacterial property exhibited by these peptides make them excellent candidates for future peptide antibiotics. However, by proper chemical engineering/modifications the adverse hemolytic issue should be addressed.

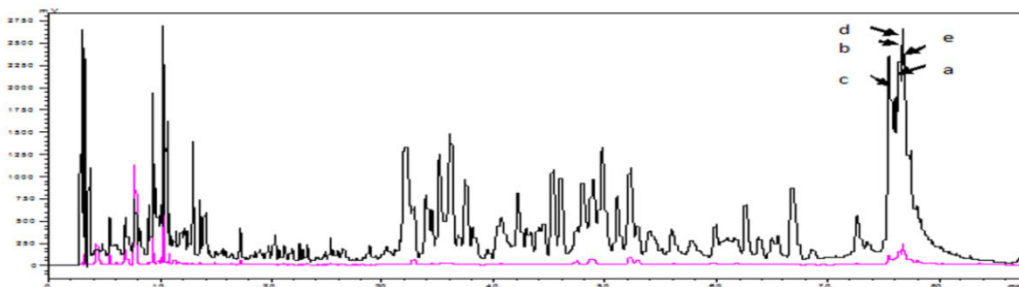


Fig. 1. RP-HPLC profile of the skin secretion of *Clinotarsus curtipes*.

Table 1. Primary Sequences of B1CTcu1-5 peptides.

Peptide	No AAs	Amino acid sequence	GRAVY	Net charge	Calculated mass (Da)	Observed mass (Da)
B1CTcu1	19	LIAGLAANFLPKLFCKITK	1.042	3	2061.6	2061.6
B1CTcu2	23	FLPLLAGLAANFLPKIFCKITRK	0.883	4	2575.2	2573.7
B1CTcu3	22	LPLLAGLAANFLPKIFCKITRK	0.795	4	2428	2426.7
B1CTcu4	23	FLPFIAGMAAKFLPKIFCAISKK	1.039	4	2542.2	2540.7
B1CTcu5	21	LIAGLAANFLPKILCKIARKC	1.067	3	2256.8	2255.5

The first step of the interaction of cationic peptides with bacterial membrane has been shown to involve negatively charged surface of the target cells. In gram negative bacteria, LPS in the outer membrane contribute significantly in this aspect. Dansyl polymyxin B displacement assay is used to quantify such kind of binding. Dansyl polymyxin B is a fluorescently tagged cationic lipopeptide, which fluoresces only when it binds to LPS and remain nonfluorescent in free solution. When the peptide binds to LPS, they displace dansyl polymyxin B, resulting in decreased fluorescence, which can be assessed as a function of peptide concentration as shown in Figure 2. The % displacement was calculated relative to polymyxin B. From Figure 3, B1CTcu1-4 exhibited a steady increase in % displacement with increase in peptide concentration. B1CTcu1-4 had more or less equal binding affinity with LPSs, but the relative binding or displacement capacity of B1CTcu5 was even lesser. Overall, in contrast to polymyxin B, the peptides had shown only a weak affinity with OM.

Table 2. Antimicrobial activity and % hemolysis of B1CTcu1-5.

	Minimum inhibitory concentration ($\mu\text{g/ml}$)							
	<i>E. coli</i> MG1655	<i>V. cholerae</i>	<i>S. aureus</i> MTCC 9542	MRSA ATCC 43300	<i>B. subtilis</i> 14416	<i>B. coagulans</i> ATCC 7050	VRE ATCC 29212	% hemo- lysis
B1 CTcu 1	8	12.5	12.5	NA	>25	6.25	NA	1
B1 CTcu 2	10	12.5	12.5	50	12.5	6.25	50	17.8
B1 CTcu 3	6.25	12.5	6.25	50	12.5	6.25	100	45
B1 CTcu 4	20	25	25	<6.25	25	NA	25	54.8
B1 CTcu 5	7	15	NA	NA	>200	6.25	NA	37.5

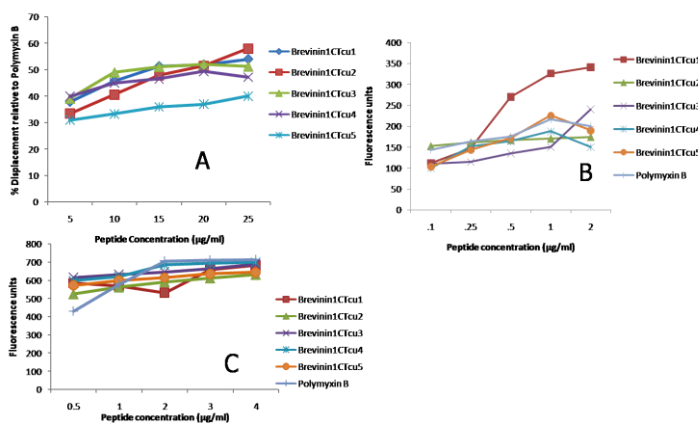


Fig 2. (A) Dansyl Polymyxin B displacement assay (B) NPN uptake assay (C) SYTOX green uptake assay.

OM permeabilisation efficiency compared to other peptides, including the positive control polymyxin. The fluorescence of SYTOX green increases drastically when it binds to intracellular nucleic acids. The extent of cytoplasmic membrane damage caused by the antimicrobial peptides can hence be studied by measuring the fluorescence produced by SYTOX green (Figure 2).

References

1. Zasloff, M. *Nature* **415**, 389-395 (2000), <http://dx.doi.org/10.1038/415389a>
2. Hancock, R.E. *The Lancet* **349**, 418-422 (1997), [http://dx.doi.org/10.1016/S0140-6736\(97\)80051-7](http://dx.doi.org/10.1016/S0140-6736(97)80051-7)
3. Wu, M., Hancock, R.E. *J. Biol. Chem.* **274**, 29-35 (1999), <http://dx.doi.org/10.1074/jbc.274.1.29>

Design and Synthesis of Lasso-Inspired Peptides with Antibacterial Activity

François Bédard¹, Riadh Hammami², Ahmed Gomaa², Muriel Subirade²,
Ismail Fliss², and Eric Biron¹

¹Faculty of Pharmacy, Université Laval and Laboratory of Medicinal Chemistry, CHU de Québec Research Centre, CHUL, Québec (QC), G1V 4G2, Canada; ²STELA Dairy Research Centre, Institute of Nutrition and Functional Foods, Université Laval, Québec (QC), G1V 0A6, Canada

Introduction

Microcin J25 (MccJ25) is a 21-residue ribosomally synthesized bactericidal peptide produced by *Escherichia coli* strains with an unusual lariat protoknot structure [1]. MccJ25 exhibits bactericidal activity toward several Gram-negative food-borne pathogens, including *Salmonella*, *Shigella* and *E. coli* [2]. The particular lasso topology of MccJ25 makes the peptide highly resistant to denaturation by high temperatures or proteolysis. These are attractive properties to both pharmaceutical and food industries. MccJ25 structure consists of an 8-residue cycle (lariat ring) formed by a lactam bond between the N-terminal amine and the Glu⁸ side chain, which is followed by a 13-residue tail that loops back to thread through the ring (Figure 1). The C-terminal tail (residues 9-21) of the peptide is tightly trapped in the lariat ring due to the presence of two aromatic side chains at positions 19 and 20. RNA polymerase appears to be the principal intracellular target of MccJ25 but other mode of actions have also been identified including inhibition of the respiratory chain [3-5]. SAR studies by site-directed mutagenesis revealed that the inhibitory activity of MccJ25 tolerates a number of residue substitutions [6]. Recent attempts to produce the lasso structure of MccJ25 by chemical synthesis have not yielded successful microbial inhibitors. Nevertheless, two synthetic peptides derived from MccJ25 without lasso folding were found to be bactericidal [7]. The current lack of information on MccJ25 structure and its essential features for antimicrobial activity could be overcome by chemical engineering and computational studies. We hypothesized that lasso formation is important but not a prerequisite for the activity of MccJ25 and that it may be possible to obtain derivatives that are active without the lasso structure [8]. In this study, we report synthetic peptides based on the MccJ25 sequence but devoid of lasso folding yet retaining activity against bacteria (*S. enterica* and *E. coli*) and specific intracellular targets (RNA polymerase and the respiration chain).

	Peptide	Sequence	Bonds	Net charge
	MccJ25	1 5 10 15 20 GGAGHVPEYFVGIGTPISFYG	1-8	-1
	1-8L	GGAGHVPE-----	-	-1
	1-10C	GGAGHVPEYF-----	1-8	-1
	9-21L	-----YFVGIGTPISFYG-NH ₂	-	0
	9-21C	-----CFVGIGTPICFYG-NH ₂	9-18	0
	8-21C	-----CYFVGIGTPICFYG	8-18	0
	7-21C	-----KCYFVGIGTPICFYG	8-18	+1
	WK7-21	GWKGKWKCYFVGIGTPICFYG	8-18	+3
	C1	CGAGHVPCYFVGIGTPISFYG	1-8	0
	C2	CGAGHVPEYFVGIGTPICFYG	1-18	-1
MccJ25	C3	GGAGHVPCYFVGIGTPICFYG	8-18	0

Fig. 1. Amino acid sequence of MccJ25 and derived-peptides used in this study. Amide and disulfide bonds are colored in blue and yellow respectively.

Table 1. Minimal inhibitory concentrations of MccJ25 and its derivatives for bacteria.

Bacterial strain	Minimal inhibitory concentration (μ M)				
	MccJ25*	C1	8-21C	7-21C	WK7-21
<i>Salmonella enterica</i> ATCC 14028	6.5	125-250	-	-	-
<i>Salmonella enterica</i> ATCC 8387	0.1	1.0	1.0	7.8-15.6	7.8
<i>Salmonella enterica</i> ATCC 29628	6.5	-	-	-	-
<i>Salmonella enterica</i> ATCC 8400	0.8	62.5-125	-	125-250	62.5
<i>Salmonella enterica</i> ATCC 9607	1.6	250	-	-	-
<i>Salmonella enterica</i> ATCC 9700	0.4	250	-	-	-
<i>Escherichia coli</i> ATCC 11229	0.2	62.5	125-250	-	250
<i>Escherichia coli</i> ATCC 25922	3.3	250.0	-	250	-
<i>Escherichia coli</i> ATCC 15144	-	-	-	-	-
<i>Escherichia coli</i> O157:H7 ATCC 35150	-	-	-	-	-
<i>Escherichia coli</i> MC4100 ATCC 35695	6.5	31.3-62.5	-	125	-
<i>Escherichia coli</i> DH5a	6.5	-	-	-	-
<i>Listeria ivanovii</i> HPB28	-	>250	-	>250	250
<i>Staphylococcus aureus</i> ATCC 6538	-	>250	-	ND	>250

*Produced by bacteria; “-” = no activity detected; ND = not determined

Results and Discussion

In this study, a series of peptides based on the primary structure of MccJ25 and lacking the lasso structure was first designed *in silico*, prepared by standard Fmoc solid-phase peptide synthesis (Figure 1) and then evaluated for antibacterial activity [8]. The peptide code is based on MccJ25 numbering. Shortened *N*-terminal and *C*-terminal sequences were included in the design since cleaved MccJ25 has been shown previously to be antibacterial [9]. The lariat ring was synthesized in linear **1-8L** and cyclized **1-10C** forms. The tail (*C*-terminal) portion was synthesized as linear peptide **9-21L**. A disulfide bond was introduced between C9 and C18 to form the head-to-tail circular peptide **9-21C**. Peptides **8-21C**, **7-21C** and **WK7-21** were designed from a tail that was scaffold-stabilized using a disulfide bond between Cys residues at positions 8 and 18. While a single Lys residue was inserted at the *N*-terminus of **7-21C**, peptide **WK7-21** was obtained by substituting the *N*-terminal portion of MccJ25 with multiple hydrophobic (Trp) and basic (Lys) and residues (H₂N-GWKGKWK) to increase solubility and possibly induce β -hairpin structure. In addition, peptides **C1**, **C2** and **C3** containing a single disulfide bond (1-8, 1-18 or 8-18) were designed to retain the core structure of the native MccJ25 peptide regardless of the lariat protoknot structure.

Table 1 summarizes the minimum inhibitory activities (MICs) of the synthesized peptides that had activity above 250 μ M in comparison to bacteria produced microcin. The MccJ25 peptide was active at μ M and nM concentrations (0.1-6.5) against Gram-negative bacteria, with *S. enterica* ATCC 8387 being the most sensitive strain (MIC = 0.1 μ M). While peptide **C2** was not inhibitory, **C1** inhibited several strains of *S. enterica* and *E. coli*. Against *S. enterica* ATCC 8387, the MICs of peptides **C1**, **C3**, **8-21C**, **7-21C** and **WK7-21** were respectively 1.0 μ M, 15.6–31.3 μ M, 1.0 μ M, 7.8–15.6 μ M and 7.8 μ M. Inhibition of *S. enterica* ATCC 8387 by MccJ25 and its derived peptides at 0.5 and 7.8 μ M is summarized in Figure 2A. At 0.5 μ M, the derived peptides were moderately inhibitory (25–50%). Similarly to MccJ25, inhibition by **C1**, **8-21C** and **WK7-21** was total at 7.8 μ M (above the MIC). Although MccJ25 was not active against Gram-positive bacteria, peptides **C1**, **7-21C** and **WK7-21** were weakly inhibitory to *Listeria ivanovii* HPB28, *Staphylococcus aureus* ATCC 6538 and *Enterococcus faecalis* ATCC 27275 (MIC \geq 250 μ M). Peptides MccJ25, **C1**, **7-21C** and **WK7-21** did

not show hemolytic activity against horse erythrocytes at concentrations up to (50 μ M), which is consistent with the low toxicity reported in the literature [10].

Of the synthetic MccJ25-derived peptides described previously, two in particular, namely GGACHVPEYFVGIGTPISEFC (**P1**, bonded 1-8, 4-20) and CGAGFHVPCYFVGRGTPISFYG (**P6**, bonded 1-9), were inhibitory to *Salmonella newport* at MICs of 25 and 30 μ M respectively [7]. While peptide **C1** of this study was designed with the replacement of the amide bond between G1 and E8 by a disulfide bond, **P6** contained besides a Phe insertion at position 5 and an Arg substitution for Ile at position 13. Although these mutations increased the solubility of **P6**, they decreased its inhibitory action. While peptide **C1** was inhibitory to Gram-negative pathogens, **P6** was 60 times less potent than MccJ25 against *S. newport* and **C1** against *S. enterica* ATCC 8387 was 10 times less potent than MccJ25. Further, **C1** showed a weak activity against Gram-positive bacteria (MIC > 250 μ M). Souday, et al. [7] also reported absence of activity for a **P6** variant with an 8-residue lariat ring. Based on our results, the Gly substitution by Phe at position 4 could explain the decrease of activity observed for **P6** and its variant compared to **C1**. The Arg substitution at position 13 has been reported previously to increase the antimicrobial activity of MccJ25 [6]. In this study, different synthetic derivatives of MccJ25 containing substitutions and/or truncations exhibited antibacterial activity against Gram-negative bacteria. Although the reduced activity of these designed synthetic derivatives compared to the native MccJ25, the lasso fold does not seem to be a prerequisite for the antimicrobial activity.

The inhibition of RNAP by MccJ25, **9-21L**, **C1**, **7-21C** and **WK7-21** was examined *in vitro* (Figure 2B). Rifampicin, an antibiotic that targets bacterial RNAP was used as a control. MccJ25 was the best inhibitor, reducing *E. coli* RNAP activity by 86.3% and 97.9% respectively at 5 and 50 μ M. Peptides **C1**, **7-21C** or **WK7-21** at a concentration of 5 μ M reduced activity by 23.4%, 37.4% and 65.0% respectively. Linear peptide **9-21L** was not inhibitory. At 50 μ M, reductions by MccJ25, **C1** and **WK7-21** were respectively 97.9%, 95.7% and 94.7%. These results suggest that the MccJ25-derived peptides could inhibit *E. coli* by interacting directly with RNAP and thereby interfering with transcription. The ability of MccJ25, **C1**, **7-21C** and **WK7-21** to inhibit respiration of *S. enterica* ATCC 8387 is shown in terms of MIC in Figure 2C. The decrease in oxygen consumption by *S. enterica* after incubation with MccJ25 was 57.2%. **WK7-21** was the strongest inhibitor among the synthetic peptides, decreasing oxygen consumption by 36.9%, followed by **C1** and **7-21C** at 32.1% and 24.2%, respectively. Inhibition of respiration by peptides **WK7-21**, **C1** and **7-21C** suggests that they share at least one mechanism of action with MccJ25. In this study, a series of MccJ25-derived peptides lacking the lasso structure was designed by an *in silico* approach. Some of the designed peptides were inhibitory to *S. enterica* and *E. coli*. Since **C1**, **7-21C** and **WK7-21** were all at least ten

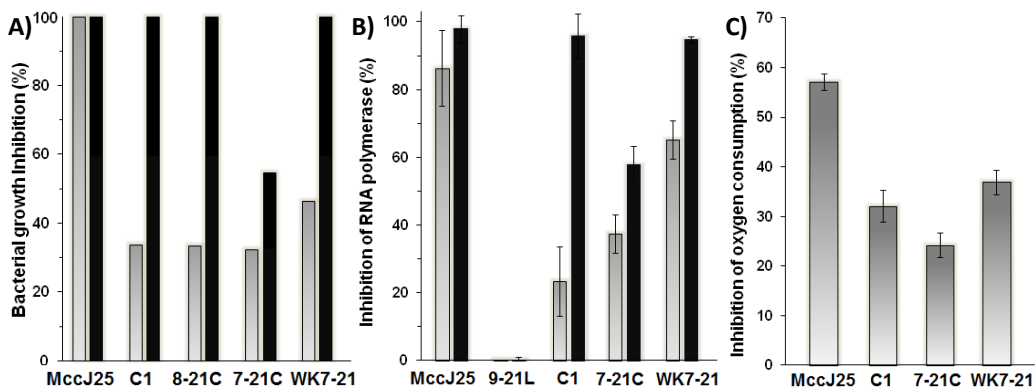


Fig. 2. A) Bacterial growth inhibition of MccJ25, **C1**, **8-21C**, **7-21C** and **WK7-21** at 0.5 μ M (gray) and 7.8 μ M (black) against *Salmonella enterica* subsp. *enterica* ATCC 8387. Data are means of triplicate measurements. B) Inhibition of *E. coli* RNA polymerase *in vitro* by MccJ25, **9-21L**, **C1**, **7-21C** and **WK7-21** at 5 μ M (gray) and 50 μ M (black). Rifampicin (200 nM) was the positive control. The values are means \pm SD of triplicate analyses. C) Inhibition of oxygen consumption by MccJ25, **C1**, **7-21C** and **WK7-21** at their respective MICs. The values are means \pm SD of triplicate analyses.

times less potent than MccJ25, the constrained lasso structure might be more than somewhat important for antibacterial action. MccJ25 inhibits transcription by binding in the secondary channel of RNAP and thereby blocking substrate access to the catalytic site. The Tyr⁹ residue of MccJ25 has been shown essential for RNAP inhibition with no compatible substitutions [6]. Other residues, namely Gly⁴, Pro⁷, Phe¹⁰ and Phe¹⁹ are reportedly important but not strictly essential for MccJ25 binding to RNAP [6]. In the present study, we observed that MccJ25-derived peptides lacking the lasso structure were able to inhibit *in vitro* RNAP at high concentrations (5 and 50 µM). Although these peptides presumably bound to RNAP, it is not possible to deduce that they share a common binding site with MccJ25. Pavlova, et al. [6] reported that the RNAP/MccJ25 interaction involves primarily hydrophobic interaction. Since the active MccJ25-derived peptides had Phe residues at positions 10 and 19 and Tyr at position 9, these might be involved in the inhibition of RNAP. On the other hand, in the case of **WK7-21**, the KWK pattern at the *N*-terminus could be involved. This pattern is known to bind to DNA [11]. The respiratory apparatus of *S. enterica* could be a target for **WK7-21**, **C1** and **7-21C**, as it is for MccJ25. Uptake of these peptides inside cells leads to increased superoxide production, oxidative damage of biologically important molecules, and ultimately cell death. Further studies are required in order to decipher the precise molecular mechanism of these and other MccJ25-derived peptides.

These findings put forward the possibility of producing MccJ25-derived peptides lacking the lasso structure but nevertheless conserving antibacterial activity. The presence of the lasso constrains the structure of MccJ25 while conferring potent antibacterial activity to the peptide. MccJ25-derived peptides lacking the lasso but otherwise constrained in a rigid overall structure, for example by disulfide bonds, could be strongly antibacterial. A rigid topology close to that of MccJ25 appears to make the molecule a more potent antibacterial agent.

Acknowledgments

François Bédard thanks the Fonds de recherche du Québec - Nature et technologies (FQRNT) and the National Sciences and Engineering Research Council of Canada (NSERC) for graduate and undergraduate scholarships, respectively. This work was supported by the FRQNT (2011-PR-139387).

References

1. Bayro, M.J., et al. *J. Am. Chem. Soc.* **125**, 12382-12383 (2003), <http://dx.doi.org/10.1021/ja036677e>
2. Sable, S., Pons, A.M., Gendron-Gaillard, S., Cottenceau, G. *Appl. Environ. Microbiol.* **66**, 4595-4597 (2000), <http://dx.doi.org/10.1128/AEM.66.10.4595-4597.2000>
3. Mukhopadhyay, J., Sineva, E., Knight, J., Levy, R.M., Ebright, R.H. *Mol. Cell* **14**, 739-751 (2004), <http://dx.doi.org/10.1016/j.molcel.2004.06.010>
4. Bellomio, A., Vincent, P.A., de Arcuri, B.F., Farías, R.N., Morero, R.D. *J. Bacteriol.* **189**, 4180-4186 (2007), <http://dx.doi.org/10.1128/jb.00206-07>
5. Niklison Chirou, M., Bellomio, A., Dupuy, F., Arcuri, B., Minahk, C., Morero, R. *FEBS J.* **275**, 4088-4096 (2008), <http://dx.doi.org/10.1111/j.1742-4658.2008.06550.x>
6. Pavlova, O., Mukhopadhyay, J., Sineva, E., Ebright, R.H., Severinov, K. *J. Biol. Chem.* **283**, 25589-25595 (2008), <http://dx.doi.org/10.1074/jbc.M803995200>
7. Soudy, R., Wang, L., Kaur, K. *Bioorg. Med. Chem.* **20**, 1794-1800 (2012), <http://dx.doi.org/10.1016/j.bmc.2011.12.061>
8. Hammami, R., Bédard, F., Gomaa, A., Subirade, M., Biron, E., Fliss, I. *Amino Acids*, **47**, 417-428 (2015), <http://dx.doi.org/10.1007/s00726-014-1877-x>
9. Blond, A., Cheminant, M., Destoumieux-Garzón, D., Ségalas-Milazzo, I., Peduzzi, J., Goulard, C., Rebuffat, S. *Eur. J. Biochem.* **269**, 6212-6222 (2002), <http://dx.doi.org/10.1046/j.1432-1033.2002.03340.x>
10. Lopez, F.E., Vincent, P.A., Zenoff, A.M., Salomón, R.A., Farías, R.N. *J. Antimicrob. Chemother.* **59**, 676-680 (2007), <http://dx.doi.org/10.1093/jac/dkm009>
11. Johnson, N.P., Mazarguil, H., Lopez, A. *J. Biol. Chem.* **271**, 19675-19679 (1996), <http://dx.doi.org/10.1074/jbc.271.33.19675>

Non-Natural D-Amino Acids to Control Bacterial Virulence

Michael A. Bertucci¹ and Kareem March²

¹Department of Chemistry, Moravian College, Bethlehem, PA, 18018, USA;

²Department of Chemistry, Hartwick College, Oneonta, NY, 13810, USA

Introduction

The progressive slowing of antibiotic development and the increase of bacterial drug resistances poses a major threat to human health [1]. Bacteria aggregate to form potent virulent communities bound by an extracellular polymeric substance composed of sugars, proteins, and other secreted biomolecules. The resultant structure, a biofilm, is responsible for an estimated 80% of known bacterial infections. This formed barrier is resistant to changes in temperature, salinity, and antimicrobial agents, protecting proliferating cells on the interior of the structure. Thus, dismantling biofilms can serve as a means of impeding pathogenicity [2].

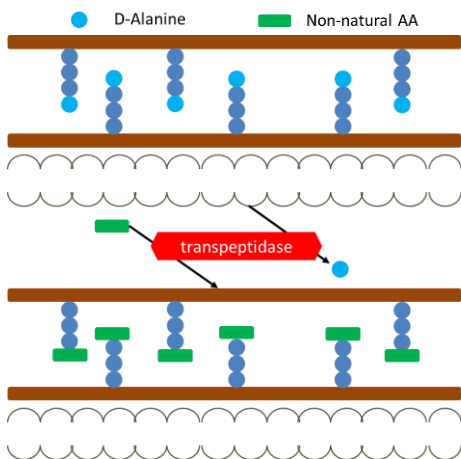


Fig. 1. The incorporation of non-natural amino acids into the peptidoglycan layer of the gram-positive bacterial cell wall.

only the enantiomers of the twenty canonical amino acids have been screened, providing optimal space for the development of synthetically modified side chain residues to enhance potency.

In this study, we report a preliminary investigation into synthetic D-amino acids for biofilm disruption. Modified from a parent glutamic acid structure, three novel amino acids were prepared and screened in cultures of the opportunistic pathogen *S. epidermidis* to probe their antimicrobial capabilities.

Results and Discussion

To expediently develop a small set of novel D-amino acids for screening, glutamic acid was used as a handle for coupling a variety of primary and/or secondary amines to afford a *de novo* amide bond. Inspiration for the selection of amine coupling partners was taken from previously reported biofilm disruptors, like D-tyrosine and D-leucine that contain aromatic or larger aliphatic side chains (Figure 2) [4]. The amines were added to a cooled solution of 1-ethyl-3-(3-dimethylaminopropyl)carbodiimide (EDC), triethylamine, and Boc-D-glutamic acid methyl ester to yield the corresponding protected amino acid. In the presence of concentrated hydrochloric acid, the Boc and methyl ester moieties were cleaved to produce the free amino acid.

Solutions of the purified amino acids (0.4 μ M to 400 μ M) were prepared by serial dilution and combined with *S. epidermidis* biofilms, grown for 24 h, in a simple crystal violet well-plate assay. After another 24 h incubation, the plates were read at 580 nm to determine the minimum inhibitory concentration of each synthetic amino acid. The combined data from 8 replicate trials reveals only modest variation in the biofilm surface (Figure 3). Both KM01 and the positive control D-tyrosine

displayed a small but global reduction in absorbance, while KM02 and EM01 showed no significant decrease in biofilm density relative to the control. The discrepancy in the activity from D-tyrosine and KM01 to KM02 implies that the carboxylate moiety in KM02 reduces biofilm disassembly, perhaps indicating the benefit of an electron-rich arene.

However, a weak correlation was displayed between amino acid concentration and antibiofilm activity. In addition, the magnitude of biofilm reduction in all cases is minimal compared to the degree of biofilm disassembly described in previous reports. Amino acids, such as D-tyrosine, were shown to eradicate biofilms at concentrations as low as 10 μM , which was simply not represented in our control experiments [4,5].

A study published concurrently by Sarkar and colleagues cites similar difficulties obtaining comparable potencies as those initially reported for D-amino acid mediated biofilm disassembly. After screening 96 natural and non-natural D-amino acids in three species of gram-positive pathogens (*S. epidermidis*, *S. aureus*, and *B. subtilis*), no significant biofilm reduction was observed [5]. These results call into question the effectiveness of employing D-amino acids as antimicrobials.

Despite the dissension in the field regarding the potential of D-amino acids to serve as biofilm disruptors, the pathway for the incorporation of non-natural amino acids into the peptidoglycan layer of gram-positive bacteria has been verified. The well-known epitope 2,4-dinitrophenylalanine (DNP) was introduced into the internal oligopeptides of *B. subtilis*, promoting assembly of endogenous antibodies at the cell surface [6]. The flexibility of the transpeptidase enzyme mediating this process

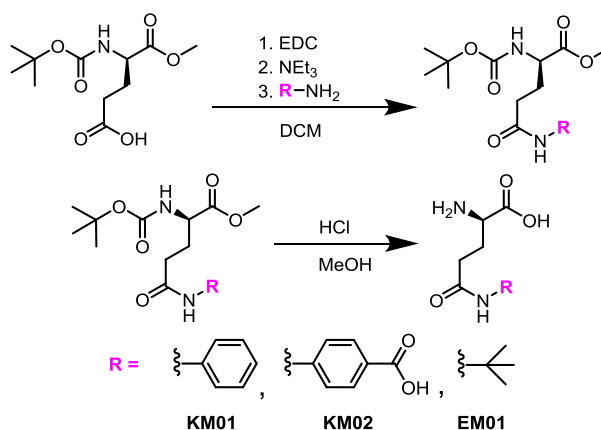


Fig. 2. Scheme for the synthesis of D-glutamic acid analogs KM01, KM02, and EM01.

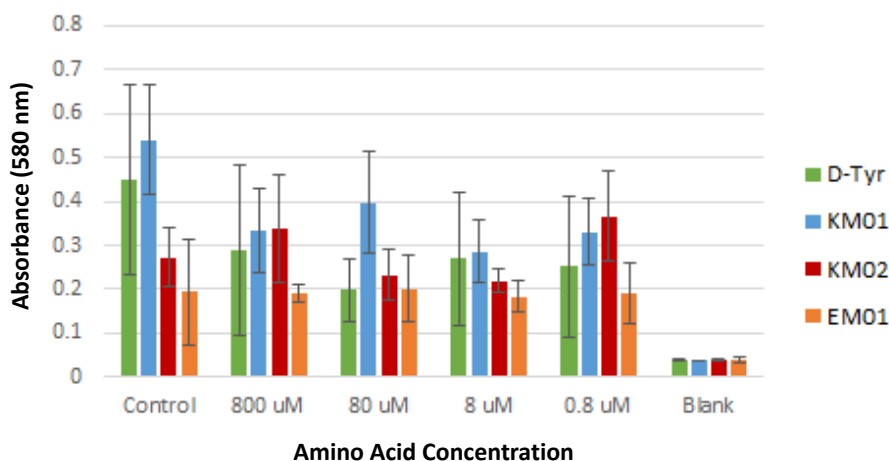


Fig. 3. Decrease in *S. epidermidis* biofilm density (absorbance) after incubated for 24 h with D-tyrosine and three D-glutamic acid derivatives KM01, KM02, and EM01.

was further employed to modify extracellular peptides at their C-termini, largely altering the topography of the bacterial cell wall [7].

In this initial investigation of synthetic D-amino acids as biofilm disruptors, three novel glutamic acid derivatives were designed and screened in *S. epidermidis*. Although the analogs only displayed slight perturbations in biofilm densities, the feasibility of inserting synthetically modified amino acids into the gram-positive cell wall has been verified in the literature. By integrating previous research in peptide science and chemical biology in bacteria, the peptidoglycan layer remains an open canvas for antimicrobial decoration.

Acknowledgments

We would like to thank the Department of Chemistry at Hartwick College and the Rochester Academy of Sciences for funding as well as Professor Mary Allen for the materials and facility to conduct the biofilm degradation assays. Future work on the project will be complete with support from the Department of Chemistry at Moravian College.

References

1. Centers for Disease Control and Prevention. (2013) Drug Resistance. Retrieved from <http://www.cdc.gov/media/releases/2013/p0916-untreatable.html>
2. Costerton, J.W., Stewart, P.S., Greenberg, E.P. *Science* **284**, 1318-1322 (1999), <http://dx.doi.org/10.1126/science.284.5418.1318>
3. Kolodkin-Gal, I., et al. *Science* **328**, 627-629 (2010), <http://dx.doi.org/10.1126/science.1188628>
4. Leiman, S.A., et al. *J. Bacteriology* **195**, 5391-5395 (2013), <http://dx.doi.org/10.1128/jb.00975-13>
5. Sarkar, S., Pires, M.M. *PLOS One* **10** (2015), <http://dx.doi.org/10.1371/journal.pone.0117613>
6. Fura, J.M., Sabulski M.J., Pires, M.M. *ACS Chem. Biol.* **9**, 1480-1489 (2014), <http://dx.doi.org/10.1021/cb5002685>
7. Pidgeon, S.E., et al. *ACIE* **54**, 6158-6162 (2015), <http://dx.doi.org/10.1002/anie.201409927>

Angiotensin I-Converting Enzyme Inhibitory Activity of Enzymatic Hydrolysates of Whey Milk, Casein and Egg Albumin by Microbial Enzymes and a Commercial Enzyme

Y.A.A. Hamin-Neto and H. Cabral

Department of Pharmaceutical Sciences, School of Pharmaceutical Sciences of Ribeirao Preto, University of Sao Paulo, do Café Avenue, Ribeirao Preto, 14040-903, Brazil

Introduction

Hydrolases, particularly proteases, are among the most widely sold enzymes [1]. These enzymes represent approximately 60% of the enzymes sold worldwide [1]. Proteases can be used in different industrial sectors, such as food, detergents, leather, medicines [2], bioremediation [3], and in production of bioactive peptide by enzymatic proteolysis of milk proteins [4]. Bioactive peptides are peptides that have activities similar to drugs or hormones, modulating physiological functions by interacting with specific receptors on target cells inducing answers [5]. Bioactive peptides have emerged on the market in the 70s, when Novartis launched Lypressin®, an analogue of vasopressin. Hypertension affects about one quarter of the world population, it is a major risk factor for cardiovascular disease and related complications [5,6]. The angiotensin I-converting enzyme (ACE) catalyses the conversion of angiotensin I to angiotensin II, a potent vasoconstrictor and has an important role in regulating blood pressure in mammals [6]. Inhibitor peptides of ACE were released from milk casein and whey proteins from goat milk by use of two commercial enzymes subtilisin (Alcalase 2.4 L FG, EC 3.4.21.62) and pancreatic trypsin (PTN 6.0 S Salt free; EC 3.4. 21.4) [7]. The aim of this study was to obtain peptides produced from egg albumin, casein and whey protein, by action of two microbial enzymes and a commercial enzyme, and to evaluate the inhibition of angiotensin I-converting enzyme using fluorescent substrate (Abz-FRK(Dnp)P-OH) in the presence of these hydrolysates.

Results and discussion

Protein hydrolysates were obtained from egg albumin, casein and whey protein. Enzymes, isolated from submerged extract of fungi *Eupenicillium javanicum* and *Myceliophthora thermophila* and commercial trypsin (Sigma-Aldrich®), were used to proteolysis. The hydrolysates were evaluated to ACE inhibitory activity using a synthetic FRET (fluorescence resonance energy transfer) peptide substrate (Abz-FRK(Dnp)P-OH), specific to this enzyme. The reaction occurred in spectrofluorimeter,

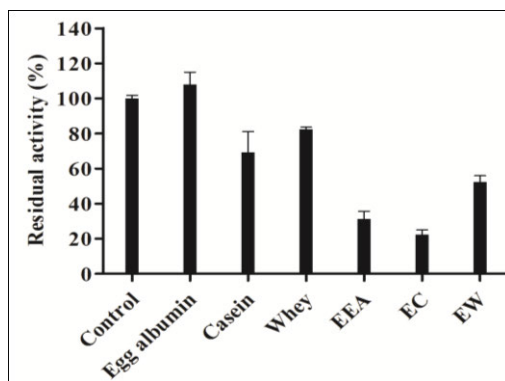


Fig. 1. ACE inhibitory activity of protein and their hydrolysates (0.8 mg/mL) produced from egg albumin (EEA), casein (EC) and whey protein (EW), using an enzyme produced by the fungus *Eupenicillium javanicum*. The test was conducted with ACE (Sigma-Aldrich®) in spectrofluorometer, pH 7.0 at 37°C with a synthetic FRET peptide substrate (Abz-FRK(Dnp)P-OH).

Lumina fluorescence spectrometer (Thermo Scientific) at 37°C. The hydrolysates, produced by action of *Eupenicillium javanicum* enzyme, showed ACE inhibitory activity from all substrates, egg albumin (EEA), casein (EC) and whey protein (EW) were able to inhibit the ACE, about 70, 80, and 50%, respectively (Figure 1).

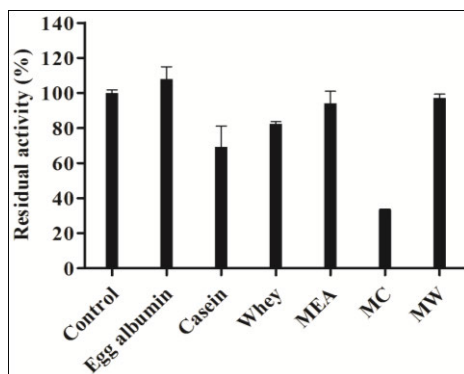


Fig. 2. ACE inhibitory activity of protein and their hydrolysates (0.8 mg/mL) produced from egg albumin (MEA), casein (MC) and whey protein (MW), using an enzyme produced by the fungus *Myceliophthora thermophila*. The test was conducted with ACE (Sigma-Aldrich®) in spectrofluorometer, pH 7.0 at 37°C with a synthetic FRET peptide substrate (Abz-FRK(Dnp)P-OH).

Analyzing the results of hydrolysates produced by *Myceliophthora thermophila*, only the products of casein cleavage were able to inhibit the ACE activity, about 70% (Figure 2).

The results of hydrolysates produced by commercial trypsin were similar to *Myceliophthora thermophila* enzyme, only products derived from casein hydrolyses presented capacity to inhibit the ACE enzyme, about 85% (Figure 3).

The hydrolysates from all substrates produced in the presence of the enzyme from the fungus *Eupenicillium javanicum* and casein hydrolysates produced by enzymes, from fungus *Myceliophthora thermophila* and trypsin, were able to inhibit angiotensin I-converting enzyme. Each enzyme presents a specificity and affinity to substrates. These characteristics define the capacity to cleave the substrate and the cleavage site. The positions of hydrolysis are related to peptides sequences produced, and these amino acids sequences and its physics and chemistry characteristics are directly linked with the biological activity.

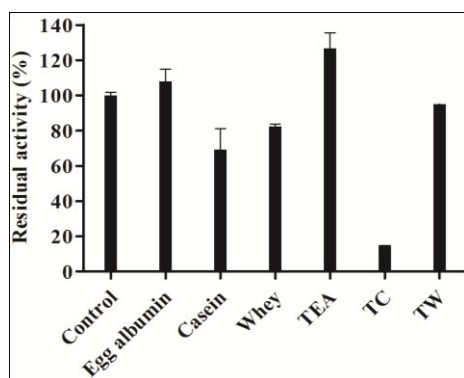


Fig. 3. ACE inhibitory activity of proteins and their hydrolysates (0.8 mg/mL) produced from egg albumin (TEA), casein (TC) and whey protein (TW), using an enzyme commercial trypsin (Sigma-Aldrich®). The test was conducted with ACE (Sigma-Aldrich®) in spectrofluorometer, pH 7.0 at 37°C with a synthetic FRET peptide substrate (Abz-FRK(Dnp)P-OH).

According to Li and Yu (2015), the catalytic site of ACE has three amino acids that are corresponding to hydrophobic amino acids from angiotensin I in C-terminal, only when the amino acids of bioactive peptides interact with these subunits, they can present inhibitory activity. The sequence of three amino acids in the C-terminal influences this inhibition. Aromatic or alkaline amino acids in the N-terminal improve the inhibitory activity. Leucine, isoleucine and valine in the N-terminal influence positively in the inhibitory activity, while proline in this position influences negatively. According to the results, the used proteins derived in products that showed potential application as ACE enzyme inhibitors, other studies are necessary to isolate and to sequence the peptides that presented activity.

Acknowledgements

The authors would like to acknowledge financial support provided by Fundação de Amparo à Pesquisa do Estado de São Paulo, (FAPESP) (2012/18278-2, 2012/24703-8 and 2011/06986-0 process) and Conselho Nacional de Desenvolvimento Científico e Tecnológico, CNPq, (308078/2012-8 process).

References

1. Rao, M.B., et al. *Microbiol. Mol. Biol. Rev.* **62**, 597-635 (1998).
2. Rai, S.K., Mukherjee, A.K. *Biochem. Eng. J.* **54**, 47-56 (2011), <http://dx.doi.org/10.1016/i.bei.2011.01.007>
3. Gupta, R., et al. *Appl. Microbiol. Biotechnol.* **60**, 381-395 (2002), <http://dx.doi.org/10.1007/s00253-002-1142-1>
4. Korhonen, H. *J. Funct. Foods* **1**, 177-187 (2009), <http://dx.doi.org/10.1016/j.jff.2009.01.007>
5. Fitzgerald, R., Murray, B. *Int. J. Dairy Technol.* **59**, 118-125(2006).
6. Hartmann, R. Meisel, H. *Curr. Opin. Biotechnol.* **18**, 163-169(2007), <http://dx.doi.org/10.1016/j.copbio.2007.01.013>
7. Espejo-Carpio, F., et al. *Int. Dairy J.* **32**, 175-183(2013).
8. Li, Y., Yu, J. *J. Med. Food* **18**(2), 147-156(2015), <http://dx.doi.org/10.1089/jmf.2014.0060>

Fluorescent Delta Selective Opioid Peptides from a Cyclic Peptide Combinatorial Library

M. Cazares*, A. Gioseffi*, A. Bunnell*, Y. Li*, and C.T. Dooley*#

*Torrey Pines Institute for Molecular Studies, Port Saint Lucie, FL, 34987, USA

#Brilliant Biosciences, Port Saint Lucie, FL, 34987, USA

Introduction

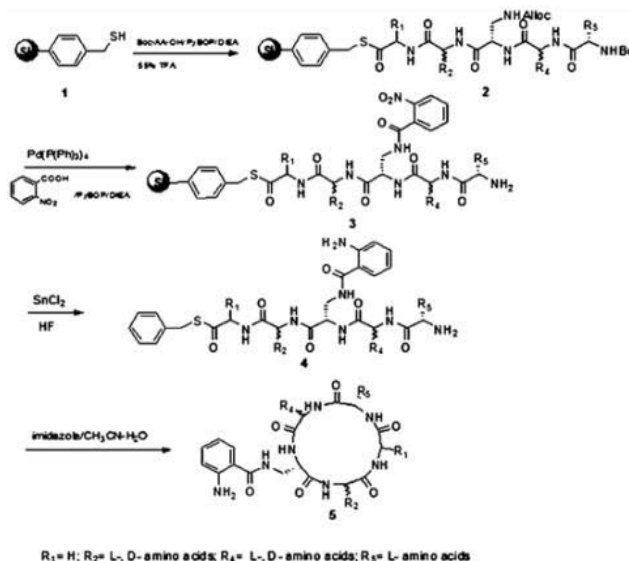
There has been an increased interest in cyclic peptides as potential therapeutic compounds, largely due to their enhanced binding affinity and specificity to G-coupled receptors when compared to their linear equivalents [1], as well as their increased stability *in vivo*. Some cyclic peptides of therapeutic value include daptomycin, cyclosporine A, polymyxin, and octreotide.

While clearly of significant value, cyclic peptides may be limited by the difficulty of their synthesis. The ground-state E geometry of the peptide bond limits the peptides from reaching the ring-like conformation that is necessary for cyclization [2]. Additionally, oligomerization often occurs as a side reaction during macrocyclization. These obstacles for synthesis have previously thwarted the development of novel therapeutic macrocycles and prevented the establishment of cyclic peptide-based libraries. Previously, few studies have been reported where cyclic peptide libraries have been used to identify ligands which may be of therapeutic interest [3]. A majority of the cyclic peptide libraries described were constructed by phage display strategies rather than de novo chemical synthesis [4]. Given this, the necessity of a simple synthetic strategy for the synthesis of cyclic peptide libraries is evident.

We have previously described an imidazole-promoted cyclization approach for synthesizing cyclic peptides from their fully unprotected linear peptide thioesters [5]. This method was shown to be highly efficient for the synthesis of cyclic peptides ranging from 5 to 11 amino acid residues. Additionally, this method of imidazole-promoted cyclization minimized the oligomerization side reaction. In our pursuit of new potent ligand tools for opioid receptors, we designed, synthesized, and screened a fluorescent anthraniloyl labeled cyclic peptide library in the positional scanning format using the imidazole-promoted cyclization method.

Results and Discussion

Boc-amino acids were coupled on the resin by using the PyBOP/DIEA activation method. Glycine was defined at the first position as R1=H. 19 L- and 17 D-amino acids were used as a mixture at the second and fourth positions as R2 and R4. 19 L-amino acids were used as a mixture at the fifth position as R5. A Boc-Dap(Alloc) was incorporated into the linear peptide at the third position. Its side chain was reacted with 2-nitrobenzoic acid to form a resin bound peptide. After being reduced by SnCl₂ and treated with anhydrous HF, the linear anthraniloyl fluorescent peptide was cyclized in a mixture solution of 1.5 M aqueous imidazole and acetonitrile (1:7 in volume) at a concentration of 1 mM for 72 h, resulting in the fluorescent cyclic peptide (Scheme 1).



Scheme 1. (1) Boc-AA-OH/PyBOP/DIEA; 55% TFA. (2) Pd(PPh₃)₄/PhSiH₃; 2-nitrobenzoic acid/DIC. (3) SnCl₂/DMF; 55% TFA. (4) HF (anhydrous)/anisole, 0°C, 2h. (5) 1.5 M imidazole (aq)/acetonitrile (1:7 v/v), r.t. 72h.

The mixture library was screened at the δ -opioid receptor. Sprague-Dawley rat brains, with cerebellums removed, were homogenized using 50 mM DPDPE buffer, pH 7.4, and centrifuged at 16,500 rpm for 10 min. The pellets were resuspended in fresh buffer and incubated at 37°C for 30 min. Following incubation, the suspensions were centrifuged as before, the resulting pellets resuspended in 100 volumes of DPDPE buffer, and the suspensions combined. Membrane suspensions were prepared and used on the same day. Each assay tube contained 0.5ml of membrane suspension, 2.7nM [3 H] DPDPE, 1 mg/ml compound, and 50 mM DPDPE in a final volume of 0.65ml. The assay tubes were incubated for 2.5hrs at 25°C. Unlabeled DPDPE was used as a competitor to generate a standard curve and determine nonspecific binding. The reaction was terminated by filtration through GF-B filters on a Tomtec Harvester 96 (Orange, CT). The filters were subsequently washed with 6ml of 50mM DPDPE buffer, pH 7.4. Bound radioactivity was counted on a Wallac Betaplate Liquid Scintillation Counter (Piscataway, NJ).

Synthetic Approach to Anthraniloyl (Ant) Labeled Cyclic Penta-Peptide. As described in our previous studies [6], the anthraniloyl group was chosen as our extrinsic fluorescent probe because of its well characterized features, such as a high quantum yield at 415nm (excitation at 330nm) for its small size and hydrophilicity, as well as the tendency of its fluorophore to not affect the overall structural characteristics of a peptide or interfere with its biological activity. The synthetic strategy for the anthraniloyl-labeled peptide is illustrated in Scheme 1. The anthraniloyl group is generated by coupling of an *o*-nitrobenzoic acid to an amino group of the peptide, followed by reduction with tin chloride(II). This reduction is mild under near neutral conditions, and is suitable for use with both Boc-and Fmoc-chemistry [7].

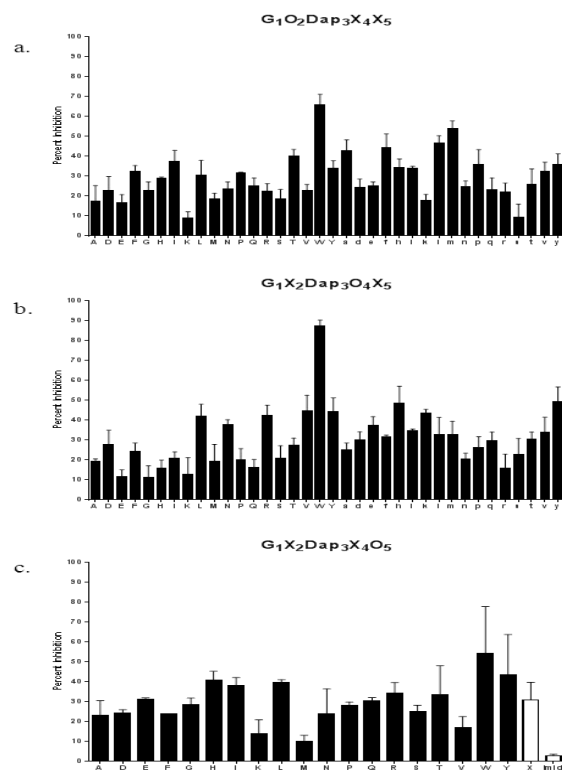
Synthesis and Deconvolution of a Positional Scanning Synthetic Combinatorial Library of Anthraniloyl-Labeled Cyclic Peptides. The synthetic strategy described in scheme 1 was applied to the construction of an anthraniloyl-labelled cyclic pentapeptide library in the positional scanning

Table 1. Deconvolution of the most active amino acids derived from the screening data in the delta receptor.

R1	R2	R3	R4	R5
L-Gly	L-Trp	L-Dap	D-Tyr	L-His
	D-Leu		L-Arg	L-Trp
	D-Met		D-His	
	D-Phe		L-Tyr	
			L-Trp	

$$4 \times 5 \times 2 = 40$$

Chart 1. (a) Position 2; (b) 4; (c) 5 in a competitive delta radio receptor binding assay.



format [8]. Position 1 was fixed with glycine to ensure efficient cyclization [5]. Position 3 was fixed with 2,3-diaminopropionic acid. Its 3-amino was coupled with the fluorescent anthraniloyl-group. This library was composed of three sublibraries, in which each of the three positions (2, 4, or 5) were defined with either a single amino acid (O) or a mixture of amino acids (X). For each of the three sublibrary mixtures, the two remaining positions were made up of a mixture of amino acids (X). Positions 2 and 4 contained 36 L- and D- amino acids, while position 5 contained 19 naturally occurring L-amino

Table 2. *K_i Values for the most active (crude) individual compounds from the cyclic peptide library at the delta receptor.*

Peptide #	R1	R2	R3	R4	R5	K _i (nM)	STD
1	L-Gly	L-Trp	L-Dap	D-Lys	L-Tyr	11	5
2	L-Gly	D-Phe	L-Dap	D-Lys	L-Tyr	11	6
3	L-Gly	D-Met	L-Dap	D-Lys	L-Trp	18	6
4	L-Gly	D-Phe	L-Dap	D-His	L-Tyr	20	4
5	L-Gly	D-Phe	L-Dap	L-Tyr	L-Trp	21	1
6	L-Gly	D-Met	L-Dap	L-Tyr	L-Trp	31	8
7	L-Gly	D-Phe	L-Dap	D-Trp	L-Trp	33	2
8	L-Gly	D-Met	L-Dap	D-His	L-Trp	36	7
9	L-Gly	D-Met	L-Dap	D-Tyr	L-Trp	76	2

the abundance of imidazole remaining in each mixture, the effect of imidazole on the delta opioid receptor binding assay was tested prior to screening of the library. This experiment determined that 1mg/mL (14.7mM) imidazole did not have a significant effect in the binding assay. Thus, it was shown that imidazole at this concentration exhibited negligible inhibition.

Each mixture in the library was screened at a concentration of 1mg/mL. The screening results for the delta selective binding assay are shown in Chart 1. Several mixtures at each position exhibited percent inhibitions above that of the all X mixture in which all cyclic peptides are present as a single mixture (all X). One mg/mL imidazole was demonstrated not to have a significant effect in the binding assay, exhibiting negligible inhibition.

When a cutoff value of 45% inhibition was used, the most active amino acids for the mixture making up position 2 were L-Trp, D-Leu, D-Met, and D-Phe; at position 4 they were D-Tyr, L-Arg, D-His, L-Tyr, and L-Trp; while L-His and L-Trp were the most active at position 5. IC₅₀ values were not required to differentiate activities in this case because the percent inhibitions observed were on the linear portion of the competition curve (i.e., between 20 and 80% inhibition).

Individual Peptides from the Cyclic Library. A total of 40 individual peptides were synthesized in parallel by the combination of the most active amino acids identified at the three positions 4×5×2 (as shown in Table 1). The individual peptides were tested prior to purification in the binding assay for the delta opioid receptor. The results for the most active crude compounds are shown in Table 2.

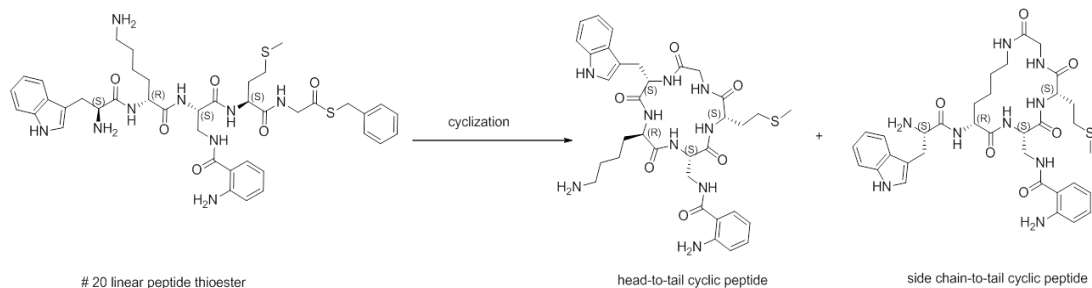
Table 3. *Opioid receptor selectivity.*

	DOR K _i (nM)	MOR K _i (nM)
Peptide 3	18	249
Peptide 7	33	>10,000

Two individual cyclic peptides, #3 and #7, exhibited significant delta receptor activity and were selected for further purification. Following purification, delta and mu opioid receptor binding assays were performed to determine selectivity of the individual peptides (data shown in Table 3).

Determination of the Structure of the Most Active Compound. The HPLC profile of the active purified peptide #3 actually showed two peaks having an identical mass weight that matched the desired cyclic product. This is caused by the head-to-tail and side chain-to-tail cyclization when R⁴ is D-Lys (as shown in Scheme 2), as our previous studies have shown that the imidazole-promoted cyclization is not regioselective when Lys is an internal residue.

Scheme 2. *Two Possible Isomers of Cyclic Peptide 3 (previously referred to as peptide #20).*



acids. Thus, this positional scanning library was composed of 91 mixtures. Each mixture contained 684 head-to-tail cyclic pentapeptides at position 2 and 4 and 1296 cyclic pentapeptides at position 5. In total, this library contains 24,624 individual head-to-tail cyclic pentapeptides.

The anthraniloyl-labeled cyclic pentapeptide library was screened in a competitive radio receptor binding assay for the delta opioid receptor. Because of

Conclusion

We have identified a cyclic peptide which exhibits delta selective opioid binding. In addition to this selective cyclic peptide, a novel linear peptide of interest (peptide 7) was also synthesized which may prove equally selective and promising (Table 3). Assays are currently being performed to determine the selectivity of these peptides in the kappa opioid receptor as well.

These selective peptides are of great interest for use in FRET assays. While we were unable to purify other cyclized products, the use of these peptides in FRET experiments is still possible regardless of their structure, as the fluorescent tag is exposed in either conformation. The availability of selective opioid peptides with fluorescent tags allows for their use in innovative kinetic and binding studies *in situ*.

References

1. (a) Dong, M., Pinon, D.I., Asmann, Y.W., Miller, L.J. *Mol. Pharmacol.* **70**, 206-213 (2006), <http://dx.doi.org/10.1124/mol.105.021840>; (b) Millward, S.W., Fiocco, S., Austin, R.J., Roberts, R.W. *ACS Chem. Biol.* **2**, 625-634, (2007), <http://dx.doi.org/10.1021/cb7001126>
2. White, C.J., Yudin, A.K. *Nat. Chem.* **3**, 509-524, (2011), <http://dx.doi.org/10.1038/nchem.1062>
3. (a) Joo, S.H., Xiao, Q., Ling, Y., Gopishetty, B., Pei, D. *J. Am. Chem. Soc.* **128**, 13000-13009, (2006), <http://dx.doi.org/10.1021/ja063722k>; (b) Liu, T., Joo, S.H., Voorhees, J.L., Brooks, C.L., Pei, D. *Bioorg. Med. Chem.* **17**, 1026-1033, (2009), <http://dx.doi.org/10.1016/j.bmc.2008.01.015>; (c) Xiao, Q., Pei, D. *J. Med. Chem.* **50**, 3132-3137, (2007), <http://dx.doi.org/10.1021/jm070282e>; (d) Xiao, W., Wang, Y., Lau, E.Y., Luo, J., Yao, N., Shi, C., Meza, L., Tseng, H., Maeda, Y., Kumaresan, P., Liu, R., Lightstone, F.C., Takada, Y., Lam, K.S. *Mol. Cancer Ther.* **9**, 2714-2723, (2010), <http://dx.doi.org/10.1158/1535-7163.MCT-10-0308>; (e) Fluxa, V.S., Raymond, J.L. *Bioorg. Med. Chem.* **17**, 1018-1025, (2009), <http://dx.doi.org/10.1016/j.bmc.2008.01.045>; Eichler, J., Lucka, A.W., Pinilla, C., Houghten, R.A. *Mol. Diversity* **1**, 233-240, (1995), <http://dx.doi.org/10.1007/BF01715527>; Eichler, J., Lucka, A.W., Houghten, R.A. *Pept. Res.* **7**, 300-307 (1994).
4. (a) Scott, C.P., Abel-Santos, E., Jones, A.D., Benkovic, S.J. *Chem. Biol.* **8**, 801-815, (2001), [http://dx.doi.org/10.1016/S1074-5521\(01\)00052-7](http://dx.doi.org/10.1016/S1074-5521(01)00052-7); (b) Meyer, S.C., Gaj, T., Ghosh, I. *Chem. Biol. Drug Des.* **68**, 3-10, (2006) <http://dx.doi.org/10.1111/j.1747-0285.2006.00401.x>; (c) Bonetto, S., Spadola, L., Buchanan, A.G., Jermutus, L., Lund, J. *FASEB J.* **23**, 575-585, (2009), <http://dx.doi.org/10.1096/fj.08-117069>; (d) Kritzer, J.A., Hamamichi, S., Michael McMaffery, J., Santagata, S., Naumann, T.A., Caldwell, K.A., Caldwell, G.A., Lindquist, S. *Nat. Chem. Biol.* **5**, 655-663, (2009), <http://dx.doi.org/10.1038/nchembio.193>; (e) Kohli, R.M., Walsh, C.T., Burkart, M.D. *Nature* **418**, 658-661, (2002), <http://dx.doi.org/10.1038/nature00907>; (f) Guillen Schlippe, Y.V., Hartman, M.C.T., Josephson, K., Szostak, J.W. *J. Am. Chem. Soc.* **134**, 10469-10477, (2012), <http://dx.doi.org/10.1021/ja301017y>; (g) Kolodziej, A.F., Nair, S.A., Graham, P., McMurry, T.J., Ladner, R.C., Wescott, C., Sexton, D.J., Caravan, P. *Bioconjug. Chem.* **23**, 548-556, (2012), <http://dx.doi.org/10.1021/bc200613e>; (h) Giebel, L.B., Cass, R.T., Milligan, D.L., Young, D.C., Arze, R., Johnson, C.R. *Biochemistry* **28**, 15430-15435, (1995), <http://dx.doi.org/10.1021/bi00047a006>
5. Li, Y., Yongye, A., Giulianotti, M., Martinez-Mayorga, K., Yu, Y., Houghten, R.A. *J. Comb. Chem.* **11**, 1066-1072, (2009), <http://dx.doi.org/10.1021/cc900100z>
6. Li, Y., Dooley, C.T., Misler, J.A., Debevec G., Giulianotti, M.A., Cazares, M.E., Maida, L., Houghten, R.A. *ACS Comb. Sci.* **14**, 673-679, (2012) <http://dx.doi.org/10.1021/co300110t>
7. Isidro-Llobet, A., Álvarez, M., Albericio, F. *Tetrahedron. Lett.* **46**, 7733-7736, (2005), <http://dx.doi.org/10.1016/j.tetlet.2005.09.043>
8. (a) Houghten, R.A., Pinilla, C., Blondelle, S.E., Appel, J.R., Dooley, C.T., Cuervo, J.H. *Nature* **354**, 84-86, (1991), <http://dx.doi.org/10.1038/354084a0>; (b) Dooley, C.T., Chung, N.N., Wilkes, B.C., Schiller, P.W., Bidlack, J. M., Pasternak, G.W., Houghten, R.A. *Science* **266**, 2019-2022, (1994), <http://dx.doi.org/10.1126/science.7801131>; (c) Nazif, T., Bogyo, M. *Proc. Natl. Acad. Sci. USA* **98**, 2967-2972, (2001), <http://dx.doi.org/10.1073/pnas.061028898>

Mechanistic Proposal for Restricted Peptides Action on Parasite Membrane

Marcelo D. T. Torres¹, Adriana F. Silva¹, Flávio L. Alves², Antonio Miranda²,
Margareth L. Capurro³, Rodrigo M. Cordeiro¹, and Vani X. Oliveira Jr.¹

¹Universidade Federal do ABC, Santo André, 09210-580, Brazil; ²Universidade Federal de São Paulo, São Paulo, 04021-001, Brazil; ³Universidade de São Paulo, São Paulo, 05508-000, Brazil

Introduction

Malaria is an infectious disease responsible for approximately one million deaths annually. Peptides such as angiotensin II (AII) and its analogs are known to have antimalarial effects against *Plasmodium gallinaceum* [1] and *Plasmodium falciparum* [2]. However, their mechanism of action is still not fully understood at the molecular level. In this work, we investigated this issue by comparing the antimalarial activity of angiotensin II with that of: *i*) its enantiomer formed by only D-amino acids; *ii*) its isomer with reversed sequence; and *iii*) its analogs restricted by lactam bridges - the so-called VC5 peptides.

Results and Discussion

The peptides were synthesized manually with the *t*-Boc strategy on Merrifield resin (Table 1). AII could inactivate 88% of the *Plasmodium gallinaceum* sporozoites, which is consistent with its known antimalarial properties. Similar anti-plasmodial effects were measured for ent-AII and other peptides (Figure 1). In contrast to AII, *ent*-AII and *retro*-AII could not interact with the membrane AII-receptors (Figure 2).

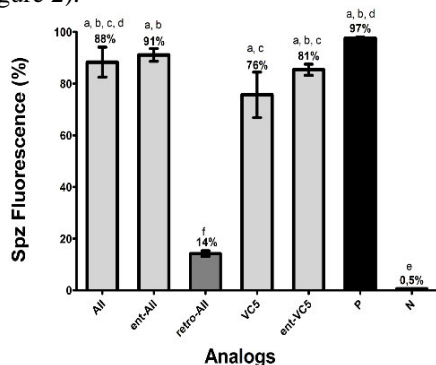


Fig. 1. Effects of AII analogs on membrane permeability expressed as the percent of fluorescent mature sporozoites (mean \pm standard deviation of 9 independent measurements). Letters indicate the results that are not significantly different from each other at the $p < 0.05$ level. Positive control group (+): digitonin/PBS; negative control group (-): PBS.

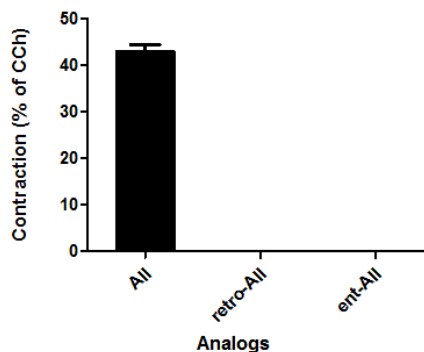


Fig. 2. Effects of peptides on contractile responses during muscle tissue incubation compared to carbachol (CCh) activity. AT_1 receptor recognition was analyzed via pre-incubation with Losartan (mean \pm standard deviation, $N = 2$).

This indicates that the anti-plasmodial effects of AII analogs depend on direct peptide-phospholipid interactions. This hypothesis was also supported by the anti-plasmodial activities recorded for the lactam bridge-restricted analogs VC5 and *ent*-VC5. These were comparable to that of AII. A significant change in the anti-plasmodial activity was observed only for *retro*-AII, which was ~6-fold less effective than AII. We used CD experiments to show that the β -turn was the most frequent

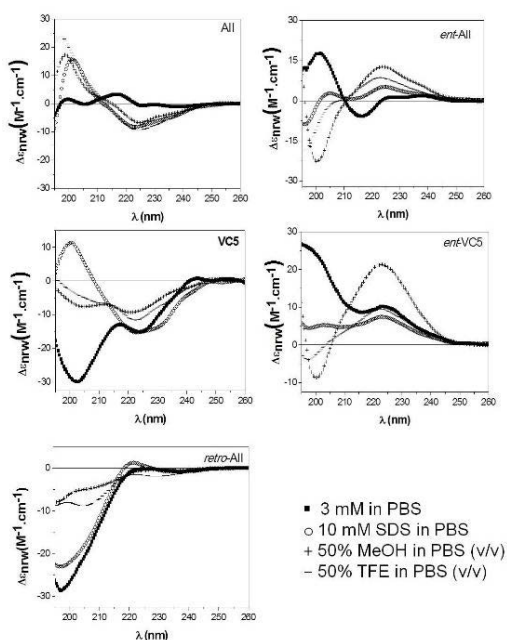


Fig. 3. Circular dichroism spectra of AII analogs. All peptides were analyzed in the following four solutions: 15 mmol L⁻¹ PBS, 10 mmol L⁻¹ SDS/PBS, 50% TFE/PBS, and 50% MeOH/PBS. The peptide concentration was approximately 10⁻⁴ mol L⁻¹.

conformation adopted by peptides in aqueous and organic solvents. Moreover, the β -turn conformation was correlated with a larger anti-plasmodial activity.

In the presence of SDS micelles, AII had a β -turn conformation while *retro*-AII presented a random coiled conformation (Figure 3). Consistently, molecular dynamic simulations revealed that the AII chains were slightly more bent than *retro*-AII at the surface of a model phospholipid bilayer (Figure 4). We did not observe spontaneous pore formation in either case. This may be an indication that this process involves larger time scales and possibly the organization of the peptide chains into larger assemblies. However, qualitative differences were identified between the behavior of AII and *retro*-AII by pulling both peptides across the phospholipid bilayer. At the hydrophobic membrane interior, the *retro*-AII chain was severely coiled and rigid. AII was much more flexible and could experience both straight and coiled conformations. Interactions between AII and phospholipid head groups were kept for a longer time even in the membrane interior. It is conceivable that stronger peptide-head group interactions might be more effective at stabilizing a pore in longer time scales. This contributes to the larger anti-plasmodial activity of AII versus *retro*-AII. We hope that our results can be used for the systematic design of novel compounds with antimalarial activity.

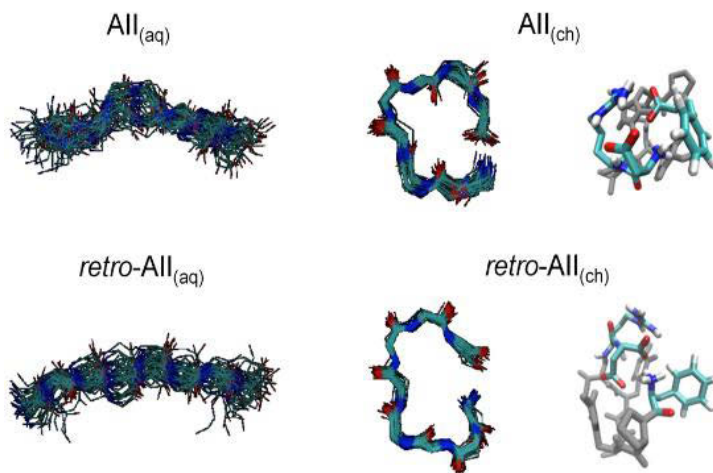


Fig. 4. Conformations of the backbone atoms of AII and *retro*-AII in water (left) and cyclohexane (center). The conformations recorded during the last 5 ns of simulation were overlaid. Selected conformers in cyclohexane (right) are represented in grey with Asp, Arg and Phe residues highlighted in color. Color code: C (cyan), N (blue), O (red), H (white).

Table 1. Mass characterization and purities of peptides synthesized.

Peptide	Sequence	HPLC Purity (%) ^a	Mass Characterization	
			Calculated Mass (Da)	Observed Mass (m/z) ^b
AII	Asp-Arg-Val-Tyr-Ile-His-Pro-Phe	-	1045.5	-
ent-AII	DAsp-DArg-DVal-DTyr-DIle-DHis-DPro-DPhe	99	1045.5	1047.5
retro-AII	Phe-Pro-His-Ile-Tyr-Val-Arg-Asp	100	1045.5	1047.5
VC5	Asp-Arg-Asp-Val-Lys-Tyr-Ile-His-Pro-Phe	95	1271.5	1272.5
ent-VC5	DAsp-DArg-DAsp-DVal-DLys-DTyr-DIle-DHis-DPro-DPhe	99	1271.5	1272.5

^aHPLC: Column Supelcosil C18 (4.6 x 150 mm), 60 Å, 5 µm; Solvent System: A (0.1% TFA/H₂O) and B (0.1% TFA in 60% ACN/H₂O); Gradient: 5-95% B in 30 minutes, Flow: 1.0 mL/min; λ = 220 nm; Injection Volume: 50 µL and Sample Concentration: 1.0 mg/mL.

^bLC/ESI-MS: Micromass instrument, model ZMD coupled on a Waters Alliance, model 2690 system. Conditions of mass measurements: positive mode; range between 500 and 2000 m/z; nitrogen gas flow: 4.1 L/h; capillary: 2.3 kV; cone voltage: 32 V; extractor: 8 V; source heater: 100 °C; solvent heater: 400°C; ion energy: 1.0 V and multiplier: 800 V.

Acknowledgments

We thank Fundação de Amparo à Pesquisa do Estado de São Paulo (FAPESP). Supported by grant #2014/04507-5 and #2014/12938-6.

References

1. Maciel, C., et al. *Plos One* **3**, e3296 (2008), <http://dx.doi.org/10.1371/journal.pone.0003296>
2. Chamlian, M., et al. *J. Pept. Sci.* **19**, 575-580 (2013), <http://dx.doi.org/10.1002/psc.2534>

Linear Peptides Related to Angiotensin II with Antiplasmodial Activity

**Adriana F. Silva¹, Marcelo D. T. Torres¹, Leandro S. Silva², Flávio L. Alves³,
Ana A. S. Pinheiro², Antonio Miranda³, Margareth L. Capurro⁴,
Vani X. Oliveira, Jr.¹**

¹Centro de Ciências Naturais e Humanas, Universidade Federal do ABC, 09210580, Santo André, Brazil;

²Centro de Ciências da Saúde, Instituto de Biofísica Carlos Chagas Filho, Universidade Federal do Rio de Janeiro, 21941902, Rio de Janeiro, RJ, Brazil; ³Departamento de Biofísica, Universidade Federal de São Paulo, 04044020, São Paulo, SP, Brazil; ⁴Instituto de Ciências Biomédicas II - Universidade de São Paulo, 05508000, São Paulo, SP, Brazil

Introduction

The antiplasmodial activities of angiotensin II and its analogs have been extensively investigated in *Plasmodium gallinaceum* and *Plasmodium falciparum* parasite species. Angiotensin II cannot be used as an antimalarial drug due to its vasoconstrictor effect [1,2]. Ten peptides related to it were synthesized by Fmoc solid phase strategy, purified by RP-HPLC, characterized by LC/ESI-MS and tested against mature *Plasmodium gallinaceum* sporozoites and *Plasmodium falciparum* early trophozoites.

Results and Discussion

From the Ang II primary sequence (DRVYIHPF), we synthesized ten peptides (Table 1). Peptide 1 (DRVY**H**IPF) and peptide 2 (DRVYPF) were designed to verify if the hydrophobic cluster exerts some influence on the parasite membrane. We inverted the position of the His and Ile amino acid residues in peptide 1. We observed that this change promotes an increase in the antiplasmodial activity (94%), about 7% that presented by native Ang II (Figure 1a). Instead, in the peptide 2 which had deleted His and Ile amino acid residues, this modification decreased the antiplasmodial activity (64%), about 15% of native Ang II and about 26% of the peptide 1.

Peptide 3 (RYPF) was designed to verify if the R, Y, P and F residues are relevant in native Ang II [3,4] and peptide 4 (RY**H**IPF) was designed to verify if the hydrophobic cluster exerts some influence on the peptide-parasite interaction (Figure 1a). Peptide 4 did not have more activity than peptide 3 (77% and 76% antiplasmodial activity, respectively). This was probably due to the influence of the cation- π interactions between Tyr and Arg residues providing greater stability [5], i.e., the effect of the cluster (Ile and His inverted residues) was not significant on biological activity because the interactions between Arg-Tyr residues are more effective than the interactions between Tyr-His residues [6].

Silva and colleagues suggested that the aromatic or hydrophobic residues can promote peptide-parasite interactions [4]. Thus, peptide 5 (YHPF) and peptide 6 (VIPF) were designed based on this information. We observed that both peptides could maintain the Ang II and peptide 1 antiplasmodial activity (89% and 94%, respectively). We studied the effects of each amino acid residue on the VIPF (peptide 6). The unusual amino acid 2-naphthylalanine (2-Nal) scan libraries of four VIPF analogs were synthesized (Peptides 7 to 10 - Table 1). Their activities against mature *P. gallinaceum* sporozoites were performed (Figure 1a) as well as CD studies (data not shown). The unusual amino acid (2-Nal) was chosen because it is similar to quinine, a potent antimalarial drug.

Table 1. Purity of peptides determined by LC/MS.

Entry	Name	Sequence	HPLC Purity ^a (%)	Calcd. Mass ^b (g.mol ⁻¹)	Obsd. Mass ^b (g.mol ⁻¹)
1	[Ile ⁶ ,His ⁵]-AII	DRVYHIPF	98	1045.5	1046
2	des-Ile ⁵ ,His ⁶ -AII	DRVYPF	98	795.4	796
3	des-Asp ¹ ,Val ³ ,Ile ⁵ ,His ⁶ -AII	RYPF	99	581.3	582
4	[Ile ⁴ ,His ³]-des-Asp ¹ ,Val ³ -AII	RYHIPF	98	831.4	833
5	des-Asp ¹ ,Arg ² ,Val ³ ,Ile ⁵ -AII	YHPF	99	562.2	563
6	des-Asp ¹ ,Arg ² ,Tyr ⁴ ,His ⁶ -AII	VIPF	99	474.3	475
7	[2-Nal ¹]- des-Asp ¹ ,Arg ² ,Tyr ⁴ ,His ⁶ -AII	(2-Nal)-IPF	97	572.3	574
8	[2-Nal ²]- des-Asp ¹ ,Arg ² ,Tyr ⁴ ,His ⁶ -AII	V-(2-Nal)-PF	99	558.3	559
9	[2-Nal ³]- des-Asp ¹ ,Arg ² ,Tyr ⁴ ,His ⁶ -AII	VI-(2-Nal)-F	97	574.3	575
10	[2-Nal ⁴]- des-Asp ¹ ,Arg ² ,Tyr ⁴ ,His ⁶ -AII	VIP-(2-Nal)	98	523.3	524

^aHPLC profiles were obtained under the following conditions: Column Supelcosil C18 (4.6 x 150 mm), 60 Å, 5 µm; Solvent System: A (0.1% TFA/H₂O) and B (0.1% TFA in 60% ACN/H₂O); Gradient: 5-95% B in 30 minutes; Flow: 1.0 mL/min; λ=220 nm; Injection Volume: 50 µL and Sample Concentration: 1.0 mg/mL. ^bThe masses were determined by LC/ESI-MS using a Micromass instrument (model ZMD) coupled to a Waters Alliance (model 2690) system. Mass measurements were performed in a positive mode with the following parameters: mass range between 300 and 2000 m/z; nitrogen gas flow: 4.1 L/h; capillary: 2.3 kV; cone voltage: 32 V; extractor: 8 V; source heater: 100 °C; solvent heater: 400 °C; ion energy: 1.0 V and multiplier: 800 V.

We observed that all replacements affected peptide 6 integrity. The substitution in a C-terminal extremity decreased peptide-parasite interaction (peptide 9 and peptide 10-70% and 73%, respectively). This behavior was observed by Chamlian, et al [7]. The antiplasmodial activity decreased in comparison to VIPF (analog 6), analog 7 and 8 had activity ≥ 75%.

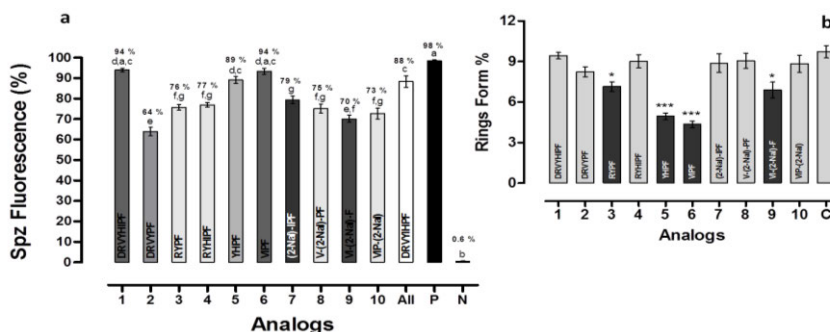


Fig. 1. Peptides activities on *Plasmodium gallinaceum* (a) and *Plasmodium falciparum* (b). (a) Effects of AII analogues on membrane permeability of the mature sporozoites. Data were expressed in mean ± standard deviation of fluorescent sporozoites percentage/blade (n=9). Different letters and colors indicate significant difference between the groups treated with AII. Peptide analogues and positive control group (P, treated with digitonin and PBS) and negative (N, treated with PBS), respectively (ANOVA followed by Tuckey test, $p < 0.05$). (b) The percentage of rings was determined after 24 hours incubation of erythrocyte cultures infected with 2-3% schizonts in the absence (control) or in the presence of 10-8 mol L⁻¹ peptides. * Statistically significant compared with control value $p < 0.05$.

***Statistically significant compared with control value $p < 0.001$. Dark grey shading indicates that the result is statistically significant compared with control. (mean \pm standard deviation, $n=2$).

From the CD studies, peptides that tend to form β -turn conformations present higher interactions with *P. gallinaceum* sporozoites membrane ($>75\%$) [3,4,8,9]. Our results indicate the same characteristics in the peptides studied here.

To verify if some peptides influence the same stage, all peptides were tested *in vitro* on red blood cells infected with *P. falciparum* species. Four peptides presented some activity in the parasite rings form reduction between 27% and 53% (Figure 1b), and this contribution was seen only by ultra-short peptides containing Val, Ile, Pro, Phe, Tyr, Arg and His amino acid residues in their primary sequences. Our results also concur with the Perez-Picaso observations [10].

The results indicate two peptides with antiplasmodial activity in both models: peptide 5 (YHPF), with 89% biological activity against *Plasmodium gallinaceum* sporozoite and 50% against *Plasmodium falciparum* early throphozoite and peptide 6 (VIPF), with 94% against *Plasmodium gallinaceum* and 53% against *Plasmodium falciparum*.

The conformational studies by Circular Dichroism spectra suggested that all the peptides presented β -turn conformation tendency in different solutions except peptide 2 (DRVYPF), which presented an α -helix conformation tendency and presented lower biological activity (63% in *Plasmodium gallinaceum* only – data not shown).

The IC₅₀ values of antiplasmodial activity for peptides 5 and 6 were also obtained and the absence of hemolysis or contractile response was observed (data not shown). In conclusion, when the hydrophobic portion and/or the Arg, Tyr, Pro or Phe residues are present on peptide primary sequence, it increases the antiplasmodial activity. These peptides are promising candidates for *in vivo* testing and offer a new direction for the design of potential antimalarial drugs.

Acknowledgments

Supported by FAPESP.

References

1. Maciel, C., Oliveira, V.X., Fázio, M.A., Nacif-Pimenta, R., Miranda, A., Pimenta, P.F., Capurro, M.L. *PLoS ONE* **3**, e3296 (2008), <http://dx.doi.org/10.1371/journal.pone.0003296>
2. Saraiva, V.B., Silva, L.S., Ferreira-DaSilva, C.T., Silva-Filho, J.L., Teixeira-Ferreira, A., Perales, J., Souza, M.C., Henriques, M.G., Caruso-Neves, C., Pinheiro, A.A.S. *PLoS ONE* **6**, e17174 (2011), <http://dx.doi.org/10.1371/journal.pone.0017174>
3. Ferreira, L., Silva, A., Torres, M., Pedron, C., Capurro, M., Alves, F., Miranda, A., Oliveira, V., Jr., *Int. J. Pep. Res. Therap.* **20**, 553-564 (2014), <http://dx.doi.org/10.1007/s10989-014-9425-9>
4. Silva, A.F., Bastos, E.L., Torres, M.D., Costa-da-Silva, A.L., Ioshino, R.S., Capurro, M.L., Alves, F.L., Miranda, A., de Freitas, Fischer Vieira, R., Oliveira, V.X., Jr. *J. Pept. Sci.* **20**, 640-648 (2014), <http://dx.doi.org/10.1002/psc.2641>
5. Gromiha, M.M. *Biophysical Chemistry* **103**, 251-258 (2003), [http://dx.doi.org/10.1016/S0301-4622\(02\)00318-6](http://dx.doi.org/10.1016/S0301-4622(02)00318-6)
6. Tayubi, I.A., Sethumadhavan, R. *Biochemistry (Mosc)* **75**, 912-918 (2010), <http://dx.doi.org/10.1134/S000629791007014X>
7. Chamlian, M., Bastos, E.L., Maciel, C., Capurro, M.L., Miranda, A., Silva, A.F., Torres, M.D.T., Oliveira, V.X. *J. Pept. Science* **19**, 575-580 (2013), <http://dx.doi.org/10.1002/psc.2534>
8. Torossian Torres, M., Silva, A., Alves, F., Capurro, M., Miranda, A., Oliveira, V., Jr. *Int. J. Pept. Res. Therap.* **20**, 277-287 (2014), <http://dx.doi.org/10.1007/s10989-014-9392-1>
9. Torres, M.D.T., Silva, A.F., Alves, F.L., Capurro, M.L., Miranda, A., Vani, Xavier, O. *Chem. Biol. Drug Design* **85**, 163-171 (2015), <http://dx.doi.org/10.1111/cbdd.12354>
10. Pérez-Picaso, L., Velasco-Bejarano, B., Aguilar-Guadarrama, A.B., Argote-Ramos, R., Rios, M.Y. *Molecules* **14**, 5103-5114 (2009), <http://dx.doi.org/10.3390/molecules14125103>

Antiplasmodial Activity of Angiotensin II Analogs

Danieli Melo de Freitas and Vani Xavier Oliveira Junior

Centro de Ciências Naturais e Humanas, Universidade Federal do ABC, Santo André, 09210-580, Brazil

Introduction

Malaria is an infectious disease caused by parasites of the genus *Plasmodium*. According to the World Health Organization, 584,000 people died of malaria in the world, and 78% of these cases were children under five [1]. Antimalarial compounds have been studied including angiotensin II (AII) with 88% inactivation efficiency towards *P. gallinaceum* parasites [2]. Other authors have studied the importance of each amino acid residue applying the Ala-scan method as well as amino acid deletions of the molecule [3,4].

The malaria cycle in the intermediate host begins with a bite from female mosquitos. Protozoa in the form of sporozoites are present in the salivary gland of the mosquito. These enter the bloodstream and reach the liver cells. The sporozoites begin to divide several times resulting in a large number of parasites in the form of merozoites. The liver merozoites invade red blood cells and initiate the so-called erythrocytic cycle. At this stage, the infected individual has mainly anemia and sporadic fever [5].

Based on this information, the present work proposes an analysis into a better hydrophobic/hydrophilic balance in angiotensin analogs (DRVYIHPF) to increase the antimalarial activity in the sporozoites of *Plasmodium gallinaceum*. This technology increases efficacy without side-effects [6].

Results and Discussion

The peptides were synthesized manually by Fmoc strategy with Wang resin. The amino acid couplings were carried out with a 2.5-fold molar excess of the Fmoc-protected amino acid with DIC/HOBt in DCM/DMF for 2h at room temperature. Peptides were cleaved from the resin in a reaction with 90% TFA, 5% water and 5% anisole comprising a concentration of 10 ml/g of peptidyl resin. At the end of reaction, the peptide was treated with ethyl ether, extracted with 0.1 % TFA/60 % ACN in water and lyophilized. The analogs of thirteen of these were satisfactory, and the resulting peptides had a chromatographic purity higher than 95%; mass characterization by LC/MS-ESI confirmed that the purified peptides were in agreement with the expected theoretical values. The antiplasmodial activity was determined *in vitro* by fluorescence microscopy after 1h of incubation of the parasites with each peptide in the presence of ethidium bromide. The results are reported as percent fluorescent sporozoites. A conformational study of peptides was done with the circular dichroism (CD) technique for peptides in 15 mmol PBS, 10 mmol SDS, 50% MeOH (v/v), and 50% TFE (v/v).

The hydrophobic/hydrophilic balance was studied by replacing the six amino acid residues with amino acids of different polarity. The amino acids proline and arginine were not modified. The antiplasmodial activity was reduced when these amino acids as well as phenylalanine and tyrosine were replaced by Ala. Clearly, these amino acids are important to the structure of the molecule [3]. The amino acid deletion study also showed the importance of proline to antiplasmodial activity of the molecule. The altered sequence had 14% residual activity; the arginine deletion showed an activity of 43% [4]. These studies have shown that any amino acid deletion causes a reduction in activity - this is more pronounced for proline and arginine. The [Arg²]-AII favors electrostatic interactions between the peptide ends [3].

The synthesized analogs had their biological activity tested in sporozoites of *P. gallinaceum*, and the activity was calculated from the total fluorescent sporozoites. The synthetic analogs showed a significant difference in antimalarial activity versus AII.

Replacement of any amino acid in AII decreased antiplasmodial activity. Analogs 1 - [His¹]-AII and 8 - [Asn¹]-AII activities were 35% and 71% of baseline, respectively. This relative decrease may be because AII has a compact folded structure due to the proximity of their amino terminus and carboxy-terminus [7].

Conformational analysis indicates that the angiotensin peptides with a greater antiplasmodial activity form a β structure [8]. Analogs 1 and 8 also had a tendency to form β structures.

Modifications of the analogs 9 - [Lys³], 11 - [Glu³] and 12 - [Ser³] showed decreased activity. The hydrophobic character of valine (the peptide containing the region Asp-Arg-Val) is important to break the plasmodium membrane. AII can interact with the negatively-charged membrane *via* the positively charged *N*-terminal portion [3]. The deletion of valine decreased the antiplasmodial activity by 23% [4]. The decrease in antiplasmodial activity may impede the interaction between the proline and valine in the chain [7]. This promotes the stabilization of the folded conformation of AII as evidenced by the conformational change in the circular dichroism.

Tyrosine plays an important role in the conformation of the molecule forming a hydrophobic cluster isoleucine and histidine. Analog 7 - [Phe⁴]-AII showed an activity of 62%, but there was no difference in conformation. Position 4 is important for peptide activity, and Tyr 4 may expose the guanidine portion of Arg to be an important interaction for the overall peptide activity [3].

Analog 6 [Tyr⁸]-AII 68% activity was statistically equal to 7. The analog position 8 is important for the biological activity of this molecule. It showed a similar difference in conformation. Although a difference has occurred, it was not very pronounced because the change involved two aromatic compounds. These amino acids with aromatic side chains may also play an important role in the peptide structure and its interaction with the membrane.

Analog 4- [Trp⁶]-AII, 5 [Asp⁶]-AII and 13- [Ser⁶]-AII had 40% activity. The conformational study showed that conformational changes occur.

Analog 2- [Arg⁵]-AII, 3- [Ans⁵]-AII and 10- [Asp⁵]-AII showed an activity of 70%, 52%, and 21%. This altered a bulky isoleucine - its substitution may affect the amphipathic properties of the AII because this amino acid is one of the hydrophobic residues in the trainer cluster. The conformational analysis showed that for the three analogs, there was a change in the conformation of the molecule. The substitution of isoleucine by other polar amino acids can prevent the formation of the hydrophobic cluster. It changes the conformation of the molecule and reduces its biological activity. In addition, its side chain interacts with the terminal amino group of aspartic acid [9].

With occasional changes made in the AII structure, we found that these synthesized analogs showed changes in biological activity versus AII. These results allow a better understanding of the importance of each of the residues in AII. The analogs exhibit a reduction in biological activity for all the sequences studied. This highlights the importance of amino acid residues.

Acknowledgments

This research was supported by Coordenação de Aperfeiçoamento de Pessoal de Nível Superior (Capes) and Fundação de Amparo a Pesquisa (FAPESP).

References

1. World Malaria Report. http://www.who.int/malaria/world_malaria_report_2014/worldmalaria_report2014.pdf
2. Maciel, C., Oliveira, V.X. Jr., Fázio, M.A., Nacif-Pimenta. R., Miranda. A., Pimenta, P.F., Capurro, M.L. *PLoS ONE* **3**, e3296, (2008), <http://dx.doi.org/10.1371/journal.pone.0003296>
3. Silva, A.F., Bastos, E.L., Torres, M.T., Costa-da-Silva, A.L., Ioshino, R.S., Capurro, M.L., Alves, F.L., Miranda, A., Freitas, R.F., Oliveira, V. *J. Pept. Science* **2**, 640-648 (2014), <http://dx.doi.org/10.1002/psc.2641>
4. Ferreira, L.H., Silva, A.F., Torres, M.T., Pedron, C.N., Capurro, M.L., Alves, F.L., Miranda, A., Oliveira, V.X. Jr. *Inter. J. Pept. Res. Therap.* **20**, 553-564 (2014), <http://dx.doi.org/10.1007/s10989-014-9425-9>
5. Garcia, L.S. *Clin. Lab. Med.* **30**, 93-129 (2010), <http://dx.doi.org/10.1016/j.cll.2009.10.001>
6. Vukelic, S., Griendling, K.K. *Circ. Res.* **114**, 754-757 (2014), <http://dx.doi.org/10.1161/CIRCRESAHA.114.303045>
7. Tzakos, A.G., Bonvin, A.M.J.J., Troganis, A., Cordopatis, P., Amzel, M.L., Gerothanassis, I.P., Nuland, N.A.J. *Eur. J. Biochem.* 849-860 (2003), <http://dx.doi.org/10.1046/j.1432-1033.2003.03441.x>
8. Greff, D., Fermandjian, S., Fromageot, P., Khosla, M.C., Smeby, R.R., Bumpus, F.M. *Eur. J. Biochem.* **61**, 297-305 (1976), <http://doi/10.1111/j.1432-1033.1976.tb10022.x>
9. Tzakos, A.G., Gerothanassis, I.P., Troganis, A.N. *Curr. Top Med. Chem.* **4**, 431-444 (2004), <http://dx.doi.org/10.2174/1568026043451375>

Effects of Methyl and Halogens in Analgesic Peptide Molecules for Their Potent Agonist Activities at MOR/DOR and Antagonist Activity at NK1R

Aswini Kumar Giri¹, C.R. Apostol¹, P. Davis², D. Rankin², G. Molnar²,
 T.W. Vanderah², F. Porreca², and V.J. Hruby¹

¹Departments of Chemistry and Biochemistry, University of Arizona, Tucson, AZ, 75721, USA;

²Department of Pharmacology, University of Arizona, Tucson, AZ, 85724, USA

Introduction

Treating pain has been always challenging, especially when it becomes chronic in nature. Current drugs (e.g. opioid drugs) cannot treat this problem effectively. In addition, constant use of these drugs has deadly side effects including drowsiness and mental clouding, nausea and emesis, and constipation [1]. Development of analgesic tolerance and hyperalgesia in many patients as the results of taking these drugs are also a serious concern. Overexpression of substance P and its receptor has been observed during prolonged pain states. Studies revealed that co-administration of cocktails of drugs containing μ/δ opioid agonist and NK1 antagonist can provide better analgesic effects in rat model while reducing side effects [2-4]. Herein, we report design, synthesis and SARs of few multifunctional ligands having μ/δ opioid agonist (μ -preferring) and NK1 antagonist activities. The detail of this study has already been communicated to *J. Med. Chem.* for publication [5]. We anticipate that these ligands will show better analgesia while reducing the adverse side effects. Our drug design principle is based on overlapping and adjacent pharmacophores (Figure 1) and we considered our previously published μ -selective (binding) ligand **TY012** (H-Tyr-D-Ala-Gly-Phe-Pro-Leu-Trp-NH-Bn(3',5'-(CF₃)₂)) [6].

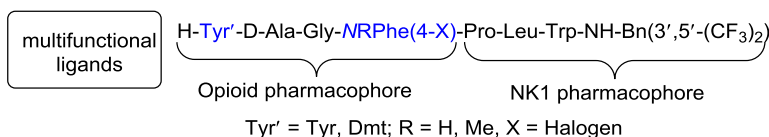


Fig. 1. Design of multifunctional ligands.

Synthesis of the ligands

Linear peptides [Boc-Tyr(^tBu)-(AA)_n-Pro-Leu-Trp(Boc)-OH] were synthesized using Fmoc/^tBu solid phase chemistry on a 2-chlorotrityl resin. The C-terminal carboxylic acid was amidated in solution phase. Removal of all protecting groups followed by purification afforded the pure ligands required for biological study. The ligands we designed and synthesized are given in Figure 2.

AKG117: H-Tyr-D-Ala-Gly-NMePhe-Pro-Leu-Trp-NH-Bn(3',5'-(CF₃)₂)
AKG115: H-Dmt-D-Ala-Gly-NMePhe-Pro-Leu-Trp-NH-Bn(3',5'-(CF₃)₂)
AKG116: H-Dmt-D-Ala-Gly-Phe-Pro-Leu-Trp-NH-Bn(3',5'-(CF₃)₂)
AKG127: H-Dmt-D-Ala-Gly-Phe(4-F)-Pro-Leu-Trp-NH-Bn(3',5'-(CF₃)₂)
AKG128: H-Dmt-D-Ala-Gly-NMePhe(4-F)-Pro-Leu-Trp-NH-Bn(3',5'-(CF₃)₂)
AKG190: H-Tyr-D-Ala-Gly-Phe(4-F)-Pro-Leu-Trp-NH-Bn(3',5'-(CF₃)₂)

Fig. 2. Structures of our multifunctional ligands.

Results and Discussion

The present study was designed to synthesized μ -selective ligands while maintaining the antagonist activity at NK1 receptor. To achieve our goal we considered our previously published μ -selective (binding) ligand **TY012** [6] and structural modification was conducted in the opioid pharmacophore moiety. We introduced Dmt at the 1st position, and NMe-Phe or halogenated-Phe at the 4th position

(Figure 2) to achieve our desired selectivity with high potency at all receptors. **AKG117** having NMe-Phe at 4th position showed a small increase in μ -agonist activity (Table 1). **AKG115** having Dmt at the 1st position and NMe-Phe at the 4th position showed selectivity (both binding and functional) for MOR over DOR (Table 1) while **AKG116** containing Dmt at the 1st position and Phe at the 4th position lacked selectivity in binding assay and displayed higher agonist activity at DOR compared to that at MOR (Table 1). **AKG127** containing Dmt at the 1st position and Phe(4-F) at the 4th position showed no selectivity in binding assay. However, it showed higher agonist activity for DOR compared to that at MOR (Table 1). **AKG128** containing Dmt at the 1st position and NMe-Phe(4-F) at the 4th position showed no improvement in selectivity. Replacement of Dmt with Tyr at the 1st position of **AKG127** produced the ligand **AKG190**, which became selective for DOR over MOR in functional assay (Table 1).

Table 1. Binding affinities of the multivalent ligands at MOR, DOR, and NK1R.

Ligand ID	K_t^μ (nM)	K_t^δ (nM)	K_t^{hNK1} (nM)	IC_{50}^μ (nM) (Agonist)	IC_{50}^δ (nM) (Agonist)	IC_{50}^{NK1} (nM) (Antagonist)
TY012	9.5	72	0.6	350	45	8.5
AKG117	27	260	3.4	230	102	21
AKG115	1	5	2.2	21	31	9.7
AKG116	3	1	1.4	81	3.1	25
AKG127	1	1	0.9	42	2	5.3
AKG128	0.4	4	2.6	77	11	11
AKG190	4	7	5.6	65	12	5.8

For binding studies, each sample was run three times at each receptor except AKG190 which was run for twice at MOR. For functional activity studies, each sample was run four times.

We have designed and synthesized novel multifunctional ligands, which are highly potent at the receptors of our interest with desired activities. Ligand **AKG115** has shown selectivity at MOR over DOR in binding as well as in functional assays. *In vivo* study with this ligand is now in progress to evaluate its analgesic activity.

Acknowledgments

We thank US Public Health Service, National Institute of Health (NIH) for supporting this research (Grant No.: 2P01 DA 006284 & R01 DA 013449). An international patent application has been filed with this discovery.

References

- Giri, A.K., Hruby, V.J. *Expert Opinion on Investigational Drugs* **23**, 227-241 (2014), <http://dx.doi.org/10.1517/13543784.2014.856879>
- Misterek, K., Maszczynska, I., Dorociak, A.; Gumulka, S.W., Carr, D.B., Szyfelbein, S.K. Lipkowski, A.W. *Life Sci.* **54**, 939-944 (1994), [http://dx.doi.org/10.1016/0024-3205\(94\)00494-3](http://dx.doi.org/10.1016/0024-3205(94)00494-3)
- Powell, K.J., Quirion, R., Jhamandas, K. *Eur. J. Neurosci.* **18**, 1572-1583 (2003), <http://dx.doi.org/10.1046/j.1460-9568.2003.02887.x>
- Ripley, T.L., Gadd, C.A., De Felipe, C., Hunt, S.P., Stephens, P.H. *Neuropharmacology* **43**, 1258-1268 (2002), [http://dx.doi.org/10.1016/S0028-3908\(02\)00295-2](http://dx.doi.org/10.1016/S0028-3908(02)00295-2)
- Giri, A.K., Apostol, C.R., Davis, P., Rankin, D., Molnar, G., Olson, K.M., Wang, Y., Forte, B.L., Largent-Milnes, T.M., Vanderah, T.W., Porreca, F., Hruby, V.J. *J. Med. Chem.* (communicated).
- Yamamoto, T., Nair, P., Vagner, J., Largent-Milnes, T.M., Davis, P., Ma, S.-w., Navratilova, E., Moye, S., Tumati, S., Lai, J., Yamamura, H.I., Vanderah, T.W., Porreca, F., Hruby, V.J. *J. Med. Chem.* **51**, 1369-1376 (2008), <http://dx.doi.org/10.1021/jm070332f>

Structure Activity Relationship of Stable Dynorphin A-(2-13) Analogues Interacting at the Bradykinin-2 Receptor

Sara M. Hall¹, Yeon Sun Lee¹, Cyf Nadine Ramos Colón¹, Frank Porreca²,
 Josephine Lai², and Victor J Hruby¹

¹Department of Biochemistry and Chemistry; ²Department of Pharmacology,
 University of Arizona, Tucson, AZ, 85721, USA

Introduction

Neuropathic pain affects 100 million Americans and imposes a significant public health problem. This type of pain results from the dysfunction of the central nervous system (CNS) or the peripheral nervous system (PNS) that can occur in the presence or absence of an initial injury. Some of the current treatments for neuropathic pain involve opioids, non-steroidal anti-inflammatory drugs (NSAIDs), and anticonvulsants, namely gabapentin and pregabalin [1]. Many of these treatments are highly efficacious for acute pain but are not very effective in neuropathic pain and have serious side effects caused by long-term administration. Treatment for this disease is difficult with conventional methods, partly because the mechanism of this disease is not well known.

One target for neuropathic pain treatment may be the blockade of Dynorphin A (Dyn A) (Figure 1). Dyn A, a proteolytic fragment derived from prodynorphin, has both inhibitory and excitatory effects in the spinal cord. The inhibitory effects of Dyn A are thought to act primarily through the opioid receptors, with the *N*-terminal tyrosine being essential for its high affinity and agonist activity. The opioid action of Dyn A is abolished by removing the *N*-terminal tyrosine, as the des-tyrosyl fragments of Dyn A do not bind to the opioid receptors ($IC_{50} > 10 \mu M$) [2]. However, these fragments are biologically active both *in vitro* and *in vivo*, and being neuroexcitatory and neurotoxic, suggest a non-opioid pathway. These des-tyrosyl fragments of Dyn A have been found to bind to the bradykinin 2 receptor (B2R) and cause an influx of calcium [3]. In a chronic pain model, Dyn A was found to be up-regulated and contributes to the maintenance of neuropathic pain [3,4]. Therefore, the development of B2R antagonists can be used to block the agonist actions of Dyn A which may lead to therapeutics for chronic pain.

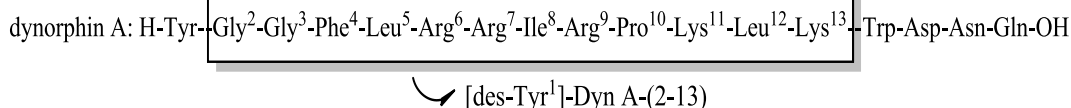


Fig. 1. Structure of Dyn A. Box shows non-opioid fragment, Dyn A-(2-13).

Results and Discussion

Structure Activity Relationship (SAR) of Dyn A Analogues at the B2R

To explore novel therapeutics for neuropathic pain, a SAR study was performed with Dyn A analogues at the B2R in rat brain membranes. It was previously found that **LYS1044** ([des-Arg⁷] Dyn A-(4-11), H-Phe⁴-Leu-Arg-Ile-Arg-Pro-Lys¹¹-OH) ($IC_{50} = 150 \text{ nM}$) is the shortest pharmacophore for binding at the B2R. This ligand was effective *in vivo* by blocking Dyn A-induced hyperalgesia in naïve animals and reversing thermal and tactile hypersensitivities in a dose-dependent manner in nerve injured animals [5]. Although this ligand was efficacious, it is composed of natural amino acids and therefore is susceptible to degradation by peptidases. In an effort to improve the peptide's stability, Dyn A analogues were designed and synthesized. It was found that *N*-terminal acetylation as well as replacement of the non-natural Nle in place of Leu/Ile retained affinity at the B2R ($IC_{50} \sim 150 \text{ nM}$). C-Terminal amidation as well as inverso modifications resulted in a complete loss of affinity at the B2R ($IC_{50} > 10,000 \text{ nM}$). Although a complete reverse of chirality resulted in loss of affinity, a D amino acid scan found that a single substitution of D-Phe⁴, D-Leu⁵, or D-Arg⁶ resulted in a retention of affinity ($IC_{50} \sim 200 \text{ nM}$), whereas substitutions with the D-isomer at other positions resulted in a loss of affinity ($IC_{50} = 800 - 10,000 \text{ nM}$).

Stability Assay of Analogues

To test the stability of the ligands, an *in vitro* stability assay in rat plasma was carried out. As expected, the lead ligand, **LYS1044** was quickly degraded with a $t_{1/2} = 0.7$ hr. Ligands that were substituted with D-isomers near the *N*-terminus and retained affinity at the B2R were found to be much more stable than the parent ligand (Figure 2). In particular **SH146**, was extremely stable ($t_{1/2} = 160$ hr) with 99% of the peptide remaining after 24 hrs. This ligand was substituted with DLeu⁵. The importance of modifications at this position was further confirmed when a ligand with substitution of *N*-methylation Leu⁵ was tested and 99% of the peptide was intact after a 24 hr incubation. Similar results were also found in human plasma.

Conclusions

We have performed an SAR study and have found a lead ligand for the B2Rs as well as ligands that were modified for stability. A ligand modified at Leu⁵ was found to be more stable than the parent ligand ($t_{1/2} = 0.7$ hr vs 16 hr) and was also found to be non-toxic in an *in vitro* cell assay. Further studies will be carried out to test the ligand's effectiveness as an analgesic.

Acknowledgments

We thank Andy Ambrose, Robert Kupp, and Lindsay Lebaron for their help in synthesis and bioassay of ligands. Supported by grants from the U.S. Public Health Services, NIH, and NIDA (P01DA006248). We also thank APS and the GPSC at the University of Arizona for their support in attending the conference.

References

1. Chavkin, C., Goldstein, A. *Science* **215**, 413 (1982), <http://dx.doi.org/10.1126/science.6120570>
2. Lai, J., Luo, M.C., Chen, Q.M., Ma, S.W., Gardell, L.R., Ossipov, M.H., Porreca, F. *Nature Neuroscience* **9**, 1534-1540 (2006), <http://dx.doi.org/10.1038/nn1804>
3. Luo, M.C., Chen, Q.M., Ossipov, M.H., Rankin, D.R., Porreca, F., Lai, J. *J. Pain* **9**, 1096-1105 (2008), <http://dx.doi.org/10.1016/j.jpain.2008.06.005>
4. Lee, Y.S., Muthu, D., Hall, S.M., et al. *J. Am. Chem. Soc.* **136**, 6608-6616 (2014), <http://dx.doi.org/10.1021/ja501677q>

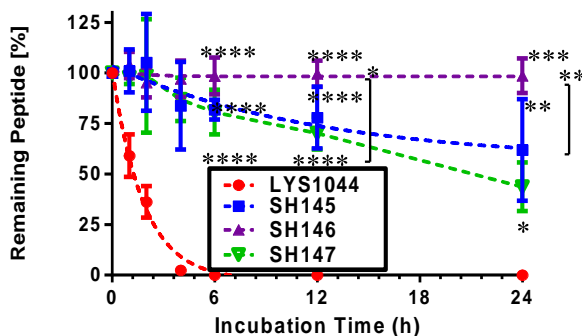


Fig. 2. Stability assay in rat plasma. **LYS1044**, the lead ligand, had a short $t_{1/2}$ whereas substitution with D-isomer (**SH145-Sh147**) lead to large increases in stability.

Structure-Activity Relationships of Constrained Dermorphin Analogues Containing an α -Alkyl- β -Substituted Alanines

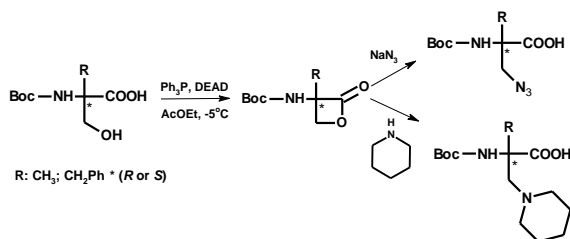
Anika Lasota¹, Oliwia Frączak¹, Adriana Muchowska², Aleksandra Misicka²,
 Michał Nowakowski³, Maciej Maciejczyk⁴, Andrzej Ejchart⁵,
 and Aleksandra Olma¹

¹Institute of Organic Chemistry, Lodz University of Technology, Zeromskiego, 116,90-924, Lodz; ²Mossakowski Medical Research Centre, Polish Academy of Sciences, Pawinskiego 5, 01-793, Warsaw; ³Centre of New Technologies, University of Warsaw, Zwirki i Wigury 93, 02-089, Warsaw; ⁴Chair of Physics and Biophysics, University of Warmia and Mazury ul. Oczapowskiego 4, 10-719, Olsztyn; ⁵Institute of Biochemistry and Biophysics, Polish Academy of Sciences, Pawinskiego 5A, 02-106, Warsaw, Poland

Introduction

Narcotic analgesics produce pain relief through the activation of μ -opioid receptors (MOR), but the use of these drugs is limited by their side effects. Endogenous opioid peptides have been studied since their discovery with a view to developing effective analgesics. Dermorphin, an opioid heptapeptide (Tyr-(*R*)-Ala-Phe-Gly-Tyr-Pro-Ser-NH₂) isolated from the skin of a South American frog, shows remarkably high μ selectivity and an extremely potent antinociceptive effect [1]. To understand the interactions between MOR ligands and the receptor, more than 100 dermorphin analogues have been synthesized and their structure-activity relationships have been investigated. The use of peptides as drugs is restricted because of their rapid biodegradation and low selectivity connected to high conformational freedom. These disadvantageous properties can be remedied by the synthesis of peptidomimetics, which are biologically active compounds with high selectivity and long half-lives. Non-coded amino acids offer a convenient tool for the modification of bioactive peptides and for conformational studies as they can be used to induce certain conformations. In these applications, of particular importance are α,α -disubstituted glycines. This work reports the synthesis and receptor binding of dermorphin analogues containing (*R*) or (*S*)- α -alkyl- β -(azido, 1-piperidiny)alanines at position 2 or 3 (Figure 1).

Results and Discussion



Scheme 1. Synthesis of α -alkyl- β -(azido, 1-piperidiny)alanines.

An efficient method of synthesizing multifunctional α,α -disubstituted glycines from easily accessible α -alkylserines has been developed by our research team [2]. Racemic *N*-Boc- α -alkylserine has been resolved by fractional crystallization of diastereoisomeric salts with (-)-ephedrine. The cyclization of (*R*) or (*S*)-Boc- α -alkylserines under Mitsunobu conditions leads to the corresponding β -lactones in high yields. The ring opening of *N*-protected (*R*) or (*S*) α -alkylserine β -lactones

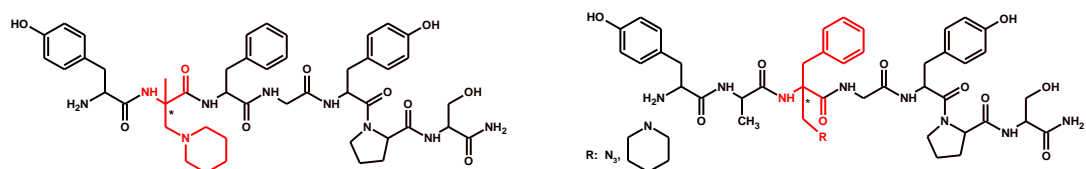
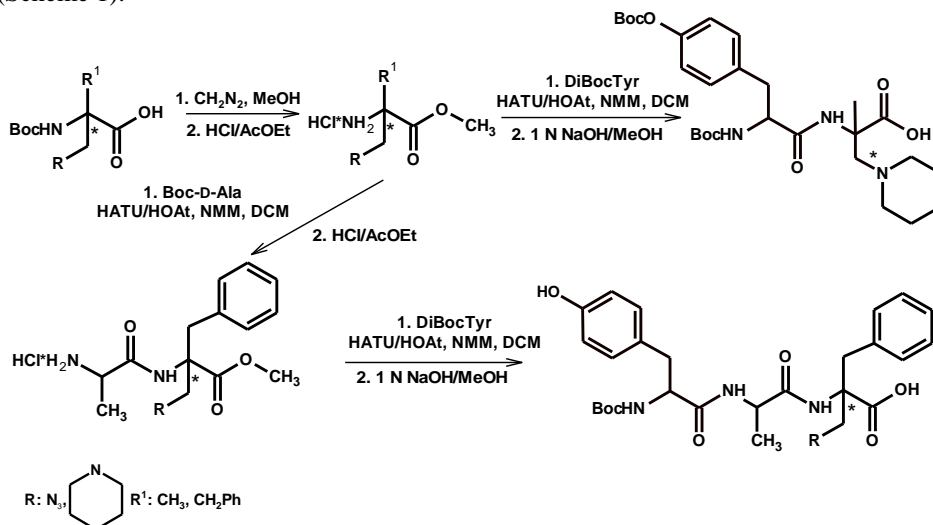


Fig. 1. Primary structures of synthesized dermorphin analogues modified at position 2 or 3 with (*R*) or (*S*)- α -alkyl- β -(1-piperidiny)alanines.

with sodium azide or piperidine as a nucleophile gives a variety of unnatural α , β -disubstituted amino acids (Scheme 1).



Scheme 2. Synthesis of di- and tripeptides containing (R) or (S) α -alkyl- β -azido(1-piperidinyl)alanine.

Our preliminary experiments showed that the classic (step-by-step) synthesis of deltorphin I containing α -methyl- β -azidoalanine on solid phase using the Boc strategy was not effective. The inability to control a critical stage (the acylation of the α , α -disubstituted amino group in the amino acid) forced us to change the strategy of synthesis. We decided to synthesize dipeptides and tripeptides containing α , α -disubstituted amino acids in solution (Scheme 2), using reagents for difficult couplings (HATU/HOAt). The *N,O*-protected di(tri)peptides were used for the acylation of penta(tetra)peptides (Gly-Tyr-Pro-Ser-NH₂, Phe-Gly-Tyr-Pro-Ser-NH₂) in manual solid-phase peptide synthesis (SPPS). The crude peptides were purified by RP-HPLC. The purity of the final TFA salts was assessed by analytical HPLC (purity 97%-99%) and ESI-MS. The new analogues of dermorphin were tested for selectivity and affinity to δ - and μ -opioid receptors in a standard displacement test on receptors in rat brain homogenates (Table 1). It was found that the introduction of (*R* or *S*)- α -methyl- β -(1-piperidinyl)alanines at position 2 in DERM causes a significant decrease of activity. The effect of substituting Phe³ with α -benzyl- β -azido(or 1-piperidinyl)alanines in dermorphin depends on the chirality of the amino acid. The incorporation of (*R*) enantiomers results in analogues with higher selectivity and affinity to opioid receptors (**I** and **III**), whereas analogues with the (*S*) configuration are less potent (**II** and **IV**). This can be explained by analogy between (*R*)- α -benzyl- β -azido(or 1-piperidinyl)alanines and (*S*) phenylalanine, which have the same steric orientation of the aromatic ring. The incorporation of (*R*)- α -benzyl- β -azidoalanine at position 3 in dermorphin gives an active analogue with μ selectivity, but with moderate affinity to the δ -receptor.

NMR experiments were conducted with the two most biologically active analogues modified with α -benzyl- β -(*R* and *S*)-azidoalanines (**I** and **II**). The nuclear Overhauser effect (NOE) has become the method of choice in studying conformations of organic and biological molecules. Short linear peptides are usually characterized by high structural flexibility. Therefore, long range correlations in their NOESY/ROESY spectra have been seldom observed. Nevertheless, one could expect increased conformational rigidity in peptides containing α , α -disubstituted amino acid residues. In order to explain this issue, an NMR study was carried out for the dermorphin analogue containing (*R*)- α -benzyl- β -azidoalanine (**I**) and its diastereoisomer modified with (*S*)- α -benzyl- β -azidoalanine (**II**). An initial analysis of the spectrum revealed two distinct sets of signals due to *cis:trans* isomerization of the Tyr⁵-Pro⁶ amide bond in 1:4 ratio. The distinction between *cis:trans* isomers was based on C γ and C δ chemical shifts and the relative intensity of the signals (Table 2).

Table 1. Binding affinities of new dermorphin analogues to δ - and μ -opioid receptors.

PEPTIDE	IC ₅₀ (nM)		
	μ^a	δ^b	Select.
Tyr-(R)-Ala-Phe-Gly-Tyr-Pro-Ser-NH ₂ (dermorphin) [3]	1.22	178.6 ^c	146
Tyr-(R)-Ala-(R)- α -benzyl- β -azidoAla-Gly-Tyr-Pro-Ser-NH ₂ [4] (I)	4.29	22.6	5.27
Tyr-(R)-Ala-(S)- α -benzyl- β -azidoAla-Gly-Tyr-Pro-Ser-NH ₂ [4] (II)	151	1057	7
Tyr-(R)-Ala-(R)- α -benzyl- β -(1-piperidinyl)Ala-Gly-Tyr-Pro-Ser-NH ₂ (III)	52.48	>10000	>191
Tyr-(R)-Ala-(S)- α -benzyl- β -(1-piperidinyl)Ala-Gly-Tyr-Pro-Ser-NH ₂ (IV)	208.9	>10000	>48
Tyr-(R)- α -methyl- β -(1-piperidinyl)Ala-Phe-Gly-Tyr-Pro-Ser-NH ₂ (V)	204.2	>10000	>52
Tyr-(S)- α -methyl- β -(1-piperidinyl)Ala-Phe-Gly-Tyr-Pro-Ser-NH ₂ (VI)	>10000	>10000	-

^aversus [³H]DAMGO, ^bversus [³H]DELT, ^cversus DADLE.

Table 2. ¹H and ¹³C chemical shifts (in ppm) of Tyr-(R)-Ala-(S and R)- α -benzyl- β -azidoAla-Phe-Asp-Val-Val-Gly-NH₂ (Aaa= α -benzyl- β -azidoalanine).

AA	HN	H α	H β	H γ	H δ	H ϵ	H ζ	C α	C β	C γ	C δ	C ϵ	C ζ
Tyr ¹ S			3.057	---	7.112	6.869	---	n.a.	n.a.	n.a.	133.44	118.65	n.a.
R	n.a.	4.087	3.120	---	7.108	6.867	---	57.54	38.91	n.a.	133.43	118.62	n.a.
	n.a.	4.090	3.071										
			3.123										
Ala ² S		4.251	1.161	---	---	---	---	52.36	19.09	---	---	---	---
R	8.413	4.277	1.176	---	---	---	---	52.33	n.a.	---	---	---	---
	8.364												
Aaa ³ S		benzyl	3.093	---	7.087	7.322	7.321	benzyl	40.72	n.a.	132.98	131.30	130.45
	8.825	CH ₂ N ₃	3.262	---	---	---	---	CH ₂ N ₃	54.93	---	---	---	---
			3.613	---	7.085	7.313	7.313	benzyl	40.71	n.a.	133.01	131.26	130.40
R		benzyl	3.659	---	---	---	---	CH ₂ N ₃	54.37	---	---	---	---
	8.360	CH ₂ N ₃	3.112										
			3.202										
			3.647										
			3.768										
Gly ⁴ S		3.707	---	---	---	---	---	45.24	---	---	---	---	---
R	8.291	3.897	---	---	---	---	---	45.33	---	---	---	---	---
	8.306	3.741											
		3.866											
Tyr ⁵ S		4.844	2.891	---	7.128	6.820	---	n.a.	n.a.	---	133.44	118.25	---
R	7.806	n.a.	3.055	---	7.147	6.812	---	n.a.	38.28	---	133.32	118.38	---
	7.890		2.854										
			3.089										
Pro ⁶ S	---	4.426	1.952	1.983	3.547	---	---	n.a.t;	32.03t;	27.27t;	50.63	---	---
R	---	4.447	2.259	1.977	3.755	---	---	62.81c	34.20c	24.67c	50.57	---	---
			1.959		3.543			n.a.	32.02t;	27.32t;			
			2.255		3.742				33.98c	24.54c			
Ser ⁷ S		4.338	3.808	---	---	---	---	58.35	64.00	---	---	---	---
R	8.243	4.343	3.838	---	---	---	---	n.a.	63.93	---	---	---	---
	8.252		3.821										
			3.845										
NH ₂ S	7.137	---	---	---	---	---	---						
R	7.529	---	---	---	---	---	---						
	7.131												
	7.520												

Nearly complete assignment of ¹H and proton-bearing ¹³C nuclei in the *trans* form of dermorphin analogues was obtained from TOCSY, ROESY and ¹H/¹³C HSQC spectra. NMR-based structural studies of Tyr-(R)-Ala-(S and R)- α -benzyl- β -azidoAla-Phe-Asp-Val-Val-Gly-NH₂ will be continued.

The presented results demonstrate that (R)- α -benzyl- β -azido(1-piperidinyl)alanine can be used as a successful tool for modulating the affinity and selectivity of peptide ligands.

Acknowledgments

This research was supported by the National Science Centre (NCN, Poland), grant Preludium 2 (2011/03/N/ST5/04701).

References

1. Erspamer, V. *Int. J. Dev. Neurosci.* **10**, 3-30 (1992), [http://dx.doi.org/10.1016/0736-5748\(92\)90003-I](http://dx.doi.org/10.1016/0736-5748(92)90003-I)
2. Olma, A., et al. *Amino Acids* **42**, 2525-2528 (2012), <http://dx.doi.org/10.1007/s00726-011-1055-3>; Kudaj, A., Olma, A. *Tetrahedron Lett.* **48**, 6794-6797 (2007), <http://dx.doi.org/10.1016/j.tetlet.2007.07.078>
3. Lazarus, L., et al. *J. Biol. Chem.* **264**, 354-362 (1989).
4. Lasota, A., et al. *J. Pept. Sci.* **20**(S1), 171 Abstract P096 (2014).

Dimeric Dermorphin Analogues Containing β^3 -*homo*-Amino Acids: Synthesis, Binding Affinities and Metabolic Stability

Oliwia Frączak¹, Anika Lasota¹, Adriana Muchowska², Piotr Kosson²,
 Dagmara Tymecka³, Aleksandra Misicka^{2,3} and Aleksandra Olma¹

¹Institute of Organic Chemistry, Lodz University of Technology, Zeromskiego 116, Lodz 90-924, Poland;

²Mossakowski Medical Research Centre, Polish Academy of Sciences, Pawlinskiego 5, Warsaw 01-793, Poland;

³Faculty of Chemistry, University of Warsaw, Pasteura 1, Warsaw 02-093, Poland

Introduction

Opioids are widely used for the treatment of moderate to severe chronic pain, although they exhibit a large number of side effects. There are three major types of opioid receptors: μ (MOR), δ (DOR), and κ (KOR). The main target for analgesia is the MOR. Opioid receptors can form homo- and heterodimers. Specially designed ligands capable of penetrating the BBB are used to study the physiological consequences of opioid receptor homo- and heterodimerization, and are also applied as new analgesics.

Dermorphin (Tyr-D-Ala-Phe-Gly-Tyr-Pro-Ser-NH₂) is a heptapeptide first isolated from the skin of South American frogs of the genus *Phyllomedusa* [1]. The peptide is a natural opioid that binds as an agonist to the μ opioid receptor with high potency and selectivity. Dermorphin is about 30-40 times more potent than morphine but is theoretically less likely to produce drug tolerance and addiction, due to its high potency [2].

Dimeric dermorphin analogues linked by a bridge of varying length were described by Lazarus, et al. [3]. Several dimeric dermorphin pentapeptides connected “tail-to-tail” by a hydrazine bridge exhibit higher μ -affinities than either dermorphin or DAGO. The most active in this series is (Tyr-D-Ala-Phe-Gly-Tyr-NH)₂.

In the present study, we designed and synthesized a new dimeric dermorphin pentapeptides containing β^3 -*homo*-amino acids. The synthesis of α/β hybrid peptides, containing homologated proteinogenic amino acids is a useful tool in drug design. Various β^3 -*homo*-amino acids have been used in the design of several classes of ligands, including opioid peptides [4]. The incorporation of β^3 -*homo*-phenylalanine or its analogues at the 4,4' positions of biphalin resulted in good opioid receptor affinities and antinociceptive activity [5].

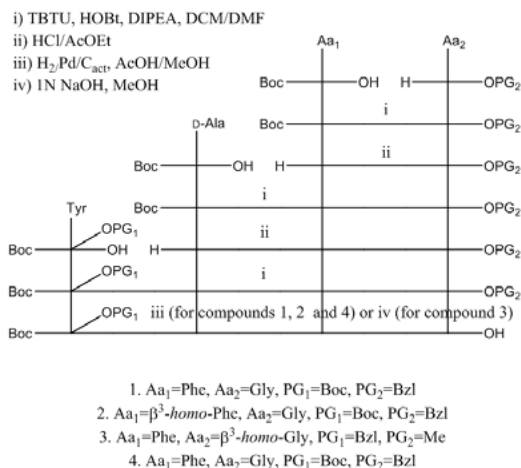


Fig. 1. Synthesis of *N,O*-protected tetrapeptides.

Results and Discussion

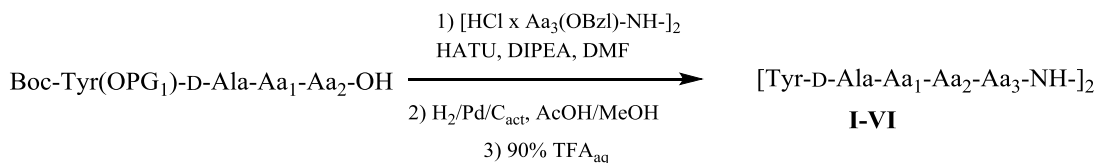
Enantiomerically pure, protected β^3 -*homo*-amino acids were synthesized from protected proteinogenic α -amino acids in two-step Arndt–Eistert homologation. Dimeric dermorphin analogs I–V were synthesized using a convergent synthetic strategy (Figure 2). The tetrapeptide precursors were obtained by stepwise elongation starting from glycine methyl or benzyl ester (Figure 1). *N*-Protected bridged dimers were synthesized by one-pot cross-coupling reaction of hydrazine, Boc- α - or β^3 -*homo*-Tyr(Bzl) and TBTU/HOBt/DIPEA in DMF. Cross-coupling reactions were conducted between *N*-unprotected bridged dimers and appropriate tetrapeptides to yield the corresponding *N,O*-protected dimeric dermorphin analogs. After deprotection, the crude peptides were purified on a preparative RP-HPLC column. The purity of the final TFA salts of analogs I–V was assessed by analytical RP-HPLC and FAB-MS.

Table 1. Biological activity of dimeric dermorphin analogues.

	Peptide	IC50 (nM)		δ/μ
		μ vs DAMGO	δ vs DELT	
	Dermorphin	1.22±0.13 [3]	178.6±18 [3]	146.4
I	(Tyr-D-Ala-Phe-Gly-Tyr-NH) ₂	0.243±0.005 0.27±0.04 [3]	8.754±0.26 7.88±0.07 [3]	36.0 29.2
II	(Tyr-D-Ala-β ³ - <i>h</i> -Phe-Gly-Tyr-NH) ₂	18.20 ± 0.43	203.7 ± 9.4	11.2
III	(Tyr-D-Ala-Phe-β ³ - <i>h</i> -Gly-Tyr-NH) ₂	3.543 ± 0.169	85.34 ± 1.83	24.1
IV	(Tyr-D-Ala-Phe-Gly-β ³ - <i>h</i> -Tyr-NH) ₂	0.302 ± 0.006	20.55 ± 1.22	68.0
V	(Tyr-D-Ala-β ³ - <i>h</i> -Phe-Gly-β ³ - <i>h</i> -Tyr-NH) ₂	11.2 ± 0.68	>10000	-
VI	(Tyr-D-Ala-Phe-β ³ - <i>h</i> -Gly-β ³ - <i>h</i> -Tyr-NH) ₂	40.7 ± 2.9	645 ± 45.8	15.8

The new dermorphin analogues were tested for selectivity and affinity to μ - and δ -opioid receptors. Binding affinities to μ - and δ -opioid receptors were determined by displacing [³H]-DAMGO and [³H]-DELT in standard displacement tests on receptors in rat brain homogenates. The results are shown in Table 1. Peptides **I** and **IV** are the most active and show higher affinity for MOR and DOR than dermorphin. The introduction of two additional methylene groups at positions 5,5' is well tolerated. On the other hand, the presence of four additional methylene groups (**V**, **VI**) leads to a mild reduction of affinity to MOR and a significant reduction of affinity for DOR.

The stability of peptides is important if a drug candidate is to be considered for therapeutic use. Compounds **I** and **IV**, the two most active peptides in the series, were selected for a study of their stability in human serum (Figure 3). The activity of the serum was tested on endomorphin-2. Z-Val was used as an internal standard. EM-2 underwent degradation in just 20 minutes. Stability studies of peptides **I** and **IV** were done in triplicate to ascertain accuracy. Both analogues are highly stable in human serum, but the peptide containing β³-*h*-Tyr at positions 5,5' (**IV**) is extremely stable over 96 h.



I Aa₁=Phe, Aa₂=Gly, Aa₃=Tyr

II Aa₁=β³-*homo*-Phe, Aa₂=Gly, Aa₃=Tyr

III Aa₁=Phe, Aa₂=β³-*homo*-Gly, Aa₃=Tyr

IV Aa₁=Phe, Aa₂=Gly, Aa₃=β³-*homo*-Tyr

V Aa₁=β³-*homo*-Phe, Aa₂=Gly, Aa₃=β³-*homo*-Tyr

VI Aa₁=Phe, Aa₂=β³-*homo*-Gly, Aa₃=β³-*homo*-Tyr

Fig. 2. Synthesis of dimeric dermorphin analogs.

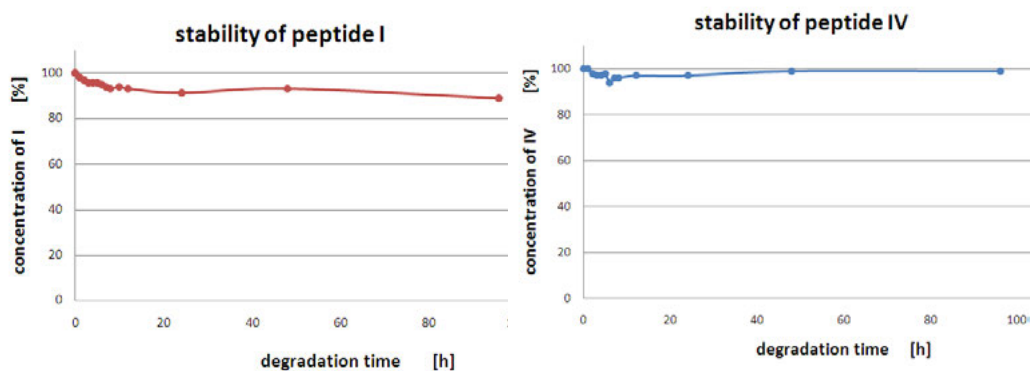


Fig. 3. The stability of peptide I and IV in human serum.

Acknowledgments

This research was supported by: Young Scientists' Fund No W-3/FMN/5G/2014 at the Faculty of Chemistry, Lodz University of Technology (Poland) and Scholarship No RNB/WFS/19/2014 from Internal Scholarship Fund at the Lodz University of Technology (Poland).

References

1. Melchiorri, P., et al. *Gen. Pharmacol.* **27**, 1099-1107 (1996), [http://dx.doi.org/10.1016/0306-3623\(95\)02149-3](http://dx.doi.org/10.1016/0306-3623(95)02149-3)
2. Broccardo, M., et al. *Br. J. Pharmacol.* **73**, 625-631 (1981), <http://dx.doi.org/10.1111/j.1476-5381.1981.tb16797.x>
3. Lazarus, L., et al. *J. Biol. Chem.* **264**, 354-362 (1989), PMID:2563375
4. For example see: Wilczyńska, D., et al. *J. Pept. Sci.* **15**, 777-782 (2009), <http://dx.doi.org/10.1002/psc.1175>; Podwysocka, D., et al. *J. Pept. Sci.* **18**, 556-559 (2012), <http://dx.doi.org/10.1002/psc.2433>
5. Frączak, O., et al. *Peptides* **66**, 13-18 (2015), <http://dx.doi.org/10.1016/j.peptides.2015.02.004>; Mollica, A., et al. *J. Med. Chem.* **56**, 3419-3423 (2013), <http://dx.doi.org/10.1021/jm301456c>

Amphipathic Non-opioid Dynorphin A Analogs to Inhibit Neuroexcitatory Effects at Central Bradykinin Receptors

Yeon Sun Lee¹, Sara M. Hall¹, Cyf Lamos-Colon¹, Michael Remesic¹,
Alexander Kuzmin¹, David Rankin², Todd W. Vanderah², Frank Porreca²,
Josephine Lai², and Victor J. Hruby¹

¹Department of Chemistry and Biochemistry; ²Department of Pharmacology,
University of Arizona, Tucson, AZ, 85721, USA

Introduction

Nerve injury and inflammation cause up-regulation of dynorphin A (Dyn A, H-Tyr¹-Gly-Gly-Phe-Leu-Arg-Arg-Ile-Arg-Pro-Lys-Leu-Lys-Trp-Asp-Asn-Gln¹⁷-OH) in the spinal cord, which results in hyperalgesia *via* the interaction with bradykinin receptors (BRs) [1]. This is a non-opioid neuroexcitatory effect that cannot be blocked by an opioid antagonist, naloxone. On the basis of the fact, systematic structure-activity relationship study on Dyn A was performed to develop BRs antagonists that can block the hyperalgesia. As a result, **LYS1044**, [des-Arg⁷]-Dyn A-(4-11), was identified as a lead ligand along with key insights into structural features for the BRs recognition (i.e. amphipathicity) [2-4]. Intrathecal administration of the lead ligand reversed thermal hyperalgesia and mechanical hypersensitivity in nerve injured animals and inhibited non-opioid Dyn A-induced motor impairment and hyperalgesia in naïve animals. Yet, this ligand showed very low metabolic stabilities in plasma and was completely degraded within 4 hours of incubation (half-life < 1 hour). Therefore, in an effort to improve the metabolic stability and also to enhance the blood brain barrier permeability, various modifications were performed on Dyn A structure. Here we report design and synthesis of cyclic Dyn A analogues and their biological activities.

Results and Discussion

To utilize potential advantages of cyclic peptide ligands, we first designed and synthesized two carba Dyn A analogues (**ML72-4** and **ML72-5**), which contain a 17-membered ring (Figure 1). In these structures, three Lys residues were allocated to position the side amino groups exposed but two hydrophobic amino acid residues were consumed for the cyclization, since positive charges were considered to play an important role in the BRs recognition. These two analogues lost binding affinities at the receptors (IC₅₀ > 10,000 nM), which suggests that 17-membered ring may be too small or hydrophobic residues are also necessary to retain amphipathicity for the BRs. Therefore, to conserve the amphipathicity by exposing the hydrophobic alkyl chain together with positive charges, we designed cyclic Dyn A analogues (17- or 20-membered ring) in which the Pro moiety of **LYS1044** is involved in a cyclization with the *N*-terminus (Figure 2). The main consideration in our design was to enhance the turn structure around the Pro residue and to expose positive charges and hydrophobic groups properly for the ligand amphipathicity.

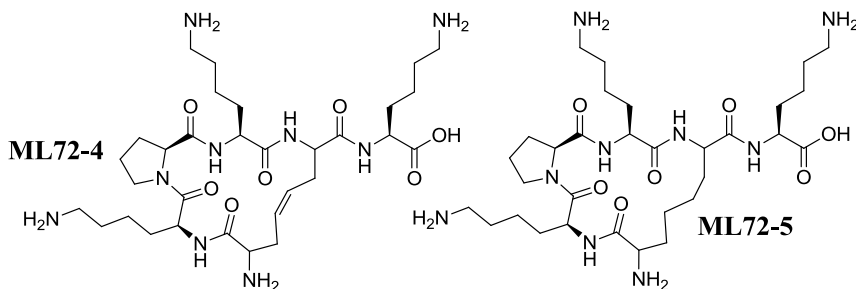


Fig. 1. Structures of Carba Dyn A Ligands.

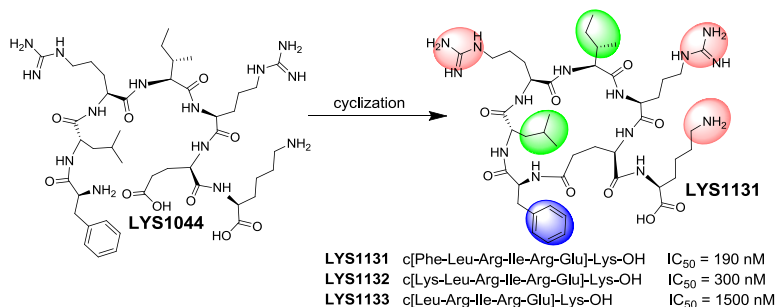


Fig. 2. Binding affinities of cyclic Dyn A analogues at BRs. Radioligand competition assays were carried out at pH 6.8 using [³H]Bradykinin in rat brain membranes.

Cyclic Dyn A analogues (**LYS1131**, **LYS1132**, and **LYS1133**) were synthesized by solid phase synthesis using Fmoc-chemistry with Pip, Pbf, and Boc group as a side protecting group for Glu, Arg, and Lys, respectively, on Fmoc-Lys(Boc)-attached Wang resin. Couplings were carried out with 3 equiv HBTU / 3 equiv HOBt / 6 equiv DIPEA for 50 min and *N*^α-Fmoc groups were deprotected by 20% piperidine in DMF for 20 min. After chain elongations, Pip groups on Glu residues were deprotected by 5% TFA for 5 min 3 times and the resulting acids were consumed for a cyclization with a *N*^α-amino group using 5 equiv DIC / 5 equiv HOBt for 3 hours. The cyclic analogues were cleaved by a cocktail solution containing 90% TFA, 5% thioanisole, 3% EDT, and 2% anisole and purified by RP-HPLC to afford more than 95% pure cyclic Dyn A analogues. Binding affinities of cyclic Dyn A analogues were determined by radioligand competition analysis using [³H]Bradykinin in rat brain membranes. Data was analyzed by nonlinear least-squares analysis using GraphPad Prism 4 and IC₅₀ values were determined from nonlinear regression analysis of data collected from three independent experiments.

Ligand **LYS1131**, which contains a 20-membered ring, retained the same range of binding affinity (IC₅₀ = 190 nM) for BRs as **LYS1044** (IC₅₀ = 97 nM). Ligand **LYS1132** with the same size ring as **LYS1131** also showed the same range of affinity (IC₅₀ = 300 nM) for the BRs. Even with the slight loss of affinities, it is clear that the cyclization between Pro residue position and the *N*-terminus is well tolerated for the receptor. Ligand **LYS1133** which contains a 17-membered ring, decreased affinity (IC₅₀ = 1500 nM), but showed better affinity than two carba cyclic analogues **ML72-4** and **ML72-5**. This SAR results indicate that hydrophobic residues play a role in the BRs recognition, too. Taken together, it is suggested that 20-membered ring and amphipathicity are key structural features of cyclic Dyn A analogues for the BRs recognition.

Acknowledgments

Supported by grants from the U.S.Public Health Services, NIH, and NIDA (P01DA006248).

References

1. Lai, J., Luo, M., et al. *Nat. Neurosci.* **9**, 1534-1540 (2006), <http://dx.doi.org/10.14800/rci.517>
2. Lee, Y.S., Muthu, D., et al. *J. Am. Chem. Soc.* **136**, 6608-6616 (2014), <http://dx.doi.org/10.1021/ja501677q>
3. Lee, Y.S., Rankin, D., et al. *Bioorg. Med. Chem. Letts.* **24**, 4976-4979 (2014), <http://dx.doi.org/10.1016/j.bmcl.2014.09.033>
4. Lee, Y.S., Hall, S.M., et al. *Bioorg. Med. Chem. Letts.* **25**, 30-33 (2015), <http://dx.doi.org/10.1016/j.bmcl.2014.11.026>

***Bauhinia bauhinioides* Kallikrein Inhibitor Fragments with Bradykinin-Like Activities**

Flavio A. Lopes¹, Jones M. Silva¹, Maria Luiza V. Oliva², and Antonio Miranda¹

¹Department of Biophysics and ²Department of Biochemistry, Federal University of São Paulo, São Paulo, SP, 04044-020, Brazil

Introduction

Medicinal plants extracts contain many proteinase inhibitors that could be an interesting source of new drugs. Structural modifications in some of this kind of macromolecule could also lead to compounds with interesting biological properties [1]. In this work, we studied one peptide fragment (BbKI₅₁₋₆₂) of *Bauhinia bauhinioides* kallikrein inhibitor (BbKI) [2,3] and its analogue (P₂) that was designed by the insertion of a proline residue in order to mimic the *N*-terminal region of the bradykinin (BK) molecule. Both retro inverse counterparts Ri-BbKI₅₁₋₆₂ and Ri-P₂ were also included. We evaluated the capability of the peptides to induce contraction on stomach fundus of mouse as well as their capability to induce calcium release from guinea pig ileum cell culture. Both biological effects induced by the fragments were compared with the ones caused by BK.

Results and Discussion

Peptides (Table 1) were manually synthesized by using the Boc-strategy [4]. After RP-HPLC purification, they were characterized by LC-ESI-MS. Stomach fundus was isolated from mouse and mounted into organ bath containing modified Krebs-Ringer solution at 37°C (pH 7.4). The maximal effect was obtained from comparison of contractile responses induced by carbachol 10⁻⁶ M (Figure 1A). Calcium release was determined by Fluo-4 dye. Fluorescence was determined by a FlexStation 3 System (Molecular Devices) (Figure 1B). Peptides resistance to degradation by enzymes presents on human blood were also evaluated (data not shown). Conformational studies by Circular Dichroism in different environments were performed (data not shown). The full results of this study is presented elsewhere [5].

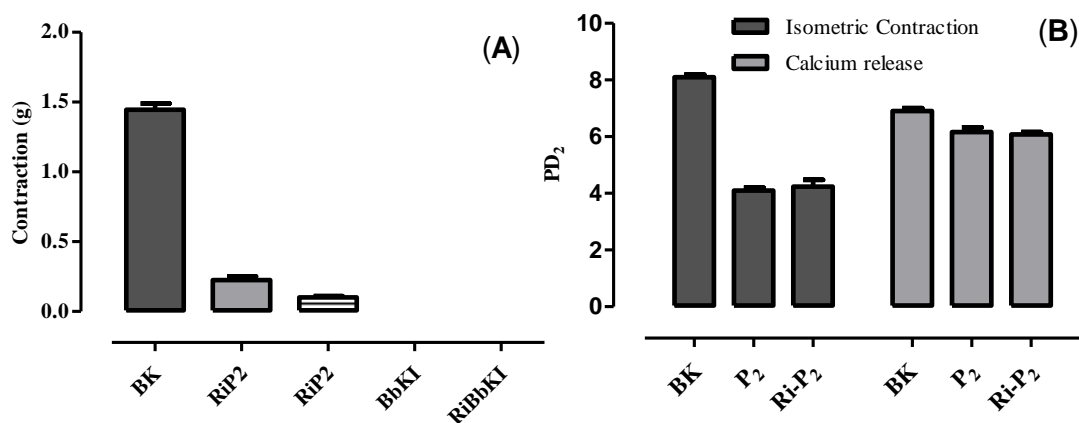


Fig. 1. Isometric contraction induced by BK and BbKI related fragments with maximum contraction at 10⁻⁵ M concentration (A) and their corresponding pD₂ values for isometric contraction and calcium release (B).

Table 1. BbKI related peptide fragments studied.

Name	Sequence ^a
BK	R-P-P-G-F-S-P-F-R
BbKI ₅₁₋₆₂	R-P-G-L-P-V-R-F-E-S-P-L-NH ₂
Ri-BbKI ₅₁₋₆₂	l-p-s-e-f-r-v-p-l-g-p-r-NH ₂
P ₂	R-P-P-G-L-P-V-R-S-F-S-P-L-R-NH ₂
Ri-P ₂	r-l-p-s-f-s-r-v-p-l-g-p-p-r-NH ₂

^asmall letters correspond to D-amino acids.

Neither BbKI₅₁₋₆₂ nor Ri-BbKI₅₁₋₆₂ presented bradykinin-like activity, but as expected, the retro-inverso compound was resistant to the enzymes presented in the blood plasma. P₂ and Ri-P₂ were able to induce a contractile response on gastric smooth muscle, maybe acting via B2 BK-receptor activation. P₂ and Ri-P₂ also produce calcium release from Guinea pig ileum muscle cells in a similar way than BK. Circular Dichroism conformational studies did not show a direct correlation between the biological effects and the peptides structure since all compounds presented a CD profile of disordered conformations.

Acknowledgments

This work was supported by grants and fellowships from CNPq and FAPESP.

References

1. Oliva, M.L.V., et al. *Current Protein & Peptide Science* **12**, 348-357 (2011), <http://dx.doi.org/10.2174/138920311796391061>
2. Oliva, M.L.V., et al. *Immunopharmacology* **45**, 163-169 (1999), [http://dx.doi.org/10.1016/S0162-3109\(99\)00075-2](http://dx.doi.org/10.1016/S0162-3109(99)00075-2)
3. Andrade, S.S., et al. *Biological Chemistry* **393**, 943-957 (2012), <http://dx.doi.org/10.1515/hsz-2012-0126>
4. Fazio, M.A., et al. *Biopolymers* **84**, 205-218 (2006), <http://dx.doi.org/10.1002/bip.20396>
5. Alves, F.L., et al. *J. Peptide Science* **21**, 495-500 (2015), <http://dx.doi.org/10.1002/psc.2766>

Active Leptin Fragments Resistant to Proteolytic Enzymes Present in Human Plasma

Paula Y. Tokuyama¹, Edgar J. Paredes-Gamero², and Antonio Miranda¹

¹Department of Biophysics; ²Department of Biochemistry, Federal University of São Paulo, São Paulo, SP, 04044-020, Brazil

Introduction

Leptin is a hormone produced and secreted predominantly from white adipose tissue and plays an important role in the regulation of energy homeostasis, food intake, body temperature and body weight maintenance. The tertiary structure of the leptin molecule shows the existence of a bundle of four helices that are characteristic of cytokines [1,2]. The main goal of this work is to study the structure-activity relationship of fragments of leptin. Peptides were designed taking into account preliminary studies involving the fragment Ac-hLEP₈₉₋₉₈-NH₂ (Ac-VLAFSKSSHL-NH₂) developed by our group [3-5]. Peptides (Table 1) were synthesized by the solid-phase methodology, purified by HPLC and characterized by LC/ESI-MS and Amino Acid Analysis [6]. Resistance to proteolytic degradation assays were performed in human plasma in the absence and in the presence of enzymes class inhibitors (PMSF, E64, ortho-phenanthroline and pepstatin). The immunomodulatory capacity of the fragments against hematopoietic stem cells and mature populations were also evaluated. The progenitor cell count was made after treatment of bone marrow cells with 10⁻⁷ M peptides in methylcellulose for 7 days [7,8].

Results and Discussion

Resistance to proteolytic degradation assays were performed in plasma in the absence and in the presence of enzymes class inhibitors (PMSF, E64, ortho-phenanthroline and pepstatin). Degradation kinetics profiles were followed by LC/ESI-MS (Figure 1A). LEP1 and LEP5 showed to be very stable even after 6 hours of incubation. On the other hand, LEP2; LEP3; LEP4 and LEP6 (mouse sequence) were very instable and were degraded in just a few minutes of incubation. Only solutions of the peptides incubated in the presence of ortho-phenanthroline preserved the stability of the peptides, showing that metalloproteases should be responsible by the degradation of the leptin fragments. Figure 1B shows the results obtained with LEP3 and LEP4 that were taken as examples.

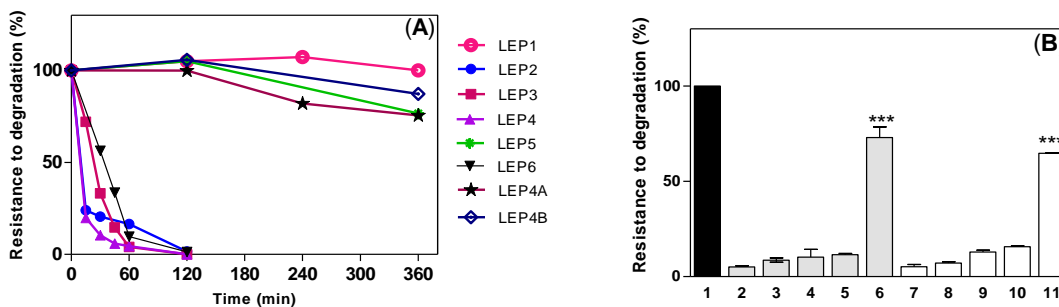


Fig. 1. Degradation profile in the absence (A) and in the presence (B) of proteolytic inhibitors of leptin fragments in plasma. Negative control; (2) LEP4; (3) LEP4+E64; (4) LEP4+Pepstatin; (5) LEP4+PMSF; (6) LEP4+Ortho-phenanthroline; (7) LEP3; (8) LEP3+E64; (9) LEP3+Pepstatin; (10) LEP3+PMSF; and (11) LEP3+Ortho-phenanthroline.

Due to its better performance in the biological activities evaluations, LEP4 was chosen to undergo chemical modification in order to increase its resistance to degradation, resulting in the compounds: LEP4A and LEP4B. Structure modification of LEP4A, was based on our knowledge of the cleavage site found by LC/ESI-MS. On LEP4A both serine residues were replaced by their corresponding D-counterpart. In contrast, LEP4B is the retro-inverso counterpart of LEP4. Both LEP4A and LEP4B

Table 1. Leptin fragments.

Abrev.	Name	Sequence ^a
LEP1	[D-Leu ⁴]-OB3 ^b	S-C-S-l-P-Q-T-NH ₂
LEP2	Ac-hLEP ₁₁₃₋₁₂₂ -NH ₂	Ac-F-S-K-S-C-H-L-P-W-A-NH ₂
LEP3	Ac-[Ser ⁹⁶]-hLEP ₈₉₋₉₈ -NH ₂	Ac-V-L-A-F-S-K-S-S-H-L-NH ₂
LEP4	Ac-[D-Phe ⁹² ,Ser ⁹⁶]-hLEP ₈₉₋₉₈ -NH ₂	Ac-V-L-A-f-S-K-S-S-H-L-NH ₂
LEP4A	Ac-[D-Phe ⁹² ,D-Lys ⁹⁴ ,D-Ser ^{95,96}]-hLEP ₈₉₋₉₈ -NH ₂	Ac-V-L-A-f-S-k-s-s-H-L-NH ₂
LEP4B	Ri-Ac-[D-Phe ⁹² ,Ser ⁹⁶]-hLEP ₈₉₋₉₈ -NH ₂	Ac-l-h-s-s-k-s-F-a-l-v-NH ₂
LEP5	[Ser ² ,D-Leu ⁴]-OB3	S-S-S-l-P-Q-T-NH ₂
LEP6	Ac-[D-Phe ⁹² ,Ser ⁹⁶]-mLEP ₈₉₋₉₈ -NH ₂	Ac-L-L-A-f-S-K-S-S-S-L-NH ₂

^aSmall letters correspond to D-amino acid; ^bLeinung and Grasso [9].

showed to be very stable to proteolytic action for more than 12 hours. The clonogenic capacity was evaluated and only LEP2 could increase the CFU-GM. Conformational studies by circular dichroism technique did not indicate a clear correlation between biological activities, since all compounds presented a random conformation spectra profile.

Acknowledgments

This work was supported by grants and fellowships from CNPq and FAPESP.

References

1. Zhang, F.M., et al. *Nature* **387**, 206-209 (1997), <http://dx.doi.org/10.1038/387206a0>
2. Kline, A.D., et al. *FEBS Letters* **407**, 239-242 (1997), [http://dx.doi.org/10.1016/S0014-5793\(97\)00353-0](http://dx.doi.org/10.1016/S0014-5793(97)00353-0)
3. Oliveira, V.X., et al. *Regulatory Peptides* **127**, 123-132 (2005), <http://dx.doi.org/10.1016/j.regpep.2004.11.001>
4. Oliveira, V.X., et al. *J. Pept. Sci.* **14**, 617-625 (2008), <http://dx.doi.org/10.1002/psc.957>
5. Martins, M., et al. *Regulatory Peptides* **153**, 77-82 (2009), <http://dx.doi.org/10.1016/j.regpep.2008.11.013>
6. Miranda, A., et al. *J. Med. Chem.* **40**, 3651-3658 (1997), <http://dx.doi.org/10.1021/Jm970311t>
7. Dias, C.C., et al. *Peptides* **50**, 24-27 (2013), <http://dx.doi.org/10.1016/j.peptides.2013.09.012>
8. Dias, C.C., et al. *J. Cell. Biochem.* **116**, 1334-1340 (2015), <http://dx.doi.org/10.1002/jcb.25090>
9. Leinung, M.C.P. *Grasso Regulatory Peptides* **179**, 33-38 (2012), <http://dx.doi.org/10.1016/j.regpep.2012.08.006>

Leptin Fragment Increase Hematopoietic Stem Cell Population and Improve its Engraftment Ability

Carolina C. Dias¹, Amanda Nogueira-Pedro¹, Edgar J. Paredes-Gamero¹, and Antonio Miranda²

¹Department of Biochemistry; ²Department of Biophysics, Federal University of São Paulo, São Paulo, SP, 04044-020, Brazil

Introduction

Several studies have shown the important actions of cytokine leptin that regulates food intake and energy expenditure. Additionally, the ability to modulate hematopoiesis has also been demonstrated increasing hematopoietic progenitors. Previous reports of our group have shown that some synthetic sequences of leptin molecules can activate leptin receptor [1-3]. Herein, decapeptides encompassing amino acids from positions 98 to 122 of the leptin molecule were constructed to evaluate their effects on hematopoiesis [4].

Results and Discussion

All leptin related peptide fragments were synthesized manually by the t-Boc Strategy. Peptides were intraperitoneally administrated in C57BL/6 mice at a dose of 1 mg/kg for 3 days. After treatment bone marrow cells populations were evaluated. Immunophenotyping was performed by Flow Cytometry (FACSCalibur) in order to quantify hematopoietic stem cells (HSC: Lin⁻c-Kit⁺Sca-1⁺FLK2⁻Thy1.1^{low}). As observed in Figure 1A the percentage of HSC was increased by the treatment of LEP F. Other peptides (Table 1) did not have effects to alter the percentage of HSC in bone marrow. Additionally, clonogenic assay in methylcellulose was also assessed (Figure 1B).

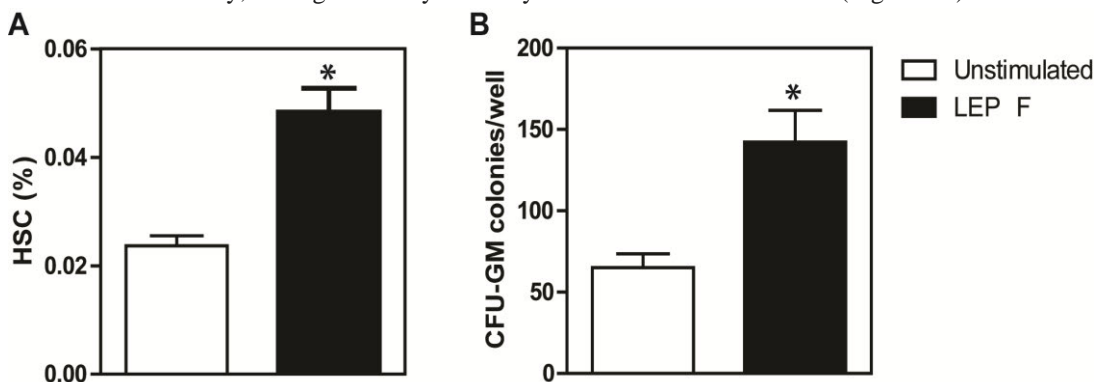


Fig. 1. Effect of LEP F on primitive hematopoietic populations (A) Percentage of HSC (B) The capacity to form primitive CFU-GM.

Each colony formed is related with the ability of progenitors to proliferate and differentiate to mature progenies. Treatment of bone marrow cells with LEP F also increase the ability of hematopoietic progenitors to produce colonies. Furthermore, LEP F also improves the grafting of HSC in bone marrow, but did not accelerate the recovery of bone marrow after ablation (data not shown). This results show that this decapeptide have the ability to increase HSC and improve bone marrow transplantation. These features can be helpful in different medical procedures such as bone marrow transplant. The synthetic peptide LEP F was the only peptide that possessed the ability to increase the percentage of hematopoietic stem cells (HSC). Moreover, LEP F also produced an increase of granulocyte/macrophage colony-forming units and activated leptin receptor. Furthermore, LEP F also improves the grafting of HSC in bone marrow, but did not accelerate the recovery of bone

Table 1. Peptide sequence of the synthetic leptin fragments studied.

<i>Abrev.</i>	<i>Name</i>	<i>Sequence</i>
LEP A	Ac-mLep ₉₈₋₁₂₂ -NH ₂	Ac-A-H-D-L-E-N-L-R-D-L-L-H-L-L-A-F-S-K-S-C-S-L-P-Q-T-NH ₂
LEP B	Ac-mLep ₉₈₋₁₀₇ -NH ₂	Ac-A-H-D-L-E-N-L-R-D-L-NH ₂
LEP C	Ac-mLep ₁₀₁₋₁₁₀ -NH ₂	Ac-L-E-N-L-R-D-L-L-H-L-NH ₂
LEP D	Ac-mLep ₁₀₄₋₁₁₃ -NH ₂	Ac-L-R-D-L-L-H-L-L-A-F-NH ₂
LEP E	Ac-mLep ₁₀₇₋₁₁₆ -NH ₂	Ac-L-L-H-L-L-A-F-S-K-S-NH ₂
LEP F	Ac-mLep ₁₁₀₋₁₁₉ -NH ₂	Ac-L-L-A-F-S-K-S-C-S-L-NH ₂
LEP G	Ac-mLep ₁₁₃₋₁₂₂ -NH ₂	Ac-F-S-K-S-C-S-L-P-Q-T-NH ₂

marrow after ablation with 5-fluorouracil. These results show that LEP F is a positive modulator of the *in vivo* expansion of HSC and could be useful in bone marrow transplantation [5].

Acknowledgments

This work was supported by grants and fellowships from CNPq and FAPESP.

References

1. Oliveira, V.X., et al. *Regulatory Peptides* **127**, 123-132 (2005), <http://dx.doi.org/10.1016/j.regpep.2004.11.001>
2. Martins, M.N.C., et al. *Regulatory Peptides* **153**, 77-72 (2009), <http://dx.doi.org/10.1016/j.regpep.2008.11.013>
3. Oliveira, V.X., et al. *J. Pept. Sci.* **14**, 617-625 (2008), <http://dx.doi.org/10.1002/Pse.957>
4. Dias, C.C., et al. *Peptides* **50**, 24-27 (2013), <http://dx.doi.org/10.1016/j.peptides.2013.09.012>
5. Dias, C.C., et al. *J. Cellular Biochemistry* (2015), <http://dx.doi.org/10.1002/jcb.25090>

Biological Studies of Angiotensin II Analogs Using Nanostructured Micelles

Cibele Nicolaski Pedron, Daniele Ribeiro Araújo, and Vani Xavier Oliveira Jr.

Centro de Ciências Naturais e Humanas, Universidade Federal do ABC, Santo André, 09210580, Brazil

Introduction

Malaria is an acute infectious disease caused by the protozoa of the genus *Plasmodium*. In humans, five species are responsible for malaria: *P. falciparum*, *P. vivax*, *P. ovale*, *P. malariae* and *P. knowlesi*. Due to resistance to antimalarial drugs, it is important to develop new treatments including peptides. The antiplasmodial action of angiotensin II ($\text{H}_3\text{N}^+\text{-Asp-Arg-Val-Tyr-Ile-His-Pro-Phe-COO}^-$) and its analogs has been reported. It inhibits the development of *Plasmodium gallinaceum* in *Aedes aegypti* mosquitoes [1,2].

To protect the peptides from protease action and promote sustained release, thermoreversible synthetic copolymers can be used as a drug delivery system. A drug delivery system is defined as a formulation or device that allows the administration of a therapeutic substance and provides better efficacy and safety by controlling the speed, time and place of release of the drug in the body [3]. This study describes the encapsulation of the antiplasmodial analogs of angiotensin II *via* preparation of formulations for slow release of peptides aiming for intramuscular administration.

Results and Discussion

The peptides were manually synthesized in the solid-phase method using Fmoc strategy and Wang and Rink Amide resins. The couplings are successful and used the coupling agents *N,N'*-diisopropylcarbodiimide (DIC) and *N*-hydroxybenzotriazole (HOBt). The syntheses were satisfactory with the peptides resulting a chromatographic purity higher than 95%; mass characterization by LC/MS-ESI confirmed that the purified peptides agreed well the expected theoretical values (Table 1).

Thermoreversible hydrogels from Poloxamer (PL) are efficient systems for the prolonged release of drugs. These were prepared at concentrations of PL 407 25%, PL 407 23% + PL 403 2% and PL 407 23% + PL 188 2%. Mixed micellar systems are formed by mixing two binary copolymers and exhibit synergistic properties including increased stability of the micelles and efficient drug encapsulation versus systems with only one copolymer [4,5].

The peptide-poloxamer characterization was performed by photon correlation spectroscopy. At 25°C, the formulation showed an average diameter ranging from 33 to 225 nm. At 37°C, the diameter decreased to 21- 40 nm (Table 2) proving the aggregation and micelle formation at body temperature. With the incorporation of peptides, the average micelle diameter was not changed at either temperature. The polydispersity index ranged from 0.1 to 0.4 indicating a homogeneous particle population.

The *in vitro* permeation assays were carried out with a vertical diffusion Franz-type cell. The receptor medium was Hepes buffer, and the membranes were cellulose acetate. The peptide $\text{H}_3\text{N}^+\text{-Val-Tyr-Ile-His-Pro-Phe-COO}^-$ had a release profile that was similar to the three formulations. The 24 h release concentrations of PL 407, PL 407 + PL 403 and PL 407 + PL 188 were $61.5 \pm 1.8 \mu\text{g/mL}$, $67.0 \pm 10.6 \mu\text{g/mL}$ and $50.3 \pm 4.8 \mu\text{g/mL}$, respectively.

The release results showed that release flow for poloxamer formulations were lower than that obtained for free peptide. The sequence VYIHPF in the poloxamer systems formed by PL 407, PL 407 + PL 403 and PL 407 + PL188 released 51, 56 and 42%, respectively, relative to free peptide. This indicates that these systems are effective models for this class of compound.

Table 1. Analogs characterization.

	Peptide	Purity HPLC ^a	Molecular weight (MW)	(m + H ⁺) ^b
1	H ₃ N ⁺ -Asp-Arg-Val-Tyr-Ile-His-Pro-Phe-CONH ₂	99%	1045.5	1047
2	H ₃ N ⁺ -Asp-Arg-Val-Tyr-His-Ile-Pro-Phe- CONH ₂	99%	1045.5	1047
3	H ₃ N ⁺ -Tyr-His-Pro-Phe- CONH ₂	99%	562.2	563
4	H ₃ N ⁺ -Ile-His-Pro-Phe- CONH ₂	98%	512.3	513
5	H ₃ N ⁺ -Val-Tyr-Ile-His-Pro- CONH ₂	99%	627.3	629
6	H ₃ N ⁺ -Val-Tyr-Ile-His-Pro-Phe-COO ⁻	98%	774.4	775
7	H ₃ N ⁺ -Asp-Arg-Val-Tyr-Ile-His-Pro-Phe-COO ⁻	99%	979.5	980

^aHPLC profiles were obtained under the following conditions: Column Supelcosil C₁₈ (4.6 x 150 mm), 60Å, 5 µm; Solvent System: A: 0.1% TFA/H₂O, B: 0.1% TFA in 60%ACN/H₂O; Gradient: 5-95% B in 30 minutes; Flow: 1.0 mL/min; λ = 220 nm; Injection volume: 50 µL and sample concentration: 1.0 mg.mL⁻¹; ^bMass measurements were performed in a positive mode with the following parameters: Column Waters Nova-Pak C₁₈ (2.1 x 150 mm), 60 Å, 3.5 µm; Solvent System: A: 0.1% TFA/H₂O, B: 0.1% TFA in 60%ACN/H₂O; Gradient: 5-95% B in 30 minutes; Flow:0.4 mL/min; λ = 220 nm; Injection volume: 30 µL; Sample concentration: 1.0 mg.mL⁻¹; mass range between 200-2000 Daltons.

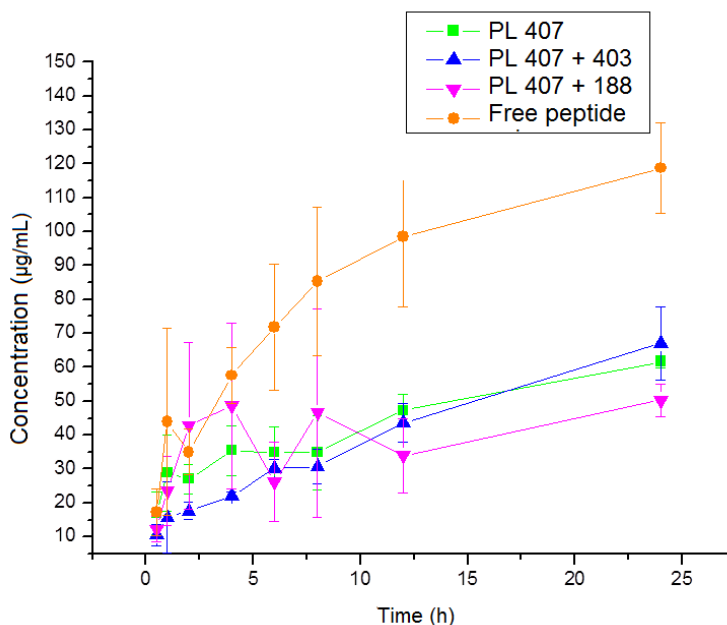


Fig. 1. Release profile of the formulations and peptide H₃N⁺-Val-Tyr-Ile-His-Pro-Phe-COO⁻.

Table 2. Diameter and size distribution percentage obtained at 25 and 37°C.

	25°C		37°C	
	Diameter	% Intensity	Diameter	% Intensity
PL 407	43 ± 0.9	86 ± 0.7	21 ± 0.1	100 ± 0.0
PL 407 + PL 403	39 ± 0.4	96 ± 3.5	37 ± 1.1	97 ± 0.9
PL 407 + PL 188	45 ± 0.5	84 ± 0.3	40 ± 0.7	97 ± 2.5
PL 407 + Peptide 2	43 ± 2.0	44 ± 0.6	27 ± 0.2	74 ± 0.6
PL 407 + PL 403 + Peptide 2	39 ± 0.8	93 ± 0.7	36 ± 0.5	91 ± 2.3
PL 407 + PL 188 + Peptide 2	41 ± 1.3	84 ± 0.6	25 ± 2.0	100 ± 0.2
PL 407 + Peptide 3	52 ± 4.1	81 ± 4.1	24 ± 2.1	100 ± 0.4
PL 407 + PL 403 + Peptide 3	54 ± 2.2	91 ± 0.2	35 ± 2.0	98 ± 0.5
PL 407 + PL 188 + Peptide 3	62 ± 3.9	76 ± 2.5	25 ± 1.5	100 ± 0.0
PL 407 + Peptide 6	188 ± 20	68 ± 2.2	27 ± 0.5	99 ± 0.7
PL 407 + PL 403 + Peptide 6	33 ± 1.0	68 ± 1.2	27 ± 1.4	99 ± 1.1
PL 407 + PL 188 + Peptide 6	197 ± 31	74 ± 5.0	28 ± 0.9	97 ± 0.6
PL 407 + Peptide 7	170 ± 14	77 ± 2.9	28 ± 0.5	94 ± 3.2
PL 407 + PL 403 + Peptide 7	34 ± 1.5	68 ± 2.5	32 ± 0.7	86 ± 0.8
PL 407 + PL 188 + Peptide 7	225 ± 69	74 ± 25	35 ± 1.8	82 ± 1.2

Data presented as (mean ± SD, n=3). The measurements of the hydrodynamic diameter was performed by Zetasizer particle analyzer ZS (Malvern® Instruments) at an angle of 173° at temperatures of 25 and 37°C.

Acknowledgments

We thank Universidade Federal do ABC (UFABC), Universidade de São Paulo (USP), Universidade Federal de São Paulo (UNIFESP), Coordenação de Aperfeiçoamento de Pessoal de Nível Superior (CAPES) and Fundação de Amparo à Pesquisa do Estado de São Paulo (FAPESP).

References

1. Maciel, C., et al. *PLoS ONE* **3**, e3296 (2008), <http://dx.doi.org/10.1371/journal.pone.0003296>
2. Silva, A.F., et al. *J. Pept. Science* **20**, 640-648 (2014), <http://dx.doi.org/10.1002/psc.2641>
3. Jain, K.K., *Methods Mol. Biol.* **437**, 1-50 (2008), http://dx.doi.org/10.1007/978-1-59745-210-6_1
4. Kulthe, S.S., et al. *Colloids Surf. B:Biointerfaces* **88**, 691-696 (2011), <http://dx.doi.org/10.1016/j.colsurfb.2011.08.002>
5. Lee, E.S., et al. *Colloids Surf. B:Biointerfaces* **82**, 190-195 (2011), <http://dx.doi.org/10.1016/j.colsurfb.2010.08.033>

Cyclotides from *Pombalia*, *Noisettia* and *Viola* Genus: Discovery and Inhibitors of Cellular Migration

Meri Emili F. Pinto¹, Jenny Najas Z. Garavito², Luma G. Magalhães³,
Adriano D. Andricopulo³, Christian W. Gruber⁴, Eduardo M. Cilli¹,
Angelo C. Pinto², and Vanderlan S. Bolzani¹

¹Institute of Chemistry, São Paulo State University - UNESP, Araraquara, 14800-060, Brazil; ²Institute of Chemistry, Federal University of Rio de Janeiro - UFRJ, Rio de Janeiro, 21941-909, Brazil; ³Institute of Physics of São Carlos, The University of São Paulo - USP, São Carlos, 13563-120, Brazil; ⁴Center for Physiology and Pharmacology, Medical University of Vienna, Vienna, 1090, Austria

Introduction

Violaceae is a rich source of cyclotides and are ubiquitous among all species of this plant family [1]. This protein group is characterized by a peculiar cyclic structure, collectively known as cyclic cystine motif (CCK) conferring them with remarkable stability. These properties together with a number of bioactivities have attracted enormous attention from both the scientific community and pharmaceutical industry for using cyclotides in drug development [2]. In this context, this work describes the identification of cyclotides in fractions of *Pombalia calceolaria*, *Viola cerasifolia*, *Viola submdmiata* and *Noisettia orchidflora*, as well as their potential anticancer properties.

Results and Discussion

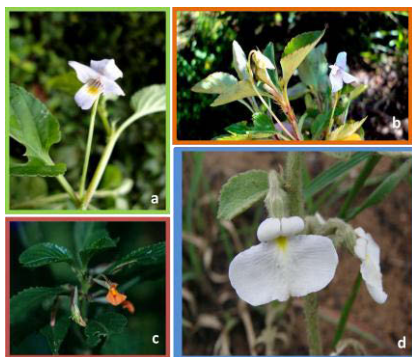


Fig. 1. a) *V. submdmiata*. b) *V. cerasifolia*. c) *N. orchidflora*. d) *P. calceolaria*.

The work presented here contributes to our understanding about the diversity and distribution of cyclotides in the *Pombalia calceolaria* (leaves, stems, seeds and roots), *Viola cerasifolia* (leaves, stems and roots), *Viola submdmiata* (leaves, stems and roots) and *Noisettia orchidflora* (roots) sourced from Forest Atlantic (Rio de Janeiro, Brazil). Although an array of pharmaceutical relevant bioactivities has been ascribed to cyclotides, their key purpose in plants is supposed to be as antibiotic agents to fend off plant pests and pathogens [3].

In order to check the possible presence and differences in the expression of cyclotide in these four plants and your tissues, approximately 60g of each plant part was ground prior to solvent extraction, yielding thirteen crude extracts. For *V. cerasifolia* were obtained three extracts named 1L (leaves), 1C (stems) and 1R (roots). For *V. submdmiata*, 2L (leaves), 2C (stems) and 2R (roots), *N. orchidflora*, 3L (leaves), 3C (stems) and 3R (roots) and *P. calceolaria* 4L (leaves), 4C (stems), 4S (seeds) and 4R (roots). The analysis by RP-HPLC and MALDI-TOF MS showed that these extracts contained a diversity of cyclotides identified bases on their mass, cysteine content and hydrophobicity. The cysteine content was in accordance with established diagnostic methodology whereupon after reduction and carbamidomethylation reaction it is possible to observe mass increase of 348 Da indicating the presence of three intramolecular disulfide bonds in the corresponding proteins. Thus, the extracts showed a wide diversity of peptides with masses in the range of 2900-3600 Da as analysed by MALDI-TOF mass spectrometry (MS), typically the range of masses expected for cyclotides. In general, the expression of the peptides appeared to vary with the plant tissues, according the Table 1.

Preparative RP-HPLC chromatography of crude extract allowed isolating four bracelet cyclotides, (m/z 3143; 3157; 3166) from roots of *P. calceolaria* and (m/z 3145) from *N. orchidflora*. Cyclotide sequencing was performed by reduction, alkylation and enzymatic digest with endoproteinases Glu-C, trypsin, and chymotrypsin and followed by MS/MS analysis.

Table 1. Peptide masses obtained by MALDI for *V.cerasifolia* 1L (leaves), 1C (stems) and 1R (roots), *V. subdmidiata*, 2L (leaves), 2C (stems) and 2R (roots), *N. orchidflora*, 3L (leaves), 3C (stems) and 3R (roots) and *P. calceolaria* 4L (leaves), 4C (stems), 4S (seeds) and 4R (roots).

1F	1G	1R	2F	2G	2R	3F	3G	3R	4F	4G	4R	4S
3108.182		3108.198		2841.653				3145.320	3070.288		3072.172	
3126.218	3124.474	3125.215		2847.027					3085.197		3084.188	
3136.257	3133.181	3135.201		2855.288		3171.399			3093.166		3093.162	
3150.227	3149.162	3148.194		2858.170					3095.106		3096.178	
3153.218		3151.209		2863.715			3178.579	3181.036	3105.174			3105.285
3166.225	3164.226	3166.215	2877.052	2877.088	2878.246	3193.396	3193.904		3109.097		3109.135	3107.981
	3180.225	3180.187	2879.052						3112.156		3112.174	
3191.261			2891.66	2891.119	2891.349			3207.354				3123.954
3195.729			2893.067	2894.014	2894.197		3209.291	3210.964		3125.102	3125.249	
3208.689			2905.079	2905.142	2906.254				3128.516		3128.254	
3214.244			2907.103						3133.607			
3223.274			2909.025	2908.033			3222.666	3223.127	3140.013			
3241.284			2915.056		2915.221			3244.616				
3249.295			2923.054	2923.092						3142.227	3143.263	
3269.744			2929.052		2929.228			3249.168	3150.228		3149.202	
3281.292			2938.066	2938.088			3273.285		3157.000		3157.232	
3288.951			2943.052	2943.289					3166.198	3166.185	3166.212	3165.291
				3070.245		3282.430	3282.753	3282.615			3174.233	
3292.760				3114.229						3180.198	3181.200	
3296.756				3139.202				3295.273	3190.257	3190.291	3190.208	
3312.300	3310.269	3311.254			3148.122			3313.015	3205.247	3205.219	3205.035	
3346.349				3171.294						3208.222		
3356.784					3180.342		3341.959				3225.223	
3369.815				3195.138				3344.560	3303.276		3229.212	
3411.346				3302.272							3328.229	

A bioassay was conducted based on cellular migration, a feature related to the metastasis process, which is involved in 90% of all cancer deaths. Thus, for qualitative evaluation of directional cell migration, MDA-MB-231 cells were seeded at a density of 1×10^5 cells/well in 24-well culture plates (TPPTM) and allowed to reach a confluent monolayer. Then, a scratch was inflicted in the wells using a sterile 100 μ L pipette tip. The medium was removed and a fresh medium without FBS was added to clean the debris. Sequentially, cells were incubated for 22h at 37°C with supplemented medium (10% FBS) and concentration of extracts (200 μ g/mL) and colchicine at 10 mM has been used as a control. When measuring the wound closure, pictures of the wells were taken under a 4X objective (Optiphaser) at 0 and 22h. The images were analyzed using

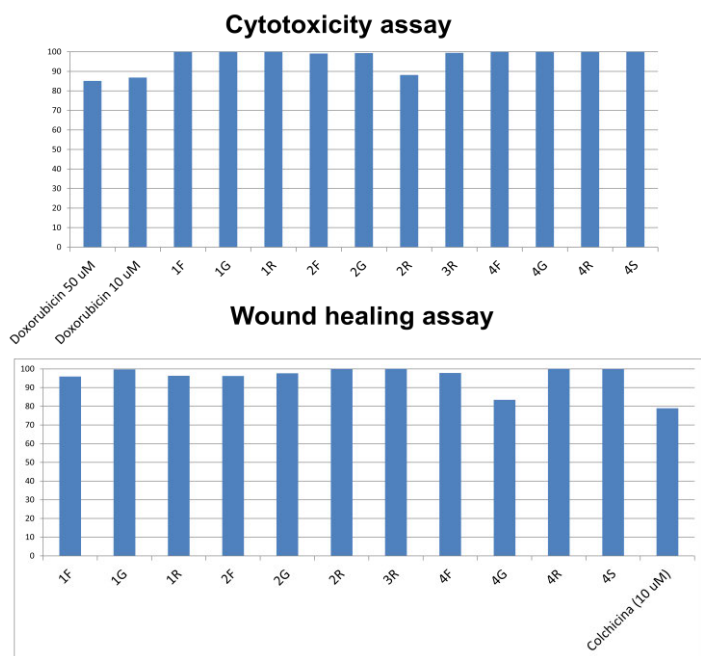


Fig. 2. Percentage of cell migration inhibition and cytotoxicity assays with MDA-MB 213 human breast tumor cells.

Image J software and two independent experiments were conducted in triplicate. All fractions demonstrated high inhibition of cellular migration between 80 to 100%, according to Figure 2. The fractions were evaluated for their cytotoxicity against MDA-MB-231 and DU-145 cancer cell lines and the percentage of unviable cells was determined in relation to the control wells. All fractions exhibited high potency as in the migration assays and cytotoxicity.

Acknowledgments

This work was supported with grants from CEPID-FAPESP grant# 2010/52327-5 and 2013/07600-3, SISBIOTA-CNPq-FAPESP grant# 2010/52327-5, and CAPES grant# BEX: 9875/11-5. The authors are also grateful to CNPq, CAPES and FAPESP (2011/22339-4 and 2012/13739-1) for scholarships and financial support, as well as to Prof. Norberto. P. Lopes (USP-Ribeirão Preto) for HRESIMS measurements. This research was also supported by resources supplied by the Center for Scientific Computing (NCC/GridUNESP) of the São Paulo State University (UNESP).

References

1. Simonsen, S.M., et al. *Plant Cell* **17**, 3176-3186 (2005), <http://dx.doi.org/10.1105/tpc.105.034678>
2. Pinto, M.F.S., et al. *Journal Evidence-Based Complementary and Alternative Medicine* **17**, 40-53 (2012), <http://dx.doi.org/10.1177/2156587211428077>
3. Burman, R., et al. *J. Natural Products* **77**, 724-736 (2014), <http://dx.doi.org/10.1021/np401055j>

Mitsunobu Reaction on Solid Support for Peptide *N*-Terminal Farnesylation

Julien Poupart and William D. Lubell

Department of chemistry, Université de Montréal, Montreal, Canada

Introduction

Prenylation is an important post-translational modification of peptide structures. For example, farnesylated and geranylgeranylated peptides and proteins bind to cell membranes by way of the prenyl subunit. Prenylation is involved in a wide variety of biological process and diseases, including cancer [1,2] and Alzheimer's disease [2]. Prenylated peptides have been shown to be generally non-toxic and to exhibit cell permeable properties [3]. Prenylated protein libraries have been used to study various biochemical mechanisms that involve post-translational prenylation [4]. Prenylated peptides have also been used as prenyltransferase inhibitors [5]. Prenylated peptides may exhibit ability to localize in membranes, which may enhance their metabolic stability and biological presentation.

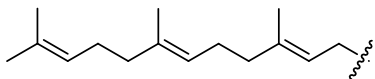


Fig. 1. Farnesyl group.

The conventional way to introduce a prenyl group onto a peptide chain involves nucleophilic displacement by a cysteine residue thiol side chain on a proper prenyl bromide [3]. Prenyl bromides are relatively expensive and unstable. Prenylation on nitrogen has been less well studied, but may offer an alternative way for introducing the lipid moiety onto peptides. In an effort to explore *N*-terminal prenylation, we have explored the Mitsunobu reaction in order to employ the relatively more stable alcohols instead of their prenyl halide counterparts.

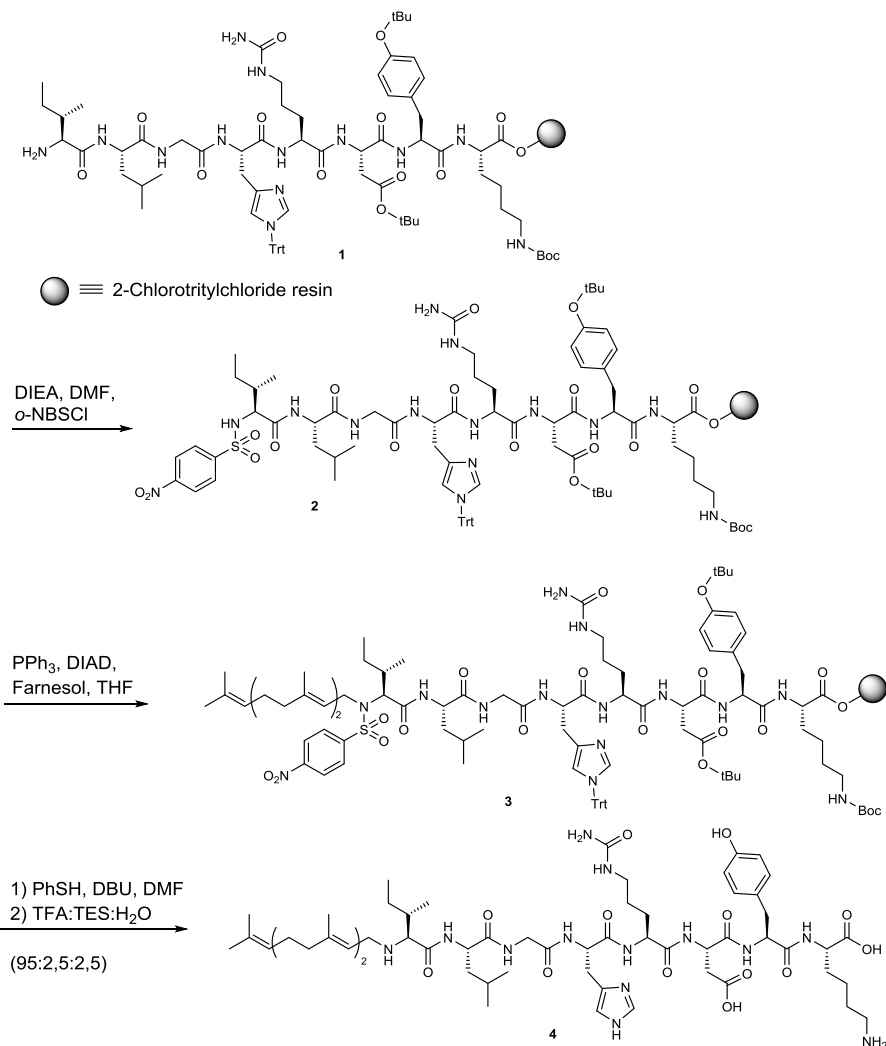
For this study, the L-enantiomer (L-PDC-31, Ile-Leu-Gly-His-Cit-Asp-Tyr-Lys) of the D-peptide PDC-31 was chosen [6], in part because this prostaglandin F₂ α receptor modulator has completed successfully phase 1b clinical trials in which toxicity was assessed in women suffering from primary desmenorea [7]. Hypothesizing that the L-isomer may be active, yet rapidly degraded in biological tissues, a farnesyl chain at the *N*-terminal nitrogen has been examined to increase metabolic stability of the peptide. Herein, the Mitsunobu reaction has been employed to farnesylate a solid supported peptide using farnesol as a shelf stable and relatively inexpensive reagent in order to prepare farnesyl peptide **4**.

Results and Discussion

Peptide **1** was prepared by standard solid-phase synthesis using a Fmoc/tBu strategy on 2-chlorotrityl chloride resin (Scheme 1) [8]. After removal of the *N*-terminal Fmoc protection, an *para*-nitrosulfonyl (Nosyl) group was installed by treating the resin-bound peptide with nosyl chloride and di-*iso*-propylethylamine in DMF [9,10]. The Mitsunobu reaction was performed using farnesol, diethylazodicarboxylate and triphenylphosphine in THF to install the farnesyl chain. The nosyl group was cleaved using thiophenol and DBU in DMF [11]. Farnesylated peptide **4** was cleaved from the resin using a cocktail of 95:2.5:2.5 TFA/TES/H₂O, precipitated in cold ether, centrifuged, filtered and washed with ether. Purification by RP-HPLC gave farnesyl peptide **4** in 89% purity and 2.5% overall yield: HRMS Calcd. (C₆₀H₉₆N₁₃O₁₃)⁺ = 1206.7245, found = 1206.7263 (M+H)⁺.

Conclusion

In conclusion, a novel solid-supported lipidation by *N*-alkylation using a Mitsunobu reaction between an alcohol and a nosyl-protected amine was developed and used to install a farnesyl residue on a model peptide. This method provides a viable alternative to the use of costly and unstable farnesyl bromide. The potential for *N*-prenylation to improve metabolic stability and membrane association of peptides is being explored and will be reported in due time.



Scheme 1. Synthesis of farnesyl peptide.

Acknowledgments

The authors would like to thank the Natural Sciences and Engineering Research Council of Canada (NSERC), the Canadian Institutes of Health Research (CIHR), and the March of Dimes foundation

References

- Hottman, D.A., Li, L. *Mol. Neurobiol.* **50**, 177-185 (2014), <http://dx.doi.org/10.1007/s12035-013-8627-z>
- Xu, N., et al. *Sci. China. Life Sci.* **58**, 328-335 (2015), <http://dx.doi.org/10.1007/s11427-015-4836-1>
- Wollack, J.W., et al. *J. Am. Chem. Soc.* **131**, 7293-7303 (2009), <http://dx.doi.org/10.1021/ja805174z>
- Yi, L., et al. *Chem. Biochem.* **12**, 2413-2417 (2011), <http://dx.doi.org/10.1002/cbic.201100466>
- Dolence, E.K., et al. *J. Comb. Chem.* **2**, 522-536 (2000), <http://dx.doi.org/10.1021/cc000026m>
- Peri, K., et al. *Semin. Perinatol.* **26**, 389-397 (2002), <http://dx.doi.org/10.1053/sper.2002.37307>
- Böttcher, B., et al. *Hum. Reprod.* **29**, 2465-2473 (2014), <http://dx.doi.org/10.1093/humrep/deu205>
- Lubell, W.D., et al. (2005) "Peptides" *Science of Synthesis 21.11, Chemistry of Amides*. Thieme, Stuttgart, 713-809.
- Bisegger, P., et al. *Tetrahedron* **64**, 7531-7536 (2008), <http://dx.doi.org/10.1016/j.tet.2008.05.119>
- Arya, P.W., et al. *J. Comb. Chem.* **6**, 65-72 (2004), <http://dx.doi.org/10.1021/cc0340067>
- Lencina, C.L., et al. *Tetrahedron: Asymm.* **19**, 1689-1697 (2008), <http://dx.doi.org/10.1016/j.tetasy.2008.06.030>

Structure-Activity Relationship Studies of Dynorphin A Analogs at the Kappa Opioid Receptor

Cyf N. Ramos Colon^{1,2}, Yeon Sun Lee², Sara M. Hall², Josephine Lai³,
Frank Porreca³, and Victor J. Hruby²

¹College of Pharmacy, Departments of ²Chemistry and Biochemistry, ³Pharmacology,
University of Arizona, Tucson, AZ, USA

Introduction

Chronic pain is the most ubiquitous disease with an incidence of 100 million people in the U.S. Opiate therapy is the mainly prescribed treatment for chronic neuropathic pain. However opioids do not address the mechanisms of neuropathic pain and thus have limited efficacy against this type of pain [1]. While opioids may reduce the pain states experienced by the patients, they have adverse effects such as tolerance, addiction, and medication overuse with long-term administration. It has been found that by blocking the κ opioid receptor (KOR) a reduction in tolerance and depressive affective states that can occur with opioid administration [2]. With this in mind we are working towards the development of a KOR selective antagonist with variable duration of action.

Dynorphin A (Dyn A, Tyr-Gly-Gly-Phe-Leu-Arg-Arg-Ile-Arg-Pro-Lys-Leu-Lys-Trp-Asp-Asn-Gln) is one of three endogenous opioid peptides with high affinities for the μ (MOR), δ (DOR), and κ opioid receptors, with a preference for the KOR. Dyn A mediates an inhibitory effect through the opioid receptors resulting in nociception. Some have studied the importance of consecutive polar residues as is found in Dyn A and found that these were important for binding and function [3].

Dyn A has been extensively studied in the search for KOR ligands. Our approach is different in that our main target is a shorter peptide with an amino acid residue deletion in the middle of the sequence. The deleted residue happens to be one of the key residues determined by studies of the relative importance of the amino acid residues in Dyn A sequence. It was previously believed that residues Arg⁷, Lys¹¹, and Lys¹³ were the most important residues for binding and potency at the KOR [4]. The importance of these residues was determined by the binding affinity of truncated analogs of Dyn A. In our approach we are completely deleting the amino acid residue and this is very interesting because usually residue deletions would have unfavorable effects to the binding of a peptide due to changes in conformation and charge distributions.

Results and Discussion

Dyn A analogs were synthesized by standard solid phase peptide synthesis using Fmoc-chemistry and cleaved by a 95% TFA cocktail solution containing 2.5% TIS, 2.5% water. Crude peptides were purified by RP-HPLC using 10-50% of acetonitrile in water containing 0.1% TFA. Radioligand competition binding assays were done for synthesized analogs using [³H] DAMGO for MOR, [³H] DeltorphinII for DOR, and [³H] U69,593 for KOR using transfected cell membranes.

We have identified that Arg 7 is not important nor necessary for binding at KOR as previously believed [4]. We also tested modification of the C-terminal acid to amide (**CYF110**, **CYF111**, and **CYF112**), which showed increased binding affinity at all three opioid receptors. Substitutions of the N-terminal amine group with (2S)-2-methyl-3-(2,6-dimethyl-4-hydroxyphenyl)propanoic acid (MDP) or Acetyl (Ac) groups increased KOR selectivity (**CYF111**, **CYF112**). It has been previously shown that N-terminal amine substitution of agonist opioid peptides can reverse their functions to antagonists [5].

After finding that the presence of Arg⁷ was not as important as previously thought, we went back to the literature to find other modifications that would improve binding and selectivity at the KOR and also produce antagonists at the receptor. It has been published that a substitution with a Pro at the third position improved selectivity and also showed weak antagonist function [6]. Another modification that has been shown to improve selectivity for the KOR is to reverse the chirality of residues 8 and 10. These residues are in the C-terminal region also known as the “address” region since they determine the selectivity of the peptide for a given opioid receptor [6]. We went ahead and tested D-amino acid substitutions, as well as peptide constraining substitution with Pro, and saw that they are well tolerated

Table 1. SAR of Dyn A analogs at the KOR, MOR, and DOR.

Dyn A	Structure	KOR (nM)	MOR (nM)	DOR (nM)
(1-11)	H-Tyr-Gly-Gly-Phe-Leu-Arg-Arg-Ile-Arg-Pro-Lys-OH	0.12	-	-
(1-11)-NH ₂	H-Tyr-Gly-Gly-Phe-Leu-Arg-Arg-Ile-Arg-Pro-Lys-NH ₂	0.10	-	-
CYF107	H-Tyr-Gly-Gly-Phe-Leu-Arg-Ile-Arg-Pro-Lys-OH	0.2	6	6
CYF110	H-Tyr-Gly-Gly-Phe-Leu-Arg-Ile-Arg-Pro-Lys-NH ₂	0.08	0.94	3
CYF111	Mdp-Gly-Gly-Phe-Leu-Arg-Ile-Arg-Pro-Lys-NH ₂	62	1600	210
CYF112	Ac-Tyr-Gly-Gly-Phe-Leu-Arg-Ile-Arg-Pro-Lys-NH ₂	74	820	2200

on the [des-Arg⁷]-Dyn A analogs but only when done one at a time. Our data suggests that modifying both the “message” and the “address” region in a single molecule are detrimental for binding affinity at the KOR.

In conclusion, we have shown that Arg⁷ is not necessary for binding at the KOR as previously believed and that *N*-terminal substitution combined with *C*-terminal amidation selectivity and binding at the KOR is retained. We also have insights on modifications of the message and address regions that can be done to the [des-Arg⁷] Dyn A analogs. We have already started the search for a [des-Arg⁷]-Dyn A minimum pharmacophore with very promising results. In our future studies we will continue to modify the structures to improve binding and selectivity of the shorter peptides for the KOR. Functional activity studies are also underway.

Acknowledgments

Funding was provided by grants from the US Public Health Services, NIH, and NIDA (RO1 DA13449 and NIDA Diversity Supplement). We also thank APS as Cyf Ramos Colón was a recipient of an APS Travel Award.

References

1. Hanlon, K.E., Herman, D.S., Agnes, R.S., Largent-Milnes, T.M., Kumarasinghe, I.R., Ma, S.W., et al. *Brain Res.* **1395**, 1-11 (2011), <http://dx.doi.org/10.1016/j.brainres.2011.04.024>
2. Tejeda, H.A., Shippenberg, T.S., Henriksson, R. *Cell. Mol. Life Sci.* **69**, 857-896 (2012), <http://dx.doi.org/10.1007/s00018-011-0844-x>
3. Oka, T., Negishi, K. *Life Sci.* **31**, 1707-1710 (1982), [http://dx.doi.org/10.1016/0024-3205\(82\)90191-6](http://dx.doi.org/10.1016/0024-3205(82)90191-6)
4. Chavkin, C., Goldstein, A. *Proc. Natl. Acad. Sci.* **78**, 6543 (1981).
5. Schiller, P.W., Weltrowska, G., Nguyen, T.M.-D., Lemieux, C., Chung, N.N., Lu, Y. *Life Sci.* **73**, 691-698 (2003), [http://dx.doi.org/10.1016/S0024-3205\(03\)00389-8](http://dx.doi.org/10.1016/S0024-3205(03)00389-8)
6. Naqvi, T., Haq, W., Mathur, K.B. *Peptides* **19**, 1277-1292 (1998), [http://dx.doi.org/10.1016/S0196-9781\(98\)00042-4](http://dx.doi.org/10.1016/S0196-9781(98)00042-4)

Design and Synthesis of a Novel Tetrapeptide with Improved Selectivity Towards the hMC1R

Jonathon R. Sawyer, Saghar Mowlazadeh Haghighi, Yang Zhou,
Kaitlyn McLeod, Victor J. Hruba, and Mingyong Cai

Department of Chemistry and Biochemistry, University of Arizona, Tucson, AZ, 85721, USA

Introduction

The melanocortin system plays vital roles with regard to maintaining homeostasis. The endogenous melanotropin peptides (α -, β -, γ -melanocyte stimulating hormones (MSH) are derived from the proopiomelanocortin (POMC) prohormone gene. These melanotropin peptides all contain the same core pharmacophore amino acid sequence: His-Phe-Arg-Trp [1,2]. This sequence is important for binding to the five human melanocortin receptors (MC1R, MC2R, MC3R, MC4R, and MC5R). Binding of the endogenous melanotropin peptides to these melanocortin receptors results in several responses depending on which receptor is activated. Such responses involve feeding behavior, learning behavior, pain modulation, pigmentation, and sexual function. The primary native ligand for all five of the melanocortin receptors is α -MSH. Unfortunately, α -MSH along with the other endogenous melanotropin peptides do not possess high selectivity for any of the melanocortin receptors as well as are biologically unstable. Thus, the quest to discover potent, biologically stable, and highly selective peptides began.

Results and Discussion

Peptide Design. Previous research led to a breakthrough discovery of a more biologically stable and potent derivative of α -MSH as seen in NDP- α -MSH (MT-I) with the key modifications of 4-norleucine and 7-D-phenylalanine [3]. Currently, MT-I is a marketed drug under the name of Afamelanotide for the treatment of congenital erythropoietic porphyria. However, MT-I does not have high selectivity to any one of the melanocortin receptor subtypes, which can lead to unexpected side effects. Because the tetrapeptide pharmacophore sequence of NDP- α -MSH is necessary for binding affinity to the melanocortin receptors but with poorer potency and selectivity to all subtypes of hMCRs, modifying the tetrapeptide structure will be of critical importance to improve the potency and the selectivity. Our earlier studies demonstrated that the electrostatic interaction, Arg(L)-Asp(R), between the Arg⁸ of the NDP- α -MSH and the Asp122, Asp126 of the hMC4R is of critical importance to achieve binding and receptor activation [4]. Similarly, a key interaction between the Arg⁸ of the NDP-MSH and the D154 as well as the D158 of the MC3R is necessary for binding [5]. Therefore, switching the arginine in the tetrapeptide to a neutrally charged amino acid, in particular norleucine, should reduce binding towards the hMC3R and the hMC4R. We envision that enhanced selectivity towards the MC1R can be reached with reduced electrostatic interaction between the Arg⁸(L)-Asp(R) of the tetrapeptide and the respective aspartic acids on the MC3R and MC4R receptors.

NDP- α -MSH (MT-I) has been well developed with potent binding and cAMP activities towards all subtypes of hMCRs (Figure 1). However, it does not have selectivity to hMCRs. Earlier studies demonstrated that the pharmacophore of NDP- α -MSH is His-D-Phe-Arg-Trp, a tetrapeptide shown here as peptide **1**, which maintains binding as well as cAMP activities to all subtypes of hMCRs but with much lower potency and efficacy. To improve the selectivity of hMCRs, herein we made a leading peptide **2**, which has replaced Arg⁸ with Nle⁸. Our biological studies demonstrate that peptide **2** has cAMP activity and selectivity towards the hMC1R, weak activity at the hMC4R (ten orders of magnitude weaker), and no functional cAMP activity at the hMC3R and the hMC5R (Table 1). The observed result indicates that changing the Arg⁸ to Nle⁸ in the peptide **2** improves the functional selectivity of hMC1R. Hence, abolishing the positive charge of the amino acid in the tetrapeptide, His-D-Phe-Arg-Trp, improves selectivity towards the hMC1R. Further research, which involves structural modifications of peptide **2**, is going on in order to produce a more potent and selective MC1R agonist/antagonist activity.

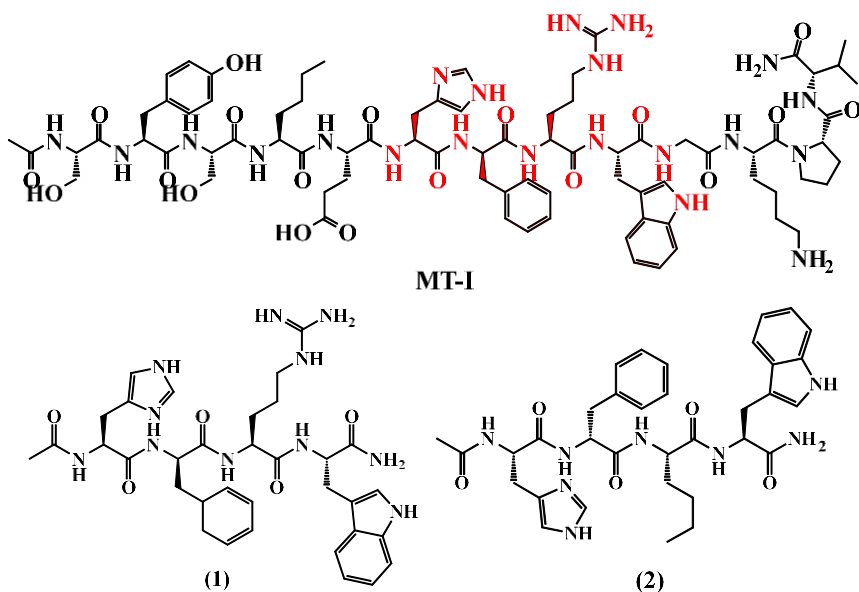


Fig. 1. Chemical structures of **MT-I** (known as NDP- α -MSH), tetrapeptide **(1)**, and the MC1R selective peptide **(2)**.

Peptide Synthesis. Standard solid-phase methods were used. Fmoc chemistry was used and the peptide was synthesized on Rink Amide resin. The resin was first deprotected using 20% (v/v) piperidine in DMF solution followed by coupling of the first amino acid. The Kaiser Test was performed to ensure that coupling went to completion. Once it was determined that coupling was complete, the growing peptide chain was deprotected using 20% (v/v) piperidine in DMF solution followed by coupling of the second amino acid. The remaining amino acids were added to the growing peptide chain in the same manner. Each coupling reaction included the amino acid, HCTU, and DIPEA. After the final amino acid was coupled, the *N*-terminus was acetylated. The peptide was cleaved from the resin and all side-chain protecting groups were removed using the cleavage cocktail of 95% TFA, 2.5% TIS, and 2.5% water.

Table 1. cAMP Assays of **MT-I** (known as NDP- α -MSH), tetrapeptide **1**, MC1R selective peptide **2**, and **MT-II** towards Melanocortin Receptors.

	MC1R cAMP		MC3R cAMP		MC4R cAMP		MC5R cAMP	
	EC ₅₀	% Act	EC ₅₀	% Act	EC ₅₀	% Act	EC ₅₀	% Act
MT-1	-	100	0.8 ± 0.3	100	0.2 ± 0.04	100	1 ± 0.3	100
1	4.5	100	7.1	100	607	100	2788	35
2	261	58	NA	0	2874	100	NA	0
MT-II	1.02 ± 0.4	100	5.1 ± 0.3	100	2.1 ± 0.6	100	5.7 ± 2.2	100

^aMT-II = Ac-Nle-c[Asp-His-D-Phe-Arg-Trp-Lys]-NH₂. EC₅₀ = Effective concentration of peptide that was able to generate 50% maximal intracellular cAMP accumulation (N = 4). Act% = % of cAMP produced at 10 μ M ligand concentration, in relation to MT-II. NA = 0% cAMP accumulation observed at 10 μ M. The peptides were tested at a range of concentration from 10⁻¹⁰ to 10⁻⁵ M.

Acknowledgements

Supported in part by a grant from the U.S. Public Health Service, National Institutes of Health, DK017420, GM 108040 and DA06284.

References

1. Hraby, V.J. *Nat. Rev. Drug Discov.* **1**, 847-858 (2002), <http://dx.doi.org/10.1038/nrd939>
2. Hraby, V.J., Wilkes, B.C., Hadley, M.E., Al-Obeidi, F., Sawyer, T.K., Staples, D.J., deVaux, A.E., Dym, O., Castrucci, A., Hintz, M.F., Riehm, J.P., Rao, K.R. *J. Med. Chem.* **30**, 2126-2130 (1987), <http://dx.doi.org/10.1021/jm00394a033>
3. Sawyer, T.K., Sanfilippo, P.J., Hraby, V.J., Engel, M.H., Heward, C.B., Burnett, J.B., Hadley, M.E. *Proc. Natl. Acad. Sci. USA* **77**, 5754-5758 (1980), <http://dx.doi.org/10.1073/pnas.77.10.5754>
4. Chen, M., Cai, M., Aprahamian, C.J., Georgeson, K.E., Hraby, V., Harmon, C.M., Yang, Y. *J. Biol. Chem.* **282**, 21712-21719 (2007), <http://dx.doi.org/10.1074/jbc.M702285200>
5. Chen, M., Aprahamian, C.J., Celik, A., Georgeson, K.E., Garvey, W.T., Harmon, C.M., Yang, Y. *Biochemistry* **130**, 1128-1137 (2006). <http://dx.doi.org/10.1021/bi0521792>

Alcohol Abrogates Intracellular Ca^{2+} Elevation by Angiotensin II and ATP in Cultured Rat Astrocytes

Steve Wu¹, Zhiqian Wu², and Desuo Wang²

¹PharmD Candidate PCOM School of Pharmacy Class 2017; ²Department of Pharmaceutical Sciences, Philadelphia College of Osteopathic Medicine School of Pharmacy, Suwanee, GA, 30024, USA

Introduction

Astrocytes have a robust and dynamic intracellular Ca^{2+} activity in response to stimulation by various neurotransmitters and neuromodulators such as angiotensin II, glutamate, and ATP [1-4]. ATP evokes Ca^{2+} bursts in astrocytes by activation of purinergic receptors [4] and angiotensin II (AngII) by stimulation of AT1 receptors [2]. Intracellular Ca^{2+} mobilization by the peptide and high energy purine signaling molecules enhances astrocyte cycling excitatory neurotransmitter glutamate, which governs the social behavior and cognitive ability [5-7]. Acute alcohol overdose alters users' social behavior and affects abusers' cognition [8,9]. We hypothesize that alcohol impairs the intracellular Ca^{2+} handling in astrocytes particularly in response to neurotransmitter/neuromodulator stimulation, which may play an important role in understanding alcohol intoxication. The impairment may relate to the development of alcohol addiction, dependence and tolerance. In this work, we studied the alteration of intracellular Ca^{2+} signaling by alcohol treatment in cultured rat hippocampal astrocytes. The findings of this study enrich our understanding of ethanol intoxication and may lead to a new treatment target for alcoholism.

Results and Discussion

Rat hippocampus astrocytes (GFAP immunocytofluorescence positive) from Creative Bioarray (CSC-C8055L) were used to measure intracellular Ca^{2+} transients at $33 \pm 0.5^\circ\text{C}$. The cells were continuously perfused with Hank's solution containing 2.0 mM CaCl_2 (pH=7.4) and loaded with 1 μM Fura-2 AM (Thermo Fisher Scientific, Life Technologies, F-1201) in 0.1 mM Ca^{2+} Hank's solution containing 1 nM pluronic acid at 37°C for 30 min. Intracellular Ca^{2+} concentration ($[\text{Ca}^{2+}]_i$) was measured as a ratio of 340- over 380-nm wavelength fluorescence signals and digitized and recorded using an IonOptix PMT system.

In control experiments (without alcohol treatment), both Ang II and ATP concentration-dependently elevated $[\text{Ca}^{2+}]_i$ in the cultured astrocytes. The responsive Ca^{2+} signals occurred reliably in almost every single cell tested ($n > 20$) and the elevation of $[\text{Ca}^{2+}]_i$ was repeatable in the same cell when it was challenged second time with Ang II or ATP as shown in Figure 1.

Peptidergic neurotransmitter angiotensin II produced a peak and a prolonged plateau elevation in $[\text{Ca}^{2+}]_i$. In comparison, purinergic neuromodulator ATP caused a brief and steeper Ca^{2+} peak with a much faster recovery phase (i.e., lack of prolonged plateau elevation of $[\text{Ca}^{2+}]_i$). These results confirmed our previous work and were consistent with the data published by other investigators [2, 10,11]. The commercially available primary culture of glial fibrillary acidic protein (GFAP)-positive astrocytes is

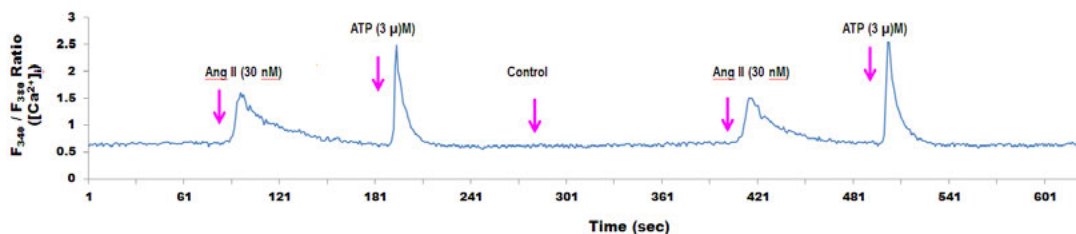


Fig. 1. Puff-application of Ang II (30 nM) or ATP (3 μM) or control vehicle caused increase in $[\text{Ca}^{2+}]_i$ in an astrocytes (a typical control experiment). The vertical axis is the ratio of fluorescence signal (F_{340}/F_{380}), an up-deflection indirectly indicates an increase in $[\text{Ca}^{2+}]_i$ relative to baseline. The horizontal axis is the real time elapsed after the experiment begins. Arrows indicate the puff-application of the test agents.

a convenient and reliable experimental model for studying the regulation of $[Ca^{2+}]_i$ by neurotransmitters and neuromodulators. Brain ACE/Ang II/AT1 axis plays an important role in stimulating the elevation of $[Ca^{2+}]_i$. When the cells were challenged with another angiotensin peptide Ang(1-7), there was no intracellular Ca^{2+} mobilization (data not shown). This indicates that the ACE2/Ang(1-7)/mas axis does not alter intracellular Ca^{2+} homeostasis in astrocytes [12].

We noticed that puff-application of ATP at micromolar concentration (1 to 100 μ M) is a dependable positive control for measurement of astroglial $[Ca^{2+}]_i$. In this cell culture model, astrocytes that responded to ATP stimulation also faithfully answered the challenge by Ang II. However, it is worth to point out that although peptidic Ang II and non-peptidic ATP stimulation both can activate astrocytes by elevation of $[Ca^{2+}]_i$, the Ca^{2+} transient signals elicited by these two stimuli are distinguishable by their peak amplitude and duration (Figure 1).

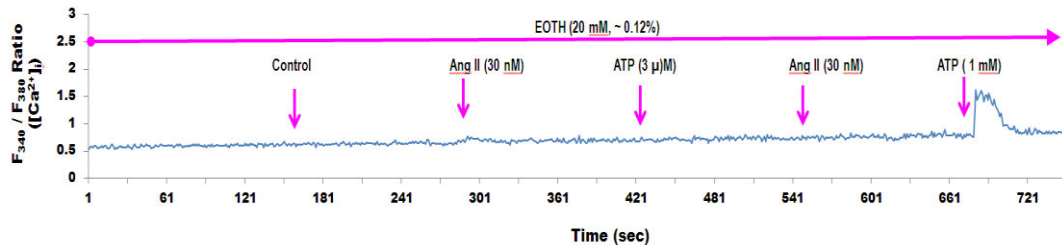


Fig. 2. Alcohol (EOTH) treatment abolishes intracellular Ca^{2+} signal triggered by both Ang II and AT. Same results were recorded from three cells ($n=3$). The horizontal arrow indicates the length of the EOTH application. The vertical arrows mark the puff of test agents.

The spatial and temporal differences in Ca^{2+} mobilization in the same cell demonstrate the diversity in the regulation of $[Ca^{2+}]_i$ even though activation of AT1 receptor by Ang II and P2Y receptor by ATP both are coupled to Gq-PLC-IP3 signaling transduction pathway [2,4]. What is/are the underlying mechanism(s) for these differences are not clear and it is worth to be elucidated in future studies.

Alcohol treatment (for 5-10 min) markedly affects ACE/Ang II/AT1 Ca^{2+} signaling in astrocytes (Figure 2). Ethanol (EOTH) itself did not cause any dynamic $[Ca^{2+}]_i$ fluctuation. However, in the presence of alcohol (20 mM, approximately equal to 0.12% plasma alcohol level), both the peak and the plateau phases of $[Ca^{2+}]_i$ elevation by angiotensin II (30 nM) were completely abolished (Figure 2 and 3). Application of higher concentration of Ang II (300 nM) did not counteract EOTH inhibition. The impact of alcohol on ATP-stimulated Ca^{2+} signal is more complicated. In one group of cells, EOTH abrogated physiologically relevant micromolar ATP-triggered $[Ca^{2+}]_i$ elevation [13] and only blunted $[Ca^{2+}]_i$ elevation when cells were challenged with much higher concentration of ATP (1 mM, Figure 2). In another group of cells, EOTH treatment only abolished peptidergic Ang II signal but had no impact on micromolar purinergic ATP-stimulated Ca^{2+} signaling (Figure 3). It is interesting

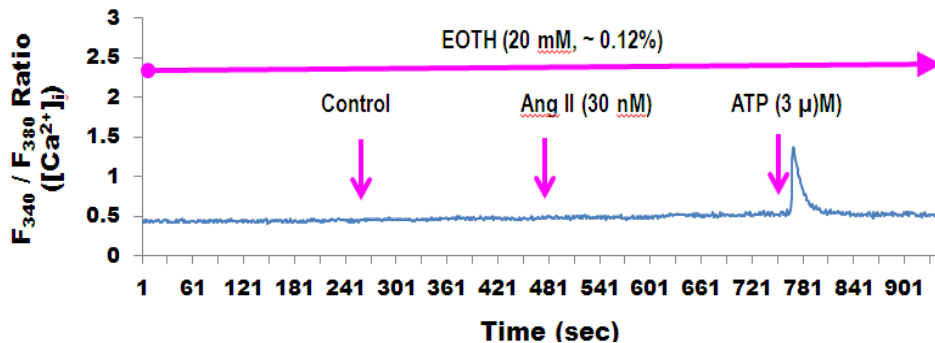


Fig. 3. Ethanol (EOTH) treatment abolishes intracellular Ca^{2+} signal triggered by Ang II. However, in this group of cells, EOTH exposure does not affect the effect of ATP on Ca^{2+} mobilization. Same results were recorded from three cells ($n=3$). The horizontal arrow indicates the length of the EOTH application. The vertical arrows mark the puff of test agents.

to find out the mechanism(s) that underlie the distinguishing influence of ethanol intoxication on Ang II-induced Ca^{2+} signaling and ATP-stimulated Ca^{2+} elevation in astrocytes in future study.

We noticed that EOTH (20 mM) treatment seemed to slightly elevate the baseline $[\text{Ca}^{2+}]_i$ in the time course of experimental recordings (Figure 2 and 3). This could be due to the non-specific impact of ethanol on lipid membrane or other Ca^{2+} transporting mechanisms in astrocytes. The small elevation of baseline $[\text{Ca}^{2+}]_i$ does not affect the dynamic Ca^{2+} signaling as shown in Figure 3.

The concentration of ethanol (20 mM) used in this study is approximately equal to 0.12% plasma alcohol level, which is relevant to alcohol intoxication. When blood alcohol content is in the range of 0.06-0.15%, drinkers may have moderate memory impairments, significant impairments in driving skills, impaired speech, balance, coordination and attention [14]. How the alteration of intracellular Ca^{2+} handling in astrocytes is correlated to these social behavioral and cognitive symptoms of alcohol intoxication is not clear. We suggest that acute ethanol exposure not only impairs the function of neurons but also disrupts the regulation of $[\text{Ca}^{2+}]_i$ by neurotransmitters and neuromodulators in astrocytes of the brain [15,16]. The later may play a significant role in alcoholism. As suggested by Agulhon, et al. [17], astrocytic G_q GPCR-mediated Ca^{2+} elevations may trigger the release of gliotransmitters through unresolved pathways. Astrocyte-released gliotransmitters may then signal back to neurons by activating presynaptic or postsynaptic (extrasynaptic) neuronal receptors to modulate synaptic transmission. Ethanol abrogates G_q GPCR-mediated Ca^{2+} elevations (panel B of Figure 4) and disrupts the normal signal communication between neurons and astrocytes.

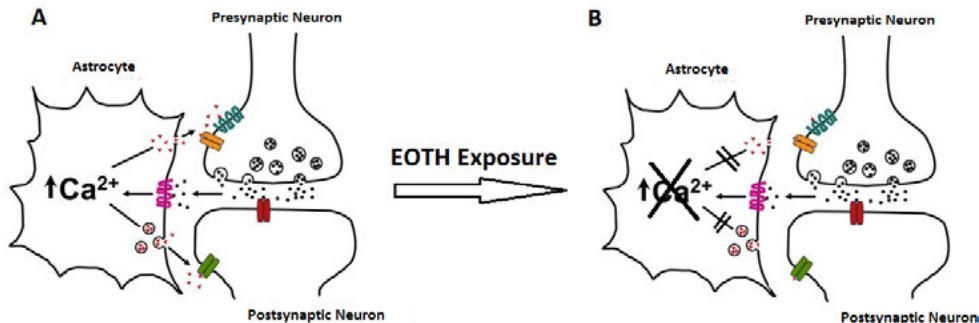


Fig. 4. Schematic depiction of the impact of EOTH exposure on neuro-astrocyte interaction (modified from Agulhon et al 2008).

In summary, our results are the first to demonstrate that acute alcohol exposure affects G_q GPCR-mediated Ca^{2+} elevations by Ang II and ATP (at least in some cells for the latter). The alcohol-caused alteration in the regulation of $[\text{Ca}^{2+}]_i$ by neurotransmitters and neuromodulators in astrocytes may have a significant role in alcohol intoxication. These study findings enrich our understanding of ethanol intoxication and may open up new treatment modalities for alcoholism.

Acknowledgments

SW was supported by the federal work study program. This work is supported by a research grant funded by the Research Division of Chief Science Officer in Philadelphia College of Osteopathic Medicine (Georgia Campus).

References

1. *Neural-Immune Interactions in Brain Function and Alcohol Related Disorders*. Cui, C., Grandison, L., Noronha, A. (Eds.), Springer, 2013, <http://dx.doi.org/10.1007/978-1-4614-4729-0>
2. Wang, D., et al. *J. Neurochem.* **67**, 996-1004 (1996), <http://dx.doi.org/10.1046/j.1471-4159.1996.67030996.x>
3. Shigetomi, E., et al. *Nat. Neurosci.* **13**, 759-766 (2010), <http://dx.doi.org/10.1038/nn.2557>
4. Franke, H., et al. *Purinergic Signal.* **8**, 629-657 (2012), <http://dx.doi.org/10.1007/s11302-012-9300-0>
5. Lee, L., et al. *J. Alzheimers Dis.* **38**, 49-62 (2014), <http://dx.doi.org/10.3233/JAD-130740>
6. Yadav, R., et al. *PLoS One* **7**, e32969 (2012), <http://dx.doi.org/10.1371/journal.pone.0032969>
7. Gupta, S.C., et al. *Neuropharmacology* **93**, 274-284 (2015), <http://dx.doi.org/10.1016/j.neuropharm.2015.02.013>
8. Cash, C., et al. *J. Psychopharmacol.* **29**, 436-446 (2015), <http://dx.doi.org/10.1177/0269881115570080>
9. Archimi, A., Kuntsche E. *Addict. Behav.* **39**, 713-716 (2014), <http://doi/10.1016/j.addbeh.2013.11.011>

10. Hamilton, N. *Glia*. **56**, 734-749 (2008), <http://doi/10.1002/glia.20649>
11. Park, H., et al. *J. Neurosci.* **29**, 13063-13073 (2009), <http://doi/10.1523/JNEUROSCI.3193-09.2009>
12. Ohishi, M., et al. *Curr. Pharm. Des.* **19**, 3060-3064 (2013), <http://doi/10.2174/1381612811319170013>
13. Yegutkin, G.G., et al. *Mol. Biol. Cell.* **17**, 3378-3385 (2006), <http://doi/10.1091/mbc.E05-10-0993>
14. <http://pubs.niaaa.nih.gov/publications/AlcoholOverdoseFactsheet/Overdosefact.htm>
15. Muñoz, G., et al. *Neurobiol. Aging* **36**, 845-856 (2015), <http://doi/10.1016/j.neurobiolaging.2014.10.017>
16. Llorente, J., et al. *Mol. Pharmacol.* **84**, 252-260 (2013), <http://doi/10.1124/mol.113.085936>
17. Agulhon, C., et al. *Neuron*. **59**, 932-946 (2008), <http://doi/10.1016/j.neuron.2008.09.004>

Designing AMPed: The Practical Antimicrobial Peptide Editable Database

**Tripti Garg^{1,2}, George Konstantinidis², Joan Peckham², Admir Monteiro³,
Roxanne LaCroix¹, and Lenore M. Martin¹**

¹Dept. of Cell & Molecular Biology; ²Dept. of Computer Science & Statistics; ³Electrical, Computer, & Biomedical Engineering, The University of Rhode Island, Kingston, RI, 02881, USA

Introduction

Peptide data are stored in various online repositories. Researchers typically need to sift through numerous databases containing large quantities of unwanted information before locating the exact data they need. Routine access to vital data is a very complex and daunting challenge. Individual researchers, experimenting with innovative search and data filtering strategies, have built up their own local databases, adding to an ever-increasing volume of highly dispersed, partially overlapping, peptide datasets. None of the existing online databases uniformly annotates their data, making correlating entries for identical proteins or peptides from one dataset to another a staggering task. Bioinformaticians have developed software to simplify cross-database searching, but the problem of locating useful antimicrobial peptide research-related entries buried inside general databases remains. Presently, AMPed consists of data obtained by bulk downloads of proteins less than 100 residues from four large online portals: UniProt (www.uniprot.org), NCBI (www.ncbi.nlm.nih.gov), EBI (www.ebi.ac.uk), and KEGG (www.genome.jp).

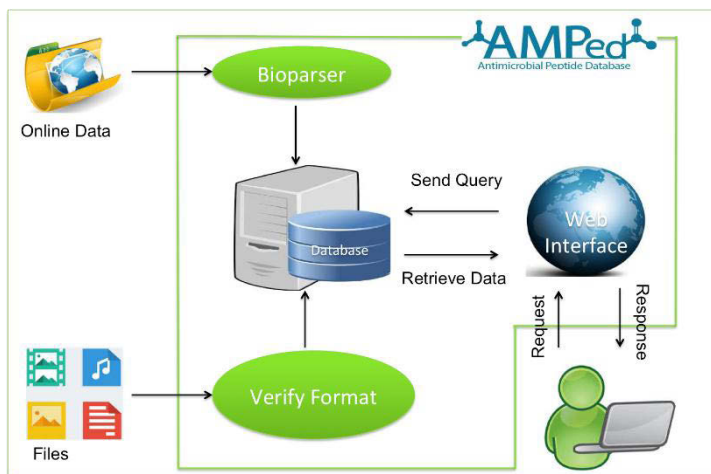


Fig. 1. The overall view of the AMPed system.

AMPed is under development at URI to support our ongoing research program on antimicrobial peptides. This work will enhance antimicrobial data access, facilitate long-distance collaborations, improve the search speed, and eliminate the need to manually correlate information gathered from multiple data sources, thereby greatly reducing the time researchers have to spend to locate and evaluate the desired data sets.

The integration of Bioparser, the AMPed database, and its web-based Interface is defined as the AMPed system (Figure 1). Bioparser, built in GO language, parses the bulk data downloaded from online repositories, converts it into a harmonious format and builds some connections. The AMPed database, developed in MySQL, is a highly normalized relational database that stores peptide data. The secure web-based interface, built using PHP & HTML5, provides easy access to the AMPed database

in the cloud. The new intuitive web interface is designed to help researchers easily formulate combinations of frequent database queries to meet their specific needs.

Navigation: A user-friendly interface for AMPed works equally well for both novice and expert users. The screens are organized logically to help users perform tasks efficiently. The navigation scheme for the AMPed interface is depicted in Figure 2.

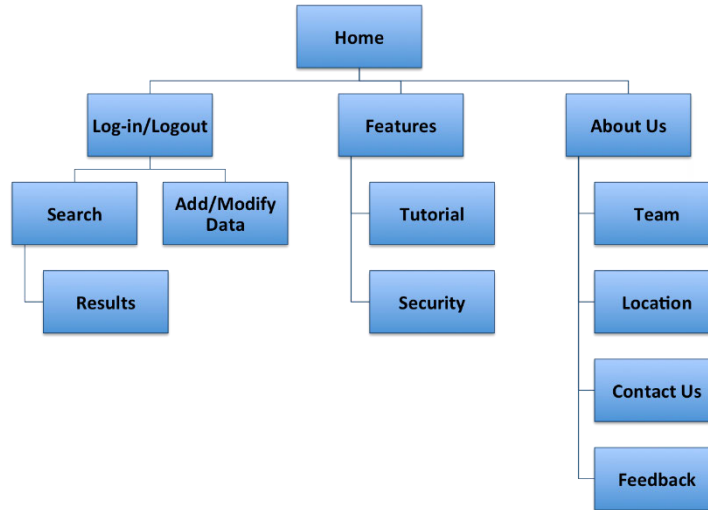


Fig. 2. Displays navigation scheme of webpages of the AMPed web interface.

The latest focus of the AMPed development project, is to build an easy, secure and intuitive user interface suitable for novice through expert researchers to efficiently search, display, manipulate, and eventually upload their own data into AMPed. The user interface project incorporates insights into various aspects of use of the current data set, and adds on and evaluates the utility of diverse visual displays of data.

Interface Design: There have been several empirical studies that identified basic psychological factors that should be considered when designing a Graphical User Interface (GUI). To design the AMPed GUI, we considered the following three primary contributing human factors:

- **Physical limits of visual acuity** - Visual acuity is the ability of the eye to resolve detail. The retina of the human eye can only focus on a small portion of a computer screen. The AMPed GUI will limit the size of icons, menus, dialog boxes etc. to ensure they fit into the limited area the human eye can take in at any one time. The design will also group related material to maintain user focus on one section of the screen. This will ensure that the user does not have to repeatedly move their eyes across the screen, causing eye fatigue due to unnecessary movements.
- **Limits of absolute memory** - Once the user has a desired fixation point, there is a limit to the amount of information that the person can store and process at one viewing. A GUI design “rule of thumb” is that the range of options or choices should never exceed five or six. AMPed GUI will chunk the information presented to the user (e.g. search results) into logical groups and will ensure not to crowd screen with data. It will also optimize the number of menu options (e.g. number of search criteria) on the page to develop clean and simple intuitive designs.
- **Gestalt Principle** - The Gestalt Principle states that people use a top-down approach to organizing data. AMPed GUI will leverage the Gestalt principle of ‘continuation’ by organizing the data in a top-down approach. It will leverage the principle of ‘similarity’ via using a template-driven approach to help users easily find like items, for example home link, log-in, log-out and search functions, at a consistent place across all screens. It will use the principle of ‘proximity’ to place similar search results close together so they are perceived as a logical group.

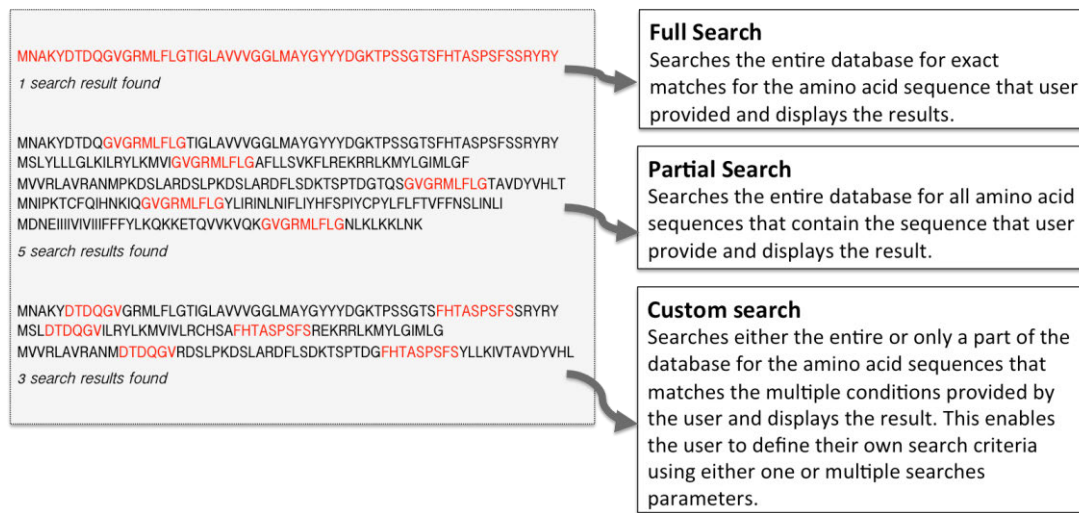


Fig. 3. A view of amino acid sequence search results.

Search Types: The full to custom search option allows researchers to easily parse through huge amounts of data quickly, efficiently and accurately. The example above (Figure 3) highlights how a full, partial or custom string search using an amino acid sequence provides different results when searched via AMPed.

Search Queries: The user interface provides the ability for a user to choose search strategies ranging from simple queries to complex combinations. The search function within AMPed consists of multiple pre-written SQL queries that are optimized for speed and accuracy. The results are sorted and viewed directly in the webpage or reports are offered that may be downloaded in multiple formats.

Data Security: The AMPed interface is designed to be highly secure and to meet the needs of different users by incorporating the following security mechanisms:

- Provides secure access to ensure data integrity and proper user authorization.
- Has CAPTCHA to protect from DOS (denial of service) attacks by robotic scripts.
- Provides tiered access levels for users: professors, students, experts & creators.
- Maintains access and audit logs for system managers to observe user trends

AMPed Website: An open source, user-friendly and well-secured website meant to provide access to the AMPed database by novice and expert users. The idea of “AMPed” (Anti-Microbial Peptide Editable Database) is to create a targeted annotated database consisting of uniquely focused information about antimicrobial peptides with the primary purpose of data storage uniformity and coherence. AMPed will be an open source public database with a simple and secure web interface that peptide researchers can use to locate and download sequences, structures, and biological information relevant to antimicrobial research, linked to the original data sources. AMPed is powered by a software tool called “Bioparser” that automatically extracts, sorts, and allows users to annotate data derived from online repositories.

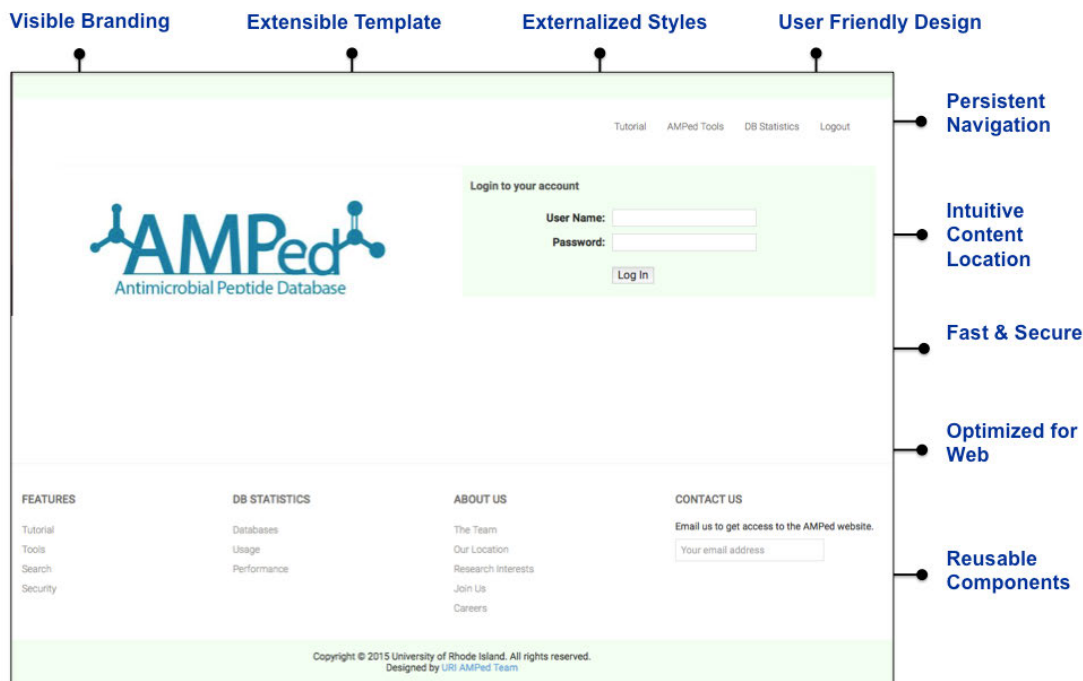


Fig. 4. The Home webpage of the AMPed web based user interface.

Acknowledgments

George Konstantinidis for designing Bioparser, & population of the AMPed database. BCH-CSC522 students for helping us take the first steps in this project. Professors Lenore M. Martin, Jean-Yves Hervé & Joan Peckham for valuable guidance & advice.

References

1. 2012, www.bbcm.univ.trieste.it/~tossi/pag1.htm, AMSDb, A Tossi, Trieste.
2. 2015, www.peptideatlas.org, Peptide Atlas, E Deutsch, Seattle.
3. 2012, aps.unmc.edu/AP/main.php, Antimicrobial Peptide Database, G Wang, Nebraska
4. 2012, 159.226.149.45/other1/kizapd/, Antimicrobial Peptide Database, Kunming Institute of Zoology, China
5. 2015, *Nucleic Acids Research*, Vol 43, Database Issue
6. 2014, George Konstantinidis; Thesis
7. 1998, E Tufte; *Visual Explanation: Images & Quantities, Evidence & Narrative*, CT
8. *International Journal of Man-Machine Studies*, Benbasat, I& P Todd; *An Experimental Investigation of Interface Design Alternatives*
9. 2010, Roman Pichler; *Agile Product Management with Scrum: Creating Products that Customers Love*, Addison-Wesley Professional, Boston

Comparing Structures of Two Antimicrobial Peptides Using a Self-Organized Mapping Approach

Faramarz Joodaki¹, Preston Steele², Lenore M. Martin³, and
Michael L. Greenfield¹

¹Department of Chemical Engineering; ²Department of Electrical, Computer, and Biomedical Engineering;

³Cell and Molecular Biology, University of Rhode Island, Kingston, RI, 02881, USA

Introduction

Antimicrobial peptides (AMP) show future potential as drugs against diverse kinds of bacteria [1]. The AMP mechanism of action is specified by its structure, which continues to change (folding process) during its attack on the membrane of bacteria [2]. Hence, the structure of AMPs has a crucial role in their functionality. Although this bacterial attack mechanism has been studied with experiments and some models have been hypothesized to explain it, a full understanding of the details has not been achieved [3-5]. Molecular modeling is a promising tool that can contribute to the better understanding of peptide structures and mechanisms of interaction with cell membranes [5].

A wide range of low energy conformations is usually obtained during molecular modeling, and each conformation may have different structural characteristics. Interpreting this huge set of simulation results from biological and biochemical perspectives is challenging because of the numerous small differences among conformations. The k-means clustering algorithm is a useful strategy to classify modeling data via physical and biological descriptors into different semi-homogeneous clusters on the basis of the distance from each data point to the center of each group. Each cluster is a region with a high density of data points which represent peptide conformations [6].

In this work, the structures of novel hybrid AMPs LM7-1 and LM7-2 [7], which were designed using combinations of pieces of naturally occurring AMPs, are investigated. These two AMPs differ in sequence at the 15th residue: glycine in LM7-1 compared to lysine in LM7-2. These AMPs do not adopt an amphiphilic helical shape until they contact a bacterial membrane [7]. Here, molecular modeling and data clustering are used to compare the structures of these two AMPs to study how this small sequence difference affects their range of accessible conformations and the ability to attain helical structures.

Results and Discussion

Monte Carlo (MC) simulation as a molecular modeling tool was applied using the Towhee program [8] to sample from low energy structures of LM7-1 at room temperature (298K) and of LM7-2 at both room temperature (298K) and biological temperature (310K). Charmm27 force field was used for calculating the potential energy. Towhee implements MC moves that include configurational bias for conformation rearrangement, pivots along dihedral angles, and atom displacements. It attempts random movements in each MC step to sample the potential energy surface of each AMP.

Figure 1 and 2 respectively show the changes in the total energy and the end-to-end distances of the two simulated AMP molecules after 800,000 cycles of MC steps. The steady fluctuations in the potential energy (Figure 1) suggest that each peptide molecule has equilibrated during the simulation. This is only one measure, however; the end-to-end distance during these three simulations continues to decrease and has not yet equilibrated at the end of the simulation. Since the conformations for these three simulations were still evolving at the end of 800,000 steps (Figure 2), equilibration cannot be determined using energy monitoring alone. The current three simulations sample among multiple AMP configurations of similar potential energies. However it is clear that continuing the MC simulations further to reach steady fluctuations in all variables, i.e. equilibration, is required. Further research to pursue such calculations is ongoing.

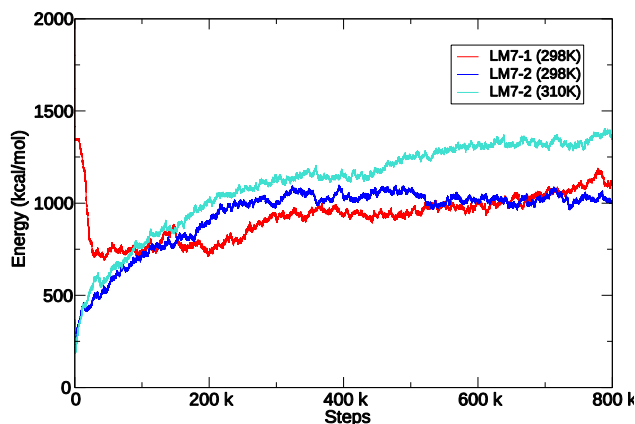


Fig. 1. Total energy distance of LM7-1 (at 298K) and LM7-2 (at 298 and 310K) during the MC simulation.

To facilitate the biological investigation of the current set of simulated peptide conformations, the Clustering Peptides and Proteins Software (CPP software) with graphic user interface (GUI) was developed using MATLAB. Just using the positions of all atoms (information found in the pdb files from the MC simulations), the CPP software calculates and displays some important physical and biological characteristics of the antimicrobial peptides: potential energies; propensities for specific secondary structures such as extended chains, alpha helices, pi helices, parallel and anti-parallel beta sheets; radii of gyration; end-to-end distances; and such shape parameters as acylindricity and asphericity. The CPP software then applies the K-means clustering algorithm based on a particular set of three calculated characteristics chosen by the user to aggregate closely related conformations from the simulation results and plot them on the (Self) organized 3-D map.

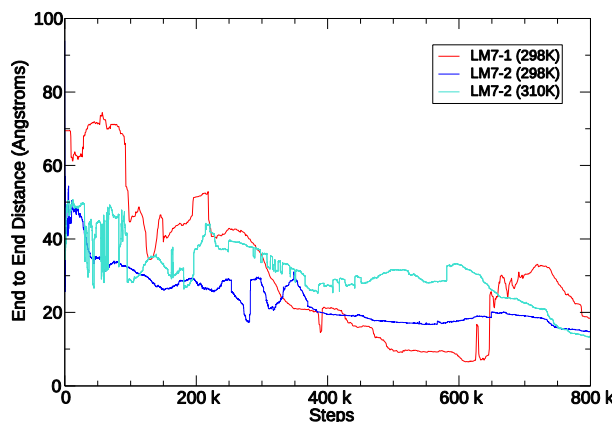


Fig. 2. End-to-end distance of LM7-1 (at 298K) and LM7-2 (at 298 and 310K) during the MC simulation.

The CPP software was first applied to 1,000 MC simulation conformations (between 35,000 to 800,000 steps at 298 K) of LM7-1 and then to 8,000 MC simulation conformations (between 0 to 800,000 steps at 310 K) of LM7-2. Figures 3 and 4, respectively, show examples of k-clustering results generated by the CPP software with radius of gyration (r_g), asphericity (bshape) and energy as the chosen three parameters. Although the initial structures for LM7-1 and LM7-2 during each MC simulation differ, the red clusters in both figures have some similar characteristics: the center point of the red cluster in figure 3 is $r_g = 10.0\text{\AA}$, bshape = 0.09 and energy = 1375 kcal/mol, while in Figure 4 $r_g = 9.28\text{\AA}$,

bshape = 0.33 and energy = 1316 kcal/mol. The energy and the radius of gyration for these clusters of conformations of the two peptides are quite similar, while the shape characteristics are very different. The LM7-1 structure has a more spherical shape, while LM7-2 tends to have more of a coin-shape. The cause of this shape difference and how it will tend to change in the presence of a lipid membrane are both interesting questions that are currently under investigation. Additional clusters in the LM7-1 simulation results show an overall trend from an initially extended chain conformation to a more compact conformation as the simulation proceeds. Some clusters for LM7-2 show much lower energies than for LM7-1. Figure 1 indicates that these low energy structures arise early in the simulation, near an initial α -helix conformation. The spontaneous rise in energy observed in Figure 1 from 0 to 200,000 steps indicates that this initial low-energy region is shallow compared to the thermal energy $k_B T$, at least without a hydrophilic or aqueous environment surrounding the peptide.

Several interesting observations can be obtained from analysis of the clustering based on groups of three chosen sets of diverse parameters over the course of the molecular modeling simulations. We are continuing to improve the CPP software and the next version will be open source and freely distributed. Adding the capability to choose additional meaningful biological parameters, such as hydrophobicity, is also currently under development.

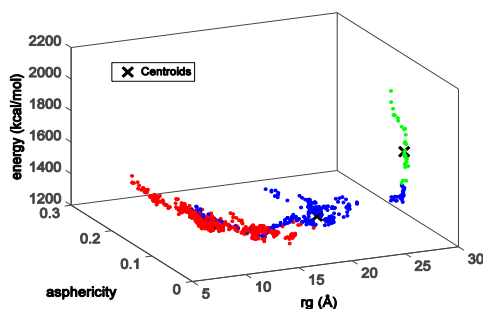


Fig. 3. Clustering results for 1000 conformations of LM7-1 (between 35,000-800,000 steps).

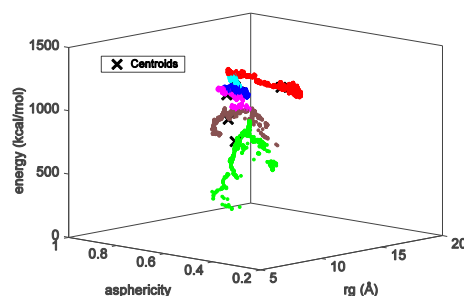


Fig. 4. Clustering results for 8000 conformations of LM7-2 (between 0-800,000 steps).

Acknowledgments

We thank the students in BCH-CSC522 Bioinformatics for helpful discussions and criticism. We thank Professor Jean-Yves Hervé for suggesting the k-means clustering algorithm, and Professors Martin and Greenfield for guiding stimulating discussion about the relevant propensities that could be plotted to better understand the changes in the peptide conformations and their effects during simulation.

References

1. Jenssen, H., Hamill, P., Hancock, R.E.W. *Clin. Microbiol. Rev.* **19**, 491-511 (2006), <http://dx.doi.org/10.1128/CMR.00056-05>
2. Powers, J.S., Hancock, R.E.W. *Peptides* **24**, 1681-1691 (2003), <http://dx.doi.org/10.1016/j.peptides.2003.08.023>
3. Leontiadou, H., Mark, A.E., Marrink, S.J. *J. Am. Chem. Soc.* **128**, 12156-2161 (2006), <http://dx.doi.org/10.1021/ja062927q>
4. Wang, K.F., Nagarajan, R., Camesano, T.A. *Biophys. Chem.* **196**, 53-67 (2015), <http://dx.doi.org/10.1016/j.bpc.2014.09.003>
5. Wang, Y., Zhao, T., Wei, D., Strandberg, E., Ulrich, A.S., Ulmschneider, J.P. *Biochim. Biophys. Acta - Biomembr.* **1838**, 2280-2288 (2014), <http://dx.doi.org/10.1016/j.bbmem.2014.04.009>
6. Likas, A., Vlassis, N., Verbeek, J.J. *Pattern Recognit.* **36**, 451-461 (2003).
7. LM7-1 and LM7-2 peptides were designed and synthesized by L. M. Martin and D. Ryder, *University of Rhode Island, Dept. of Cell Mol. Biol.*
8. Martin, M.G. "MCCCS Towhee: a tool for Monte Carlo molecular simulation," *Mol. Simul.* **39**, 212-1222 (2013), <http://dx.doi.org/10.1080/08927022.2013.828208>

Multi-Variable Individual Heating Conditions Tested in Parallel Provide Rapid Process Optimization on the Prelude® X

Daniel Martinez, James P. Cain, Elizabeth Restituyo-Rosario, Katya
Karankevich, Peter Bergwall, and Nathaniel Cosper

Protein Technologies, Inc., Tucson, AZ, 85714, USA, Website: www.ptipep.com, Email: info@ptipep.com

Introduction

Despite their high selectivity and low toxicity compared to their small molecule counterparts, a pressing problem when looking at the design of peptide drugs is their poor oral bioavailability and short *in vivo* half-life. Significant progress has been made to address the disadvantages of peptide drugs through modifications such as head-to-tail cyclization, backbone *N*-methylation, and “stapling” through a ring-closing metathesis (RCM) reaction, all of which can increase the synthetic difficulty. The application of heat represents an additional tool to optimize the production of challenging synthetic peptides, and a new heating technology, induction heating, has been introduced on the Prelude X. Induction heating allows for independent, simultaneous and rapid heating of multiple reactors with increased efficiency. Different heating conditions, at 25°C, 60°C and 90°C were used for the synthesis of the difficult JR(1-10)peptide (Figure 1) [1].



Fig. 1. Sequence of JR(1-10) peptide synthesized with heat on the Prelude X® platform.

Results and Discussion

Experimental results show a vast improvement in crude purity as temperature was increased. The highest purity was found for the synthesis at 90°C. Compared to 25°C, 90°C produced a 51% improvement in the purity. From the tested conditions, applying heat at 90°C improved crude purity more than four-fold when compared to the synthesis performed at room temperature (Figure 2). Importantly, rapid process optimization was attained through the use of independently heated parallel synthesis.

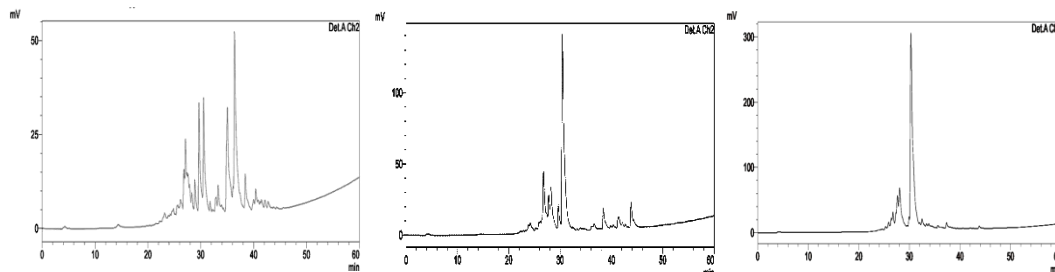


Fig. 2. HPLC traces of JR(1-10) peptide synthesized with heat on the Prelude X® platform at 25°C, 60°C and 90°C (left to right).

References

1. Redemann, T., Jung, G. In Ramage, R., Epton, R., Eds., *Peptides 1996, Proceedings of the 24th European Peptide Symposium*, Mayflower Scientific Ltd, Kingswinford, UK, 1998, p. 749.

Labeling and Expression of Opioid Receptors Using N-Terminal Fusion of Fluorescent Proteins

C.T. Dooley^{1,2}, A. Gioseffi¹, and Y. Li¹

¹Torrey Pines Institute for Molecular Studies, Port Saint Lucie, FL, 34987, USA;

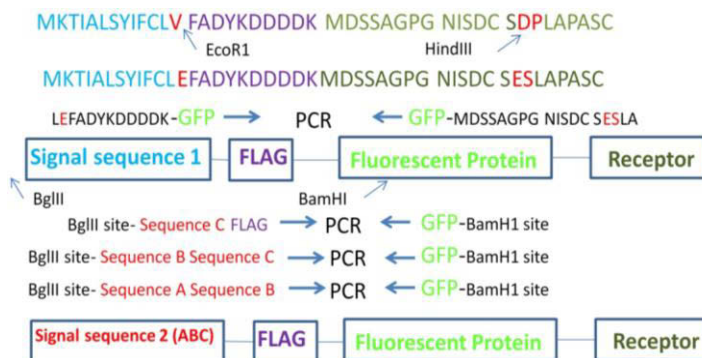
²Brilliant Biosciences, Port Saint Lucie, FL, 34987, USA

Introduction

The most efficient fluorescent based binding assay requires detection of Förster resonance energy transfer (FRET) or Luminescence Resonance Energy Transfer (LRET) between two matched fluorescent ligands in the former or a chelated lanthanide donor and fluorescent acceptor in the latter, one attached to the receptor and one attached to the ligand. Although there is an abundance of fluorescent based functional assays for G-coupled protein receptors (GPCRs) [1,2], there are few fluorescent based receptor binding assays, the only commercial fluorescent based binding assay contains SNAP tags [3,4], although capable of FRET it requires the expression of a heterologous protein which is subsequently labeled with a fluorescent tag. Many of the GPCRs including the opioid receptors have short *N*-terminal tails, usually 20-50 amino acids. Early attempts to fuse FP to the receptors yielded poor results such that today fusion to the *C*-terminal tail is the preferred method of labeling receptors. There are notable exceptions such as class II GPCRs that naturally have large extracellular domains such as vasoactive intestinal peptide receptor (VPAC1), these receptors readily accept fusion of a FP to the *N*-terminal tail [5]. GPCRs with large extracellular domains usually have a cleavable signal peptide that enables cell surface expression. Increasing receptor expression at the cell surface by inserting a cleavable signal sequence to heterologous receptors was first described for adrenergic receptors [6] and is now a widely used method for receptor expression. Early studies described for the mu opioid receptor (MOR) with a FP fused to the *N*-terminal of the receptor by insertion of the FP between the signal sequence of the insect endogenously expressed Immunoglobulin Heavy Chain Binding Protein (BiP) and MOR. Cell surface expression was achieved but FP-MOR was limited to insect cells and receptors were observed to be trapped within intracellular compartments [7]. In mammalian cells it appeared that insertion of a signal sequence interfered with the natural regulation of expression via glycosylation [8,9] or alternate strategies such as binding to p24A through the acidic residues at the second extracellular loop [10].

Results and Discussion

Cloning: The nucleotide sequence for GFP was inserted into a plasmid (pN1) already containing mouse MOR (Scheme 1). An EcoRI site was first created in the initial *N*-terminal sequence (MKTIALSYIFCLEF) by replacing the valine (V) by glutamic acid (E) to generate GAATTC and a HindIII site within the receptor sequence ISDCSDPLAPA replacing the amino acids aspartic acid and proline (DP) with glutamic acid and serine (ES) to generate AAGCTT using site directed mutagenesis. GFP nucleotide sequence with the two flanking restriction sites was generated by PCR, using a forward primer with a EcoRI site and a reverse primer with a HindIII site. The PCR product was inserted into the plasmid. Our signal peptide was inserted using nested PCR reactions with a BamHI site engineered into the MOR receptor sequence and a BglII site located in the multiple cloning site of pN1. The human clones of DOR, KOR



Scheme 1. Molecular cloning strategy for production of fluorescent labeled receptor at the N-terminus with custom signal peptide.

and OXR2 fusions were generated by exploiting the BsrG1 site on the 3' of the GFP sequence and NotI in the pN1 vector (an internal NotI site in DOR was first removed). Further optimization of the signal sequence was achieved using site directed mutagenesis (proprietary information).

MOR binding assay: Rat cortices were homogenized using 50 mM Tris, pH 7.4, and centrifuged at 16,500 rpm for 10 min. The pellets were resuspended in fresh buffer and incubated at 37°C for 30 min. Following incubation, the suspensions were centrifuged as before, the resulting pellets resuspended in 100 volumes of 50 mM Tris, pH 7.4 plus 2 mg/ml bovine serum and the suspensions combined. Each assay tube contained 0.5 ml of membrane suspension, 2 nM [³H]-DAMGO, in a total volume of 0.65 ml.

Imaging: Experiments were carried out on a Zeiss Axiovert Microscope equipped with a scanning stage, an incubation chamber, an ultra-high speed Lambda DG-4 wavelength switcher, and an AxioCam CCD camera (Zeiss, Gottingen, Germany) all controlled by Axiovision software 4.8. Cells were maintained during imaging at 37°C in a 5% CO₂ atmosphere. Filters used were; green excitation (480/20nm) green emission (530/20nm) and orange excitation (531/40nm), orange emission (593/40nm) and the dichroics used were FF495 and FF559 respectively (Semrock, Rochester, NY).

Results and Discussion

GFP-labeled MOR

We have optimized a signal sequence that allows for efficient extracellular expression of FP-fused GPCRs with short amino terminal tails. For GFP-MOR, the green fluorescent protein was fused to the N-terminal end of the receptor by preparation of a cloning vector (pN1), a 23 amino acid sequence was inserted immediately following the initiating methionine, a linker of 2 amino acids was used between the signal sequence and GFP, a second linker (Gly-Ser-Gly) was used between the GFP and the first amino acid of the opioid receptors. Expression of the vector in COS cells revealed a high number of cells expressing the fluorescent receptor at the cell surface. External presentation of the GFP was confirmed using antibodies raised against the Flag tag sequence (FADYKDDDDK) present on the sequence between the signal peptide and GFP (Figure 1).

To test whether the external GFP interfered with binding to the receptor we compared the binding affinity of DAMGO, a standard opioid ligand, at the N-terminal fused GFP-MOR compared to the receptor with the fluorescent protein fused to the C-terminal. The binding affinity of GFP-MOR ($K_i = 3.06$ nM), did not differ from that of the C-terminal fused receptor ($K_i = 2.96$ nM) as determined in a radioreceptor binding assay (Figure 2). Differences observed in the total bound values are due to expression of the GFP-MOR by transient transfection versus a stable clone cell line

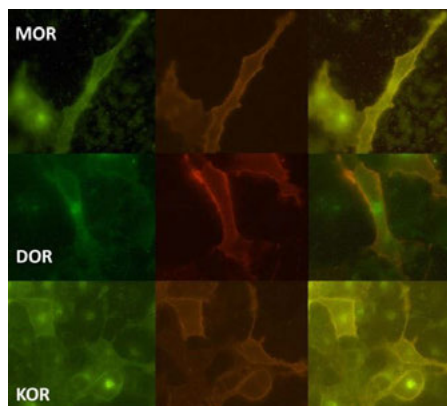


Fig. 1. Surface expression in COS7 cells of opioid receptors (OPR) with GFP fused to the N-terminal of the receptor. Left panel: Green fluorescent intensity for GFP-OPR. Middle panel: Fluorescent intensity for red FP-labeled antibodies bound to flag-tag on GFP-OPR. Antibodies are bound to non-permeabilized fixed cells demonstrating the external expression of the GFP. Right panel: Merge of images demonstrating overlap of GFP and RFP fluorescence.

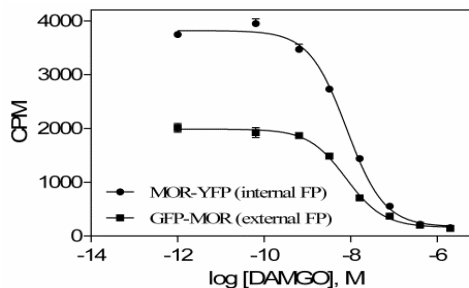


Fig. 2. Radioreceptor binding assay for GFP-MOR expressed in HEK293 cells. ³H-DAMGO was observed to bind to cells expressing MOR with similar affinities whether the fluorescent protein was fused to N- or C-terminal. Graphs represent the average \pm sem of three replicates.

for MOR-YFP. We have successfully applied the *N*-terminal fusion method to all 3 opioid receptors (MOR, DOR, and KOR) and the orexin 2 receptor.

Use of Fluorescent labeled cyclic peptide for FRET.

We have previously designed, synthesized, and identified a fluorescent labeled MOR ligand from a mixture-based penta-cyclic peptide library [11]. Screening and de-convolution of a penta-cyclic peptide library identified a potent and selective MOR ligand (Figure 3) exhibiting a binding affinity of $K_i=14$ nM. We prepared analogues of this peptide in which the anthraniloyl group was replaced with Rhodamine, the binding affinity was not adversely affected by the addition of the fluorescent dye.

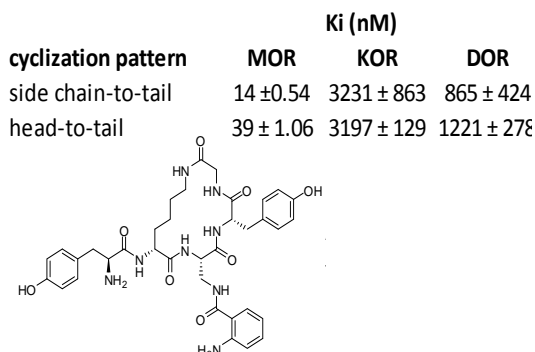


Fig. 3. Selective MOR ligand.

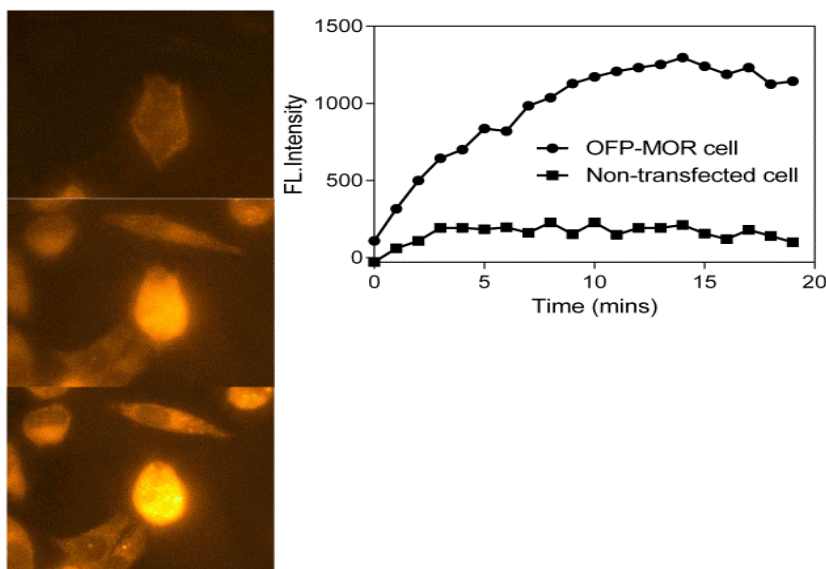


Fig. 4. Binding of Rhodamine labeled cyclic peptide to CHO cells. Cells transfected with OFP labeled MOR were exposed to 100 μ M peptide and images taken at 1 minute intervals for 20 mins. Filters used were; 559/34 for excitation; 607/36 for emission and a GFP Dichroic FF593.

To determine that cells expressing the *N*-terminal fusion protein were capable of binding the rhodamine labeled cyclic peptide we performed a time-lapsed imaging experiment in which we compared the increase in red fluorescence on the cell surface between cells transfected with the FP-MOR and non-transfected cells. There was a fivefold increase in the level of rhodamine fluorescence observed on the cells expressing the *N*-terminal GFP fusion (Figure 4). We then used a combination of the rhodamine labeled MOR ligand and the *N*-terminal fusion of GFP to the mu opioid receptor to determine if there was FRET between the ligand and the externally expressed GFP. FRET between GFP-labeled MOR and Rhodamine labeled cyclic peptide was demonstrated in HEK293 cells using live cell imaging, cells expressing the *N*-terminal GFP-MOR were labeled with the cyclic peptide for 30 minutes (images taken at 5 min intervals), then the fluorescent ligand was washed out and cells

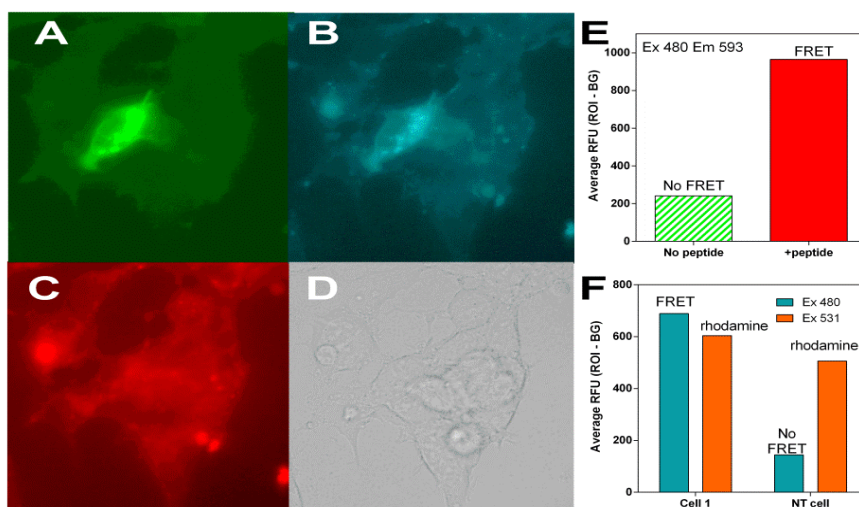


Fig. 5. Binding of rhodamine-labeled MOR peptide demonstrates FRET with GFP-labeled MOR receptor. A. GFP labeled HEK293 cells. Demonstrate cell surface expression (708ms). B. Use of excitation at green wavelength (489/20nm) and emission at red wavelength (593/40nm) reveals FRET in all GFP expressing cells (1300ms Can). C. Excitation at rhodamine channels (531/40nm) and emission at red channel before addition of peptide demonstrates a small leak through for the brightest cell, but FRET values increase 5 fold upon addition of rhodamine labeled peptide (all exposures 1300ms). F. Comparison of Fret (cyan) and red channels (red) demonstrate the occurrence of efficient FRET correlates with the expression of MOR-GFP. Fret is observed in GFP labeled cells but minimal in non-transfected cells (NT, all exposures 1300 ms).

imaged for another 15 minutes (Figure 5). Images were taken using excitation and emission of for Green fluorescence and red fluorescence and excitation at green and emission at red wavelengths, FRET was observed between the ligand and receptor in transfected cells but not in non-transfected cells (Figure 5F).

References

- Alvarez-Curto, E., Pediani, J.D., Milligan, G. *Anal. Bioanal. Chem.* **398**, 167-180 (2010), <http://dx.doi.org/10.1007/s00216-010-3823-4>
- Castro, L.R., Guiot, E., Polito, M., Paupardin-Tritsch, D., Vincent, P. *Biotechnol. J.* **9**, 192-202 (2014), <http://dx.doi.org/10.1002/biot.201300202>
- George, N., Pick, H., Vogel, H., Johnsson, N., Johnsson, K. *J. Am. Chem. Soc.* **126**, 8896-8897 (2004), <http://dx.doi.org/10.1021/ja048396s>
- Gautier, A., Juillerat, A., Heinis, C., Correa, I.R., Jr., Kindermann, M., Beaufils, F., Johnsson, K. *Chem. Biol.* **15**, 128-136 (2008), <http://dx.doi.org/10.1016/j.chembiol.2008.01.007>
- Couvineau, A., Rouyer-Fessard, C., Laburthe, M. *Regul. Pept.* **123**, 181-185 (2004), <http://dx.doi.org/10.1016/j.regpep.2004.06.025>
- Guan, X.M., Kobilka, T.S., Kobilka, B.K. *J. Biol. Chem.* **267**, 21995-21998 (1992).
- Perret, B.G., Wagner, R., Lecat, S., Brillet, K., Rabut, G., Bucher, B., Pattus, F. *Protein Expr. Purif.* **31**, 123-132 (2003), [http://dx.doi.org/10.1016/S1046-5928\(03\)00140-2](http://dx.doi.org/10.1016/S1046-5928(03)00140-2)
- Ge, X., Loh, H.H., Law, P.Y. *Mol. Pharmacol.* **75**, 1307-1316 (2009), <http://dx.doi.org/10.1124/mol.108.054064>
- Huang, P., Chen, C., Mague, S.D., Blendy, J.A., Liu-Chen, L.Y. *Biochem. J.* **441**, 379-386 (2012), <http://dx.doi.org/10.1042/BJ20111050>
- Luo, W., Wang, Y., Reiser, G. *J. Neurochem.* **117**, 71-81 (2011), <http://dx.doi.org/10.1111/j.1471-4159.2011.07173.x>
- Li, Y., et al. *ACS Comb. Sci.* **14**, 673-679 (2012), <http://dx.doi.org/10.1021/co300110t>

B7H6: A Bio-Marker for the Development of Cancer-Targeted Immunotherapy Applications

Mariana Phillips¹, Constantine Bitsakis², and David Sabatino¹

¹*Department of Chemistry and Biochemistry; ²Department of Biological Sciences, Seton Hall University,
400 South Orange Ave, South Orange, NJ, 07079, USA*

Introduction

Natural Killer (NK) cells are a class of cytotoxic lymphocytes with the ability to rapidly eliminate transformed or infected cells upon activation [1]. A key mediator of the NK cell line activity, NKp30, is a member of the natural cytotoxicity receptors (NCRs) that signal pro-inflammatory cytokine and chemokine production, as well as the release of cytotoxic agents that leads to tumor cell death [2]. The active search of NKp30-dependent immunostimulatory ligands led to chemical cross-linking studies followed by tryptic digestion, tandem mass spectrometry and proteomic analyses of the leukemia cell line K562 with soluble NKp30-Fc fusion protein which revealed B7H6 as a cell membrane expressed protein ligand of the NKp30 receptor [3]. Mechanistic studies demonstrated that upon binding of B7H6 to NKp30, the association of a transmembrane arginine residue of NKp30 to an ITAM bearing protein, such as CD3 ζ , initiated a signaling cascade that resulted in the reorganization of the NK cells' cytoskeleton and initiation of Ca²⁺ flux that ultimately led to the secretion of inflammatory cytokines [4]. Consequently, the discovery of the B7H6-NKp30 binding interaction offers a new opportunity in the development of tumor immunotherapy applications [5]. This study will highlight our most recent achievements in validating B7H6 as a lead protein biologic in cancer immunotherapy.

Results and Discussion

Flow cytometry was used to investigate the binding interactions of the soluble free form of B7H6 with the NK92-MI cells known to overexpress the cell surface NKp30 receptor. In a direct binding assay, Alexa Fluor 488-labeled B7H6 demonstrated similar binding to NK92-MI cells' (85%) compared to the human APC-labeled antiNKp30 monoclonal antibody (95%) (Figure 1). These initial results confirmed the NK cells' binding affinity of the B7H6 ligand. A competitive binding assay was next conducted in order to determine the NKp30 receptor binding specificities of the B7H6 ligand. In this assay, the NK92-MI cells were incubated with the Alexa Fluor 488-labeled B7H6 ligand, followed by treatment with the APC-labeled antiNKp30 monoclonal antibody. Flow cytometry analyses demonstrated partial displacement of B7H6 (~70%) upon addition of the antiNKp30 monoclonal antibody (Figure 2). Interestingly, when the NK92-MI cells were first incubated with the APC-labeled antiNKp30 monoclonal antibody, followed by treatment with the Alexa Fluor 488-labeled B7H6 ligand, no displacement was observed, suggesting allosteric binding of both ligands to the NKp30 receptor. Nevertheless, the ability for B7H6 to induce inflammatory responses on the NK92-MI cells was next evaluated by ELISA. In this assay, the NK92-MI cells were left untreated (negative control), and incubated with the soluble free form of B7H6 (test sample). Following a 24 h incubation period, the cells were harvested and media was tested for the secretion of the pro-inflammatory cytokines TNF α and IFN γ . In this assay, B7H6 was found to activate NK92-MI cells resulting in the release of pro-inflammatory cytokines TNF α and IFN γ (Figure 3). These results supports B7H6 as an immunostimulatory ligand of the NK92-MI cells for the development of cancer-targeted immunotherapy approaches. Moreover, B7H6 will be studied as a synergistic activator of pro-inflammatory cytokines as well as a trigger of potent immunological activities within diverse tumor microenvironments.

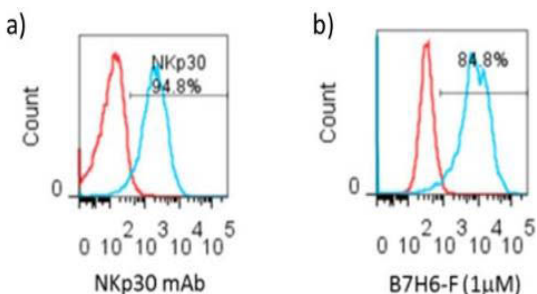


Fig. 1. Direct binding studies: Flow cytometry analyses of A. Anti-NKp30 APC labeled monoclonal antibody (2 μ L) and B. Alexa Fluor 488 labeled B7H6 ligand (1 mM, 20 μ L in PBS) with NK92-MI cells.

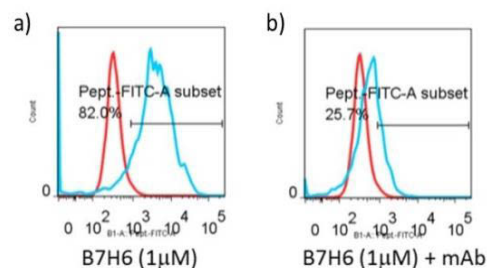


Fig. 2. Competitive binding studies: Flow cytometry analyses of A. Alexa Fluor 488 labeled B7H6 ligand (1 mM, 20 μ L in PBS) and B. Anti-NKp30 APC labeled monoclonal antibody (2 μ L) in the presence of Alexa Fluor 488 labeled B7H6 ligand (1 mM, 20 μ L in PBS) with NK92-MI cells.

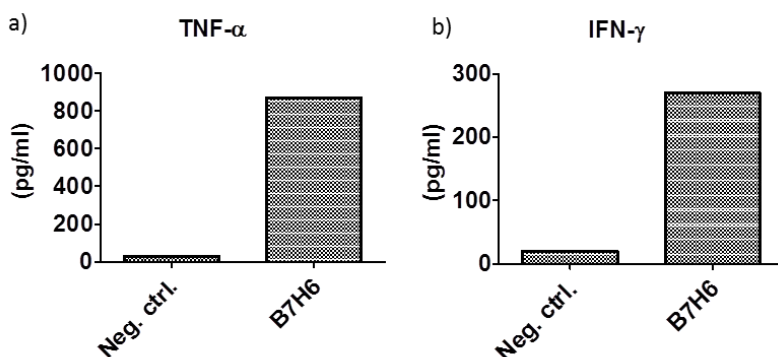


Fig. 3. Immunostimulatory Activity: ELISA of the NK92-MI cell excretion of A. TNF α and B. IFN- γ in the presence of B7H6 ligand (0.5mM, 100 μ L).

Acknowledgments

The authors would like to thank the Department of Chemistry and Biochemistry at Seton Hall University for continued support. The authors are also grateful to the 24th APS for accommodating our research presentation.

References

1. Vivier, E., Tomasello, E., Baratin, M., Walzer, T., Ugolini, S. *Nat. Immunol.* **9**, 503-510 (2008), <http://dx.doi.org/10.1038/ni1582>
2. Pende, D., Parolini, S., Pessino, A., Sivori, S., Augugliaro, R., Morelli, L., Marcenaro, E., Accame, L., Malaspina, A., Biassoni, R., Bottino, C., Moretta, L., Moretta, A. *J. Exp. Med.* **190**, 1505-1516 (1999), <http://www.ncbi.nlm.nih.gov/pmc/articles/PMC2195691/>
3. Li, Y., Wang, Q., Mariuzza, A. *J. Exp. Med.* **208**, 703-714 (2011), <http://dx.doi.org/10.1084/jem.20102548>
4. Kaifu, T., Escaliere, B., Gastinel, L.N., Vivier, E., Baratin, M. *Cell. Mol. Life Sci.* **68**, 3531-3539 (2011), <http://dx.doi.org/10.1007/s00018-011-0802-7>
5. Brandt, C.S., Baratin, M., Yi, E.C., Kennedy, J., Gao, Z., Fox, B., Haldeman, B., Ostrander, C.D., Kaifu, T., Chabannon, C., Moretta, A., West, R., Xu, W.F., Vivier, E., Levin, S.D. *J. Exp. Med.* **206**, 1495-1503 (2009), <http://dx.doi.org/10.1084/jem.20090681>

Structural Determinants of Furin Inhibitors Derived from Influenza Hemagglutinin

Monika Lewandowska-Goch¹, Anna Kwiatkowska², Teresa Łepeć¹,
Adam Prahl¹, and Robert Day²

¹Faculty of Chemistry, University of Gdańsk, Poland; ²Institut de Pharmacologie de Sherbrooke (IPS),
Université de Sherbrooke, Sherbrooke (QC), Canada

Introduction

Furin belongs to a small family of the proprotein convertases (PCs) and is the best-characterized member with a ubiquitous tissue distribution. Furin is responsible for posttranslational transformation and activation of proproteins into biologically active proteins and regulation of many physiological processes in living organisms [1]. In addition to their normal physiological role, furin and related convertases contribute to the maturation of many diseases-related proteins and are involved in tumorigenesis, neurodegenerative disorders, diabetes and atherosclerosis [2]. Moreover, furin is also required for the activation of many bacterial and viral toxin precursors (including *Pseudomonas aeruginosa*, pathogenic Ebola strains, Marburg, HIV gp160, the avian influenza virus hemagglutinin) [3]. Studies have shown that the hemagglutinin of avian influenza virus A contains a TPRERRRKKRTGL sequence, which is a furin cleavage site. The optimization of TPRERRRKKRTGL peptide led to the discovery of a potent inhibitor with the following sequence: Ac-RARRRKKRT-NH₂ [4,5]. In the present work, the structural determinants for furin inhibition were investigated using positional-scanning approach. We synthesized peptide libraries substituted by each natural amino acid residue (with the exception of the Cys) in the P5-P8 positions, while maintaining the furin recognition motif (the P4-P1 positions) and we determined inhibitor activity of the resulting peptides towards recombinant furin.

Results and Discussion

The peptides were prepared by solid-phase synthesis and inhibition constants (K_i) were determined *via* competitive kinetic assays using recombinant human furin. The results of kinetic studies (Figure 1) contain four series of analogs, which were modified at the P5 (A), P6 (B), P7 (C) and P8 (D) position. The most potent peptides are indicated in dark blue and our initial peptide (control) is indicated in green. The most potent inhibitors derived from this study include analogs modified at the P5 position with small hydrophobic residues. Moreover, almost all of the peptides substituted at the P8 position possessed improved inhibitory activity towards furin with the exception of compound containing Trp, Phe and Tyr.

The results of the kinetic studies showed that the incorporation of the small, hydrophobic residues like Leu, Ile and Val at the P5 position led to the most potent furin inhibitors. Therefore, in order to improve the stability of our analogs we decided to substitute this position with the unnatural amino acid residues with the similar character (Figure 2).

Screening the P5 to P8 libraries with recombinant furin revealed that only the modification of the P5 or P8 position might have a beneficial effect on the inhibitory activity of the resulting analogs. We demonstrated that the incorporation of small, hydrophobic residues at the P5 position led to analogs with improved potency towards furin, whereas at the P8 position almost all of the residues used enhanced inhibitory activity, with the exception of the aromatic amino acids residues. Keeping in mind that polybasic peptides like our initial inhibitor suffer from poor metabolic stability, we designed an additional series of compounds having the unnatural substitutions at the P5 position. From this group, the peptide modified with the Abu residue displayed improved inhibitory activity. The next step of this project will be to combine the most efficient modifications at the P5 and P8 position in order to obtain even more potent inhibitor. Then, the plasma stability studies of the leading compounds will be assessed. We believe that our results could be a solid basis for further structure optimization aiming at improving potency and stability of furin inhibitors and might lead to a new drug candidate to treat infectious disease.

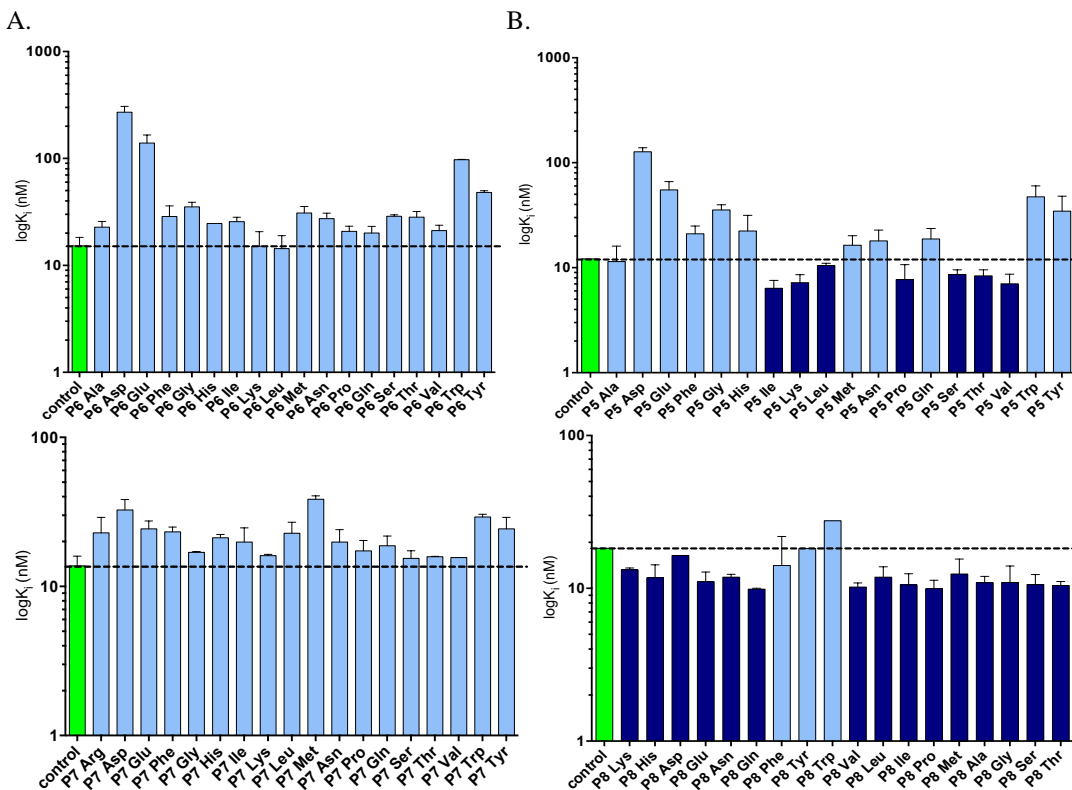


Fig. 1. Screening the P5 to P8 libraries with recombinant furin presented in comparison to our initial inhibitor (Ac-RARRRKKRT-NH_2).

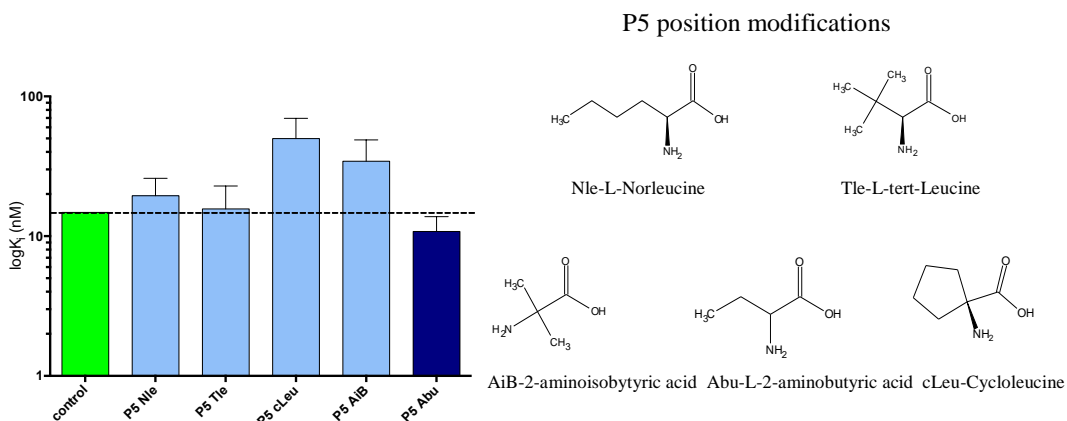


Fig. 2. Inhibition of furin by analogs modified at the P5 position by unnatural amino acids residues. The most potent inhibitor was the peptide containing L-2-aminobutyric acid that is marked by dark blue color.

Acknowledgments

The authors thank Nicolas Dory for help with enzyme kinetic studies. This work was supported by the National Science Centre grant no, UMO-2012/05/N/ST5/01995. Anna Kwiatkowska holds a Heart and Stroke Foundation postdoctoral fellowship.

References

1. Couture, F., et al. *Biomol. Concepts* **2**, 421-438 (2011), <http://dx.doi.org/10.1515/BMC.2011.034>
2. Thomas, G. *Nat. Rev. Mol. Cell Biol.* **3**, 753-766 (2002), <http://dx.doi.org/10.1038/nrm934>
3. Artenstein, A.W., Opal S.M. *N. Eng. J. Med.* **365**, 2507-25183 (2011), <http://dx.doi.org/10.1056/NEJMr1106700>
4. Remacle, A.G., et al. *Int. J. Biochem. Cell Biol.* **42**, 987-995 (2010), <http://dx.doi.org/10.1016/j.biocel.2010.02.013>
5. Gagnon, H., et al. *J. Med. Chem.* **57**, 29-41 (2014), <http://dx.doi.org/10.1021/jm400633d>

A Dual Photochemical Ring-Opening/Cleavage Approach for the Synthesis and Decoding of One-Bead-One-Compound Cyclic Peptide Libraries

Xinxia Liang, Simon Vézina-Dawod, François Bédard, and Eric Biron

Faculty of Pharmacy, Université Laval and Laboratory of Medicinal Chemistry, CHU de Québec Research Centre, CHUL, Québec (QC), G1V 4G2, Canada

Introduction

With a great therapeutic potential, peptide macrocycles have gained a lot of interest in drug discovery. Compared to their linear counterparts, cyclic peptides show improved resistance to proteases and their increased conformational rigidity lowers the entropic cost of binding, making them tighter-binding to a given macromolecule [1,2]. The great degree of molecular diversity and complexity that can be accessed by simple changes in their sequence has prompted the use of cyclic peptides in combinatorial chemistry. The one-bead-one-compound (OBOC) approach, in which each bead carries many copies of a unique compound, has become a powerful tool in the drug discovery process [3]. However, the use of cyclic peptides in combinatorial OBOC libraries has been limited by difficulties in sequencing hit compounds after the screening. Lacking a free N-terminal amine, Edman degradation sequencing cannot be used on cyclic peptides and complicated fragmentation patterns are obtained by tandem mass spectrometry (MS/MS). This problem has been initially overcome by using a bead topological segregation strategy [4,5]. More recently, different strategies have been reported to avoid encoding by using a ring-opening approach to allow a simultaneous linearization and compound release from the bead [6-9]. Most of the reported methods require post-screening chemical reactions that could lead to side chain modification. Based on these strategies, we were looking for an efficient, single step and chemical reagent free ring-opening approach that would be compatible with free amino acid side chains.

Results and Discussion

Our approach utilizes the photocleavable β -amino acid 3-amino-3-(2-nitrophenyl)propionic acid (ANP) as a linker and within the macrocycle (Figure 1). The strategy is to use UV irradiation to simultaneously convert cyclic peptides into their linear counterpart and release them from the beads. The generated linear peptides could then be sequenced by MS/MS. To evaluate the ring-opening upon UV irradiation, a model cyclic peptide with the sequence ANP-Leu-Gly-Tyr-Gly-Lys-Phe-Glu was first synthesized on Rink Amide AM polystyrene resin.

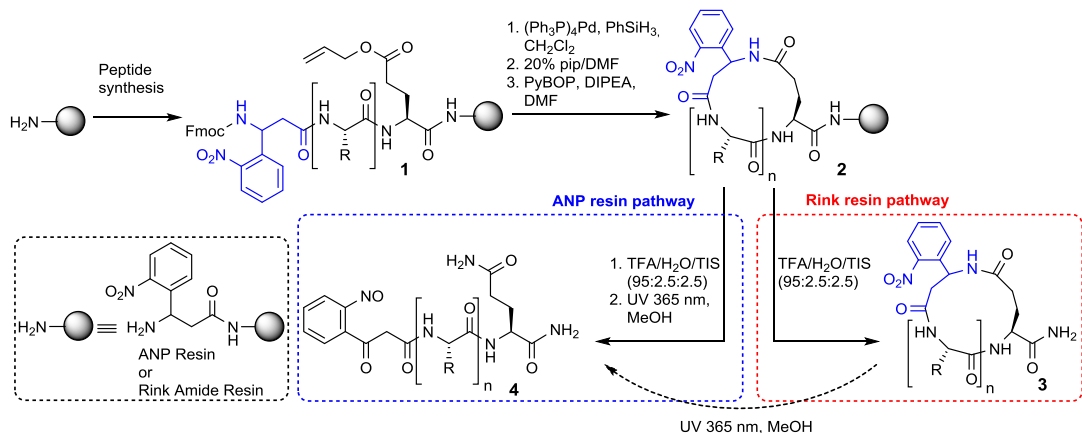


Fig. 1. Synthetic route to cyclic peptides with ANP residue and ring-opening upon UV irradiation.

Linear peptide **1** was synthesized on solid support by standard Fmoc chemistry. After removing the allyl and Fmoc protecting groups, the peptide was cyclised on resin with PyBOP. After cyclization, the side chains protecting groups were removed and the compound cleaved from the resin with a TFA cocktail. The released cyclic peptide **3** was then analysed by HPLC and electrospray ionization MS (ESI-MS) to confirm the absence of linear peptide (Figure 2a). Cyclic peptide **3** was then subjected to UV-irradiation at 365 nm in MeOH for ring cleavage. HPLC analysis confirmed the transformation of the cyclic peptide into its linear counterpart **4** (Figure 2b). The observed main peak was a doublet with both peaks having the same mass. This result led us to presume the formation of two diastereomers during ring-opening. Since the cyclic and linearized peptides have exactly the same elemental composition, the use of MS to differentiate cyclic **3** from linear compound **4** is theoretically limited. Surprisingly, after MS analysis of the generated linear peptide **4**, the anticipated molecular ion was not obtained and the most important peak was observed at $M+H^++14$ Da (Figure 2b). This observation led us to suspect that the reaction did not stop at the nitroso product as expected. Further analysis of the photocleavage reaction mechanism of *ortho*-nitrophenyl derivatives, proposed that the +14 Da peak is generated during UV irradiation from the addition of MeOH (32 Da) on a dehydrated specie ($M+H^+-18$) of the nitroso derivative **4**. This hypothesis was supported by the following results: 1) when methanol- d_4 (36 Da) was used as solvent, the adduct peak was observed at +18 Da; and 2) only the M-18 peak was observed in absence of MeOH during MALDI-TOF MS analysis. Further investigations to understand this reaction are underway.

To evaluate the efficiency of the simultaneous ring-opening/cleavage strategy, the model cyclic peptide **2** was synthesized on TentaGel S NH_2 resin bearing the ANP as linker. After cyclization and side chains deprotection, a small amount of resin **2** was subjected to UV-irradiation and the released peptide analysed by HPLC and ESI-MS to confirm the presence of linear peptide **4**. Next, a single bead was picked up from the resin **2** and exposed to UV-irradiation in MeOH. The crude product released from a single bead was immediately subjected to MALDI-TOF MS. Surprisingly, the mass spectra did not show the peak of the MeOH adduct ($M+H^++14$) but the dehydrated product ($M-18+H^+$) was observed as the major peak (Figure 3a). These results suggest that the adduct product is modified into the dehydrated specie when exposed to the laser during ionisation in the MALDI instrument. The ability of the MALDI's Nd:YAG laser to induce photochemical reaction has been shown and used by a few groups for synthesis monitoring and structural elucidation of biomolecules [10,11]. MS/MS analysis of the dehydrated product molecular ion yielded high-quality spectra from which the linearized peptide **4** could be unambiguously sequenced manually and by using *de novo* sequencing with the Peaks software (Figure 3b) [12].

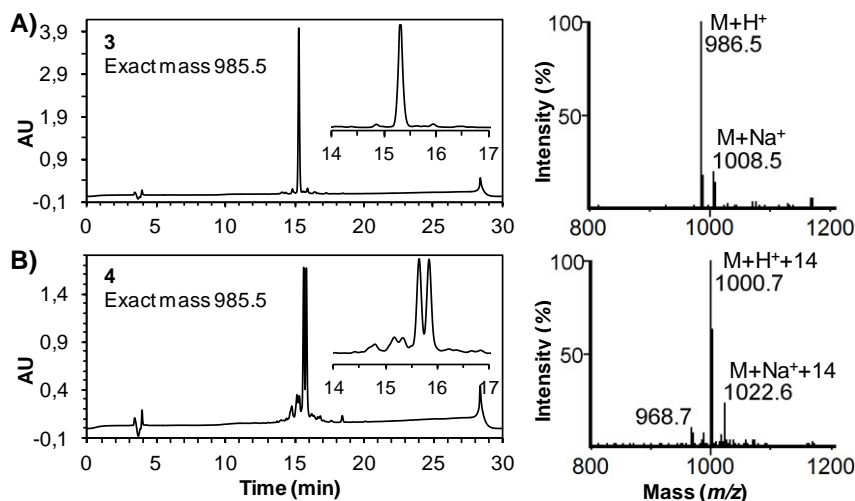


Fig. 2. HPLC and ESI-MS profiles of crude products showing cyclization and ring-opening. (A) cyclo[ANP-Leu-Gly-Tyr-Gly-Lys-Phe-Glu]- NH_2 **3**. (B) 3-oxo-3-(2-nitrosophenyl)propionyl-Leu-Gly-Tyr-Gly-Lys-Phe-Gln- NH_2 **4**.

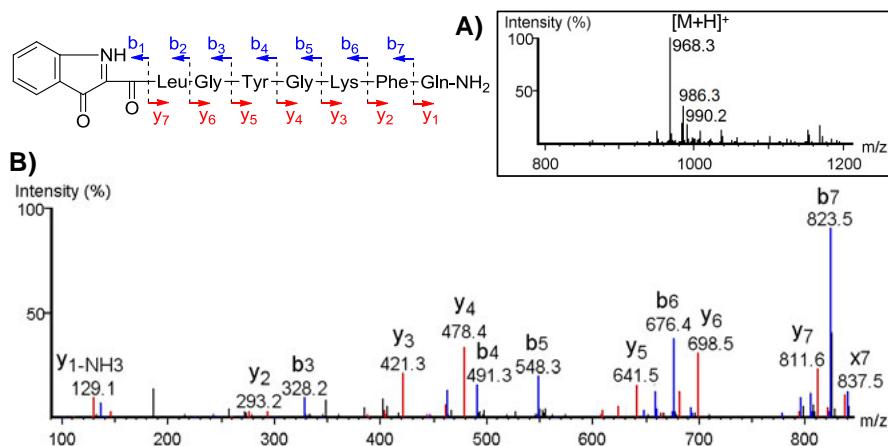


Fig. 3. MS and MS/MS spectra obtained after dual ring opening/cleavage on a single bead of cyclic peptide 2. (A) MS of the crude product; (B) MS/MS of the dehydrated specie $[M-18+H]^+$ (968.3 Da).

In summary, we report the use of a photolabile residue as a linker and within a cyclic peptide to allow a simultaneous ring-opening of the macrocycle and cleavage from the resin upon UV irradiation. The linearized peptides can then be efficiently sequenced by MS/MS analysis. This approach reduces the need for post-screening chemical modification for sequencing and allows a fast sequence determination of cyclic peptides from combinatorial libraries by MS/MS. As previously reported [6-9], compared to topological segregated bilayer beads, the re-opening strategy in OBOC libraries eliminates the risks of interference by the tag during screening since the same molecules are displayed inside and on the surface of the beads. Simple and affordable for any peptide science or combinatorial chemistry laboratory, the described procedure is compatible with commonly used amino acid side chains and could be readily used for the synthesis of cyclic peptoid or other peptidomimetic OBOC libraries. The compatibility of our strategy with OBOC library synthesis and screening is currently investigated.

Acknowledgments

Xinxia Liang, Simon Vézina-Dawod and François Bédard respectively thank the China Scholarship Council (CSC), the Fond d'enseignement et de recherche de la Faculté de pharmacie de l'Université Laval (FER) and the Fonds de recherche du Québec – Nature et technologies (FRQNT) for graduate scholarships. This work was supported by the National Sciences and Engineering Research Council of Canada (NSERC) (371503-2010).

References

- Adessi, C., Soto, C. *Curr. Med. Chem.* **9**, 963-978 (2002), <http://dx.doi.org/10.2174/0929867024606731>
- Pauletti, G.M., et al. *Adv. Drug Delivery Rev.* **27**, 235-256 (1997), [http://dx.doi.org/10.1016/S0169-409X\(97\)00045-8](http://dx.doi.org/10.1016/S0169-409X(97)00045-8)
- Lam, K.S., Krchnak, V., Lebl, M. *Chem. Rev.* **97**, 411-448 (1997), <http://dx.doi.org/10.1021/cr9600114>
- Liu, R., Marik, J., Lam, K.S. *J. Am. Chem. Soc.* **124**, 7678-7680 (2002), <http://dx.doi.org/10.1021/ja026421t>
- Joo, S.H., et al. *J. Am. Chem. Soc.* **128**, 13000-13009 (2006), <http://dx.doi.org/10.1021/ja063722k>
- Lee, J.H., Meyer, A.M., Lim, H.S. *Chem. Comm.* **46**, 8615-8617 (2010), <http://dx.doi.org/10.1039/C0CC03272G>
- Simpson, L.S., Kodadek, T. *Tetrahedron Lett.* **53**, 2341-2344 (2012), <http://dx.doi.org/10.1016/j.tetlet.2012.02.112>
- Liang, X., Girard, A., Biron, E. *ACS Comb. Sci.* **15**, 535-540 (2013), <http://dx.doi.org/10.1021/co4000979>
- Lee, K.J., Lim, H.S. *Org. Lett.* **16**, 5710-5713 (2014), <http://dx.doi.org/10.1021/ol502788e>
- Fitzgerald, M.C., Harris, K., Shevlin, C.G., Siuzdak G., *Bioorg. Med. Chem. Lett.* **6**, 979-982 (1996), [http://dx.doi.org/10.1016/0960-894X\(96\)00152-7](http://dx.doi.org/10.1016/0960-894X(96)00152-7)
- St-Hilaire P.M., Lowary, T.L., Meldal, M., Bock, K. *J. Am. Chem. Soc.* **33**, 13312-13320 (1998), <http://dx.doi.org/10.1021/ja980387u>
- Ma, B., Lajoie, G. *Rapid Commun. Mass Spectrom.* **17**, 2337-2342 (2003), <http://dx.doi.org/10.1002/rcm.1196>

Optimized Method to Generate Synthetically Challenging Macrocyclic Tetrapeptides That Do Not Have a Turn Inducer

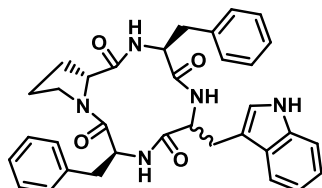
Sanjeewa N. Senadheera¹, and Jane V. Aldrich^{1,2}

¹Department of Medicinal Chemistry, The University of Kansas, Lawrence, KS, 66045, USA;

²Department of Medicinal Chemistry, University of Florida, Gainesville, FL, 32610, USA

Introduction

Natural and synthetic cyclic peptides represent an important class of bioactive molecules that exhibit a broad range of biological activities [1] and are considered as promising lead compounds in the search for new drugs. In particular, macrocyclic tetrapeptides (MTPs) have potential for development into therapeutic agents because of their low molecular weight, small organic molecule-like properties, membrane permeability, selectivity, expected metabolic stability to proteases, and improved pharmacokinetic properties *in vivo* [1,2]. However, the small 12-membered ring size can make their synthesis difficult, often resulting in low yields of the desired MTP with resulting dimers and oligomers as the major products [3-5]. Generally MTPs in which the amino acids are all the same chirality are more difficult to synthesize because the conformations of the linear precursor tetrapeptides limit the close approach of the *N*- and *C*-termini needed for macrocyclization to occur [5]. Also to date, almost all reported synthesized MTPs contain at least one turn inducing residue such as Pro, an *N*-alkyl amino acid, a *D*-amino acid or an unusual amino acid that favors macrocyclization [1,6].



L-Trp = CJ-15,208

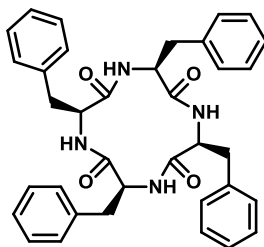
D-Trp = [D-Trp]CJ-15,208

Fig. 1. Structure of CJ-15,208 and its *D*-Trp isomer [4].

As part of our long standing interest in peptide ligands for kappa opioid receptors (KOR) we are synthesizing analogs of the natural product macrocyclic tetrapeptide CJ-15,208 (Figure 1) which exhibits modest affinity for KOR [4,7]. We use an improved synthetic protocol to prepare larger quantities of the macrocyclic tetrapeptide CJ-15,208, [D-Trp]CJ-15,208 and their analogs for detailed pharmacological evaluation *in vivo* [8-10]. To demonstrate the broad applicability of this methodology, here we describe the challenging syntheses of two all *L*-amino acid macrocyclic tetrapeptides (all *L*-AA MTPs, Figure 2) based on the CJ-15,208 scaffold that do not contain a turn inducer to promote macrocyclization.

Results and Discussion

The cyclic tetrapeptides were synthesized by a combination of solid phase synthesis of the linear peptide precursors on the 2-chlorotrityl chloride resin, followed by cyclization in solution [3,4,9]. The crucial cyclization step was optimized by modifying the reaction conditions reported previously (HATU, DIEA, DMF) [3,4].



cyclo[Phe-Phe-Phe-Phe], 1

Fig. 2. Structure of an all *L*-AA MTP derived from CJ-15,208 that does not have a turn inducing residue.

Table 1. Improvements in the isolated yield of all L-AA MTPs using the optimized protocol for synthesis and purification.

Peptide	Yield of pure cyclic peptide using the modified method (%)
<i>cyclo</i> [Phe-Phe-Phe-Phe], 1	15 ^a
Analog of 1	40 ^b

^aReported yield for MTP **1** was <1% [11]; ^bThere is no previously reported synthesis for this all L-AA MTP.

In our optimized procedure we found that several experimental parameters have an influence on the yield in the crucial cyclization, namely the concentration and addition rate of the linear tetrapeptide to the reaction mixture, and the reaction temperature as well as reaction time. Depending on the particular tetrapeptide sequence these four experimental parameters for the cyclization step may have to be adjusted to generate the desired macrocyclic tetrapeptide in good yield. Accordingly, the addition rate of the linear peptide to the reaction and the concentration of the linear peptide were optimized to minimize dimer formation and to increase the yields. The temperature of the cyclization step was also slightly increased (from rt to 30-37°C after addition of the linear peptide). The crude MTPs were purified using normal phase column chromatography on silica gel. The syntheses of the all L-AA MTPs were successfully achieved in modest yields (Table 1). The all L-AA MTP *cyclo*[Phe-Phe-Phe-Phe], **1**, was generated in significantly higher yield compared to the previously reported minimal yield of this cyclic peptide [11]. An analog of **1** which has not been previously prepared was obtained in substantially higher yield.

In conclusion, the use of these optimized conditions for the crucial cyclization step permitted the synthesis of these all L-AA MTPs that do not contain a turn inducing residue. *cyclo*[Phe-Phe-Phe-Phe], **1**, was obtained in substantially higher yield than the reported method (15% vs. <1% [11]), and an analog of **1** was also synthesized for the first time in good yield (40%). This generally applicable optimized synthetic methodology could facilitate the development of a variety of synthetically challenging MTPs for potential therapeutic applications.

Acknowledgments

This research was supported by grant R01 DA018832 (National Institute on Drug Abuse).

References

- White, C.J., Yudin, A.K. *Nature* **3**, 509-524 (2011), <http://dx.doi.org/10.1038/nchem.1062>
- Bockus, A.T., McEwen, C.M., Lokey, R.S. *Curr. Top. Med.* **13**, 821-836 (2013), <http://dx.doi.org/10.2174/1568026611313070005>
- Kulkarni, S.S., et al. *Adv. Exp. Med. Bio.* **611**, 269-270 (2009), http://dx.doi.org/10.1007/978-0-387-73657-0_121
- Ross, N.C., et al. *Tetrahedron Lett.* **51**, 5020-5023 (2010), <http://dx.doi.org/10.1016/j.tetlet.2010.07.086>
- Haddadi, M.E., et al. *J. Peptide Sci.* **6**, 560-570 (2000), [http://dx.doi.org/10.1002/1099-1387\(200011\)6:11<560::AID-PSC275>3.0.CO;2-I](http://dx.doi.org/10.1002/1099-1387(200011)6:11<560::AID-PSC275>3.0.CO;2-I)
- Fairweather, K.A., et al. *Org. Lett.* **12**, 3136-3139 (2010), <http://dx.doi.org/10.1021/ol101018w>
- Ross, N.C., et al. *Br. J. Pharmacol.* **165**, 1097-1108 (2012), <http://dx.doi.org/10.1111/j.1476-5381.2011.01544.x>
- Aldrich, J.V., et al. *J. Nat. Prod.* **76**, 433-438 (2013), <http://dx.doi.org/10.1021/np300697k>
- Senadheera, S.N., et al. in Lebl, M. (Ed.) *Peptides: Building Bridges (Proceedings of the 22nd American Peptide Symposium)*, American Peptide Society, San Diego, 2011, pp. 346-347.
- Aldrich, J.V., et al. *Br. J. Pharmacol.* **171**, 3212-3222 (2014), <http://dx.doi.org/10.1111/bph.12664>
- Cavelier-Frontin, F., et al. *THEOCHEM* **286**, 125-130 (1993), [http://dx.doi.org/10.1016/0166-1280\(93\)87158-A](http://dx.doi.org/10.1016/0166-1280(93)87158-A)

Towards the Development of Cell Permeable Macrocyclic Scaffolds: Probing the Structural Requirements for Enhancing Cellular Uptake

Simon Vézina-Dawod^{1,3}, Sophie Fortin^{1,3}, Marie Perrin^{1,3},
Louis-Jean Bordeleau^{2,3}, Stéphane Gobeil^{2,3}, and Eric Biron^{1,3}

¹Faculty of Pharmacy, Université Laval, Quebec (QC), G1V 0A6, Canada; ²Department of Molecular Medicine, Université Laval, Quebec (QC), G1V 0A6, Canada; ³CHU de Québec Research Centre, CHUL, Quebec (QC), G1V 4G2, Canada

Introduction

Peptide macrocycles are useful tools in chemical biology and for the development of therapeutic compounds. Compared to their linear counterparts, cyclic peptides are more resistant to proteases and their increased conformational rigidity makes them tighter-binding to a given macromolecule [1,2]. However, the relatively high polarity of the secondary amide bonds through the cyclic peptide backbone often results in poor cellular uptake. Since many therapeutic targets are found inside cells, drugs often need to cross multiple hydrophobic membranes to reach their site of action. To cross a membrane, a molecule must first break its interactions with water to go into the hydrophobic media. In many bioactive cyclic peptides, some amide bonds undergo intramolecular hydrogen bonding (IHB), thus internalizing the polarity [3,4]. Other amide bonds are free to interact with water and bring an energetic cost to cross the membrane in a passive way. *N*-Methylation of free amide bonds (not involved in IHB) is a promising approach to improve cellular uptake [5,6]. Another approach is to use peptoid residues (*N*-substituted glycines) to replace and mimic peptide bonds. Compared to peptides, the side chains migration to the backbone nitrogens increases proteolytic resistance and decreases the global polarity [7,8]. However, the replacement of the chiral C α to CH₂ and the display of tertiary amide bonds lead to a lost in conformational definition as *N*-alkylglycine oligomers are more flexible. Considerable efforts have been achieved to rigidify peptoids, by incorporating rigid monomers that induce dihedral angle preferences. Amongst these monomers, *N*-arylglycine was reported to significantly rigidify linear and cyclic peptoids [9]. Kirshenbaum and coworkers have shown that electronic repulsion is occurring between the amide bond oxygen and the aromatic ring, inducing a strong energetic preference for the *trans*-amide bond [9]. With the aim of developing macrocyclic scaffolds that could mimic the functional and conformational space found in peptide structures, we were interested in studying the relationships between the incorporation of rigid *N*-aryl monomers into cyclic peptoids, the induced conformations and their effects on cellular uptake.

Results and Discussion

For the study, the cyclic peptide motif c[Xaa⁵-Phe⁶-Pro¹-Phe²-pXaa³-Xaa⁴] was selected for its ability to induce a type II' β -turn upon amino acids 3 and 4. Based on this motif, the sequence c[Glu⁵-Phe⁶-Pro¹-Phe²-DTyr³-Lys⁴(Dns)] was chosen as model peptide **1**. Next, different modifications such as *N*-methylation or the introduction of peptoid residues were performed on the model peptide **1** to evaluate and compare their impact on cellular uptake (Table 1).

Table 1. Sequences of the synthesized peptide and peptoid analogs for the cellular uptake study.

	Cyclic <i>N</i> -methylated analogs		Cyclic peptoid analogs
2	c[(<i>N</i> -Me)Glu-Phe-Pro-Phe-DTyr-Lys(Dns)]	7	c[Nlys(Dns)-Ntyr-Nphe-Pro-Nphe-Nglu]
3	c[Glu-(<i>N</i> -Me)Phe-Pro-Phe-DTyr-Lys(Dns)]	8	c[Nglu-Nphe-Pro-Nphe-Ntyr-Nlys(Dns)]
4	c[Glu-Phe-Pro-(<i>N</i> -Me)Phe-DTyr-Lys(Dns)]	9	c[Nglu-Nphg-Pro-Nphe-Ntyr-Nlys(Dns)]
5	c[Glu-Phe-Pro-Phe-(<i>N</i> -Me)DTyr-Lys(Dns)]	10	c[Nglu-Nphe-Pro-Nphg-Ntyr-Nlys(Dns)]
6	c[Glu-Phe-Pro-Phe-DTyr-(<i>N</i> -Me)Lys(Dns)]	11	c[Nglu-Nphg-Pro-Nphg-Ntyr-Nlys(Dns)]

A first series of *N*-methylated analogs was prepared by standard solid phase peptide synthesis on 2'-chlorotrityl polystyrene resin using the procedure described by Biron, et al. for selective *N*-methylation on solid support and HATU as coupling reagent [10]. After cleavage from the resin with a HFIP solution, the *N*-methylated peptides were successively cyclized with PyBOP, deprotected with a solution of TFA and labeled on the lysine side chain with a dansyl moiety in solution to afford analogs **2-6**. To prepare peptoid analogs **7-11**, a dansyl labeled Mlys monomer was synthesized in solution and coupled to the resin during oligomerization on solid-support. Briefly, *o*-NBS-Mlys(Dns)-OH was synthesized from commercial glycine *tert*-butyl ester by protection of the amine with *o*-nitrobenzenesulfonyl group (*o*NBS) followed by *N*-alkylation with *N*-(4-bromobutyl)phtalimide. After removal of the phtalyl protecting group, the side chain amine was labeled with dansyl chloride followed by *tert*-butyl ester cleavage with TFA to afford the *N*^ε-labeled *N*^α-*o*NBS-*N*^α-substituted glycine monomer. After coupling the monomer to the solid support, peptoid analogs **7-11** were prepared by the submonomer approach (Figure 1) [11]. In the case of *N*phg residues, due to electronic deactivation of the aniline submonomer, bromide displacement was performed over 16 h instead of 30 min to ensure complete reaction and bromoacetylation on *N*-arylglycine 90 min instead of 30 min. Coupling of Fmoc-Pro-OH on *N*phg residues was achieved using bis(trichloromethyl)carbonate (BTC) to generate the acyl chloride *in situ*. Among the various coupling reagents like HATU, DIC and others that have been tested, BTC was significantly the most efficient one. After cleavage from resin with a HFIP solution, head-to-tail cyclisation and side chain deprotection were performed in solution as described above to afford cyclic peptoid analogs **7-11**. To evaluate the effect of cyclisation on cellular uptake, a linear peptoid **12** and a linear analog of the model peptide **13** were also synthesized.

After their purification and characterization by LC-MS, the ability of compounds **1-13** to penetrate inside cells was evaluated by flow cytometry. The cellular uptake study was performed by incubating human cervical carcinoma (HeLa) cells with compounds **1-13** at a final concentration of 50 μM or DMSO alone and TAT peptide (Dns-YGRKKRRQRRR) as negative and positive controls, respectively. After incubation for 2 h at 37°C, the cells were washed, trypsinized, fixed, and resuspended. The level of cellular uptake was evaluated in flow cytometry using median fluorescence and the standard deviation from triplicates gave the error (Figure 2). The results were compared to model peptide **1** and showed that *N*-alkylation has a major impact on cellular uptake. As expected, *N*-methylated analogs **2-6** yielded variable uptake results, depending on the *N*-methyl group position.

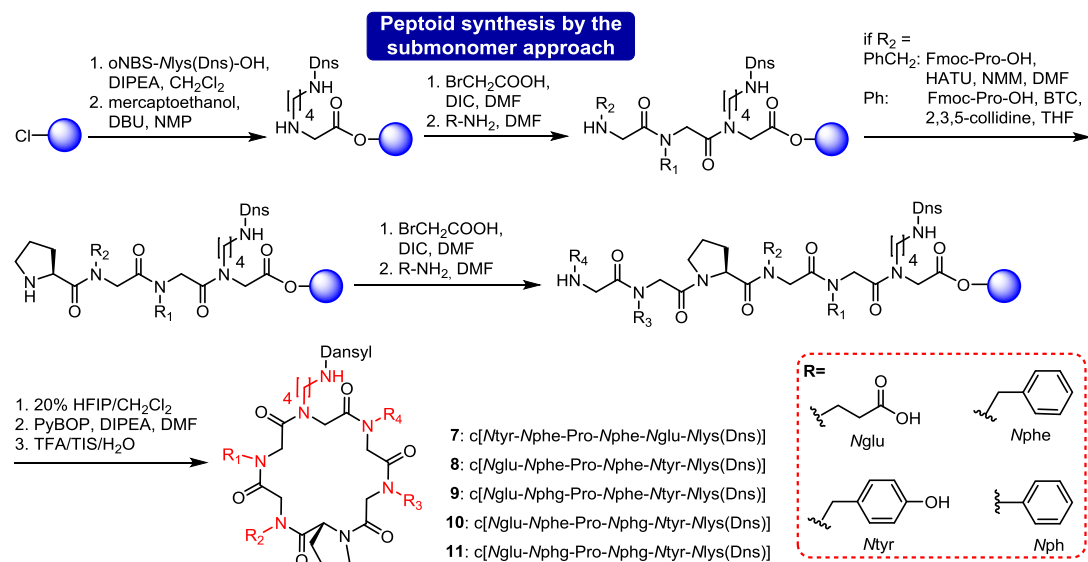


Fig. 1. Synthesis of the cyclic peptoid analogs **7-11**.

Compared to model peptide **1**, a loss of 41% in cellular uptake was observed for the *N*-methylated Glu⁵ analog **2** while no significant difference was observed for *N*-methylation on Phe⁶ (**3**). On the other hand, analogs with *N*-methylated Phe² (**4**), Tyr (**5**) and Lys (**6**) residue showed an increase in cellular uptake of 196, 255 and 251%, respectively. These results suggest that some positions are more sensible to *N*-alkylation than others and that their modification lead to a loss of IHB or an important conformational change. It is reasonable to think that N-H bond in position 5 might undergo IHB and amide N-H in position 2, 3 and 4 are more susceptible to interact with water. No significant difference was observed between the full peptoid **8** and the retropeptoid **7**, but compared to compound **1**, they presented increased uptake of 235% and 264%, respectively.

Interestingly, compared to cyclic peptoid **8**, substitution of *N*phe² by a *N*-phenylglycine (*N*pHg) resulted in a gain of 162% for compound **10** while the same substitution at position 6 yielded a loss of 66% for compound **9**. Substitution of *N*pHe residues at positions 2 and 6 by *N*pHg (**11**) gave intermediate result with a small loss of 16% compared to cyclic peptoid **8**. When compared to model peptide **1**, the cyclic peptoid **10** showed a 383% increase in cellular uptake. By comparison, with a *N*pHg at position 6, the cellular uptake for the cyclic peptoid analog **9** was comparable to model peptide **1**. These results suggest that rigidification of the peptoid scaffold with an *N*-aryl residue can significantly increase the cellular uptake and that its position in the macrocycle is very important. Finally, linear analogs **12** and **13** are slightly above the negative control and the results showed that cyclisation of peptide **13** enhanced the cellular uptake by 203% (**1** vs **13**) while cyclisation of peptoid **12** increased uptake by 487% (**8** vs **12**). No significant difference was observed between linear peptide and peptoid oligomers, suggesting that cyclisation and overall conformation have a greater impact on cellular uptake than only *N*-substitution. From this study, showing nearly a 5 fold increase in cellular uptake compared to its peptide counterpart, the most promising candidate for cell penetration is the *N*-aryl analog **10**.

In summary, a series of macrocyclic *N*-alkylated peptide and peptoid analogs labeled with a dansyl moiety was synthesized and their ability to penetrate cells evaluated by flow cytometry. The results showed that the amide bond at position 2 in the model peptide **1** seems to play a very important role in the cell penetration capability. Indeed, its modification by *N*-methylation, *N*-substitution and *N*-arylation yielded significant increase in cellular uptake. *N*-Methylation of the Phe², Tyr or Lys residue yielded 2-2.5 fold increases in cellular uptake.

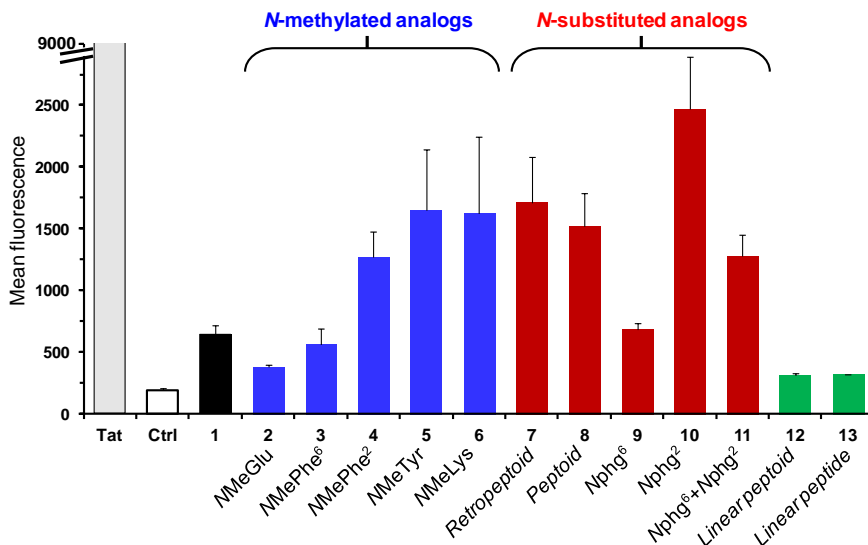


Fig. 2. Comparative cellular uptake of compounds **1-13** on HeLa cells as measured by flow cytometry with excitation at 360 nm. Emission was monitored with 525/50 band-pass filter and fluorescence intensity is expressed as median fluorescence.

The cyclic peptoid analogs showed also a 2.5 fold increase in cellular uptake but the most significant improvement was observed when the peptoid macrocycle was rigidified by the introduction of an *N*-aryl residue. Here again the position of the modification is important and the best result was obtained when the *N*-aryl residue was incorporated at position 2. In this case a 5 fold increase in cellular uptake was observed. These results strongly suggest that the conformation of a peptide-based macrocyclic compound plays a critical role in its ability to penetrate cells in a passive manner. The relation between conformation and the ability to cross membranes has also been reported for *N*-methylated peptides [5,6,12]. The position of the modification has an impact on the macrocycle's conformation that will affect IHB and the total polarity surface area. The described study showed that the ability of a cyclic peptide to penetrate cells can be rapidly and significantly improved by doing the appropriate modifications. Compared to its peptide counterpart, a 5 fold increase in cellular uptake has been observed for the *N*-arylated cyclic peptoid **10**. Finally, conformational studies are currently underway to characterize the structural changes in the analogs and define a relation between the modifications and their impact on the overall conformation.

Acknowledgments

Simon Vézina-Dawod and Sophie Fortin thank the Fond d'enseignement et de recherche de la Faculté de pharmacie de l'Université Laval (FER) and the National Sciences and Engineering Research Council of Canada (NSERC) for research scholarships. This work was supported by the NSERC of Canada (371503-2010).

References

1. Adessi, C., Soto, C. *Curr. Med. Chem.* **9**, 963-978 (2002), <http://dx.doi.org/10.2174/0929867024606731>
2. Tyndall, J.D., Nall, T., Fairlie, D.P. *Chem. Rev.* **105**, 973-999 (2005), <http://dx.doi.org/10.1021/cr040669e>
3. Alex, A., Millan, D.S., Perez, M., Wakenhut, F., Whitlock, G.A. *MedChemComm* **2**, 669 (2011), <http://dx.doi.org/10.1039/c1md00093d>
4. Kuhn, B., Mohr, P., Stahl, M. *J. Med. Chem.* **53**, 2601-2611 (2010), <http://dx.doi.org/10.1021/jm100087s>
5. Biron, E., et al. *Angew. Chem. Int. Ed.* **47**, 2595-2599 (2008), <http://dx.doi.org/10.1002/anie.200705797>
6. White, T.R., et al. *Nat. Chem. Biol.* **7**, 810-817 (2011), <http://dx.doi.org/10.1038/nchembio.664>
7. Miller, S.M., Simon, R.J., Ng, S., Zuckermann, R.N., Kerr, J.M., Moos, W.H. *Bioorg. Med. Chem. Lett.* **4**, 2657-2662 (1994), [http://dx.doi.org/10.1016/S0960-894X\(01\)80691-0](http://dx.doi.org/10.1016/S0960-894X(01)80691-0)
8. Kwon, Y.U., Kodadek, T. *Chem. Biol.* **14**, 671-677 (2007), <http://dx.doi.org/10.1016/j.chembiol.2007.05.006>
9. Shah, N.H., Butterfoss, G.L., Nguyen, K., Yoo, B., Bonneau, R., Rabenstein, D.L., Kirshenbaum, K. *J. Am. Chem. Soc.* **130**, 16622-16632 (2008), <http://dx.doi.org/10.1021/ja804580n>
10. Biron E, Chatterjee J, Kessler H. *J. Peptide Sci.* **12**, 213-219 (2006), <http://dx.doi.org/10.1002/psc.711>
11. Zuckerman, R.N., Kerr, J.M., Kent, S.B.H., Moos, W.H. *J. Am. Chem. Soc.* **114**, 10646-10647 (1992), <http://dx.doi.org/10.1021/ja00052a076>
12. Rezai, T., Yu, B., Millhauser, G.L., Jacobson M.P., Lokey, R.S. *J. Am. Chem. Soc.* **128**, 2510-2511 (2006), <http://dx.doi.org/10.1021/ja0563455>

Stability Evaluation of Immobilized Peptides Towards Proteases by Mass Spectrometry

Silvana L. Giudicessi¹, María L. Salum², María C. Martínez-Ceron¹,
Osvaldo Cascone¹, Rosa Erra-Balsells², and Silvia A. Camperi^{1*}

¹NANOBIOTEC Institute, UBA-CONICET, Cathedra of Biotechnology, School of Pharmacy and Biochemistry, UBA, Junín 956, 1113, Buenos Aires, Argentina; ²CIHIDECAR-CONICET, Dept. of Organic Chemistry, School of Exact and Natural Sciences, UBA, 1428, Buenos Aires, Argentina

*scamperi@ffyb.uba.ar

Introduction

Short peptides are widely used as ligands in affinity chromatography purification of proteins [1,2]. However, peptidases and proteases present in the crude sample may degrade immobilized peptides, shortening the affinity support useful life. Then, peptide ligand stability must be evaluated before its use in a purification process. Commonly, enzymatic stability is evaluated with the peptide in solution, which may differ from the resin-bound peptide behavior [3]. Further, as the peptides to be evaluated are in solution in the reaction mixture, the study of the peptide degradation products requires purification steps before their analysis [4].

In this work we developed a strategy to evaluate immobilized peptide stability using electrospray ionization (ESI) and matrix assisted laser desorption/ionization (MALDI) mass spectrometry (MS).

Results and Discussion

ChemMatrix (CM) was used as the solid support due to its chemical stability. This PEG-based matrix allowed peptide synthesis in organic solvents and stability peptide evaluation in aqueous solvents [5]. 4-Hydroxymethylbenzoic acid (HMBA) [6] was used as the linker in order to introduce a cleavage site to release the peptides from the beads before MS analysis. The model peptide H-Phe-Lys-Phe-Arg-Tyr-Thr-Ala-His-Ser-Gly-Ala-Ser-Gly-NH₂ with known trypsin and chymotrypsin cleavage sites [7] was synthesized on HMBA-CM resin (0.63 mmol/g) by using the Fmoc strategy as we have previously described [1]. Ser-Gly-Ala-Ser-Gly was incorporated as a spacer arm at the C-terminal. After peptide elongation, protecting groups were removed with trifluoroacetic acid (TFA)/triisopropylsilane (TIS)/H₂O (95:2.5:2.5 v/v/v), leaving the unprotected peptides anchored to the resin. Peptide beads were washed with dichloromethane (DCM), N,N-dimethylformamide (DMF), H₂O:DMF (3:7; 5:5; 7:3 v/v) and H₂O. Then, 0.1 mg of peptidyl-resin

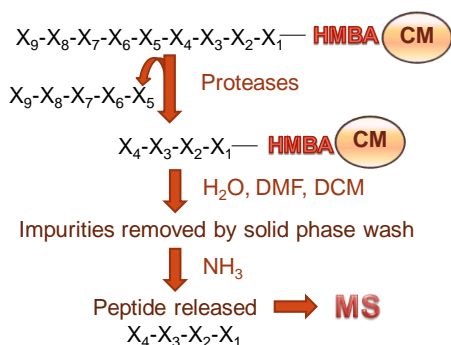


Fig. 1. Strategy for immobilized peptide stability evaluation.

and H₂O. Then, 0.1 mg of peptidyl-resin (approximately 100 peptidyl-beads) was incubated with solution A (trypsin 40 μM in Tris-HCl 40 mM, pH 8.1, CaCl₂ 10 mM buffer) or B (chymotrypsin 40 μM in Tris-HCl 40 mM, pH 8.1, CaCl₂ 10 mM buffer) overnight. The peptidyl-beads were then thoroughly washed with H₂O, H₂O:DMF (7:3; 5:5; 3:7 v/v), DMF and DCM. Later on, peptides were detached with ammonia vapor. Released peptides were eluted by adding acetic acid/acetonitrile (CH₃CN) / H₂O (3:4:3 v/v/v) (Figure 1). Eluted peptides were analyzed by mass spectrometry (MS). ESI mass spectra were recorded in a Bruker microTOF-Q II (Bruker Daltonics GmbH, Leipzig, Germany). 5 μL aliquot of eluted peptide was injected and analyzed in positive mode. MALDI mass spectra were recorded in an Ultraflex II TOF/TOF (Bruker Daltonics GmbH, Leipzig, Germany). 1 μL Aliquot of eluted peptide from 100 beads was loaded onto the sample plate, air-dried at room temperature, and then 1 μL of MALDI matrix solution was added on the sample dry layer (successive-dry-layers deposit method). Two matrices solutions were assayed: a) Commercial E-α-cyano-4-hydroxycinnamic acid (CHCA) 4

mg/mL in CH₃CN/H₂O (1:1 v/v) with 0.1% TFA and b) Z-sinapinic acid (SA) [8,9] 5 mg/mL in MeOH/H₂O (7:3 v/v). Mass spectra were acquired in the MS reflectron positive ion mode.

Figure 2 shows the ESI mass spectra obtained before and after subjecting the peptide-beads with chymotrypsin and trypsin. ESI-MS allowed the detection of the whole peptides (Figure 2 A) as well as their C-terminal enzymatic degradation products (Figures 1 B and C) obtained after incubation with trypsin and chymotrypsin.

When analyzing the peptide and their degradation products with MALDI-MS, E- α -cyano-4-hydroxycinnamic acid matrix clusters interfered in MALDI-MS analysis of low molecular weight products. On the other hand, Z-sinapinic acid matrix allowed their analysis (Figures 1 D and E).

The method here developed allowed a fast evaluation of peptide ligands stability in solid phase towards the proteases that may be present in the crude sample before their use in affinity chromatography. Due to the high sensitive of mass spectrometry, only a small sample of peptidyl-resin is required to evaluate its stability. As the enzymatic degradation is performed in solid-phase, none hard purification protocols are needed before analysis.

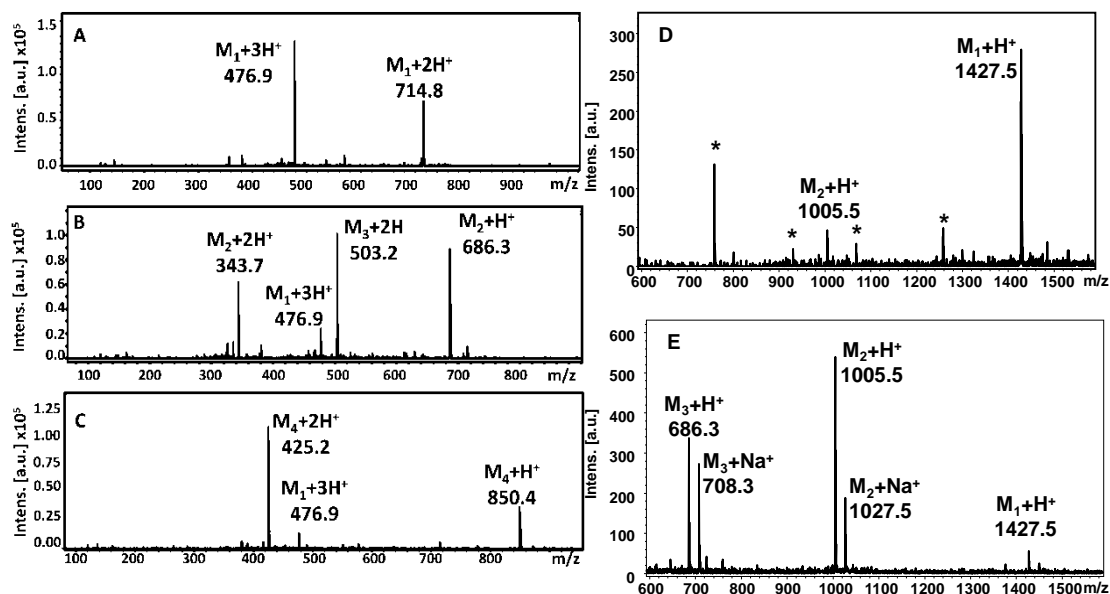


Fig. 2. ESI mass spectra of peptide H-Phe-Lys-Phe-Arg-Tyr-Thr-Ala-His-SerGly-Ala-Ser-Gly-NH₂ before (A) and after treatment with chymotrypsin (B) and trypsin (C). The signals at m/z 476.9 and 714.8 correspond to the whole peptide FKF₁RYTAHSGASG [M_1+3H^+] and [M_1+2H^+] respectively. The signals at m/z 343.7 and 686.3 correspond to the degradation product TAHSGASG [M_2+2H^+] and [M_2+H^+] respectively and 503.2 correspond to the degradation product RYTAHSGASG [M_3+2H^+]. The signals at m/z 425.2 and 850.4 correspond to the degradation product YTAHSGASG [M_4+2H^+] and [M_4+H^+]. MALDI mass spectra of peptide FKF₁RYTAHSGASG after treatment with chymotrypsin using α -cyano-4-hydroxycinnamic acid matrix (D) or using Z-sinapinic acid matrix (E). The signal at m/z 1427.5 corresponds to the whole peptide FKF₁RYTAHSGASG [M_1+H^+]. The signals at m/z 1005.5 and 1027.5 correspond to the degradation product RYTAHSGASG [M_2+H^+] and [M_2+Na^+] respectively. The signals at m/z 686.3 and 708.3 correspond to the degradation product TAHSGASG [M_3+H^+] and [M_3+Na^+] respectively. The signals marked with an asterisk (*) correspond to the matrix matrices clusters.

Acknowledgments

This work was partially supported by the National Scientific and Technological Research Council (Consejo Nacional de Investigaciones Científicas y Técnicas de la República Argentina) (CONICET), PIP 11220130100119CO, the University of Buenos Aires (20020130100060BA and PB03-PDTS-PCTI-74). S.L.G., M.L.S., M.C.M.C., O.C., R.E.B. and S.A.C. are researchers of the CONICET. We thank Simon Côté from Matrix Innovation Inc. for a generous donation of HMBA-ChemMatrix resin.

References

1. Camperi, S.A., et al. in Labrou, N. (Ed.) *Methods in Molecular Biology: Protein Downstream Processing*, Humana Press Inc. Springer, New York, 2014, Vol 1129, p. 277-302, http://dx.doi.org/10.1007/978-1-62703-977-2_22
2. Huang, P.Y., Carbonell, R.G. *Biotechnol. Bioeng.* **47**, 288-297 (1995), <http://dx.doi.org/10.1002/bit.260470303>
3. Bell, L.N. *Biotechnol. Prog.* **13**, 342-346 (1997), <http://dx.doi.org/10.1021/bp970057y>
4. Knör, S.A., et al. *J. Thromb Haemost.* **6**, 470-477 (2008), <http://dx.doi.org/10.1111/j.1538-7836.2008.02893.x>
5. Camperi, S.A., et al. *Tetrahedron Lett.* **46**, 1561-1564 (2005), <http://dx.doi.org/10.1016/j.tetlet.2004.12.105>
6. Atherton, E., et al. *J. Chem. Soc. Perkin Trans.* **1**, 538-546 (1981), <http://dx.doi.org/10.1039/P19810000538>
7. Sweeney, P.J. and Walker, J. M. in: Michael, M.B. (Ed.), *Methods in Molecular Biology: Enzymes of Molecular Biology*, Humana Press Inc. Springer, New York, 2014, Vol 16, p. 277-303, <http://dx.doi.org/10.1385/0896032345>
8. Salum, M.L., et al. *Org. Lett.* **12**, 4808-4811 (2010), <http://dx.doi.org/10.1021/ol1019508>
9. Salum, M.L., et al. Application of Z-sinapinic matrix in short peptide MALDI-MS analysis. Manuscript under preparation.

Multicomponent Dipeptide Supramolecular Hydrogels as Fibronectin-Mimetic Biomaterials

Wathsala Liyanage and Bradley L. Nilsson

Department of Chemistry, University of Rochester, Rochester, NY, 14627, USA

Introduction

Self-assembled supramolecular peptide hydrogels are important biomaterials that have been designed as matrices for tissue engineering and regenerative medicine [1-4]. Hydrogels derived from low molecular weight dipeptides or functionalized amino acids are a subset of self-assembled peptide hydrogels that have garnered significant recent interest [5-7]. Serious effort has been directed toward engineering low molecular weight hydrogelators that rival peptides in terms of their emergent viscoelastic and biochemical properties. Biochemical cell signaling motifs are often incorporated into supramolecular peptide hydrogels to facilitate cell adhesion, migration, and differentiation. The fibronectin-derived Arg-Gly-Asp (RGD) motif has been frequently incorporated into these types of materials to enable cell adhesion by interacting with integrin receptors.

Herein, we discuss two-component supramolecular hydrogels that functionally bind cell surface integrins in a fibronectin-like manner without the explicit display of the RGD peptide [8]. These hydrogels are composed of Fmoc-3F-Phe-Asp-OH (**1**) and Fmoc-3F-Phe-Arg-NH₂ (**2**) dipeptides (Figure 1) that coassemble to form a fibril network. These fibrils display Asp and Arg at the surface to spatially mimic the Asp and Arg residues in the RGD motif. NIH 3T3 fibroblast cells adhere to the hydrogel surface via integrin binding in a demonstration of the fibronectin-like biochemical behavior of these materials.

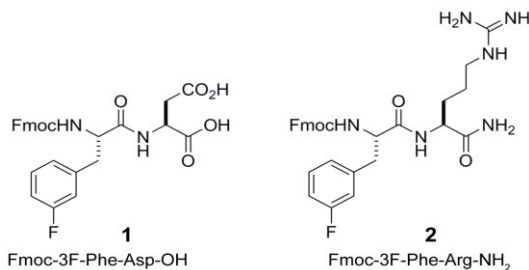


Fig. 1. Structures of Fmoc-3F-Phe-Asp-OH (**1**) and Fmoc-3F-Phe-Arg-NH₂ (**2**).

Results and Discussion

The central hypothesis of this study is that supramolecular fibrils that display Asp and Arg in an appropriate spatial approximation of the fibronectin RGD motif will functionally mimic fibronectin in the extracellular matrix and facilitate cell adhesion by binding to integrins. In order to test this hypothesis, we examined coassembly of Fmoc-3F-Phe-Asp-OH (**1**) and Fmoc-3F-Phe-Arg-NH₂ (**2**) dipeptides (Figure 1). We have previously found that Fmoc-3F-Phe effectively self-assembles to form self-supporting hydrogels in water [9]. We reasoned that appending either Asp or Arg to the Fmoc-3F-Phe assembly motif, giving dipeptides **1** and **2**, would facilitate coassembly of these dipeptides based on complementary charge between the Asp and Arg residues. Further, we anticipated that the resulting fibrils would display these hydrophilic charged residues at the surface where they would be exposed to integrins on cells cultured on these fibrils.

Coassembly and hydrogelation was initiated by dilution of solutions of **1** and **2** from DMSO into water (9.8 mM combined **1** and **2**, 4% DMSO/H₂O v/v). We varied the ratio of **2**:**1** (1:1, 3:2, 7:3, 4:1, 9:1) in order to assess the hydrogelation capacity of mixtures of these dipeptides. Upon dilution, each of the mixtures initially formed an opaque suspension that became optically transparent, self-supporting hydrogels within 10 minutes. Dipeptide **1** self-assembled to form self-supporting hydrogels, but dipeptide **2** failed to self-assemble independently. The hydrogel forming mixtures were composed of nanotape fibrils with diameters of 10-21 nm. The rheological viscoelasticity of each of the hydrogels was characterized to ensure that the resulting gels would be adequate for cell culture applications. The viscoelasticity of dipeptide hydrogels was measured using dynamic frequency sweep experiments. The gels had storage moduli (G') values of ~1400-2500 Pa and loss moduli (G'') values of ~20-200 Pa. The hydrogels were sufficiently rigid to support cell culture at the surface of the resulting materials.

The utility of these hydrogels for cell culture applications was then evaluated [8]. The hydrogels, which were formed in unbuffered water, were perfused by incubation with DMEM in order to remove DMSO from the gels and to prepare them for the introduction of cells [10]. Mouse embryonic fibroblast cells (NIH 3T3) were seeded onto the surface of each coassembled hydrogel (50,000 cells/cm²). As a control, cells were also grown on standard tissue culture plates. After 24 h of cell seeding, cells incubated on self-assembled hydrogels of dipeptide **1** or 9:1 mixtures of **2:1** were found to adopt spherical morphologies indicative of poor cell attachment (Figure 2A and 2B). In contrast, cells grown on 1:1 mixtures of **2:1** (Figure 2D) adopted spindle/polyhedral morphologies identical to those observed on tissue culture plates (Figure 2C), indicative of good cell attachment. The cells remained viable and were shown to continue to proliferate after >5 days of incubation on the hydrogel surfaces.

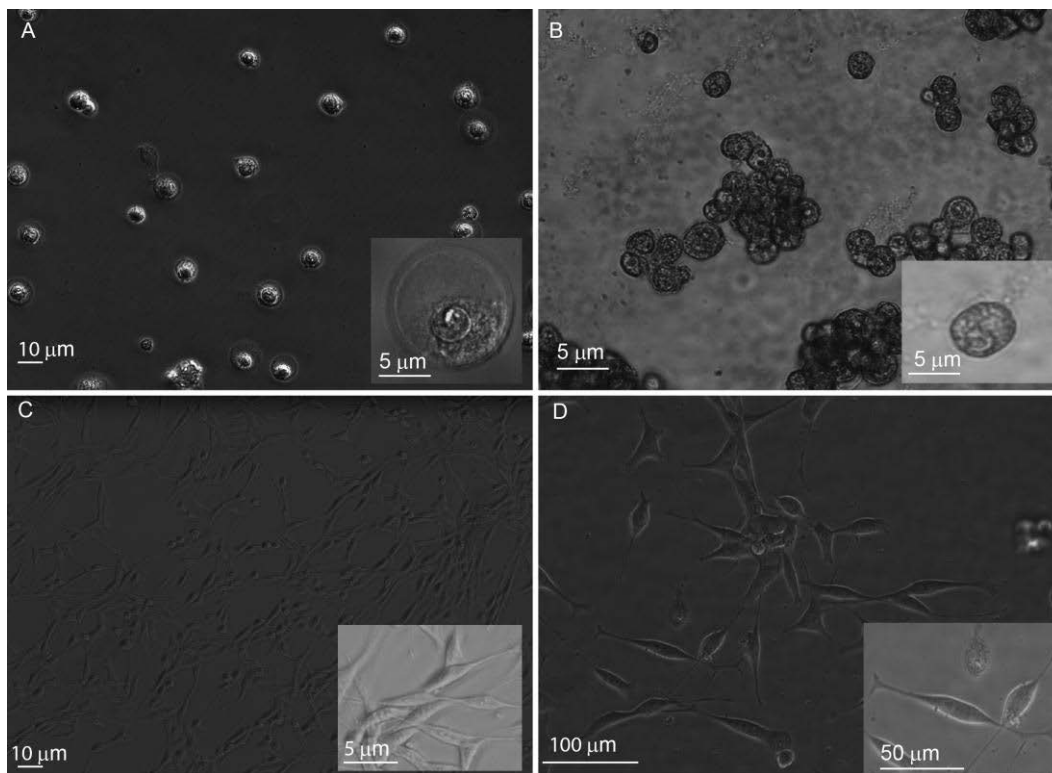


*Fig. 2. Images of NIH 3T3 cells seeded on hydrogels of dipeptides **1** and **2**. A. Cells seeded on a self-assembled hydrogel of dipeptide **1** (20× magnification); B. Cells seeded on a 9:1 hydrogel of **2:1** (20× magnification); C. Cells seeded on a tissue culture plate as a control (10× magnification); D. Cells seeded on a 1:1 hydrogel of **2:1** (20× magnification).*

The mechanism of cell adhesion to the hydrogels was examined to determine if the gels exhibit fibronectin-like binding to cellular integrins [8]. Integrin-blocking antibodies were used to conduct these cell adhesion analyses (Figure 3). Untreated cells (no integrin blocking) and cells blocked with anti- $\alpha 5$ and - $\beta 1$ integrin antibodies were found to adhere to the 1:1 gels of dipeptides **2:1**, while cells blocked with αv and $\beta 3$ integrin antibodies failed to adhere to the Arg/Asp coassembled nanofiber surfaces and exhibited spherical instead of spindle-like morphologies as shown in Figure 2D. This study suggests that integrin $\alpha v \beta 3$ is responsible for cell adhesion to the Arg/Asp coassembled gels, consistent with many RGD-functionalized materials. Thus, these hydrogels exhibit fibronectin-mimetic properties by the noncovalent display of Arg and Asp at the nanofiber surface.

These studies demonstrate that noncovalent supramolecular display of Arg and Asp provides materials that can effectively mimic the cell adhesive functions of the fibronectin RGD peptide, without covalent connection between the Arg and Asp amino acids. Specifically, we have utilized designed dipeptides (**1** and **2**, Fmoc-3F-Phe-Asp and Fmoc-3F-Phe-Arg respectively) that are composed of an Fmoc-3F-Phe derivative that functions as an effective assembly motif to arrange the appended Asp and Arg residues at the surface of the resulting fibrils in an alternating fashion. This display of Asp and Arg effectively mimics the spatial arrangement of these residues within covalent RGD peptides. The data indicates that fibrils that have nearly equimolar ratios of Asp and Arg provide hydrogel surfaces that support cell attachment and spreading as well as proliferation. In addition, integrin-blocking assays show that the cells bind to these surfaces in an integrin-dependent manner, similar to RGD-modified materials. These multicomponent coassembled hydrogel materials expand the possibilities for design of novel materials for tissue engineering.

Acknowledgments

The National Science Foundation supported this research (DMR-1148836). We gratefully acknowledge Karen Bentley (URMC Electron Microscopy Research Core) for her assistance with TEM and SEM imaging and Dr. Scott Kennedy for assistance with CD experiments.

References

1. Hirst, A.R., Escuder, B., Miravet, J.F., Smith, D.K. *Angew. Chem. Int. Ed. Engl.* **47**, 8002-8018 (2008), <http://dx.doi.org/10.1002/anie.200800022>
2. Branco, M.C., Schneider, J.P. *Acta Biomaterialia* **5**, 817-831 (2009), <http://dx.doi.org/10.1016/j.actbio.2008.09.018>
3. Stupp, S.I. *Nano Letters* **10**, 4783-4786 (2010), <http://dx.doi.org/10.1021/nl103567y>
4. Zhao, X., Pan, F., Xu, H., Yaseen, M., Shan, H., Hauser, C.A.E., Zhang, S., Lu, J.R. *Chem. Soc. Rev.* **39**, 3480-3498 (2010), <http://dx.doi.org/10.1039/b915923c>
5. Ryan, D.M., Nilsson, B.L. *Polym. Chem.* **3**, 18-33 (2012), <http://dx.doi.org/10.1039/c1py00335f>
6. Xu, B. *Langmuir* **25**, 8375-8377 (2009), <http://dx.doi.org/10.1021/la900987r>
7. Fleming, S., Ulijn, R.V. *Chem. Soc. Rev.* **43**, 8150-8177 (2014), <http://dx.doi.org/10.1039/c4cs00247d>
8. Liyanage, W., Vats, K., Rajbhandary, A., Benoit, D.S.W., Nilsson, B.L. *Chem. Commun.* **51**, 11260-11263 (2015), <http://dx.doi.org/10.1039/c5cc03162a>
9. Ryan, D.M., Anderson, S.B., Nilsson, B.L. *Soft Matter* **6**, 3220-3231 (2010), <http://dx.doi.org/10.1039/c0sm00018c>
10. Liyanage, W., Nilsson, B.L., in Lebl, M. (Ed.) *Peptides: Peptides Across the Pacific (Proceedings of the 23rd American Peptide Symposium)*, American Peptide Society, San Diego, 2013, pp. 158-159, <http://dx.doi.org/10.17952/23APS.2013/158>

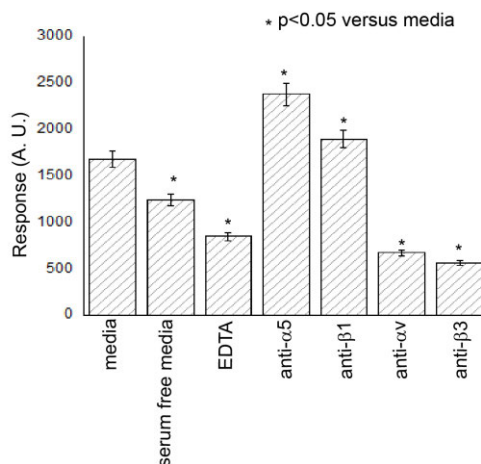


Fig. 3. Integrin-blocking cell adhesion assay. Coassembled hydrogels of 1:1 mixtures of dipeptides **2**:**1** were integrated with integrin-blocking antibodies (anti-α5, anti-β1, anti-αv, and anti-β3) [8]. Media, serum-free media, and EDTA controls were conducted on cells incubated in tissue-culture plates. After 2 h of incubation, cells were stained with 2 mM calcein to quantify live cells.

One-Bead-One-Peptide Library to Purify *Crotalus durissus terrificus* Phospholipase A2

María C. Martínez-Ceron^{1*†}, Soledad L. Saavedra¹, Lucía Ávila^{2†},
Silvana L. Giudicessi¹, Fernando Albericio^{3,4}, Silvia A. Camperi¹
and Osvaldo Cascone^{1,2}

¹NANOBIOTEC Institute, UBA-CONICET, Cathedra of Biotechnology, School of Pharmacy and Biochemistry, UBA, CABA, 1113, Argentina; ²National Institute of Biologicals Production, ANLIS-Malbrán, CABA, 1281, Argentina; ³IRB-PCB, UB. Barcelona, 08028, Spain; ⁴School of Chemistry, Yachay Tech,

Yachay City of Knowledge, Urcuqui, 100650, Ecuador

*camartinez@ffyb.uba.ar, †both contributed equally to this work

Introduction

Crotalus durissus terrificus (Cdt) is the only species of that genus in Argentina. Crotoxin represents more than 50% of the dry weight of its venom. This protein has two subunits: A (phospholipase A2, PLA2), and B (crotopotin). The venom protein profile differs according to geographical regions and contain several biologically active molecules [1,2]. Muller, et al [3] evaluated the antiviral activity of isolated toxins from Cdt and found that PLA2 strongly inhibits the yellow fever and dengue viruses growth in VERO E6 cells.

The aim of this work was to design a high performance purification method of Argentinean Cdt PLA2 by affinity chromatography with ligands selected from the screening of peptidic combinatorial libraries. Affinity chromatography is the better choice to purify proteins from complex mixtures like

snake venoms. Short peptides, as affinity ligands, are stable and resistant to proteases and can be produced in high quantities and purity. The challenge is to find a peptide ligand with enough affinity to use in industrial-scale chromatography [4]. Divide-couple-recombine (DCR) method allows obtaining a library with all possible combinations of the amino acids in the form of "one bead-one peptide". Peptide ligands can be selected from library screening [5,6]. We have developed a rapid and non-expensive strategy for the identification of peptides contained on positive beads by using matrix-assisted laser desorption/ionization time-of-flight mass spectrometry (MALDI-TOF-MS), and 4-hydroxymethylbenzoic acid (HMBA) as the linker in order to introduce a cleavage site to release the peptides from matrix before MS analysis [7,8].

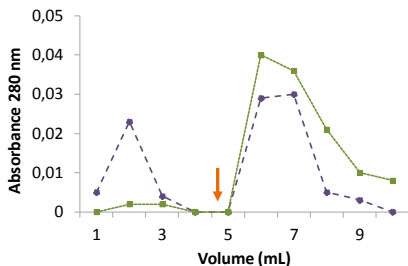


Fig. 1. Pure PLA2 chromatography on P1-Sepharose (---●---) (adsorption buffer: 20 mM sodium phosphate, pH 7.0) and on P2-Sepharose (—■—) (adsorption buffer: 20 mM sodium phosphate, pH 8.0). The arrow indicates the buffer change.

Results and Discussion

A combinatorial library containing the decapeptides XXXXXGGAGG where X= A, E, F, H, L, N, P, R, S, T, V or Y was synthesized on HMBA-ChemMatrix resin by the DCR method using Fmoc chemistry as previously described [4]. The screening was carried out using pure PLA2 labeled with NHS-Biotin. Those peptidyl-beads with affinity for the protein were revealed using Streptavidin-Peroxidase and α -Chloronaphthol/H₂O₂. Those beads that turned to violet colour were isolated to release the peptides from HMBA-ChemMatrix resin using ammonia vapor. Then, the peptides were analyzed by MALDI-TOF MSMS to determinate their sequence. We sequenced 50 peptides and studied their amino acid frequencies and moieties. Peptide 1 and Peptide 2 were selected to be immobilized in Sepharose.

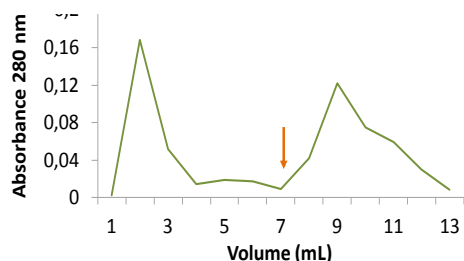
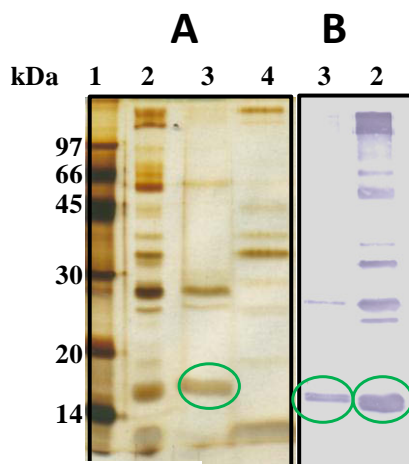


Fig. 2. Cdt whole venom chromatography on P2-Sepharose (adsorption buffer: 20 mM sodium phosphate, pH 8.0, buffer) and PLA2 purification. The arrow indicates buffer change.



1. MW marker
2. Cdt venom
3. Eluted fraction
4. Pass-through fraction

Fig. 3. (A) SDS-PAGE of Cdt's venom fractionation Silver staining and (B) Western Blot analysis of whole venom and elution fraction. The circle indicates the PLA2 band.

References

1. Faure, G., et al. *Eur. J. Biochem.* **223**, 161-164 (1994), <http://dx.doi.org/10.1111/j.1432-1033.1994.tb18978.x>
2. Hernandez-Oliveira, S., et al. *Protein J.* **24**, 233-242 (2005), <http://dx.doi.org/10.1007/s10930-005-6718-z>
3. Müller, V.D.M., et al. *Toxicon* **59**, 507-515 (2012), <http://dx.doi.org/10.1016/j.toxicon.2011.05.021>
4. Camperi, S.A., et al. Labrou, N. (Ed.) *Methods in Molecular Biology: Protein Downstream Processing*, Humana Press Inc. Springer, New York, 2014, Vol. 1129, p. 277-302, http://dx.doi.org/10.1007/978-1-62703-977-2_22
5. Furka, A., et al. *Int. J. Peptide Protein Res.* **37**, 487-493 (1991), <http://dx.doi.org/10.1111/j.1399-3011.1991.tb00765.x>
6. Lam, K.S., et al. *Nature* **354**, 82-84 (1991), <http://dx.doi.org/10.1038/354082a0>
7. Marani, M.M., et al. *J. Comb. Chem.* **11**, 146-150 (2009), <http://dx.doi.org/10.1021/cc800145c>
8. Martínez-Ceron, M.C., et al. *Anal. Biochem.* **400**, 295-297 (2010), <http://dx.doi.org/10.1016/j.ab.2010.01.029>

Pure samples of PLA2 in equilibrating buffer were loaded on columns (0.5 × 5 cm) filled with Peptide 1-Sepharose (P1) or Peptide 2-Sepharose (P2). The columns were washed with equilibrating buffer until the absorbance at 280 nm reached its initial value. The equilibrating buffers assayed were 20 mM sodium phosphate, pH 7.0, and 20 mM sodium phosphate, pH 8.0. The elution was performed with 100 mM sodium acetate buffer, pH 3.0, 0.25 M NaCl.

The best result for P1-Sepharose matrix was achieved by employing 20 mM sodium phosphate, pH 7.0, as the adsorption buffer and for P2-Sepharose by using 20 mM sodium phosphate, pH 8.0 buffer. A 97% of PLA2 adsorption was achieved with P2-Sepharose matrix, while the adsorption percentage with P1-Sepharose was only 70% (Figure 1). Therefore, P2-Sepharose matrix was used for further experiments.

A Cdt's whole venom dilution (100 µL of 5 mg/ml) in equilibrating buffer was loaded on a chromatographic column filled with P2 matrix, and

Figure 2 shows the chromatogram obtained. The PLA2 was adsorbed and eluted quantitatively. When Cdt venom was applied to P2 matrix, the SDS-PAGE analysis showed that the band corresponding to PLA2 only appears in the elution fraction (Figure 3 A). The identity was determined by Western Blot analysis performed with crotalic horse antivenom and rabbit antihorse IgG-peroxidase (Figure 3 B).

The results obtained indicate that affinity chromatography with peptide ligands are an efficient method to purify, in only one step, Argentinean Cdt PLA2. This matrix can be used to purify Cdt PLA2 for possible uses as antiviral against several tropical diseases.

Acknowledgements

This work was partially supported by the National Scientific and Technological Research Council (Consejo Nacional de Investigaciones Científicas y Técnicas de la República Argentina) (CONICET), ANPCyT PICT. PICT-2012-1881, PIP 11220130100119CO, the University of Buenos Aires (20020130100060BA and PB03-PDTS-PCTI-74). M.C.M.C., S.L.G., S.A.C. and O.C. are researchers of the CONICET. We thank Simon Côté from Matrix Innovation Inc. for generous donation of HMBA-ChemMatrix resin.





Detection of Protease Activity by Concentration Quenching-Based Substrates

Daisuke Sato, Wu Zhe, and Tamaki Kato

Graduate School of Life Science and Systems Engineering, Kyushu Institute of Technology, 2-4 Hibikino,
Wakamatsu-ku, Kitakyushu, 808-0196, Japan

Introduction

Concentration quenching-based substrates have been developed for protease assays [1,2]. The substrate fluorescence is quenched by concentration quenching resulting from highly assembled fluorophores on the substrates. The release of these concentrated fluorophores by proteases leads to fluorescence recovery, thereby allowing detection of protease activity. In this study, we designed and synthesized model compounds as concentration quenching-based substrates. They are composed of two fluorescein isothiocyanates (FITCs) and one or two substrate peptides (β -Ala-L-Ala-L-Phe-L-Ala) (Figure 1). Two types of concentration quenching-based substrates were designed: short-type substrates and long-type substrates. The short-type substrates are comprised of one FITC-linked substrate peptide and FITC on each edge of the core respectively. The long-type substrates are comprised of two FITC-linked substrate peptides. These substrates include hexamethylenediamine or ethylenediamine as the core.

		Short type	Long type	Feature
Core	C ₆	 6-Short dimer (1)	 6-Long dimer (2)	Longer core
	C ₂	 2-Short dimer (3)	 2-Long dimer (4)	Shorter core
Features		1 peptide moiety 1 cleavage point	2 peptide moieties 2 cleavage points	




Fig. 1. Concentration quenching-based substrates developed in this study and their features.

Results and Discussion

For the synthesis of **1** and **3**, the corresponding *N*-Boc-alkyldiamine was coupled with a Boc-protected peptide (Boc- β -Ala-L-Ala-L-Phe-L-Ala). FITC was then linked after the deprotection of the Boc group from the previously obtained compound. A similar synthetic route was applied to synthesize **2** and **4**, using the corresponding unprotected diamine and the Boc-protected peptides.

First, the fluorescence spectra upon excitation at 495 nm of each substrate before the addition of chymotrypsin were measured. All of the substrate solutions were prepared as an equimolar solution of FITC (1 μ M) in 200 mM Tris-HCl buffer with 5 mM CaCl₂ and 0.01% Tween 20 (pH 8.0). All of the substrates showed quenched fluorescence by intramolecular concentration quenching (Figure 2).

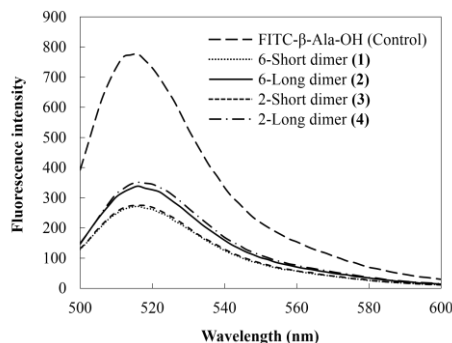


Fig. 2. Fluorescence spectra of each substrate prior to cleavage.

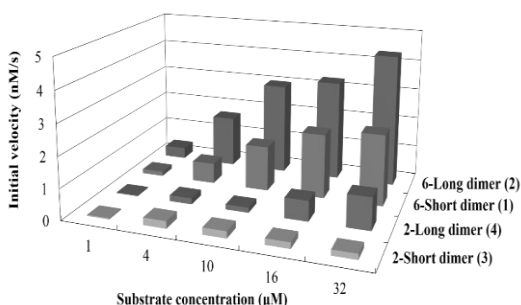


Fig. 3. Initial velocities of chymotrypsin cleavage.

quenching efficiency than the substrates with two peptide moieties. The differences in the length of the core barely affected the quenching efficiency.

Next, the increase in the fluorescence intensity at 535 nm upon excitation at 485 nm of different concentrations of substrates during chymotrypsin cleavage was monitored, and the initial velocities were calculated. The concentration of the substrates were prepared at 1, 4, 10, 16, and 32 μM, and the concentration of chymotrypsin was adjusted to 150 nM with 50 mM Tris-HCl buffer containing 100 mM NaCl, 5 mM CaCl₂, and 0.01% Tween 20 (pH 8.0). Compound **2** showed the fastest reaction rate of all the substrates. One explanation was that **2** had two cleavage sites for chymotrypsin compared with one site in **1**, and was the least sterically hindered because of its longer core (Figure 3). Comparatively, compound **3**, which possessed one peptide moiety and a shorter core, had the lowest initial velocity. This might be because **3** had only one cleavage site for chymotrypsin, and was sterically hindered. These observations were consistent with the k_{cat}/K_m values (Table 2). The kinetic

Table 2. Kinetic parameters of chymotrypsin cleavage of each substrate.

Substrate	K_m (μM)	V_{max} (nM/s)	k_{cat} (s ⁻¹)	k_{cat}/K_m (μM ⁻¹ s ⁻¹)
6-Short dimer (1)	13.1	3.41	2.27×10^{-2}	1.73×10^{-3}
6-Long dimer (2)	9.71	5.58	3.72×10^{-2}	3.83×10^{-3}
2-Short dimer (3)	n.d.	n.d.	n.d.	n.d.
2-Long dimer (4)	n.d.	n.d.	n.d.	n.d.

n.d.: not determined.

parameters of **3** and **4** could not be determined because the signal/noise (S/N) ratio was too low to calculate kinetic parameters reliably. These results indicate that the substrates consisting of two peptide moieties can be used for the detection of protease activity because of their faster reaction rates compared with the substrates consisting of one peptide moiety.

Table 1. Quenching efficiencies of the substrates.

Substrate	Quenching efficiency
6-Short dimer (1)	64%
6-Long dimer (2)	52%
2-Short dimer (3)	63%
2-Long dimer (4)	55%

References

1. Ternon, M., Diaz-Mochon, J.J., Belsom, A., Bradley, M. *Tetrahedron* **60**, 8721-8728 (2004), <http://dx.doi.org/10.1016/j.tet.2004.05.105>
2. Galande, A.K., Hilderbrand, S.A., Weissleder, R., Tung, C.-H. *J. Med. Chem.* **49**, 4715-4720 (2006), <http://dx.doi.org/10.1021/jm051001a>

A New Concept: A Peptide Monolayer for Accurate Positioning of Electroactive Probes at Close Distance from a Gold Surface

M. Caruso¹, E. Gatto¹, A. Palleschi¹, M. Scarselli², M. De Crescenzi²,
K. Wright³, E. Longo⁴, M. De Zotti⁴, F. Formaggio⁴, C. Toniolo⁴,
and M. Venanzi¹

¹Department of Chemical Sciences and Technologies, University of Rome 'Tor Vergata', 00133, Rome, Italy;

²Department of Physics, University of Rome 'Tor Vergata', 00133, Rome, Italy; ³Institute Lavoisier de Versailles, UMR 8180, University of Versailles, 78035, Versailles, France;

⁴Department of Chemistry, University of Padova, 35131, Padova, Italy

Introduction

Thio-gold chemistry is the most extensively employed method to generate organic layers stably linked to gold. Peptide functionalization at the *N*- and/or *C*-terminus with thiol linkers has been widely utilized, as well as with the side chains of sulfur containing proteinogenic amino acids (as Cys or Met). Among the several linkers to gold, dithiolane (with an S-S bridge) has been exploited for its ability to induce strong bidentate ligation. In this connection, lipoic acid has been the most popular compound for realizing this kind of linkage. At the beginning of the 1970s, a family of new dithiolane-containing cyclic structures, and among them the 4-amino-1,2-dithiolane-4-carboxylic acid (herein called Adt), was originally synthesized as an organic building block. Belonging to the class of C^{α,α}-cyclized, C^α-tetrasubstituted α-amino acids [1], Adt is expected to stabilize 3₁₀-helical structures in short peptides.

Beside its unique conformational properties, the presence of an S-S dithiolane group on the side chain ring makes Adt the best candidate for developing a new approach to peptide functionalization of gold surfaces. The short separation of the S-S linker from the peptide backbone allows the design of peptide layers much closer to the metal surface as compared to those formed by peptides using lipoic acid as the linker. Furthermore, bidentate ligation should anchor the peptide chain to the gold surface more rigidly than would a flexible linker like Cys. We therefore synthesized a hexapeptide, denoted in the following as Fc-CO-6Adt2, formed by two -Adt-Ala-Aib- triads and functionalized with an electroactive ferrocenoyl (Fc) group at the *N*-terminus [Fc-CO-(Adt-Ala-Aib)₂-OMe]. The presence in the oligopeptide sequence of four C^α-tetrasubstituted residues, *i.e.* the two Adt and the two Aib residues, gives a strong propensity to the main chain to attain a 3₁₀-helix conformation both in solution and in the crystal state, and consequently to locate the two Adt residues in the correct positions to link to the gold surface.

Results and Discussion

The predominant population of a 3₁₀-helical conformation in Fc-CO-6Adt2 was confirmed by FTIR absorption and 2D-NMR (NOESY, TOCSY) experiments in solution and by X-ray diffraction crystal studies on the synthetic pentapeptide precursor. X-Ray Photoelectron Spectroscopy (XPS) and Scanning Tunneling Microscopy (STM) techniques were used to characterize the binding of the peptide to the gold surface and the morphology of the peptide layer, respectively. In particular, XPS data indicate separate components for the S(2p) element: the signals at 161.5eV (36%) and 162.5 eV (4%) that can be assigned to Au-bonded sulfur atoms (thiolate bonded to the Au hollow sites), and the signal at 163.7 (40%) typical of non-bonded or weakly interacting sulfur atoms. A fourth component at 165.3 eV (20%) can be assigned to disulfide groups or oxidized (sulfoxides or sulfones) sulfur atoms. STM measurements on the Fc-CO-6Adt2-modified substrate revealed that extended regions of the gold surface appeared strongly altered by the presence of the peptide layer, which exhibits a rich morphology, *i.e.* emerging clusters of peptides of nanometric size and ordered stripe-like structures.

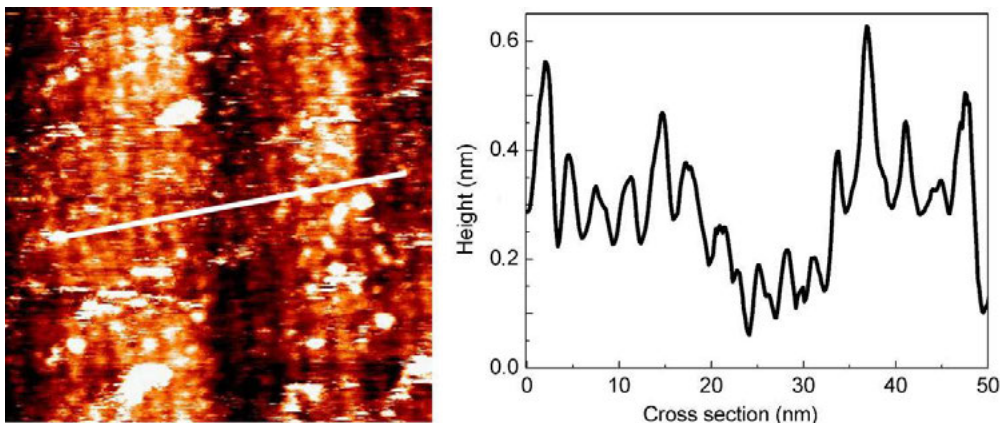


Fig. 1. Left: STM image of a stripe domain of the Fc-CO-6Adt2 film on gold. Bright spots of 1-nm width and 0.5-nm height can also be seen in the image ($55 \times 55 \text{ nm}^2$, $V_s = 1 \text{ V}$, $I = 300 \text{ pA}$). Right: Height profile taken along the line drawn in the image reported on the left side.

Interestingly, stripe domains (Figure 1) showed ordered flat structures of 2-3 nm width and sub-nanometric height, *i.e.* the actual size dimensions of peptides horizontally layered on the gold surface. Cyclic Voltammetry (CV) experiments carried out on the Fc probe showed that the current intensity increases linearly with the CV scan rate, indicating that the Fc discharge is not affected by diffusive processes at the electrode/peptide interface, *i.e.* that the peptide is stably chemisorbed on the surface.

Chronoamperometry (CA) experiments were also carried out on a three-electrode electrochemical cell using an Fc-CO-6Adt2-modified gold electrode as the working electrode. We found that CA experiments were adequately reproduced by a bi-exponential decay law, obtaining $k_{0,1(a)} = 11.2 \pm 0.4 \text{ s}^{-1}$ under anodic conditions, *i.e.* $\text{ET Fc} \rightarrow \text{Au}$, and $k_{0,1(c)} = 12.3 \pm 0.4 \text{ s}^{-1}$ under cathodic conditions, *i.e.* $\text{ET Au} \rightarrow \text{Fc}$ for the faster time component of the current intensity decay and $k_{0,2(a)} = 0.9 \pm 0.2 \text{ s}^{-1}$ and $k_{0,2(c)} = 1.2 \pm 0.3 \text{ s}^{-1}$ under anodic and cathodic conditions, respectively, for the slower time component. The appearance in the plot of frequency-normalized current intensity *vs.* frequency, obtained by pulsed Square Wave Voltammetry (SWV), of a maximum at a critical frequency of about 100 Hz, strongly suggests that most of the Fc probes are rigidly positioned at a relatively close distance from the gold surface.

Conclusions

In this contribution we described a new strategy for functionalizing a solid substrate with a peptide layer characterized by the main chain being rigidly disposed in a parallel orientation with respect to the surface. This result was achieved by inserting in the peptide sequence two Adt residues in the correct position to realize two bidentate linkages to the gold surface through the two dithiolane sulfur atoms in the Adt side chain. The main achievement of this new strategy of functionalizing solid substrates is to make possible an accurate positioning of an electroactive probe in the proximity of the gold surface. We proved this situation by analyzing by several electrochemical techniques the properties of a Fc group covalently linked to the peptide chain at its *N*-terminus.

Acknowledgments

This work was supported by the Italian Ministry of University and Research (MIUR), PRIN 2010-2011 No. 2010FM738P, 'Photophysical and photochemical properties of organic and biological compounds in solution and in organized systems'.

References

1. Toniolo, C., Crisma, M., Formaggio, F., Peggion, C. *Biopolymers (Pept. Sci.)* **60**, 396-419 (2001), [http://dx.doi.org/10.1002/1097-0282\(2001\)60:6<396::AID-BIP10184>3.0.CO;2-7](http://dx.doi.org/10.1002/1097-0282(2001)60:6<396::AID-BIP10184>3.0.CO;2-7)

Comparison of the Effects of Myristoylated and Transactivating Peptide (TAT) Conjugated Mitochondrial Fission Peptide Inhibitor (P110) in Myocardial Ischemia/Reperfusion (I/R) Injury

Israel Benjamin, Jonathan Vu, Christina Lipscombe, Devon Stutzman, Carly Schmidgall, Harsh Patel, Samir Patel, Qian Chen, Cathy J. Hatcher, Robert Barsotti, and Lindon H. Young

Division of Research, Department of Bio-Medical Sciences, Philadelphia College of Osteopathic Medicine (PCOM), Philadelphia, PA, 19131, USA

Introduction

Mitochondrial dynamics, mitochondrial fusion and fission may be involved in myocardial ischemia/reperfusion (MI/R) injury. In particular, mitochondrial fission is associated with mitochondrial fragmentation and decreased ATP production leading to cardiac contractile dysfunction and increased infarct size in MI/R [1-3]. During ischemic events, coronary blood flow is restricted causing cardiomyocytes to enter a hypoxic state. This change in cellular respiration causes a buildup of lactic acid and a decrease in pH. The acidic conditions developed during ischemia prevent the opening of the mitochondrial permeability transition pore (MPTP) and cause cardiomyocyte hypercontracture. When blood flow and oxygen delivery are restored during reperfusion, reactive oxygen species (ROS) are generated which leads to the loss of mitochondrial membrane potential and opening of the MPTP, which potentiates mitochondrial fission in MI/R (Figure 1). Therefore inhibiting mitochondrial fission, which results from the vital act of reperfusion, may be a strategy to salvage damaged cardiomyocytes and protect them from MI/R injury. P110 (DLLPRGT) is a mitochondrial fission peptide inhibitor that acts by selectively inhibiting the interaction between human fission protein (Fis1), which is located on the outer mitochondrial membrane and dynamin related protein 1 (Drp1), a GTPase (Figure 2).

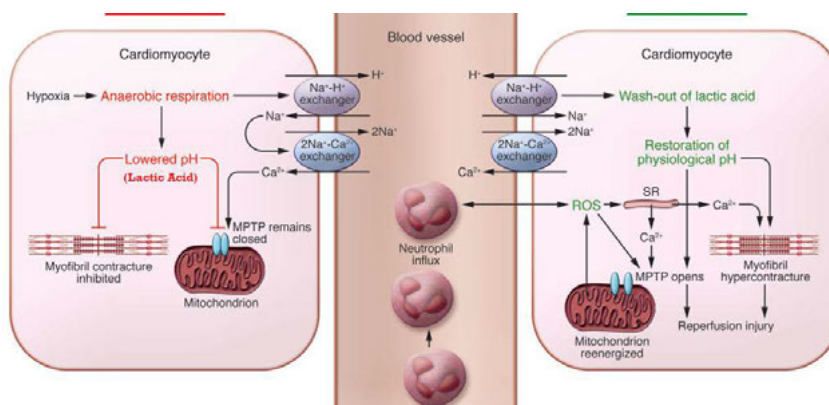


Fig. 1. Acute myocardial ischemia results in a decrease in pH from anaerobic conditions. The acidic conditions during ischemia prevent the opening of the mitochondrial permeability transition pore (MPTP) and cardiomyocyte hypercontracture at this time. Reperfusion results in rapid restoration of physiological pH, which promotes opening of the MPTP, reactive oxygen species (ROS) release, Ca²⁺ overload, and cardiomyocyte hypercontracture. Neutrophils accumulate in the infarcted myocardial tissue in response to the release of chemoattractants, and generate ROS leading to further tissue damage. Adapted from Hausenloy and Yellon, 2013 [1].

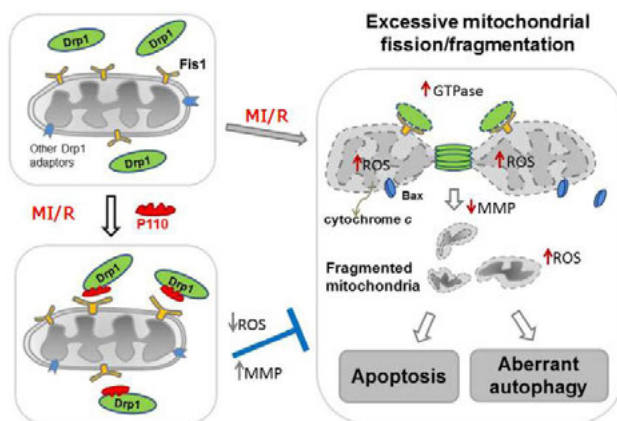


Fig. 2. Mechanism of mitochondrial fission in myocardial ischemia/reperfusion (MI/R) and P110's inhibition of interaction between dynamin related protein 1 (Drp1) and human fission protein (Fis1). Mitochondrial membrane potential (MMP) is increased and reactive oxygen species (ROS) are decreased with P110. Adapted from Qi, 2013 [3].

It is well known that adding myristic acid (Myr) or TAT carrier peptide to native peptides will facilitate cell membrane permeability required for targeting intracellular substrates. The addition of a glycine-glycine spacer between the TAT and cargo portion of the peptide is reported to facilitate delivery of the cargo sequence (i.e., DLLPRGT) [3,4]. Myristic acid conjugated peptides enter into cells by simple diffusion whereas TAT-conjugated peptides enter into cells via an endocytosis-like mechanism involving interactions with positively-charged amino acids (i.e., RKKRRQRRR) and negatively charged plasma cell membrane [4,5]. Native peptides enter through facilitated diffusion (Figure 3). We have previously shown that myristic acid conjugated caveolin-1 and PKC β II and ζ peptide inhibitors significantly attenuated leukocyte chemotactic receptor stimulated superoxide release compared to their native counterparts [5]. However, it is not known if differences exist in the effectiveness of myristic acid versus TAT-conjugated peptides compared to their native counterparts or untreated controls in MI/R. In the current study, we compared the effects of TAT-conjugated P110 (MW= 2427g/mol), Myr-P110 (MW=981 g/mol), and Native-P110 (MW=771 g/mol) on cardiac function and infarct size in isolated perfused rat hearts. Previously it was shown that TAT-P110 exerted a modest (i.e. one-third) reduction in infarct size compared to untreated controls; however, cardiac function was not reported in the study, nor was there a comparison of TAT-P110 to native peptide in isolated perfused rat hearts subjected to MI(30min)/R(90min) [2].

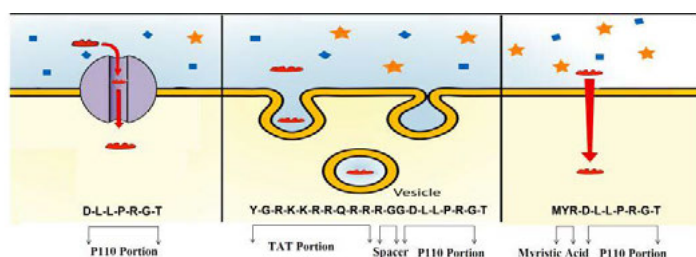


Fig. 3. Cell entry mechanisms for Native, TAT, and Myr-P110. The a.a. sequence of TAT, GG spacer, and P110 is depicted above.

Results and Discussion

Male Sprague Dawley rats (275-325 g, Charles River, Springfield, MA) were anesthetized with pentobarbital sodium (60 mg/kg) and anti-coagulated with sodium heparin (1,000 U) injection intraperitoneally. Each heart was rapidly excised, immersed in a 160 mL water-jacketed reservoir and subjected to retrograde perfusion via the aorta with a modified Krebs-Henseleit buffer. The perfusate was maintained at 37°C, kept at 80 mmHg constant pressure, aerated with 95% O₂-5% CO₂, and equilibrated at a pH of 7.35-7.45. A flow meter (T106, Transonic Systems, Inc., Ithaca, NY) placed in the inflow line monitored coronary flow. Left ventricular end-systolic pressure (LVESP), left ventricular end-diastolic pressure (LVEDP), heart rate, and peak rates of rise and fall in the first derivative (dP/dt_{max} and dP/dt_{min}, respectively) of left ventricular developed pressure (LVDP) were monitored using a pressure transducer (SPR-524, Millar Instruments, Inc., Houston, TX) positioned in the left ventricular cavity and recorded using a Powerlab Station acquisition system (ADInstruments,

Grand Junction, CO). LVDP was calculated by subtracting LVEDP from LVESP. Sham hearts were not subjected to global ischemia. At the end of reperfusion, five heart slices (2 mm/slice) were subjected to 1% triphenyltetrazolium chloride (TTC) staining to detect non-viable (unstained) and viable (red stained) area. Infarct size was expressed as the percentage of non-viable tissue to the total tissue weight [6]. All data are presented as means \pm SEM. Cardiac function and TTC staining data were analyzed by ANOVA using post hoc analysis with the Student-Newman-Keuls test. Probability values of <0.05 were considered statistically significant.

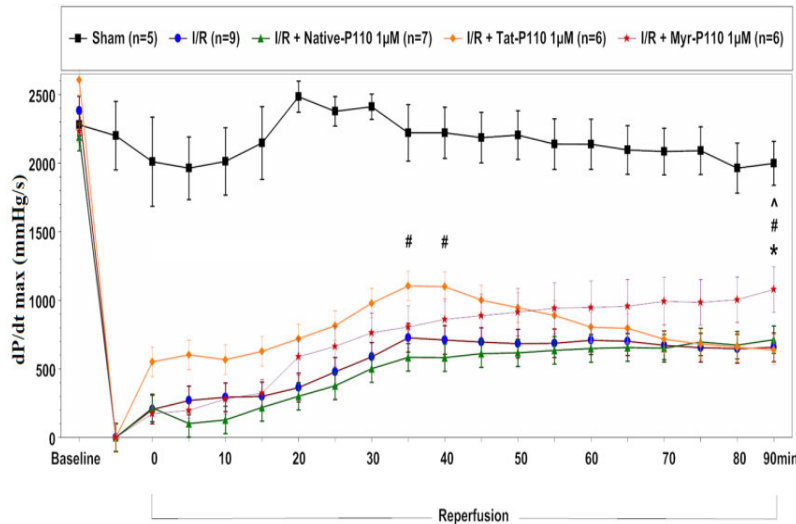


Fig. 4. Time course of dP/dt_{max} for Sham, MI/R and MI/R + Tat-P110, Myr-P110 and Native P110 hearts. (* $p<0.05$ compared to untreated I/R hearts; # $p<0.05$ compared to Native hearts; ^ $p<0.05$ compared to TAT-P110 hearts).

Figure 4 shows that Myr-P110 significantly improved post-reperused dP/dt_{max} compared to untreated MI/R, TAT-P110, and Native-P110 hearts. Sham hearts maintained cardiac function throughout the experimental protocol ($87\pm 9\%$ of initial LVDP (data not shown) and $89\pm 8\%$ of initial dP/dt_{max}). We found that Myr-P110 (1 μ M; $n=6$) given for 10 min before ischemia and for 20 min post-reperfusion, significantly restored dP/dt_{max} to $49\pm 7\%$ compared to TAT-conjugated P110 (1 μ M $n=6$), Native P110, and untreated controls ($n=9$), which only recovered to $26\pm 5\%$, $35\pm 6\%$, $28\pm 4\%$ of baseline values at 90 min post-reperfusion respectively. TAT-P110 transiently improved post-reperused dP/dt_{max} at 40-45 minutes compared to untreated controls, but this effect diminished by the end of reperfusion.

Weight ratios of infarcted to area at risk left ventricular tissue in MI/R were determined by TTC staining. Myr-P110 significantly reduced infarct size to $28\pm 2\%$ compared to untreated MI/R controls which had an infarct size of $46\pm 3\%$ ($p<0.01$). Whereas, TAT-conjugated P110 and Native P110 treated hearts had an infarct size of $35\pm 3\%$ and $34\pm 3\%$ respectively, and was not statistically different from controls using ANOVA analysis. Coronary flow (ml/min) (data not shown) was not statistically different among the experimental groups during initial baseline or reperfusion. It is known that coronary flow in the *ex vivo* isolated perfused rat heart model can have a wide variation of post-reperfusion coronary flow (i.e. 7 to 14 ml/min) and this variable is independent of post-reperused cardiac function within the 7-14 ml/min range among all MI/R study groups [7].

In summary, these data suggest that mitochondrial fission may contribute to MI/R injury and that inhibition of mitochondrial fission by Myr-P110 significantly improved post-reperused dP/dt_{max} and reduced infarct size as compared to untreated control, TAT, and Native P110 MI/R hearts. Interestingly, TAT-P110 transiently improved post-reperused cardiac function but did not significantly reduce infarct size compared to Native P110. The data suggest that TAT-P110 had limited intracellular entry compared to Myr-P110, and therefore only transiently improved cardiac function and was marginally effective in reducing infarct size. Future studies will be aimed at attaching a

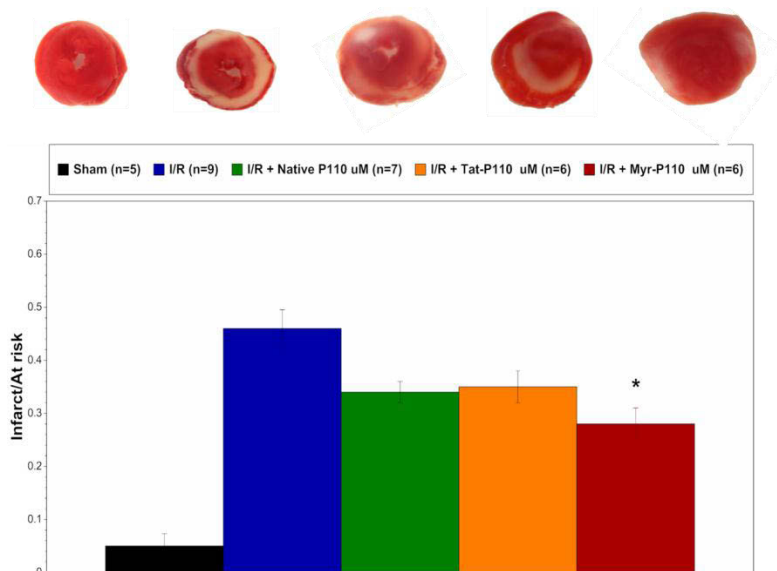


Fig. 5. Representative 1% triphenyltetrazolium chloride (TTC) stained heart sections displayed above from sham, control MI/R and MI/R + P110 treated hearts were used to assess infarct size after cardiac function experiments ($p < 0.05$ compared to untreated MI/R hearts.) Myr-P110 $1\mu\text{M}$ significantly reduced infarct size compared to untreated MI/R hearts. Sham hearts had minimal cell death ($< 5\%$) at the end of the experimental protocol.*

fluorescent probe to both TAT and Myr-P110 peptides to monitor intracellular targets and the time course of cell entry and degradation of both peptide formulations. Moreover, additional studies using higher concentrations, i.e. $5\mu\text{M}$ of both TAT and Myr-P110 will be tested in our MI/R model. The data suggests that Myr-P110 is the more effective formulation and may be an attractive strategy to attenuate MI/R injury and salvage heart tissue in MI patients.

Acknowledgments

This study was supported by the Center for Chronic Disorders of Aging and the Department of Bio-Medical Sciences at PCOM. Special thanks to PCOM DO/Biomed students Stephanie Liu, Joseph Venditto, and Gregory Stoner for assistance in the preparation of this manuscript.

References

1. Hausenloy, D.J., Yellon, D.M. *J. Clin. Invest.* **123**, 92-100 (2013), <http://dx.doi.org/10.1172/JCI62874>
2. Disatnik, M.H., et al. *J. Am. Heart Assoc.* **2**, e000461 (2013), <http://dx.doi.org/10.1161/JAHA.113.000461>
3. Qi, X., et al. *J. Cell Sci.* **126**, 789-802 (2013), Advance Online Article December 13, 2012, <http://dx.doi.org/10.1242/jcs.114439>
4. Taraballi, F., et al. *Frontiers in Neuroengineering* **3**, (2010), <http://dx.doi.org/10.3389/neuro.16.001.2010>
5. Perkins, K.A., et al. in Lebl, M. (Ed.) *Building Bridges (Proceedings of the 22nd American Peptide Symposium)*, American Peptide Society, San Diego, 2011, p. 288-289.
6. Blakeman, N., et al. *Am. J. Biomed. Sci.* **4**, 249-261 (2012), <http://dx.doi.org/10.5099/aj120300252>
7. Peterman, E.E., Taormina, II P., Harvey, M., Young, L.H. *J. Cardiovasc. Pharmacol.* **43**, 645-656 (2004), <http://dx.doi.org/10.1097/00005344-200405000-00006>

Myristoylated PKC β II Peptide Inhibitor Exerts Dose-Dependent Inhibition of N-Formyl-L-Methionyl-L-Leucyl-L-Phenylalanine (fMLP) Induced Leukocyte Superoxide Release

Chinyere B. Ebo, Carly Schmidgall, Christina Lipscombe, Harsh Patel,
Qian Chen, Robert Barsotti, and Lindon H. Young

Department of Bio-Medical Sciences, Philadelphia College of Osteopathic Medicine,
4170 City Avenue, Philadelphia, PA, 19131, USA

Introduction

Phosphorylation of polymorphonuclear leukocyte (PMN) NADPH oxidase by protein kinase C (PKC) is essential to generate superoxide (SO) release. Inhibition of PMN SO release attenuates inflammation mediated vascular tissue injury during myocardial ischemia/reperfusion (MI/R) injury. PMNs express five isoforms of PKC (α (α), β I (β I), β II (β II), δ (δ) and ζ (ζ)) and their role regulating this response have not been fully elucidated. PKC α , β II and ζ are thought to positively regulate PMN SO release, whereas PKC δ negatively regulates PMN SO release. [1,2] PKC β I, in contrast to the other four isoforms, translocates to the nucleus after second messenger stimulation [1]. PKC β II, a classical isoform, is activated by calcium and diacylglycerol (DAG) following PMN chemotactic receptor stimulation with fMLP peptide (Figure 1) [1]. Activated PKC β II will phosphorylate PMN NADPH oxidase to produce SO. Selective PKC β II peptide inhibitor has been developed based on its binding sites to receptor for activated C kinase (RACK) domain (Figure 2) [3]. RACK shuttles cytosolic PKC β II to interact with cell membrane substrates (e.g., NADPH oxidase).

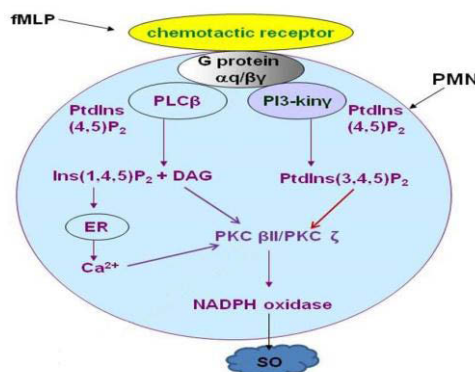


Fig. 1. Schematic representation of PKC activation generating SO release in PMN. PMN chemotactic G-protein receptors are activated by fMLP. The G-protein subunits α_q and $\beta\gamma$ disassociate after stimulation and activate phospholipase C beta (PLC β) to produce inositol 1,4,5 trisphosphate (Ins(1,4,5)P₂) plus DAG respectively from phospholipids phosphatidylinositol 4,5 bisphosphate (PtdIns(4,5)P₂). Ins(1,4,5)P₂ stimulates Ca²⁺ release from the endoplasmic reticulum (ER). Ca²⁺ and DAG directly activate PKC β II while PKC ζ is activated by phosphatidyl inositol trisphosphate (PtdIns(3,4,5)P₂). Activated PKC β II phosphorylates NADPH oxidase to release SO (Adapted from Young, et al.).

Myristoylation of peptides is known to be an effective strategy to enable simple diffusion through cell membranes to affect PKC function [4,5]. The cell permeable myristoylated (myr) PKC β II peptide inhibitor is known to inhibit PMN SO release at doses that correlated with restoration of post-reperused cardiac function following global MI(20 min)/R(45 min) in leukocyte mediated cardiac MI/R dysfunction and more recently in prolonged MI(30 min)/R(90 min) in isolated rat hearts [1,6,7]. However, a full dose-response curve with Myr-PKC β II peptide inhibitor has not been indicated previously. Characterizing the full dose-response effects is essential in identifying putative mechanisms responsible for attenuating vascular and tissue injury following I/R.

Hypothesis

We hypothesized that Myr-PKC β II peptide inhibitor would dose-dependently attenuate fMLP induced PMN SO release, and these effects would not be associated with a decrease in cell viability.

Results and Discussion

Isolation of PMNs

Male Sprague-Dawley rats (350-400 g, Charles River), used as PMN donors, were anesthetized with 2.5% isoflurane and given a 16 ml intraperitoneal injection of 0.5% glycogen (Sigma Chemical; St. Louis, MO) dissolved in PBS. Rats were reanesthetized with isoflurane 16-18 h later, and the PMNs were harvested by peritoneal lavage in 30 ml of 0.9% NaCl, as previously described [4,6].

Measurement of SO Release from Rat PMNs

The SO release from PMNs was measured spectrophotometrically (model 260 Gilford, Nova Biotech; El Cajon, CA) by the reduction of ferricytochrome c [4,6]. The PMNs (5×10^6 cells) were resuspended in 450 μ l PBS and incubated with ferricytochrome c (100 μ M, Sigma Chemical; St. Louis, MO) in a total volume of 900 μ l PBS in the presence or absence of myr PKC β II inhibitor (0.2 to 20 μ M; N-myr-SLNPEWNET, 1300 g/mol) for 15 min at 37°C in spectrophotometric cells. The PMNs were stimulated with 1 μ M fMLP (MW= 438 g/mol Calbiochem; La Jolla, CA) in a final reaction volume of 1.0 ml. Absorbance at 550 nm was measured every 30 sec for up to 120sec for fMLP and the change in absorbance (SO release) from PMNs was determined relative to time 0. Cell viability among all study groups was determined microscopically by 0.3% trypan blue exclusion at the end of the SO release assay. Viable cells remained unstained and non-viable cells stained blue.

Statistical Analysis

All data in the text and figures are presented as means \pm S.E.M. The data were analyzed by ANOVA using post hoc analysis with Fisher's PLSD test. Probability values of <0.05 are considered to be statistically significant.

Figures 3 and 4 illustrate the dose-dependent effects of Myr-PKC β II peptide inhibitor (0.5-20 μ M) on fMLP-stimulated PMN SO release. Untreated fMLP control stimulates SO release which increases absorbance and the reaction reached plateau at 60-90 sec. As shown in Figure 3, Myr-PKC β II peptide inhibitor dose dependently inhibited SO release from untreated controls by 21-26 \pm 12% (0.5 μ M; 30-120 sec), 43-46 \pm 19% (1 μ M; 30-120 sec), 58-69 \pm 9% (2 μ M; 30-120 sec), 71-75 \pm 12%

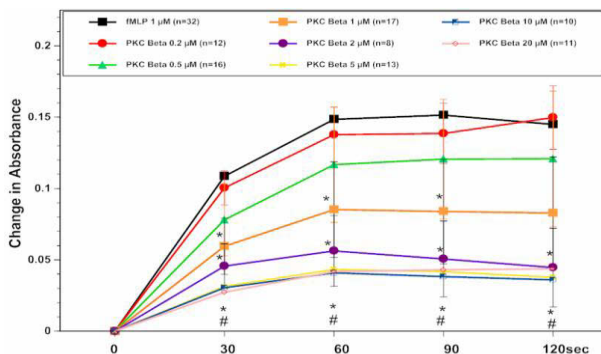


Fig. 3. The time course response of fMLP (1 μ M)-induced SO release in PMNs. * $p<0.05$ compared to untreated controls; # $p<0.05$ (5 to 20 μ M) compared to the lowest dose group (0.2 μ M); n=number of trials.

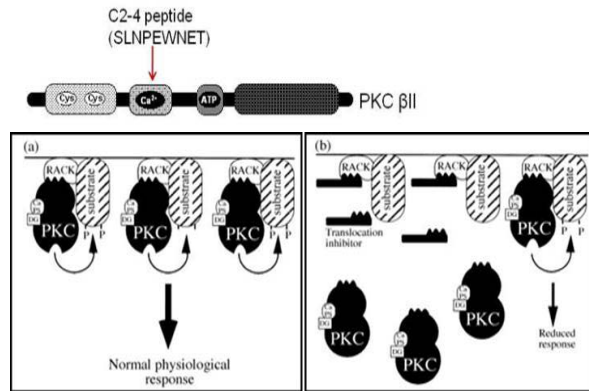


Fig. 2. Top: Illustration of PKC β II peptide inhibitor. The Ca^{2+} binding domain for PKC β II peptide inhibitor (i.e., C2-4 region) is unique for PKC β II translocation to the cell membrane when activated (Adapted from Young et al.) Bottom: PKC β II peptide inhibitor mechanism of action. The peptide inhibitor is intended to inhibit PKC β II translocation from cytosol to the sites where PKC β II interacts with substrates such as leukocyte NADPH oxidase (Adapted from Csukai and Mochly-Rosen).

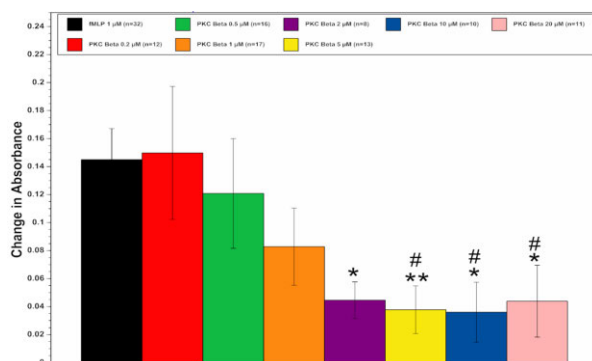


Fig. 4. fMLP (1μM)-induced peak response (120 sec) SO release in PMNs. * $p<0.05$, ** $p<0.01$ compared to untreated controls; # $p<0.05$ compared to the lowest dose group (0.2 μM).

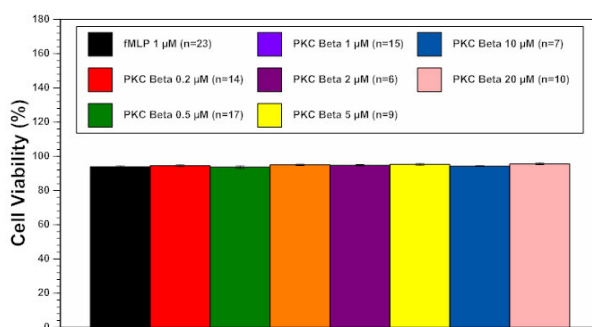


Fig. 5. The effects of Myr-PKC β II peptide inhibitor (0.2-20 μM) on cell viability in fMLP (1 μM)-induced SO release in PMNs. Cell viability ranged between 94-96% \pm 1 and was not different amongst study groups, suggesting that the inhibition of leukocyte SO release at higher doses was not due was not related to cell death.

(5-20 μM; 30-120 sec). Myr-PKC β II peptide inhibitor (1 to 20 μM) significantly reduced the PMN SO release compared to the control (all, $p<0.05$) Furthermore, PKC β II peptide inhibitor high dose groups (5-20 μM) were significantly different from the low dose group (0.2 μM) from 30-120 sec. Myr-PKC β II peptide inhibitor dose-dependently inhibited the fMLP-induced SO release from PMNs. A linear decrease in PMN SO release was observed when the doses increased from 0.2 to 2 μM, whereas the inhibition reached a plateau phase of 71-75 \pm 12% in the 5 to 20 μM dose range. Moreover, the higher dose range (5-20 μM) had no toxicity on PMN cell viability. These results suggest that activation of NADPH oxidase via PKC β II is the dominant pathway following stimulation of the PMN chemotactic receptor, and that PKC β II peptide inhibitor functions as an anti-inflammatory agent that can be used in vascular complications associated with I/R, hypertension and diabetes.

Acknowledgments

This study was supported by the Center for Chronic Disorders of Aging and the Department of Bio-Medical Sciences at PCOM. Special thanks to PCOM DO/Biomed students Stephanie Liu, Joseph Venditto, and Gregory Stoner for assistance with editing the manuscript.

References

- Young, L., et al. *Cardiovasc. Drug Rev.* **23**, 255-272 (2005), <http://www.ncbi.nlm.nih.gov/pubmed/16252018>
- Kilpatrick, L., et al. *Am. J. Physiol. Cell Physiol.* **279**, C2011-C2018 (2000), <http://www.ncbi.nlm.nih.gov/pubmed/11078718>
- Csukai, M, Mochly-Rosen, D. *Pharmacol. Res.* **39**, 253-259 (1999), <http://www.ncbi.nlm.nih.gov/pubmed/10208754>
- Perkins, K.A., et al. in Michal Lebl (Editor), *Proceedings of the 22nd American Peptide Symposium*, American Peptide Society, San Diego, 288-289, 2011.
- Eichholtz, T., et al. *J. Biol. Chem.* **268**, 1982-1986 (1993), <http://www.ncbi.nlm.nih.gov/pubmed/8420972>
- Omiyi, D., et al. *J. Pharm. Exp. Ther.* **314**, 542-551 (2005), <http://www.ncbi.nlm.nih.gov/pubmed/15878997>
- Lipscombe, C., et al., in Ved Srivastava, Andrei Yudin, and Michal Lebl (Editors), *Proceedings of the 24th American Peptide Symposium*, American Peptide Society, San Diego, 2015. *In press*.

Comparing the Effectiveness of TAT and Myristoylation of gp91ds on Leukocyte Superoxide (SO) Release

Harsh Patel, Kyle Bartol, Amelie Bottex, Ryan Remarcke, William Chau, Sydney Walker, Qian Chen, Robert Barsotti, and Lindon Young

Department of Bio-Medical Sciences, Philadelphia College of Osteopathic Medicine,
 4170 City Avenue, Philadelphia, PA, 19131, USA

Introduction

SO release from leukocytes via NADPH oxidase activation contributes to oxidative stress under various diseases, such as ischemia/reperfusion (I/R) injury and vascular complications in diabetes. NADPH oxidase has seven isoforms with NOX2 being the predominant isoform of NADPH oxidase in polymorphonuclear leukocytes (PMNs). Activation of NOX2 requires the assembly of cytosolic subunits (p47^{phox}, p40^{phox}, p67^{phox}, Rac) to plasma membrane subunits (gp91^{phox} and p22^{phox}) [1]. NADPH oxidase is activated during I/R injury via cytokine receptor stimulation or chemotactic factor (N-formyl-L-methionyl-L-leucyl-L-phenylalanine (fMLP, MW= 438 g/mol) and utilizes molecular oxygen to produce SO [2] (Figure 1).

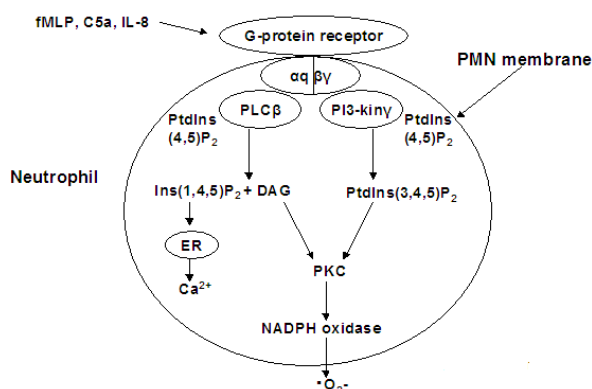


Fig. 1. Schematic representation of PKC activation generating SO release in PMN. PMN chemotactic G-protein receptors are activated by fMLP, C5a and interleukin 8. The G-protein subunits α_q and $\beta\gamma$ disassociate after stimulation and activate phospholipase C beta (PLC β) and phosphatidylinositol-3-kinase gamma (PI-3kiny) to produce inositol 1,4,5 trisphosphate (Ins(1,4,5)P₂) plus DAG and PtdIns(3,4,5)P₂ respectively from phospholipids phosphatidylinositol 4,5 bisphosphate (PtdIns(4,5)P₂). Ins(1,4,5)P₂ stimulates Ca²⁺ release from the endoplasmic reticulum (ER). Ca²⁺/DAG

and PtdIns(3,4,5)P₂ directly activate PKC. Activated PKC phosphorylates NADPH oxidase to release SO anion ($\bullet\text{O}_2^-$). Adapted from Young, et al. [2].

Gp91ds conjugated with tat or myristic acid + pegylated linker (myr-peg) are cell permeable peptide formulations which selectively inhibit NADPH oxidase assembly by blocking p47^{phox} interaction with gp91^{phox} (Figure 2).

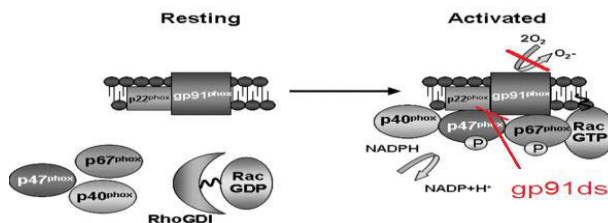


Fig. 2. Schematic showing the inactive and active forms of NADPH oxidase. Red-lines denote areas of inhibition performed by gp91ds. Adapted from Wilkinson, et al. [1]

It is well known that adding myristic acid or a tat carrier peptide to native peptides facilitates cell membrane permeability which is required for effectively targeting intracellular substrates. The

addition of a glycine-glycine (gg) spacer between the tat and cargo portion of the peptide is reported to facilitate delivery of the cargo sequence (i.e., CSTRIRRQL) [3,4] (Figure 3).

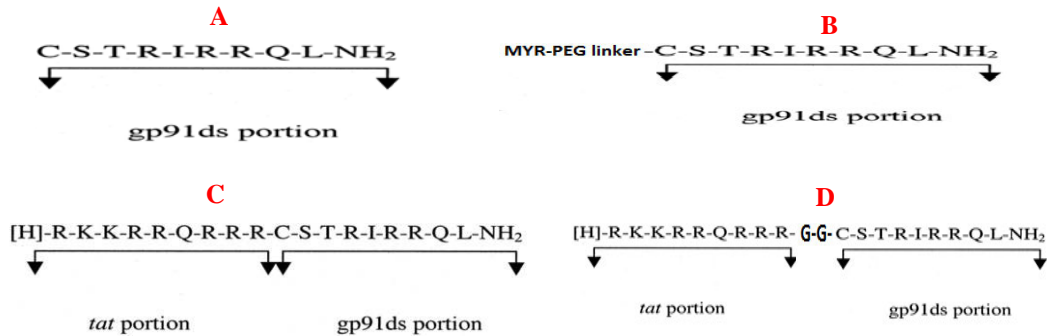


Fig. 3. A: native gp91ds (MW=1131 g/mol). B: myr-peg linker-gp91ds (MW=1486 g/mol). C: gp91ds-tat sequence (MW= 2452 g/mol). D: gp91ds-tat gg spacer (MW=2566 g/mol). Adapted from Rey, et al. [3].

We have previously shown that myristic acid conjugated caveolin-1 and protein kinase C (PKC) beta II and zeta peptide inhibitors significantly attenuated fMLP-induced SO release compared to their native counterparts [5]. However, it is not known if differences exist in the effectiveness of myristic acid versus tat conjugated gp91 ds-tat peptides compared to their native counterparts or untreated controls. We hypothesized that myr-gp91ds (2-10 μ M) would dose-dependently attenuate fMLP induced PMN SO release at lower concentrations compared to tat conjugated or tat conjugated gg spacer-gp91ds peptides. Moreover, we also predict that both myristic acid and tat conjugated gg spacer gp91ds peptides would significantly attenuate fMLP-induced leukocyte SO release compared to native or untreated controls without affecting cell viability.

Results and Discussion

Isolation of PMNs

Male Sprague-Dawley rats (350–400 g, Charles River), used as PMN donors, were anesthetized with 2.5% isoflurane and given a 16 ml intraperitoneal injection of 0.5% glycogen (Sigma Chemical) dissolved in PBS. Approximately 16 h later, the rats were reanesthetized with isoflurane and the PMNs were harvested by peritoneal lavage in 30 ml of 0.9% NaCl, as previously described [2,5].

Measurement of SO Release from Rat PMNs

The SO release from PMNs was measured spectrophotometrically (Gilford model 260, Nova Biotech; El Cajon, CA) by the reduction of ferricytochrome c [2,5]. The PMNs (5×10^6 cells) were suspended in 450 μ l PBS and incubated with 100 μ M ferricytochrome c (Sigma Chemical; St Louis, MO) in a total volume of 900 μ l PBS in the presence or absence of myr-peg conjugated (2 to 10 μ M), tat conjugated (80 μ M) or native gp91ds (80 μ M) for 15 min at 37°C in spectrophotometric cells. Thereafter, absorbance at 550 nm was measured every 30 sec for up to 120 sec following fMLP 1 μ M (Calbiochem; La Jolla, CA) stimulation and the change in absorbance (SO release from PMNs) was determined relative to time 0 in a final reaction volume of 1 ml. Cell viability among all study groups was determined by 0.3% trypan blue exclusion at the end of the SO release assay.

Myr-peg gp91 (5 & 10 μM) significantly attenuated untreated and native gp91ds induced SO release by $56-57 \pm 8\%$ and $52-54 \pm 9\%$ respectively. Myr-peg gp91 (2 μM), gp91ds-tat (80 μM), and gg spacer (80 μM) significantly inhibited untreated by $36 \pm 11\%$ compared to untreated controls and was not different from native gp91ds (see Figure 4). Concentrations of tat conjugated peptides $\leq 40 \mu\text{M}$ did not exert significant inhibition of PMN SO release. (Data not shown)

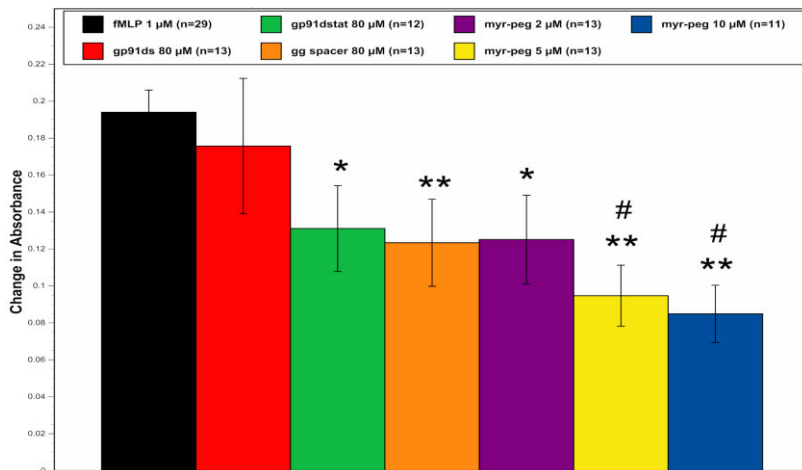


Fig. 4. fMLP (1 μM)-induced peak response SO release in PMNs. Probability values of <0.05 are considered to be statistically significant (* $p<0.05$, ** $p<0.01$ compared to untreated controls; # $p<0.05$ compared to native gp91ds). All data in the text and figures are presented as means \pm S.E.M. The data were analyzed by analysis of variance using post hoc analysis with the Fisher's test and n = number of trials.

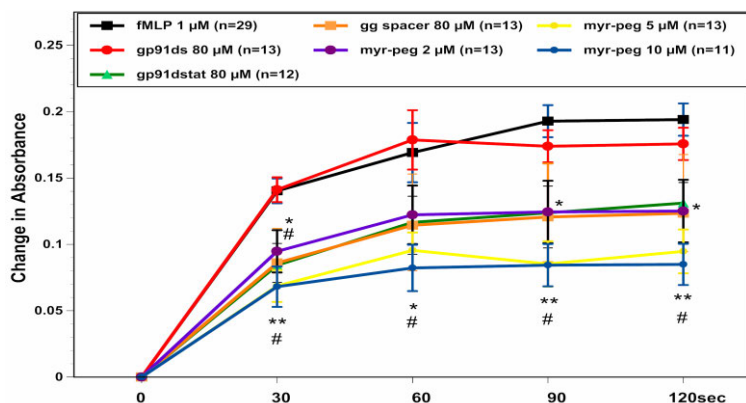


Fig. 5. The time course response of fMLP (1 μM)-induced SO release. * $p<0.05$, ** $p<0.01$ compared to untreated controls; # $p<0.05$ compared to native gp91ds.

Myr-peg gp91 (5 & 10 μM) significantly inhibited untreated and native gp91 by 44-56% and 46-52% respectively from 30-120 sec. Myr-peg gp91ds (2 μM), gp91dstat (80 μM), and gp91ds-tat with gg spacer (80 μM) significantly inhibited untreated by 33-36% from 30-120 sec and was only different from native gp91 at 30 sec (Figure 5).

We also observed that TAT (R-K-K-R-R-Q-R-R; MW=1321g/mol, $n=7$) alone decreased fMLP-induced absorbance by $48 \pm 9\%$ and cell viability was $92 \pm 1\%$ (data not shown). Although cell viability was not significantly different from untreated and other tat conjugated gp91ds groups, we observed a significant degree of cell clumping, which in turn would decrease the absorbance. Therefore

the measured decrease in absorbance was likely due to the effect of cell clumping rather than a decrease in fMLP induced SO release. By contrast, cell clumping was not observed in the other tat conjugated gp91ds groups suggesting that in these groups leukocyte SO release was attenuated. These results suggest that tat alone may potentiate cell aggregation.

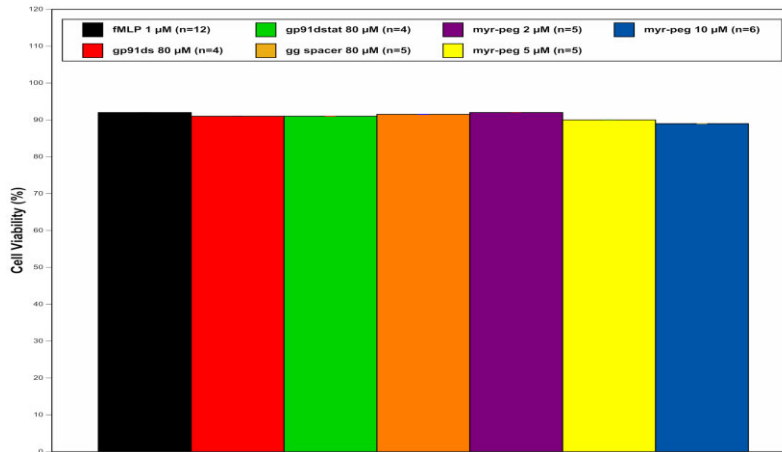


Fig. 6. The effects of native, tat, and myr-peg conjugated gp91ds on cell viability in fMLP (1 μ M)-induced SO release in PMNs. Cell viability ranged between 90-93 \pm 1% and was not different amongst study groups indicating that the reduction in SO release was not related to cell death.

Unconjugated native sequence did not inhibit the fMLP induced SO response at the highest dose tested (80 μ M). Myr-peg gp91ds NADPH oxidase peptide inhibitor significantly attenuated leukocyte SO release dose dependently compared to untreated or native sequence (myr-peg-gp91ds; 2-10 μ M). The tat conjugated gp91ds inhibitors (both 80 μ M) significantly attenuated fMLP-induced leukocyte SO release, but to a lesser extent than the myr-peg linked inhibitor and were not different from native gp91ds at 60-120 sec. Moreover, we expected to see greater inhibition with gp91ds-tat with gg spacer compared to gp91ds-tat since the gg spacer is reported to facilitate delivery of the cargo sequence. However, this subtle difference in cargo sequence delivery may be masked with respect to inhibition of leukocyte SO release in this assay. Collectively, these results suggest that native gp91ds requires conjugation of myr-peg or tat in order to effectively inhibit the intracellular target of p47^{phox} and gp91 interaction. Additionally, myr-peg-gp91ds is more cell permeable and therefore can inhibit fMLP-induced SO release from leukocytes at lower doses compared to gp91ds-tat and gg spacer gp91ds-tat. Future studies will be aimed at comparing myr and tat conjugated peptides that have other intracellular targets i.e. mitochondria in myocardial ischemia-reperfusion.

Acknowledgments

This study was supported by the Center for Chronic Disorders of Aging and the Department of Bio-Medical Sciences at PCOM. Special thanks to PCOM DO/Biomed students Kevin Kucharski, Stephanie Liu and Gregory Stoner for assistance with editing the manuscript.

References

1. Wilkinson, B.L., Landreth, G.E. *J. Neuroinflammation* **3**, 30 (2006), <http://dx.doi.org/10.1186/1742-2094-3-30>
2. Young, L.H., et al. *Cardiovascular Drug Reviews* **23**, 255-272 (2005), <http://www.ncbi.nlm.nih.gov/pubmed/16252018>
3. Rey, F.E., et al. *Circulation Research* **89**, 408-414 (2001), <http://www.ncbi.nlm.nih.gov/pubmed/?term=Novel+Competitive>
4. Taraballi, F., et al. *Frontiers in Neuroengineering* (2010), <http://dx.doi.org/10.3389/neuro.16.001.2010>
5. Perkins, K.A., et al., in Lebl, M. (Ed.) *Peptides: Building Bridges (Proceedings of the 22nd American Peptide Symposium)*, American Peptide Society, San Diego, 2011, p. 288-289, http://www.5z.com/22APS/proceedings/22APS_full_color_v5.pdf

Pancreatic β -cell Imaging with High Affinity Peptide Ligands to the GLP-1 Receptor

Bikash Manandhar¹, William Silvers², Amit Kumar², Su-Tang Lo²,
 Xiankai Sun², and Jung-Mo Ahn^{1*}

¹Dept. of Chemistry and Biochemistry, University of Texas at Dallas, Richardson, TX, 75080, USA;

²Dept. of Radiology, University of Texas Southwestern Medical Center, Dallas, TX, 75390, USA

Introduction

In both type 1 and type 2 diabetes, early diagnosis and monitoring of the pancreatic beta-cell mass (BCM) change during the disease progression may be highly beneficial. As a specific beta-cell biomarker, glucagon-like peptide-1 receptor (GLP-1R) is found to be highly expressed in the pancreatic beta-cells and can serve as a suitable target for the development of molecular imaging probes [1]. Its natural ligand, glucagon-like peptide-1 (GLP-1), is an incretin and interacts with GLP-1R with nanomolar affinity, which makes it an outstanding candidate. There are several GLP-1 based PET imaging probes reported, but high renal uptake of these PET agents has been a concern for developing them for clinical use. As the beta-cells are dispersed throughout the pancreas and constitute less than 2% of the total mass, non-specific uptake by nearby tissues and organs like kidney and liver may decrease contrast of the signal dramatically. In our prior studies, we have demonstrated that strategically positioned lactam bridges at the *N*- and *C*-terminus of GLP-1 can increase receptor affinity by stabilizing the helical structures in the peptide and enhance proteolytic stability. Based on the findings, we designed a bicyclic GLP-1 analog EM2198 having two lactam bridges between residues 18-22 and 30-34 [2,3]. D-Ala⁸ was also introduced to prevent the degradation by DPP-IV. The resulting bicyclic GLP-1 analog EM2198 was found to be remarkably stable, and a PET imaging agent for the pancreatic β -cells was developed by conjugating to DOTA and labeling with ⁶⁴Cu [4].

Results and Discussion

To lower non-specific uptake by nearby organs, we have modified our previously reported bicyclic GLP-1 analog EM2198 (**1**), by introducing hydrophilic tails, such as penta-glutamic acids (**2**), penta-serines (**3**) and penta-lysines (**4**). These modifications were found to make no change in receptor activation capability (Figure 1). These peptides were examined for their utility as PET agents for imaging the β -cells. PET/CT imaging probes were constructed by conjugating to NOTA. After labeling with Ga-68, static PET/CT scans were acquired on a Siemens Inveon PET/CT multimodality system using normal C57BL/6 mice.

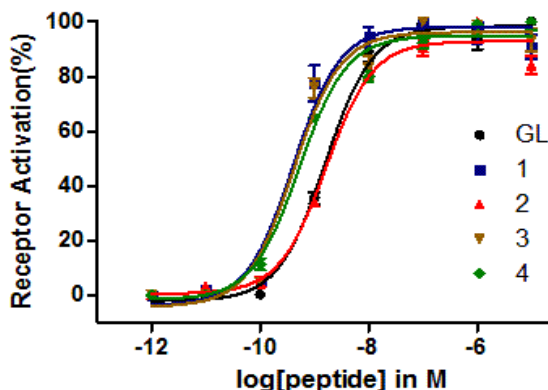


Fig. 1. GLP-1R activation by the GLP-1 analogs with hydrophilic tails.

PET tracers derived from these peptides were examined for their capability of enhancing the specific pancreatic uptake and lowering non-specific adsorption to nearby organs. Increase in polarity by introducing the hydrophilic tails appears to enhance imaging quality presumably by decreasing plasma protein binding and diminishing non-specific uptake by other organs like liver and lungs. The pancreas to kidney uptake ratios (Table 1) of the modified peptides **2-4** were found to be comparable to the parent peptide **1**. The increased hydrophilicity may have slightly promoted clearance *via* renal route. The peptide bearing hydroxyl groups **3** appeared to be marginally superior to the other peptides with charged tails **2** and **4** (Figure 2).

Table 1. Specific uptake ratios of GLP-1 based PET tracers.

Uptake ratio	GLP-1 analogs			
	1	2	3	4
Pancreas/Liver	0.76	1.06	1.19	1.21
Pancreas/Lungs	0.60	1.15	1.37	0.86
Pancreas/Kidney	0.05	0.02	0.04	0.02

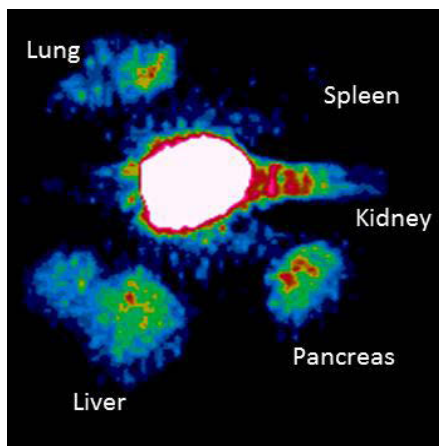


Fig. 2. Ex vivo PET image of peptide 3 in normal mice.

Acknowledgments

This work was supported in part by the Welch Foundation (AT-1595), the Juvenile Diabetes Research Foundation (37-2011-20, 37-2011-632), and National Institutes of Health (R01 DK092163-01).

References

1. Manandhar, B., Ahn, J.-M. *J. Med. Chem.* **58**, 1020-1037 (2015), <http://dx.doi.org/doi:10.1021/jm500810s>
2. Murage, E.N., et al. *Bioorg. Med. Chem.* **16**, 10106-10112 (2008), <http://dx.doi.org/doi:10.1016/j.bmc.2008.10.006>
3. Murage, E.N., et al. *J. Med. Chem.* **53**, 6412-6420 (2010), <http://dx.doi.org/doi:10.1021/jm100602m>
4. Manandhar, B., et al., in Lebl, M. (Ed.) *Peptides: Peptides Across the Pacific (Proceedings of the 23rd American Peptide Symposium)*. American Peptide Society, San Diego, 2013, p. 172, <http://dx.doi.org/10.17952/23APS.2013.172>

Development of a Troponin-Specific Probe for Early Detection of Cardiac Injuries

Lara Pes^{1,§}, Young Kim^{1,2,§}, and Ching-Hsuan Tung^{1,*}

¹Molecular Imaging Innovations Institute, Department of Radiology, Weill Cornell Medical College, New York, NY, 10021, USA; ²Department of Pathology, Chonnam National University

Medical School, 671, Jebongno, Dong-Gu, Gwangju, 501-757, Korea

[§]These authors contributed equally to the development of the project.

Introduction

Cardiac troponin I (cTnI) is an important cardiomyocyte-specific protein responsible for heart muscle contraction. It is released into the bloodstream subsequently to heart damage; for this reason, it is widely used as a biomarker in the early detection of myocardial injuries [1,2]. Recently a novel peptide termed myocyte targeting peptide (MTP, Figure 1), which has unusual affinity to cardiomyocytes was identified by us [3,4]. This prototype MTP contains three residues of the non-natural amino acid biphenylalanine (Bip) and its selectivity towards cardiac tissues is thought to be due to the ability of Bip to bind cTnI. With the aim of early heart injury diagnosis, a library of MTP derivatives was designed in order to optimize the affinity and specificity of the troponin binding. Assisted by a fluorescein (FITC) label, the specific selectivity of the MTP analogs to myocardium over skeletal muscle tissues was assayed by fluorescence imaging. The improved MTP could potentially be used to detect circulating cTnI after cardiac injury.

Results and Discussion

Despite the good results previously obtained with MTP in selectively binding cTnI in cardiac muscle tissues, a new library of derivatives was developed (Figure 2) in order to investigate the role of the unusual Bip amino acid and the number of phenyl groups in the peptide structure and better understand structure-activity relationship. MTP peptides were prepared on Rink Amide MBHA resin using Fmoc chemistry, HBTU and piperidine were employed as coupling reagent and deprotecting agent respectively. All the compounds were labeled with a FITC on their termini. Troponin specific binding was performed on sliced frozen sections of cardiac and skeletal muscle tissue (the latter used as a control) for 1h with the MTP derivatives in PBS, at concentrations from 2 to 10 μ M. Fluorescence images were taken and the fluorescence intensity was calculated using the software Image J.

To evaluate the ability of the Bip amino acid alone to interact with cTnI, the fluorescent tag was grafted directly to its *N*-terminus, with and without a spacer (BipHA and BipAA respectively), but in tissue study no fluorescence was registered, indicating that Bip alone does not provide a strong enough binding. A Bip dimer was then prepared and a short peptide chain was added (sBip2) to improve solubility and mimic the original MTP, in which the Bip are part of a peptide structure. The newly prepared sBip2 was able to preferentially stain cardiac muscles over skeletal muscle tissues. At the same time, other analogs of sBip2 were synthesized aiming to understand the importance of the number of phenyl groups; in sPheBip and sGlyBip, one Bip was replaced with a phenylalanine or glycine, bringing the number of aryls from four to three and two respectively and in sPhePhe, both Bip residues were substituted with phenylalanine. Consistent with previous findings, a decrease in the ability of staining cardiac muscle with a decrease in the number of phenyl groups was observed. In the case of sGlyTrip, where a triphenyl moiety was used, the selectivity towards cardiac muscles was lost. Finally the PEG5Bip2 analog, synthesized in solution over 5 steps, substituting the Bip amino acid with Bip amine and the peptide chain with an equivalent length PEG, showed binding, but no selectivity.

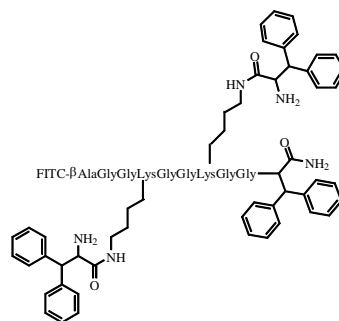


Fig. 1. Structure of MTP.

Among the first series of compounds, the best results in fluorescence intensity and selectivity were obtained with sBip2, but still the solubility was not as hoped. A positively charged poly-arginine chain was thus introduced to improve solubility and, as expected, both Bip1 and Bip2 were fully soluble. In addition, Bip1 and Bip2, which have one and two Bip amino acid residues respectively, showed significantly improved binding to cardiac muscle tissues and selectivity over skeletal muscles. Bip2 was found to be the best derivative from this set of the library (Figure 3).

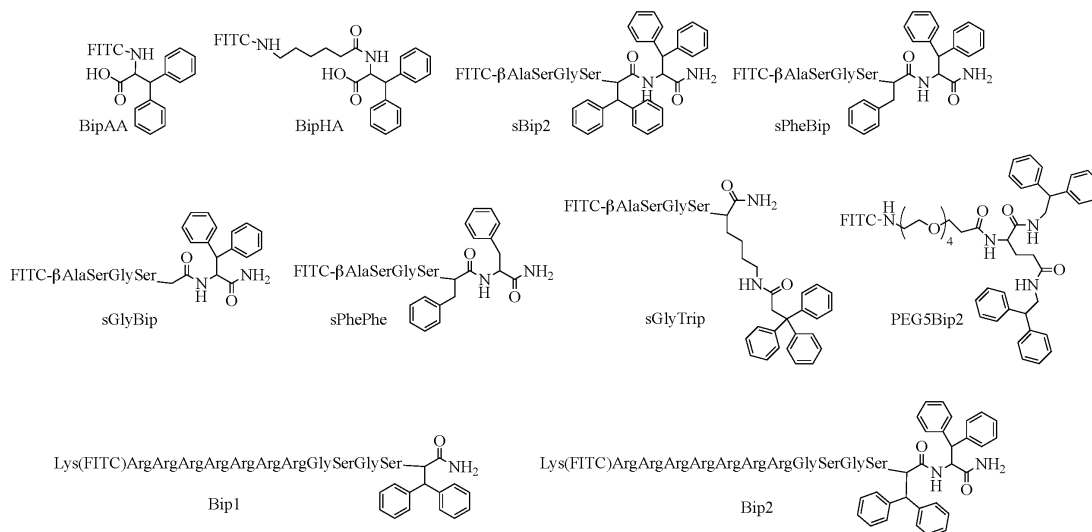


Fig. 2. Structures of the MTP derivatives.

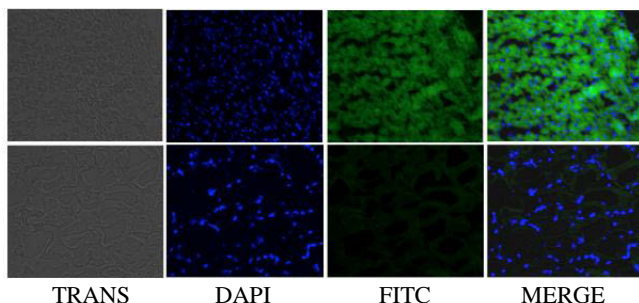


Fig. 3. Fluorescence microscope images, 20x at 30 ms exposure time, of frozen sections of cardiac muscles (top) and skeletal muscles (bottom) after 1 h staining with 2 μ M solutions in PBS of the most active MTP derivative Bip2.

References

1. De Lemos, J.A. *JAMA* **309**, 2262-2269 (2013), <http://dx.doi.org/10.1001/jama.2013.5809>
2. Mahajan, V.S., Jarolim, P. *Circulation* **124**, 2350-2354 (2011), <http://dx.doi.org/10.1161/CIRCULATIONAHA.111.023697>
3. Chen, J., et al. *PLoS ONE* **6**, e19097 (2011), <http://dx.doi.org/10.1371/journal.pone.0019097>
4. Abd-Elgalil, W.R., Tung, C.H. *Mol. Biosyst.* **8**, 2629-2632 (2012), <http://dx.doi.org/10.1039/c2mb25178g>

Effects of Mitochondrial-Targeted Antioxidants on Real-Time Blood Nitric Oxide and Hydrogen Peroxide Release in Acute Hyperglycemic Rats

Matthew L. Bertolet, Michael Minni, Tyler Galbreath, Robert Barsotti,
 Lindon H. Young, and Qian Chen

Division of Research, Department of Bio-Medical Sciences, Philadelphia College of Osteopathic Medicine
 (PCOM), Philadelphia, PA, 19131, USA

Introduction

Diabetes and prediabetes are major public health concerns worldwide due to the high risk of developing micro- and macro-vascular complications. Hyperglycemia, the major criteria for diabetes diagnosis, is causally related to the pathogenesis of vascular complications in diabetic patients. An early event during hyperglycemia is vascular endothelial dysfunction. Normally, the vascular endothelium facilitates blood flow principally by releasing endothelial-derived nitric oxide (NO) via vascular endothelial NO synthase (eNOS) in the presence of an essential co-factor, tetrahydrobiopterin (BH₄). By contrast, acute and chronic hyperglycemia increase oxidative stress and reduce NO bioavailability [1,2]. The reduced endothelial-derived NO bioavailability promotes vasoconstrictive, pro-inflammatory, and pro-thrombotic events, initiating inflammation, thereby recruiting leukocytes, resulting in tissue/organ damage (Figure 1). Therefore, reduction of oxidative stress during hyperglycemia will mitigate vascular endothelial dysfunction and organ damage. Crabtree, et al. [1] found that mitochondria-derived superoxide (SO) contributes to hyperglycemia-induced oxidative stress in cultured vascular endothelial cells. Subsequently, the overproduction of SO promotes the oxidation of BH₄ to dihydrobiopterin (BH₂). The reduced BH₄/BH₂ ratio leads to BH₂, not BH₄, binding to oxygenase domain of eNOS, which causes eNOS to shift its product profile from NO to SO [1] (Figure 1). However, the role of mitochondria in acute hyperglycemia-induced oxidative stress and blood NO reduction has not been evaluated *in vivo*. Recently, our lab showed that mitoquinone (MitoQ) and SS31 (Szeto-Schiller, D-Arg-Dmt-Lys-Phe-Amide) peptide (Figure 2), mitochondria-targeted antioxidants, significantly reduced blood H₂O₂ (an index of oxidative stress) and increased blood NO levels in a hind limb ischemia/reperfusion (I/R) animal model [3]. Oxidative stress is also an important cause of reperfusion injury during I/R. Thus, we hypothesize that MitoQ and SS-31 will reduce blood oxidative stress and increase blood NO levels under acute hyperglycemic conditions.

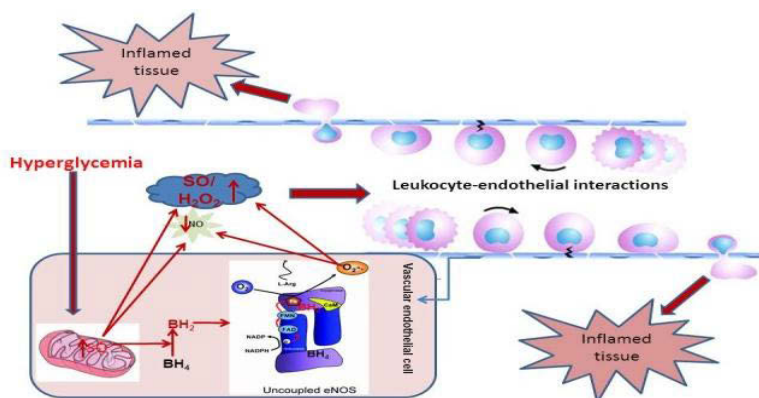


Fig. 1. The putative role of mitochondrial-derived SO in hyperglycemia-induced oxidative stress, vascular endothelial dysfunction and tissue inflammation.

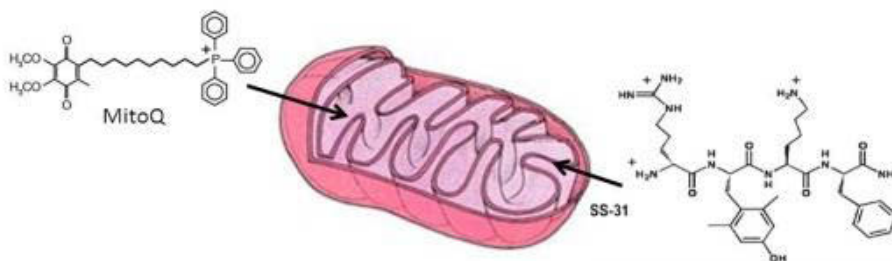


Fig. 2. Chemical structure of MitoQ and SS-31 [4,5].

Results and Discussion

Male Sprague-Dawley rats (275 to 325g, Charles River, Springfield, MA) were anesthetized with 60 mg/kg of pentobarbital sodium with 1000 units of heparin via intraperitoneal (i.p.) injections. The jugular vein was catheterized to allow for the infusion of saline, 20% D-glucose, or 20% D-glucose with 1.86 mg/kg MitoQ (MW=600 g/mol; complexed with cyclodextrin to improve water solubility, total MW=1714 g/mol) or with 2.7 mg/kg SS-31 (MW=640 g/mol, Genemed Synthesis, Inc., San Antonio, TX). The continuous infusion of 20% D-glucose solution was used to maintain a hyperglycemic state around 200 mg/dL for about 180 min. MitoQ or SS-31 was added to the 20% D-glucose infusate to achieve a blood concentration of approximately 13 μ M and 50 μ M, respectively. Both femoral veins were exposed and catheterized in order to randomly place calibrated NO or H₂O₂ microsensors (100 μ m diameter, WPI Inc., Sarasota, FL) into each femoral vein. These microsensors were connected to an Apollo 4000 free radical analyzer (WPI Inc., Sarasota, FL) to monitor blood NO and H₂O₂ levels in real-time. NO, H₂O₂ were monitored continuously while glucose levels were recorded at baseline and at 20 minute intervals throughout the 180 minute infusion period [2].

The changes of blood NO (nM) and H₂O₂ (μ M) levels were expressed as the relative change to the saline group. All the data were represented as a mean \pm SEM, and then analyzed by ANOVA using post hoc analysis with the Student Newman Keuls test. $p < 0.05$ was considered significant.

The time course change in blood glucose in different experimental groups is illustrated in Figure 3. The blood glucose level in the saline group remained at baseline values of 80-100 mg/dl throughout the experiment. In contrast, after 20 min infusion of 20% D-glucose with or without the drug, the blood glucose levels rose to hyperglycemic levels at \sim 200 mg/dl. All hyperglycemic rats urinated between 20-40 min after glucose infusion.

The time course change in blood NO levels relative to the saline infusion among the different experimental groups is shown in Figure 4. There was a significant decrease in blood NO levels in the

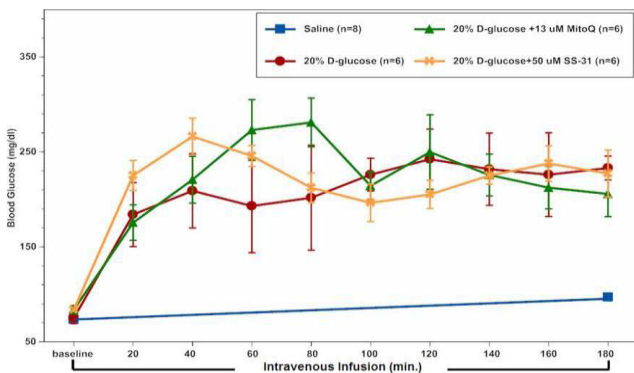


Fig. 3. Blood glucose level among saline and 20% glucose infusion groups.

20% glucose group (n=9) compared to the saline group (n=7) at 120 min (43.7 ± 11.3 nM lower), followed by a continued decrease throughout the infusion (all $p < 0.05$). At 180 min, blood NO level was 68 ± 13.5 nM lower relative to that in saline group ($p < 0.01$). However, the co-infusion of MitoQ (13 μ M, n=5) or SS-31 (50 μ M, n=6) with 20% glucose significantly reduced the fall in blood NO levels from 120 min or 140 min, respectively, which was sustained during the rest of the infusion time compared to those in the 20% glucose group. The NO levels in both MitoQ and SS-31

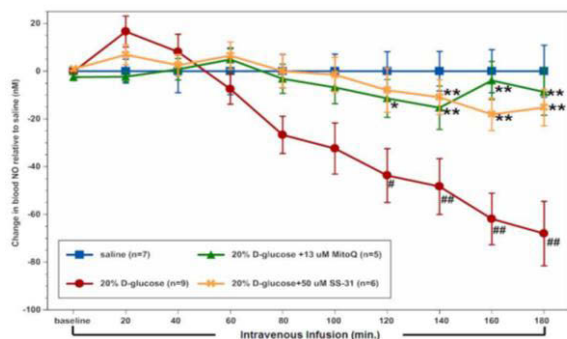


Fig. 4. The comparison of change in blood NO levels relative to saline group among 20% D-glucose, 20% D-glucose with MitoQ (13 μ M), and 20% D-glucose with SS-31 (50 μ M) (# p <0.05, ##<0.01 vs saline; * p <0.01 vs D-glucose).

blood H_2O_2 levels only at 160 min and 180 min by comparing to those in the 20% glucose group (both p <0.05). SS-31 treatment did show a trend of smaller increases in blood H_2O_2 levels compared to MitoQ treatment, but was not significant. Moreover, the H_2O_2 levels in both MitoQ and SS-31 treatment groups were not significantly different from H_2O_2 levels in the saline group throughout the experimental time course.

Researchers have shown that acute hyperglycemia can cause systemic oxidative stress and vascular dilatory dysfunction in non-diabetic human subjects [6,7]. By placing NO/ H_2O_2 sensors in rat femoral veins, we established the time course of blood NO and H_2O_2 levels during acute hyperglycemia. Blood H_2O_2 levels serve as an index of oxidative stress because H_2O_2 is principally derived from SO by SO dismutase. We found that acute hyperglycemia significantly increased blood H_2O_2 and reduced blood NO levels compared to the saline group. Moreover, increased blood H_2O_2 levels occurred earlier than reduction of blood NO levels during hyperglycemia. This result suggests that reduced blood NO levels may be due to direct quenching effect of free radicals on blood NO levels and/or eNOS product profile changing from NO to SO when BH_4 is oxidized to BH_2 (see Figure 1). Mitochondria may be a site of free radicals overproduction during hyperglycemia. Both MitoQ and

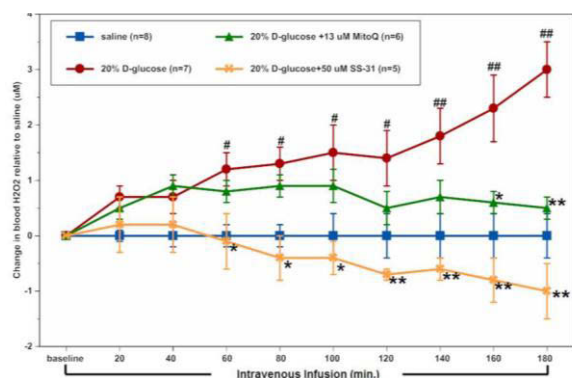


Fig. 5. The comparison of change in blood H_2O_2 levels relative to saline group among 20% D-glucose, 20% D-glucose with MitoQ (13 μ M), and 20% D-glucose with SS-31 (50 μ M) (# p <0.05, ## p <0.01 vs saline; * p <0.01 vs D-glucose).

treatment groups were similar to the NO levels in the saline group throughout the experimental time course.

The time course change in blood H_2O_2 levels relative to the saline infusion among the different experimental groups is shown in Figure 5. There was a significant increase in blood H_2O_2 levels in the 20% glucose group (n =7) compared to the saline group (n =8) at 60 min (1.2 ± 0.3 μ M higher), followed by a continued increase throughout the infusion. At 180 min, blood H_2O_2 level was 3.0 ± 0.5 μ M higher relative to that in saline group. However, the addition of SS-31 (50 μ M, n =5) significantly reduced the increase in blood H_2O_2 levels from 60 min to 180 min compared to those in 20% glucose group (all p <0.05). Furthermore, the addition of MitoQ (13 μ M, n =6) significantly reduced

SS-31 have been indicated as mitochondrial-targeted antioxidants by selectively diffusing into the mitochondria after administration [6,7]. We found that administration of MitoQ or SS-31 during hyperglycemia significantly reduced blood H_2O_2 levels and improved blood NO levels, similar to the saline group. Previous research has indicated that MitoQ possesses positive charges and lipophilic properties, and both facilitate its diffusion into the mitochondria. Meanwhile, MitoQ may collapse mitochondrial membrane potential at higher doses which slows its further concentration in the mitochondria [6]. By contrast, SS-31 has an alternating cationic-aromatic amino acid sequence which allows it to concentrate into the mitochondria without relying on mitochondrial membrane potential [4,5]. The different mechanism of action

between MitoQ and SS-31 may explain the observation in this study that SS-31 exerted earlier and better reduction in blood H₂O₂ levels compared to MitoQ. In summary, the data suggest that mitochondrial derived SO is a significant source of oxidative stress and vascular endothelial dysfunction under acute hyperglycemic conditions. Moreover, treatment with mitochondrial-targeted antioxidants, MitoQ or SS-31, may be beneficial to attenuate hyperglycemia-induced oxidative stress and vascular endothelial dysfunction.

Acknowledgments

This study was supported by Division of Research, Department of Bio-Medical Sciences, and Center for Chronic Disorders of Aging at Philadelphia College of Osteopathic Medicine.

References

1. Crabtree, M.J., et al. *Am. J. Physiol. Heart Circ. Physiol.* **294**, H1530-1540 (2008), <http://dx.doi.org/10.1152/ajpheart.00823.2007>
2. Minni, M., et al., in Lebl, M. (Ed.) *Proceedings of the 22nd American Peptide Symposium*, American Peptide Society, San Diego, 2011; 280-281.
3. Galbreath, T., et al., in Lebl, M. (Ed.) *Proceedings of the 23rd American Peptide Symposium* American Peptide Society, San Diego, 2013, p. 46-47, <http://dx.doi.org/10.17952/23APS.2013/046>
4. Szeto, H.H. *Antioxidants and Redox Signaling* **10**, 601-619 (2008), <http://dx.doi.org/10.1089/ars.2007.1892>
5. Adlam, V.J., et al. *FASEB J.* **19**, 1088-1095 (2005), <http://www.fasebj.org/content/19/9/1088.full.pdf>
6. Title, L.M., et al. *J. Am. Coll. Cardiol.* **36**, 2185-2191 (2000), [http://dx.doi.org/10.1016/S0735-1097\(00\)00980-3](http://dx.doi.org/10.1016/S0735-1097(00)00980-3)
7. Marfella, R., et al. *J. Clin. Invest.* **108**, 635-636 (2001), <http://dx.doi.org/10.1172/JCI13727>

Investigating Metabolic Gender Differences with Melanocortin Antagonist SKY 2-23-7

Cody J. Lensing, Skye R. Doering, Danielle N. Adank, and
Carrie Haskell-Luevano

Department of Medicinal Chemistry, University of Minnesota, Minneapolis, MN, 55455, USA

Introduction

The melanocortin system has been implicated in various physiological functions including pigmentation [1,2], sexual function [3], cardiovascular function [4], memory [5], and energy homeostasis [6-10]. The energy homeostasis functions have been attributed to the melanocortin 3 (MC3R) and melanocortin 4 receptors (MC4R) [6-10]. The intracerebroventricular (ICV) administration of melanocortin agonists has been reported to significantly decrease food intake, whereas administration of antagonists is reported to significantly increase food intake [9,10]. Therefore, melanocortin agonist ligands could serve as a potential treatment for obesity, and melanocortin antagonist ligands could serve as a treatment for cachexia. However, some limitations of the melanocortin ligands do exist such as modulating sexual function [3] and blood pressure [4]. It is, therefore, of interest to develop melanocortin ligands with unique pharmacologies which are void of these undesired effects.

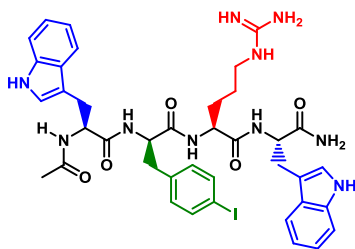


Fig. 1. Structure SKY2-23-7 Ac-Trp-(pI)DPhe-Arg-Trp-NH₂.

SKY 2-23-7 is a tetrapeptide which was identified in our laboratory with the sequence Ac-Trp-(p-I)DPhe-Arg-Trp-NH₂ (Figure 1) [11]. It was discovered through a double substitution strategy of the melanocortin core His-Phe-Arg-Trp sequence. SKY 2-23-7 was characterized as a weak antagonist ($pA_2=5.43\pm0.16$) at the mMC3R and a strong antagonist ($pA_2=7.83\pm0.16$) at the mMC4R (Figure 2). Distinctly there was minimal mMC3R agonist activity up to 100 μ M which is not commonly observed for a mMC3R/mMC4R antagonist such as SHU9119 [11]. The current study investigated the *in vivo* effects of this unique pharmacology *via* intracerebroventricular (ICV) administration of SKY 2-23-7 in male and female mice which gave evidence of sex specific differences.

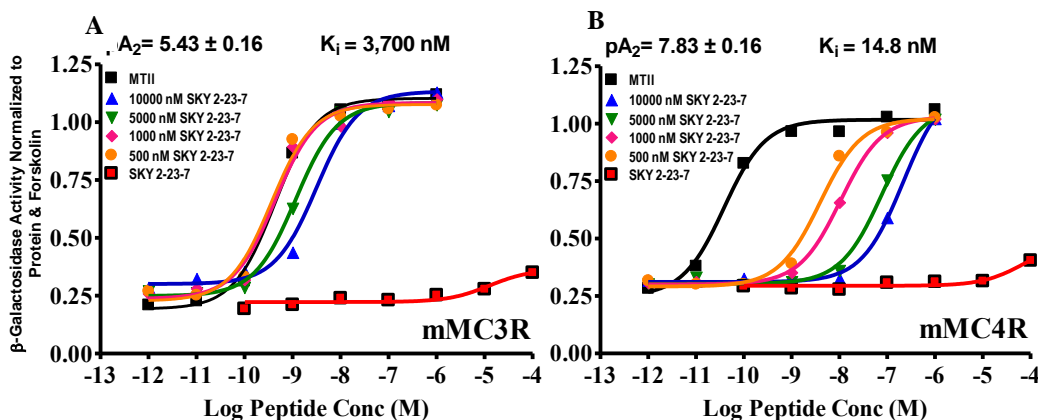


Fig. 2. Reported *in vitro* pharmacology of SKY2-23-7 at the mMC3R and mMC4R [11]. The pA_2 values were found by a Schild analysis [12]. The K_i was calculated by the equation $pA_2=-\log(K_i)$. Figure modified from Doering, et al. 2015.

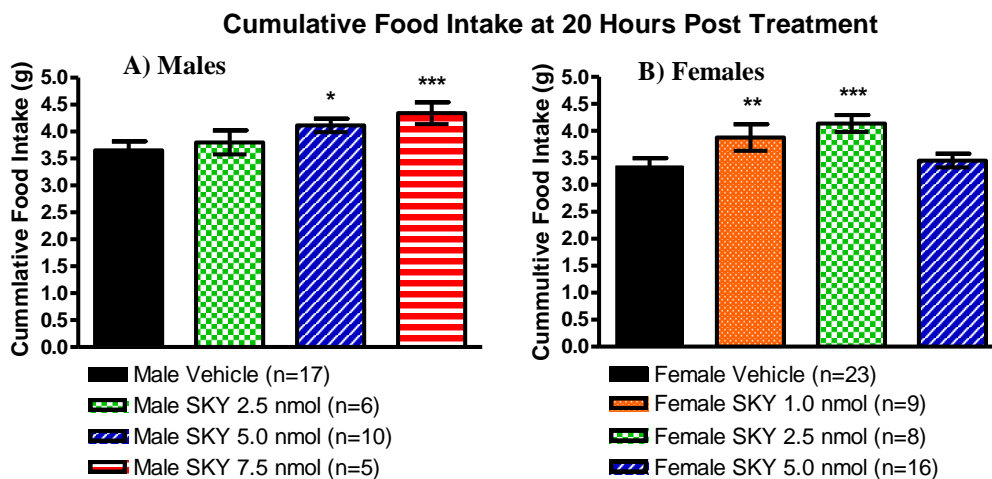


Fig. 3. Cumulative food intake 20 hours after receiving SKY 2-23-7 in 3 μ L vehicle vs 3 μ L of vehicle (<1.0% DMSO in water) via ICV administration in both wild type (A) male and (B) female mice. Data shown as mean \pm SEM. * p <0.05 ** p <0.01 *** p <0.001.

Results and Discussion

Both male and female wild type mice underwent surgery to implant a cannula into the lateral ventricle as previously described [9]. After a one week recovery, placement of the cannula was validated via human PYY₃₋₃₆ (Bachem) administration as described by Marsh, et al. [10]. Cannula placement validation was characterized by at least 0.9 g increase in food intake following hPYY treatment versus saline treatment. Mice which passed validation were then administered SKY 2-23-7 after a 1 week washout period. The experiments were performed following a Latin-square paradigm. Vehicle was sterile water with less than 1% DMSO. Mice were housed in TSE PhenoMaster metabolic cage systems (TSE Systems, Berlin Germany). The TSE PhenoMaster system measured the food intake, oxygen uptake, and carbon dioxide production in 15 minute bins following treatment for 96 hours. From the oxygen uptake and carbon dioxide production, the energy expenditure (calories burned) were calculated. Preliminary statistical analyses for compound concentration over time were performed using two-way ANOVA followed by Bonferroni post tests. The analyses showed statistical significant differences for both cumulative food intake and energy expenditure over 24 hours. The data from individual time points were then compared on the bar graphs shown. Individual time point data were analyzed by a one-way ANOVA followed by a Bonferroni post test to compare each treatment group to vehicle treated animals. Statistical significance was considered p <0.05.

SKY 2-23-7 displayed a unique pharmacological profile in which it affects male and female mice differently. In male mice, a dose dependent increase in cumulative food intake 20 hours after administration is seen with statistical significance at the 5 and 7.5 nmol doses (Figure 3A). This is consistent with previous reports of mMC4R antagonists increasing food intake [6,9]. In female mice, the 1.0 and 2.5 nmol dose significantly increases food intake (Figure 3B). The same 2.5 nmol dose in males had minimal effect on food intake. Surprisingly, the higher 5 nmol dose in female mice had no effect on food intake which was different from the significant increase in food intake seen in male mice.

Analysis of the energy expenditure in male and female mice also showed sex specific differences. The calories burned in 24 hours was higher in female than in male mice after vehicle administration when normalized for body weight differences (p =0.001). When comparing the doses which most significantly affected food intake (7.5 nmol for males; 2.5 nmol for females) opposing effects can be

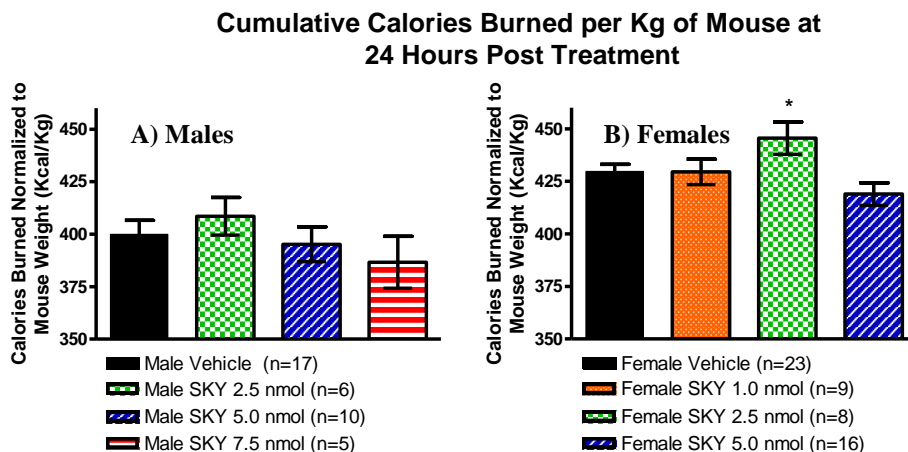


Fig. 4. Cumulative calories burned normalized to mouse body weight (Kcal/Kg) 24 hours after receiving SKY 2-23-7 in 3 μ L vehicle vs 3 μ L of vehicle (<1.0% DMSO in water) via ICV administration in both (A) male and (B) female wild type mice. Data shown as mean \pm SEM. * p <0.05.

seen (Figure 4). The 2.5 nmol dose of SKY2-23-7 in female mice significantly increased the calories burned in 24 hours after ICV administration (Figure 4B). In contrast, the ICV administration of the 7.5 nmol dose of SKY2-23-7 in male mice trended towards decreasing calories burned albeit not significantly (Figure 4A).

These initial findings suggest that ICV administration of SKY 2-23-7 affect male and female mice differently. Due to the observed sex specific responses in food intake and energy expenditure, it can be postulated this compound may have sex specific differences in the side effects of melanocortin ligands related to blood pressure and sexual function. Further probing into a melanocortin sex specific pharmacology could provide a potential avenue to overcome the previously established limitations of melanocortin ligands for their therapeutic use.

Acknowledgments

We would like to thank Katie Freeman and Stacey Wilber for mouse breeding and colony maintenance. This research was supported by National Institutes of Health grant R01DK091906.

References

- Mountjoy, K.G., et al. *Science* **257**, 1248-1251 (1992), <http://dx.doi.org/10.1126/science.1325670>
- Lerner, A.B., et al. *Nature* **189**, 176-179 (1961), <http://dx.doi.org/10.1038/189176a0>
- Van der Ploeg, L.H., et al. *Proc. Natl. Acad. Sci. USA* **99**, 11381-11386 (2002), <http://dx.doi.org/10.1073/pnas.172378699>
- Greenfield, J.R., et al. *N. Engl. J. Med.* **360**, 44-52 (2009), <http://dx.doi.org/10.1056/NEJMoa0803085>
- Gonzalez, P.V., et al. *Brain Behav. Immun.* **23**, 817-822 (2009), <http://dx.doi.org/10.1016/j.bbi.2009.03.001>
- Fan, W., et al. *Nature* **385**, 165-168 (1997), <http://dx.doi.org/10.1038/385165a0>
- Huszar, D., et al. *Cell* **88**, 131-141 (1997), [http://dx.doi.org/10.1016/S0092-8674\(00\)81865-6](http://dx.doi.org/10.1016/S0092-8674(00)81865-6)
- Chen, A.S., et al. *Nat. Genet.* **26**, 97-108 (2000), <http://dx.doi.org/10.1038/79254>
- Irani, B.G., et al. *Eur. J. Pharmacol.* **660**, 80-87 (2001), <http://dx.doi.org/10.1016/j.ejphar.2010.10.101>
- Marsh, D.J., et al. *Nat. Genet.* **21**, 119-122 (1999), <http://dx.doi.org/10.1038/5070>
- Doering, S.R., et al. *ACS Med. Chem. Lett.* **6**, 123-127 (2015), <http://dx.doi.org/10.1021/ml500340z>
- Schild, H.O. *Br. J. Pharmacol. Chemother.* **2**, 189-206 (1947), <http://dx.doi.org/10.1111/j.1476-5381.1947.tb00336.x>

Protein Kinase C Beta II (PKC β II) Peptide Inhibitor Exerts Cardioprotective Effects in Myocardial Ischemia/Reperfusion Injury

Christina Lipscombe, Israel Benjamin, Devon Stutzman, Amelie Bottex,
Chinyere Ebo, William Chau, Harsh Patel, Qian Chen, Cathy J. Hatcher,
Robert Barsotti, and Lindon H. Young

Division of Research, Department of Bio-Medical Sciences, Philadelphia College of Osteopathic Medicine
(PCOM), Philadelphia, PA, 19131, USA

Introduction

Coronary heart disease is the leading cause of death worldwide, and is primarily attributable to the detrimental effects of tissue infarct after an ischemic insult. The most effective therapeutic intervention for reducing infarct size associated with myocardial ischemia injury is timely and effective reperfusion of blood flow back to the ischemic heart tissue. However, the reperfusion of blood itself can induce additional cardiomyocyte death that can account for up to 50% of the final infarction size. Currently, there are no effective clinical pharmacologic treatments to limit myocardial ischemia/reperfusion (MI/R) injury in heart attack patients [1]. Reperfusion injury is initiated by decreased endothelial-derived nitric oxide (NO) which occurs within 5 min of reperfusion [2], and may in part be explained by PKC β II mediated activation of NADPH oxidase, which occurs upon cytokine release during MI/R [3]. PKC β II activity is increased in animal models of MI/R and known to exacerbate tissue injury [4,5]. PKC β II is known to increase NADPH oxidase activity in leukocytes, endothelial cells and cardiac myocytes *via* phox47 phosphorylation, and decrease endothelial NO synthase (eNOS) activity *via* phosphorylation of Thr 495 [6-8]. NADPH oxidase produces superoxide (SO) and quenches endothelial derived NO in cardiac endothelial cells. Moreover, PKC β II phosphorylation of p66Shc at Ser 36 leads to increased mitochondrial reactive active oxygen species (ROS) production, opening of the mitochondrial permeability transition pore (MPTP), and pro-apoptotic factors leading to cell death and increased infarct size [9] (Figure 1 left). Therefore, using a pharmacologic agent that inhibits the rapid release of PKC β II mediated ROS, would attenuate endothelial dysfunction and downstream pro-

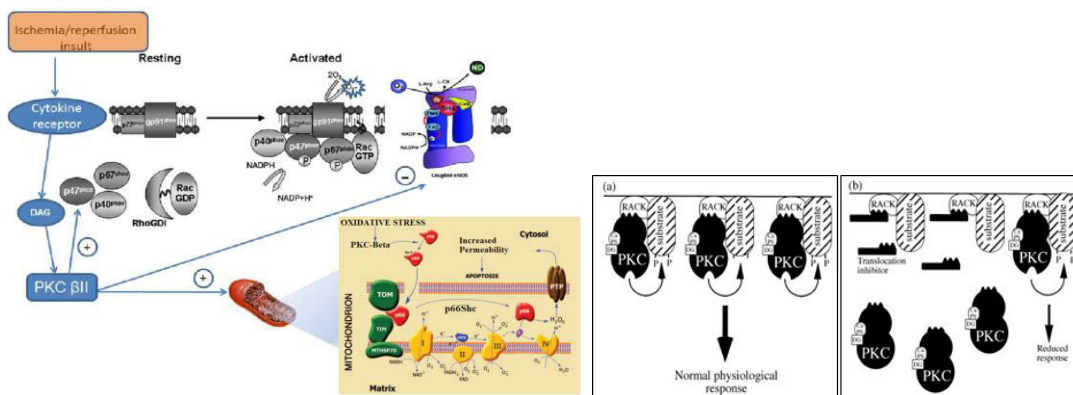


Fig. 1. Left: Schematic representation of PKC β II mediated activation in myocardial ischemia and reperfusion (MI/R). MI/R induces cytokine receptor activation within minutes leading to activation of PKC β II via diacylglycerol (DAG). PKC β II increases reactive oxygen species (ROS) release from damaged mitochondria and NADPH oxidase, respectively, and reduces coupled eNOS activity. (Adapted from [9]). Right: Mechanism of action of PKC β II peptide inhibitor. PKC β II peptide inhibitor attenuates the translocation of PKC β II to cellular substrates (e.g., NADPH oxidase) by competing for the receptor for activated C kinase (RACK), adapted from [10].

apoptotic pathways when given during reperfusion and should be an ideal candidate to attenuate MI/R injury. PKC β II peptide inhibitor mechanism of action (Figure 1 right) is to inhibit PKC β II translocation to cellular substrates such as eNOS, NADPH oxidase, and mitochondrial p66Shc protein that increase ROS leading to opening of the MPTP which in turn leads to consequent release of pro-apoptotic factors into the cytosol [9,10]. We've previously shown that PKC β II peptide inhibitor restored post-reperfused cardiac function and reduced polymorphonuclear leukocyte (PMN) infiltration in isolated rat hearts subjected to MI(20min)/R(45min) reperfused with PMNs [8]. In addition, the use of PKC β II peptide inhibitor (10-20 μ M) correlated with the inhibition of SO release from isolated leukocytes suggesting that this dose range maybe effective in attenuating ROS production [11].

We extended our research in the current study by using a MI (30min)/R (90min) isolated perfused rat heart model. A cell permeable PKC β II peptide inhibitor (10-20 μ M) was given at the beginning of reperfusion for five minutes. Post-reperfused cardiac function and infarct size were measured and compared to untreated control MI/R hearts.

Hypothesis

We hypothesize that PKC β II peptide inhibitor will improve post-reperfused cardiac function and reduce infarct size in isolated perfused rat hearts (*ex vivo*) subjected to global MI/R compared to non-drug control MI/R hearts in MI(30min)/R(90min) studies.



Fig. 2. PKC β II peptide inhibitor location resides in the Ca^{2+} binding domain (C2-4 region) of RACK (N-Myr-SLNPEWNET), adapted from [8].

Methods

Isolated Rat Heart Preparation

Male Sprague Dawley rats (275-325g, Charles River, Springfield, MA) were anesthetized with pentobarbital sodium (60mg/kg) and anti-coagulated with sodium heparin (1,000 U) injection intraperitoneally. Hearts were rapidly excised and perfused at a constant pressure of 80 mm Hg with a modified physiological Krebs' buffer aerated with 95% O_2 -5% CO_2 maintained at 37°C and pH 7.3-7.4 by Langendorff preparation. Hearts were subjected to 15 min of baseline perfusion, 30 min of ischemia, and a 90 min reperfusion period [8]. Five ml of plasma (control MI/R hearts), or plasma containing cell-permeable PKC β II peptide inhibitor (N-Myr-SLNPEWNET, MW=1300 g/mol, 10-20 μ M Genemed Synthesis Inc., San Antonio, TX) (Figure 2) were infused during the first 5min of reperfusion by a side arm line proximal to the heart inflow at a rate of 1ml/min. Coronary flow, left ventricular developed pressure (LVDP), maximal and minimal rate of LVDP ($+\text{dP}/\text{dt}_{\text{max}}$ and $-\text{dP}/\text{dt}_{\text{min}}$), and heart rate were taken every 5min during baseline and reperfusion using a flow meter (T106, Transonic Systems, Inc., Ithaca, NY) and pressure transducer (SPR-524, Millar Instruments, Inc., Houston, TX), respectively. Data were recorded using a Powerlab Station acquisition system (ADInstruments, Grand Junction, CO).

Sham hearts experienced no ischemia, received no drug and were infused with plasma at the same time point as I/R hearts. To evaluate tissue viability, the left ventricle was isolated at the end of the cardiac function experiment and cross sectioned into five 2mm thick slices from apex to base. The slices were subjected to 1% triphenyltetrazolium chloride (TTC) staining for 15min at 37°C (viable tissue stained red, infarct left unstained (white)). Infarct size was expressed as the percentage of dead tissue to the total tissue weight.

Statistical Analysis

All data in the text and figures are presented as means \pm S.E.M. Analysis of variance using post hoc analysis with the Student-Newman-Keuls test was used for heart function and infarct size in the MI(30min)/R(90min) study. Probability values of <0.05 are statistically significant.

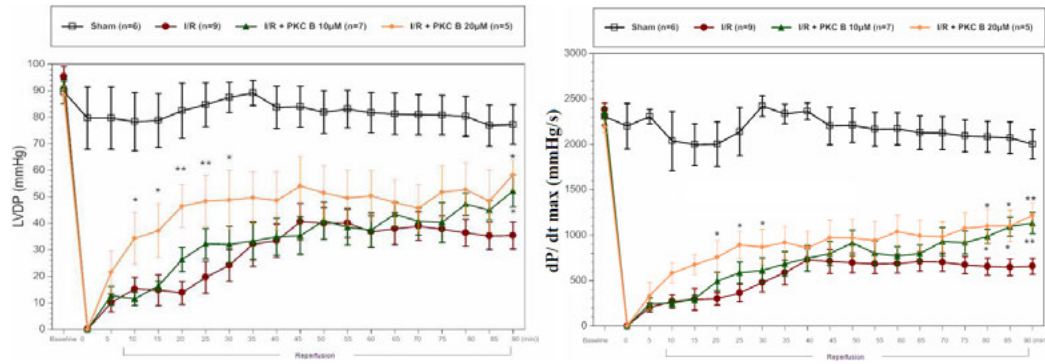


Fig. 3. Time course of LVDP (left) and dP/dt max (right) in sham, control MI/R and MI/R+PKC β II inhibitor (10 and 20 μ M) perfused rat hearts. LVDP and dP/dt max data at initial (baseline) and reperfusion from 0 to 90 min following 30 min ischemia are shown. (* p <0.05; ** p <0.01 compared to untreated control MI/R hearts).

Results and Discussion

This study focused on the inhibition of PKC β II in MI/R injury. Figure 3 shows that PKC β II inhibitor (10 and 20 μ M) significantly improved cardiac function compared to untreated control MI/R hearts. Sham hearts ($n=6$) maintained cardiac function throughout the experimental protocol (i.e., $87 \pm 9\%$ of initial LVDP and $89 \pm 8\%$ of initial dP/dt_{max}). MI/R+PKC β II inhibitor hearts (10 μ M, $n=7$; 20 μ M, $n=5$) exhibited a significant improvement in LVDP $66 \pm 8\%$ and dP/dt_{max} $56 \pm 8\%$ (20 μ M) and $57 \pm 7\%$ and $48 \pm 5\%$ (10 μ M) compared to control MI/R hearts ($n=9$) that only recovered to $38 \pm 6\%$ (LVDP) and $28 \pm 4\%$ (dP/dt_{max}) at 90 min post-reperfusion of initial baseline. MI/R+PKC β II inhibitor hearts (20 μ M) significantly improved post-reperused LVDP at 10-30 and 90 minutes and dP/dt_{max} at 20-30 and 80-90 minutes compared to untreated MI/R controls. MI/R+PKC β II inhibitor hearts (10 μ M) significantly improved post-reperused LVDP at 90 minutes and dP/dt_{max} at 80-90 minutes compared

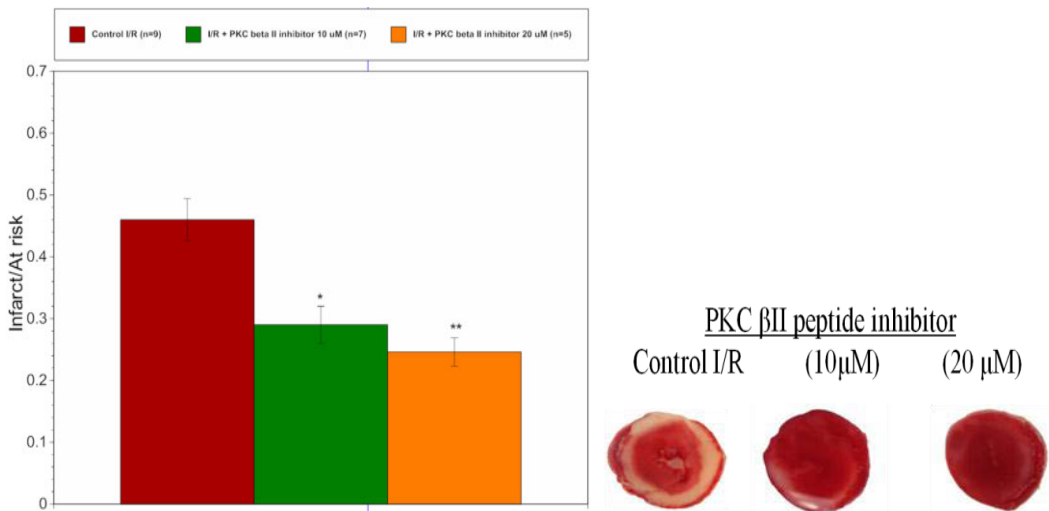


Fig. 4. Representative TTC stained heart sections displayed above from control MI/R and MI/R+PKC β II inhibitor hearts were assessed after cardiac function experiments to determine infarct size. Viable tissue stained red and infarcted tissue was unstained (white). (* p <0.05 and ** p <0.01 compared to I/R control).

to untreated MI/R controls. Also, PKC β II inhibitor hearts displayed a significantly reduced infarct size ($29 \pm 3\%$, $10 \mu\text{M}$; $25 \pm 3\%$, $20 \mu\text{M}$) and compared to untreated I/R hearts that had an infarct size of $46 \pm 3\%$ (Figure 4). Sham hearts had minimal cell death ($<0.05\%$) at the end of the experimental protocol (data not shown).

In conclusion, PKC β II peptide inhibitor was shown to improve post-reperfused cardiac function and decrease infarct size. Reperfusion injury following myocardial ischemia has been shown to be a pathologic condition resulting in contractile dysfunction and myocardial cell death in animal models and patients suffering from a myocardial infarction. PKC β II peptide inhibitor given at the beginning of reperfusion significantly improved contractile function and decreased infarct size compared to MI/R untreated controls at 90 min post-reperfusion following 30 min global ischemia. These data suggest that PKC β II inhibition during reperfusion attenuates MI/R injury by improving cardiac function and salvaging heart tissue. These effects may be related to inhibiting ROS release in MI/R. Therefore, PKC β II inhibitor will be an effective therapeutic tool to ameliorate cardiac contractile dysfunction and tissue damage in heart attack, coronary bypass, and organ transplant patients.

Acknowledgments

This study was supported by the Center for Chronic Disorders of Aging and the Department of Bio-Medical Sciences at PCOM. Special thanks to PCOM DO/Biomed students Stephanie Liu, Christine Adekayode, and Gregory Stoner for assistance in the preparation of this manuscript.

References

1. Hausenloy, D.J., Yellon, D.M. *J. Clin. Invest.* **123**, 92-100 (2013), <http://dx.doi.org/10.1172/JCI62874>
2. Lefer, A.M., Lefer, D.J. *Cardiovasc. Res.* **32**, 743-751 (1996), [http://dx.doi.org/10.1016/S0008-6363\(96\)00073-9](http://dx.doi.org/10.1016/S0008-6363(96)00073-9)
3. Frangogiannis, N.G., et al. *Circulation* **98**, 699-710 (1998), <http://dx.doi.org/10.1161/01.CIR.98.7.699>
4. Kong, L., et al. *Am. J. Physiol. Heart Circ. Physiol.* **294**, H1862-870 (2008), <http://dx.doi.org/10.1152/ajpheart.01346.2007>
5. Rui, T., Tang, Q. *PLoS One* e56089 (2013), <http://dx.doi.org/10.1371/journal.pone.0056089>
6. Korchak, H.M., Kilpatrick, L.E. *J. Biol. Chem.* **276**, 8910-8917 (2001), <http://dx.doi.org/10.1074/jbc.M008326200>
7. Chiasson, V.L., et al. *J. Pharmacol. Exp. Ther.* **337**, 718-723 (2011), <http://dx.doi.org/10.1124/jpet.110.178095>
8. Young, L.H., et al. *Cardiovasc. Drug Rev.* **23**, 255-272 (2005), <http://dx.doi.org/10.1111/j.1527-3466.2005.tb00170.x>
9. Cosentino, F., et al. *Arterioscler. Thromb. Vasc. Biol.* **28**, 622-628 (2008), <http://dx.doi.org/10.1161/ATVBAHA.107.156059>
10. Csukai, M., Mochly-Rosen, D. *Pharmacol. Res.* **39**, 253-259 (1999), <http://dx.doi.org/10.1006/phrs.1998.0418>
11. Ebo, C., et al. in Srivastava, V., Yudin, A. and Lebl, M. (Eds) *Proceedings of the 24th American Peptide Symposium*, American Peptide Society, San Diego, 2015, *in press*.

Reduced Cycle Times & Solvent Consumption for the Synthesis of ⁶⁵⁻⁷⁴ACP on the Symphony X®

Daniel Martinez, James P. Cain, Elizabeth Restituyo-Rosario,
Katya Karankevich, Peter Bergwall, and Nathaniel Cosper

Protein Technologies, Inc., Tucson, AZ, 85714, USA, Website: www.ptipep.com, Email: info@ptipep.com

Introduction

High demand for peptides as research tools and lead compounds has increased the need for fast production of peptides in high purity. The challenge has been answered by the Symphony X, capable of high-throughput peptide synthesis of even difficult peptides with effective cycle times of less than one minute. New and optimized methods for rapid peptide synthesis, combined with instruments capable of parallel synthesis enable the production of peptide libraries with high throughput. Herein, optimization of synthesis protocols for ⁶⁵⁻⁷⁴ACP is explored (Figure 1), using the Symphony X parallel synthesis platform, to reduce cycle times and decrease solvent consumption and waste generation by removing DMF washes after coupling steps.

Val-Gln-Ala-Ala-Ile-Asp-Tyr-Ile-Asn-Gly-NH₂

Fig. 1. Sequence of ⁶⁵⁻⁷⁴ACP peptide synthesized on the Symphony X® platform.

Results and Discussion

The synthesis of ⁶⁵⁻⁷⁴ACP was optimized by reducing the number of washes after coupling. Eliminating post-coupling washes reduced cycle times from 2.8 to 2.3 minutes and solvent consumption from 55 to 41 mL without significantly affecting the purity of the final peptides. Therefore, a 20% reduction in cycle times and a 25% reduction of solvent consumption were observed with very low impact on crude purity as shown in the HPLC analysis (Figure 2). Importantly, these findings suggested an overall improvement in time and cost of peptide synthesis when eliminating post-coupling washes.

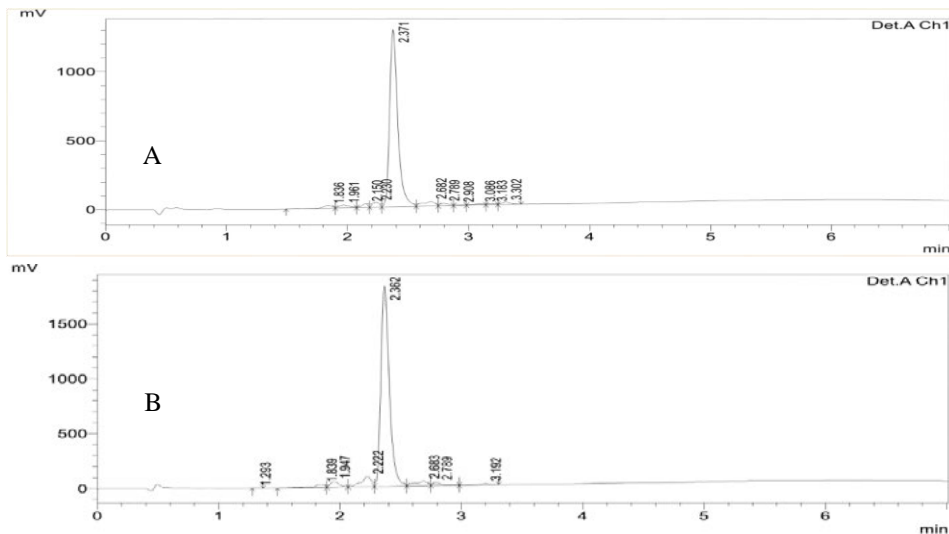


Fig. 2. HPLC traces of ⁶⁵⁻⁷⁴ACP peptide synthesized on the Symphony X® platform with A) no DMF washes after coupling steps and B) 3 DMF washes after coupling steps.

Tris-Benzamide Analogs for Inhibiting Bcl-2 Proteins in Prostate Cancer

Joongsoo Kim, Rakesh Kumar, and Jung-Mo Ahn*

Department of Chemistry and Biochemistry, University of Texas at Dallas, Richardson, TX, 75080, USA

Introduction

Apoptosis is an important cellular mechanism for tissue homeostasis and aberration in the process is well documented in cancers including castration-resistant prostate cancer (CRPC) [1]. Since it is regulated by heterodimerization of Bcl-2 family proteins, disrupting such protein complexes is attractive for therapeutic intervention. Structural studies revealed that the helical BH3 domain of pro-apoptosis proteins including Bak binds to a hydrophobic pocket in anti-apoptotic proteins like Bcl-xL [2,3]. To mimic helical BH3 domain, we have reported the synthesis and biological activity of tris-benzamides which can place three functional groups corresponding to the side chains found at the *i*, *i*+4, and *i*+7 positions in an α -helix [4,5]. To improve the activity of tris-benzamides, we have modified them by introducing additional side chain group at either end of molecules or changing one of side chain group. This library of tris-benzamide analogs as BH3 peptidomimetics was then examined for their binding affinity to anti-apoptotic Bcl-xL protein, inhibition of cell proliferation of various prostate cancer cell lines, mechanism of action, and *in vivo* efficacy. We have identified several leading compounds that showed strong binding affinity as well as high metabolic stability and cell permeation. These compounds were found to be effective in inhibiting cell growth of several prostate cancer cell lines and provided evidence of inducing apoptosis. These results show a potential of BH3 mimetics in treating prostate cancer.

Results and Discussion

We have designed and synthesized a number of tris-benzamides as peptidomimetics of BH3 domains of pro-apoptotic Bcl-2 proteins like Bak, Bad, Bim, Bik, Bid, Puma, and Noxa, and several compounds were found to be capable of inhibiting Bcl-xL from making a complex with Bak. To increase their potency, we have derivatized one of the leading compounds. We have introduced a variety of functional groups at each end of the molecule in order to improve its inhibitory potency. Among many functional groups surveyed, a carboxylate either at the *N*- or *C*-terminus was found to be the most effective.

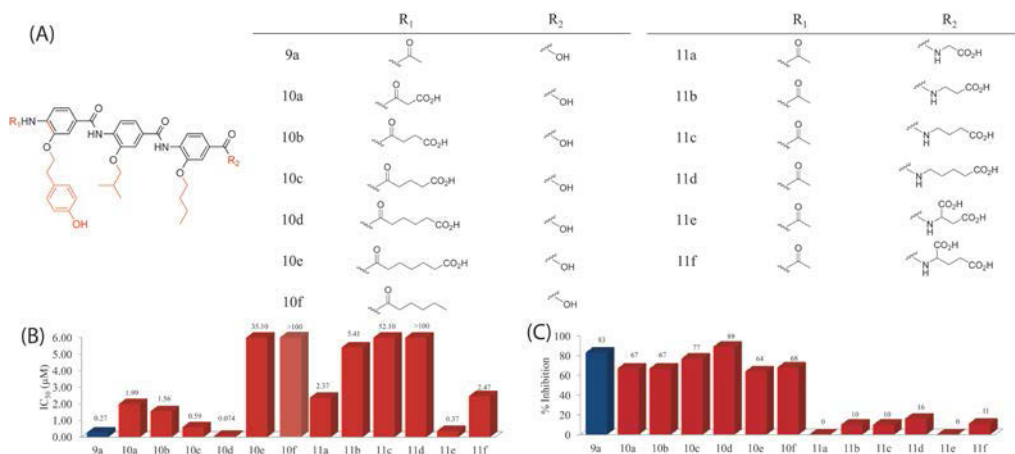


Fig. 1. (A) Structures of structural analogs of BH3 peptidomimetics and (B) their binding affinity to Bcl-xL and (C) cytotoxicity on a prostate cancer cell line DU145.

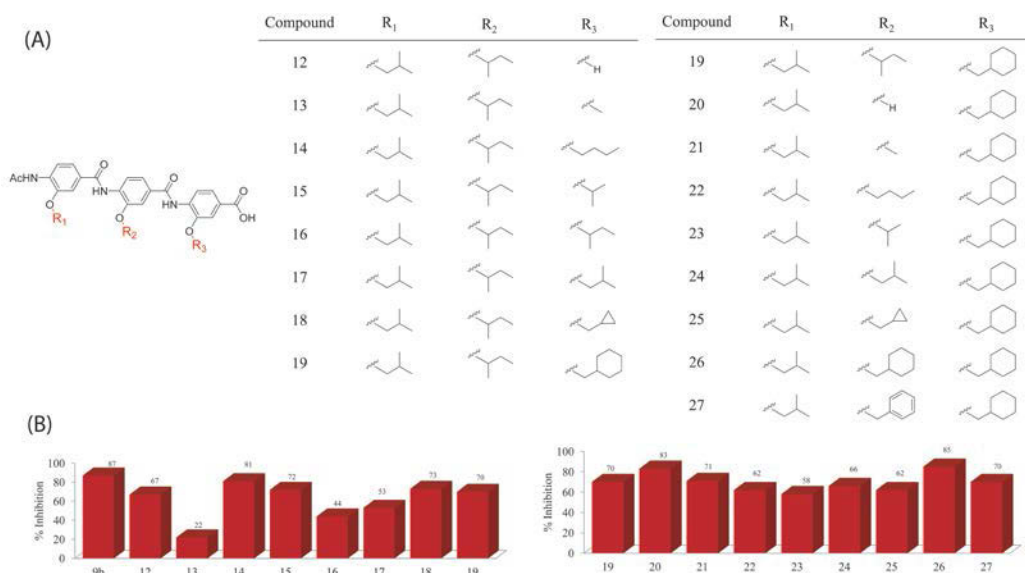


Fig. 2. (A) Selected structures of small chemical library of tris-benzamides and (B) their cytotoxicity on a prostate cancer cell line DU145.

In addition, we also constructed a small chemical library of tris-benzamides. Three substituents of the tris-benzamide scaffold were varied to create topologically diverse hydrophobic surfaces of an α -helix. A number of tris-benzamides were synthesized and tested on protein binding assays on Bcl-xL and cytotoxicity on a prostate cancer cell line DU145. Several potent compounds were identified for high cell proliferation inhibition as shown in Figure 2.

Acknowledgments

This work was supported in part by the Cancer Prevention and Research Institute of Texas (RP100718) and the Welch Foundation (AT-1595).

References

1. Thompson, C.B. *Science* **267**, 1456-1462 (1995), <http://dx.doi.org/doi:10.1126/science.7878464>
2. Liu, X., et al. *Immunity* **19**, 341-352 (2003), [http://dx.doi.org/doi:10.1016/S1074-7613\(03\)00234-6](http://dx.doi.org/doi:10.1016/S1074-7613(03)00234-6)
3. Petros, A.M., et al. *Protein Sci.* **9**, 2528-2534 (2000), <http://dx.doi.org/10.1110/ps.9.12.2528>
4. Ahn, J.-M., Han, S.-Y. *Tetrahedron Lett.* **48**, 3543-3547 (2007), <http://dx.doi.org/10.1016/j.tetlet.2007.03.108>
5. Marimnganti, S., et al. *Org. Lett.* **11**, 4418-4421 (2009), <http://dx.doi.org/10.1021/ol901785v>

Peptide Coupling Challenges on Route to Aza-Pipecolyl Smac Mimetic

Ramesh Chingle and William D. Lubell*

Département de Chimie, Université de Montréal, C.P. 6128, Succursale Centre-Ville,
Montréal, QC, H3C 3J7, Canada

Introduction

Azopeptides are reactive peptide analogs bearing a diazo dicarbonyl moiety as a dehydro *N*-(acyl)amino acid surrogate [1]. Azopeptides have been employed in the synthesis of peptide analogs bearing semicarbazides as amino amide surrogates, so called azapeptides [2]. For example, the Diels-Alder reaction of a diazine residue with cyclopentadiene provided aza-methano-pipecolyl peptide **5** (Scheme 1) [1]. In the context of research towards anticancer drugs, we perceive the aza-methano-pipecolyl structure as a constrained valine analog for insertion into a mimic of the *N*-terminal AVPI binding motif of the second mitochondria-derived activator of caspases (Smac). Coupling to the aza-methano-pipecolyl residue proved however challenging during efforts to prepare Smac mimetic **4**.

Results and Discussion

The AVPI peptide amide **1** has served as a lead for the development of Smac mimetics that bind the inhibitor of apoptosis protein-3 and induce apoptosis (Figure 1) [3-6]. Considering the turn conformation adopted by this peptide on receptor binding, constrained analogs such as indolizidinone amino acids have been used to rigidify the Val-Pro dipeptide to enhance potency (e.g., **2**) [7-9]. Although such bicyclic amino acid analogs represent an important class of Smac mimetics, their multiple step synthesis has restricted analog development. Employing aza-amino acyl proline analogs as indolizidinone amino acid surrogates, azapeptide smac mimetics (e.g., **3**) have been developed that induce cell death by a caspase-9 mediated apoptotic pathway [6]. In the interest to further restrict the conformation of the aza-amino acid residue, aza-methano-pipecolate was pursued as a rigid valine analog in smac mimetic **4**.

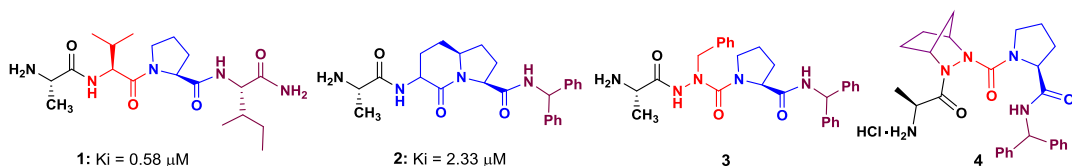
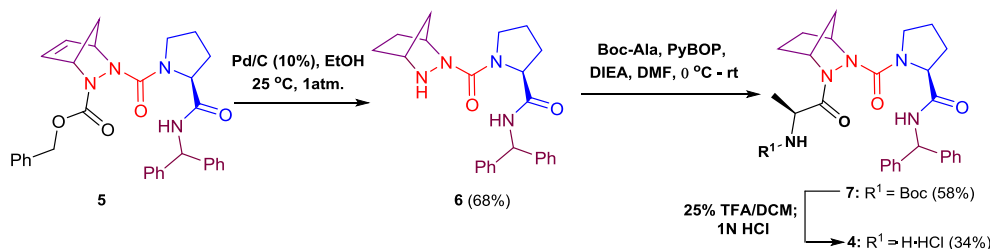


Fig. 1. AVPI-NH₂ and peptide mimetic activators of caspase-9.

Hydrogenation aza-Diels-Alder adduct **5** removed the Cbz group and reduced the olefin to provide bicyclic semicarbazide **6** (Scheme 1). The acylation of semicarbazide **6** with Boc-Ala proved particularly challenging presumably because of the combination of steric hindrance and electronic deactivation. A variety of coupling condition was examined to achieve acylation, albeit with minimal success. For example, various coupling conditions failed to afford the Boc protected aza-tripeptide amide **7**: TBTU/HOBT [10], EDCI/HOBT [11], and DIC/AtOH [12]. Moreover, attempts were unsuccessful using the mixed anhydride generated from Boc-Ala, *iso*-butyl chloroformate and *N*-methylmorpholine [13,14]. On the other hand, PyBOP and di-*iso*-propyl ethyl amine (DIEA) proved effective in the reaction of semicarbazide **6** with Boc-Ala, and gave tripeptide amide **7** in 58% yield [15]. Removal of the Boc group with 25% TFA in dichloromethane, salt exchange using 1N HCl for 30 min and freeze-drying afforded hydrochloride salt **4** (HRMS m/z calculated for $\text{C}_{27}\text{H}_{34}\text{N}_5\text{O}_3$ $[\text{M}+\text{H}]^+$ 476.2656; found 476.2663).

Scheme 1. Synthesis of aza-methano-pipecolyl Smac mimetic 4.



In conclusion, we have disclosed the incorporation of a novel constrained valine into an azapeptide Smac mimetic analog. Application of PyBOP surmounted difficulties in coupling to the bulky and electron deficient aza-methano-pipecolyl residue. Smac mimetic analog 4 will be examined for bioactivity to probe further structure-activity relationships at the AVPI binding site towards the development of improved therapy for treating cancer.

Acknowledgments

This research was supported by the Natural Sciences and Engineering Research Council of Canada (NSERC).

References

- Chingle, R., Lubell, W.D. *Submitted*.
- Proulx, C., Sabatino, D., Hopewell, R., Spiegel, J., García Ramos, Y., Lubell, W.D. *Future Med. Chem.* **3**, 1139-1164 (2011), <http://dx.doi.org/10.1021/jm300557t>
- Kerr, J.F., Wyllie, A.H., Currie, A.R. *Br. J. Cancer* **26**, 239-257 (1972), <http://dx.doi.org/10.1038/bjc.1972.33>
- Fadeel, B., Orrenius, S. *J. Intern. Med.* **258**, 479-517 (2005), <http://dx.doi.org/10.1111/j.1365-2796.2005.01570.x>
- Deveraux, Q.L., Reed, J.C. *Genes Dev.* **13**, 239-252 (1999), <http://dx.doi.org/10.1101/gad.13.3.239>
- Bourguet, C.B., Boulay, P.-L., Claing, A., Lubell, W.D. *Bioorg. Med. Chem. Lett.* **24**, 3361-3365 (2014), <http://dx.doi.org/10.1016/j.bmcl.2014.05.095>
- Sun, H., Nikolovska-Coleska, Z., Yang, C.-Y., Xu, L., Tomita, Y., Krajewski, K., Roller, P.P., Wang, S. *J. Med. Chem.* **47**, 4147-4150 (2004), <http://dx.doi.org/10.1021/jm0499108>
- Sun, H., Nikolovska-Coleska, Z., Yang, C.-Y., Xu, L., Liu, M., Tomita, Y., Pan, H., Yoshioka, Y., Krajewski, K., Roller, P.P. *J. Am. Chem. Soc.* **126**, 16686-16687 (2004), <http://dx.doi.org/10.1021/ja047438>
- Khashper, A., Lubell, W.D. *Org. Biomol. Chem.* **12**, 5052-5070 (2014), <http://dx.doi.org/10.1039/C4OB00777H>
- Bourguet, C.B., Sabatino, D., Lubell, W.D. *Peptide Science* **90**, 824-831 (2008), <http://dx.doi.org/10.1002/bip.21103>
- Chakraborty, T.K., Ghosh, A., Sankar, A.R., Kunwar, A.C. *Tetrahedron Lett.* **43**, 5551-5554 (2002), [http://dx.doi.org/10.1016/S0040-4039\(02\)01141-3](http://dx.doi.org/10.1016/S0040-4039(02)01141-3)
- Hemmerlin, C., Cung, M.T., Boussard, G. *Tetrahedron Lett.* **42**, 5009-5012 (2001), [http://dx.doi.org/10.1016/S0040-4039\(01\)00917-0](http://dx.doi.org/10.1016/S0040-4039(01)00917-0)
- Anderson, G.W., Zimmerman, J.E., Callahan, F.M. *J. Am. Chem. Soc.* **89**, 5012-5017 (1967), <http://dx.doi.org/10.1021/ja00995a032>
- Zaitsev, A.B., Adolfsson, H. *Org. Lett.* **8**, 5129-5132 (2006), <http://dx.doi.org/10.1021/ol062227q>
- Coste, J., Le-Nguyen, D., Castro, B. *Tetrahedron Lett.* **31**, 205-208 (1990), [http://dx.doi.org/10.1016/S0040-4039\(00\)94371-5](http://dx.doi.org/10.1016/S0040-4039(00)94371-5)

Structure-Based Design, Synthesis and Evaluation of Novel Peptidic Inhibitors of Thrombin-Induced Activation of Platelets Aggregation

Janet Gonzalez¹, Anna Babinska², Ebenezer L.V. Ewul³, Edem Timpo²,
Alhassan Jallow¹, Zhiyong Qiu¹, Radoslaw Bednarek⁴, Maria Swiatkowska⁴,
Moro O. Salifu², Manfred Philipp³, and Cristina C. Clement³

¹Department of Natural Sciences, LaGuardia Community College, New York, NY, 11104, USA; ²Division of Nephrology, Department of Medicine, State University of New York, Downstate Medical Center, Brooklyn, NY, 11203, USA; ³Department of Chemistry, Lehman College of the City University of New York, Bronx, NY, 10468, USA; ⁴Medical University of Lodz Department of Cytobiology and Proteomics, Lodz, Poland

Introduction

Thrombosis-related disorders such as myocardial infarction, stroke and pulmonary embolism remain a major cause of mortality and morbidity worldwide [1]. This has driven the interest on thrombin inhibitors as potential antithrombotic drugs [2]. However, to date, discovery of safe, selective and orally available inhibitors has proven difficult to accomplish, therefore limiting their therapeutic use [3,4]. Newer direct thrombin inhibitors (DTIs) are attempting to fine tune thrombin's activity by targeting allosteric sites or by site-specific targeting of clotting. Advancements in formulations and production processes have attempted to make traditional DTIs more cost effective to produce. Today, the research focused on optimizing anti-thrombosis drugs reveals a trend to develop a thrombin

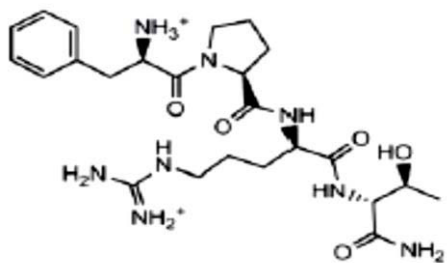


Fig. 1. Structure of the lead DTI [D-Phe-Pro-D-Arg-D-Thr-CONH₂](fPrt) characterized in complex with human alpha thrombin (3U8O.pdb [1]).

'modulator' rather than an 'inhibitor' [2-4]. Recently, our research group described the biochemical and structural characterization of three peptidic non-covalent direct thrombin inhibitors (DTI) that contain the common sequence D-Phe(P₃)-Pro-(P₂)-D-Arg(P₁)-P₁'-CONH₂ ([1] and Figure 1). The three-dimensional structures of three complexes of human alpha-thrombin with the lead peptidic competitive inhibitors (with L-isoleucine, L-cysteine or D-threonine at the P₁' position) highlighted all inhibitors adopting a substrate-like orientation in the active site of thrombin [1]. Moreover, other collaborators in the field developed biomaterials with enhanced haemocompatibility containing our lead peptidic DTI [D-Phe-Pro-D-Arg-D-Thr-CONH₂] (fPrt) [6]. The research proved that the immobilization of the thrombin inhibitor (fPrt) onto

nanostructured surfaces induces selective and reversible adsorption of albumin, delaying the clotting time when compared to peptide-free surfaces [5]. To further improve the potency and selectivity of the peptidic DTI and assess their future potential as scaffolds for developing biomaterials with improved haemocompatibility for the blood-contacting medical devices, we performed a structure-based drug design (SBDD) and structure-activity relationship (SAR) evaluation of novel peptidic DTI by optimizing the P₃ position within the original scaffold "D-Phe(P₃)-Pro-(P₂)-D-Arg(P₁)-P₁'-CONH₂" with other un-natural D-Phe analogs (such as D-3,3-Diphenylalanine) (Figure 2).

Results and Discussion

Thrombin is known to induce the activation of platelets to aggregate by binding to and cleaving the extracellular N-terminal domains of protease-activated receptors 1 and 4 (PAR1 and PAR4) [3]. To date many DTI proved to also be potent inhibitors of the thrombin mediated activation of platelet aggregation. Such DTI can be used as pharmacological agents for the management of acute coronary syndrome (ACS) [3].

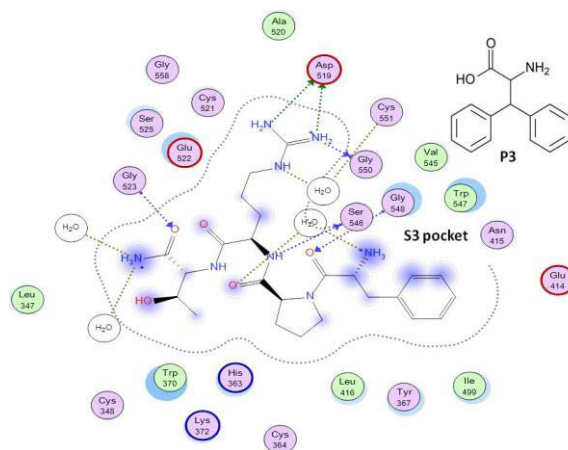


Fig. 2. Illustration of the lead compound [D-Phe(P3)-Pro(P2)-D-Arg(P1)-D-Thr(P1')-CONH₂] DTI (fPrt) in complex with human alpha thrombin (3U8O.pdb) (1). The main interactions with the amino acids within 5Å of the thrombin's active site are displayed. The S3 pocket is occupied by D-Phe which is replaced by D-3,3-Diphenylalanine (DIP) in P3 position.

This research presents the structure-based drug design (SBDD), synthesis and evaluation of novel tetrapeptides DTI inhibitors of thrombin-activated platelet aggregation. Analogs of the lead DTI, [D-Phe(P₃)-Pro(P₂)-D-Arg(P₁)-D-Thr(P₁')-CONH₂], have been designed to improve the hydrophobic driven interactions with the S3 pocket of thrombin by replacing the D-Phe (in P₃) with D-3,3-Diphenylalanine (DIP) among other unnatural amino acids (such as D-3,5-difluorophenylalanine, (L)/(D)-Tic [1,2,3,4-tetrahydro-isoquinoline-3-carboxylic acid], (L)/(D)-Thi [Thienylalanine], D-Naphthylalanine (D-Nal(1) and D-Nal(2)) and 1,2,3,4-tetrahydronorharman-3-carboxylic acid (D-Tpi). The new peptidic DTIs were designed and developed by means of "in silico" SBDD approach where the X-ray structure of the DTI lead compound [D-Phe-Pro-D-Arg-D-Thr-CONH₂] (fPrt) in complex with human alpha-thrombin (3U8O.pdb) was used as a template for rigid docking experiments performed with AutoDock Vina [6]. The docking experiments provided the free energy of interaction between each ligand and thrombin template (Table 1).

The new lead DTIs were synthesized using standard solid-phase fluorenylmethyloxycarbonyl (Fmoc) chemistry in collaboration with Karebay Biochem, Inc. as described earlier (1). Two types of binding experiments were performed to assess the inhibitory constant (K_i): (1) kinetics of alpha-thrombin inhibition of chromogenic substrate S2238; and (2) surface plasmon resonance (SPR) with immobilized alpha-thrombin. All D-3,3-Diphenylalanine-DTI analogs competitively inhibited alpha-thrombin's cleavage of the S2238 chromogenic substrate with K_i of 500-24 nM (Table 1). Moreover, the kinetic constants and the binding affinities for the interaction between the two lead synthetic peptides and immobilized thrombin monitored by surface plasmon resonance (SPR) revealed that the K_d (dissociation constant) was in the order of 290 to 40-50 nanomolar (Table 2). Remarkably the new DTIs proved to inhibit the alpha thrombin activation of platelets aggregation.

Table 1. Summary of some of the lead peptidic DTIs and the corresponding experimental and predicted K_i (nM).

Peptide sequence (ID)	Experimental K _i (nM)	Predicted (AutoDock Vina) K _i (nM)
D-3,3-Diphenylalanine-Pro-D-Arg-D-Cys-CONH ₂	65.5 ± 0.3	40.2
D-3,3-Diphenylalanine-Pro-D-Arg-D-Ala-CONH ₂	130.6 ± 0.5	85
D-3,3-Diphenylalanine-Pro-D-Arg-D-Thr-CONH ₂	104.4 ± 1.5	50.2
D-3,3-Diphenylalanine-Pro-D-Arg-D-Val-CONH ₂	102.2 ± 5.5	45
D-3,3-Diphenylalanine-Pro-D-Arg-D-Ile-CONH ₂	64.2 ± 2.5	35
D-3,3-Diphenylalanine-Pro-D-Arg-D-Leu-CONH ₂	540.2 ± 2.4	350
D-3,3-Diphenylalanine-Pro-D-Arg-D-Thi-CONH ₂	312.5 ± 0.8	120

Table 2. Summary of kinetic constants and binding affinities for the interaction between two synthetic DTI peptides and immobilized thrombin monitored by surface plasmon resonance (SPR). K_D was calculated as the ratio (k_d/k_a) of dissociation and association rate constants as $K_A = K_D^{-1}$. Sensorgrams were analyzed with BIA evaluation 4.1.1 software and the constants were determined by global fitting of the data using the Langmuir binding model ($k_d/k_a = K_A = K_D^{-1}$).

Peptide DTI	$k_a (M^{-1} \times s^{-1})$	$k_d (s^{-1})$	$K_A (M^{-1})$	$K_D (M)=K_i$
D-3,3-Diphenylalanine-Pro-D-Arg-D-Cys-CONH ₂	7.16×10^4	3.00×10^{-5}	2.39×10^9	4.19×10^{-10}
D-3,3-Diphenylalanine-Pro-D-Arg-D-Ala-CONH ₂	1.82×10^5	5.36×10^{-2}	3.39×10^6	2.95×10^{-7}

Washed human platelets ($4 \times 10^8/\text{ml}$ from healthy donors) were incubated with Tyrode's buffer (vehicle), or each DTI peptide (50-0.1 μM final concentration) for 1 minute stirring at 37°C followed by the stimulation with alpha-thrombin in presence of fibrinogen. The new DTI lead compounds (Tables 1 and 2) completely inhibited threshold alpha-thrombin-induced platelet aggregation at concentrations of 8000-25 nM (Figure 3). SAR analysis proved that selected amino acids substitutions in P1' position determine the potency of peptidic DTIs.

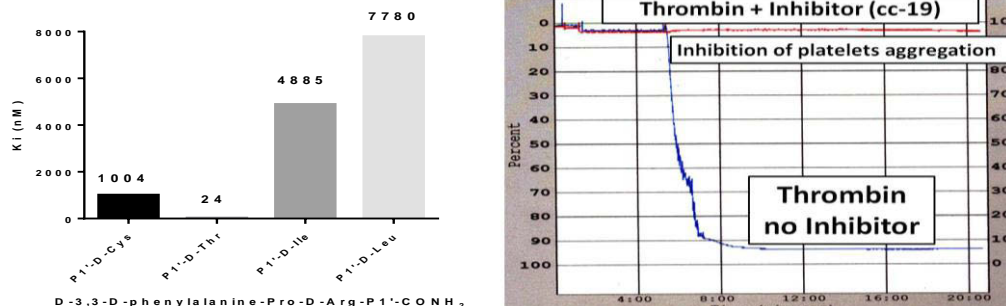


Fig. 3. The K_i for the inhibition of the thrombin activated platelets aggregation for some of the lead compounds containing DIP in P3 position showed that selected amino acids substitutions in P1' affect the potency of the peptidic DTIs (left). Representative platelets aggregation assay view in the absence and presence of one selected DTI (cc19: [D-3,3-Diphenylalanine-Pro-D-Arg-D-Thr-CONH₂]) (right).

This research demonstrated the proof of principle for using potent peptidic DTI (K_i in the hundreds to two digits nM range) to inhibit thrombin activated platelet aggregation. Specific amino acid substitutions required for activity against platelet aggregation have been identified for P1' positions, and lead compounds having D-3,3-Diphenylalanine in P3 position have been developed. These lead compounds completely inhibited threshold alpha-thrombin-induced platelet aggregation at concentration 10-24nM. These novel DTI tetrapeptides could be used as future pharmacophore scaffolds for the development of inhibitors of thrombin-mediated platelet aggregation for treatment of acute coronary syndrome (ACS).

Acknowledgments

CCC gratefully acknowledges the Chemistry department from Lehman College of CUNY for the continuous financial support through the appointment at the level of Adjunct Assistant Professor (2006-2015).

References

1. Figueiredo, A.C., et al. *PLoS One* **7**, e34354 (2012), <http://dx.doi.org/10.1371/journal.pone.0034354>
2. Mehta, A.Y., et al. *Expert Opin. Ther. Pat.* **24**, 47-67 (2014), <http://dx.doi.org/10.1517/13543776.2014.845169>
3. Girmys, E.A., et al. *Bioorg. Med. Chem.* **19**, 7425-7434 (2011), <http://dx.doi.org/10.1016/j.bmc.2011.10.045>
4. Clement, C.C., Babinska, A., Kornecki, E., Philipp, M. *Adv. Exp. Med. Biol.* **611**, 579-580 (2009).
5. Freitas, S.C., et al. *Acta Biomater.* **10**, 1227-1237 (2014), <http://dx.doi.org/10.1016/j.actbio.2013.11.023>
6. Trott, O., Olson, A.J. *J. Comput. Chem.* **31**, 455-461 (2010), <http://dx.doi.org/10.1002/jcc.21334>

Peptide Ring Closing Metathesis: Minimizing Side Reactions in Arodyn Analogs

Solomon A. Gisemba^{1,2} and Jane V. Aldrich^{1,2}

¹Department of Medicinal Chemistry, The University of Kansas, Lawrence, KS, 66045, USA;

²Department of Medicinal Chemistry, University of Florida, Gainesville, FL, 32610, USA

Introduction

Kappa (κ) opioid receptor (KOR) ligands, particularly antagonists, have received increasing attention due to their therapeutic potential in stress related conditions [1]. The acetylated dynorphin A (Dyn A) analog arodyn (Ac[Phe^{1,2,3},Arg⁴,D-Ala⁸]Dyn A(1-11)-NH₂, Figure 1), shows potent KOR antagonism *in vitro*. Arodyn has high affinity (K_i = 10 nM) and selectivity (K_i ratio ($\kappa/\mu/\delta$) = 1/174/583) for KOR [2]. Clinical development of KOR antagonists has been hampered partly because prototypical small molecule KOR antagonists such as JDTic exhibit long-lasting antagonism, lasting for weeks after a single dose [1]. Conversely, linear peptide KOR antagonists such as arodyn are rapidly metabolized and inactivated. Conformational constraint of the flexible linear peptide by ring closing metathesis (RCM) cyclization was expected to enhance its metabolic stability and potentially stabilize the bioactive conformation. Aromatic residues in arodyn contribute to affinity at KOR [4]; we are exploring RCM cyclization employing Tyr(All) residues which retain the aromatic nature of the N-terminal region.

In contrast to high yields observed in RCM using allylglycine in Dyn A analogs [5], a mixture of side products (Figure 2) compromised the RCM product yield of arodyn analogs containing Tyr(All) [4]. Olefin isomerization due to degradation products of the Grubbs catalyst could lead to the observed side products [6].

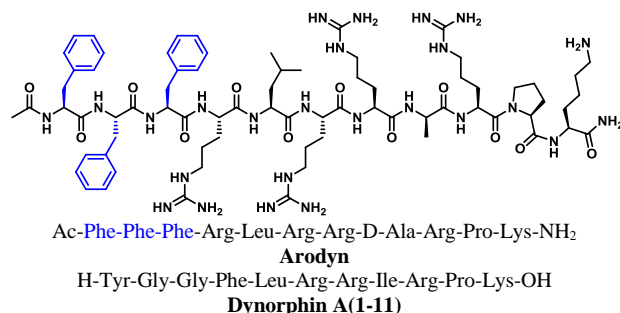


Fig. 1. Structure of arodyn and dynorphin A (1-11), a fragment of the endogenous KOR ligand.

A model dipeptide, Fmoc-Tyr(All)-Tyr(All), was employed to explore reaction conditions to enhance yields of the cyclic RCM product, conditions which were subsequently applied to arodyn analogs. Here, we present the results of different strategies to minimize the side reaction, including examination of reagents reported to suppress isomerization [6,7] as well as microwave heating.

Results and Discussion

The model peptide was synthesized by standard Fmoc SPPS and cyclized on resin using second generation Grubbs catalyst (G II). The reaction conditions used for arodyn analogs containing allylglycine (40mol% and 3mM of catalyst at 60°C for 2 days) [5] gave only 20% of the desired RCM

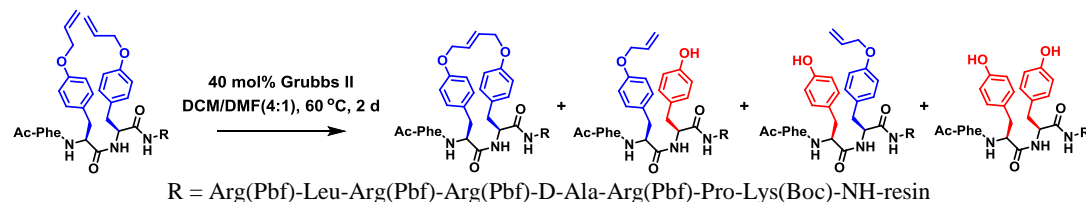


Fig. 2. Products resulting from RCM of [Tyr(All)^{2,3}]arodyn.

product for the model dipeptide plus a number of desallyl side products (Figure 2), as determined by HPLC. Different reaction parameters and strategies to enhance the yield of the RCM product were then examined on the model dipeptide. Generally, higher yields of the RCM product were observed at a lower temperature (40°C) in the presence of phenol and at a low catalyst concentration (0.3mM) in dichloromethane. A four-fold increase in yield was observed under the optimized conditions with the model dipeptide. A similar increase in yield was observed when second generation Hoveyda-Grubbs catalyst (HG II) was used under the optimized reaction conditions. Unlike G II, HG II was active at a higher temperature (60°C), presumably due to its higher stability compared to G II [8].

The optimized conditions when applied to [Tyr(All)^{2,3}]arodyn gave much higher yields (56-71%) of the cyclic product compared to the initial conditions (30%). The highest yields were observed using G II (71%), and thus G II was used in the synthesis of subsequent analogs containing Tyr(All) or *m*-Tyr(All). In initial reactions, reasonable yields (52-64%) of the cyclic products were obtained for [Tyr(All)²,*m*-Tyr(All)³]-, [*m*-Tyr(All)^{2,3}]-, and [Tyr(All)^{1,2}]arodyn. However, lower yields were observed for [*m*-Tyr(All)²,Tyr(All)³]- and [Tyr(All)¹,*m*-Tyr(All)²]arodyn (22-35%) where *m*-Tyr(All) is the second residue of arodyn. Generally, the olefins were in the *trans* configuration. A negligible amount (<10%) of the cyclic product was observed for [Tyr(All)^{1,3}]arodyn.

Microwave heating was also examined as a strategy to increase the yield of the RCM products. In preliminary studies, negligible yields of the RCM product were observed when G II was used, whereas HG II gave high yields under both closed and open-vessel microwave heating at 60°C in dichloroethane. HG II was therefore used in subsequent microwave assisted RCM. Moderate to high yields (44-72%) were observed under microwave heating with reduced reaction times (3-5h at 60°C) compared to conventional heating (2d at 40°C). Notably, a two-fold increase in yield was observed for [Tyr(All)¹,*m*-Tyr(All)²]arodyn (44%) under microwave heating. However, a negligible yield of [Tyr(All)^{1,3}]arodyn (<10%) was still observed. Pharmacological evaluation of the synthesized RCM products is in progress.

In summary, using the optimized RCM conditions developed for the model dipeptide generally resulted in higher yields of arodyn analogs containing Tyr(All)/*m*-Tyr(All). While sequence dependent effects were observed under both microwave and conventional heating, microwave heating offered the advantage of shorter reaction times for generally comparable yields compared to conventional heating.

Acknowledgments

We thank Dmitry Yakovlev for assistance in HPLC analysis and Justin Douglas of the University of Kansas NMR laboratory for assistance with configurational assignments based on NMR data. Research supported by grant R01 DA018832 (National Institute on Drug Abuse).

References

1. Aldrich, J.V., et al. *AAPS J.* **11**, 312-322 (2009), <http://dx.doi.org/10.1208/s12248-009-9105-4>
2. Bennett, M.A., et al. *J. Med. Chem.* **45**, 5617-5619 (2002), <http://dx.doi.org/10.1021/jm025575g>
3. Bennett, M.A., et al. *J. Pept. Res.* **65**, 322-332 (2005), <http://dx.doi.org/10.1111/j.1399-3011.2005.00216.x>
4. Fang, W.J. et al., in Valle, D.S. et al. (Ed.) *Peptides: Peptides for Youth (Proceedings of the 20th American Peptide Symposium)*, American Peptide Society, Montreal, 2009, p. 279, <http://dx.doi.org/10.1007/978-0-387-73657-0>
5. Fang, W.J., et al. *J. Med. Chem.* **52**, 5619-5625 (2009), <http://dx.doi.org/10.1021/jm900577k>
6. Hong, S.H., et al. *J. Am. Chem. Soc.* **127**, 17160-1716 (2005), <http://dx.doi.org/10.1021/ja052939w>
7. Schmidt, B., Hauke, S. *Org. Biomol. Chem.* **11**, 4194-4206 (2013), <http://dx.doi.org/10.1039/c3ob40167g>
8. Vougioukalakis, G.C., Grubbs, R.H. *Chem. Rev.* **110**, 1746-1787 (2010), <http://dx.doi.org/10.1021/cr9002424>

Design and Construction of a Selection Peptide Library Based on the Human Thymic Hormone Thymopoietin Domain

Chunjie Gong, Jianhao Xu, Ling Li, Qianhui Li, Huiling Guo, Li Zheng, Honghao Sun*, and Zhengding Su*

The Key Laboratory of Fermentation of the Ministry of Education and Collaborative Innovation Center of Industrial Fermentation, Hubei University of Technology, Wuhan, 430068, China

Introduction

The activity sites of thymic hormone thymopoietin (TPN) [1] have different biological functions depending on different amino acid sequences, providing a new scaffold for designing peptide inhibitors. In this study, we constructed TPN-based peptide library displayed on the surface of *Escherichia coli* strain using FimH fusion protein [2]. In principle, the activity site residues of TPN were substituted with randomized peptide sequences and each bacterial cell displayed multiple copies of the same peptide. We checked the bacterial expression on surface of *E. coli* and the feasibility of the peptide library using a histidine₈-tag and SDS-PAGE analysis. The histidine₈ fusion scaffold protein visualized by scanning transmission electron microscopy (STEM) with Ni-NTA-modified magnetic nanoparticles demonstrates that a large fraction of our library expresses to be membrane protein. Furthermore, we proved that the library expressed on the surface of *E. coli* with SDS-PAGE analysis of expression cultures show a large ratio of protein to be insoluble. As expected, the TPN-peptide library was also confirmed to contain 3×10^4 peptides of random 7-amino acid sequences. The results indicate that many kinds of peptide sequences containing in the TPN scaffold is an efficient technique for screening of peptide drugs.

Results and Discussion

In this work, we constructed a peptide display library described in Figure 1, and tried to select peptide drugs using the library. We designed the peptide library using the attachment protein FimH of *E. coli* and human TPN activity site. As for the gene of FimH, it was amplified by polymerase chain reaction (PCR). The gene of TPN was synthesized and integrated with the sequence of FimH by PCR, and cloned into vector pET20b(+). After transformation, the FimH protein was fused with the scaffold protein TPN, and expressed on the surface of *E. coli*.

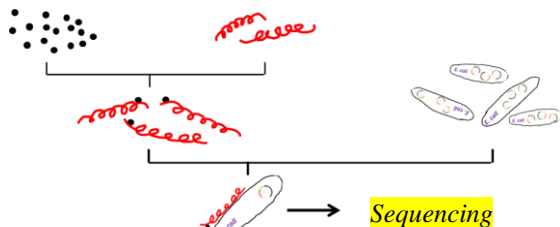


Fig. 1. Schematic showing the design principle of selection peptide library. The peptides were displayed on the surface of *E. coli*. Then the expressed peptides were selected with target proteins which bind to Ni-NTA-modified magnetic nanoparticles.

fraction of His tagged protein was expressed as membrane protein or inclusion body. To prove the expression of membrane protein, we examined the bacterial expression characteristics of this library using Ni-NTA modified magnetic nanoparticles (5 nm). The expression of the FimH-TPN-His₈ on the surface of *E. coli* was confirmed by scanning transmission electron microscopy. The binding between *E. coli* carrying plasmid FimH-TPN-His₈ and nanoparticles was observed. The fusion protein with Histidine₈ expressed on the surface suggested the feasibility of the peptide library.

Furthermore, the library containing a great deal of small peptides at various sequences expressed via the scaffold protein was designed. We constructed the model peptide expression library based on the TPN sequence, in which restriction digestion site *Bam*HI was inserted to facilitate other construction. The construction was confirmed by PCR and sequencing. To confirm the feasibility of the library, a nucleotide encoding Histidine₈-tag was integrated into the activity site of TPN to construct an expression plasmid, FimH-TPN-His₈. SDS-PAGE analysis suggests that a large

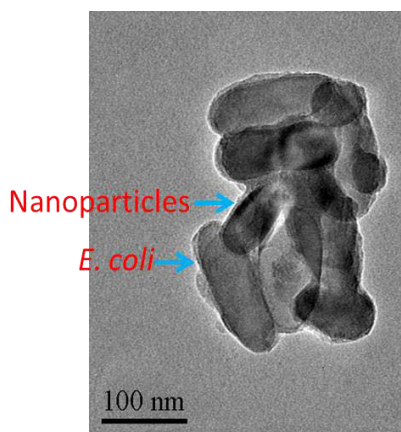


Fig. 2. Nanoparticles bound to E.coli suggests that peptides are expressed on the surface of E. coli.

Based on the vector FimH-TPN containing the BamHI site, we constructed a peptides expression library to generate FimH-TPN-Random using random primers containing random 21-synthetic-nucleotides. The diversity of the library was confirmed by sequencing of thirty clones. The vector FimH-TPN-Random were introduced into recombination *E. coli* DH5 α to prepare random peptide expression library, and stored at -80°C until use.

The peptide display on the surface is a powerful tool for library selection and protein engineering especially using yeast and phage [3,4]. In this study, our work is the first time to construct a peptide library using the combination of FimH and TPN. The construction facilitates the display of peptides on the surface of *E. coli*. We observed a large fraction of insolubility for the proteins in our library. The random peptide expression library was proposed to screen the target proteins. Although the transformation affected the amount of the peptides of the library, we thought it is effective for selection of peptide drugs. Overall, our results demonstrate the design of a peptide library using human TPN activity site and the feasibility of the library for screening of peptide drugs.

Acknowledgments

This work was supported by the starting fund from Hubei University of Technology.

References

1. Li, J., et al. *Protein Expression and Purification* **84**, 1-8 (2012), <http://dx.doi.org/10.1016/j.pep.2012.04.013>
2. Dagmara, I., et al. *PLOS Pathogens* (2015), <http://dx.doi.org/10.1371/journal.ppat.1004857>
3. Rhiel, L., et al. *PLOS ONE* (2014), <http://dx.doi.org/10.1371/journal.pone.0114887>
4. Clackson, T., et al. *Nature* **352**(6336), 624-628 (1991), <http://dx.doi.org/10.1038/352624a0>

Antimicrobial and Hemolytic Activity of Cysteine-Deleted Tachyplesin (CDT) Analogues in the Pursuit of Therapeutic Selectivity

Deborah Heyl, Yeji Park, Jennifer Garvey, Rebecca Newman,
and Yllka Vladaj

Department of Chemistry, Eastern Michigan University, Ypsilanti, MI, 48197, USA

Introduction

Because of the increasing resistance of bacteria to antibiotics, antimicrobial peptides (AMPs) may provide an alternative to traditional therapy. Tachyplesin is an AMP found in horseshoe crabs that can permeabilize the cell membrane [1]. Its positively charged residues are attracted to the negatively charged bacterial membrane. The hydrophobic amino acids then can insert into the nonpolar region of the membrane bilayer, forming pores or pulling the membrane apart. Human cell membranes are more zwitterionic, so the peptide does not affect them to the same extent. However, better selectivity for bacterial over mammalian cells is clearly desirable. Due to the mechanism by which AMPs act, bacteria are less able to develop resistance. Starting with a linear tachyplesin analogue that had the cysteine residues deleted and retained activity (CDT) [2], this study examines variations in end capping, sequence reversal, and the inclusion of D-amino acids.

Results and Discussion

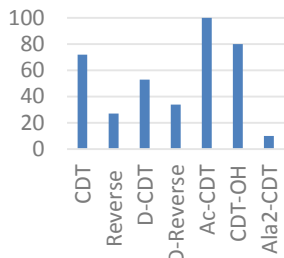


Fig. 1. Percent liposome dye leakage caused by 20 μ M peptide.

All analogues of CDT were synthesized by solid phase peptide synthesis using an Fmoc protection strategy on a PS3 Automated Peptide Synthesizer by Protein Technologies. They were then cleaved from the resin by trifluoroacetic acid, purified by RP-HPLC, and tested for effects on model membranes as well as for antimicrobial and hemolytic activity. Sequences can be found in Table 1. To test for the ability to disrupt liposomes, carboxy-fluorescein encapsulated vesicles were made using a 3:1 mixture of POPC:POPG (palmitoyloleylphosphocholine and glycerol, respectively); dye leakage was measured in the presence of 20 μ M peptide and compared to that caused by a Triton-X detergent control (Figure 1). Antimicrobial activity was assessed by determining the minimum inhibitory concentration of peptide for gram positive *S. aureus* and gram negative *E. coli* strains (Table 1). Serial dilutions of the peptides were added to wells containing specific concentrations of bacteria. The cultures were allowed to grow

overnight and turbidity readings were taken to measure bacterial growth. Damage to eukaryotic cells was evaluated spectrophotometrically by measuring hemolysis of sheep red blood cells compared to Triton-X treated controls (Table 1). Relative selectivity for bacterial over mammalian cells is represented in Figure 2, where the selectivity index was calculated by dividing the maximum concentration of peptide which caused less than 1% red blood cell hemolysis (where a high value is advantageous) by the MIC (where a low value indicates greater effectiveness).

Results for the first set of analogues show that reversing the amino acid sequence had virtually no effect on MIC values (CDT vs. Reverse CDT or All D-CDT vs. All D- Reverse CDT). However, the reverse sequences were less selective for bacteria, making them less promising as therapeutics.

Altering the stereochemistry, on the other hand, improved antimicrobial activity and selectivity. All-D Reverse CDT showed more selectivity than Reverse CDT, and All-D CDT exhibited a significant increase in selectivity over CDT. Changing the stereochemistry of amino acids did not improve membrane permeabilization (as expected, since membrane interaction does not involve specific binding), yet led to greater antibacterial activity in All D-CDT. This suggests that this D-amino acid containing peptide may have a secondary mechanism that targets bacterial cells.

Table 1. Sequences of the antimicrobial peptides, effective minimum concentrations to inhibit bacterial growth (MIC), and concentration producing less than 1% hemolysis.

Analog	Sequence	MIC (μ M)		<1% Hemolysis (μ M)
		<i>E. coli</i> C25	<i>S. aureus</i> ATCC 25923	
CDT	KWFRVYRGIYRRR-NH ₂	7.1	14	67
Reverse CDT	RRRYIGRYVRFWK-NH ₂	8.4	16.8	8.4
All-D CDT	kwfrvyrgiyr-rr-NH ₂	2.1	8.4	540
All-D Reverse CDT	rrryigryvrfwk-NH ₂	8.4	16.8	67
Ac-CDT	Ac-KWFRVYRGIYRRR-NH ₂	16.5	4.11	8.2
CDT-OH	KWFRVYRGIYRRR-OH	33.7	67.3	17
Ala ² -CDT	KAFRVYRGIYRRR-NH ₂	71.8	144	72

Capping the *N*-terminus (Ac-CDT) or removal of the natural *C*-terminal “capping” carboxamide (CDT-OH) led to decreased selectivity for bacterial cells. Both peptides showed greater membrane disrupting ability *in vitro*, and more mammalian cell membrane permealization (hemolysis). Although acetylated CDT (Ac-CDT) showed slightly increased activity against *S. aureus* (the only analogue to show selectivity for the gram positive over the gram negative strain), these analogues, which both reduce overall positive charge, generally decreased both antimicrobial activity and selectivity, especially the CDT-OH with its *C*-terminal negative charge.

Replacement of Trp at the 2nd position in CDT (Ala²-CDT) reduced overall antimicrobial action. Ala²-CDT exhibited the lowest antibacterial activity of all CDT analogues here (10-fold reduction relative to CDT), and also displayed very little hemolytic activity. The low dye leakage from vesicles also indicates that a lack of tryptophan at this position significantly decreases membrane permeabilization. The observation is consistent with the published literature, which states that Trp in

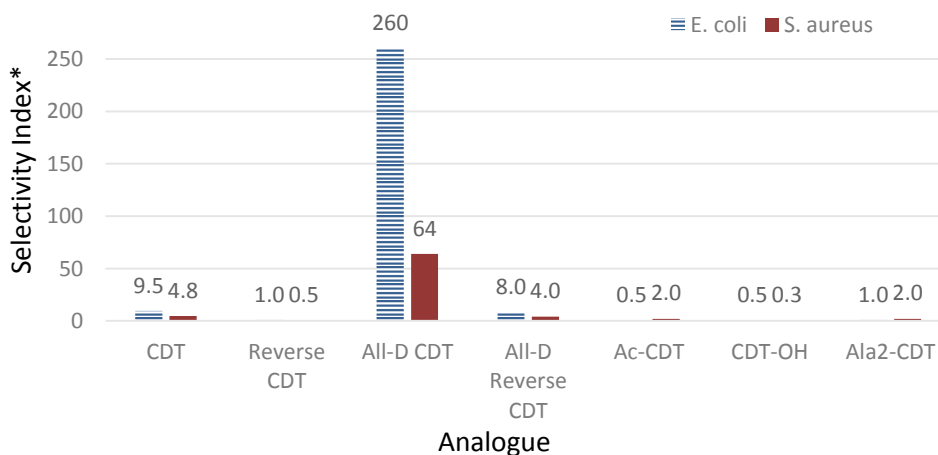


Fig. 2. Relative selectivity of each analogue for bacterial over mammalian cells; for example, at 64 times the concentration required to kill *S. aureus*, All-D CDT causes <1% RBC hemolysis.

*S.I. is calculated by dividing the concentration of peptide for which there is <1% hemolysis by the MIC. This gives an indication of selectivity for bacterial over mammalian cells.

antimicrobial peptides, including CDT, enhances membrane permeabilization and strengthens antimicrobial activity [3].

All D-CDT exhibited the best bactericidal activity and highest selectivity index of all CDT analogues developed thus far [4]. While the MIC is improved only about 1.5 to 3-fold against *S. aureus* and *E. coli*, respectively, its selectivity was significantly better than that of CDT itself since it caused virtually no damage to red blood cells, even at much higher concentrations than those required to kill the bacteria. D-amino acids also afford resistance against enzymatic breakdown and less immunogenicity. This analogue therefore shows broad spectrum activity with the potential to be developed into a potent nontoxic therapeutic drug.

Acknowledgments

Sincere thanks to Dr. Jim Vandenbosch for help with the MIC assays. This work was supported by the Eastern Michigan University Graduate School, and the Provost's Research Support and Chemistry Department Seller's Funds.

References

1. Nakamura, T., Furunaka, H., Miyata, T., Tokunaga, F., Muta, T., Iwanaga, S., Niwa, M., Takao, T., Shimonishi, Y. *J. Biol. Chem.* **263**, 16709-6713 (1988), <http://www.ncbi.nlm.nih.gov/pubmed/3141410>
2. Ramamoorthy, A., Thennarasu, S., Tan, A., Gottipati, K., Sreekumar, S., Heyl, D.L., An, F., Shelburne, C.E. *Biochemistry* **45**, 6529-6540 (2006), <http://dx.doi.org/10.1021/bi052629q>
3. Saravanan, R., Mohanram, H., Joshi, M., Domadia, P., Torres, J., Ruedl, C., Bhattacharjya, S. *Biochim. Biophys. Acta* **1818**, 1613-1624 (2012), <http://dx.doi.org/10.1016/j.bbamem.2012.03.015>
4. Wood, S.J., Park, Y.A., Kanneganti, N.P., Mekkisa, H.R., Crisman, L.L., Davis, S.E., Vandenbosch, J.L., Scaglione, J., Heyl, D.L. *Int. J. Peptide Res. Ther.* **20**, 519-530 (2014), <http://dx.doi.org/10.1007/s10989-014-9419-7>

Synthesis of *N*-Methyl and Azasulfuryl Urotensin-II₍₄₋₁₁₎ Derivatives

Francesco Merlino^{1,2}, Ali M. Yousif^{1,2}, Salvatore Di Maro¹, Stéphane Turcotte², Julien Dufour-Gallant^{2,3}, David Chatenet³, Paolo Santicioli⁴, Ettore Novellino¹, Paolo Grieco¹, and William D. Lubell²

¹Department of Pharmacy, University of Naples "Federico II", Naples, 80131, Italy; ²Département de Chimie, Université de Montréal, Montréal, H3C 3J7, Canada; ³INRS-Institut Armand-Frappier, Institut National de la Recherche scientifique, Université du Québec, Laval, H7V 1B7, Canada; ⁴Department of Pharmacology, Menarini Ricerche, Florence, I-50131, Italy

Introduction

Human urotensin-II (*hU*-II) is a cyclic peptide that is able to regulate cardiovascular homeostasis [1]. The shortest active sequence required for biological activity of *hU*-II contains residues 4-11 in a cycle featuring a disulfide bond between Cys⁵-Cys¹⁰, Asp-c[Cys-Phe-Trp-Lys-Tyr-Cys]-Val-OH (Figure 1), and is suggested to adopt a β -hairpin conformation of prime relevance for interaction with the urotensin-II receptor (UT) [2]. Employing the minimal active sequence, we have developed synthetic strategies to prepare new derivatives in which *N*-methylated (**1**) and azasulfuryl (**2**) residues have been inserted into the cyclic peptide core region (Figure 1). Mono and multiple *N*-methylation of the amide bonds and insertion of *N*-aminosulfamide residues into *hU*-II₍₄₋₁₁₎ have been performed to survey their influences on intra- and inter-molecular hydrogen bonds, geometry and interactions with UT.

Results and Discussion

A solid-phase procedure was used to install *N*-methyl groups on amides at residues 5-10 consisting of three fundamental steps: i) amine protection with the *o*-nitrobenzenesulfonyl group (*o*-NBS), ii) amine alkylation with methylsulfate and 1,8-diazabicycloundec-7-ene (DBU) as base, and iii) selective removal of the *o*-NBS group on solid support (Scheme 1) [3].

N-Aminosulfamides are peptidomimetics in which the C α H and the carbonyl of an amino amide residue are respectively replaced by a nitrogen atom and a sulfuryl group. Azasulfurylphenylalanine (AsF) analogue **8** was synthesized by an approach consisting of two phases: i) the synthesis of the AsF tripeptide building block **5** by solution phase chemistry with protected functional groups compatible

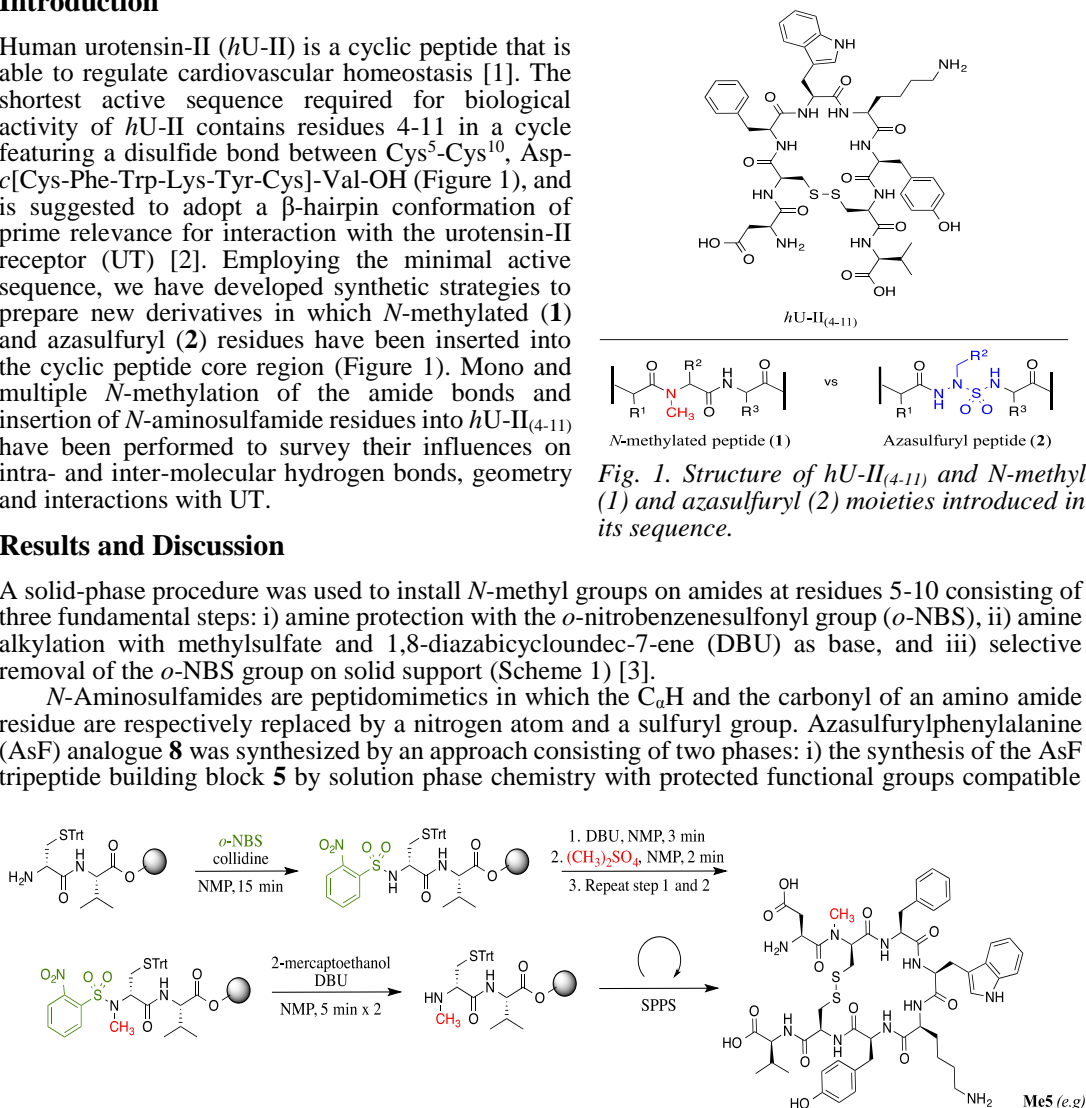
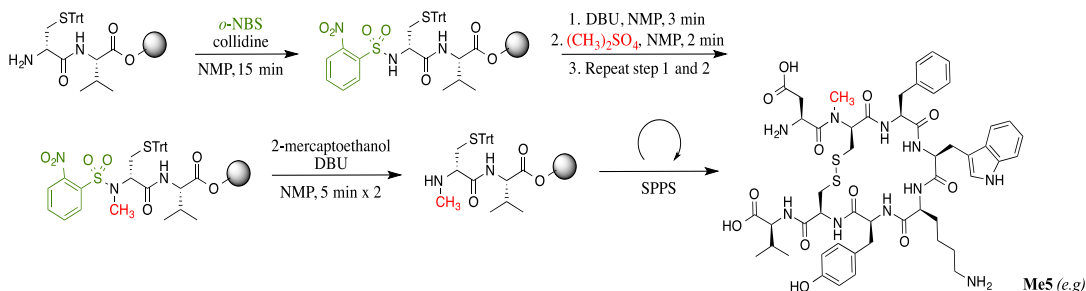
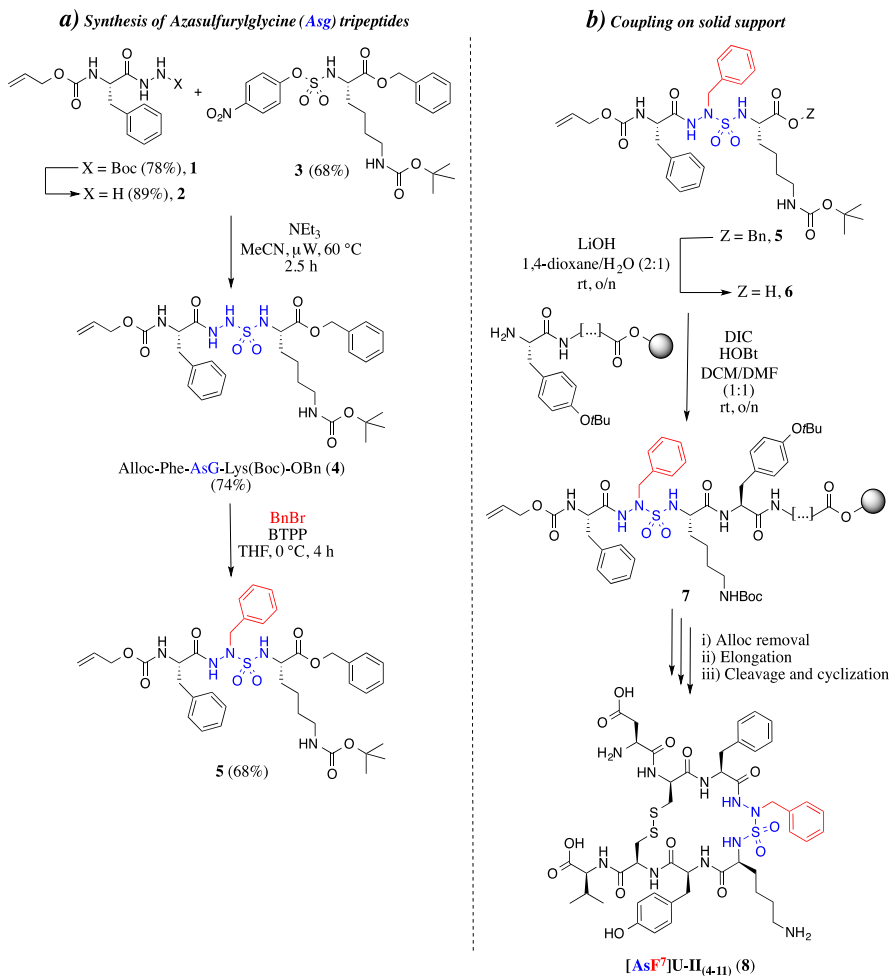


Fig. 1. Structure of *hU*-II₍₄₋₁₁₎ and *N*-methyl (1) and azasulfuryl (2) moieties introduced in its sequence.



Scheme 1. Three-step procedure for the synthesis of *N*-methylated *U*-II analogues is illustrated for the preparation of [N-(Me)Cys⁵]*hU*-II₍₄₋₁₁₎ (**Me5**).

with solid phase peptide synthesis (Scheme 2a); ii) incorporation of AsF tripeptide **6** into the peptide sequence on solid support using a Fmoc/*t*Bu orthogonal protection strategy (Scheme 2b). In [AsF⁷]hU-II₍₄₋₁₁₎ (**8**), the Trp⁷ residue was replaced by azasulfurylphenylalanine with the phenyl group serving as a mimic of the indole moiety. Initially, the AsF tripeptide building block **5** was synthesized using a solution-phase approach featuring chemoselective alkylation of azasulfurylglycine (AsG) **4** with benzyl bromide and *tert*-butylimino-tri(pyrrolidino)phosphorane (BTTP) as base [4].



Scheme 2. Synthesis of [AsF⁷]hU-II₍₄₋₁₁₎ (**8**): a) preparation of azasulfurylphenylalanine (AsF) tripeptide **5**; b) introduction of AsF tripeptide into [AsF⁷]U-II₍₄₋₁₁₎ (**8**).

With AsF tripeptide building block **6** in hand, solid phase chemistry was performed on Rink amide resin. Azasulfuryl tripeptide **6** was coupled to the Tyr⁹ residue using di-*iso*-propylcarbodiimide and hydroxybenzotriazole. Subsequently, the *N*-terminal Alloc group was removed using palladium catalysis and the sequence was elongated by conventional solid phase peptide synthesis (SPPS) [5]. Cleavage and disulfide bond formation were accomplished in a one-pot reaction using a cocktail of 10% DMSO in TFA in the presence of anisole as scavenger to afford azasulfuryl peptide **8**, which was purified by HPLC on a C18 bonded silica column and characterized by LCMS and HRMS analysis [*t*_R = 14.18 min, 20 to 80% methanol (0.1% formic acid) in water (0.1% formic acid) over 15 min;

Table 1. Biological data for mono *N*-methylated *hU-II*₍₄₋₁₁₎ analogues.

Peptide	Sequence	Biological data	
		<i>pEC</i> ₅₀ ^a	<i>pK</i> _D / <i>pK</i> _i ^b
<i>hU-II</i>₍₄₋₁₁₎	Asp-c[Cys-Phe-Trp-Lys-Tyr-Cys]-Val-OH	8.20±0.01	8.34±0.04
Me5	Asp-c[(NMe)Cys-Phe-Trp-Lys-Tyr-Cys]-Val-OH	8.26±0.03	8.53±0.08
Me6	Asp-c[Cys-(NMe)Phe-Trp-Lys-Tyr-Cys]-Val-OH	6.36±0.04	6.64±0.10
Me7	Asp-c[Cys-Phe-(NMe)Trp-Lys-Tyr-Cys]-Val-OH	8.50±0.05	8.76±0.07
Me8	Asp-c[Cys-Phe-Trp-(NMe)Lys-Tyr-Cys]-Val-OH	4.91±0.18	=5
Me9	Asp-c[Cys-Phe-Trp-Lys-(NMe)Tyr-Cys]-Val-OH	5.25±0.07	=5
Me10	Asp-c[Cys-Phe-Trp-Lys-Tyr-(NMe)Cys]-Val-OH	8.31±0.08	8.45±0.05

^afunctional activity was tested on the rat thoracic aorta; ^bbinding affinity was evaluated on UT receptors expressed on CHO cell line.

calculated mass: 1059.3733, found: 1059.3706]. Similar procedures are being pursued to broaden the library of azasulfuryl peptide mimics of the *hU-II*₍₄₋₁₁₎ sequence.

Biological data for the *N*-methyl *U-II*₍₄₋₁₁₎ analogs was acquired through experiments performed on CHO cell lines expressing the human UT receptor for binding affinity, and on rat thoracic aorta for functional activity, according to experimental procedures previously described [6]. In agreement with the hairpin conformation, *N*-methylation of amide bonds of *U-II*₍₄₋₁₁₎ at Phe⁶ and Tyr⁹ decreased binding affinity and consequently reduced vasoconstriction in the rat thoracic aorta assay (Table 1).

In contrast, *N*-methylation of Trp⁷ (e.g., **Me7**) improved affinity relative to the parent peptide. On the other hand, *N*-methylation of the amide bonds at position 8, which is normally occupied by Lys, decreased affinity, and reduced vasoconstriction in the rat thoracic aorta assay. *N*-Methylation of the Cys residues at positions 5 and 10 gave more active analogs (e.g., **Me5** and **Me10**) without significant change in binding affinity. Preliminary data inspired investigation of a set of di-methylated analogs, which were synthesized by a similar process and are presently being investigated for biological activity. The influence of *N*-methylation on conformation is also being analyzed by NMR spectroscopy.

Other azasulfuryl amino acids are being inserted into the cyclic portion of the *hU-II*₍₄₋₁₁₎ sequence by replacement of the Trp⁷ and Lys⁸ amino acid residues. Their synthesis and activity will be reported in due time.

Information from *N*-methylation and *N*-aminosulfamide studies is designed to provide a detailed view of the influences of hydrogen-bonding in the *hU-II*₍₄₋₁₁₎ sequence. In preliminary results, removal of the N-H group of Trp⁷ by methylation enhanced interaction with the UT receptor. Further investigation of the urotensin analogues is ongoing and their impact on structure-activity relationships of the urotensinergic system will be reported in due time.

Acknowledgments

This work was supported in part by the Italian Ministry of Education, University and Research (PRIN2010MCLBCZ_002), a grant from “Regione Campania” - Laboratori Pubblici progetto “Hauteville”, and the Natural Sciences and Engineering Research Council of Canada (NSERC).

References

1. Vaudry, H., et al. *Pharmacol. Rev.* **67**, 214-258 (2015), <http://dx.doi.org/10.1124/pr.114.009480>
2. Carotenuto, A., et al. *J. Pept. Sci.* **19**, 293-300 (2013), <http://dx.doi.org/10.1002/psc.2498>
3. Miller, S., Scanlan, T.S. *J. Am. Chem. Soc.* **119**, 2301-2302 (1997), <http://dx.doi.org/10.1021/ja9635443>
4. Turcotte, S., et al. *Org. Lett.* **14**, 1318-1321 (2012), <http://dx.doi.org/10.1021/ol3001987>
5. Lubell, W.D., et al. (2005) “*Peptides*” *Science of Synthesis 21.11, Chemistry of Amides*. Thieme, Stuttgart, 713-809.
6. Carotenuto, A., et al. *J. Med. Chem.* **57**, 5965-5974 (2014), <http://dx.doi.org/10.1021/jm500218x>

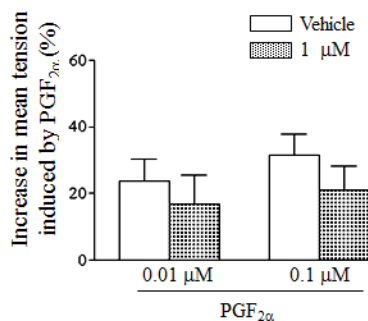
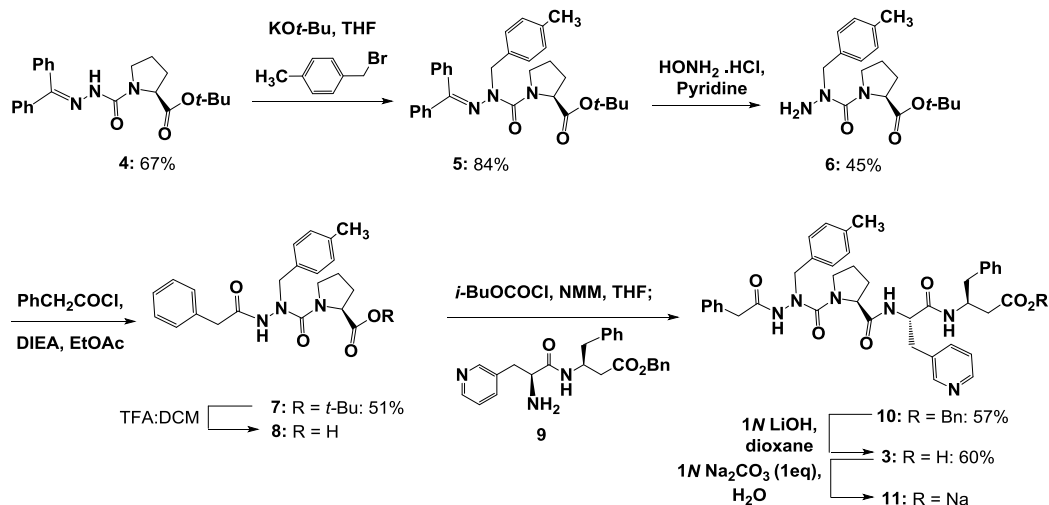


Fig. 2. Preliminary test of biological activity of sodium salt **11**.

Due to limited solubility in water, azapeptide **3** was converted to sodium salt **11** by titrating with a 1N solution of Na₂CO₃. In the myometrial contraction assay, in contrast to aza-Phe analogue **2**, sodium salt **11** did not significantly reduce the mean tension of PGF_{2α}-induced myometrial contractions.

Conclusion

In conclusion, we have synthesized aza-4-methylphenylalanine peptide **11**, and examined its ability to curb myometrial contractions. The subtle addition of a *para*-methyl substituent onto aza-Phe analogue **2** significantly diminished antagonistic activity, illustrating the consequences of aromatic structure on modulator ability. The synthesis and further examination of other aromatic analogs are ongoing to further probe the structural requirements for modulating FP activity.



Scheme 1. Synthesis of aza-4-methylphenylalanine analogue **11**.

Acknowledgments

This research was supported by the Natural Sciences and Engineering Research Council of Canada (NSERC), Canadian Institutes of Health Research (CIHR), the March of Dimes foundation and Bill and Melinda Gates foundation.

References

- Requejo, C., Rubens, Menon, R., Van, L.P.F.A. *Bull World Health Organ.* **88**, 31-38 (2010), <http://dx.doi.org/10.2471/BLT.08-62554>
- Pathe-Neushäfer-Rube, A., Neushäfer-Rube, F., Püschel, G.P. *Biochem. J.* **388**, 317 (2005), <http://dx.doi.org/10.1042/BJ20041321>
- Goupil, E., et al. *J. Biol. Chem.* **285**, 25624-25636 (2010), <http://dx.doi.org/10.1074/jbc.M110.115196>
- Bourguet, C.B., Goupil, E., Tassy, D., Hou, X., Thouin, E., Polyak, F., Hebert, T.E., Claing, A., Laporte, S.A., Chemtob, S., Lubell, W.D. *J. Med. Chem.* **54**, 6085-6097 (2011), <http://dx.doi.org/10.1021/jm200608k>
- Bourguet, C.B., Sabatino, D., Lubell, W.D. *Biopolymers, Peptide Science* **90**, 824-831 (2008), <http://dx.doi.org/10.1002/bip.21103>
- Bourguet, C.B., Proulx, C., Kloczek, S., Sabatino D., Lubell, W.D. *J. Peptide Sci.* **16**, 284-296 (2010), <http://dx.doi.org/10.1002/psc.1235>

Table 1. Binding and cAMP Assays of Novel Peptides toward Melanocortin Receptors.

	MC1R				MC3R				MC4R				MC5R			
	Binding		cAMP		Binding		cAMP		Binding		cAMP		Binding		cAMP	
	IC ₅₀	%BE	EC ₅₀	Act %	IC ₅₀	%BE	EC ₅₀	Act %	IC ₅₀	%BE	EC ₅₀	Act %	IC ₅₀	%BE	EC ₅₀	Act %
(1)	1621	61	9.6	100	NB	0	111	93	189	46	40	79	NB	0	NA	0
(2)	1053	81	8.5	100	>10000	45	102	87	NB	0	19	55	NB	0	NA	0
MT-II	1 ± 0.1	100	1.02 ± 0.4	100	2.0 ± 0.1	100	5.1 ± 0.3	100	2.3 ± 0.85	100	2.1 ± 0.6	100	4.2 ± 1.3	100	5.7 ± 2.2	100

^aMT-II = Ac-Nle-c[Asp-His-D-Phe-Arg-Trp-Lys]-NH₂. ^bIC₅₀ = concentration of peptide at 50% specific binding (N = 4). NB = 0% of 125I-NDP- α -MSH displacement observed at 10 μ M. %BE (binding efficiency) = maximal % of 125I-NDP- α -MSH displacement observed at 10 μ M. EC₅₀ = Effective concentration of peptide that was able to generate 50% maximal intracellular cAMP accumulation (N = 4). Act% = % of cAMP produced at 10 μ M ligand concentration, in relation to MT-II. NA = 0% cAMP accumulation observed at 10 μ M. The peptides were tested at a range of concentration from 10⁻¹⁰ to 10⁻⁵ M.

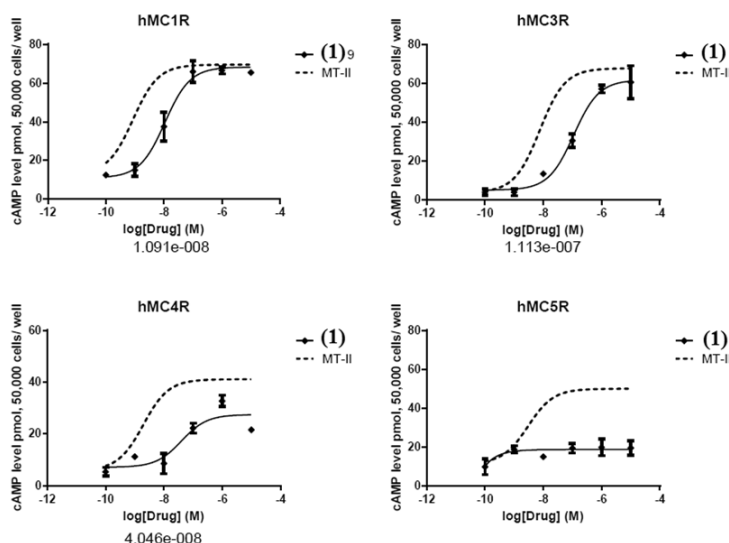


Fig. 2. The comparison between Melanocortin activity of synthesized Peptides and MT-II.

Acknowledgments

Supported in part by a grant from the U.S. Public Health Service, National Institutes of Health, DK017420, GM 108040 and DA06284.

References

- Norton, H.L., Friedlaender, J.S., Merriwether, D.A., Koki, G., Mgone, C.S., Shriver, M.D. *Am. J. Physical Anthropology* **130**, 254-268 (2006), <http://dx.doi.org/10.1002/ajpa.20343>
- Rinne, P., Ahola-Olli, A., Nuutinen, S., Koskinen, E., Kaipio, K., Eerola, K., Juonala, M., Kähönen, M., Lehtimäki, T., Raitakari, O.T., Savontaus, E. *Arterioscler. Thromb. Vasc. Biol.* **35**, 1678-1686 (2015), <http://dx.doi.org/10.1161/ATVBAHA.114.305064>
- Ying, J., Gu, X., Cai, M., Dedek, M., Vagner, J., Trivedi, D.B., Hraby, V.J. *J. Med. Chem.* **49**, 6888-6896 (2006), <http://dx.doi.org/10.1021/jm060768f>
- Morgan, A.A., Rubenstein, E. *PLoS One* **8**, 53785 (2013), <http://dx.doi.org/10.1371/journal.pone.0053785>
- Pulka, K., et al. *Tetrahedron* **63**, 1459-1466 (2007), <http://dx.doi.org/10.1016/j.tet.2006.11.069>

Solid-Phase Peptide Synthesis and Structural Analyses by Circular Dichroism Spectroscopy of the Cytotoxic D-(KLAKLAK)₂ Sequence

Niki Rana and David Sabatino

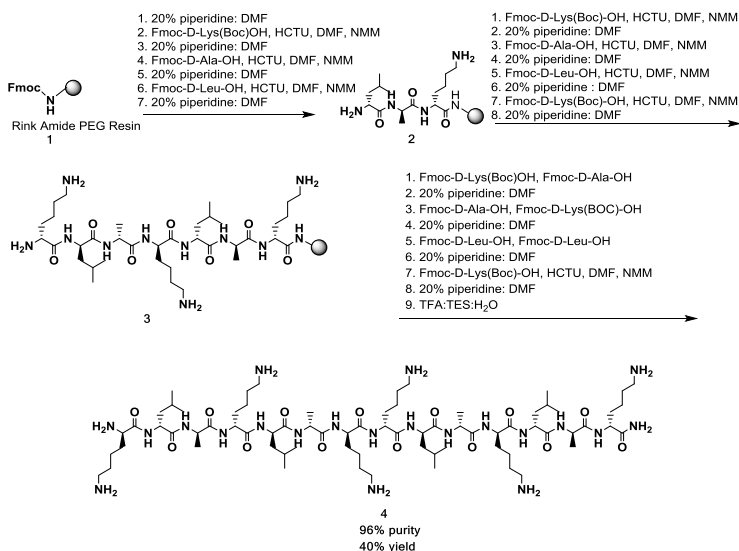
Department of Chemistry and Biochemistry, Seton Hall University, South Orange, NJ, 07079, USA

Introduction

The apoptosis inducing (pro-apoptotic) peptide sequence, D-(KLAKLAK)₂, has been classified as a potent antimicrobial agent [1]. Moreover, it was found to trigger cell death in bacteria without inducing cytotoxicity in mammalian cell types. The chemical basis for this selectivity has been associated with the poly(cationic) amphiphilic nature of this peptide sequence, which facilitates cell permeability in negatively charged bacterial membranes and not within the zwitterionic lipid bilayers of mammalian cell types [1,2]. Upon cell internalization, the positively charged D-(KLAKLAK)₂ sequence accumulates on the surface of the mitochondria and induces depolarization of the negatively charged mitochondrial membrane [3]. This depolarization compromises the mitochondrial membrane integrity and triggers the release of cell death effectors, including cytochrome c, second mitochondrial derived activator of caspase and the apoptosis-inducing factor (AIF) which ultimately results in the programmed cell death response [4]. Considering the potential of this antimicrobial peptide sequence in the treatment of infectious diseases, an optimized solid-phase peptide synthesis and structure analyses by Circular Dichroism (CD) spectroscopy is revealed in this study.

Results and Discussion

The D-(KLAKLAK)₂ peptide sequence may prove to be a synthetic challenge by conventional Merrifield peptide synthesis. These types of amphiphilic peptides have been shown to aggregate during the course of peptide synthesis on the non-polar polystyrene-based resins causing diminished purities and yields [5]. Therefore, the polar poly (ethylene) glycol (PEG) resin which was shown to afford excellent crude purities and yields of synthetically challenging amphiphilic peptide sequences was adopted for our solid-phase peptide synthesis strategy [6] (Scheme 1).



Scheme 1. Solid-phase peptide synthesis of the D-(KLAKLAK)₂ sequence.

Peptide synthesis was conducted on a PSI 200C Peptide Synthesizer (Fairfield, NJ) with *O*-(6-Chlorobenzotriazol-1-yl)-*N,N,N',N'*-tetramethyluronium hexafluorophosphate, HCTU, as activator and coupling reagent, *N*-methylmorpholine, NMM, as base in *N,N*-dimethylformamide, DMF, as solvent for the coupling reactions [5]. The deprotection steps of the fluorenylmethoxycarbonyl, Fmoc, group were completed with piperidine in DMF. Following peptide synthesis, cleavage and deprotection of the peptide from the solid support was achieved with trifluoroacetic acid, TFA, with water and triethylsilane scavenging any unreacted side chain protecting groups (Scheme 1). The desired peptide sequence, **4**, was synthesized in good purities (96%) and acceptable yields (40%) following RP-HPLC. Peptide identity was confirmed by molecular weight following LCMS analyses.

The structure and stability properties for the D-(KLAKLAK)₂ peptide sequence were next evaluated. Circular Dichroism (CD) spectroscopy of the peptide (30–200 μ M) in water and phosphate buffered saline (PBS) validated the anticipated α -helix peptide secondary structure in more dilute conditions (30 μ M) and β -sheets at higher concentrations (120–200 μ M) Figure 1a [1]. Peptide structural stability was next examined with the addition of a surfactant, sodium dodecyl sulfate, SDS, which serves to mimic the cell membrane microenvironment [1]. These conditions demonstrated a stable peptide secondary structure, maintaining the canonical α -helix conformation, Figure 1b. These results demonstrates the adaptive structural properties of this important peptide sequence that are likely needed for cell translocation activity.

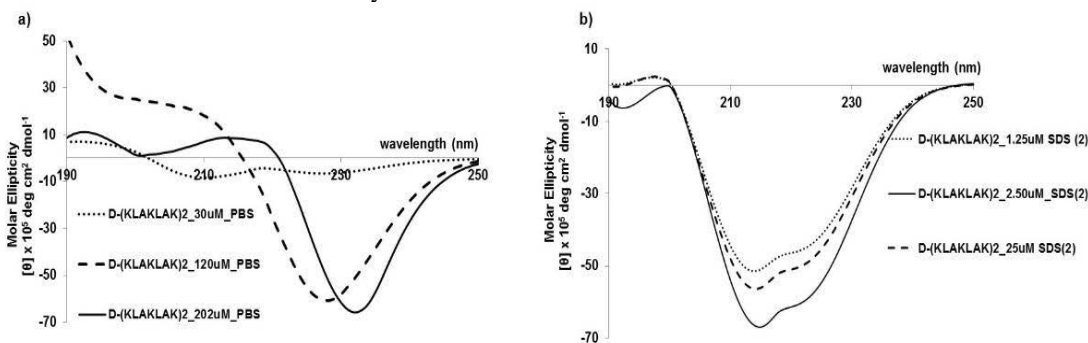


Fig. 1. CD spectroscopy of D-(KLAKLAK)₂ in a) PBS (30–200 μ M) and b) SDS (1.25–25 μ M).

Acknowledgments

The authors would like to thank Seton Hall University for continued support. The authors are also grateful to the 24th APS for accommodating our research presentation.

References

- Javaddpour, M.M., Juban, M.M., Lo, W.C., Bishop, S.M., Albertv, J.B., Cowell, S.M., Becker, C.L., McLaughlin, M.L. *J. Med. Chem.* **39**, 3107–3113 (1996), <http://dx.doi.org/10.1021/jm9509410>
- Glukhov, E., Stark, M., Burrows, L.L., Deber, C.M. *J. Biol. Chem.* **280**, 33960–33967 (2005), <http://dx.doi.org/10.1074/jbc.M507042200>
- Trapp, S., Horobin, R.W. *Eur. Biophys. J.* **34**, 959–966 (2005), <http://dx.doi.org/10.1007/s00249-005-0472-1>
- Costantini, P., Jacotot, E., Decaudin, D., Kroemer, G. *J. Natl. Cancer Inst.* **92**, 1042–1053, (2000), <http://dx.doi.org/10.1093/jnci/92.13.1042>
- Joseph, S.C., Blackman, B.A., Kelly, M.L., Phillips, M., Beaury, M.W., Martinez, I., Parronchi, C.J., Bitsaktsis, C., Blake, A.D., Sabatino, D. *J. Pept. Sci.* **20**, 736–745 (2014), <http://dx.doi.org/10.1002/psc.2665>
- García-Martín, F., Quintanar-Audelo, M., García-Ramos, Y., Cruz, L.J., Gravel, C., Furic, R., Côté, S., Tulla-Puche, J., Albericio, F. *J. Comb. Chem.* **8**, 213–220 (2006), <http://dx.doi.org/10.1021/cc0600019>

Lasso Peptides and Murein Peptide Ligase Inhibitors as Novel Anti-Mycobacterial Agents

Francesca Scotti^{1,2}, Sanjib Bhakta², and John P. Malkinson¹

¹UCL School of Pharmacy, 29-39 Brunswick Square, WC1N 1AX, London, UK;

²Birkbeck College, Malet Place WC1E 7HX, London, UK

Introduction

Despite the existence of vaccinations, diagnostic tools and treatments, tuberculosis (TB) prevalence is increasing because of the increased circulation of people, the misuse of antibacterials - giving rise to growing numbers of drug resistant strains of *Mycobacterium tuberculosis*, low compliance with the lengthy therapy - four different drugs for six months, and deadly liaisons with other health concerns (AIDS, diabetes, cancer, etc.). There is therefore a pressing need to look for new strategies against TB, in the hope of finding new drugs with novel mechanisms of action or ways to potentiate the activity of existing drugs and to reduce treatment duration. Recently, among the class of lasso peptides, interesting stable cyclic peptides of bacterial origin were reported, including the anti-mycobacterial lariatins A and B, followed by the newly-discovered anti-TB pseudo-lasso peptide lassomycin [1-3]. Furthermore the identification in *M. tuberculosis* of an orthologue of an enzyme found in *E. coli* [4,5] involved in peptidoglycan recycling encouraged us to try to identify and evaluate its activity and find potential inhibitors.

Results and Discussion

The choice of potential inhibitors of Mpl was based on structural analogy with the putative natural peptide substrates identified in *E. coli* [4,5]. These small peptides have been synthesised *via* solid-phase synthesis and have been tested using *M. aurum* through the SpotI whole-cell high-throughput screening assay [6].

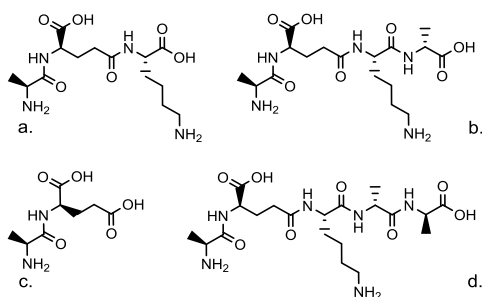


Fig. 1. First structural analogues of putative Mpl natural substrates synthesized.

upon the use of the semi-permanent Dmab protecting group. Unfortunately the use of this group was associated with troublesome side-reactions, including chain termination by pyroglutamate formation (lariatins) and aspartimide formation (lassomycin), requiring modification of the strategy and use of an allyl ester.

The SpotI whole-cell high-throughput screening assay, on a valid mycobacterial surrogate [7], will be used to evaluate whether these synthetic molecules adopt their appropriate bioactive conformations and whether the linear precursor retains their anti-mycobacterial activity.

The intention is to characterise Mpl activity in *M. tuberculosis* in order to confirm its substrates and evaluate the activity of analogues at the enzyme level. In order to achieve this, recombinant *M. tuberculosis* Mpl has been heterologously expressed in *E. coli* BL21(DE3)-pLysS competent cells and purified. Automated solid-phase peptide synthesis has been utilised to rapidly synthesise multiple short branched peptide analogues in parallel which have been tested on *M. aurum* using the SpotI high-throughput screening assay [6]. The results so far show no significant inhibiting activity.

Lariatins A, lariatins B and lassomycin as well as their linear precursors have been synthesised *via* solid-phase synthesis. Initial efforts adopted an on-resin head-to-side chain cyclisation strategy based

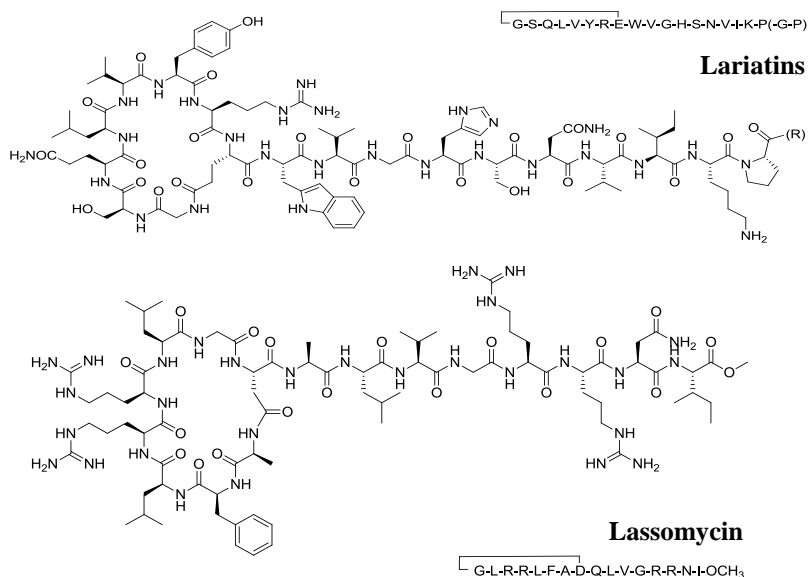


Fig. 2. Schematic representation of lariatins and lassomycin structure.

Acknowledgments

This work was supported by Bloomsbury Colleges Consortium, London, UK. F.S. is grateful to APS and UCL School of Pharmacy for providing travel funds.

References

1. Maksimov, M.O., et al. *Proc. Natl. Acad. Sci. USA* **109**, 15223-15228 (2012), <http://dx.doi.org/10.1073/pnas.1208978109>
2. Iwatzuki, M., et al. *J. Am. Chem. Soc.* **128**, 7486-7491 (2006), <http://dx.doi.org/10.1021/ja056780z>
3. Gavriš, E., et al. *Chem. Biol.* **21**, 509-518 (2014), <http://dx.doi.org/10.1016/j.chembiol.2014.01.014>
4. Das, D., et al. *PLoS One* **6**, e17624 (2011), <http://dx.doi.org/10.1371/journal.pone.0017624>
5. Hervé, M., et al. *Biochimie* **95**, 1120-1126 (2013), <http://dx.doi.org/10.1016/j.biochi.2012.12.011>
6. Gupta, N., et al. *J. Antimicrob. Chemother.* **67**, 1380-1391 (2012), <http://dx.doi.org/10.1093/jac/dks056>
7. Gupta, N., et al. *J. Antimicrob. Chemother.* **64**, 774-781 (2009), <http://dx.doi.org/10.1093/jac/dkp279>

Discovery of Novel, Potent and Long Acting CCK Analogs

Robert Hunter¹, Andrew Carpenter¹, Erin Swiger¹, Makda Mebrahtu¹,
Robert Wiard¹, Andrea Acker¹, Shane Roller^{1,2}, Mark Paulik^{1,2},
and Ved Srivastava^{*,1,2}

¹GlaxoSmithKline, 5 Moore Dr. Research Triangle Park, NC, 27709, USA;

²Phoundry Pharmaceuticals Inc., 6 Davis Dr., Research Triangle Park, NC, 27709, USA

Introduction

Cholecystokinin (CCK) is a sulfated neuropeptide hormone and neurotransmitter synthesized by cells in the mucosal epithelium of the small intestine and secreted in the duodenum. The C-terminal fragment CCK-8, inhibits gastric emptying as well as other physiological processes involved in satiety.

Results and Discussion

While the physiological effects of inhibiting gastric emptying, decreasing gastric acid secretion and satiety make CCK-8 an interesting peptide for the treatment of obesity, the anxiolytic effect which is normally attributed to the Cholecystokinin B receptor, complicate its use. In our research, we sought to synthesize a long acting peptide CCK agonist which was selective for the CCK-A receptor, had desired potency and sufficient solubility to be dosed using an implanted osmotic mini pump. To do this, we used much of the data which has been previously reported and attempted to systematically assemble it into a single peptide agonist with the desired pharmacokinetic profile.

- Potency in vitro (>9.5 pIC₅₀)
- 200 fold selectivity over CCK-B
- 45 min or better t_{1/2} (CCK-8 = 20 min)
- Equal or better food intake reduction than CCK-8
- Solubility >160 mg/mL

A screening of the literature provided the following information:

- Sulfation of Tyr27 is required for biological activity of the native peptide at the CCK-A receptor [1]
- Non hydrolyzable Sulfated Tyr27 mimetics are desired for synthetic ease, chemical stability [1]
- Activity is restored to non-sulfated CCK-4 when Met31 is replaced with a Lys(Tac) residue [2]
- Hexapeptide analogs retain potency when both Met28 and Met31 are replaced with norleucine [3]
- N-methyl-Phenylalanine enhances metabolic stability [4]
- N-terminal pGlu-Gln enhances metabolic stability [5]

The literature modifications were systematically incorporated, resulting in peptide 34 (Table 1) which had the desired potency, selectivity, food intake reduction and a solubility > 150 mg/mL. While endogenous CCK-8 lacks the selectivity duration of action and solubility to be used as an effective tool compound in combination studies, the introduction of modifications to the peptide sequence gleaned from the literature enabled us to generate a suitable molecule.

Table 1. Key analogs.

ID	SEQUENCE	CCK CCK Selec.			A.F.I.	A.F.I.	A.F.I.
		A	B	A/B	(DIO) 6hr	(DIO) 15hr	(DIO) 30hr
1	D(Y-SO ₃ H)MGWMDF-NH ₂ (CCK-8)	10.5	9.8	5	-59	-26	-10
33	(pGlu)KKKRD(F-CH ₂ SO ₃ H)LGW(K-Tac)D(mePhe)-NH ₂	9.8	7.5	200	-91	-69	-48
34	(pGlu)KKKKKRD(F-CH ₂ SO ₃ H)LGW(K-Tac)D(mePhe)-NH ₂	9.9	7.5	251	-100	-90	-68
35	(pGlu)KKKKKKKRD(F-CH ₂ SO ₃ H)LGW-(K-Tac)D(mePhe)-NH ₂	9.6	7	398	-100	-95	-73

The novel peptide 34 (Figure 1) demonstrated a pEC_{50} of 9.9 and a duration of action greater than 60h in an acute DIO mouse model. The improvements to CCK-8 translate to an ED_{50} 0.09 mg/kg/day and an observed weight loss of 23% when dosed in combination with Exendin-4 in the 14 day DIO rat model (Figure 2).

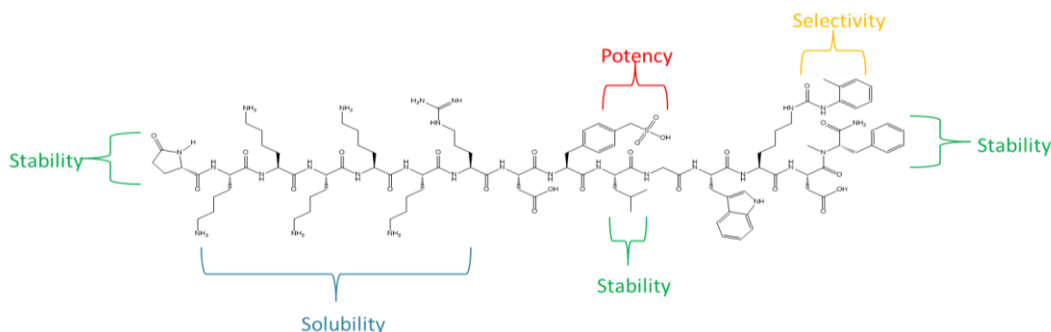


Fig. 1. Peptide 34.

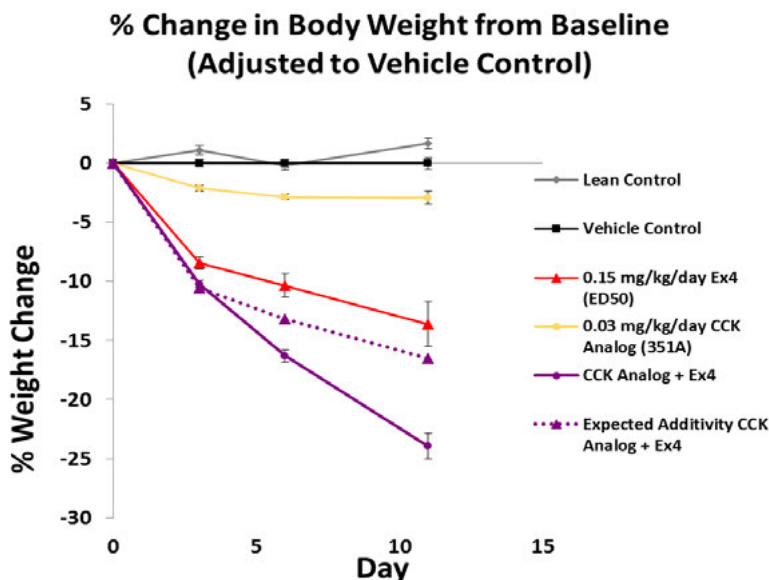


Fig. 2. In vivo results.

References

1. Marseigne, I., Roy, P., Dor, A., Durieux, C., Pelaprat, D., Reibaud, M., Blanchard, J.C., Roques, B.P. *J. Med. Chem.* **32**, 445-449 (1989), <http://dx.doi.org/10.1021/jm00122a026>
2. Sugg, E.E., Kimery, M.J., Jian, Mei Ding, Kenakin, D.C., Miller, L.J., Queen, K.L., Rimele, T.J. *J. Med. Chem.* **38**, 207-211 (1995), <http://dx.doi.org/10.1021/jm00001a027>
3. Pierson, M.E., Comstock, J.M., Simmons, R.D., Kaiser, F., Julien, R., Zongrone, J., Rosamond, J.D. *J. Med. Chem.* **40**, 4302-4307 (1997), <http://dx.doi.org/10.1021/jm970477u>
4. Simmons, R.D., Blosser, J.C., Rosamond, J.R. *Pharmacology Biochemistry and Behavior* **47**, 701-708 (1994), [http://dx.doi.org/10.1016/0091-3057\(94\)90176-7](http://dx.doi.org/10.1016/0091-3057(94)90176-7)
5. Irwin, N., Frizelle, P., Montgomery, I.A., Moffett, R.C., O'Harte, F.P.M., Flatt, P.R. *Diabetologia* **55**, 2747-2758 (2012), <http://dx.doi.org/10.1007/s00125-012-2654-6>

Discovery of Novel and Long Acting GLP-1 Analogs

Robert Hunter¹, Andrew Carpenter¹, Erin Swiger¹,
Makda Mebrahtu¹, Robert Wiard¹, Andrea Acker¹, Shane Roller^{1,2},
Mark Paulik^{1,2}, and Ved Srivastava^{1,2*}

¹GlaxoSmithKline, 5 Moore Dr. Research Triangle Park, NC, 27709, USA;

²Phoundry Pharmaceuticals Inc, 6 Davis Dr., Research Triangle Park, NC, 27709, USA

Introduction

Glucagon Like Peptide-1 (GLP-1) is a 30 amino acid gut hormone produced by intestinal L cells and pancreatic α cells. GLP-1 induces post prandial glucose-dependent insulin secretion and inhibits gastric secretion and motility, thus reducing circulating glucose levels and increasing satiety. These physiological effects make GLP-1 an interesting target for both diabetes and obesity therapy. However, GLP-1 lacks the therapeutic potential due to its very short half-life. Described are our efforts using ortholog screening and fragment substitution to discover novel and long acting GLP-1 analogues with modifications in the GLP-1 sequence,

HGEGTFTSDLTEYLEEEAVREFIEWLKNNGPKKIRYS-NH₂.

These analogs have desired potency and efficacy over endogenous GLP-1 with a 15h duration of action in an acute food intake reduction mouse model.

Results and Discussion

The World Health Organization estimates that as of 2008, 347 million people have diabetes mellitus [1] and by 2030, type II diabetes mellitus (T2DM) is projected be one of the leading non-communicable causes of death [2]. Comorbidities of T2DM include heart disease, fatty liver disease, hypertension and, importantly, obesity. While the physiological effects make GLP-1 therapy an interesting target for both diabetes and obesity, infusion studies in healthy subjects show rapid degradation of GLP-1 by the enzyme DPP-4 making the endogenous peptide unsuitable as a therapy. Exenatide (Byetta) and Liraglutide (Victoza) are stabilized versions of native GLP-1 and have shown utility in T2DM. Sitagliptin (Januvia) and Linagliptin (Tradjenta), inhibitors of DPP-4, are also marketed agents for T2DM. In addition Liraglutide is being investigated for obesity. Herein we describe our efforts in the discovery of novel, stable GLP-1 mimetics for the treatment of T2DM and obesity.

Infusion studies in healthy subjects demonstrate GLP-1(7-36) t_{1/2} to be around 2 minutes [3], due to rapid degradation by the enzyme DPP-4. DPP-4 cleaves dipeptide segments from the *N*-terminus of polypeptides containing a proline or alanine in the 2 position. Known GLP-1 cleavage products of DPP-4 and NEP (Neutral Endopeptidase) [5] are reasonable starting points for modification to enhance the stability of GLP-1 analogs.

Exendin-4, a uniquely stable peptide with a considerably longer half-life in human plasma [4] is a good example of the benefits of the ability to withstand DPP-4 degradation as it contains a glycine in the 2 position of the *N*-terminus. While one could attempt to stabilize hGLP-1 through analogs to address the DPP-IV and NEP cleavage sites, our search for a stabilized GLP-1 mimetic began with the selection of a series of GLP-1 orthologs from various species. The thought being that nature has preselected acceptable modifications. Selected Orthologs (Table 1) were prepared and screened in a melanophore assay using hGLP-1 as a standard. Orthologs with confirmed potency were then screened in an overnight acute food intake reduction mouse model (6h and 15h time points) using Exendin-4 as a control. The overnight food intake reduction model was employed as a crude measure of stability, making the assumption that a longer duration of action would require greater stability in general.

It has been suggested that the *C*-terminal tail portion of Exendin-4 is partially responsible for its plasma stability. To investigate the importance of the tail region, analogs of G-2 modified human 3-36 GLP-1 were synthesized with the Exendin-4 tail (PSSGAPPPS-NH₂), Cane Toad tail (*Bufo Marinus*, PKKQRLS-NH₂), and African Clawed Frog tails (*X. Laevis* 1A and 1B, PSKEIIS-NH₂, PKKIRYS-NH₂ respectively). The analogs prepared with both the toad and frog tails outperformed the analog with the Exendin-4 tail at the 15h time point in the overnight food intake assay, suggesting enhanced peptide stability (Table 2).

A group of 5 GLP-1 orthologs with either desired potency or potential stability was chosen as the basis of a strategy in which each peptide was divided into 5 amino acid segments. The C-terminal tail portion was selected from *X. Laevis* 1b GLP-1 (PKKIRYS-NH₂). A set of 23 novel analogs were then constructed by combining a mixture of the 5 amino acid segments. The first 5 amino acids were maintained as HEGGT as protection from DPP-4. The peptides were screened in both the melanophore assay and overnight food intake assay. Chimeric peptides 12 and 21 were then selected and used in a two-fold strategy: 1) Improve potency of peptide 12 and maintain stability and 2) Improve stability of peptide 21 and maintain potency via single point mutations in the peptide sequence. Chimeric peptides 25, 26, and 27 were then scaled and run in a 14 day DIO rat model to determine the ED₅₀ of the optimized GLP-1 analogs.

While endogenous GLP-1 lacks the stability to be used as an effective therapy, the introduction of modifications to the peptide sequence gleaned from natural GLP-1 orthologs is a highly effective way to generate analogs of GLP-1 which have a superior stability profile. The incorporation of two 5 amino acid sections (11-15 and 21-25), the KKIRYS-NH₂ tail from *X. Laevis* and a single E21 modification yielded a GLP-1 peptide analog with apparent protection from NEP and DPP-4. The novel peptide 27 (Chimera-12, E21) demonstrated a pEC₅₀ of 10.5 and a duration of action greater than 15h in an acute DIO mouse model (Table 3). The improvements translate to a 0.21 mg/kg/day and a calculated weight loss at the ED₅₀ of 13.5% compared to the 0.08 mg/kg/day and 8.4% calculated weight loss demonstrated by Exendin-4 in the 14 day DIO rat model (Figure 1).

Table 1. Selected orthologs.

Sequence						Species
HAEGT	FTSDV	SSYLE	GQAAK	EFIAW	LVKGR	Human
HGEGT	FTSDL	SKQME	EEAVR	LFIEW	LKNGG	PSSGAPPPS-NH2
HSEGT	FTNDV	TRLLE	EKATS	EFIAW	LLKGL	Platypus
HGEGT	YTSDI	SSYLQ	DQAAQ	NFVAW	LKSGQ	F.Minnow
HGEGT	YTNDV	TEYLE	EKATK	AFIEW	LIK GK	X.Laeviss 1b

Table 2. Tail scanning.

Sequence	pEC ₅₀	6h	15h
HGEGTFTSDVSSYLEGQAAKEFIAWLVKGRPKKIRYS-NH2	9.9	-44	-20
HGEGTFTSDVSSYLEGQAAKEFIAWLVKGRPSKEIIS-NH2	10.4	-48	-21
HGEGTFTSDVSSYLEGQAAKEFIAWLVKGRPKKQRLS-NH2	10.3	-53	-22
HGEGTFTSDVSSYLEGQAAKEFIAWLVKGRPSSGAPPPS-NH2	10.7	-60	-11

Table 3. Chimeras.

ID		Single point changes in Ch12	pEC ₅₀	6h	15h
12	Ch-12	HGEGT FTSDL TEYLE EEAVR AFIEW LKNGG PKKIRYS-NH2	9.8	-97	-83
21	Ch-21	HGEGT YTNDV SKQLE EEAVR EFIAW LKSGQ PKKIRYS-NH2	11.4	-56	-30
25	Ch-12, S28	HGEGT FTSDL TEYLE EEAVR AFIEW LKSGG PKKIRYS-NH2	10.4	-74	-67
26	Ch-12, A24	HGEGT FTSDL TEYLE EEAVR AFIAW LKNGG PKKIRYS-NH2	10.0	-96	-79
27	Ch-12, E21	HGEGT FTSDL TEYLE EEAVR EFIEW LKNGG PKKIRYS-NH2	10.5	-94	-79

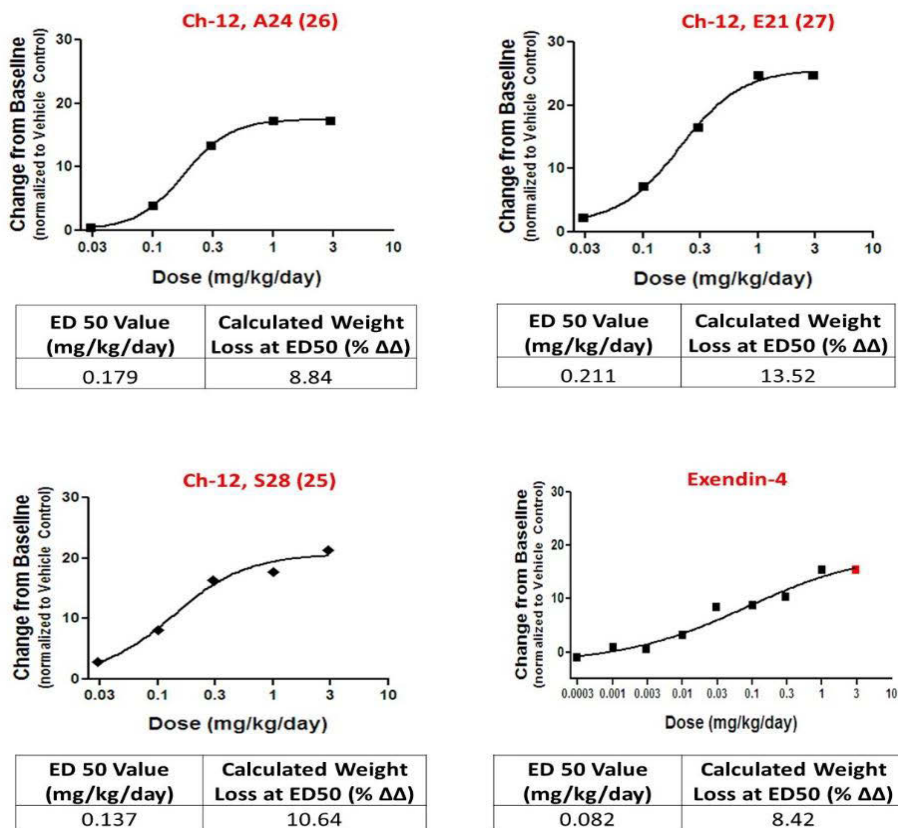


Fig. 1. In vivo results body weight / ED₅₀ data (DIO rat).

References

1. Danaei, G., Finucane, M.M., Lu, Y., Singh, G.M., Cowan, M.J., Paciorek, C.J., et al. *Lancet* **378**, 31-40 (2011), [http://dx.doi.org/10.1016/S0140-6736\(11\)60679-X](http://dx.doi.org/10.1016/S0140-6736(11)60679-X)
2. *Global status report on noncommunicable diseases 2010*. Geneva, World Health Organization, 2011 ISBN: 978 92 4 156422 9.
3. Baggio, L.L., Drucker, D.J., *Gastroenterology* **132**, 2131-2157 (2007), <http://dx.doi.org/doi:10.1053/j.gastro.2007.03.054>
4. Chen, J., Ling, Y., Wang, L., Fang, X., Li, L., Li, W. *Protein Pept. Lett.* **14**, 19-25 (2007), <http://dx.doi.org/10.2174/092986607779117272>
5. Hupe-Sodmann, K., McGregor, G.P., Bridenbaugh, R., Göke, R., Göke, B., Thole, H., Zimmermann, B., Voigt, K. *Regulatory Peptides* **58**, 149-156 (1995), [http://dx.doi.org/10.1016/0167-0115\(95\)00063-H](http://dx.doi.org/10.1016/0167-0115(95)00063-H)

Mono and Bis-Triazoles Incorporated into Chimeric AGRP-Melanocortin Peptide Template as Disulfide-Bridge Mimetics

Srinivasa R. Tala, Anamika Singh, Sathya M. Schnell, Katie Freeman,
and Carrie Haskell-Luevano

Department of Medicinal Chemistry, University of Minnesota, Minneapolis, MN, 55455, USA

Introduction

The melanocortin receptor (MCR) family consists of five receptor subtypes (MC1R-MC5R), endogenous agonists and antagonists. These receptors are involved in important biological pathways such as skin and hair pigmentation, food intake, energy homeostasis, erectile function, and exocrine glands function [1]. The MC3 and MC4 receptors are expressed in the brain and regulate weight and energy homeostasis as well as feeding behavior [2]. Our laboratory is involved in the design, synthesis and characterization of ligands to probe selectivity and potency at these functionally overlapping receptors [3-5]. The [1,2,3]-triazole-based bridge was previously utilized as a disulfide-bridge replacement in the sunflower trypsin inhibitor-1 peptide [6]. More recently, [1,2,3]-triazole-bridge was introduced into a synthetic melanocortin agonist, MT-II template as a type-I β -turn mimetic [7]. In our ongoing efforts to identify potent and selective lead compounds at melanocortin receptors, we designed and synthesized mono- and bis-triazoles incorporated chimeric AGRP-Melanocortin peptides. It was hypothesized that triazole-bridge may serve as a viable replacement for the disulfide-bridge in the AGRP-melanocortin chimeric peptide template.

Results and Discussion

This study utilized the chimeric peptide template Tyr-c[Cys-His-DPhe-Arg-Trp-Asn-Ala-Phe-Cys]-Tyr-NH₂ (AMW3-130), which we previously identified as a subnanomolar potent agonist for the melanocortin receptors [4,5]. This template is derived from the antagonist hAGRP(109-118) decapeptide sequence with amino acid residues His-Phe-Arg-Trp from the melanocortin agonists incorporated in the place of the Arg-Phe-Phe amino acids. It contains a single disulfide bridge between the two Cys side chains [4,5]. The cyclic peptide AMW3-130 (Table 1) is equipotent to α -MSH at the mMC1R and more potent than α -MSH at the mMC4R. Here, we designed 1,4-disubstituted and 1,5-disubstituted mono-[1,2,3]-triazole-bridged cyclic peptides **1**, and bis-[1,2,3]-triazole-bridged cyclic peptides **2** (Figure 1). Linear peptides were synthesized using microwave-assisted Fmoc-solid phase peptide methodology. Copper(I)-catalyzed intramolecular azide-alkyne cycloaddition was used to afford 1,4-disubstituted [1,2,3]-triazole-bridged cyclic peptides. Ruthenium(II)-catalyzed azide-alkyne cycloaddition was used to obtain 1,5-disubstituted [1,2,3]-triazole-bridged cyclic peptides. The

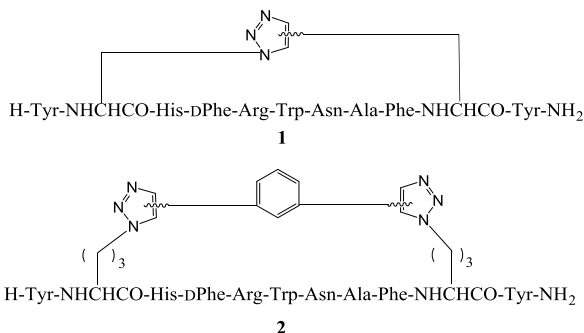


Fig. 1. The mono-[1,2,3]- and bis-[1,2,3]-triazole-bridged cyclic peptides.

purified peptides were at least 95% pure as determined by RP-HPLC in two diverse solvent systems and possessed the correct molecular weights as determined by mass spectrometry. The synthesized peptides were tested for agonist pharmacology using the cAMP-based AlphaScreen assay at the mouse melanocortin receptors (mMC3R and mMC4R) [8]. This study resulted in several compounds with interesting pharmacology (Table 1; Figure 2) at mMC3R and mMC4R. The 1,5-disubstituted [1,2,3]-triazole-bridged peptide SRT4-79-1cy showed increased agonist activity at the mMC3R and mMC4R compared to the linear compound SRT4-79-2-lin having the azido and alkynyl side chains.

The 1,5-disubstituted triazolyl peptide SRT4-79-1cy resulted in equipotent functional activity (within experimental error) at the mMC3R and 5-fold reduced potency at the mMC4R versus the disulfide bridged peptide AMW3-130 (Table 1). The 1,5-disubstituted triazolyl peptide (SRT4-79-1cy) was 4-fold more potent at the mMC3R, but retained equipotency at the mMC4R in comparison to the 1,4-disubstituted triazolyl peptide (SRT4-79-2cy). The bis-[1,2,3]-triazole-bridged peptides SRT4-154-1cy (1,5-disubstituted) and SRT4-154-2cy (1,4-disubstituted) (Figure 1) were designed to improve selectivity at the melanocortin receptors. However, incorporation of the bulky group resulted in reduced agonist potency at both mMC3 and mMC4 receptors (Table 1, Figure 2).

Table 1. Pharmacology of the peptides at the mouse MC3 and MC4 Receptors.

Compound	Agonist Potency (nM)	
	mMC3R	mMC4R
α -MSH	0.15	2.7
AMW3-130	2.2	0.43
SRT4-79-2-lin	51	29
SRT4-79-1cy	6.4	2.0
SRT4-79-2cy	28	6.0
SRT4-154-1cy	1944	971
SRT4-154-2cy	2744	539

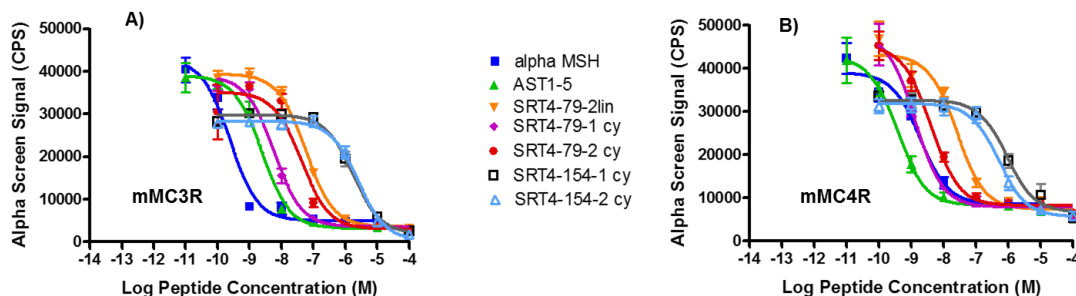


Fig. 2. Illustration of the pharmacological agonist dose-response curve for the synthesized peptides characterized in this study at the A) mMC3R and B) mMC4R.

In conclusion, we synthesized 1,4- and 1,5-disubstituted triazole-bridged macrocyclic peptides using Cu(I)-catalyzed and Ru(II)-catalyzed cycloadditions respectively. We demonstrated that the 1,2,3-triazole-bridge is a viable mimetic for disulfide-bridge replacement in melanocortin chimeric peptide template. These triazole-bridged peptides may serve as a probe for *in vivo* studies.

Acknowledgments

This study was supported by NIH Grant NIHRO1DK091906.

References

- Irani, B.J., et al. *Curr. Pharma. Design* **10**, 3443-3479 (2004), <http://dx.doi.org/10.2174/1381612043382891>
- Huszar, D., et al. *Cell* **88**, 131-141 (1997), [http://dx.doi.org/10.1016/S0092-8674\(00\)81865-6](http://dx.doi.org/10.1016/S0092-8674(00)81865-6)
- Xiang, Z., et al. *Biochemistry* **46**, 8273-8287 (2007), <http://dx.doi.org/10.1021/bi7007382>
- Wilczynski, A., et al. *J. Med. Chem.* **47**, 2194-2207 (2004), <http://dx.doi.org/10.1021/jm0303608>
- Singh, A., et al. *J. Med. Chem.* **54**, 1379-1390 (2011), <http://dx.doi.org/10.1021/jm101425m>
- Empting, M., et al. *Angew. Chem. Int. Ed.* **50**, 5207-5211 (2011), <http://dx.doi.org/10.1002/anie.201008142>
- Testa, C., et al. *J. Med. Chem.* **57**, 9424 (2014), <http://dx.doi.org/10.1021/jm501027w>
- Singh, A., et al. *ACS Med. Chem. Lett.* **6**, 568-578 (2015), <http://dx.doi.org/10.1021/acsmchemlett.5b00053>

Solid-Phase Synthesis of Aza-Lysine Peptide Analogue of Trypsin Substrate

Mariam Traoré and William D. Lubell

Département de Chimie, Université de Montréal, C.P. 6128, Succursale Centre-Ville,
Montréal, QC, H3C 3J7, Canada

Introduction

Lysine residues play critical roles in biological processes, such as protein post-translational modifications, enzymatic cleavage, and cell penetration. Constrained Lys residues may thus serve as tools for studying the structural requirements for such phenomenon. Azapeptides contain semicarbazide residues that may favor turn geometry, enhance molecular recognition and prevent protease degradation [1]. We have developed general methods for inserting aza-lysine residues and various side chain derivatives anywhere within a peptide sequence (Figure 1) [2-4].

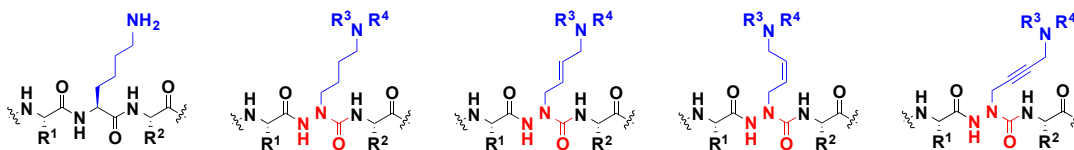
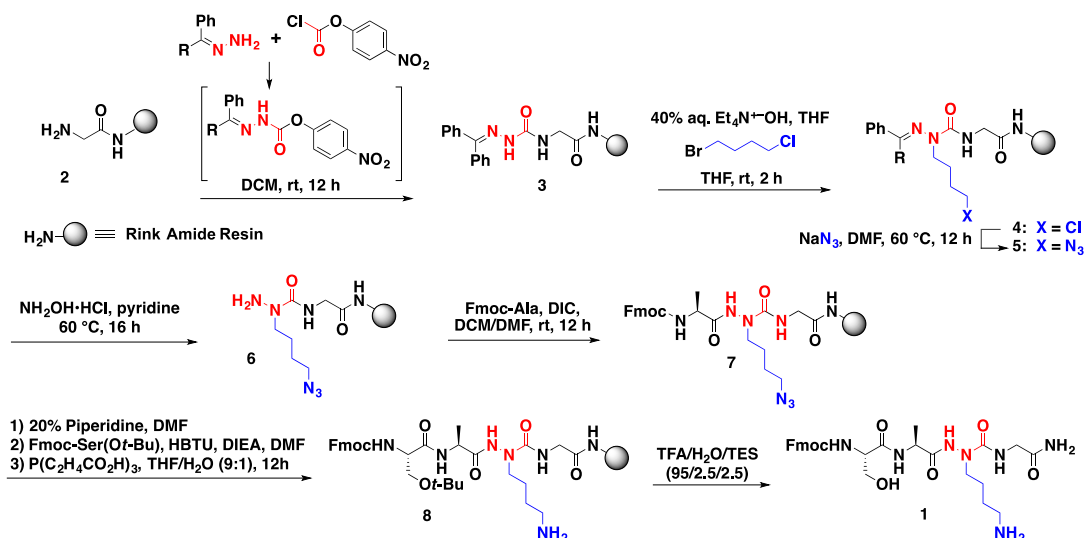


Fig. 1. To study the role of Lys residues (left) in peptides, aza-lysine residues possessing different amine and alkyl side chains have been prepared [2,3].

Results and Discussion

Trypsin is a serine protease that normally cleaves peptides at the carboxyl terminal of Lys and Arg residues. Trypsin is involved in cell growth, cell death, and immune defense. Imbalanced trypsin activity has been implicated in ovarian, colorectal and pancreatic cancers [5]. Azapeptides have previously been studied as tools for modulating trypsin activity. For example, the azatripeptide Boc-Lys-azaPhe-Leu was examined as a trypsin substrate [6]. In comparison with the parent peptide Boc-Lys-Phe-Leu, the azapeptide counterpart was digested more rapidly [6]. Complete cleavage to form the azaPhe-Leu and Phe-Leu dipeptides were respectively observed after 24 h and 48 h. Considering that semicarbazides may serve as better leaving groups, we plan to examine a trypsin substrate in which the Lys residue itself is replaced by azaLys.

The tetrapeptide Fmoc-Ser-Ala-Lys-Gly-NH₂ was studied, because of its relationship to the previously synthesized substrate Fmoc-Ser-Pro-Arg-Gly [7] that could be monitored effectively in trypsin digestion experiments. To study the influence of aza-residues on trypsin cleavage, we have now synthesized Fmoc-Ser-Ala-azaLys-Gly (**1**) on Rink amide resin (Scheme 1). Semicarbazone resin **3** was obtained after Fmoc deprotection from Rink amide resin using a solution of 20% piperidine in DMF. Acylation of the amine resin with 4-nitrophenyl 2-(diphenylmethylidene)carbazate, which was prepared from the reaction of benzophenone hydrazone with p-nitrophenylchloroformate, gave semicarbazone resin **3**, which was alkylated with 1-bromo-4-chlorobutane (320 mol %) employing tetraethylammonium hydroxide (300 mol %, of a 40% aqueous solution) as base in THF for 2 h at room temperature to provide the chloroalkyl semicarbazone **4**. Chloride displacement with sodium azide (600 mol %) in DMF at 60 °C for 12 h provided dipeptide resin **5**. The semicarbazone protecting group was removed using a 1.5 M solution of hydroxylamine hydrochloride in pyridine, and the resulting semicarbazide **6** was coupled to Fmoc-Ala by using diisopropylcarbodiimide (DIC) to provide azatripeptide **7**, which after Fmoc removal, was coupled to Fmoc-Ser(tBu) using HBTU (300 mol%) and DIEA (600 mol%). Azide was reduced with tris(2-carboxy)ethylphosphine (TCEP) (300 mol%) in THF/H₂O (9/1) for 12 h to provide the corresponding amine **8**. After cleavage from resin using TFA/H₂O/TES (9.5:0.25:0.25), tetrapeptide **1** (86% crude purity) was purified by HPLC on a C18-column and isolated in 4% overall yield and >98% purity: LCMS [20-50% MeOH (1% FA) in water (1% FA) over 12 min] RT = 7.7 min.



Scheme 1. Synthesis of trypsin substrate analogue, Aza-Lys peptide 1.

Efficient methods were developed for making azapeptides bearing aza-lysine residues, and were employed in the synthesis of an aza-analog of a trypsin substrate. This synthetic method and azapeptides bearing aza-amino acid residues, such as aza-Lys and aza-Arg, should find interesting applications for studying other peptides, particularly those involved in protein post-translational modifications and in cell-penetration processes.

Acknowledgments

This research was supported by the Natural Sciences and Engineering Research Council of Canada (NSERC), the Ministère du développement économique de l'innovation et de l'exportation du Québec (#878-2012, Traitement de la dégénérescence maculaire) and Amorchem.

References

- Proulx, C., Sabatino, D., Hopewell, R., Spiegel, J., Garcia-Ramos, Y., Lubell, W.D. *Future Med. Chem.* **3**, 1139-1164 (2011), <http://dx.doi.org/10.4155/fmc.11.74>
- Traore, M., Doan, N.-D., Lubell, W.D. *Org. Lett.* **16**, 3588-3591 (2014), <http://dx.doi.org/10.1021/ol501586v>
- Zhang, J., Proulx, C., Tomberg, A., Lubell, W.D. *Org. Lett.* **16**, 298-301 (2014), <http://dx.doi.org/10.1021/ol403297v>
- Doan, N.-D., Zhang, J., Traore, M., Kamdem, W., Lubell, W.D. *J. Pept. Sci.* **21**, 387-391 (2015), <http://dx.doi.org/10.1002/psc.2711>
- Goldberg, D.M. *Clin. Chim. Acta* **291**, 201-221 (2000), [http://dx.doi.org/10.1016/S0009-8981\(99\)00229-6](http://dx.doi.org/10.1016/S0009-8981(99)00229-6)
- Dutta, A.S., Giles, M.B. *J. Chem. Soc. Perkin* **1**, 244-248 (1976), <http://dx.doi.org/10.1039/P19760000244>
- Adjemian, J., Anne, A., Cauet, G., Demaille, C. *Langmuir* **26**, 10347-10356 (2010), <http://dx.doi.org/10.1021/la100397g>

In Vitro Evaluation of New, Potent, and Selective V₂ Receptor Agonists

Kazimierz Wiśniewski, Hiroe Tariga, Glenn Croston, Diane M. Hargrove,
Pierre J-M. Rivière, Gebhard Neyer, and Claudio D. Schteingart

Ferring Research Institute, San Diego, CA, 92121, USA

Introduction

The vasopressin analogue desmopressin (dDAVP, **1**) is a potent V₂ receptor agonist that also activates the related V_{1b} receptor [1]. dDAVP is approved in many countries for the treatment of diabetes insipidus, primary nocturnal enuresis, nocturia, and coagulation disorders including hemophilia A and von Willebrand's disease.

In search of novel, potent, selective and pharmacologically useful peptidic V₂R agonists, we synthesized a series of C-terminally truncated [Val⁴]dDAVP (**2**) [2] analogs modified in positions 2, 3, 7 and/or at the disulfide bridge. The peptides were evaluated for *in vitro* potency at the human V₂ receptor (hV₂R) and selectivity versus related receptors (hV_{1a}R, hV_{1b}R, hOTR). Here we present comprehensive *in vitro* data for the new compounds and describe synthetic methods used to prepare the analogues.

Results and Discussion

Analogues **3-24** (Table 1) were synthesized by a combination of solid and solution phase chemistry. The linear precursors of compounds **3-13**, **22** were assembled on H-Aaa-O-2-ClTrt resins by standard Fmoc chemistry using DIC/HOBt mediated couplings. The carba thioether modifications of the disulfide bridge (X or Y = CH₂, Figure 1) were introduced to the peptide sequence by coupling Fmoc-

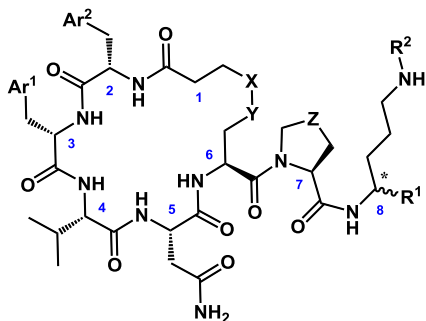


Fig. 1. General structure of new analogues **3-24**. Sequence positions numbered at α -carbons.

Cys((CH₂)₃-COOtBu)-OH or Fmoc-Hcy((CH₂)₂-COOtBu)-OH [3]. Fully protected peptide C-terminal acids were cleaved with 30% HFIP/DCM. For compounds **3-10** the carboxylic group was reduced to the hydroxymethyl group using mixed anhydride method [4]. For compounds **11-13** the C-terminal acids were coupled with agmatine and for analogue **22** the linear fragment was coupled with H-D-Arg(Pbf)-NEt₂. The protecting groups were removed with the TFA/TIS/H₂O 95/2.5/2.5 cocktail and the linear peptides were cyclized in DMF using HBTU/DIPEA method. The linear precursor of peptide **14** was assembled on 1,4-diaminobutane-2-ClTrt resin. After cleavage from the resin the C-terminal amino function was temporarily protected with the TFA resistant Z(2-Cl) group. The peptide was deprotected and cyclized as described above. The Z(2-Cl) group was removed with TMSBr/thioanisole/TFA (1/1/6) [5]. The linear precursors of compounds **15-21**, **23** and **24** were synthesized on BAL resin which was

reductively alkylated with an appropriate primary amine prior to the peptide assembly. The peptides were cleaved with concomitant side chain protecting group removal using the TFA cocktail and cyclized as described above. All peptides were purified by preparative HPLC and lyophilized.

The pharmacological profile of **1** was determined in *in vitro* assays and was consistent with the literature data [1]. **1** was particularly selective vs. the V_{1a}R (>1000-fold) presumably due to the desamino modification [6]. The Val⁴ analogue of **1** ([Val⁴]dDAVP, **2**) has been reported to be more potent and selective than **1** in rat *in vivo* models [7]. This profile is consistent with our *in vitro* studies at the human receptors (Table 1). Manning, et al. investigated the impact of the C-terminal Gly residue removal on the antidiuretic activity of **1**, **2** and related peptides in rats [7]. The corresponding desglycine analogues retained 10 - 50% initial antidiuretic activity, suggesting C-terminal truncation could be a good strategy to design novel V₂R agonists.

Table 1. Structure and in vitro pharmacological profile of analogs **1-24**.

Analog	Structure ^a		Config of *C	hV ₂ R		Selectivity ^b vs. receptor		
	Ar ¹	R ¹		EC ₅₀ (nM)	E _{max} (%)	hV _{1a} R	hV _{1b} R	hOTR
1	dDAVP			0.20	100	>5000 ^c	55	550
2	[Val ⁴]dDAVP			0.05	89	>20000 ^c	480	7000
3	Ph(4-OH)	CH ₂ OH	S	0.10	92	>10000 ^c	520	2300
4	Ph(4-OH)	CH ₂ OH	R	0.08	93	>12000 ^c	720	2000
5	Ph(4-Cl)	CH ₂ OH	R	0.10	102	>10000 ^c	1400	>100000 ^c
6	Ph(4-Cl)	CH ₂ OH	R	0.08	115	>12000 ^c	800	>120000 ^c
7	Ph(4-Cl)	CH ₂ OH	S	0.14	96	>7100 ^c	2700	>71000 ^c
8	Ph(4-Cl)	CH ₂ OH	R	0.35	102	>2800 ^c	620	>28000 ^c
9	Ph(4-Me)	CH ₂ OH	R	0.39	104	>25000 ^c	2000	>25000 ^c
10	Ph(4-Et)	CH ₂ OH	S	0.35	110	>2800 ^c	>28000 ^c	>28000 ^c
11	Ph(4-Cl)	H	NA	0.31	89	>3200 ^c	450	>32000 ^c
12	Ph(4-Cl)	H	NA	0.07	104	>140000 ^c	1500	>140000 ^c
13	Ph(4-Cl)	H	NA	0.12	106	>83000 ^c	1100	>83000 ^c
14	Ph(4-OH)	H	NA	0.19	94	>5200 ^c	>52000 ^c	3400 ^c
15	Ph(4-Cl)	C(=O)NHMe	R	0.27	106	>3700 ^c	1200	>37000 ^c
16	Ph(4-Cl)	C(=O)NHEt	R	0.29	92	>3400 ^c	580	>34000 ^c
17	Ph(4-Cl)	C(=O)NHPr	R	0.33	92	>3000 ^c	750	>30000 ^c
18	Ph(4-Cl)	C(=O)NHcPr	R	0.23	86	>4300 ^c	2000	>43000 ^c
19	Ph(4-Cl)	C(=O)NH _i Pr	R	0.45	81	>2200 ^c	1200	>22000 ^c
20	Ph(4-Cl)	C(=O)NHBu	R	0.26	98	>38000 ^c	730	>38000 ^c
21	Ph(4-Cl)	C(=O)NH _i Bu	R	0.22	100	>45000 ^c	950	>45000 ^c
22	Ph(4-Cl)	C(=O)NEt ₂	R	0.25	102	>40000 ^c	2100	>40000 ^c
23	Ph(4-Cl)	C(=O)NHBzl	R	0.19	100	>52000 ^c	780	>52000 ^c
24	Ph(4-Cl)	C(=O)NHEt	R	0.10	103	>100000 ^c	1600	>100000 ^c

^a XY=CH₂S for analogues **3, 5, 7-24** and SCH₂ for **4, 6**; Ar²=2-thienyl for **3-7, 9, 10, 12-24** and 4-fluorophenyl for **8, 11**; R²=C(=NH)NH₂ for all new compounds except for **14** where R²=H; ^b Ratio EC₅₀(receptor)/EC₅₀(hV₂R); ^c No agonism up to 1 μM or 10 μM, the highest concentration tested.

First, the C-terminal group R¹ (–C(=O)-Gly-NH₂) in compound **2** was replaced with the hydroxymethyl function and the analogues were also modified in position 2, 3 and at the disulfide

bridge (compounds **3-10**). The disulfide bridge modifications (X, Y) as well as the configuration of the ¹³C chiral carbon had very little impact on potency and selectivity profiles. Compounds in this series were potent hV₂R agonists with **9** and **10** (Ar¹ = 4-alkylphenyl) being about 2-fold less potent at the V₂R than **1**. Analogues **3-10** displayed improved selectivity versus both the hV_{1b}R (all partial agonists) and hOTR except for the Tyr² compounds **3** and **4** (Ar¹ = 4-hydroxyphenyl) that were less selective vs. hOTR than **2**. Peptide **8** where Ar² = 4-fluorophenyl was less potent as an hV₂R agonist than its 2-thienyl counterpart **5**.

Next, we investigated if the substituent R¹ is actually required to preserve high agonistic potency at the hV₂R (compounds **11-14**). Compound **12** (R¹ = H, Ar¹ = 4-chlorophenyl, Ar² = 2-thienyl) was found to be very potent and considerably more selective than **2**. The Thz⁷ modification (Z = S) was found to be neutral in this series as analogues **12** and **13** had very similar pharmacological profiles. In addition we demonstrated that the guanidino function (R² = -C(=NH)NH₂) does not appear to be essential to preserve hV₂R agonism (compound **14**, R² = H). Lastly, we explored if the C-terminal glycine amide could be replaced with alkyl groups (R¹ = -C(=O)-NR³R⁴; compounds **15-24**). Based on the initial results the cyclic part of the new analogues was fixed with the consensus structure (Ar¹ = 4-chlorophenyl, Ar² = 2-thienyl, X = CH₂, Y = S). Somewhat surprisingly a variety of R³, R⁴ substituents were well tolerated and rather shallow SAR was observed. The isopropyl compound **19** (R³ = iPr, R⁴ = H) was the least potent V₂R agonist in this subset. The Thz⁷ modification was advantageous as exemplified by a 3-fold increase in potency for peptide **24** (Z = S) vs. **16** (Z = CH₂). Double alkylation, e.g. compound **22** (R³ = R⁴ = Et), was also well tolerated while maintaining excellent selectivity vs. the related receptors.

In conclusion, a series of novel C-terminally truncated dDAVP analogues with improved *in vitro* pharmacological profile has been identified. The novel compounds retain the potent V₂ receptor agonism activity of dDAVP, **1**. Compounds **5-13** and **15-24** display substantially improved selectivities vs. hV_{1a}R, hV_{1b}R and hOTR as compared to **1** and **2**.

References

1. Saito, M., Tahara, A., Sugimoto, T. *Biochem. Pharm.* **53**, 1711-1717 (1997), [http://dx.doi.org/10.1016/s0006-2952\(97\)00070-1](http://dx.doi.org/10.1016/s0006-2952(97)00070-1)
2. Sawyer, W.H., et al. *Endocrinology* **94**, 1106-1115 (1974), <http://dx.doi.org/10.1210/endo-94-4-1106>
3. Wiśniewski, K., Stalewski, J., and Jiang, G. PCT WO2003072597 (2003).
4. Rodriguez, M., et al. *Tetrahedron Lett.* **32**, 923-926 (1991), [http://dx.doi.org/10.1016/S0040-4039\(00\)92121-X](http://dx.doi.org/10.1016/S0040-4039(00)92121-X)
5. Fujii, N., et al. *Chem. Pharm. Bull.* **35**, 3880-3883 (1987).
6. Wiśniewski, K., et al. *J. Med. Chem.* **54**, 4388-4398 (2011), <http://dx.doi.org/10.1021/jm200278m>
7. Manning, M., et al. *Peptide Chemistry* 585-590 (1988).

Novel Macrocyclic Peptides Active at Human Melanocortin Receptors: A Preliminary SAR Study

A.M. Yousif¹, M. Cai², F. Merlino¹, P. Grieco¹, and V.J. Hruby²

¹Dept. of Pharmacy, University of Naples "Federico II", Naples, Italy;

²Dept. of Chemistry, University of Arizona, Tucson, AZ, USA

Introduction

The melanocortins are a group of structurally related peptides derived from proopiomelanocortin (POMC), their name from their melanotropic and corticotropic activities and are comprised of adrenocorticotrophic hormone (ACTH), α -melanocyte stimulating hormone (α -MSH), β -MSH, and γ -MSH. The effects of melanocortins are mediated by activation of a family of melanocortin receptors (MCRs). Five MCR (MC1R, MC2R, MC3R, MC4R, and MC5R) (Figure 2) genes have been cloned and the receptors pharmacologically characterized [1]. All the melanocortin ligands conserve the core sequence, Trp-Arg-Phe-His. Previous SAR study on melanotropins, in particular on α -MSH, led to the small cyclic peptide MT-II, a potent and non-selective agonist at MCRs.

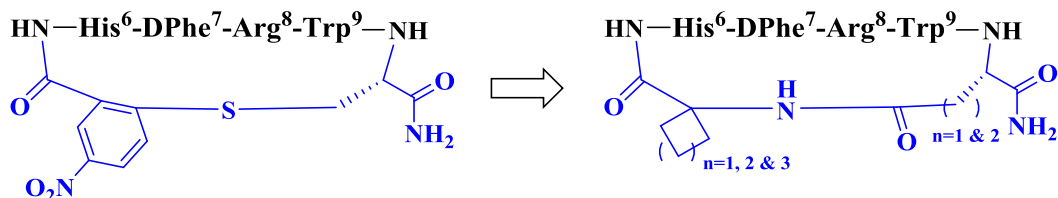


Fig. 1. New cyclic lactam peptide analogues of α -MSH containing α,α -disubstituted amino acids.

Similarly, the lactam analogue, SHU-9119, is an antagonist at MCRs 3 and 4 receptors. Subsequently, we developed a series of novel 20-membered macrocycles formally derived from MTII and SHU9119, containing an alkylthioaryl bridge. Based on these considerations, herein we synthesized a new cyclic lactam peptide analogues of α -MSH containing α,α -disubstituted amino acids to provide further SAR study.

Design, Synthesis and Peptide Library

The cyclization approach by disulphide bond, and lactam on melanocortins led to interesting results. Previously, our research group has developed melanocortin peptide analogues in which 2-fluoro-5-nitro benzoic acid was used for the macrocyclization reaction, side chain to tail cyclization (Figure 1) [2]. Among these compounds, PG10N, represents a potent analogue which has different conformation compared with MTII and shown to be selective for the MC5R. In the present study, we synthesized a new 18 lactam macrocyclic analogues of α -MSH by the introduction of α,α -disubstituted amino acids such as Fmoc-1-amino-1-cyclobutane carboxylic acid, Fmoc-1-amino-1-cyclopentane carboxylic acid, and Fmoc-1-amino-1-cyclohexane carboxylic acid. Furthermore, we investigated the role of the ring dimension on the biological activity by the replacement of Asp residue with Glu turning from 19-membered macrocyclic ring to 20-membered ring (Table 1).

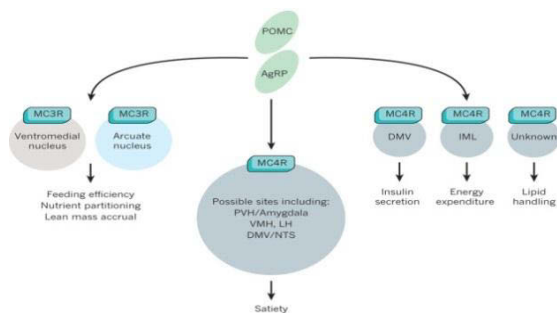


Fig. 2. Melanocortin receptors and their functions.

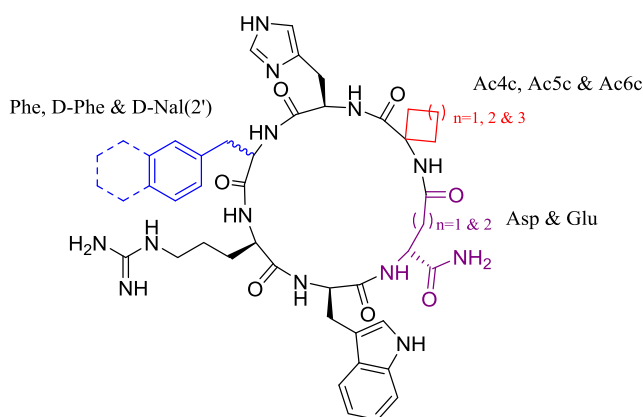


Table 1. Macrocyclic peptide library.

Peptide	Sequence
1	[Ac4c-His-Phe-Arg-Trp-Asp]-NH ₂
2	[Ac5c-His-Phe-Arg-Trp-Asp]-NH ₂
3	[Ac6c-His-Phe-Arg-Trp-Asp]-NH ₂
4	[Ac4c-His-Nal(2')-Arg-Trp-Asp]-NH ₂
5	[Ac5c-His-Nal(2')-Arg-Trp-Asp]-NH ₂
6	[Ac6c-His-Nal(2')-Arg-Trp-Asp]-NH ₂
7	[Ac4c-His-D-Phe-Arg-Trp-Asp]-NH ₂
8	[Ac5c-His-D-Phe-Arg-Trp-Asp]-NH ₂
9	[Ac6c-His-D-Phe-Arg-Trp-Asp]-NH ₂
10	[Ac4c-His-D-Nal(2')-Arg-Trp-Asp]-NH ₂
11	[Ac5c-His-D-Nal(2')-Arg-Trp-Asp]-NH ₂
12	[Ac6c-His-D-Nal(2')-Arg-Trp-Asp]-NH ₂
13	[Ac4c-His-D-Phe-Arg-Trp-Glu]-NH ₂
14	[Ac5c-His-D-Phe-Arg-Trp-Glu]-NH ₂
15	[Ac6c-His-D-Phe-Arg-Trp-Glu]-NH ₂
16	[Ac4c-His-D-Nal(2')-Arg-Trp-Glu]-NH ₂
17	[Ac5c-His-D-Nal(2')-Arg-Trp-Glu]-NH ₂
18	[Ac6c-His-D-Nal(2')-Arg-Trp-Glu]-NH ₂

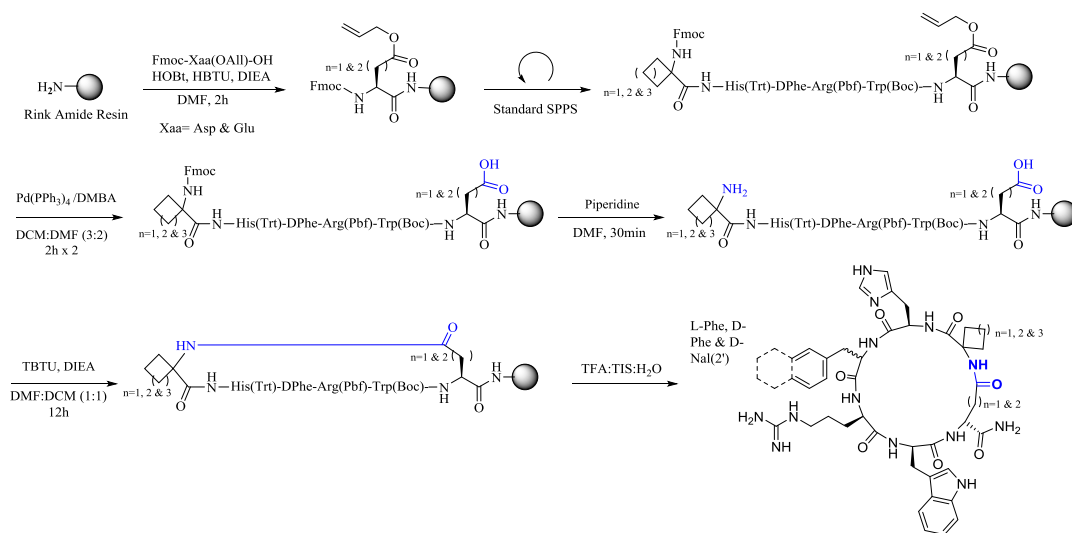
acids instead of 2-fluoro-5-nitro benzoic acid could be determinant to get additional selective compounds at hMCRs. In this study, we evaluated the role of ring dimension in binding activity, turning from 19- to 20- membered ring dimension. In fact, the preliminary biological data showed that the ring dimension could have a key role on biological activity also in these series of compounds.

The synthesis was accomplished using Fmoc chemistry in solid phase. The first coupling was carried out using Fmoc-Xaa(OAll)-OH (Xaa: Asp or Glu), activating groups, in presence of Hunig's base in DMF for 2 hours. After the elongation of peptide on resin by standard solid phase synthesis. The allyl protecting group was removed by treating the resin with tetrakis(triphenylphosphine)-palladium (0) and *N,N'*-dimethylbarbituric acid in DCM/DMF under nitrogen atmosphere for 2 hours and the procedure was repeat again. The side chain to tail cyclization was carried out directly on solid support using HBTU as and Hunig's base for 12 hours. The peptide was released using a cocktail of TFA/TIS/H₂O (95:2.5:2.5, v/v/v) for 3 hours. All crude peptides were purified by RP-HPLC and the final products were characterized by LC-MS (Scheme 1).

Results and Discussion

In this study we prepared a number of cyclic melanotropin analogues in which an α,α -disubstituted amino acids was used for the macrocyclization reaction. These compounds conserve the core sequence His-Phe-Arg-Trp which is responsible for the biological activities. All synthesized compounds were evaluated for their binding affinities at human melanocortin receptors in competitive binding assays for their potency in cAMP assays employing the HEK293 cells expressing the receptors. The results are reported in Table 2.

In conclusion, we have designed and synthesized new macrocyclic melanocortin ligands. The introduction of an α,α -disubstituted amino



Scheme 1. The synthesis was accomplished using Fmoc chemistry in solid phase.

Table 2. Biological results.

	hMC1R			hMC3R			hMC4R			hMC5R		
	Binding	cAMP		Binding	cAMP		Binding	cAMP		Binding	cAMP	
	IC ₅₀ (nM)	EC ₅₀ (nM)	Act %	IC ₅₀ (nM)	EC ₅₀ (nM)	Act %	IC ₅₀ (nM)	EC ₅₀ (nM)	Act %	IC ₅₀ (nM)	EC ₅₀ (nM)	Act %
1	39.12	370	>100	NB	>10000	>100	2380	217	>100	2.21	0.1	30
2	5.71	43.16	16.8	NB	NA	-20.9	1454	NA	30	1.93	<0.01	14.5
3	1748	60.89	28.5	NB	NA	12.5	<0.01	NA	35.1	17.43	3.02	58
4	22.89	0.4632	24	NB	NA	-21.7	>10000	NA	43.3	1.82	<0.01	65.9
5	1.063	226.1	80	919.9	NA	-14.8	39.1	NA	13.9	NB	<0.01	72.5
6	>10000	1.223	33.1	NB	NA	-20.6	2584	3977	19.6	0.54	0.55	82.9
8	4906±400	17	100	279	5.1	100	1902	311	100	NB	NA	0
9	2744±104	12	100	234	23.4	100	836	122	96	NB	NA	0
10	1256±97	25	100	100±6	3.4	50	783	331	70	>10000	1536	100
11	3303±297	13	100	61	3.3	68	590	0.52	67	1374	214	100
12	1583±174	11	100	23	12.5	91	449	3.4	67	>10000	182	100
14	1036±63	3.9	100	1173±148	0.93	100	1274	372	100	NB	NA	0
17	3140±414	3.4	100	24±3	8.5	82	1126	669	74	>10000	47	100

References

- Grieco, P., Han, G., Weinberg, D., Van der Ploeg, L.H., Hruby, V.J. *Biochem. Biophys. Res. Commun.* **292**, 1075-1080 (2002), <http://dx.doi.org/10.1006/bbrc.2002.6739>
- Grieco, P., Cai, M., Liu, L., Mayorov, A., Chandler, K., Trivedi, D., Lin, G., Campiglia, P., Novellino, E., Hruby, V.J. *J. Med. Chem.* **51**, 2701-2707 (2008), <http://dx.doi.org/10.1021/jm701181n>

A Study on the Structural Stability of the Peptide 2.0₅-Helix by Infrared Absorption Spectroscopy

M. De Zotti¹, B. Di Napoli², C. Mazzuca², A. Palleschi², G. M. L. Messina³,
G. Marletta³, and F. Formaggio¹

¹Department of Chemistry, University of Padova, Padova, I-35131, Italy; ²Department of Sciences and Chemical Technologies, University of Rome "Tor Vergata", Rome, I-00133, Italy; ³Laboratory for Molecular Surfaces and Nanotechnology, Department of Chemical Sciences, University of Catania, Catania, I-95125, Italy

Introduction

C^α-Tetrasubstituted residues are known to induce the onset of helical structures in peptides with sequences even as short as 4-5 residues [1]. Due to their rigidity, such conformationally-constrained oligopeptides are often employed as spacers [2], or as simple models to study the stability and behavior of biologically-relevant helical structures [3]. C^{α,α}-diethylglycine (Deg) is one of such residues. Its homo-peptides were found to adopt a rather unusual helical conformation, the 2.0₅-helix, also known as fully-extended conformation [4]. The 2.0₅-helix, characterized by ϕ and ψ backbone torsion angles of 180°, is indeed the longest conformation a peptide of a given number of residues can adopt. Recently, we found that Deg homo-peptides are also able to switch their conformation between 2.0₅- and 3₁₀-helices in response to a change in solvent polarity [5]. Here, we present preliminary results obtained in our FT-IR study on the stability and behavior of the (Deg)_n 2.0₅-helix in the solid state. We found that the conformation adopted by our model peptide **Deg₅** [Tfa-(Deg)₅-OtBu (Tfa, trifluoroacetyl)] in CDCl₃ solution is not maintained when it is deposited as a film, and that we can govern the conformational equilibrium by applying an electric field (EF) during the deposition process [6].

Results and Discussion

To study the influence of both the physical state and an applied electric field (EF=7.5 V/m) on the 3D-structure adopted by **Deg₅**, we performed FTIR experiments under different experimental conditions. We chose to employ this spectroscopy because peptides have several IR active vibrational modes, some of which (amide I at 1700-1600 cm⁻¹ and amide II at 1600-1480 cm⁻¹) are sensitive to the variation of secondary structure [7].

Experimentally, the FTIR spectrum of **Deg₅** in CDCl₃ solution at 0.1mM peptide concentration has been obtained in the transmission mode using a NaCl cell, while that of **Deg₅** as a film has been recorded using an ATR apparatus equipped with a ZnSe cell. In the latter case, CDCl₃ peptide solutions were deposited on the cell, and the solvent allowed to evaporate in the presence or absence of an external EF.

Analysis of the amide I and II regions of the **Deg₅** FTIR spectrum as a film was performed and compared with the spectrum of the same peptide in CDCl₃ solution. In solution, the number, position, and relative intensities of the absorption bands in the two spectral regions are diagnostic of the presence of a fully-extended conformation [8,9]. One clear proof for the onset of a 2.0₅-helix is indeed the presence in the amide I region of the FTIR spectrum of two, strong peaks near 1650 and 1670 cm⁻¹, as shown in Figure 1-I (dashed line).

For the peptide film, however, the FTIR spectrum in the amide I region is clearly different (Figure 1-I). The peptide changes its most populated conformation, assuming a mainly $\alpha/3_{10}$ -helical structure (a strong absorption band for $\alpha/3_{10}$ -helices is usually seen in the 1655-1670 cm⁻¹ range). The minor component at about 1680 cm⁻¹ may be assigned to type-III β -turn and/or non H-bonded carbonyl groups [10,11]. An inspection of the intensities of the amide II bands (Figure 1-II), in comparison with those in the amide I region, confirms this conclusion, as the strong band near 1490 cm⁻¹, expected for a fully-extended conformation, is much less evident in the peptide film.

When an external electric field is applied during the process of film formation, the FTIR spectrum of **Deg₅** seems to indicate a somewhat increased helical content. This conclusion stems from a decrease in the intensity of the band centered at about 1680 cm⁻¹, attributed to the 2.0₅-helix, and a concomitant

shift of the band in the amide II region to higher wavenumbers with respect to 1500 cm^{-1} , confirming the reduced presence of fully-extended structures.

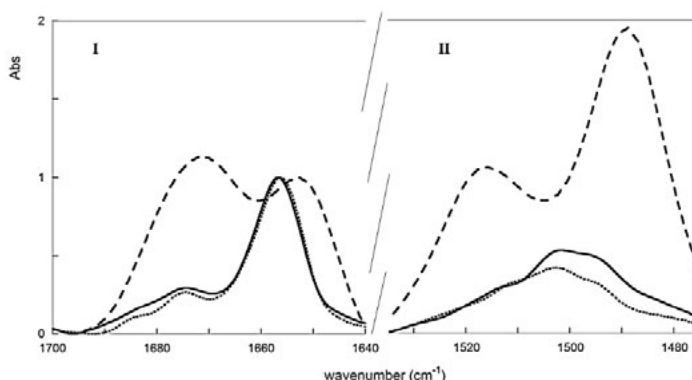


Fig. 1. Amide I (panel I) and Amide II (panel II) regions of the FTIR normalized spectra of *Deg5* (0.1mM) in CDCl_3 solution (---) and in film obtained by a CDCl_3 peptide solution in the absence (—) and presence (---) of an external electric field. Curves are normalized to the intensity at 1656 cm^{-1} for film, and at 1653 cm^{-1} for solution spectra.

Acknowledgments

We gratefully acknowledge MIUR for financial support (FIRB project RBF13RQXM: Peptide-based Conformational Switches: Design, Synthesis, and Applications).

References

1. Toniolo, C., Crisma, M., Formaggio, F., Peggion, C. *Biopolymers (Pept. Sci.)* **60**, 396-419 (2001), [http://dx.doi.org/10.1002/1097-0282\(2001\)60:6<396::AID-BIP10184>3.0.CO;2-7](http://dx.doi.org/10.1002/1097-0282(2001)60:6<396::AID-BIP10184>3.0.CO;2-7)
2. Toniolo, C., Crisma, M., Formaggio, F., Peggion, C., Broxterman, Q.B., Kaptein, B. *Biopolymers (Pept. Sci.)* **76**, 162-176 (2004), <http://dx.doi.org/10.1002/bip.10575>
3. Parthasarathy, R., Chaturvedi, S., Kuantee, G. *Prog. Biophys. Mol. Bio.* **64**, 1-54 (1995), [http://dx.doi.org/10.1016/0079-6107\(95\)00009-7](http://dx.doi.org/10.1016/0079-6107(95)00009-7)
4. Peggion, C., Moretto, A., Formaggio, F., Crisma, M., Toniolo, C. *Biopolymers (Pept. Sci.)* **100**, 621-636 (2013), <http://dx.doi.org/10.1002/bip.22267>
5. Peggion, C., Crisma, M., Toniolo, C., Formaggio, F. *Tetrahedron* **68**, 4429-4433 (2012), <http://dx.doi.org/10.1016/j.tet.2011.12.087>
6. Toschi, F., Lugli, F., Biscarini, F., Zerbetto, F. *J. Phys. Chem. B* **113**, 369-376 (2009), <http://dx.doi.org/10.1021/ct1001335>
7. Krimm, S., Bandekar, J. *Adv. Protein Chem.* **38**, 181-364 (1986), [http://dx.doi.org/10.1016/S0065-3233\(08\)60528-8](http://dx.doi.org/10.1016/S0065-3233(08)60528-8)
8. Formaggio, F., Crisma, M., Ballano, G., Peggion, C., Venanzi, M., Toniolo, C. *Org. Biomol. Chem.* **10**, 2413-2421 (2012), <http://dx.doi.org/10.1039/c2ob06863j>
9. Maekawa, H., Ballano, G., Toniolo, C. and Ge, N.-H. *J. Phys. Chem. B* **115**, 5168-5182 (2011), <http://dx.doi.org/10.1021/jp105527n>
10. Pispisa, B., Palleschi, A., Stella, L., Venanzi, M., Mazzuca, C., Formaggio, F., Toniolo, C., Broxterman, Q.B. *J. Phys. Chem. B* **106**, 5733-5738 (2002), <http://dx.doi.org/10.1021/jp012599a>
11. Kennedy, D.F., Crisma, M., Toniolo, C., Chapman, D. *Biochemistry* **30**, 6541-6548 (1991), <http://dx.doi.org/10.1021/bi00240a026>

Mimicking the Binding Sites of Wnt Proteins: Rational Design of Wnt/Fzd-Signaling Modulators

Ana I. Fernández-Llamazares¹, Kevin C. M. Hermans², Peter Timmerman¹,
and W. Matthijs Blankesteyn²

¹Pepscan Therapeutics, Zuidersluisweg 2, 8243 RC, Lelystad; ²Dept. of Pharmacology, University of Maastricht, Universiteitssingel 50, 6229 ER, Maastricht, The Netherlands

Introduction

The interaction between Wnt proteins and Frizzled (Fzd) receptors is a key event that activates all the Wnt signaling pathways [1]. Aberrant regulation of Wnt signaling is linked to a variety of diseases, and compounds that interfere with Wnt/Fzd interactions are potentially useful for their diagnosis and therapeutics.

The aim of the present work was to develop peptides that bind to Fzds, and are able to modulate Wnt/Fzd-signaling. In order to develop such compounds, we sought to mimic the Fzd-binding sites of Wnt proteins. Although there is limited structural information on the features of Wnt/Fzd interactions, it is likely that all Wnt proteins interact with Fzds through their β 2- and β 3-loop regions [2]. These regions are highly conserved among the different Wnts, and their secondary structure is stabilized by a characteristic pattern of intraloop SS-bonds.

Herein we report the design, synthesis and biological evaluation of a library of peptide mimics for the β 2- and β 3-loop regions of Wnt3a and Wnt5a.

Results and Discussion

Peptide design: We designed a library of peptides derived from the sequences of Wnt3a and Wnt5a in their β 2- and β 3-loop regions (Tables 1 and 2). The designed mimics have the same pattern of SS-bonds as the natural Wnt ligands, and are further conformationally constrained via cyclization, for which two additional Cys were introduced at the N- and C-terminus of the Wnt-derived sequence and connected via a bivalent CLIPS scaffold (Figure 1). The variables in our library are the length of the peptide sequence, and the position of the two additional Cys. For some of the designed mimics, we also synthesized: i. linear analogs (Cys replaced by SMe-Cys), ii. scrambled analogs, iii. analogs with the N- and C-terminal Cys connected via an SS-bond, iv. mutants lacking SS-bonds (Cys replaced by Ala). Data not shown.

Peptide synthesis: We synthesized the peptides by a non-regioselective approach, employing AcM-protection for those Cys to be connected via an SS-bond. For every target peptide, we prepared the corresponding linear precursor on the Rink Amide resin by automated solid-phase peptide synthesis, using standard Fmoc/^tBu chemistry. After cleavage and purification, we cyclized the peptide via Cys-attachment onto the bivalent CLIPS scaffold, and purified the target product. Next, we removed the AcM groups under oxidative conditions (I₂). In this last synthetic step, all the SS-bonds of the peptide are formed concomitantly, which can afford several SS-bond isomers of unknown SS-bond pattern. For every target peptide, we isolated the SS-bond isomeric products formed, and we tested them separately.

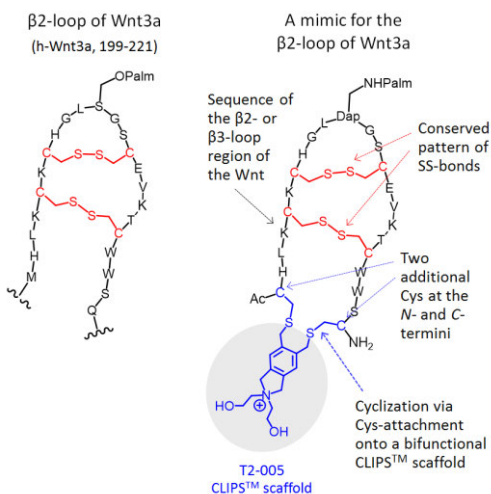


Fig. 1. Schematic representation of a Wnt-mimicking peptide.

Table 1. Wnt3a mimics designed, synthesized and tested.

Peptide	Sequence
h-Wnt3a, 199-221	¹⁹⁹ MHLK ^{C^B} K ^{C^A} HGLS(OPalm)GS ^{C^A} EVKT ^{C^B} WWSQ ²²¹
WNT3A-B2-001	Ac- ^{C^T} HLK ^{C^K} CHGLDap(NPalm)GS ^{C^E} EVKT ^{C^W} WS ^{C^T} -NH ₂
WNT3A-B2-002	Ac- ^{C^T} LK ^{C^K} CHGLDap(NPalm)GS ^{C^E} EVKT ^{C^W} W ^{C^T} -NH ₂
WNT3A-B2-003	Ac- ^{C^T} K ^{C^K} CHGLDap(NPalm)GS ^{C^E} EVKT ^{C^W} C ^T -NH ₂
WNT3A-B2-004	Ac- ^{C^T} K ^{C^K} CHGLDap(NPalm)GS ^{C^E} EVKT ^{C^{C^T}} -NH ₂
WNT3A-B2-005	Ac- ^{C^T} K ^{C^K} CHGLDap(NPalm)GS ^{C^E} EVKT ^{C^T} -NH ₂
h-Wnt3a, 312-351	³¹² ^{C^D} GRGHNARAERRREK ^{C^R} C ^R VFW ^{C^A} C ^A YVS ^{C^B} QEC ^{C^T} TRVYDVHT ^{C^D351}
WNT3A-B3-001	Ac- ^{C^T} NARAERRREK ^{C^R} C ^R VFW ^{CCYVS} CQEC ^{C^T} TRVYDVHT ^{C^T} -NH ₂
WNT3A-B3-002	Ac- ^{C^T} REK ^{C^R} C ^R VFW ^{CCYVS} CQEC ^{C^T} TRV ^{C^T} -NH ₂
WNT3A-B3-003	Ac- ^{C^T} R ^{C^R} VFW ^{CCYVS} CQEC ^{C^T} -NH ₂
WNT3A-B3-004	Ac- ^{C^T} ERREK ^{C^R} C ^R VFW ^{CCYVS} CQEC ^{C^T} TRV ^{C^T} -NH ₂
WNT3A-B3-005	Ac- ^{C^T} RREK ^{C^R} C ^R VFW ^{CCYVS} CQEC ^{C^T} TR ^{C^T} -NH ₂
WNT3A-B3-006	Ac- ^{C^T} REK ^{C^R} C ^R VFW ^{CCYVS} CQEC ^{C^T} -NH ₂
WNT3A-B3-007	Ac- ^{C^T} EK ^{C^R} C ^R VFW ^{CCYVS} CQEC ^{C^T} -NH ₂
WNT3A-B3-008	Ac- ^{C^T} AR ^{C^R} VFW ^{CCYVS} CQEC ^{C^T} -NH ₂
WNT3A-B3-009	Ac- ^{C^T} R ^{C^R} VFW ^{CCYVS} CQ ^{C^T} -NH ₂
WNT3A-B3-010	Ac- ^{C^T} VFW ^{CCYVS} C ^{C^T} -NH ₂
WNT3A-B3-011	Ac- ^{C^T} VFW ^{CCYVS} C ^T -NH ₂

Nomenclature: Dap(NPalm) = N-β-palmitoyl-L-2,3-diaminopropionic acid; CT = Cys connected via the bivalent CLIPS scaffold; C = Cys connected via an SS-bond.

Table 2. Wnt5a mimics designed, synthesized and tested.

Peptide	Sequence
h-Wnt5a, 234-256	²³⁴ ADVA ^{C^B} K ^{C^A} HGVS(OPalm)GS ^{C^A} SLKT ^{C^B} WLQL ²⁵⁶
WNT5A-B2-001	Ac- ^{C^T} DVA ^{C^K} CHGVDap(NPalm)GS ^{C^S} SLKT ^{C^W} LQ ^{C^T} -NH ₂
WNT5A-B2-002	Ac- ^{C^T} VA ^{C^K} CHGVDap(NPalm)GS ^{C^S} SLKT ^{C^W} L ^{C^T} -NH ₂
WNT5A-B2-003	Ac- ^{C^T} A ^{C^K} CHGVDap(NPalm)GS ^{C^S} SLKT ^{C^W} ^T -NH ₂
WNT5A-B2-004	Ac- ^{C^T} CK ^{C^K} CHGVDap(NPalm)GS ^{C^S} SLKT ^{C^{C^T}} -NH ₂
WNT5A-B2-005	Ac- ^{C^T} K ^{C^K} CHGVDap(NPalm)GS ^{C^S} SLKT ^{C^T} -NH ₂
h-Wnt5a, 340-379	³⁴⁰ ^{C^D} GRGYDQFKTVQTER ^{C^H} C ^H KFW ^{C^A} C ^A YVK ^{C^B} KK ^{C^C} TEIVDQFV ^{C^D379}
WNT5A-B3-001	Ac- ^{C^T} DQFKTVQTER ^{C^H} C ^H KFW ^{CCYVK} CKK ^{C^T} TEIVDQFV ^{C^T} -NH ₂
WNT5A-B3-002	Ac- ^{C^T} TER ^{C^H} C ^H KFW ^{CCYVK} CKK ^{C^T} TEI ^{C^T} -NH ₂
WNT5A-B3-003	Ac- ^{C^T} HCKFW ^{CCYVK} CKK ^{C^T} -NH ₂
WNT5A-B3-004	Ac- ^{C^T} VQTER ^{C^H} C ^H KFW ^{CCYVK} CKK ^{C^T} TEI ^{C^T} -NH ₂
WNT5A-B3-005	Ac- ^{C^T} QTER ^{C^H} C ^H KFW ^{CCYVK} CKK ^{C^T} TE ^{C^T} -NH ₂
WNT5A-B3-006	Ac- ^{C^T} TER ^{C^H} C ^H KFW ^{CCYVK} CKK ^{C^T} -NH ₂
WNT5A-B3-007	Ac- ^{C^T} ER ^{C^H} C ^H KFW ^{CCYVK} CKK ^{C^T} -NH ₂
WNT5A-B3-008	Ac- ^{C^T} AHCKFW ^{CCYVK} CKK ^{C^T} -NH ₂
WNT5A-B3-009	Ac- ^{C^T} HCKFW ^{CCYVK} CK ^{C^T} -NH ₂
WNT5A-B3-010	Ac- ^{C^T} CKFW ^{CCYVK} C ^{C^T} -NH ₂
WNT5A-B3-011	Ac- ^{C^T} KFW ^{CCYVK} C ^T -NH ₂

Nomenclature: Dap(NPalm) = N-β-palmitoyl-L-2,3-diaminopropionic acid; C^T = Cys connected via the bivalent CLIPS scaffold; C = Cys connected via an SS-bond.

Biological evaluation: We tested the peptides for their capacity to inhibit Wnt3a-mediated signaling in Fzd1/2-expressing cells. For this purpose, we used a 3T3 cell line that is specially developed for discovering modulators of canonical Wnt signaling, and expresses the TOPFlash reporter. In our assay, we first added Wnt3a-conditioned medium to the cells to induce canonical Wnt signaling, and afterwards we added the peptides at 10-100 μ M.

Several Wnt-mimicking peptides inhibited Wnt3a-mediated signaling at 10 μ M (i.e. >50% inhibitory activity). Based on their activities, we selected 4 peptides as leads for the development of potent Fzd1/2 antagonists (Table 3, Figure 2). For these 4 peptides, regioselective synthesis of the native SS-bond isomers is currently under investigation.

Table 3. Wnt3a and Wnt5a mimics selected as leads.

Peptide	Sequence	SS-isomers isolated and tested
WNT3A-B2-003	Ac- C ^T K C KCHGLDap(NPalm)GS C EVK T C W C ^T -NH ₂	a
WNT3A-B3-009	Ac- C ^T R C VFW C YV S C Q C ^T -NH ₂	a, b, c
WNT5A-B2-003	Ac- C ^T A C K C HGVDap(NPalm)GS C SLK T C W C ^T -NH ₂	a, b
WNT5A-B3-009	Ac- C ^T H C KFW C YV K C K C ^T -NH ₂	a, b

Nomenclature: Dap(NPalm) = *N*- β -palmitoyl-L-2,3-diaminopropionic acid; **C**^T = Cys connected via the bivalent CLIPS scaffold; **C** = Cys connected via an SS-bond.

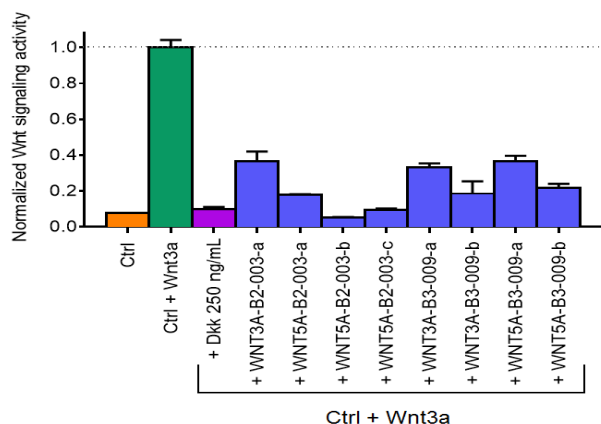


Fig. 2. Inhibitory activities of the Wnt-mimicking peptides selected as leads, when tested at 10 μ M.

In summary, we have synthesized a library of peptides derived from the sequences of Wnt3a/5a in their β 2- and β 3-loop regions. Several of these Wnt mimicking peptides inhibited Wnt3a-mediated signaling in Fzd1/2-expressing cells (10 μ M), thereby demonstrating that mimicking the Fzd-binding sites of Wnt proteins is a feasible strategy for discovering Wnt/Fzd-signaling modulators.

Acknowledgments

This work was supported by the Cyttron II research project (grant FES09088), the Dutch Heart Foundation (grant 2010B196), and the EU FP7 Marie Curie ITN program (grant 608180, 'WntsApp').

References

- MacDonald, B., Tamai, K., Xei, H. *Dev. Cell* **17**, 9-26 (2009), <http://dx.doi.org/10.1016/j.devcel.2009.06.016>
- Janda, C.Y., Waghray, D., Levin, A.M., Thomas, C., Garcia, K.C. *Science* **337**, 59-64 (2012), <http://dx.doi.org/10.1126/science.1222879>

Structural Requirement of Fibrogenic Peptide AG97 (SAKVDAIGLEIV) and B160 (VILQQSAADIAR) for Amyloid-Like Fibril Formation and Cellular Activity

Fumihiko Katagiri, Kazuki Takeyama, Nobuko Yamada, Atsushi Naito, Satomi Yamada, Kentaro Hozumi, Yamato Kikkawa, and Motoyoshi Nomizu

School of Pharmacy, Tokyo University of Pharmacy and Life Sciences, Hachioji, 1920392, Japan

Introduction

It is known that the process of amyloid fibril formation, including amyloid β (A β) and islet amyloid polypeptide, is generally associated with diseases, such as Alzheimer's disease, type II diabetes, and prion diseases. However, many proteins form amyloid-like fibrils but do not associate with amyloid-related diseases. Amyloid fibrils are elongated, insoluble structures of 7-10 nm in diameter found in extracellular plaques. Structural studies have shown that mature amyloid fibrils involve the alignment of short peptide segments, usually between 6 and 12 residues in length, from many protein monomers. Together, these aligned polypeptide stretches form the characteristic core structure of the amyloid fibril, the cross β sheet, in which β strands run perpendicular to the main axis of the fibril. Amyloid fibrils possess a characteristic UV absorbing spectrum at the peak of 540 nm with Congo red and a characteristic X-ray diffraction pattern. Thus, specific pattern of molecular interactions, rather than nonspecific hydrophobic interactions, lead to ordered structures. Nevertheless, common structural elements responsible for such organized structures have not been identified and the mechanism of amyloid fibril formation is unclear.

Previously, we screened the synthetic peptide library derived from the laminin-111 sequence, and identified five amyloidogenic peptides, A119 (LSNIDYILIKAS, mouse laminin α 1 chain, 1321-1332), A208 (AASIKVAVSADR, mouse laminin α 1 chain, 2097-2108), AG97 (SAKVDAIGLEIV, mouse laminin α 1 chain, 2942-2953), B133 (DISTKYFQMSLE, mouse laminin β 1 chain, 1367-1378), and B160 (VILQQSAADIAR, mouse laminin β 1 chain, 1607-1618) [1]. Laminins, major components of basement membranes, regulate multiple biological functions, including cell adhesion, migration, differentiation, neurite outgrowth, wound healing, angiogenesis, and tumor progression. Laminins are a family of heterotrimeric glycoproteins that consist of α , β , and γ chains. So far, five α , three β , and three γ chains have been identified and at least 16 laminin isoforms have been reported that are formed by various combinations of each chains. Here, we focused on the AG97 and B160 peptide, which exhibits amyloid-like fibril formation, heparin-dependent cell attachment activity, and neurite outgrowth activity. Our approach was to investigate the essential residues for fibril formation and cell behavior using alanine-substituted peptides.

Results and Discussion

We prepared two sets of alanine-substituted peptides for AG97 and B160 (Table 1). First, we evaluated amyloid fibril formability of those peptides using Congo red staining. Congo red is a red pigment, which has high affinity for amyloid fibrils. When Congo red binds to amyloid fibrils, the absorption peak shifts from 490 nm to 540 nm. The absorption peak of Congo red was shifted in AG97 and B160. The absorption peak of Congo red was not shifted in AG97I11A, V12A, B160V1A, I2A, L3A, Q4A, Q5A, and I10A. The Ile¹¹ and Val¹² residues of AG97, the Val¹, Ile², Leu³, Gln⁴, Gln⁵, and Ile¹⁰ residues of B160 are suggested to be critical for amyloid fibril formation. Next, we measured circular dichroism (CD) spectra of the Ala substituted peptides of AG97 and B160. The CD spectrum of AG97 showed typical β sheet structure. The CD spectra of AG97D5A, I11A and V12A showed α helix structure, and those of AG97V4A, I7A and L9A showed random coil structure. The CD spectrum of B160 showed mixed structure (α helix and β sheet). The CD spectra of B160V1A, I2A, Q4A, Q5A and I10A showed α helix structure, and B160S6A, D9A and R12A showed β sheet structure. Furthermore, we examined the amyloid-like fibrils of AG97 and B160 with a transmission electron micrograph. AG97S1A, K3A, D5A, G8A, and E10A lost the amyloid-like fibril forming ability of AG97, and B160V1A, I2A, L3A, Q4A, Q5A, and I10A lost that of B160. We hypothesize that the amyloid-like fibril formation needs

two steps; 1st step, β sheet structure formation, 2nd step, aggregation. The results suggested that important residues are different by each step.

Table 1. Synthetic peptides derived from the AG97 and B160 peptide.

Peptide	Sequence	Peptide	Sequence
AG97	SAKVDAIGLEIV	B160	VILQQSAADIAR
AG97S1A	AAKVDAIGLEIV	B160V1A	AILQQSAADIAR
AG97K3A	SAVDAIGLEIV	B160I2A	VALQQSAADIAR
AG97V4A	SAKDAIGLEIV	B160L3A	VIALQQSAADIAR
AG97D5A	SAKVDAIGLEIV	B160Q4A	VILQSAADIAR
AG97I7A	SAKVDAIGLEIV	B160Q5A	VILQSAADIAR
AG97G8A	SAKVDAIGLEIV	B160S6A	VILQQAADIAR
AG97L9A	SAKVDAIGLEIV	B160D9A	VILQSSAAIAR
AG97E10A	SAKVDAIGLEIV	B160I10A	VILQSSAADAR
AG97I11A	SAKVDAIGLEIV	B160R12A	VILQSSAADIAR
AG97V12A	SAKVDAIGLEIA		

AG97 and B160 are reported that these peptides showed cell attachment activity to human fibrosarcoma HT1080 cells [1]. These peptide promoted cell attachment to human dermal fibroblasts (HDFs). AG97K3A, I11A and V12A peptides lost, the AG97V4A and G8A peptides weakened the HDF attachment activity of AG97, and The B160I2A and R12A peptides lost, and the B160L3A and Q4A peptides weakened that of B160. The Lys³, Ile¹¹ and Arg¹² residue were critical, Val⁴ and Gly⁸ were important residues for HDF attachment activity of AG97. The Ile² and Arg¹² were critical, Leu³ and Gln⁴ were important residues for HDF attachment activity of B160. The peptides which form amyloid fibrils showed HDF attachment activity. The AG97 and B160 peptides are reported to bind heparin sulfate proteoglycans, which have negative charge on surface [1]. The results showed basic amino acid (Lys and Arg) residues, which had positive charge, were critical for HDF attachment activity.

We examined neurite outgrowth activity with rat pheochromocytoma PC12 cells. AG97K3A, V4A, I11A, and V12A peptides lost the neurite outgrowth activity of AG97. The Lys³, Val⁴, Ile¹¹, and Val¹² residue were critical residues for the neurite outgrowth activity of AG97. B160I2A, L3A, Q4A, and R12A peptides lost the neurite outgrowth activity of B160. The Ile², Leu³, Gln⁴, and Arg¹² residue were critical residues for the neurite outgrowth activity of B160. The peptides which form amyloid fibrils showed neurite outgrowth activity. The result suggested that the basic amino acids also play important role for neurite outgrowth activity.

The results suggested that the biological activities (HDF attachment and neurite outgrowth) were closely related with amyloid-like fibril formation. Furthermore, the results indicated that the Ile residue was critical for fibril formation. These findings were useful to elucidate the mechanism of amyloid-like fibril formation.

Acknowledgments

This work was supported by JSPS KAKENHI Grant Number 26870613.

References

1. Kasai, S., et al. *Biochemistry* **46**, 3966-3974 (2007), <http://dx.doi.org/10.1021/bi062097t>
2. Katagiri, F., et al. *Biochemistry* **51**, 8218-8225 (2012), <http://dx.doi.org/10.1021/bi300822d>
3. Yamada, M., et al. *FEBS Lett* **530**, 48-52 (2002), [http://dx.doi.org/10.1016/S0014-5793\(02\)03393-8](http://dx.doi.org/10.1016/S0014-5793(02)03393-8)
4. Katagiri, F., et al. *Biochemistry* **49**, 5909-5918 (2010), <http://dx.doi.org/10.1021/bi100748s>

Misfolding and Oligomerization of Amyloid β (1–40)

Sándor Lovas¹ and Charles R. Watts^{2,3}

¹Department of Biomedical Sciences, Creighton University, Omaha, NE, 68168, USA; ²College of Medicine, Mayo Clinic, Rochester, MN, 55905, USA; ³Department of Neurosurgery, Mayo Clinic Health System, La Crosse, WI, 54601, USA

Introduction

Protein misfolding and self-assembly have been identified as important factors in the development of several neurodegenerative diseases. The hallmark of many of these diseases is the deposition of amyloid fibrils and plaques within the extracellular matrix with an organized core structure consisting of β -sheets running perpendicular to the fibril axis. The histologic sign of Alzheimer's disease is the presence of senile plaques formed from Amyloid β ($A\beta$) and neurofibrillary tangles formed from hyperphosphorylated tau protein. Despite a more thorough understanding of fibril structure, $A\beta$ (1-40) belongs to an inherently disordered class of polypeptides making its structural determination in both monomeric and oligomeric forms difficult. Previous studies have been dependent on maintaining peptide solubility through the use of organic solvents or detergents which would potentially have significant effects on the overall solution structure of the peptide. Recently, a solution NMR structure of $A\beta$ (1-40) in 50 mM NaCl solution has been determined (PDB id.: 2LFM) [1]. The molecular mechanism of dimerization, subsequent oligomerization and the conformation of the multimeric peptide chains are still not known. Therefore, herein we describe the structural properties of the dimer of $A\beta$ (1-40) using 300 ns replica exchange molecular dynamics (REMD) simulation in TIP3P water as solvent using the CHARMM36 force field as implemented in the GROMACS version 4.6.4 package [2]. The dimer structure was created by randomly docking the NMR-derived solution structure with itself and relaxed with a 1.4 μ s MD simulation. The REMD simulations were performed with 70 replicas of the initial structure. The exchange probability was 0.2. The exchange temperatures were obtained from a web-based temperature predictor [3] with the lower and upper limits of 290 K and 470 K, respectively.

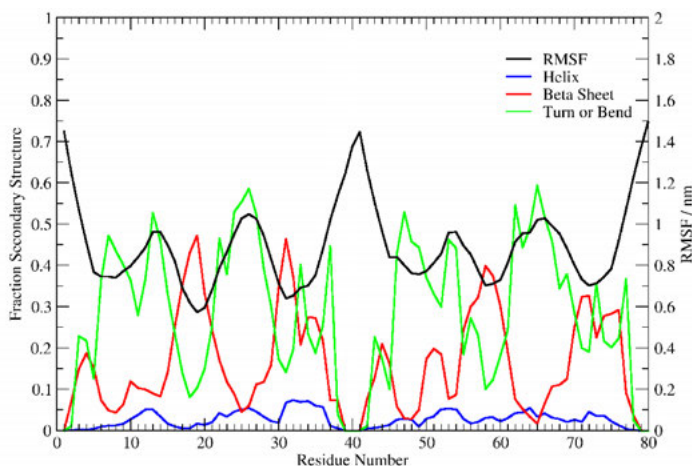


Fig. 1. Backbone RMSF (nm) for each monomer overlaid with its own average structure. The RMSF data compared to a plot of the fraction of sampled secondary structures as a function of residue number. Monomer A constitutes residues 1 through 40 and monomer B constitutes residues 41 through 80.

Results and Discussion

The backbone conformational entropy for the dimer system was calculated for all replica exchange temperatures. Two important aspects of the dimer system are evident from examination of the evolution of entropy during simulations. First, a relatively long, approximately 100000 ps, period of simulation time is required for the system to reach equilibrium. Second, the structures sampled at 310K, the physiological temperature, have a lower value of backbone entropy compared to any other replica temperature during the REMD simulations. This may indicate a slightly more stable system of sampled structures than what occurs at non-physiological temperatures. This temperature effect on the backbone entropy of the system is not unexpected and is confirmed by circular dichroism studies performed as a function of temperature [4].

The sampled secondary structure by the dimer was calculated by the DSSP method [5]. The fraction of sampled secondary structure as a function of residue number in the replica trajectory at 310 K is plotted in Figure 1. The most frequently sampled secondary structure is β -turn/ β -bend followed by β -sheet. β -Turn/ β -bend regions are prominent between residues 1 to 16 and 21 to 29 with a mixed β -sheet/ β -turn/ β -bend region between residues 32 to 38 of monomer A and residues 1 to 15 and 21 and 30 with a mixed β -sheet/ β -turn/ β -bend region between residues 30 and 38 of monomer B. β -sheet regions are prominent between residues 16 to 21 and 29 to 32 of monomer A and between residues 15 to 21 and 30 to 33 of monomer B. There is minimal sampling of helical structures in either monomer. The C-terminus of both monomers is largely unstructured with a more prominent turn structure present from residues 36 to 38 of both monomers. The root mean square fluctuation (RMSF) of the backbone atoms shows that the monomers have similar and significant flexibility. The most flexible regions have a larger proportion of β -turn/ β -bend secondary structure associated with them.

An average residue-residue distance matrix analysis for the dimer system (Figure 2) shows that many of the intra- and inter-monomer contacts occur at distances of 1.0 nm or greater indicating that the dimer system is loosely packed. Intra-monomer contacts occur between residues 4 to 19 and 15 and 36 of both monomers. There are anti-parallel contacts that occur within the dimer system between

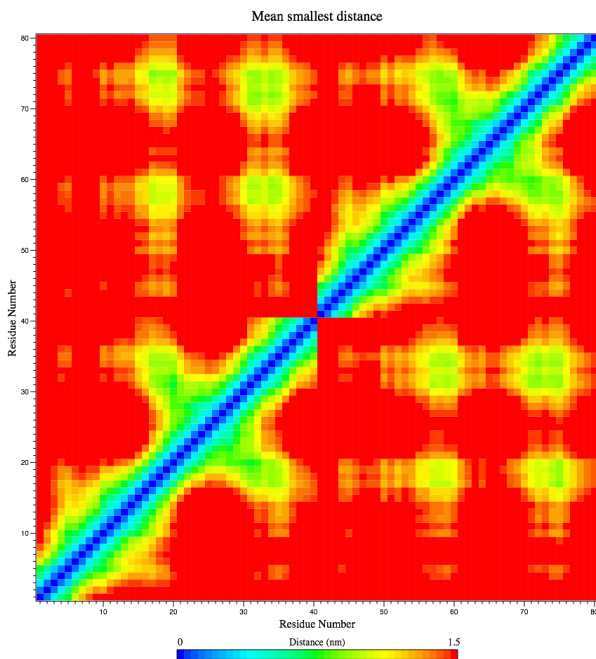


Fig. 2. Distance matrix of the residues at 310 K showing that the system samples an antiparallel global configuration.

residues 16 to 20 of monomer A with residues 17 to 20 and 31 to 36 of monomer B as well as residues 31 to 36 of monomer A with residues 17 to 20 and 30 to 36 of monomer B. The contact map is therefore consistent with a loosely packed antiparallel system that appears to be driven by collapse around the central hydrophobic core of residues 17 to 21 with the C-terminal hydrophobic core of residues 30 to 40.

The sampled configurations of the dimer and both monomers were de-convoluted using dihedral principle component analysis (dPCA) and the lowest energy configuration identified (Figure 3). Examination of the energy surface shows that the minima are relatively shallow with only 1.86 kJ/mol separating the lowest energy from the highest energy configurations. The majority of the sampled configurations are located within a broad based and shallow region with a total of six identified low energy conformations. The lowest energy configuration (Figure 3) consists of a

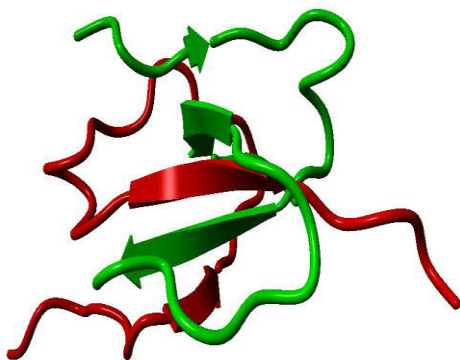


Fig. 3. Lowest energy configuration of A β (1-40) dimer. Monomer A is shown in red while Monomer B is shown in Green.

five strand anti-parallel β -sheet from 9 to 11 and 30 to 34 in monomer A and residue 5 and residues 17 to 20, 33 to 36 of monomer B. The remaining five structures from the broad based shallow region show the presence of β -sheet and anti-parallel β -sheet conformations however, the length and location tend to be variable and the majority of the monomers secondary structure is random coil with an overall loose packing of the dimer. This finding explains why the RMSF for the dimer system and individual monomers is high and the contact map demonstrates interaction distances around between 0.7 and 1.0 nm.

Dimers of A β (1-40) have a different conformation compared to that of the monomers [1]. The presence of stable β -sheet conformations indicates a misfolded state for the peptide. Furthermore, such conformations

are characteristic of the dimers. This finding is in agreement with the dynamic force spectroscopy study (DFS) which predicted the presence of stable dimers in solution with a life-time of 0.1 s at pH 7.0 [6]. The DFS analysis of A β (1-40) dimers also showed that various pathways of dimer dissociation occur indicating that the dimers are built with different conformations. The present REMD simulations not only showed relatively high conformation heterogeneity for the dimer but also indicated that the dimers are stable and only a rare and short-time dissociation event occurred at some of the replica trajectories.

Although A β (1-40) belongs to the class of natively disordered proteins, neither its monomeric or dimeric forms are entirely in a random coil conformation. Previous MD simulations of structures of monomeric A β (1-40) and A β (1-42) have demonstrated that a wide variety of conformations occurred during simulations [7]. These simulations demonstrated that the peptides sample a large population of turn type structures and that the driving force of secondary structure formation and fluctuation appears to be the collapse around the central and C-terminal hydrophobic cores with resulting “zipping” and “unzipping” of the hydrogen bonds between highly flexible areas with a propensity for β -sheet formation. It is clear that a similar mechanism is occurring in dimeric A β (1-40). The two peptides tend to collapse on each other in their most energetically favorable conformation with the driving force of collapse and secondary structure formation being antiparallel contact between the two hydrophobic regions. The fact that these interactions do not result in a stable antiparallel β -sheet dimer but rather a large ensemble of sampled conformations may be one reason that the dimer remains soluble in water.

Acknowledgments

The study was partially supported by a grant from Mayo Clinic Health System Franciscan Health Foundation and by Mayo Clinic, Department of Neurosurgery.

References

1. Vivekanandan, S., et al. *Biochem. Biophys. Res. Commun.* **411**, 312-316 (2011), <https://dx.doi.org/10.1016/j.bbrc.2011.06.133>
2. Pronk, S., et al. *Bioinformatics* **29**, 845-854 (2013), <http://dx.doi.org/10.1093/bioinformatics/btt055>
3. <http://folding.bmc.uu.se/remd/>
4. Gursky, O., Aleshkov, S. *Biochim. Biophys. Acta* **1476**, 93-102 (2000), [http://dx.doi.org/10.1016/S0167-4838\(99\)00228-9](http://dx.doi.org/10.1016/S0167-4838(99)00228-9)
5. Kabsch, W., Sander, C. *Biopolymers* **22**, 2577-2637 (1983), <http://dx.doi.org/10.1002/bip.360221211>
6. Kim, B.-H., et al. *Biochemistry* **50**, 5154-5162 (2011), <http://dx.doi.org/10.1021/bi200147a>
7. Yang, M., Teplow, D.B. *J. Mol. Biol.* **384**, 450-464 (2008), <http://dx.doi.org/10.1016/j.jmb.2008.09.039>

Structure Stabilizing Role of Aromatic Interactions is Decided by Spatial Arrangement of Aromatic Pairs: A Case Study With Designed Peptide β -Hairpins

Kamlesh Madhusudan Makwana and Radhakrishnan Mahalakshmi*

Molecular Biophysics Laboratory, Department of Biological Sciences, Indian Institute of Science Education and Research, Bhopal, 462023, India

Introduction

Interaction among aromatic side chains in the hydrophobic core of proteins is a well-known mechanism for protein structure stabilization [1]. Aromatic pairs at the non-hydrogen bonding position of designed β -hairpin peptides interact by T-shaped arrangement and usually result in structured folds [2]. However, the consequences of spatial positioning and preferred packing geometry of aromatic pairs on scaffold structure and stability are still unclear. Studies on tryptophan packing geometry have revealed that the heterogeneous indole ring preferentially occupies “face” geometry in T-shaped aromatic interactions [3]. But the fate of Trp at the sterically constrained “edge” geometry is not well understood. Using β -hairpin peptide models we describe here a detailed investigation highlighting the implication of aromatic-aromatic interactions in the formation and measured stability of β -hairpin scaffolds.

Results and Discussion

Octapeptide β -hairpins nucleated by D P-G segment and with a single non-hydrogen bonding position [4], were chosen as model systems to probe all possible aryl pair interactions involving Phe, Tyr, and Trp. All peptides were synthesized using Fmoc-chemistry on a Rink amide resin (Figure 1a). Being hydrophobic in nature, the peptides were highly soluble in methanol but not in water. This feature allowed us to investigate the preferred modes of aromatic interactions in the absence of solvent-driven hydrophobic contributions, using high-resolution NMR and CD spectroscopy. Complete assignment of the resonances was achieved using proton 1D, 2D ROESY, TOCSY and heteronuclear HSQC-TOCSY experiments. The spectra revealed that all the peptides adopted β -hairpin structures and gave rise to NOEs characteristic of β -hairpins. Comparison of fraction folded populations (Figure 1b), extent of signature downfield shifted backbone resonances, extent of glycine splitting and HPLC retention time, and anomalous chemical shifts for resonances influenced by aromatic ring current effects (Figure 2a) revealed the stabilizing and destabilizing contribution of tryptophan.

Positional permutants YW and FW pairs displayed an interconversion of Face-to-Edge (FtE) and Edge-to-Face (EtF) geometry, resulting in scaffold destabilization (Figure 2b). However, we found evidence of a single FtE geometry in the analogs WY and WF pairs, with the highest stabilizing contribution of aromatic interactions to the β -hairpin scaffold.

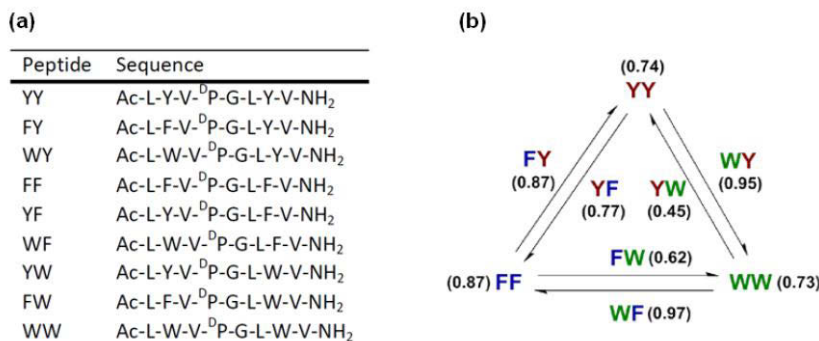


Fig. 1. Sequences of peptide β -hairpins. (b) Comparison of fraction folded populations across the peptides (provided in brackets). Reprinted (adapted) with permission from [5].

Our meticulous examination of all possible aryl-aryl interactions at a single non-hydrogen bonding position in β -hairpin scaffolds revealed a near-universal T-shaped Face-to-Edge mode of interaction among aromatic pairs. However, the indole ring, particularly in amphipathic solvents, causes destabilization of the β -hairpin structure when placed at the sterically constrained edge position. Thus, the implication of tryptophan, when interacting with non-Trp rings in β -hairpin stabilization can be contextual: *stabilizing* at “face” and *destabilizing* at “edge” geometry. Such small variations in the geometry may have a strong bearing in the hydrophobic protein interior. Our results serve as important criteria in the rational design of stable structural scaffolds.

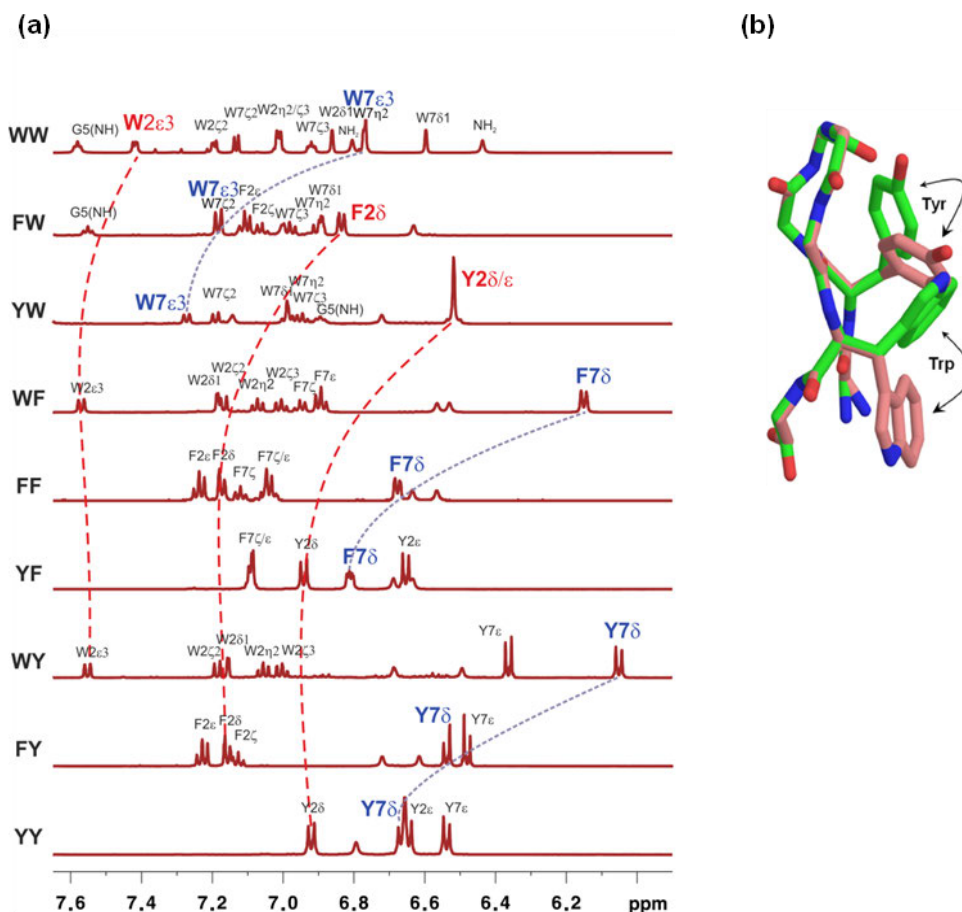


Fig. 2. (a) Comparison of signature upfield shifted aromatic proton resonances across all peptides. Stack plot of proton 1D NMR spectra at 303 K in methanol. The upfield shifted protons, $F7\delta$ and $W7\epsilon3$ is a signature of FtE geometry. The significant upfield shifted protons $Y2\delta/\epsilon$, $F2\delta$ and $W2\epsilon3$ in aro-Trp pairs is evidence for the flipped EtF geometry. Reprinted (adapted) with permission from [5]. (b) Modeled structure showing the interconversion of FtE to EtF, as what seen in Aro-W pairs. Reprinted (adapted) with permission from Makwana & Mahalakshmi [6]. Copyright (2015) American Chemical Society.

Acknowledgments

K.M.M. acknowledges the University Grants Commission, Govt. of India, for research fellowship. R.M. is a recipient of the Wellcome Trust/DBT India Alliance Intermediate Fellowship. This work was supported by intramural funds. K.M.M thanks the Department of Science and Technology, Govt. of India for International Travel Support. K.M.M. also thanks the 24th American Peptide Symposium for the APS Travel Award.

References

1. Burley, S.K., Petsko, G.A. *Science* **229**, 23-28 (1985), <http://dx.doi.org/10.1126/science.3892686>
2. Santiveri, C.M., Jimenez, M.A. *Biopolymers* **94**,779-790 (2010), <http://dx.doi.org/10.1002/bip.21436>
3. Samanta, U., Pal, D., Chakrabarti, P. *Acta Crystallogr. Sect. D Biol. Crystallogr.* **55**, 1421-1427 (1999), <http://dx.doi.org/10.1107/S090744499900726x>
4. Mahalakshmi, R., Raghothama, S., Balaram, P. *J. Am. Chem. Soc* **128**, 1125-1138 (2006), <http://dx.doi.org/10.1021/ja054040k>
5. Makwana, K.M., Mahalakshmi, R. *ChemBioChem* **15**, 2357-2360 (2014), <http://dx.doi.org/10.1002/cbic.201402340>
6. Makwana, K.M., Mahalakshmi, R. *J. Phys. Chem. B* **119**, 5376-5385 (2015), <http://dx.doi.org/10.1021/acs.jpcc.5b00554>

Differential Potencies for Endogenous Dynorphins Indicate Functional Selectivity at the Delta Opioid Receptor

Keith M. Olson¹, Justin Lavigne², John Streicher², Frank Porreca^{3*}, and Victor J. Hruby¹

¹University of Arizona, Dept. of Chemistry, Tucson, 85721, AZ, USA; ²University of New England, Dept. of Biomedical Sciences, Biddeford, ME, 04005, USA; ³University of Arizona, Dept. of Pharmacology, Tucson, AZ, 85721, USA

Introduction

Opioid receptors (ORs) are G-protein Coupled Receptors (GPCRs), which mediate analgesia, tolerance, withdrawal, GI transit. Classically, ORs couple inhibitory $G\alpha_{i/o}$ proteins and recruit β -arrestin – a multifaceted scaffold molecule implicated in opioid mediated effects including tolerance, constipation, dysphoria and nausea [1,2]. Upon activation β -arrestin and $G\alpha_{i/o}$ induce downstream signaling responses such as reduced cAMP levels. Recent drug discovery efforts identified several functionally selective exogenous opiates which prefer certain signaling pathways at a given receptor – such as $G\alpha$ stimulation – to others – such as β -arrestin recruitment and generate desired pharmacological properties [3,4]. Noting that most of the 20+ endogenous opioid peptides are non-selective and some opiates display functional selectivity, two important points emerge. First, endogenous and exogenous ligands, such as those used during studies, do not necessarily generate the same effects. Second, two different endogenous opioid peptides may differentially activate a given receptor. Dynorphin A (DynA) and Dynorphin B (DynB) are considered κ OR agonists, despite binding to the δ OR at 1.29 nM and 3.39 nM [1], respectively. The Dynorphins start with the 5 amino acid Leu-enkephalin (Leu-Enk) sequence – YGGFL – traditionally considered a δ OR agonist followed by distinct C-terminal sequences. Thus, we ask: Do Dynorphin A (1-17), Dynorphin B (1-13) and Leu-enkephalin induce functionally selective signaling at the δ OR?

Results and Discussion

We assessed DynA, DynB and Leu-Enk signaling for two ubiquitous GPCR signals – $G\alpha$ activation and β -arrestin recruitment – *in vitro*. GTP γ S stimulation assays were performed using CHO cells expressing the δ OR, analogous to previous reports [5]. β -Arrestin-2 recruitment assays (DiscoverX) were performed by manufacturer's protocol. We found DynA, DynB and Leu-Enk display different

Table 1. In Vitro Signaling Profile of Endogenous Opioids at δ OR. DynA and DynB show distinct rank orders for arrestin-recruitment, GTP γ S and cAMP; in addition DynA and DynB show distinct efficacies for cAMP inhibition relative to Leu-Enk. β -arrestin2 recruitment (n= 1), cAMP (n=3) and GTP γ S (n=2) assays performed as referenced in text.

Ligand	β -arrestin Recruitment		GTP γ S		cAMP	
	EC 50	Emax	EC 50	Emax	EC 50	Emax
Dynorphin A(1-17)	83	1.0	488	1.04	21	0.54
Dynorphin B(1-13)	330	1.0	383	1.04	122	0.52
Leu-Enkephalin	17	1.0	1.86	1.00	5.3	1.00

potency rank orders for $G\alpha$ activity and β -arrestin recruitment at the δ OR (Table 1). DynB more potently activates $G\alpha$ signaling than β -arrestin2 recruitment with EC50 values of 83 nM and 230 nM, respectively. In contrast, DynA more potently recruits β -arrestin than DynB with EC50 values of 83 and 328 nM, respectively (Table 1). A reversal in rank order between DynA and DynB likely indicates functional selectivity, such that each

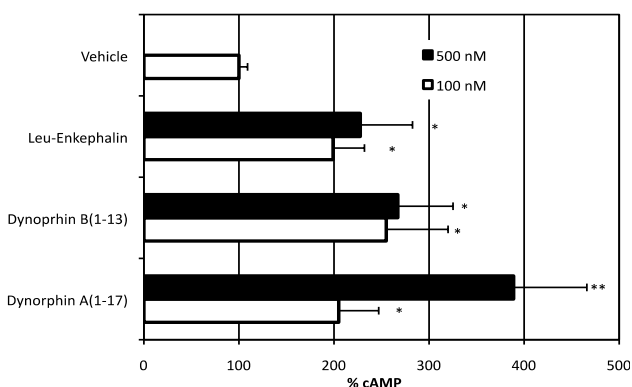


Figure 1. δ OR Mediated AC Super Activation. Cells were treated with vehicle or ligand for 24 hours - refreshing media every 8 hours - then AC was stimulated with 10 mM forskolin. Percentage of basal cAMP increase relative to vehicle was graphed and analyzed with a two-tailed t-test * $p < .05$, ** $p < .01$.

At the δ OR, chronic opioid treatment causes a compensatory increase in basal cAMP levels, referred to as *Adenylyl Cyclase (AC) super activation*. AC super activation may play a physiological role in developing opioid tolerance, dependence and withdrawal [5,6]. Chronic treatment with DynA led to greater AC super activation than treatment with DynB or Leu-Enk, which similarly induce AC super activation (Figure 1). This upregulation in forskolin-stimulated cAMP indicates that DynA and DynB induce distinct receptor regulatory events. Differences in AC super activation by endogenous ligands could be important in the physiological roles of disease and require further *in vivo* study. Thus, *in vitro* assays show endogenous opioid peptides with differing (or absent) C-terminal tails induce distinct changes in the activity of these peptides. Therefore, we show three endogenous opioids induce distinct signaling and regulatory outcomes *in vitro*. Further studies are required to understand the differences in $G\alpha$ activation, other cellular regulatory changes and potential uses as a peptide scaffold for drug design.

Acknowledgments

This work was supported by the U.S. Public Health Services, NIH, and NIDA (P01DA006284).

References

1. Lamb, K., Tidgewell, K., Simpson, D.S., Bohn, L.M., Prisinzona, T.E. *Drug and Alcohol Dependence* **121**, 181-188 (2012), <http://dx.doi.org/10.1016/j.drugalcdep.2011.10.026>
2. Raehal, K.M., Walker, J.K.L., Bohn, L.M. *J. Pharma. Exper. Therap.* **314**, 1195-1201 (2005), <http://dx.doi.org/10.1124/jpet.105.087254>
3. Lamb, K., Tidgewell, K., Simpson, D.S., Bohn, L.M., and Prisinzona, T.E. *Drug and Alcohol Dependence* **121**, 181-188 (2012), <http://dx.doi.org/10.1016/j.drugalcdep.2011.10.026>
4. Schmid, C.L., Streicher, J.M., Groer, C.E., Munro, T.A., Zhou, L., Bohn, L.M. (2013). *J. Biol. Chem.* **288**(31):22387-98, <http://dx.doi.org/10.1074/jbc.M113.476234>
5. Varga, E.V., Rubenzik, M., Grife, V., Sugiyama, M., Stropova, D., Roeske, W.R., Yamamura, H.I. *Eur. J. Pharma.* **451**, 101-102 (2002), [http://dx.doi.org/10.1016/S0014-2999\(02\)02220-3](http://dx.doi.org/10.1016/S0014-2999(02)02220-3)
6. Varga, E.V., Rubenzik, M.K., Stropova, D., Sugiyama, M., Grife, V., Hrubv, V.J., Yamamura, H.I. *J. Pharma. Exper. Therap.* **306**, 109-115 (2003), <http://dx.doi.org/10.1124/jpet.103.049643>

ligand likely induces distinct δ OR conformations. Thus a modest 3-fold potency difference, may lead to more pronounced differences downstream.

Next we probed each ligand for forskolin-stimulated cAMP inhibition - a well-established $G\alpha$ dependent pathway [6]. Acute treatment of DynA and Leu-Enk yield IC_{50} values of 21 nM and 5nM, respectively (Table 1). However, DynB exhibits a ~10 fold less potent response (IC_{50} =122 nM). DynB is a less potent agonist in the forskolin induced cAMP inhibition compared to DynA and Leu-Enk, whereas all display similar potency in the $GTP\gamma S$ assay. Based on differential cAMP inhibition potencies and efficacies, we predicted these peptides would differentially effect receptor mediated $G\alpha$ regulation.

Probing Peptide-Membrane Interaction by Neutron Scattering

Shuo Qian

Biology and Soft Matter Division, Oak Ridge National Laboratory, Oak Ridge, TN, 37831, USA

Notice: This manuscript has been authored by UT-Battelle, LLC, under Contract No. DE-AC0500OR22725 with the U.S. Department of Energy. The United States Government retains and the publisher, by accepting the article for publication, acknowledges that the United States Government retains a non-exclusive, paid-up, irrevocable, world-wide license to publish or reproduce the published form of this manuscript, or allow others to do so, for the United States Government purposes.

Introduction

Membrane-active peptides, including antimicrobial peptides, cell-penetrating peptides, pre-amyloid peptides, fusion peptides etc., interact with membrane to exert at least part of their functions. Due to their potent power to disrupt or go through cell membrane, it is of great interest to apply them as antibiotics, drug-delivery or other therapeutic agents. Moreover, the understanding of their interaction with the target membrane provides important clues on the mode of action, which affords researchers better guidance for developing new peptides with specific properties and functions.

Neutron scattering, similar to X-ray scattering techniques, is well-developed to solve molecular structural problems. Like photon in X-ray interacts with electrons in atom, neutron interacts with nuclei of atoms. It can determine the spatial distribution of atoms in molecule, or structure, from atomic to mesoscale resolution. The high penetration power of neutron and the lack of radiation damage to the sample provide an opportunity to study complex bio-system both *in vivo* and *in vitro*. Furthermore, neutron is scattered very differently by isotopes hydrogen (H) and deuterium (D), enhancing the contrast greatly in the sample with deuterium labeling. With H₂O/D₂O contrast variation and selective deuterium labeling techniques, different compositions in a membrane complex can be distinguishable, and different parts of structure can be accessed either separately or wholly. A few neutron scattering methods for studying peptide-membrane interaction introduced here are implemented at the SANS instruments located in Oak Ridge National Laboratory [1,2].

Results and Discussion

Small Angle Neutron Scattering (SANS):

SANS is a mature technique to probe the structure of biomolecules. In contrast to protein crystallography, it doesn't require crystallization or cryogenic temperature on samples. Therefore samples under physiologically relevant conditions either in solutions or in complexes with other molecules can be studied for the shapes and sizes. Model membrane systems including lipid vesicles and multilayer membranes are developed to understand the peptide-membrane interactions under various conditions by SANS.

Vesicle Solution Scattering:

In SANS with vesicle solution, SANS affords us to detect the redistribution of deuterium-labeled phospholipid across the membrane bilayer under the influence of peptide. The unilamellar vesicles (ULV), made of lipids with different charges, intrinsic curvatures and ratios of cholesterol etc., are used as a simplified model membrane system. The molecular response of lipid species under the influence of other molecules including peptides can be studied. For example, we have studied how alamethicin and melittin, two well-studied membrane-active peptides, modify the charged lipid distribution in the inner and outer leaflet of lipid bilayers [3]. It is known that they are able to form pores in membrane and exhibit anti-microbial activities at high concentrations. At much lower concentrations than the pore-forming concentrations, we have found that they are not stress-free to membrane: the disruption effect by changing the distribution of charged lipid across the bilayer could be harmful to the cell. In other studies, we also found that they can lessen the cholesterol inhomogeneity laterally on the bilayers at low concentration [4,5].

Neutron In-plane Scattering:

Many membrane-active peptides are pore-forming toxins in membrane, while many are not. Detecting pore-formation in membrane is an effective assay on elucidating the mode of action. And for those pore-forming peptides, the size and the structure of the membrane pore is of great interest. While vesicle leakage experiment with dextran can probe the pore size in a vesicle, in many cases, the presence of high concentration peptide required by stable pore formation ruptures liposomes quickly. Neutron in-plane scattering is able to detect pores at equilibrated stable poration states.

The sample is in form of multi-lamellar membrane. At the pore-forming concentration of peptide and other conditions such as appropriate buffer, lipid charge etc., the proteinous or lipidic water channel stabilized by peptide is hydrated fully with D₂O. The D₂O filled pore has distinct scattering length density from the hydrogenated peptide-lipid complex in fluid phase. The size, density, and correlation of the membrane pores can be resolved. This method has been used to understand peptides such as alamethicin, gramicidin etc. [6,7].

In one case, the membrane pore formation caused by human antimicrobial peptide LL-37 peptide is revealed by neutron in-plane scattering [8]. Previously, solid-state NMR or FTIR failed to discover the pore in multilayer membrane samples, but with sample hydrated using excessive water, the helical peptide is found to insert into membrane forming stable pores when the bilayer spacing exceeds the length of the peptide ~ 55 Å. The pore is about 23 Å in radius and about 70-84 Å away from each other depending on the concentrations of peptide. On average each membrane pore is stabilized by ~ 5 peptides.

Grazing-angle Scattering:

Grazing-angle scattering provides geometry to detect film-like samples both in-plane and out-of-plane simultaneously. Multilayer membrane samples under full hydration, similar to the samples used in neutron in-plane scattering, can be used. When multilayer samples are dehydrated, the lipidic structure complexed with peptide forms long-range ordered structure, like a lipidic crystal, which subjects to neutron and X-ray diffraction. The diffraction from such peptide-membrane system contains high resolution membrane structural information. For example, the membrane pores formed by alamethicin, melittin and a Bax protein derived peptide Bax-α5 have been solved [9-11]. The solved structure ultimately proved the existence of lipidic pore (toroidal) and proteinous pore (barrel-stave). This has shown that cooperative interaction of peptide and lipid are essential in forming toroidal pores, which is energy-efficient in establishing those structures. While those examples are solved by X-ray, we are working on interesting structures with the newly implemented neutron diffraction setup at the SANS instruments.

Other Biophysical Methods:

In addition to SANS techniques, other biophysical tools are available for users. Quasi-Elastic Neutron Scattering (QENS) is a microscopic spectroscopy technique which detects local motions from pico- to nano-seconds and in length scales from Å to tens of nm [12]. It works on lipid vesicle sample as well as multilayer membrane sample. QENS could extract information on peptide's effect on the dynamics, fluidity, and phase transition of the lipid bilayer.

Oriented Circular Dichroism is a modification of traditional Circular Dichroism [13]. Instead of using isotropic solution sample, planar multilayer on a solid substrate is used to provide a reference to the peptide orientation. Combined with other structural methods like neutron/X-ray scattering, it provides location and orientation of peptide in a planar membrane. As complementary techniques for peptide characterization in membrane, it has been implemented with relative humidity and temperature control in the user facility.

Acknowledgments

Part of the work was supported by the Laboratory Directed Research and Development program of Oak Ridge National Laboratory. The research at the Oak Ridge National Laboratory's Center for Structural Molecular Biology (F.W.P. ERKP291) is supported by the Office of Biological and Environmental Research of the US Department of Energy. The research at the High Flux Isotope Reactor (HFIR) and at the Spallation Neutron Source (SNS) of Oak Ridge National Laboratory was sponsored by the Scientific User Facilities Division, Office of Basic Energy Sciences, US Department of Energy.

References

1. Heller, W.T., et al. *J. Appl. Cryst.* **47**, 1238-1246 (2014), <http://dx.doi.org/10.1107/S1600576714011285>
2. Zhao, J.K., Gao, C.Y. Liu, D. *J. Appl. Cryst.* **43**, 1068-1077 (2010), <http://dx.doi.org/10.1107/S002188981002217X>
3. Qian, S., Heller, W.T. *J. Phys. Chem. B* **115**, 9831-9837 (2011), <http://dx.doi.org/10.1021/jp204045t>
4. Qian, S., Heller, W.T. *Biochim. Biophys. Acta (BBA) - Biomembranes* <http://dx.doi.org/10.1016/j.bbamem.2015.06.012>
5. Qian, S., Rai, D., Heller, W.T. *J. Phys. Chem. B* **118**, 11200-11208 (2014), <http://dx.doi.org/10.1021/jp504886u>
6. Harroun, T.A., et al. *Biophys. J.* **76**, 937-945 (1999), [http://dx.doi.org/10.1016/S0006-3495\(99\)77257-7](http://dx.doi.org/10.1016/S0006-3495(99)77257-7)
7. He, K., et al. *Biochemistry* **34**, 15614-15618 (1995).
8. Lee, C.-C., et al. *Biophys. J.* **100**, 1688-1696, (2011), <http://dx.doi.org/10.1016/j.bpj.2011.02.018>
9. Lee, M.-T., et al. *PNAS* **110**, 14243-14248 (2013), <http://dx.doi.org/10.1073/pnas.1307010110>
10. Qian, S., et al. *PNAS* **105**, 17379-17383 (2008), <http://dx.doi.org/10.1073/pnas.0807764105>
11. Qian, S., et al. *Biophys. J.* **94**, 3512-3522 (2008), <http://dx.doi.org/10.1529/biophysj.107.126474>
12. Sharma, V.K., et al. *J. Phys. Chem. B* **119**, 4460-4470 (2015), <http://dx.doi.org/10.1021/acs.jpcb.5b00220>
13. Wu, Y., Huang, H.W., Olah, G.A. *Biophys. J.* **57**, 797-806 (1990), [http://dx.doi.org/10.1016/S0006-3495\(90\)82599-6](http://dx.doi.org/10.1016/S0006-3495(90)82599-6)

Investigating the Effects of Aromatic Amino Acids on Amphipathic Peptide Self-Assembly and Emergent Hydrogel Viscoelasticity

Annada Rajbhandary and Bradley L. Nilsson

Department of Chemistry, University of Rochester, Rochester, 14620, USA

Introduction

Self-assembled peptides have been exploited to create novel biomaterials, including hydrogels for tissue engineering, wound-healing and drug delivery [1-3]. Amphipathic β -sheet peptides composed of alternating hydrophobic and hydrophilic amino acids (with general sequence (XZXZ)_n where X is nonpolar and Z is polar) are a privileged class of self-assembling peptide that have been widely used in the design of hydrogel materials [4]. The (FKFE)₂ peptide is a prominent member of this class of material that has been frequently studied [5,6]. This peptide self-assembles into putative β -sheet bilayer nanoribbons; molecular dynamics studies suggest that the alignment of peptides within the β -sheet structure requires the *N*-terminal Phe residue to “dangle” out of register (Figure 1) [6]. We have adopted this peptide specifically to understand the impact of general hydrophobic and more specific aromatic π - π effects on peptide self-assembly [7,8]. Our studies have shown that substitution of the Phe residues in (FKFE)₂ peptides with either aromatic or nonaromatic residues has an impact on both self-assembly propensity and on the morphology of the self-assembled materials. Self-assembly propensity can be more directly correlated to the hydrophobicity of nonpolar amino acids rather than to the aromatic character of these residues.

While these studies suggest that self-assembly propensity for this class of peptides is correlated to hydrophobicity of the nonpolar amino acids, the emergent hydrogel properties of networks of these fibrils appear to be correlated with the aromatic character of the nonpolar residues in the constituent peptides [8]. Specifically, it was found that the elasticity of hydrogels derived from Ac-(XKXX)₂-NH₂ peptides in which X was Val, Ile, Phe, pentafluoro-phenylalanine (F₅-Phe or F⁵F), or cyclohexylalanine (Cha) depended on the aromaticity of the X residue. Hydrogels of the Ac-(ChaKChaK)₂-NH₂ and Ac-(IKIK)₂-NH₂ peptides (G' values of ~75 and 230 Pa respectively) were significantly weaker than those of Ac-(FKFK)₂-NH₂ and Ac-(F⁵FKF⁵FK)₂-NH₂ (G' values of ~1640 and 1960 Pa respectively). It is not immediately apparent why this trend is observed. If hydrogel rigidity is a function of fibril density

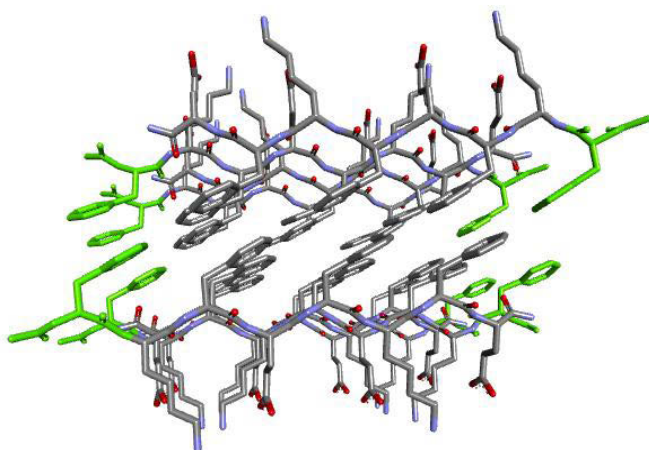


Fig. 1. Structural representation of Ac-(FKFE)₂-NH₂ β -sheet bilayer fibrils. The β -sheet axis is perpendicular to (extending from and descending into) the page. The *N*-terminal Phe residue, which is proposed to hang out-of-register, is shown in green.

alone, then the viscoelasticity of each of these hydrogels should be similar, since the degree of fibrillization for each peptide was shown to be similar [8]. These observations suggest that specific aromatic effects may influence formation of the fibril hydrogel network. Based on the proposed structure (Figure 1) that indicates β -sheet alignment with the *N*-terminal residue of the constituent peptides out of register, we postulated that specific cross-fibril interactions involving this *N*-terminal residue may occur during hydrogelation, accounting for the observed differences in elasticity between aromatic versus nonaromatic hydrogels. Our data suggests that these hypothetical interactions are apparently more favorable if aromatic residues are present at

the *N*-terminus. If this is true, then modification of only the *N*-terminal residue of these peptides could change the emergent viscoelasticity of the resulting hydrogels. For example, modifying Ac-(ChaKXChaK)₂-NH₂ (which has a reported *G'* value of 75 Pa) to Ac-FK(ChaK)₃-NH₂ would be expected to dramatically increase the elasticity of the resulting hydrogel. Herein, we report the results of an initial assessment of this hypothesis.

Results and Discussion

In order to assess our hypothesis, the peptides shown in Table 1 were designed and synthesized. The peptides were based on the aromatic Ac-(^{F5}FK^{F5}FK)₂-NH₂ or the nonaromatic Ac-(ChaKChaK)₂-NH₂ core sequences with modifications made only to the *N*-terminal nonpolar residue. Based on our central hypothesis, we predicted that changing the *N*-terminal residue of the rigid Ac-(^{F5}FK^{F5}FK)₂-NH₂ hydrogels to a nonaromatic amino acid should weaken the gels. Conversely, changing the *N*-terminal residue of the weak Ac-(ChaKChaK)₂-NH₂ hydrogels to an aromatic residue should strengthen the resulting gel.

Peptides were synthesized by standard solid phase peptide methods. The peptides were purified by high pressure liquid chromatography (HPLC) and characterized by MALDI-TOF mass spectroscopy. Peptide concentrations were determined by correlation to HPLC standard curves for each peptide that were calibrated by amino acid analysis [8]. Peptide self-assembly was initiated by dissolution in 200 mM NaCl to obtain samples with final peptide concentrations of 8 mM. TEM imaging confirmed assembly into fibrils (see Figure 2 for representative images). (Note that these cationic peptides do not spontaneously self-assemble without NaCl, which acts to shield repulsive charge effects; 200 mM NaCl was sufficient to promote assembly of each of the peptides studied herein). The samples were then vortexed (1 min) and sonicated (5 min). The cycle was repeated twice to obtain a homogenous mixture that was then stored at room temperature for 1 day to allow homogenous hydrogels to form. Hydrogel viscoelasticity was characterized by oscillatory rheology (TA instruments AR-G2 rheometer) to determine to storage (*G'*) and loss (*G''*) moduli. Frequency sweep experiments were performed on gels (150 μ L) that were transferred onto the rheology plate using a capillary piston pipettor specifically manufactured to handle viscous, soft materials. Experiments were performed using a 20 mm parallel geometry with a stage gap of 400 μ m; a solvent trap was placed over the apparatus to prevent evaporation from the gel. Frequency sweep experiments were performed at 25°C with 0.1% strain (within the linear viscoelastic region) over a frequency range of 0.1–100 rad s⁻¹.

*Table 1. Rheological storage modulus (*G'*) and loss modulus (*G''*) values for peptide hydrogels.*

<i>Peptide</i>	<i>G'</i> (Pa)	<i>G''</i> (Pa)
Ac-(ChaKChaK) ₂ -NH ₂	1325	199
Ac-FK(ChaK) ₃ -NH ₂	911	126
Ac- ^{F5} FK(ChaK) ₃ -NH ₂	638	79
Ac-IK(ChaK) ₃ -NH ₂	458	81
Ac-FK(^{F5} FK) ₃ -NH ₂	2091	161
Ac-IK(^{F5} FK) ₃ -NH ₂	615	90

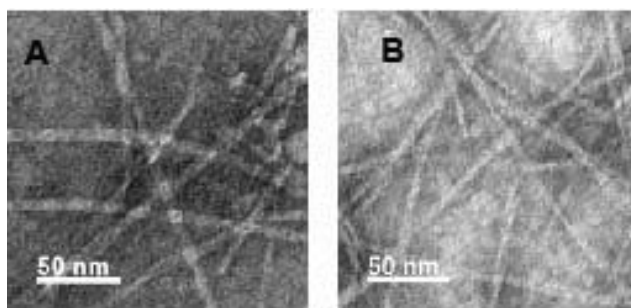


Fig. 2. Representative TEM images of fibrils formed at 8 mM peptide in 200 mM NaCl solution. A. Ac-FK(^{F5}FK)₃-NH₂ peptide fibrils and B. Ac-FK(ChaK)₃-NH₂ peptide fibrils.

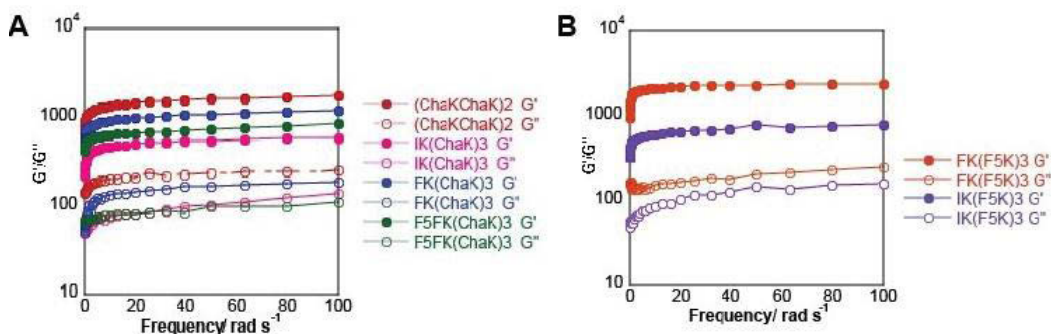


Fig. 3. Rheological frequency sweep data for: A. Modified Ac-(ChaKChaK)₂-NH₂ peptides and B. Modified Ac-(F⁵FKF⁵FK)₂-NH₂ peptides.

The rheological characterization data (Figure 3 and Table 1) was inconsistent with our previously published data [8]. In our previously published work, the Ac-(ChaKChaK)₂-NH₂ hydrogels were reported to have a weak storage modulus (G') of ~ 75 Pa (8 mM peptide, 200 mM NaCl). In contrast, in this study we found the Ac-(ChaKChaK)₂-NH₂ hydrogels to have a significantly stronger storage modulus of 1325 Pa. We found some significant differences in our experimental protocols that account for these differences. First, in our previously published work [8], the hydrogels were assessed after only several hours of maturation; in this work, the gels were allowed to stand for 24 h prior to rheological assessment. Second, in the previously reported data, the gels were applied to the rheometer stage by extrusion from plastic tubes: the gels were formed in plastic conical tubes, the bottom of the conical tubes were then cut off using razor blades, and the gel was finally squeezed from the tube onto the rheometer stage. In this study, a specialized pipettor that was designed for the handling of viscous materials was used to transfer the gels from plastic tubes onto the rheometer stage. The latter technique was shown to be much less disruptive to the mechanical integrity of the hydrogels. Thus, our previously published data showing that Ac-(ChaKChaK)₂-NH₂ hydrogels are relatively weak most likely report on gels in which the network is incompletely formed. Given enough time for maturation, the Ac-(ChaKChaK)₂-NH₂ hydrogels become significantly more rigid.

Modification of the *N*-terminal amino acid of these hydrogels did affect hydrogel rigidity. However, these effects did not strongly correlate to the aromaticity of the *N*-terminal residue as we predicted based on our postulations. As indicated above, the Ac-(ChaKChaK)₂-NH₂ hydrogels had a G' value of 1325 Pa. Peptides in which the *N*-terminal Cha residue was replaced with either Phe or F₅-Phe (Ac-FK(ChaK)₃-NH₂ and Ac-F₅K(ChaK)₃-NH₂) also formed fairly rigid gels with average G' values of 911 Pa and 638 Pa respectively. We predicted that these gels should be more rigid than the parent Ac-(ChaKChaK)₂-NH₂ hydrogels, which obviously is not true. In comparison, aromatic Ac-FK(F₅K)₃-NH₂ peptides form rigid hydrogels with G' values of 2091 Pa. When the *N*-terminus of this peptide or the Ac-(ChaKChaK)₂-NH₂ peptide was replaced with a nonaromatic Ile residue, the rigidity of the resulting hydrogels dropped significantly relative to the parent hydrogels. The Ac-IK(ChaK)₃-NH₂ and Ac-IK(F₅K)₃-NH₂ hydrogels had G' values of 458 Pa and 615 Pa respectively. While modification of the *N*-terminus does influence emergent hydrogel viscoelasticity, the trends do not strongly correlate with the aromaticity of the *N*-terminal amino acid.

This data provides insight into the relationship between the aromatic/hydrophobic character of amphipathic peptides and the emergent hydrogel properties of the assembled fibril networks. We postulated that the aromatic character of the *N*-terminal nonpolar residue potentially participates in specific noncovalent cross-linking interactions in hydrogel formation [8]. This hypothesis was based on observations from our previous work that showed a dramatic difference in hydrogel rigidity between amphipathic peptides in which the nonpolar residues are aromatic or nonaromatic; peptides with aromatic peptides tended to be more rigid [8]. However, data reported herein indicate that our previously reported data is likely a function of kinetically slower network formation (not fibril formation) for the nonaromatic peptides and not an inherent difference in specific fibril-fibril cross-linking effects. Given enough time, even the nonaromatic peptides form rigid hydrogels. In addition,

substitution of only the *N*-terminal residue of amphipathic peptides did not result in hydrogels in which the elasticity correlated strongly with the aromaticity of the *N*-terminal residue. The possibility remains that the differences are merely kinetic. That is, the fibril network that constitutes the hydrogels forms more slowly in the case of some of these peptides relative to the others. Perhaps all hydrogels approach a common maximum rigidity related to total fibril content if given enough time to mature. This work is ongoing and additional insight will be reported in due course.

Acknowledgments

We thank Karen Bentley (URMC Electron Microscope Research Core) for assistance with TEM experiments. This work was supported by the National Science Foundation (DMR-1148836).

References

1. Hirst, A.R., Escuder, B., Miravet, J.F., Smith, D. K. *Angew. Chem. Int. Ed. Engl.* **47**, 8002-8018 (2008), <http://dx.doi.org/10.1002/anie.200800022>
2. Branco, M.C., Schneider, J.P. *Acta Biomaterialia* **5**, 817-831 (2009), <http://dx.doi.org/10.1016/j.actbio.2008.09.018>
3. Zhao, X., Pan, F., Xu, H., Yaseen, M., Shan, H., Hauser, C. A.E., Zhang, S., Lu, J.R. *Chem. Soc. Rev.* **39**, 3480-3498 (2010), <http://dx.doi.org/10.1039/b915923c>
4. Bowerman, C.J., Nilsson, B.L. *Biopolymers* **98**, 169-184 (2012), <http://dx.doi.org/10.1002/bip.22058>
5. Marini, D., Hwang, W., Lauffenburger, D.A., Zhang, S., Kamm, R.D. *Nano Lett.* **2**, 295-299 (2002), <http://dx.doi.org/10.1021/nl015697g>
6. Hwang, W., Marini, D.M., Kamm, R.D., Zhang, S. *J. Chem. Phys.* **118**, 389-397 (2003), <http://dx.doi.org/10.1063/1.1524618>
7. Bowerman, C.J., Ryan, D.M., Nissan, D.A., Nilsson, B.L. *Mol. BioSyst.* **5**, 1058-1069 (2009), <http://dx.doi.org/10.1039/b904439f>
8. Bowerman, C.J., Liyanage, W., Federation, A.J., Nilsson, B.L. *Biomacromolecules* **12**, 2735-2745 (2011), <http://dx.doi.org/10.1021/bm200510k>

Peptide-Guided Design of Mdm2/MdmX Inhibitors with Anticancer Activity

Lingyun Qin, Yao Chen, Rong Chen, Jinjin Zhou, Fei Yang,
 and Zhengding Su*

Protein Engineering and Biopharmaceutical Science Laboratory, the Key Laboratory of Fermentation
 of the Ministry of Education and Collaborative Innovation Center of Industrial Fermentation,
 Hubei University of Technology, Wuhan, Hubei, China

Introduction

The N-terminal domains of MdmX or Mdm2 are highly homologous and have similar conformation (Figure 1a & b). There are three binding pockets for a p53 binding peptide (p53p), defined as F19, W23 and L26 on their surfaces. Current Mdm2 inhibitors including nutlin-3a exhibit weak binding affinity to MdmX. Nutlin-3a (Figure 1c) mimics p53p with high binding affinity to Mdm2 ($K_d \sim 20$ nM) but very weak to MdmX ($K_d \sim 29 \mu\text{M}$). The L26 pocket significantly differentiates the binding affinities of nutlin-3a between Mdm2 and MdmX, but detailed mechanism remains unclear.

Results and Discussion

Drug Target Model: A short p53p peptide (p53p^{short}, Figure 2a) can occupy the F19 and W23 binding pockets on MdmX as well as Mdm2. A small molecule compound, HG201 (Figure 2b) adopted from current Mdm2/MdmX inhibitors, mimicking p53p^{short} binding behavior, is used as a positive control.

High-Throughput Screening (HTS) of CTM Compound Library:

The Cys76 residues on Mdm2 and MdmX are labeled with fluorescence probe, ANS, respectively. The protein-peptide complexes of MdmX-ANS/ p53p^{short} and Mdm2-ANS/ p53p^{short} are used as targets for HTS.

A natural compound library containing 2400 Chinese Traditional Medicinal Compounds (CTMs) are screened for leads. The compound concentration for screening was set at 20 μM , 5 μM , 1 μM , 0.5 μM and 0.3 μM , respectively.

Identification of Leads: The compound hits are ranked by FRET attenuation between the Trp23 of the p53p^{short} and the labelled-ANS on protein (Figure 3 Left). More than 15 hits were selected from screening at 20 μM , 5 μM , 1 μM and 0.5 μM of each compound (Figure 3 Middle). The three most potent leads selected at above 0.5 μM and defined as HS201, HS202 and HS203 (Figure 3 Right), exhibited significant inhibition to the MdmX-p53 interaction.

Future Work: Resulting scaffold will be used to build a secondary model for searching target-specific functional group

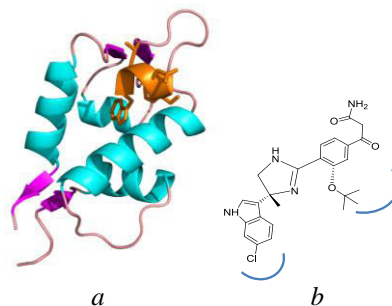


Fig. 2. (a) A protein target model is formed by a N-terminal domain in complex with a short p53p peptide. (b) A small molecule compound mimicking p53p^{short} is used as a positive control.

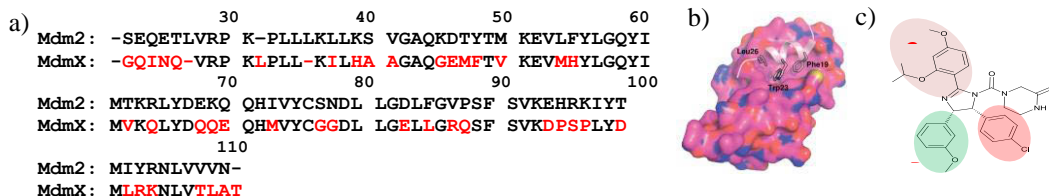


Fig. 1. (a) Alignment of N-terminal domains of Mdm2 and MdmX; (b) Three key residues, Phe18 (L19), Trp23(W23) and Leu29(L29), contribute to the high affinity of p53 peptide (p53p) binding to the domains; (c) A Mdm2 inhibitor, nutlin-3a, mimics p53p.

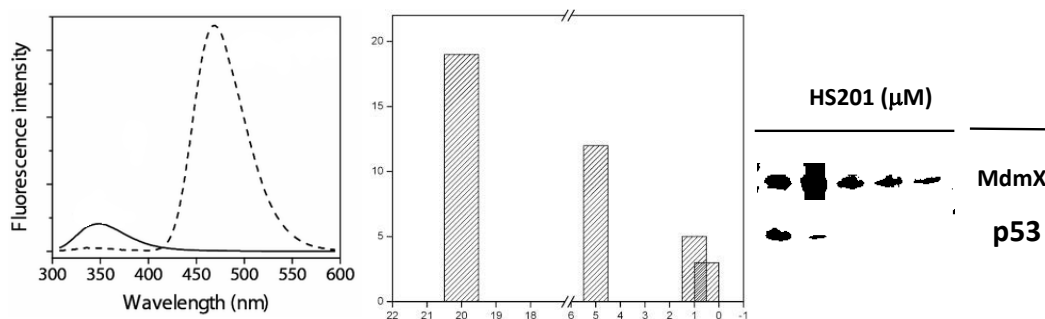


Fig. 3. Summary of HTS Hits. (Left) FRET happens between the Trp23 of p53p and the labelled-ANS on protein. (Middle) Numbers of hits decrease with decreasing threshold values; (Right) One of the three leads exhibits significant inhibition to the MdmX-p53 interaction, evaluated with western blot analysis using GST-MdmX pull-down experiment.

by screening virtual fragment library. Potent Mdm2-specific, MdmX-specific and dual specific inhibitors will be generated through fusing target-specific functional group to the scaffold. New inhibitors will be evaluated for their anticancer activities with cancer cell models.

Acknowledgments

This project was supported by Wuhan Science Research Grant (2015060101010033).

References

1. Wang, X., Jiang, X. *FEBS Letters* **586**, 1390-1396 (2012), <http://dx.doi.org/10.1016/i.febslet.2012.02.049>
2. Wade, M., Li, Y.C., Wahl, G.M. *Nature reviews Cancer* **13**, 83-96 (2013), <http://dx.doi.org/10.1038/nrc3430>
3. Hong, B., van den Heuvel, A.P., Prabhu, V.V., et al. *Current Drug Targets* **15**, 80-89 (2014).
4. Muller, P.A., Vousden, K.H. *Cancer Cell* **25**, 304-317 (2014), <http://dx.doi.org/10.1016/j.ccr.2014.01.021>
5. Wade, M., Wang, Y.V., Wahl, G.M. *Trends in Cell Biology* **20**, 299-309 (2010), <http://dx.doi.org/10.1016/j.tcb.2010.01.009>
6. Lane, D.P., Cheok, C.F., Lain, S. *Cold Spring Harbor Perspectives in Biology*, 2010, 2: a001222, <http://dx.doi.org/10.1101/cshperspect.a001222>
7. Popowicz, G.M., Domling, A., Holak, T.A. *Angewandte Chemie* **50**, 2680-2688 (2011), <http://dx.doi.org/10.1002/anie.201003863>
8. Vassilev, L.T., Vu, B.T., Graves, B., et al. *Science* **303**, 844-848 (2004), <http://dx.doi.org/10.1126/science.1092472>
9. Su, Z.D., Royappa, G., Duda, D., et al. *Symposium on Biomolecular Structure, Dynamics & Function* **1**, 2 (2012).
10. Newman, D.J., Cragg, G.M. *J. Natural Products* **75**, 311-335 (2012), <http://dx.doi.org/10.1021/np200906s>
11. Newman, D., Cragg, G. *Bioorganic & Medicinal Chemistry* **17**, 2105-2634 (2009).

Structural Characterization of PPII Helical Oligoproline

Patrick Wilhelm, Bartosz Lewandowski, and Helma Wennemers*

ETH Zurich, Laboratory of Organic Chemistry, 8093, Zurich, Switzerland

Introduction

Detailed knowledge of the geometry and conformational dynamics of molecules used as molecular scaffolds is crucial for the design of functional compounds based on this architecture. Oligoproline is such a molecular scaffold that adopts in aqueous environments a left-handed helix, the Polyproline II (PPII)-helix [1]. Powder diffraction studies provided in the 1950s valuable low-resolution information about the PPII-helix [2]. They revealed basic parameters *e.g.*, the all-*trans* configuration of the amide bonds and that every third residue is stacked on top of each other. However, in contrast to crystal structures of collagen and several other proteins with PPII-helical domains, crystallization of an oligoproline in a PPII-helical conformation had remained elusive. Our interest in the use of azidoproline-containing oligoprolines as functionalizable scaffolds [3-6] led us to revisit the crystallization of oligoprolines.

Results and Discussion

N-Terminal functionalization of a proline-hexamer with *p*-bromobenzoic acid provided *p*-Br-C₆H₄-Pro₆-OH that crystallized by vapor diffusion from acetonitrile to tetrahydropyran. This high-resolution structure provided detailed insight into the conformational properties of PPII-helical oligoprolines [7].

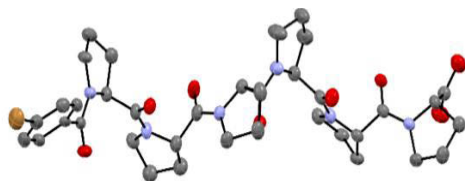
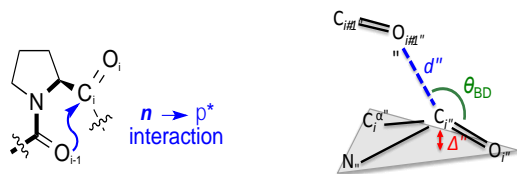


Fig. 2. Crystal structure of hexaproline *p*-Br-C₆H₄-Pro₆-OH (ORTEP).

Distance measurements between every N, C α , and C β revealed that the helical pitch between every third residue is 8.98 ± 0.14 Å in contrast to the 9.36 Å that was derived from the powder diffractogram [2]. Analysis of the distances between the carbonyl oxygens and the carbonyl carbons of neighboring residues (O_{*i-1*}...C_{*i*}) showed that they are all below the van der Waals' radii (3.2 Å) of these atoms (Figure 2). Such short distances are indicative of *n* → π^* interactions between neighboring carbonyl groups, which involve delocalization of the non-bonding electrons of O_{*i-1*} into the π^* orbital of the C_{*i*}=O_{*i*} bond [8]. Additional parameters that are indicative for *n* → π^* interactions are the degree of pyramidalization of C_{*i*} (Δ) and the trajectory angle O_{*i-1*}...C_{*i*}=O_{*i*} (θ_{BD}) between adjacent carbonyl groups. Ideal trajectory angles of $\sim 104^\circ$ were observed in Pro1 and Pro2 that also show the highest degree of pyramidalization of C_{*i*} (Δ). These values of 0.040 Å and 0.023 Å are in fact the highest ever observed values for interactions between two amides. Additionally the crystal structure showed a correlation between the ring-pucker and the backbone dihedral angles and that water is not a necessity for PPII-helical oligoproline [7].



residue	θ_{BD}	d [Å]	Δ [Å]
Pro1	102.9 °	2.958	0.040
Pro2	106.5 °	2.923	0.023
Pro3	89.8 °	3.072	0.005
Pro4	98.9 °	3.063	0.022
Pro5	88.2 °	3.173	0.010
Pro6	98.2 °	3.047	nd ^a

^aThe high anisotropy of the O atoms within the carboxylic acid did not allow for determining a meaningful Δ value.

Fig. 1. Trajectory angles O_{*i-1*}...C_{*i*}=O_{*i*} (θ_{BD}), O_{*i-1*}...C_{*i*} distances (d) and pyramidalization of C_{*i*} (Δ).

Next, we explored the dynamic behavior of oligoprolines and performed double electron-electron resonance (DEER) measurements on a series of double spin-labelled oligoprolines to measure the dipole-dipole interactions between spin labels at distances on the nanometer scale with very high precision [8]. In contrast to commonly applied FRET chromophores, these spin-labels are significantly smaller and therefore reduce label-related line-broadening on the distance distribution. We used the super high-spin complex Gd^{3+} -DOTA and the nitroxide radical 2,2,5,5-tetramethyl-3-pyrrolin-1-oxyl as spin labels and varied the distances across a series of five oligoproline of the same length (Figure 3). Narrow distance distributions were obtained from the DEER-measurements both, in trifluoroethanol (TFE) and a water/glycerol mixture with maxima at distances that were expected for PPII-helices. The narrowest distance distributions were observed for probe **P5**, with distance distribution widths increasing with the number of repeating Pro_3 units between the labels in the other probes **P8-P17**. This implies that the width and shape of the distributions of **P11**, **P14**, and **P17** are governed by the flexibility of the oligoproline backbone. This observation is typical for shape-persistent oligomers, which is predicted by the worm-like-chain model (WLC) and related to the persistence length. [10]

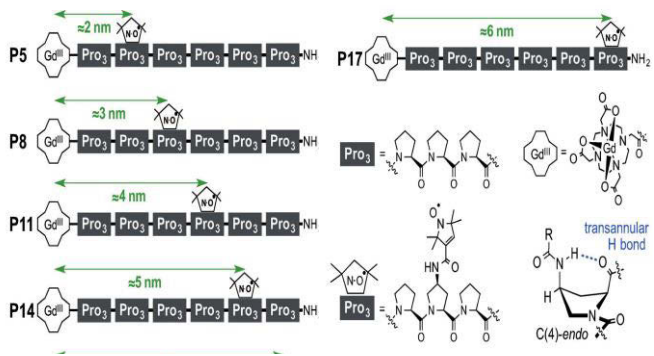


Fig. 3 a.) Double spin-labeled oligoprolines **P5**, **P8**, **P11**, **P14**, and **P17** b.) C(4)-endo pucker of (4S)Amp.

Thus, using the WLC model the persistence length at ambient temperature (298 K) was determined to be between 3.0 and 3.5 nm.

Monte Carlo Simulations allowed to separate influences of backbone flexibility and the occurrence of *cis*-amide bonds that contribute to the observed line-broadening [11]. These computational studies allowed to quantify the probability of a *cis*-amide bond to be ~2% in both solvents [12].

In conclusion, we have gained insight into the crucial parameters of oligoprolines from the first crystal-structure of a PPII-helical oligoproline [7] and determined their shape-persistence [12]. The presented data are crucial for the use of oligoprolines as molecular scaffolds and will allow for the design of even better tailored molecular systems [7,12].

References

1. M. De Zotti, M., et al. *J. Pept. Sci.* **20**, 307-322 (2014), <http://dx.doi.org/10.1002/psc.2638>
2. Cowan, P.M., et al. *Nature*, **176**, 501-503 (1955), <http://dx.doi.org/10.1038/176501a0>
3. Kumin, M., et al. *J. Am. Chem. Soc.* **129**, 466-467 (2007), <http://dx.doi.org/10.1021/ja067148o>
4. Upert, G., et al. *Angew. Chem. Int. Ed.* **51**, 4231-4234 (2012), <http://dx.doi.org/10.1002/anie.201107183>
5. Lewandowska, U., et al. *Angew. Chem. Int. Ed.* **53**, 12537-12541 (2014), <http://dx.doi.org/10.1002/anie.201408279>
6. Kroll, C., et al., *J. Am. Chem. Soc.* **135**, 16793-16796 (2013), <http://dx.doi.org/10.1021/ja4087648>
7. Wilhelm, P., et al. *J. Am. Chem. Soc.* **136**, 15829-15832 (2014), <http://dx.doi.org/10.1021/ja507405j>
8. Hinderaker, M.P., et al. *Protein Sci.* **12**, 1188-1194 (2003), <http://dx.doi.org/10.1110/ps.0241903>
9. Pannier, M., et al. *J. Magn. Reson.* **142**, 331-340 (2000), <http://dx.doi.org/10.1006/jmre.1999.1944>
10. Jeschke, G., et al. *J. Am. Chem. Soc.* **132**, 10107-10117 (2010), <http://dx.doi.org/10.1021/ja102983b>
11. Best, R.B., et al. *Proc. Natl. Acad. Sci. USA* **104**, 18964-18969 (2007), <http://dx.doi.org/10.1073/pnas.0709567104>
12. Garbuito, L., et al. *Chemistry - Eur. J.* **21**, 10747-10753 (2015), <http://dx.doi.org/10.1002/chem.201501190>

Development of Oral Available Melanotropins Based on the Cyclic Peptide Framework of Sunflower Trypsin Inhibitor-1

Minying Cai¹, David Craik², Horst Kessler³, and Victor J. Hruby¹

¹Department of Chemistry and Biochemistry, The University of Arizona, Tucson, AZ, 85721, USA; ²Queensland Tropical Health Alliance, School of Pharmacy and Molecular Sciences and Centre for Biodiscovery and Molecular Development of Therapeutics, James Cook University, Cairns, QLD 4870, Australia; ³Center of Integrated Protein Science Institute for Advanced Study at the Technische Universität München, Lichtenbergstr. 4, 85747, Garching, Germany

Introduction

The melanocortin system involves numerous physiological functions and is associated with many diseases such as skin cancer, obesity and diabetes, sexual dysfunction, neuropathic pain, inflammatory diseases etc. Our primary interests have been focusing on the human melanocortin 1 and 4 receptors (hMC1R, hMC4R) due to their direct involvement in the regulation of feeding behavior, energy homeostasis, as well as inflammatory diseases. Nevertheless, the full scope of physiological functions of these receptors is still poorly understood. There has been a resurgence of interest in peptide pharmaceuticals recently as they have an advantage of potency, selectivity and less toxicity compared with small-molecule therapeutics. The main drawback of peptides is lack of stability in biological media. Using cycloids and N-Methylation have been useful options to improve *in vivo* stability of the peptides [1]. Several new modalities in constraining peptides have been developed over recent years and this work highlights some of the new developments in our lab [2,3]. The newer grafted and methylation strategies have rendered, in some cases, oral activity, cell permeability, improved potency at the target receptor, selectivity against receptor subtypes and improved stability to enzymes. Further understanding rules governing cell permeability, oral absorption and enhancing stability of peptides can help peptides to enter the clinic for many unmet medical needs.

Results and Discussion

During the last decade, great efforts have been made to develop selective melanotropins. Nevertheless, the potential of potent and selective peptides as drug candidates is challenged by their poor pharmacokinetic properties. Many peptides have a short half-life *in vivo* and a lack of oral availability. Inspired by the excellent pharmacokinetic profile of cyclosporine, a natural, multiply N-methylated cyclic peptide, we visualized using cycloids as a stable template and grafted with multiple N-methylated pharmacophore of NDP- α -MSH, His-D-Phe-Arg-Trp, as a promising way to rationally improve key pharmacokinetic characteristics of melanotropins. The incorporation of this strategy to multiple N-methylated analogs of melanotan II (MTII) has successfully reached this goal by increasing receptor selectivity and peptide stability [4]. Here, we extended our efforts toward a grafted cycloid sunflower trypsin inhibitor-1, SFTI-1, to develop novel oral available melanocortin receptor agonists and antagonists. The melanocortin 1 receptor (hMC1R) selective ligand has great potential to prevent melanoma. We aimed to develop selective and orally available melanotropins by applying the pharmacophore of NDP- α -MSH, His-D-Phe-Arg-Trp, sequence into the SFTI-1 framework. Combined with multiple N-Methylation strategy, thirty peptides were synthesized using solid phase peptide chemistry and ¹H NMR chemical shifts were used to confirm that the structures of the peptides were similar to native SFTI-1. The analogs were tested in a series of binding and functional assays at melanocortin receptors 1 and 3, 4, 5 and several peptides showed potent agonist or antagonist activity. We discovered that several selective hMC1R agonists and hMC4R agonists [5]. As an example cyclo[C-T-A-S-I-P-I-C-H-f-R-W-R] is a nano-molar selective peptide for hMC1R (Table 1). In this peptide Arginine (R) and Tryptophan (W) are N-Methylated (Grey highlighted amino acids). The binding efficacy is showing 100% and the binding affinity is showing 48 nM, while the other types of melanocortin receptors showing no binding affinity.

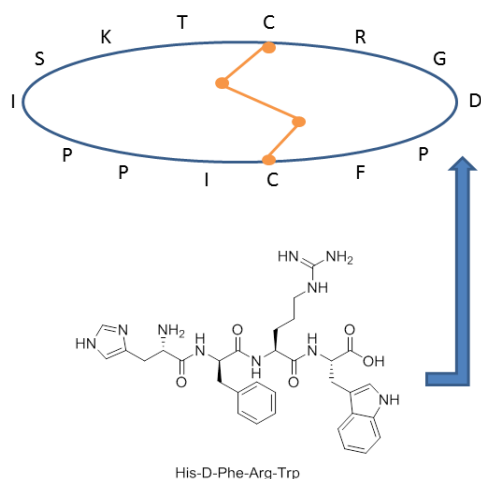


Fig. 1. Primary sequence of the SFTI-1 scaffold (Top), the disulfide bond is shown in yellow; Structure of the grafting pharmacophore of melanotropin (His-D-Phe-Arg-Trp) (Bottom).

The improvement of oral bioavailability by multiple N-methylation and using cycloid template are significant advances toward the development of peptide-based therapeutics, which has been hampered over the years due to poor pharmacokinetic properties. Cycloid grafted peptides combined with multiple N-methylation of NDP- α -MSH pharmacophore result in enhancement in the activity and selectivity of receptor subtypes using either library or designed approaches and helps in understanding the finer details of the bioactive conformation. Thus, with these diverse properties, we foresee a bright future for peptide chemistry by multiple N-methylation toward their development as therapeutic prototypes.

Table 1. Binding assay of N-methylated SHU9119 analogues at hMCRs.

	hMC1R		hMC3R		hMC4R		hMC5R	
	IC ₅₀ nM	PBE ^a	IC ₅₀ nM	PBE ^a	IC ₅₀ nM	PBE ^a	IC ₅₀ nM	PBE ^a
MTII	1±0.1	100	2±0.2	100	2.4±0.2	100	6.9±1.2	100
cyclo[C-T-A-S-I-P-P-I-C-H-f-R-W-R]	48	100	4640	100	>10,000	100	>10,000	NB

IC₅₀ = concentration of peptide at 50% specific binding (N=4). NB = 0% of ¹²⁵I-NDP- α -MSH displacement observed at 10 μ M. ^aPercent Binding Efficiency = maximal % of ¹²⁵I-NDP- α -MSH displacement observed at 10 μ M. Grey highlighted amino acids are N-methylated.

Acknowledgments

This work is supported in part by a grant from the U.S. Public Health Service, National Institutes of Health, DK017420, GM 108040 and DA06284.

References

- Kessler, H. *Angew. Chem. Int. Ed.* **21**, 512-523 (1992), <http://dx.doi.org/10.1002/anie.198205121>
- Hruby, V.J. *Nature Reviews Drug Discovery* **1**, 847-858 (2002), <http://dx.doi.org/10.1038/nrd939>
- Wang, C. K., Gruber, C. W., Cemazar, M., Siatskas, C., Tagore, P., Payne, N., Sun, G., Wang, S., Bernard, C. C., Craik, D. J. (2014). **9**: 156-163. <http://dx.doi.org/10.1021/cb400548s>
- Doedens, L., Opperer, F., Cai, M., Beck, J.G., Dedek, M., Palmer, E., Hruby, V.J., Kessler H. *J. Amer. Chem. Soc.* **132**, 8115-8128 (2010), <http://dx.doi.org/10.1021/ja101428m>
- Hruby, V.J., Lu, D., Sharma, S.D., Castrucci, A.L., Kesterson, R.A., Al-Obeidi, F.A., Hadley, M.E., Cone, R.D. *J. Med. Chem.* **38**, 3454-3461 (1995), <http://dx.doi.org/10.1021/jm00018a005>

K_v1.3 Selective Peptides Based upon N-Terminal Extension and Internal Substitutions of ShK Toxin

Rosendo Estrada¹, Redwan Huq², Rajeev Tajhya², Satendra Chauhan¹,
Christine Beeton², and Michael W. Pennington¹

¹Peptides International Inc., Louisville, KY, 40299, USA; ²Baylor College of Medicine Houston, TX, 77030, USA

Introduction

With more than 80 different types of autoimmune disorders affecting all organ systems in the human body, finding a drug which would treat patients at the root cause of these diseases has been a quest of our mutual labs for the past two decades. These diseases may range from mild skin disorders such as psoriasis, widely distributed joint damage such as in rheumatoid arthritis, destruction of specific cells such as β cells in type-1 diabetes to more complex disorders affecting central nervous system such as multiple sclerosis. Current treatments involve the use of broad immunosuppressants, which may open the door to opportunistic infections. Through work pioneered with the Chandy lab, we have shown that the channel phenotypes of these autoantigen specific T-cells have preferentially upregulated the K_v1.3 channel to balance Ca⁺² influx upon activation. A sea anemone derived peptide named ShK is one of the most potent K_v1.3 blockers described (IC₅₀ = 10 pM), however it lacks specificity and blocks K_v1.1 and K_v1.5 also at pM levels [1,2]. Through many years of engineering, we have progressed one of our peptides, Dalazatide (formerly ShK-186) to the clinic for its selective block of K_v1.3 channels as a means of treating autoimmune diseases. In our current work, we have built upon our findings to continue to improve the selectivity of ShK-derived analogs and have recently reported selectivity profiles of more than 1000x for K_v1.3 versus K_v1.1. We have improved the drugability of ShK [3,4].

Results and Discussion

Several analogs were designed to investigate the effect of Q₁₆K or K₁₈A substitution on the selectivity and potency of ShK analogs previously reported, such as ShK-192 and ShK analog with N-terminal extension EWSS (Figure 1) [3]. The analogs were designed to include a substitution that a group at Amgen had published in a patent filed in 2007. This substitution replaced Gln₁₆ with Lys. The results presented in that patent suggested that this substitution conferred on ShK a high K_v1.3 *versus* K_v1.1 specificity. Thus, we incorporated this substitution into ShK-192, which incorporated a non-hydrolyzable para-phosphono-Phe (Ppa) as the N-terminal residue, extended from the primary ShK sequence with an Aeea (aminoethoxyethoxyacetyl, mini-PegTM) linker, as well as amidation at the C-terminus (ShK-224). We also incorporated a Met₂₁ to Nle substitution into this sequence to generate an analog that would be less susceptible to oxidation (ShK-223). We also designed two more analogs by replacing the N-terminal extension of ShK-192 (Ppa-Aeea) with EWSS extension [3] and replacing Qln₁₆ with K (ShK-237), and Lys₁₈ with Ala (ShK-238). The EWSS extension consists of only common proteins amino acids, and it was designed to resemble the structure of the ShK-192 N-terminal extension [3].

All the analogs were synthesized on a Rink-mBHA resin using an Fmoc-tBu strategy, except for ShK-239 that was synthesized on a Wang resin. The solid-phase assembly proceeded smoothly with all couplings mediated by 6-Cl-HOBT and diisopropylcarbodiimide. In order to form the disulfide bonds utilizing a simple redox buffer, all Cys residues were protected with the trityl group. Following synthesis of the primary chain, each peptide was cleaved from the resin and simultaneously deprotected using an acidolytic reagent cocktail containing carbocation scavengers. The peptides were folded to the active form using a slightly basic aqueous buffer containing an equimolar ratio of reduced and oxidized glutathione. The peptide folding was done for a period of 16 h and was determined to be complete with the formation of the major front eluting peak consistent with other ShK peptides. Each peptide was purified by RP-HPLC and the purified peptides were characterized by analytical HPLC and ESI-MS.

Peptide	Sequence
ShK	H-RSCIDTIPKSRCTQFKCKHSMKYRLSFCRKTCGTC-OH
ShK-013	H-RSCIDTIPKSRCTQFACKHSMKYRLSFCRKTCGTC-NH ₂
ShK-192	H-Ppa-Aeea-RSCIDTIPKSRCTQFQCKHSNleKYRLSFCRKTCGTC-NH ₂
ShK-223	H-Ppa-Aeea-RSCIDTIPKSRCTQF FK CKHSNleKYRLSFCRKTCGTC-NH ₂
ShK-224	H-Ppa-Aeea-RSCIDTIPKSRCTQF FK CKHSMKYRLSFCRKTCGTC-NH ₂
ShK-237	H- EWSS -RSCIDTIPKSRCT FK CKHSMKYRLSFCRKTCGTC-NH ₂
ShK-238	H- EWSS -RSCIDTIPKSRCTQF QCA HSMKYRLSFCRKTCGTC-NH ₂
ShK-239	H- EWSS -RSCIDTIPKSRCTQF FK CKHSMKYRLSFCRKTCGTC-OH

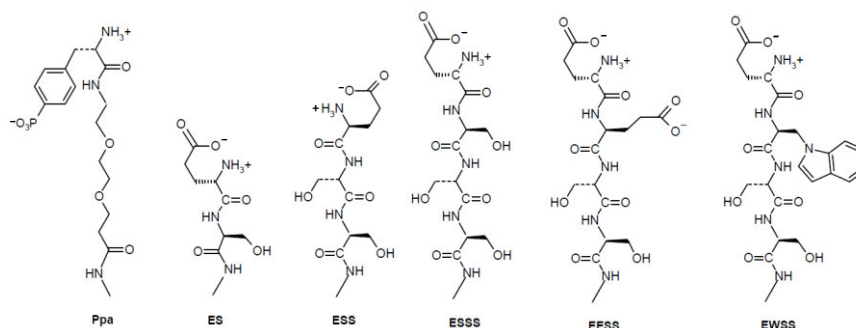


Fig. 1. N-terminal extensions of ShK analogues. Schematic illustrating the structural similarity and physicochemical properties of Ppa moiety of ShK-192 and various amino acid extensions.

We used patch-clamp electrophysiology to assess the effects of ShK-223, ShK-224, ShK-237, ShK-238 and ShK-239 on K_v1.1 and K_v1.3 channels and compare them to the parent peptide, ShK and ShK-192. Mouse fibroblasts stably expressing homotetramers of K_v1.1 or K_v1.3 were patch-clamped in the whole-cell configuration and steady-state block was measured after addition of different concentrations of the peptides. As published previously, ShK inhibited K_v1.3 currents with an IC₅₀ of 10 pM and K_v1.1 currents with an IC₅₀ of 25 pM (Table 1). ShK-224 exhibited a 16-fold loss of efficacy on K_v1.3 relative to ShK, ShK-237 a 26-fold loss, ShK-238 a 9-fold loss and ShK-239 a 3-fold loss, whereas the potency of ShK-223 on K_v1.3 was similar to that of ShK (Table 1). Unlike ShK, ShK-238 exhibited a 28-fold selectivity for K_v1.3 over K_v1.1, and ShK-239 a 158-fold selectivity, while ShK-223, ShK-224 and ShK-237 had any effect on K_v1.1 currents at concentrations up to 100 nM, representing a selectivity for K_v1.3 of >10,000-fold.

Table 1. Comparative IC₅₀ Values for K_v1.3 and K_v1.1.

Peptide	K _v 1.3 IC ₅₀ (pM)	K _v 1.1 IC ₅₀ (pM)	Ratio(K _v 1.1/K _v 1.3)
ShK	10	25	2.5
ShK-013	40	4900	122.5
ShK-192	140	22,000	157
ShK-223	25	>100,000	>4000
ShK-224	164	>100,000	>609
ShK-237	263	>100,000	>380
ShK-238	88	2480	28
ShK-239	34	5372	158

In this study we showed that ShK analogs with *N*-terminal extensions are conveniently produced *via* standard Fmoc/tBu methods. These analogs were modeled to resemble the ShK-192 with the *N*-terminal extension *para*-Phosphono-Phe with an Aeea linker or where an anionic Glu is positioned in close proximity to Trp giving a similar aromatic anionic charge positioned by two spacer Ser residues. Additionally, we have also introduced two previously determined selectivity determinants, either Q₁₆K or K₁₈A [3] coupled with these *N*-terminal additions. The *N*-terminal extension of EWSS confers a similar 100x selectivity of K_v1.3 versus K_v1.1 as that of ShK-192. The Q₁₆K substitution coupled with either the Ppa-Aeea or EWSS *N*-terminal extensions confers the greatest level of selectivity enhancement as shown in the ShK-223, ShK-224 and ShK-237. The K₁₈A coupled with the EWSS *N*-terminal extension lost more than 10x of its gain of the singly substituted ShK-K₁₈A [5].

Acknowledgments

This work was supported in part by a grant from the National Institutes of Health (NS073712 to C.B. and M.W.P.). R.H. was supported by a T32 award from the National Institutes of Health (HL007676).

References

1. Pennington, M.W., et al. *Mol. Pharmacol.* **75**, 762-773 (2009), <http://dx.doi.org/10.1124/mol.108.052704>
2. Tarcha, E.J., et al. *J. Pharmacol. Exp. Ther.* **342**, 642-653 (2012), <http://dx.doi.org/10.1124/jpet.112.191890>
3. Chang, S.C., et al. *FEBS J.* **282**, 2247-2259 (2015), <http://dx.doi.org/10.1111/febs.13294>
4. Pennington, M.W., et al. *Marine Drugs* **13**, 529-542 (2015), <http://dx.doi.org/10.3390/md13010529>
5. Rashid, H.M., et al. *PLoS One* **8**, e78712 (2013), <http://dx.doi.org/10.1371/journal.pone.0078712>

Development of Novel Broad Spectrum Anticancer Small Molecule Peptidomimetics with Nanomolar Activity

Lajos Gera¹, John Tentler², S. Gail Eckhardt², Ziqing Jiang¹,
Angelo D'Alessandro¹, and Robert S. Hodges¹

¹Department of Biochemistry and Molecular Genetics; ²Division of Medical Oncology, University of Colorado
Denver, Anschutz Medical Campus, School of Medicine, Aurora, CO, 80045, USA

Introduction

Cancer is a major public health problem in the United States and throughout the world. It is currently the second leading cause of death in the United States and is expected to surpass heart diseases in the next few years to become the leading cause of death [1]. The estimated number of new cases of invasive cancer (all types) in the United States is 1,658,370 which is equivalent of more than 4,500 new cancer diagnoses each day. In addition, the estimated number of deaths from cancer in 2015 is 589,430 corresponding to about 1,600 deaths per day [1]. Though there has been a steady increase in survival for most cancers the death rate remains unacceptable and for certain cancers i.e. lung and pancreatic cancers the 5-year relative survival is currently 18% and 7%, respectively.

Traditional chemotherapy drugs act against all actively dividing cells (normal and cancerous cells) whereas targeted cancer therapies are drugs that interfere with specific molecular targets involved in cancer cell growth, progression and spread of cancer. Most targeted therapies are either small molecules or monoclonal antibodies. However, therapeutic strategies that target single molecular pathways eventually succumb to problems of intrinsic or acquired resistance due to extensive signaling "cross talk". Thus, combination targeted therapies are more attractive, as they synergistically inhibit multiple receptors. However, overlapping toxicities and pharmacological interactions limit patient compliance, feasibility and efficacy. Clearly, there is an urgent need to develop new first-line agents with enhanced efficacy and reduced toxicity.

We support the concept that the ideal drug maybe a broad spectrum drug whose efficacy is based not on the inhibition of a single target but rather a multi-targeted drug that affects several proteins or events that contribute to the etiology, pathogenesis and progression of diseases [2]. In addition, multi-pathway targeting is one of the strategies to overcome chemo-resistance.

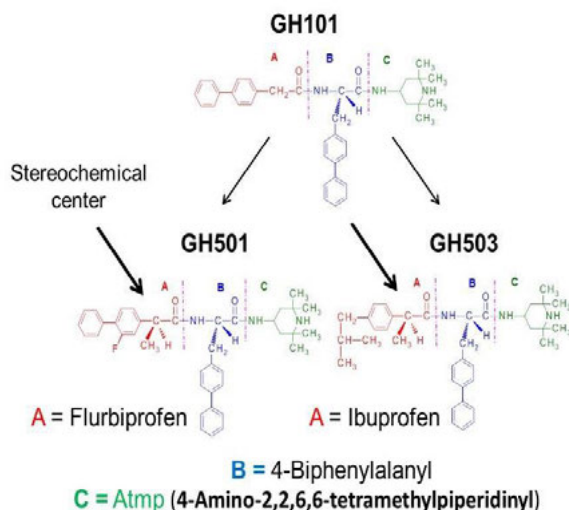
To design novel anticancer drugs with unique structural properties we have taken an innovative and nontraditional approach where we combine pharmacophoric components to create new and highly potent small molecules with a simple three component "A-B-C" structure where each pharmacophore is known to have anticancer properties on its own or when incorporated as a component of an existing drug. Our multi-component "A-B-C" drugs can target simultaneously two or more different molecular targets or molecular mechanisms in a single entity which should reduce the likelihood of drug resistance.

Results and Discussion

Five stringent criteria were established before we would consider our compounds as drug leads:

1. Nanomolar broad spectrum activity against a large variety of human tumor cell lines including breast, colon, central nervous system (CNS), leukemia, melanoma, non-small cell lung (NSCL), ovarian, prostate and renal cancers;
2. The three component "**A-B-C**" molecules must be low molecular weight (500-700 Daltons) and consist of non-natural amino acids;
3. Easy and inexpensive to manufacture requiring only two chemical steps to join the three components together via two peptide bonds;
4. The compounds must be stable to proteolysis due to the use of non-natural amino acids;
5. The new structures must demonstrate synergistic activity over individual components.

In our new generation compounds we made very subtle changes in the structure of the A-component of GH101. GH501 differs from GH101 with a methyl group on the α -carbon and a fluorine atom on the phenyl group (Figure 1, where the A-component is Flurbiprofen) [3]. GH503 differs from GH101 with a methyl group on the α -carbon and the terminal phenyl group is replaced with a 4-carbon alkyl group (Figure 1, where the A-component is Ibuprofen). These subtle changes dramatically increased the activity of GH501 and GH503 compared to the starting prototype, GH101 by 3 to 5 fold in the 60 human tumor cell lines involving 9 cancer types tested by the NCI-60 tumor cell line screen and 5-10 fold against particular cell lines in each of the 9 cancer cell types. The average GI₅₀ value for all 60 cell lines from the 9 cancer types was 498 nanomolar for GH501 and 498 nanomolar for GH503 compared to 1,350 nanomolar for our prototype, GH101. In addition, our new compounds GH501 and GH503 are also significantly more active than our first generation compound BKM570 [4] which had an average GI₅₀ value of all 60 tumor cell lines in the NCI-60 cell line screen of 1,123 nanomolar.



BKM570 remains an excellent candidate for the treatment of glioblastoma, the most aggressive brain tumor [5]. In conclusion, GH501 and GH503 are truly broad spectrum anticancer small molecules (Table 1). These results suggest that our new multi-component small molecules may have the potential to be effective in the treatment of all cancers.

Fig. 1. Two potent anticancer compounds (GH501 and GH503) were derived from our prototype, GH101 where the A-component in GH501 is Flurbiprofen and the A-component in GH503 is Ibuprofen. The B- and C- components are identical in both GH501 and GH503 and our starting prototype, GH101. The arrow shows the stereochemical center in the A-component.

We have selected melanoma as our initial disease target before advancing to other cancer types since despite recent advancements in the treatment of melanoma, there is evidence that escape mechanisms arise and alternative therapies are urgently needed. An estimated 73,870 new cases of melanomas will be diagnosed in 2015 in the US with 9,940 deaths [1]. An important molecular feature of melanoma that impacts upon clinical drug development is that ~50% of all melanomas have activating mutations in the BRAF gene [6]. Of note, GH501 was effective against cell lines harboring the V600E BRAF mutation as well as wild-type BRAF suggesting that activity is independent of BRAF status (Table 2). The NCI-60 results were validated by Tentler and Eckhardt, at the University of Colorado, School of Medicine on 10 different melanoma cell lines with known BRAF status (Table 2).

To evaluate the antitumor *in vivo* efficacy of our lead compounds we will use a unique patient-derived tumor xenograft (PDTX) melanoma bank developed by Drs. Eckhardt and Tentler [7]. Because they are never cultured on plastic, PDTX models recapitulate the human tumor from which they were derived with respect to tumor architecture, stroma, mutational status, etc. and are thus considered superior models for drug efficacy studies [7]. As we have access to both BRAF mutant and BRAF WT PDTX models, we will assess the anticancer activity of GH501 and GH503 in both populations. BRAF mutant models will be compared with vemurafenib while BRAF WT will be compared with standard chemotherapy (dacarbazine). Additionally, the effects of GH501 and GH503 will be assessed in combination with vemurafenib or as a single agent in PDTX models of tumors that were derived from patients who developed resistance to vemurafenib clinically. To date, we have established over 30 individual patient tumor samples in nude mice, making our bank one of the largest in the country.

We have taken two approaches to identify the targets and the potential mechanism of action of our unique inhibitors. First, the Open Innovation Drug Discovery Program of Lilly suggested Histone H3 (Lys 27) methyltransferase (EZH2) as a potential target for our lead compounds, GH501 and GH503. EZH2 has recently emerged as an important and one of the most frequently mutated genes in

Table 1. Average GI_{50} values for compounds GH101, GH501 and GH503 against 9 cancer types.

Cancer Type	Cell Lines Tested	Average GI_{50} (nanomolar)		
		GH101	GH501	GH503
Breast	MCF7, MDA-MB-231/ATCC, HS 578T, BT-549, T-47D, MDA-MB-468	1,394	492	607
CNS	SF-268, SF-295, SF-539, SNB-19, SNB-75, U-251	1,315	398	411
Colon	COLO 205, HCC-2998, HCT-116, HCT-15, HT-29, KM12, SW-620	1,006	446	362
Leukemia	CCRF-CEM, HL-60(TB), K-562, MOLT-4, RPMI-8226, SR	592	241	225
Melanoma	LOX IMVI, MALME-3M, M14, MDA-MB-435, SK-MEL-2, SK-MEL-5, SK-MEL-28, UACC-62, UACC-257	1,753	598	592
Non-Small Cell Lung	A549/ATCC, EKVX, HOP-62, HOP-92, NCI-H226, NCI-H23, NCI-H322M, NCI-H460, NCI-H522	1,251	373	369
Ovarian	IGROV1, OVCAR-3, OVCAR-4, OVCAR-5, OVCAR-8, NCI/ADR-RES, SK-OV-3	1,750	688	681
Prostate	PC-3, DU-145	1,600	360	415
Renal	786-0, A-498, ACHN, CAKI-1, RXF 393, SN12C, TK-10, UO-31	1,527	744	665
Average GI_{50} for 60 cell lines tested in the 9 cancer types		1,350	498	498

GI_{50} the concentration (nanomolar) that inhibits growth by 50%.

Table 2. GI_{50} values for 18 melanoma cell lines.

National Cancer Institute - NCI60		University of Colorado		
Melanoma Cell line	GH501 GI_{50} (nanomolar)	Melanoma Cell line	GH501 GI_{50} (nanomolar)	BRAF
LOX IMVI	150	HS294T	200	p.V600E
M14	260	HS695T	210	p.V600E
MDA-MB-435	267	AO4	250	WT
SK-MEL-5	377	A375	360	p.V600E
SK-MEL-28	428	MeWo	430	WT
UACC-62	882	GO4	690	p.V600E
MALME-3M	1200	1205LU	690	p.V600E
UACC-257	1220	HMCB	770	WT
		ME10538	920	p.V600E
		HS852T	1030	WT
Average GI_{50}	598		555	

Highlights are GI_{50} values less than 500 nanomolar.

melanoma, which has in turn sparked interest in targeting this molecule as a therapeutic option for this disease [8]. Second, to identify potential alternative mechanisms underlying the effectiveness of GH501 and GH503 on melanoma cell lines we will carry out metabolomics analyses. Metabolic changes closely mirror phenotypic alterations, making the metabolome a more reliable proxy than the genome, transcriptome or proteome for mechanistic studies. The main metabolic pathways related to energy and redox metabolism and how key metabolites are affected from incubation of melanoma cells with GH501 at 48 hours are shown in Figure 2.

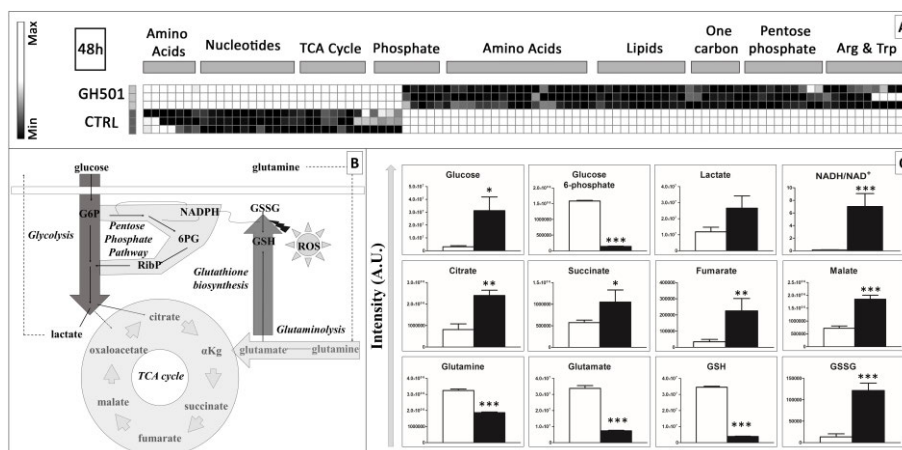


Fig. 2. Incubation of HS29T melanoma cells with GH501 for 48 h significantly altered metabolic profiles, as shown through the heat map in A (relative Z-score normalized fold changes are color coded; black=low; white=high levels). In B, we provide an overview of the main energy and redox metabolic pathways affected by the GH501 treatment (e.g. glycolysis, TCA cycle, Pentose Phosphate Pathway and glutaminolysis/glutathione homeostasis). In C, bar graphs are shown for key metabolites from these pathways for GH501-treated (black bars) and untreated cells (white). One to three asterisks indicate 95, 99 and 99.9% statistical confidence (paired T-test, $n=3$).

In summary, we have shown that our approach of creating a single multi-component “A-B-C” drug by rationally selecting pharmacophores based on general principles of our understanding of their anticancer activity, with no particular targets in mind and general screening of our compounds against the NCI-60 cell lines has provided new highly potent broad-spectrum anticancer drug candidates with nanomolar activity.

Acknowledgments

The authors are grateful to NCI for the NCI-60 human tumor cell line screening and to Eli Lilly for preliminary studies with our compounds on mechanism of action. We thank the John Stewart Endowed Chair in Peptide Chemistry to Robert S. Hodges for financial support.

References

1. Siegel, R.L., et al. *CA: A Cancer Journal for Clinicians* **65**, 5-29 (2015), <http://dx.doi.org/10.3322/caac.21254>
2. Mencher, S.K., Wang, L.G., *BMC Clin. Pharmacol.* **5**, 3 (2005), <http://dx.doi.org/10.1186/1472-6904-5-3>
3. Gera, L., Chan, D.C., Hodges, R.S., Bunn, P.A. USA 8,575,170 B2 (2013).
4. Gera, L., et al., in Martinez, J., and Fehrentz, J-A. (Eds.) *Peptides 2000: (Proceedings of the 26th European Peptide Symposium)*. EDK, Paris, France, 2001, p. 637.
5. Avdieiev, S., et al. *Bioorg. Med. Chem.*, **22**, 3815-3823 (2014), <http://dx.doi.org/10.1016/i.bmc.2014.06.046>
6. Chapman, P.B., et al., *N Engl. J. Med.* **364**, 2507-2516 (2011), <http://dx.doi.org/10.1056/NEJMoa1103782>
7. Tentler, J.J., et al., *Nat. Rev. Clin. Oncology* **9**, 338-350 (2012), <http://dx.doi.org/10.1038/nrclinonc.2012.61>
8. Tiffen, J., et al. *Pigment Cell Melanoma Res.* **28**, 21-30 (2015), <http://dx.doi.org/10.1111/pcmr.12280>

Design of New Antimicrobial Peptides (AMPs) with “Specificity Determinants” that Encode Selectivity for Gram-negative Pathogens and Remove both Gram-positive Activity and Hemolytic Activity from Broad-spectrum AMPs

Ziqing Jiang, Lajos Gera, Colin T. Mant, and Robert S. Hodges

Department of Biochemistry and Molecular Genetics, University of Colorado Denver,
Anschutz Medical Campus, School of Medicine, Aurora, CO, 80045, USA

Introduction

Antimicrobial peptides (AMPs) are widely distributed in nature, generally have broad-spectrum activity and represent a promising class of new antimicrobial agents. However, it is widely accepted that native AMPs lack specificity and may be too toxic (ability to lyse mammalian cells, normally expressed as hemolytic activity against human red blood cells) to be used for systemic treatment [1,2]. To overcome this problem, we developed the design concept of “specificity determinants” which refers to substituting positively charged residue(s) in the center of the non-polar face of amphipathic cyclic β -sheet [3,4] or amphipathic α -helical AMPs [5] to create selectivity between eukaryotic and prokaryotic membranes; that is, antimicrobial activity is improved or maintained and hemolytic activity or cell toxicity to mammalian cells is decreased or eliminated. We showed that a single valine to lysine substitution in the center of the non-polar face of an AMP dramatically reduced toxicity and increased the therapeutic index [5-7].

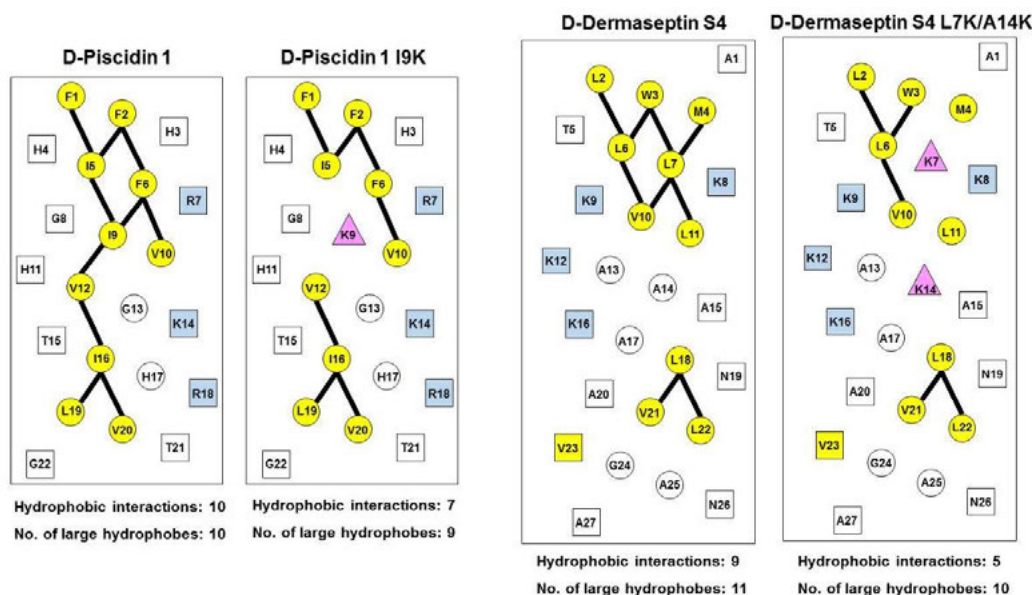
The question arose could we take such a broad spectrum AMP in the all-D conformation and use a rational design approach to enhance further the biological properties if the focus was to develop a better Gram-negative AMP rather than maintain broad-spectrum activity. Our final AMP had a 746-fold improvement (i.e., decrease) in its hemolytic activity, improved antimicrobial activity and improved therapeutic indices by 1305-fold and 895-fold against *Acinetobacter baumannii* and *Pseudomonas aeruginosa*, respectively [7]. We applied this design concept to native AMPs, piscidin 1 (isolated from mast cells of hybrid striped bass - *Morone saxatilis* male \times *Morone chrysops* female) and dermaseptin S4 (isolated from the skin of tree-dwelling, South American frogs of the *Phyllomedusa* species), where substitution of one or two lysine residues at different positions in their non-polar faces enhanced or maintained Gram-negative activity, dramatically decreased hemolytic activity and significantly improved the therapeutic indices (55-fold and 730-fold for D-piscidin 1 I9K and D-dermaseptin S4 L7K, A14K against *A. baumannii*, respectively) [8].

In the current study, we used the above 2 native AMPs and tested their activity against 2 different pathogens: 11 and 20 diverse clinical isolates of *A. baumannii*, and *Staphylococcus aureus* (12 Methicillin-sensitive *S. aureus* strains and 8 Methicillin/Oxacillin-resistant *S. aureus* strains), respectively. We showed that substitution of “specificity determinant(s)” in broad spectrum AMPs, encode selectivity for Gram-negative pathogens and simultaneously remove both Gram-positive activity and hemolytic activity of these 2 diverse amphipathic α -helical AMPs which differ dramatically in amino acid composition, net positive charge and amphipathicity, showing generality of our approach.

Results and Discussion

The peptide analogs (D-piscidin 1, D-piscidin 1 I9K, D-dermaseptin S4 and D-dermaseptin S4 L7K, A14K) (Figure 1) were synthesized by standard solid-phase peptide synthesis methodology using 9-fluorenylmethoxycarbonyl (Fmoc) chemistry on Rink amide 4-methylbenzhydrylamine resin using a CEM Liberty microwave peptide synthesizer and using Boc-chemistry on 4-methylbenzhydrylamine (MBHA) solid support. Peptides were cleaved from the resins by TFA cleavage cocktail for Fmoc chemistry or by HF for Boc chemistry. Peptide purification was performed by reversed-phase high-performance liquid chromatography (RP-HPLC) on a Zorbax 300 SB-C₈ column (250 \times 9.4 mm I.D.; 6.5 μ m particle size, 300 Å pore size; Agilent Technologies, Little Falls, DE, USA). The minimal inhibitory concentration (MIC) was measured by a standard microtiter two-fold serial dilution method

in Mueller Hinton (MH) medium after incubation at 37°C for 24h. The hemolytic activity was determined as the peptide concentration that caused 50% hemolysis (compared to human erythrocytes treated with water or 0.1% Triton-X 100 as 100% lysis) of erythrocytes after 18h (HC₅₀).



Peptide Name	Length	Sequence	MW
D-Piscidin 1	22	NH ₂ -FFHHIFRGIVHVGKTIHRLVTG-amide	2571
D-Piscidin 1 I9K	22	NH ₂ -FFHHIFRGKIVHVGKTIHRLVTG-amide	2586
D-Dermaseptin S4	27	NH ₂ -ALWMTLLKKVLKAAAKALNAVLVGANA-amide	2778
D-Dermaseptin S4 L7K, A14K	27	NH ₂ -ALWMTLLKKVLKAKAKALNAVLVGANA-amide	2851

Fig. 1. Helical net representation of D-piscidin 1 and D-dermaseptin S4 analogs. The one-letter code is used for amino acid residues. D denotes that all residues in the peptides are in the D-conformation. Positively charged residues (Lys and Arg) are colored light blue, large hydrophobic residues (Val, Ile, Leu, Phe, Met and Trp) are colored yellow. The “specificity determinant(s)” are denoted by pink triangles. The residues on the polar face are boxed and the residues on the non-polar face are circled. The $i \rightarrow i+3$ and $i \rightarrow i+4$ potential hydrophobic interactions along the helix are shown as black bars. D-dermaseptin S4 (27-mer) reported here involved a deletion of Ala18 from the 28-mer sequence reported in the literature [9]. This deletion results in 10 out of 11 large hydrophobes being located on the non-polar face with only Val23 being on the polar-face as shown above.

Antibacterial activities against 11 strains of *A. baumannii* and 20 strains of *S. aureus* are compared in Tables 1 and 2, respectively. Geometric mean of MIC values was calculated to provide an overall view of antibacterial activity of different analogs. It is clear that all four of our peptides were effective in killing Gram-negative pathogen *A. baumannii*. The single specificity determinant analog (D-piscidin 1 I9K) and D-dermaseptin S4 L7K, A14K with two specificity determinants exhibited similar or improved antibacterial activity compared to their parent peptides: D-piscidin 1 and D-dermaseptin S4 (Table 1). However, the new analogs have a dramatic decrease in antibacterial activity against Gram-positive pathogen *S. aureus* (Table 2).

As summarized in Table 3, a single “specificity determinant” had a dramatic effect in lowering the hemolytic activity of D-piscidin 1 from a HC₅₀ value of 1.8 μM to 98 μM for D-piscidin 1 I9K, a 54-fold improvement (Table 3). In addition, two “specificity determinants” in D-dermaseptin S4 gave the analog D-dermaseptin S4 L7K, A14K which decreased hemolytic activity from 0.6 μM to a HC₅₀ value of 241 μM, a 402-fold improvement in hemolytic activity (Table 3).

Table 1. Peptide antimicrobial activity (MIC^a (μM)) against Gram-negative *A. baumannii* clinical isolates.

Strain	Source	Peptide Name			
		D-Piscidin 1	D-Piscidin 1 I9K	D-Dermaseptin S4	D-Dermaseptin S4 L7K,A14K
ATCC 17978	Fatal meningitis	3.0	3.0	2.8	0.7
ATCC 19606	Urine	3.0	1.5	2.8	0.7
649	Blood	3.0	3.0	1.4	0.7
689	Groin	1.5	3.0	1.4	0.7
759	Gluteus	3.0	3.0	1.4	1.4
821	Urine	3.0	3.0	2.8	0.7
884	Axilla	3.0	3.0	2.8	1.4
899	Perineum	3.0	3.0	1.4	1.4
964	Throat	3.0	3.0	1.4	2.7
985	Pleural fluid	1.5	3.0	0.7	0.7
1012	Sputum	6.1	6.0	2.8	2.7
	GM ^b	2.8	3.0	1.8	1.1

^aMIC is minimal inhibitory concentration (μM) that inhibited growth of different strains in Mueller-Hinton (MH) medium at 37°C after 24h; MIC is given based on three sets of determinations; ^bGM is the geometric mean of the MIC values from 11 different isolates of *A. baumannii*.

Table 2. Peptide antimicrobial activity (MIC^a (μM)) against Gram-positive *S. aureus* clinical isolates.

Strain	Source	Peptide Name			
		D-Piscidin 1	D-Piscidin 1 I9K	D-Dermaseptin S4	D-Dermaseptin S4 L7K,A14K
M22315		3.0	773.4	11.3	>350.8
M22274	Spine	3.0	773.4	11.3	>350.8
M22300	Finger	3.0	773.4	5.6	>350.8
M22287	Hip	3.0	773.4	5.6	>350.8
M22312	Finger	6.1	773.4	11.3	>350.8
M21935	Resp.	3.0	386.7	5.6	>350.8
M22111	Ear	1.5	3.0	5.6	87.7
M22075	Axilla	3.0	386.7	2.8	>350.8
M21913	Finger	3.0	193.3	5.6	>350.8
BL7429	Blood	3.0	193.3	2.8	>350.8
M22097	Neck	6.1	193.3	5.6	>350.8
M21991	Resp.	6.1	193.3	5.6	>350.8
M22424	Arm	3.0	773.4	11.3	>350.8
M22111	Ear	3.0	96.7	5.6	>350.8
M22360	Labia	1.5	3.0	5.6	>350.8
M22354		3.0	773.4	5.6	>350.8
M21756	Nose	3.0	386.7	2.8	>350.8
M22130		3.0	12.1	5.6	>350.8
M22224	Leg	3.0	96.7	5.6	>350.8
M21742	Nose	3.0	96.7	5.6	>350.8
	GM ^b	3.1	180	5.8	Inactive

^aMIC is minimal inhibitory concentration (μM) that inhibited growth of different strains in Mueller-Hinton (MH) medium at 37°C after 24h; MIC is given based on three sets of determinations; ^bGM is the geometric mean of the MIC values from 12 different isolates of Methicillin-sensitive *S. aureus* (from strain M22315 to M21991) or 8 different isolates of Methicillin/Oxacillin-resistant *S. aureus* (from strain M22424 to M21742).

The corresponding therapeutic indices when comparing hemolytic activity and antimicrobial activity against *A. baumannii* showed a dramatic improvement of 55-fold and 730-fold, respectively (Table 3).

However, the antibacterial activity against the Gram-positive pathogen *S. aureus* was lost. The new peptide analogs turned into Gram-negative pathogen-selective AMPs with a Gram-negative selectivity factor of 60 for D-piscidin 1 I9K and >319 for D-dermaseptin S4 L7K, A14K (Table 3).

Table 3. Summary of biological activity.

Peptide Name	Hemolytic activity		Antimicrobial activity				Gram-negative selectivity factor ^f
			A. baumannii		S. aureus		
	HC ₅₀ ^a (μM)	Fold ^b	MIC _{GM} ^c (μM)	T. I. ^d	Fold ^e	MIC _{GM} ^c (μM)	$\frac{MIC_{GM} (S. aureus)}{MIC_{GM} (A. baumannii)}$
D-Piscidin 1	1.8	1.0	2.8	0.6	1.0	3.1	1.1
D-Piscidin 1 I9K	98	54	3.0	33	55	180	60
D-Dermaseptin S4	0.6	1.0	1.8	0.3	1.0	5.8	3.2
D-Dermaseptin S4 L7K,A14K	241	402	1.1	219	730	>351 ^g	>319

^aHC₅₀ is the concentration of peptide (μM) that results in 50% hemolysis after 18h at 37°C; ^bThe fold improvement in HC₅₀ compared to that of native D-Piscidin 1, D-Dermaseptin S4 are bolded; ^cMIC is the minimum inhibitory concentration (μM) of peptide that inhibits growth of bacteria after 24h at 37°C, MIC_{GM} is the geometric mean of the MIC values from 11 different isolates of *A. baumannii* or 20 different isolates of *S. aureus*; ^d“T.I.” denotes therapeutic index, which is the ratio of the HC₅₀ value (μM) over the geometric mean MIC value (μM), where large values indicate greater antimicrobial specificity; ^eThe fold improvement in therapeutic index compared to that of native D-Piscidin 1, D-Dermaseptin S4 are bolded; ^fThe ratio of the MIC_{GM} (*S. aureus*) versus MIC_{GM} (*A. baumannii*) indicates selectivity for Gram-negative versus Gram-positive bacteria, where the larger the value, the greater the selectivity for *A. baumannii*; ^gInactive against *S. aureus*.

In summary, we have taken two examples of native AMPs, piscidin 1 and dermaseptin S4, to demonstrate the universality of our “specificity determinant” design concept to effect a dramatic reduction in AMP hemolytic activity and antibacterial activity against the Gram-positive pathogen *S. aureus*, while maintaining or improving antibacterial activity against Gram-negative pathogen *A. baumannii* to successfully generate Gram-negative pathogen-selective AMPs as potential drug candidates. To us, the excitement in the field of amphipathic α-helical AMPs lies in our demonstration that a single or double substitution in nature’s AMP sequences can have such a dramatic effect on changing their biological profiles for drug development.

Acknowledgments

We thank the John Stewart Endowed Chair in Peptide Chemistry to Robert S. Hodges for financial support.

References

1. Gura, T. *Science* **291**, 2068-2071 (2001), <http://dx.doi.org/10.1126/science.291.5511.2068>
2. Levy, O. *Blood* **96**, 2664-2672 (2000).
3. Kondejewski, L.H., et al. *J. Biol. Chem.* **272**, 13181-13192 (1999), <http://dx.doi.org/10.1074/jbc.274.19.13181>
4. McInnes, C., et al. *J. Biol. Chem.* **275**, 14287-14294 (2000), <http://dx.doi.org/10.1074/jbc.275.19.14287>
5. Chen, Y., et al. *J. Biol. Chem.* **280**, 12316-12329 (2005), <http://dx.doi.org/10.1074/jbc.M413406200>
6. Chen, Y., Vasil, A.I., Rehaume, L., Mant, C.T., Burns, J.L., Vasil, M.L., Hancock, R.E., Hodges, R.S. *Chem. Biol. Drug Des.* **67**, 162-173 (2006), <http://dx.doi.org/10.1111/j.1747-0285.2006.00349.x>
7. Jiang, Z., Vasil, A.I., Gera, L., Vasil, M.L., Hodges, R.S. *Chem. Biol. Drug Des.* **77**, 225-240 (2011), <http://dx.doi.org/10.1111/j.1747-0285.2011.01086.x>
8. Jiang, Z., Vasil, A.I., Vasil, M.L., Hodges, R.S. *Pharmaceuticals* **7**, 366-391 (2014), <http://dx.doi.org/10.3390/ph7040366>
9. Mor, A., Nicolas P. *Eur. J. Biochem.* **219**, 145-154 (1994), <http://dx.doi.org/10.1111/j.1432-1033.1994.tb19924.x>

Structure-Based Optimization of a Potent PACE4 Inhibitor Containing a Decarboxylated P1 Arginine Mimetic

Anna Kwiatkowska, Christine Levesque, Frédéric Couture, Kévin Ly,
 Frédéric Dufour, and Robert Day

Institut de pharmacologie de Sherbrooke (IPS) et département de chirurgie/service d'urologie, Faculté de médecine et des sciences de la santé (FMSS), Université de Sherbrooke, Sherbrooke, J1H 5N4, Québec, Canada

Introduction

Our recent studies have provided direct evidence for the critical role of PACE4 in the progression of prostate cancer, identifying this enzyme as a promising target to design novel and effective treatments [1]. Moreover, we developed a potent PACE4 inhibitor with considerable selectivity (20-fold over furin) known as the Multi-Leu (ML) peptide [2]. In order to improve its pharmacological profile, we performed structure-activity relationship (SAR) studies and determined that the incorporation of the decarboxylated arginine mimetic (4-amidinobenzylamide, Amba) at the P1 position led to a more potent and stable analog [3]. Unfortunately, this inhibitor suffered from a reduced selectivity towards PACE4. To restore its specificity profile, we used a positional-scanning approach and synthesized peptide libraries by substituting each amino acid residue in the leucine core of our inhibitor. These studies revealed that we are able to enhance the specificity profile (3-fold) and preserve the inhibitory activity as well as antiproliferative properties of our inhibitor by incorporating a leucine isomer – L-isoleucine into its structure (Maluch, et al., unpublished data). Based on these results, we decided to perform further SAR studies aiming to improve the specificity and activity of our MLamba inhibitor. We focused on the leucine core (P8-P5) and its modification with unnatural amino acid residues possessing hydrophobic character (Figure 1). First we evaluated the impact of a single substitution (from the P8 to P5 position) on the inhibitory activity of the resulting peptides, and then we combined the most promising modifications. In this work, we present the synthesis and biological evaluation of a new series of MLamba analogs.

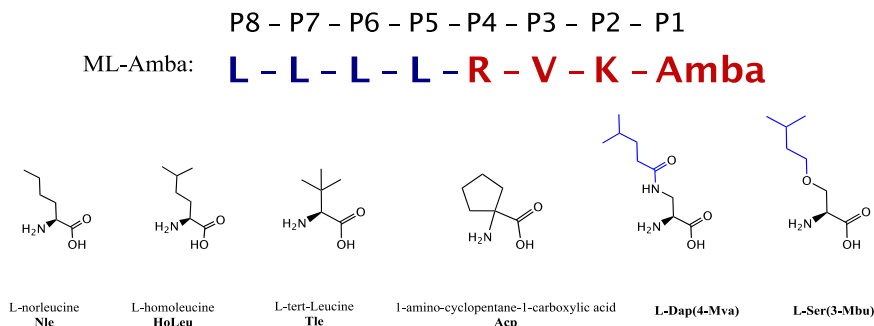


Fig. 1. The amino acid residues selected to modify the leucine core (P8-P5 position) of the MLamba inhibitor.

Results and Discussion

All peptides were obtained by a combination of solid-phase peptide synthesis and solution synthesis as previously described [3]. The scan of the P5, P6 and P7 (with the exception of the Tle^{P7}) position resulted in analogs with reduced inhibitory potency against PACE4 when compared to the initial peptide (MLamba), revealing that Leu residues at these positions provide higher binding affinity for the enzyme (Figure 2A). On the other hand, the Tle-substitution at the P7 and P8 positions had a beneficial effect and led to peptides with improved activity, while the Acp^{P8}-analog maintained potency similar to the MLamba inhibitor. In the case of analogs with combined modifications, only

one peptide substituted at the P8 and P5 positions with the Nle displayed enhanced activity against PACE4 (Figure 2B).

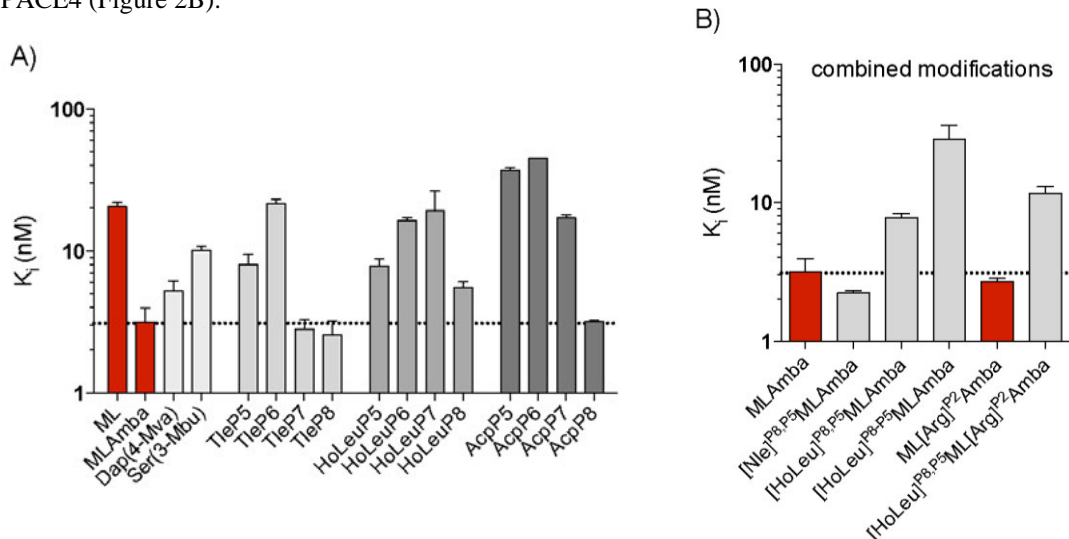


Fig. 2. Inhibitory activity of the new MLamba analogs towards PACE4. A) Positional scanning in the leucine core of the MLamba peptide. B) Activity of the analogs containing multiple substitutions. Results are means \pm SD from three independent experiments. Control peptides are indicated in red.

Regarding the antiproliferative activity, the incorporation of the Tle residue to the MLamba peptide yielded analogs with significantly diminished potency, whereas the HoLeu-substitution preserved the inhibitory activity of the resulting peptides (Table 1). In the case of the Ser(3-Mbu)^{P5}-modified peptide, its activity towards DU145 and LNCaP cells was reduced (3.2- and 4.2-fold, respectively), while the compound containing Acp^{P8} or Dap(4-Mva)^{P8} showed no inhibitory effect.

Table 1. Antiproliferative activity and cytotoxicity of the selected analogs.

Analog	IC_{50} (μ M) \pm SD (DU145)	IC_{50} (μ M) \pm SD (LNCaP)	LDH (DU145) at IC_{50} concentration
Ac-LLLLRVK[Amba]	25 \pm 10	40 \pm 15	< 5%
[Tle] ^{P5} MLamba	115 \pm 10	180 \pm 50	< 5%
[Tle] ^{P6} MLamba	150 \pm 25	N.C.	< 5%
[Tle] ^{P7} MLamba	120 \pm 5	N.C.	< 5%
[Tle] ^{P8} MLamba	130 \pm 10	N.C.	< 5%
[HoLeu] ^{P5} MLamba	30 \pm 5	50 \pm 10	< 5%
[HoLeu] ^{P6} MLamba	40 \pm 10	40 \pm 10	< 5%
[HoLeu] ^{P7} MLamba	30 \pm 5	80 \pm 25	< 5%
[HoLeu] ^{P8} MLamba	30 \pm 10	30 \pm 10	< 5%
[Acp] ^{P8} MLamba	N.C.	N.C.	< 5%
[Dap(4-Mva)] ^{P8} MLamba	N.C.	N.C.	< 5%
[Ser(3-Mbu)] ^{P5} MLamba	80 \pm 5	170 \pm 20	< 5%
[Nle] ^{P8,P5} MLamba	50 \pm 10	85 \pm 10	< 5%
[HoLeu] ^{P8,P5} MLamba	15 \pm 1	30 \pm 3	< 5%
[HoLeu] ^{P8,P5} MLamba	11 \pm 1	130 \pm 70	< 5%

IC_{50} s were calculated from the dose-response curves using DU145 and LNCaP cell lines. The lactate dehydrogenase (LDH) release (an indicator of acute cytotoxicity) was quantified relative to the untreated control. Results are means \pm SD from three independent experiments, N.C. - not calculable.

The modification of the MLamba peptide with Nle residues at the P5 and P8 position slightly reduced its antiproliferative activity, whereas the incorporation of multiple HoLeu substitutions greatly improved it. However, it was shown that some of the most potent analogs in this test exhibited not only an antiproliferative effect on cancer cells, but were also cytotoxic at higher concentration (Figure 3).

Regarding the selectivity profile of the new MLamba analogs over furin, in general the selected modifications did not result in peptides with improved selectivity with the exception of two compounds substituted with HoLeu^{P5} and Acp^{P8}, which were more selective towards PACE4 (2- and 3-fold respectively) when compared to the initial peptide.

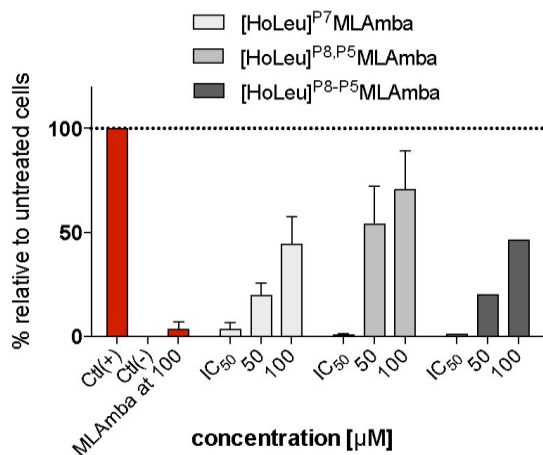


Fig. 3. Cytotoxic effect (LDH release) of the selected analogs at various concentrations on DU145 cells.

These data demonstrate that the modification of the leucine core of the MLamba inhibitor has crucial impact on the inhibitory activity of the resulting peptides. Among all the modification tested, the HoLeu residue turned out to be the most favorable. Although, HoLeu-substituted analogs did not exhibit enhanced potency in the kinetic assay with recombinant PACE4, they showed comparable or improved antiproliferative activity against prostate cancer cells. Bearing in mind that the incorporation of the unnatural amino acids into a peptide sequence should also improve its stability, we are undertaking further studies on our analogs and we will test their stability in plasma. We believe that these findings lay the foundation for future research focusing on the development of more potent, specific and stable PACE4 inhibitors with the potential to become new drug candidates to treat prostate cancer.

Acknowledgments

The authors thank Xue Wen Yuan for assistance with peptide synthesis, Roxane Desjardins for enzyme preparation, Sophie Beauchemin for the synthesis of Fmoc-L-Ser(3-Mbu) and assistance with the synthesis of the Amba modification, and Nicolas Dory for help with enzyme kinetic studies. AK holds a Heart and Stroke Foundation postdoctoral fellowship. FC holds a Banting and Charles Best Canada Graduate Scholarships (Grant #315690) from CIHR and a Graduate Studentship from Prostate Cancer Canada (Grant #GS-2015-07). FD holds a MS Student Scholarships from the FRQ-S and CIHR.

References

1. Couture, F., et al. *Neoplasia* **14**, 1032-1042 (2012). <http://dx.doi.org/10.1593/neo.121368>
2. Levesque, C., et al. *J. Med. Chem.* **55**, 10501-10511(2012), <http://dx.doi.org/10.1021/jm3011178>
3. Kwiatkowska, A., et al. *J. Med. Chem.* **57**, 98-109 (2014), <http://dx.doi.org/10.1021/jm401457n>

From Bench to Clinical Using a Combinatorial Screenings of Phage-Displayed Peptide Libraries

Nelson Santiago Vispo¹ and Hortensia Rodríguez Cabrera²

¹Prometeo Researcher SENESCYT, School of Biology, Yachay Tech, Yachay; ²School of Chemistry, Yachay Tech, Yachay City of Knowledge, Urcuqui, Ecuador

Introduction

Phage peptide display technology

Phage peptide display technology was not initially designed to develop cyclic peptide compounds when it was first introduced [1]. In this technology, each phage particle displays a unique peptide on its surface and the winner can be selected for binding toward a target molecule. Usually, peptides are displayed on the *N*-terminus, the middle, or the *C*-terminus of coat proteins, and the peptide sequence from each phage particle is directed by the DNA sequence of the same phage particle, allowing an easy sequence determination. The selection can be repeated as long as encoding DNA molecules are preserved, and this repeated procedure, called biopanning, is used to enrich the best binders. Billions of pooled peptides presented on phage particles form a phage displayed peptide library, and in contrast to regular synthetic small molecule libraries, as many as 10^{10} different peptides can be screened simultaneously for the desired activity [2].

Cyclic Peptides

Cyclic peptides are polypeptide chains taking ring structures, typically bind with much higher affinity to target proteins than linear ones, due to a smaller reduction in entropy upon binding, allowing an enhanced binding toward target molecules, or better receptor selectivity [3,4]. The ring structure can be formed by linking one end of the peptide and the other with chemically stable bonds. Head-to-tail cyclization is the amide bond formation between amino and carboxyl termini, and many biologically active cyclic peptides are formed by this way. However, cyclic peptide libraries are most easily generated by forming a disulfide bridge between two cysteine's within the peptide [5] (Figure 2).

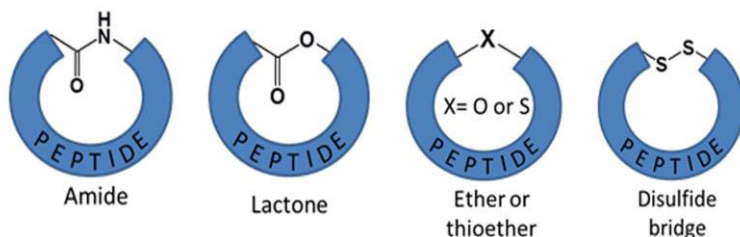


Fig. 2. Chemically stable bonds used to cyclize linear peptide sequences.

Additional advantage of the cyclic peptides:

- Higher proteolytic stability, due to the lack of both, amino and carboxyl termini. Cyclic peptides can be resistant even to endopeptidases.
- Structures less flexible (more rigid) than linear peptides, particularly important aspects for its therapeutic applications.

In order to increase the flexibility of phage display technology, it is desirable to be able to impose some structural constraints on the peptides that are presented by the phage particles. Cyclized peptides from disulfide bridges were sometimes obtained from phage display, for instance the RGD peptide, and a cyclic peptide can be prepared by designing the peptide sequences such as Cys-X₆-Cys for

platelet glycoprotein binding [6]. The phage particles are released to oxygen rich periplasmic space of bacteria, and two neighboring Cys residues would naturally form a disulfide bond to yield a cyclic peptide [7].

Using a peptide-based approach and exploiting the feasibility of cell permeable peptides as carriers, we describe the identification and characterization of proapoptotic cyclic peptide that impairs the phosphorylation by CK2 *in vitro* and that leads to regression when administered directly to solid tumors. This peptide, called CIGB 300, was originally identified by screening a 9-mer random linear and cyclic peptide phage library and by using the human papillomavirus (HPV-16) E7 acidic domain as target. The cyclic peptide obtained compared to the linear peptide selection show an increased biological activity [8]. CIGB-300 elicits antitumor activity in different animal models when administered by different routes [9]. As an investigational drug, CIGB-300 was previously tested in a First-in-Human trial where patients with high grade squamous intraepithelial lesion (HSIL) or epidermoid microinvasive cervical cancer received intralesional injections of this peptide-based drug [10]. That was the first clinical trial in which a drug was used to target the CK2 phosphoacceptor domain providing an early proof-of-principle of a possible clinical benefit. Treatment with CIGB-300 significantly reduced the B23/nucleophosmin levels in tumor specimens. CIGB-300 meets potentialities to be tested in future trials in a neoadjuvant setting prior to chemoradiotherapy in cervical cancer [11] (Figure 2).

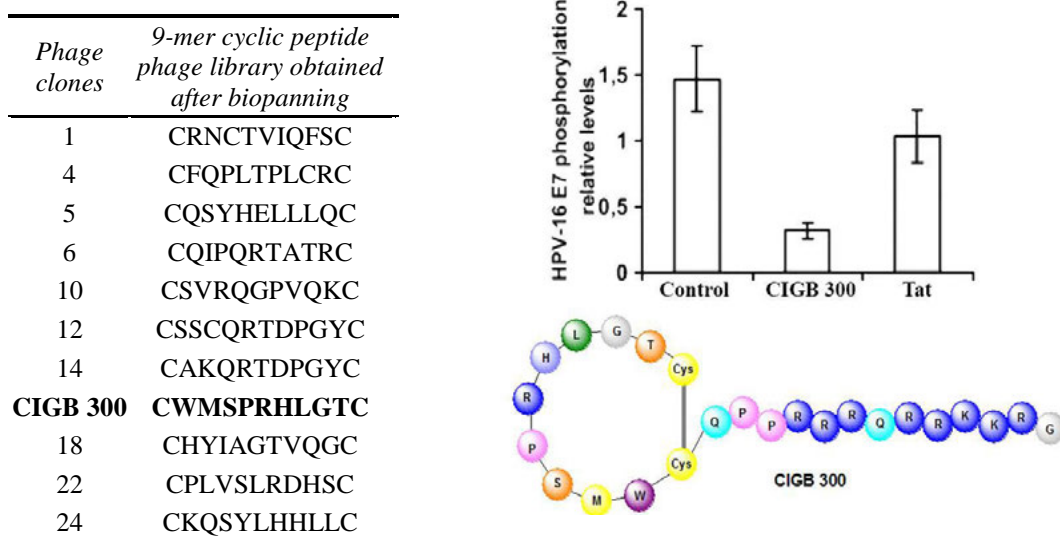


Fig. 2. Structures of cyclic peptides from the cyclic peptide phage display libraries. Phosphorylation was done with a blue stained gel. Levels of the ^{32}P -HPV16 E7-GST protein were normalized with respect to levels of the Coomassie-stained HPV-16 E7-GST. CIGB 300 cyclic peptide with penetration peptide.

Peptide Synthesis

After the selection and identification (sequention) of targeted peptides through phage displayed, the sequences have to be synthesized. Taking into account that in general, the selected peptides by this methodology have short and more or less simple sequences, in the majority of reported cases, the solid phase peptide synthesis (SPPS) is the method of choice.

From Merrifield (1963) until today, the solid-phase principle for peptide synthesis has been conceived and developed with the purpose of providing a rapid, simplified, and effective way to prepare peptides and small proteins. In this sense, Fmoc/t-Bu method, which is based on an orthogonal protecting group strategy, uses the base-labile N-Fmoc group for protection of the α -amino group and acid-labile side-chain protecting groups and resin linkage agents.

Since removal of temporary and permanent protection is effected by completely different chemical mechanisms, side-chain protecting groups and linkage agents can be employed, and are removed under considerably milder conditions than those used in the Merrifield method.

With the linear peptide in hand, the cyclization step becomes the main challenge. Certainly, this procedure, specifically through disulfide bond formation, is one of the most important step in the preparation of these compounds and many successfully strategies have been reported. It also should be mentioned that some selected cyclic sequences have been obtained in the biotinylated form [12].

Cyclization Particularities (Examples)

CIGB-300: CIGB-300 was synthesized on solid phase (Fmoc/t-Bu strategy), and an additional cyclization step was done by oxidation of the linear peptide in ammonia aqueous solution (pH 8.2) for 72 hours with agitation [13].

Cyclic Peptide Ligands for NeutrAvidin and Avidin: The selected NeutrAvidin-binding peptides were also synthesized on solid phase (Fmoc/t-Bu strategy), using RinkAmide-AM resin as solid support. Peptide cyclization was carried out by oxidation of the two cysteines to form an intramolecular disulfide bond. The peptides were shaken in phosphate-buffered saline (PBS; pH 7.4) with 10% dimethyl sulfoxide (DMSO) for 8 h at 37°C. Extent of the disulfide bond formation was monitored as a loss of free thiol using Ellman's reagent.

Others examples of the successful use of this approach are the identification of ligands of tumor necrosis factor- α (TNF- α) [14], neutravidin and avidin, and inhibitors of LEDGF/p75PPI that prevent HIV replication [15].

One drawback of phage display is that the cyclic peptides are formed by disulfide formation, not head-to-tail cyclization. In addition, phage display is limited to natural, ribosomal amino acids. Many amino acids found in biologically active cyclic peptides are non-ribosomal, and they are not accessible with phage display.

Conclusions

Cyclic peptides show better biological activity compared to their linear counterparts due to its conformational rigidity. Biologically active cyclic peptides have been identified through phage display technology and both, solid phase synthetic approaches and cyclizations strategies, have allowed to obtain this potentially biologically active structures for further studies, showing their usefulness as therapeutics and biochemical tools. Cyclic peptides have several structural features making them good drug leads, and there are several naturally occurring cyclic peptides in clinical use.

Acknowledgments

This work was sponsored by the Prometeo Project of the Secretariat for Higher Education, Science, Technology and Innovation of the Republic of Ecuador.

References

1. Smith, G.P. *Science* **228**, 1315-1317 (1985), <http://dx.doi.org/10.1126/science.4001944>
2. Azzazy, H.M., et al. *Clin. Biochem.* **35**, 425-445 (2002), [http://dx.doi.org/10.1016/S0009-9120\(02\)00343-0](http://dx.doi.org/10.1016/S0009-9120(02)00343-0)
3. Edman, P.E.H.R. *Ann. Rev. Biochem.* **28**, 69-96 (1959), <http://dx.doi.org/10.1146/annurev.bi.28.070159.000441>
4. Horton, D.A., et al. *J. Comp. Aided Mol. Des.* **16**, 415-431 (2002), <http://dx.doi.org/10.1023/A:1020863921840>
5. Wilkins, M.R., et al. *The Lancet* **349**, 1307-1310 (1997), [http://dx.doi.org/10.1016/s0140-6736\(96\)07424-7](http://dx.doi.org/10.1016/s0140-6736(96)07424-7)
6. O'Neil, K.T., et al. *Struct. Funct. Bioinform.* **14**, 509-515 (1992), <http://dx.doi.org/10.1002/prot.340140411>
7. Joo, S.H. *Biomolecules & Therapeutics* **20**, 19-26 (2012), <http://dx.doi.org/10.4062/biomolther.2012.20.1.019>
8. Perea, S.E., et al. *Cancer Res.* **64**, 7127-7129 (2004), <http://dx.doi.org/10.1158/0008-5472.CAN-04-2086>
9. Perera, Y., et al. *Inter. J. Cancer* **122**, 57-62 (2008), <http://dx.doi.org/10.1002/ijc.23013>
10. Solares, A.M., et al. *BMC Cancer* **9**, 146 (2009), <http://dx.doi.org/10.1186/1471-2407-9-146>
11. Soriano-García, J.L., et al. *J. Cancer Res. Ther.* **1**, 153-162 (2013), <http://dx.doi.org/10.14312/2052-4994.2013-25>
12. Sclavons, C., et al. *Inter. J. Pept.* **2013**, 9 (2013), <http://dx.doi.org/10.1155/2013/348409>
13. Cabrales-Rico, A., et al. *J. Pharm. Biomedical Analysis* **105**, 107-114 (2015), <http://dx.doi.org/10.1016/j.jpba.2014.11.043>
14. Meyer, S.C., et al. *Chem. Biol. Drug Des.* **68**, 3-10 (2006), <http://dx.doi.org/10.1111/j.1747-0285.2006.00401.x>
15. Desimmie, B.A., et al. *Mol. Ther.* **20**, 2064-2075 (2012), <http://dx.doi.org/10.1038/mt.2012.132>

Department of Chemistry and Biochemistry, University of Arizona, Tucson, AZ, 85721, USA

255

To understand the effect of the extra *N*-acetyl group on lipopeptide binding to TLR2/6, *in silico* molecular docking experiments were performed. The structure of Pam2CysSK4 bound to active TLR2/6 was previously determined [5] and was retrieved from Protein Data Bank (3A79). Since there are too many rotatable bonds in Pam2CysSK4, which leads to inaccuracy in Glide flexible docking, the four lysine residues which according to the crystal structure do not interact with the receptor [5] were deleted and the diacyl chains were trimmed to six carbons to generate the initial conformation of Cap2CysSer (S-[2,3-bis(capryloxy)propyl]cysteinyl-serine) molecule.

To reveal the conformation of *N*-acetyl Cap2CysSer when it binds to the TLR2/6 receptor, Glide docking with the docking flexible option was performed. This option allows all rotatable bonds on the ligand to be able to rotate in order to find out the favorable conformations. Five conformations were found to be energetically favorable with the best docking score of -10.025. Comparing to the initial position of Cap2CysSer, the *N*-acetyl Cap2CysSer is found to be more embedded into the ligand binding pocket of TLR2/6 (Figure 4). It suggests that the *N*-acetyl group on cysteine drives the lipopeptide to bury deeper into the binding pocket.

In conclusion, we developed new synthetic methods that can be used to synthesize *N*-acetyl Pam2Cys analogues. We showed that *N*-acetyl Str2Cys is able to activate TLR2/6, which makes it a promising candidate as a synthetic vaccine adjuvant. Our docking experiments provide information on the ligand-receptor interactions between *N*-acetyl Pam2Cys analogues and TLR2/6. Future work may still be required to establish the use of *N*-acetyl Str2Cys as a synthetic vaccine adjuvant.

Acknowledgments

This research was supported by U.S. Public Health Service, National Institutes of Health (GM104080).

References

1. Jackson, D.C., Lau, Y.F., Le, T., Suhrbier, A., Deliyannis, G., Cheers, C., et al. *Proc. Natl. Acad. Sci. USA* **101**, 15440-15445 (2004), <http://dx.doi.org/10.1073/pnas.0406740101>
2. Purcell, A.W., Zeng, W., Mifsud, N.A., Ely, L.K., Macdonald, W.A., Jackson, D.C. *J. Pept. Sci.* **9**, 255-281 (2003), <http://dx.doi.org/10.1002/psc.456>
3. Muhlradt, P.F., Kiess, M., Meyer, H., Süssmuth, R., Jung, G. *J. Exp. Med.* **185**, 1951-1958 (1997), <http://dx.doi.org/10.1084/jem.185.11.1951>
4. Zeng, W., Ghosh, S., Lau, Y.F., Brown, L.E., Jackson, D.C. *J. Immunol.* **169**, 4905-4912 (2002), <http://dx.doi.org/10.4049/jimmunol.169.9.4805>
5. Kang, J.Y., Nan, X., Jin, M.S., Youn, S.J., Ryu, Y.H., Mah, S., et al. *Immunity* **31**, 873-884 (2009), <http://dx.doi.org/10.1016/j.immuni.2009.09.018>

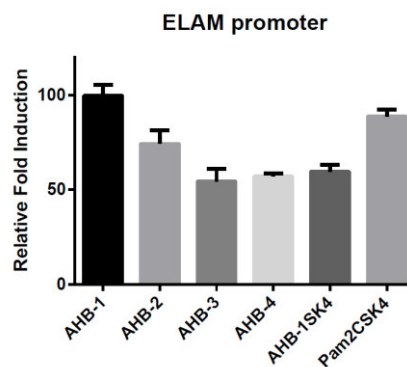


Fig. 3. TLR2/6 activation by *N*-acetyl Pam2Cys and analogues.

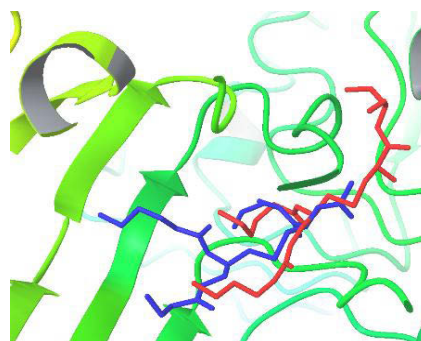


Fig. 4. Comparison of the best flexible docking result (lowest docking score) of *N*-acetyl Cap2CysSer (in blue) with the initial conformation of the Cap2CysSer (in red).

An Auxiliary-Mediated Approach for the Chemoenzymatic Synthesis of Homogenous Glycopeptides

Claudia Bello and Christian F.W. Becker

University of Vienna, Institute of Biological Chemistry, Vienna, 1090, Austria

Introduction

The development of effective methodologies for the production of homogeneous proteins carrying complex PTMs is essential for studying the role of the PTMs in protein function and malfunction. We established a strategy [1] for the synthesis of peptides carrying multiple and complex PTMs, focusing at first on the preparation of homogeneously glycosylated peptides. The tumor marker MUC1, a protein abundantly *O*-glycosylated in its extracellular domain, was chosen as a synthetic target.

Attachment of a monodisperse PEG polymer to the *N*-terminus of our MUC1 peptides changes their solubility properties and allows sequential chemoenzymatic glycosylation of the peptides in solution and their separation from glycosyltransferases and low molecular weight components by simple techniques such as spin column gel permeation chromatography (GPC) and precipitation. This method proved to be high-yielding and versatile, as it could be coupled with native chemical ligation (NCL), thereby giving access to longer site-specifically *O*-glycosylated peptides.

Herein we present the synthesis and application of a photocleavable auxiliary, based on the 1-nitrophenyl-2-sulfanylethyl scaffold previously described by the groups of Aimoto [2] and Dawson [3], that allows attachment of the PEG polymer for efficient enzymatic glycosylation, provides the functional groups for NCL, and is cleanly removed by UV irradiation [4]. Upon photolytic removal a native glycine residue remains at the ligation site (Figure 1B).

Results and Discussion

The multistep chemical synthesis of the new auxiliary was carried out starting from vanillin and opportunely modifying the phenol moiety to accommodate the PEG polymer. In order to prepare the desired auxiliary-peptide conjugate, the MUC1 tandem repeat was synthesized by solid phase peptide synthesis (SPPS) and then modified at its *N*-terminus with an iodoacetyl group. During SPPS a Thr(GalNAc) residue was used to introduce the first sugar of the glycan chain and have full control over the glycosylation site. S_N2 reaction between the iodoacetylated peptide and the auxiliary gave the expected conjugate Aux-MUC1(Tn) in good yields (Figure 1A).

Next, we demonstrated that the PEGylated auxiliary was indeed able to facilitate the fast sequential enzymatic glycosylation of the MUC1 peptides as previously described for *N*-terminally PEGylated MUC1. Glycosylation of Aux-MUC1(Tn) with human C1GalT1 gave Aux-MUC1(T) with a single T antigen (Galβ1-3GalNAcα disaccharide attached to Thr14) in excellent conversion. The incubation with a mixture of ethanol and diethyl ether at -80°C induced the precipitation of the glycopeptide, which was then collected in 95% yield by centrifugation and used in the next glycosylation step without further purification. Incubation of the product with CMPNeu5Ac in the presence of recombinant ST3Gal1 allowed efficient extension of the disaccharide to the Neu5Acα2-3Galβ1-3GalNAcα trisaccharide and gave Aux-MUC1(sT) with the sialyl-T antigen in 90% yield (Figure 1A). Using similar conditions for all glycosylation reactions but by increasing times of incubation with ethanol and ether at -80 °C (6-12h instead of 4h), the sequential glycosylation procedure was simplified by omitting the GPC spin column step. As a control we have also used MUC1(Tn) without the auxiliary in this glycosylation-precipitation procedure and only 27% yield of MUC1(T) was recovered, clearly demonstrating the advantages of PEGylation.

We then coupled glycosylation and NCL reaction. A MUC1 peptide thioester (MUC1-SR) was prepared by hydrazinolysis of the MUC1 peptidyl resin and subsequent oxidation of the obtained peptide hydrazide [5]. Aux-MUC1(Tn) was converted via sequential enzymatic glycosylation into the sialylated core 1 containing conjugate Aux-MUC1(sT), which was recovered by precipitation and directly used in a ligation reaction with the MUC1-SR thioester fragment giving the desired product MUC1-Aux-MUC1(sT) in one day and with 70% conversion. Finally, light-induced removal of the PEGylated auxiliary was accomplished by UV irradiation of the crude ligation mixture in a water/acetonitrile mixture (Figure 1B). No starting material was detectable after 30 min of irradiation

with an UV-A lamp and simultaneously a new peak formed corresponding to the desired product, which was isolated by HPLC purification.

To further explore the potential of this approach, the synthesis of fully unprotected conjugates comprising two glycosylated MUC1 peptides was accomplished (Figure 1C). A MUC1 peptide carrying the Tn antigen at position Thr7 (instead of Thr14) was synthesized and converted into a peptide α -thioester. Hydrazine cleavage, deprotection, and treatment with NaNO_2 and MesNa smoothly led to the desired MUC1-(Tn⁷)-SR in 43% yield.

This peptide thioester was used in NCL with the conjugate Aux-MUC1(Tn) to give MUC1(Tn⁷)-Aux-MUC1(Tn) in 35% yield. The ligation product was efficiently used in the glycosylation-precipitation procedure leading to MUC1(T⁷)-Aux-MUC1(T) consisting of two MUC1 tandem repeats with a T antigen at different positions. This much longer peptide with only one auxiliary was efficiently recovered by precipitation (80% recovery) under similar conditions as described above. Subsequently, it was submitted to UV irradiation at 365 nm for 6 min and the desired MUC1(T⁷)-G-MUC1(T) was obtained in 53% yield. MUC1(T⁷)-Aux-MUC1(T) was also used in a further glycosylation-precipitation step leading to sialylated MUC1(sT⁷)-Aux-MUC1(sT) (68% recovery). UV irradiation cleanly removed the auxiliary and pure MUC1-(sT⁷)-G-MUC1(sT) was obtained in 12% yield after HPLC purification (Figure 1C). These results demonstrate the power of this approach for the chemoenzymatic synthesis of glycosylated peptides and its combination with NCL to obtain larger polypeptides with different but specific glycosylation patterns.

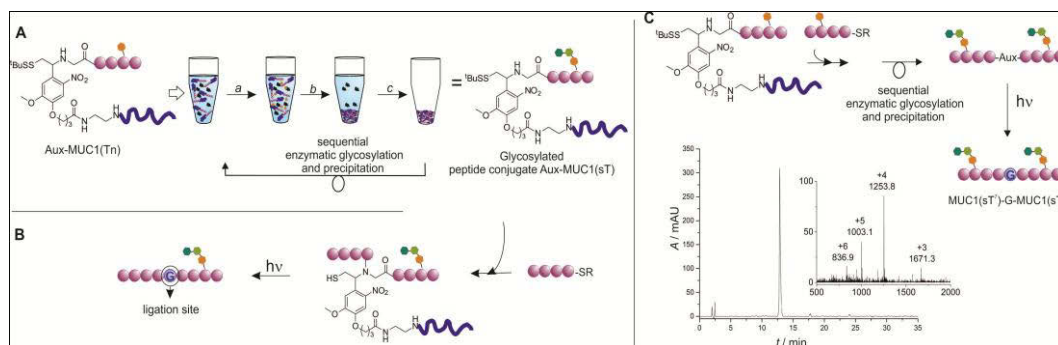


Fig. 1. Auxiliary-mediated enzymatic glycosylation (A) and ligation approach (B). HPLC chromatogram and ESI-MS spectrum of the native Mucin1 analog MUC1(sT⁷)-G-MUC1(sT) (C).

Acknowledgments

We thank the MS center of the Department of Chemistry at the University of Vienna for help with MS analysis of a variety of compounds, and M. Arndt, L. Mairhofer, and J. Cotter for help with laser experiments. The Alexander von Humboldt foundation is kindly acknowledged for financial support to C.B.

References

- Bello, C., Farbiarz, K., Moeller, J.F., Becker, C.F.W., Schwientek, T. *Chem. Sci.* **5**, 1634-1641 (2014), <http://dx.doi.org/10.1039/C3SC52641K>
- Kawakami, T., Aimoto, S. *Tetrahedron Lett.* **44**, 6059-6061 (2003), [http://dx.doi.org/10.1016/S0040-4039\(03\)01463-1](http://dx.doi.org/10.1016/S0040-4039(03)01463-1)
- Marinzi, C., Offer, J., Longhi, R., Dawson, P.E. *Bioorg. Med. Chem.* **12**, 2749-2757 (2004), <http://dx.doi.org/10.1016/j.bmc.2004.02.039>
- Bello, C., Wang, S., Meng, L., Moremen, K.W., Becker, C.F.W. *Angew. Chem. Int. Ed.* **54**, 7711-7715 (2015), <http://dx.doi.org/10.1002/anie.201501517>
- Bello, C., Kikul, F., Becker, C.F.W. *J. Pept. Sci.* **21**, 201-207 (2015), <http://dx.doi.org/10.1002/psc.2747>

High-Throughput Process Optimization and Difficult Peptide Synthesis on the Symphony® X

**Daniel Martinez, James P. Cain, Elizabeth Restituyo-Rosario,
Katya Karankevich, Peter Bergwall, and Nathaniel Cosper**

Protein Technologies, Inc., Tucson, AZ, 85714, USA, Website: www.ptipep.com, Email: info@ptipep.com

Introduction

The Symphony X® multiple peptide synthesizer offers the greatest number of independent protocols of any instrument on the market, making it an ideal platform for high-throughput process development. Furthermore, the addition of rapid IR heating provides a powerful tool for completing even the most difficult peptide sequences.

A range of conditions, including variations in the resin, deprotection and coupling reagents, activation, and reaction time was screened simultaneously to optimize the synthesis of the 31-mer C-Peptide (Figure 1). Temperature may also be varied on the Symphony X® through the use of IR heating, as applied to the synthesis of the challenging peptide thymosin $\alpha 1$ (Figure 2).

EAEDLQVGQVELGGGPGAGSLQPLALEGSLG

Fig. 1. Sequence of C-Peptide.

Ac-SDAAVDTSSSEITTKDLKEKKEVVEEAEN

Fig. 2. Sequence of Thymosin $\alpha 1$.

Results and Discussion

The power of the Symphony XTM for process optimization has been demonstrated through the synthesis of C-Peptide using multiple reaction conditions. The target 31-mer peptide was obtained with crude purities ranging from 80 to 92%. Among the variations in the 22 conditions screened, reaction time, coupling reagent, and the choice of resin all had an effect on the product purity. For example, under otherwise equivalent conditions, slightly higher purities were noted for the synthesis on Tentagel S RAM than with standard Rink MBHA polystyrene resin (Figure 3).

Illustrating the advantage of rapid heating to 85°C during deprotection and coupling, thymosin $\alpha 1$ was prepared with 80% purity (Figure 4). This is the highest purity that has been reported for the synthesis of this peptide. Impressively, this result was produced using just one minute deprotections and two minutes coupling times.

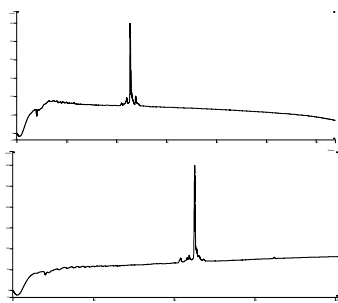


Fig. 3. HPLC traces for C-Peptide synthesized using Rink MBHA PS (left, 82% purity) and Tentagel S RAM resin (right, 88% purity).

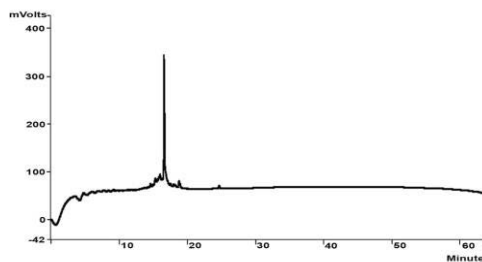


Fig. 4. HPLC trace of thymosin $\alpha 1$ synthesized in 80% purity using IR heating.

A Comparison of Heating Protocols for the Cyclization of Melanotan II on the Prelude® X

Daniel Martinez, James P. Cain, Elizabeth Restituyo-Rosario,
Katya Karankevich, Peter Bergwall, and Nathaniel Cosper

Protein Technologies, Inc., Tucson, AZ, 85714, USA, Website: www.ptipep.com, Email: info@ptipep.com

Introduction

Cyclic peptides typically offer enhanced stability as well as increased potency and selectivity for biological targets compared to their linear counterparts. A number of methods for on-resin cyclization of peptides have been described, allowing for convenient automation; however, depending on the sequence, cyclization of synthetic peptides may be a challenging and time-consuming process.

Heat-assisted synthesis has been shown to reduce the time necessary to produce high-purity linear peptides, and its application to the synthesis of cyclic peptides may provide similar advantages. To demonstrate the utility of heating in the preparation of a cyclic peptide, the potent melanocortin receptor agonist Melanotan II (MT-II) [1] has been synthesized using the Prelude® X peptide synthesizer. The Prelude® X is the first instrument to use rapid induction heating, with six parallel and independently heated channels.

Multiple temperature profiles were tested in parallel for the optimization of the cyclization reaction of MT-II, with the lactam formation *via* the Asp and Lys side chains performed for one or five minutes at both 55°C and 85°C.



Fig. 1. Sequence of MT-II peptide.

Results and Discussion

The synthesis of MT-II peptide using induction heating was found to improve cyclization times and the efficiency of the cyclization reaction. Heating at 55°C or 85°C was effective for accelerating the reaction, but the highest purity was achieved by heating to 85°C for 5 minutes (Table 1, Figure 1).

Induction heating achieved a significant decrease of cyclization time without compromising peptide crude purity. Efficient cyclization was obtained even from one minute cyclization reaction times at two different temperatures.

Table 1. Cyclization times and crude purity for MT-II peptides performed at different temperatures.

Temperature (°C)	Cyclization time	Purity (%)
55	1 min	68.7
85	1 min	69.5
55	5 min	67.8
85	5 min	72.6

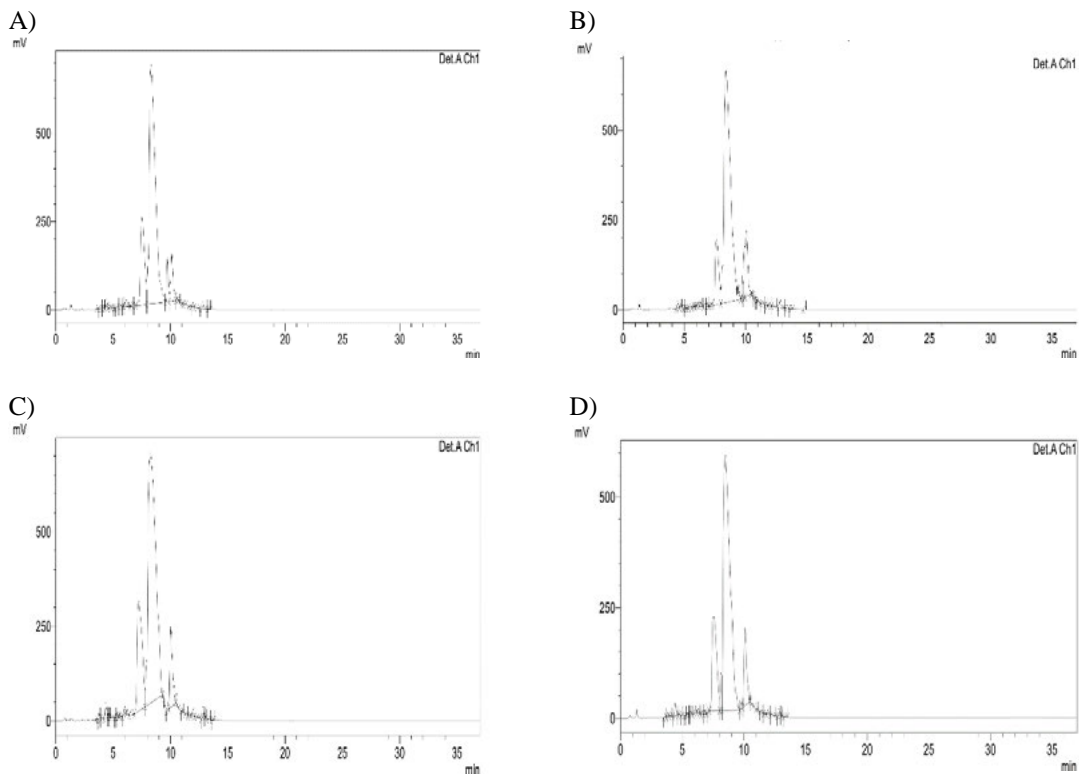


Fig. 2. HPLC analysis of the MT-II cyclic peptide utilizing different protocols. A) 1 min cyclization time at 55°C, B) 1 min cyclization time at 85°C, C) 5 min cyclization time at 55°C, and D) 5 min cyclization time at 85°C.

References

1. Al-Obeidi, F., Hadley, M.E., Pettitt, B.M., Hruby, V.J. *J. Am. Chem.Soc.* **111**, 3413-3416 (1989), <http://pubs.acs.org/doi/abs/10.1021/ja00191a044>

Identifying Immunogenic CD4⁺ T-cell Epitopes of Myeloid Cell Leukemia 1 Using Overlapping 20-mer Peptides Spanning the Whole Protein

Joshua S. Woodworth¹, Else M. Agger¹, and Paul R. Hansen²

¹Department of Infectious Disease Immunology, Statens Serum Institut, Copenhagen, DK-2200, Denmark;

²Department of Drug Design and Pharmacology, University of Copenhagen, Copenhagen, DK-2100, Denmark

Introduction

Myeloid cell leukemia 1 (Mcl-1) is an anti-apoptotic protein which is overexpressed in various leukemia and other cancers [1]. Mcl-1 has a very short half-life [2], which has been suggested as a molecular mechanism for cells to switch into either the survival or apoptotic pathways in response to different stresses [3]. Recently, it has been demonstrated that downregulation of Mcl-1 by various pharmacological agents or genetic approaches dramatically increases ABT-737 lethality in various malignant cell types [4]. Different strategies for targeting Mcl-1 include (i) small interfering RNA [5] (ii) small-molecule inhibitors [6] and (iii) peptide inhibitors [7]. In recent years, therapeutic vaccination with synthetic peptides derived from anti-apoptotic proteins such as Mcl-1 has emerged as a promising strategy against hematological cancers.

In this study, 34 overlapping 20-mer peptides, spanning the entire Mcl-1 protein, were adjuvanted with cationic liposomes [8] and tested in three different mouse strains with varied Major Histocompatibility Complex (MHC) haplotypes (FVB [H-2q], CB6F1[H-2b/d], B6CBAF1 [H-2b/k]) to identify immunogenic CD4⁺ T-cell epitopes.

Results and Discussion

The peptides were synthesized by Fmoc SPPS on a Tentagel S Ram Resin. Each amino acid was coupled in 3-fold excess using HATU, HOAt and DIEA (1:1:1.5) in DMF. Deprotection of the Fmoc group was effected by 20% piperidine in DMF. Following synthesis the peptides were cleaved from the resin for 2h using reagent TFA/TIS/DTT/H₂O (88:2:5:5). The products were then purified by preparative RP-HPLC and characterized by MALDI-TOF-MS.

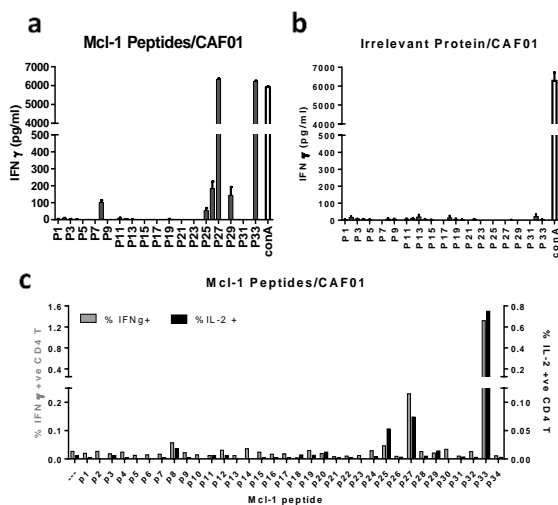


Fig. 1. Immunogenicity of Mcl-1 peptides in CB6F1 mice.

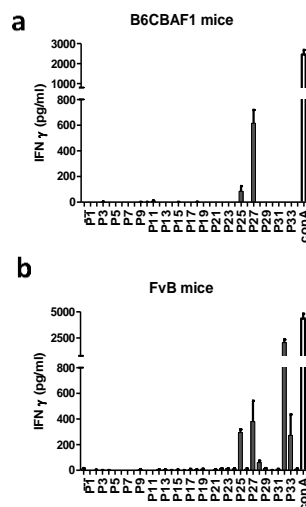


Fig. 2. Mcl-1 peptides in B6CBAF1 and FvB mice.

MFGLKRNAVI	GLNLYCGGAG	LGAGSGGATR	PGGRLLATEK	EASARREIGG
GEAGAVIGGS	AGASPPSTLT	PDSRRVARPP	PIGAEVPDVT	ATPARLLFFA
PTRRAAPLEE	MEAPAADAIM	SPEEELDGYE	PEPLGKRPAV	LPLLELVGES
GNNTSTDGSL	PSTPPPAEEE	EDDLYRQSLE	IISRYLREQA	TGAKDTKPMG
RSGATSRKAL	ETLRRVGDGV	QRNHETAFQG	MLRKLDIKNE	DDVKSLSRVM
IHFVSDGVTN	WGRIVTLISF	GAFVAKHLKT	INQESCIEPL	AESITDVLVR
TKRDWLVKQR	GWDGFVEFFH	VEDLEGGIRN	VLLAFAGVAG	VGAGLAYLIR

Mcl_1: MFGLKRNAVI GLNLYCGGAG; Mcl_2: GLNLYCGGAG LGAGSGGATR etc.

Fig. 3. Mcl-1 Sequence.

To investigate the induction of CD4 T cell responses following Mcl-1 peptide vaccination, mice were immunized s.c. with a pool of overlapping peptides spanning the human Mcl-1 sequence adjuvanted with cationic liposomes (CAF01). CAF01 is known to specifically drive a strong CD4⁺ Th1/Th17 response [9-10]. Splenocytes from immunized mice were restimulated with individual Mcl-1 peptides and IFN γ released measured after three days to evaluate peptide immunogenicity.

Initial immunizations were focused on responses in B6 x BALB/c F1 (CB6F1) mice carrying the H-2b and H-2d MHC haplotypes. Compared to mice immunized with an irrelevant protein, Mcl-1 peptide immunized mice generate distinct immune responses to several peptides, including weak responses to Mcl_8, 25, 26 and 29 and dominant responses to Mcl_27 and 33 (Figure 1a,b). Intracellular cytokine staining confirmed that these were CD4 (but not CD8) T cell responses, capable of producing IFN γ , IL-2 and TNF α (Figure 1c and data not shown). Immunization of B6 x CBA F1 (B6CBAF1, H-2b/k) mice with Mcl-1 peptides generated a weak Mcl_25- and a strong Mcl_27-specific CD4 T cell response (Figure 2a). These responses were also both seen in CB6F1 mice, suggesting they are H-2b restricted. Notably, although several additional peptides were predicted to contain H-2k binding peptides, none of these were found to be empirically immunogenic in our experiments. In FvB (H-2q) mice, Mcl_32 was uniquely immunogenic (Figure 2b), while Mcl_25 and Mcl_27 peptides displayed MHC haplotype immunogenic promiscuity.

In conclusion, we found that the ensemble of overlapping Mcl-1 peptides (Figure 3) contained many immunogenic MHC II-restricted peptides. Future experiments to confirm that these CD4⁺ T cells induced against novel epitopes can recognize Mcl-1 over-expressing cells and enhance anti-tumor immunity *in vivo* will be important to determine whether such responses are indeed effective in tumor control.

Acknowledgments

Jurgita Nørup, Katja Carlse and Sabaheta Babajic are thanked for excellent technical assistance. This work was supported by the Danish Advanced Technology Foundation (#060-2009-3).

References

1. Inuzuka, H., et al. *Oncotarget* **2**, 239-244 (2011), <http://nrs.harvard.edu/urn-3:HUL.InstRepos:10288518>
2. Yang-Yen, H.-F. *J. Biomedical Science* **13**, 201-204 (2006), <http://dx.doi.org/10.1007/s11373-005-9064-4>
3. Maurer, U., et al. *Molecular Cell* **21**, 749-760 (2006), <http://dx.doi.org/10.1016/j.molcel.2006.02.009>
4. Giménez-Bonafé, P., et al. *Curr. Cancer Drug Targets* **9**, 320-340 (2009), <http://dx.doi.org/10.2174/156800909788166600>
5. Zhou, W., et al. *BMC Cancer* **11**, 485-494 (2011), <http://dx.doi.org/10.1186/1471-2407-11-485>
6. Friberg, A., et al. *J. Med. Chem.* **56**, 15-30 (2012), <http://dx.doi.org/10.1021/im301448p>
7. Muppidi, A., et al. *J. Am. Chem. Soc.* **134**, 14734-14737 (2012), <http://dx.doi.org/10.1021/ja306864v>
8. Woodworth, J.S., et al. *J. Immunol.* **192**, 3247-3258 (2014), <http://dx.doi.org/10.4049/jimmunol.1300283>
9. Agger, E.M., et al. *PLoS ONE* **3**, e3116 (2008), <http://dx.doi.org/10.1371/journal.pone.0003116>
10. Christensen, D., et al. *Expert Review of Vaccines* **10**, 513-521 (2011), <http://dx.doi.org/10.1586/ERV.11.17>

Fmoc Solid-Phase Peptide Synthesis of Human α -Calcitonin Gene-Related Peptide and Two Fluorescent Analogs

M. Fuente-Moreno^{1,2}, A. Oddo¹, M. Sheykhzade¹, D.S. Pickering¹,
 and P.R. Hansen¹

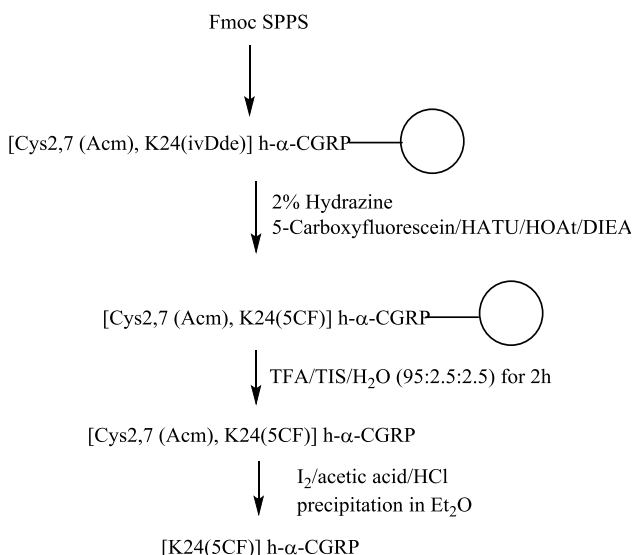
¹Department of Drug Design and Pharmacology, University of Copenhagen, Copenhagen, DK-2100, Denmark;

²Facultad De Farmacia, Universidad Complutense De Madrid, Madrid, Spain

Introduction

Human α -Calcitonin Gene-Related Peptide (h- α -CGRP) is a naturally occurring 37 amino acid vasodilatory neuropeptide amide, ACDTATCVTHRLAGLLSRSGGVVKNFVPTNVGSKAF, with a disulfide bond between residues 2 and 7. The peptide is found in primary afferent sensory nerves and is widely distributed throughout the central and peripheral nervous systems in the body [1]. Structure activity studies of h- α -CGRP have shown that the middle and C-terminal part of the peptide allow the formation of the appropriate conformation required for the interaction with the receptor, while the N-terminus is essential for biological activity and onset of signal [2]. Fluorescent h- α -CGRP analogs are useful for investigating the mechanism behind (re)uptake of h- α -CGRP into the sensory nerve terminals and monitoring trafficking of CGRP receptors. As part of an ongoing study on the mechanism of action behind h- α -CGRP-induced vasodilation, we here present an Fmoc strategy for the synthesis of [Cys2,7(Acm)] h- α -CGRP (1), h- α -CGRP (2), and two fluorescent h- α -CGRP analogs labelled with 5-carboxyfluorescein [3] (5CF) at the side-chain of K24. The first analog, [Cys2,7(Acm), 5CFK24] h- α -CGRP (3) is linear, while the second [5CFK24] h- α -CGRP (4), contains the native disulfide bond.

Results and Discussion



The peptides (1) and (2) were synthesized using standard Fmoc chemistry on a TentaGel RAM resin (50 mg, loading 0.24 mmol/g) (Figure 1). Activation of the Fmoc amino acids was carried out using HATU/HOAt/DIEA (4:4:8) [4].

Fig. 1. Strategy for the synthesis of compound (4).

Fmoc-Cys(Acm)-OH was used for residue 2 and 7. Fmoc deprotection was accomplished by treatment with 20% piperidine in DMF (3x4 min) and final wash with DMF/DCM/DMF (3x/3x/5x). The peptides were cleaved from the solid support along with the permanent side chain protection groups using TFA/H₂O/TIS (90:2.5:2.5 v/v) for 2 h. The crude peptides were purified by preparative HPLC and characterized by MALDI-TOF-MS (Figure 2). The peptides (3) and (4) were synthesized as above with the following modifications: Fmoc-Lys(ivDde)-OH was used at residue 24. Following SPPS, the ivDde was cleaved by treatment with 2% hydrazine hydrate in DMF (12x5 min). This is significantly longer than reported in the literature but a cleavage study using the model peptide Boc-A-F-S-K(ivDde)-S-F-NH-Resin showed that it was necessary. After DMF wash, 5-carboxyfluorescein was coupled overnight to the side-chain of K24 using HATU/HOAt/DIEA (5:5:10 eq). Following resin cleavage, disulfide bond formation for compound 2 and 4 was achieved by dissolving the HPLC-purified and Acm-protected peptides in I₂/acetic acid (20mM) and 60 mM HCl [5]. MALDI-TOF-MS indicated that the reaction was completed after 30 min. Next, 9 vol. eqv. of ice-cold ether was added and cooled on dry ice for 10-15 min. The suspension was then centrifuged, decanted and purified by RP-HPLC.

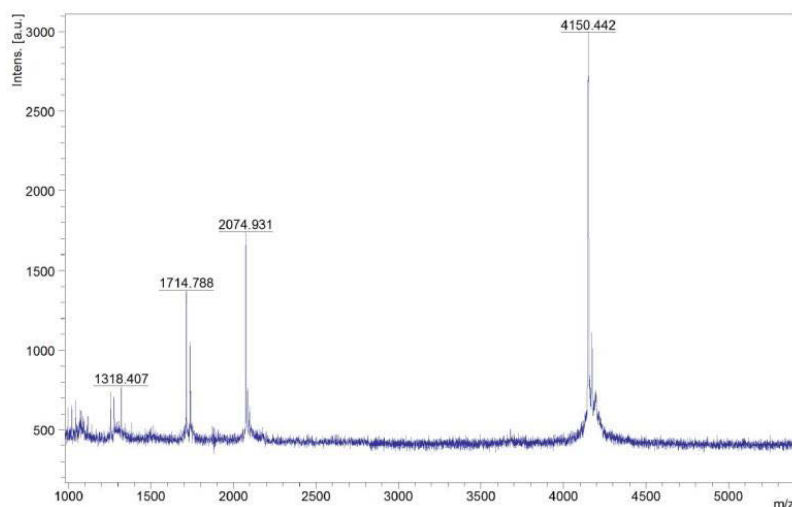


Fig. 2. MALDI-TOF-MS of compound 4.

In conclusion, we present an Fmoc strategy for the syntheses of [Cys2,7(Acm)] h- α -CGRP (1), h- α -CGRP (2), and two fluorescent h- α -CGRP analogs labeled with 5-carboxyfluorescein at the side-chain of K24. The first analog, [Cys2,7(Acm), 5CFK24] h- α -CGRP (3) is linear, while the second [5CFK24] h- α -CGRP (4), contained the native disulfide bond. However, the compounds were obtained in low yields. Additional future work will include protocol optimization and performing binding and functional studies.

Acknowledgments

Birgitte Simonsen is thanked for excellent technical assistance. This work was supported by an ERASMUS grant to M. Fuente-Moreno.

References

1. Sheykhzade, M., et al. *Eur. J. Pharmacol.* **667**, 375-382 (2011), <http://dx.doi.org/10.1016/j.ejphar.2011.06.031>
2. Watkins, H.A., et al. *British J. Pharmacol.* **170**, 1308-1322 (2013), <http://dx.doi.org/10.1111/bph.12072>
3. Fischer, R., et al. *Bioconjugate Chem.* **14**, 653-660 (2003), <http://dx.doi.org/10.1021/bc025658b>
4. Nielsen, S.L., et al. *Protein Sci.* **16**, 1969-1976 (2007), <http://dx.doi.org/10.1110/ps.072966007>
5. Zhang, S., et al. *Int. J. Pept. Res. Ther.* **14**, 301-305 (2008), <http://dx.doi.org/10.1007/s10989-008-9148-x>

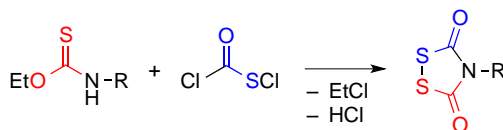
Mechanistic Insights Into the Zumach-Weiss-Kühle Synthesis of Dithiasuccinoyl (Dts)-Protected Amines

Matthew J. Henley, Michael J. Barany, Lin Chen, Robert P. Hammer,
Alex M. Schrader, Victor G. Young, Jr., and George Barany

Department of Chemistry, University of Minnesota, Minneapolis, MN, 55455, USA

Introduction

The 1,2,4-dithiazolidine-3,5-dione heterocycle was first prepared by Zumach, Weiss, and Kühle [1] by reactions of primary *O*-ethyl thiocarbamates with (chlorocarbonyl)sulfonyl chloride [Scheme 1]. Subsequently, we adopted this heterocycle as the basis for the thiolysable dithiasuccinoyl (Dts) amino protecting group, which was used for orthogonal solid-phase peptide synthesis and related applications [2-7]. We report here that when substrates are changed from primary amines to carbamates, cyclization to the title heterocycle does *not* occur, but two acyclic (chlorocarbonyl)disulfanyl species corresponding to proposed intermediates in the ZWK reaction mechanism can be isolated and structurally characterized. The present work might also provide insight into why reactions of primary amines with bis(chlorocarbonyl)disulfane fail to provide the corresponding Dts-amines, while analogous reactions with bis(trimethylsilyl)amines give Dts-amines in high yields [8].



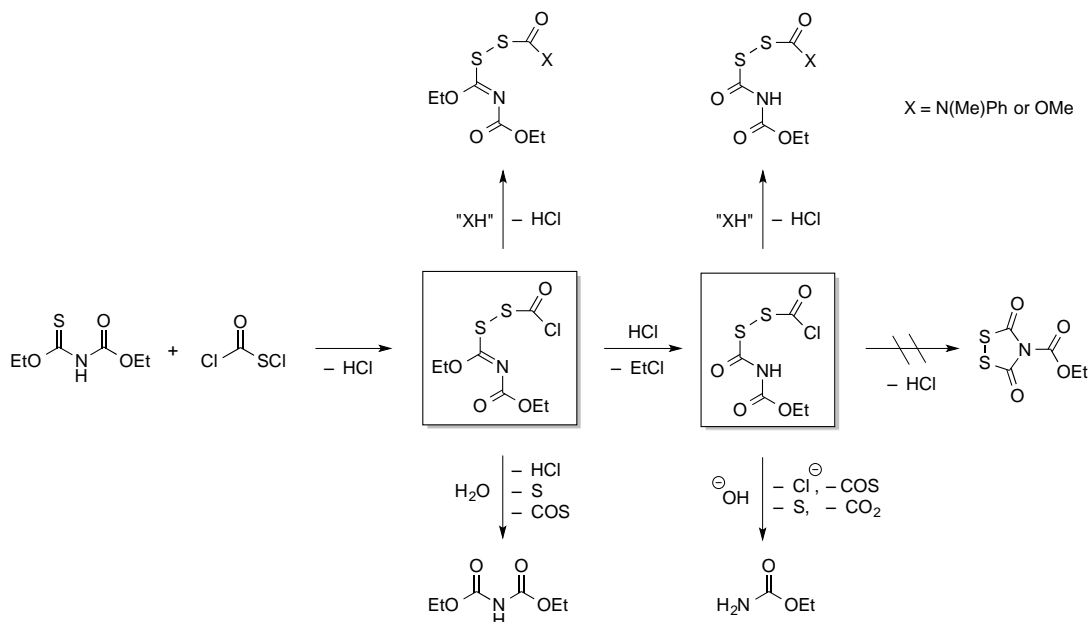
Scheme 1. Zumach-Weiss-Kühle (ZWK) reaction: Reaction of a primary thiocarbamate with (chlorocarbonyl)sulfonyl chloride results in the rapid formation of the 1,2,4-dithiazolidine-3,5-dione (Dts-amine) heterocycle, with simultaneous loss of ethyl chloride and hydrogen chloride.

Results and Discussion

In what was originally an attempt to prepare the Dts analogue of the *N*-phthaloylation reagent (*N*-ethoxycarbonyl)phthalimide (i.e., the Nefkens reagent) [9] *via* ZWK chemistry, we discovered that the principal product was actually (chlorocarbonyl)(*N*-ethoxycarbonylcarbamoyl)disulfane [second box in Scheme 2], a surprisingly stable crystalline compound. Through slight modifications to the reaction conditions, the precursor (chlorocarbonyl)[1-ethoxy-(*N*-ethoxycarbonyl)formimidoyl]disulfane [first box in Scheme 2] could be isolated and characterized as well. These two species correspond to proposed [1] intermediates in the ZWK mechanism that have never before been isolated or observed spectroscopically.

The two novel (chlorocarbonyl)disulfanyl species were characterized by their hydrolysis reactions, as well as by preparation of derivatives that substitute their respective chlorine atoms by methoxy and *N*-methylaniline moieties through direct and/or indirect chemistries. Treatment of the (chlorocarbonyl)(carbamoyl)disulfane and its derivatives with base revealed that the diacyl *N*-H is quite acidic, and that its abstraction leads to rapid decomposition of the disulfane.

The (chlorocarbonyl)(carbamoyl)disulfane, its methyl ester, and its *N*-methylanilide, along with the *N*-methylanilide of the precursor imidoyl disulfane, were all amenable to x-ray crystallography, laying the groundwork for detailed understanding of changing bond parameters in the ZWK reaction trajectory. As part of this analysis, we observed that for all four model disulfanes, the acidic proton or the lone pair electrons on the nitrogen are *trans* to the disulfane; this contrasts to the *cis* depiction in Scheme 2. A *trans* conformation will prevent the nucleophilic attack of nitrogen on the chlorocarbonyl moiety that is prerequisite to Dts formation. While we recognize that molecules may behave somewhat differently in solution, the rather stable and preferred *trans* conformation observed in the solid-state suggests a possible explanation why cyclization does not occur in the special case studied in the current work (Scheme 2).



Scheme 2. Preparation and further transformations of two novel (chlorocarbonyl)disulfanyl species [shown within the two boxes]. Transformations in quotes indicate that the products were obtained either by direct substitution, or by indirect methods in certain cases when direct substitution reactions were not successful.

From the chemical point of view, we tentatively conclude that unsuccessful attempts at preparing Dts-amines directly from the reaction of bis(chlorocarbonyl)disulfane with primary amines failed at least partly because facile deprotonation of the putative (chlorocarbonyl)(carbamoyl) disulfane intermediate by any excess primary amine would promote degradation before any cyclization could occur.

Acknowledgments

MJH thanks Phylogica for sponsoring a travel award to present this work. VGY thanks NSF MRI grant 1229400, which provided funds for a Bruker PHOTON-100 diffractometer that was used to obtain some of the crystal structures presented in this work.

References

1. Zumach, G., Kühle, E. *Angew. Chem. Int. Ed. Engl.* **9**, 54-63 (1970), <http://dx.doi.org/10.1002/anie.197000541>
2. Barany, G., Merrifield, R.B. *J. Am. Chem. Soc.* **99**, 7363-7365 (1977), <http://dx.doi.org/10.1021/ja00464a050>
3. Jensen, K.J., Hansen, P.R., Venugopal, D., Barany, G. *J. Am. Chem. Soc.* **118**, 3148-3155 (1996), <http://dx.doi.org/10.1021/ja953529i>
4. Barany, G., Albericio, F. *J. Am. Chem. Soc.* **107**, 4936-4942 (1985), <http://dx.doi.org/10.1021/ja00303a019>
5. Chen, L., Barany, G. *Lett. Pept. Sci.* **3**, 283-292 (1996), <http://dx.doi.org/10.1007/BF00127662>
6. Xu, Q., Musier-Forsyth, K., Hammer, R.P., Barany, G. *Nucleic Acids Res.* **24**, 1602-1607 (1996), <http://dx.doi.org/10.1093/nar/24.9.1602>
7. Planas, M., Bardají, E., Jensen, K.J., Barany, G. *J. Org. Chem.* **64**, 7281-7289 (1999), <http://dx.doi.org/10.1021/jo9824394>
8. Barany, M.J., Hammer, R.P., Merrifield, R.B., Barany, G. *J. Am. Chem. Soc.* **127**, 508-509 (2005), <http://dx.doi.org/10.1021/ja0455446>
9. Nefkens, G.H.L., Tesser, G.I., Nivard, R.J.F. *Rec. Trav. Chim. Pays-Bas* **79**, 688-698 (1960), <http://dx.doi.org/10.1002/recl.19600790705>

Peptide Ligation via Suzuki-Miyaura Cross-Coupling Reaction

Tae-Kyung Lee, Bikash Manandhar, and Jung-Mo Ahn*

Department of Chemistry and Biochemistry, University of Texas at Dallas, Richardson, TX, 75080, USA

Introduction

Functions of peptides can be improved or new ones be conferred by introducing molecules of different properties. Conjugation of peptides with cognate peptides, cell-permeable peptides, and PEG chains may enhance affinity to targets, cellular uptake, and metabolic stability, respectively. Furthermore, incorporation of chemical probes, such as fluorescent dyes and affinity tags, to peptides provides a useful tool for studying biological systems. Suzuki-Miyaura reaction, a palladium catalyzed cross-coupling reaction between a boronic acid and an organohalide or sulfonate, has a great potential in peptide ligations due to advantages like bio-orthogonality and tolerance toward a broad range of functional groups [1,2]. However, the Suzuki-Miyaura reaction has been seldom used in peptide synthesis presumably because of relatively incompatible reaction conditions like a high reaction temperature in organic solvents [3-6]. In this study, we developed a method for chemoselective and bioorthogonal ligation of peptides via the Suzuki-Miyaura reaction. We also employed the method to conjugate various chemical probes to peptides.

Results and Discussion

We first studied the impact of bases and solvents at a range of temperature on the cross-coupling reaction of the iodo-peptide and the peptide boronic acid (Figure 1a). As a base, K_2CO_3 was found to be quite efficient compared to KF and Et_3N . Screening of solvents showed that aqueous DMF, 2,2,2-trifluoroethanol (TFE) and 10% sodium dodecyl sulfate (SDS) solutions afforded the cross-coupled peptides in good yields, whereas 6M urea solution was not effective for the ligation. In particular, the coupling reaction at 40°C in 10% aqueous SDS solution achieved a remarkably high yield (95%, Figure 1a). The concentration of SDS can be lowered to 0.3% without compromising the high yield. On the other hand, Triton and glycerol [5] were less efficient for the cross-coupling reactions. With the optimized reaction conditions in hand (K_2CO_3 , 10% SDS), we then evaluated various Pd catalysts such as $PdCl_2(dppf)$, $Pd(PPh_3)_4$, $PdCl_2(dba)_3$, $Pd(OAc)_2$, and $PdCl_2(PPh_3)_2$ for the efficiency of the ligation reaction. Whereas all of the tested catalysts gave the cross-coupled peptide in moderate to high yield, $PdCl_2(dppf)$ turned out to be the most effective one.

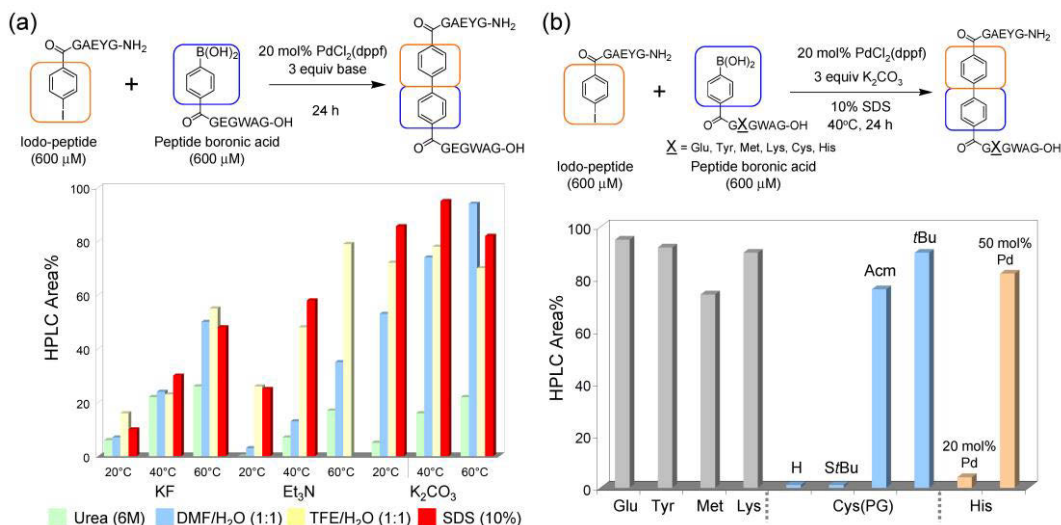


Fig. 1. Optimization of Suzuki-Miyaura cross-coupling reactions of peptides. (a) Screening of base, solvent, and temperature. (b) Effect of amino acids on the cross-coupling reaction.

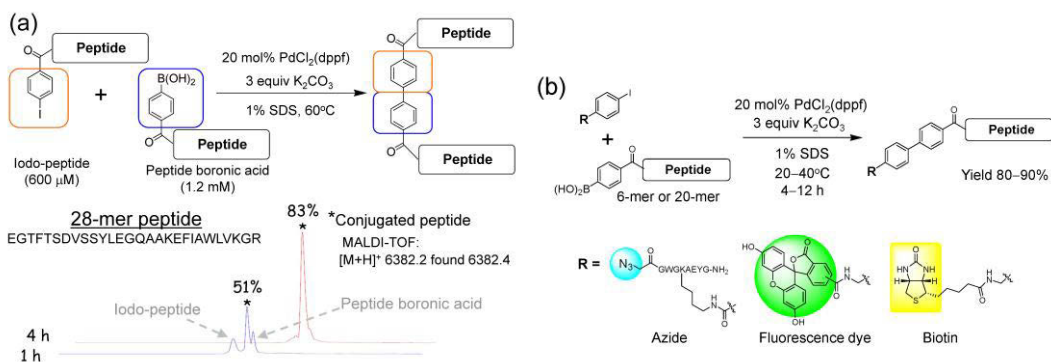


Fig. 2. (a) Suzuki-Miyaura ligation of long peptides. (b) Orthogonal labeling of peptides.

In order to study the effect of amino acids on the cross-coupling reaction, we prepared a series of peptide boronic acids bearing various side chain functional groups (Figure 1b). Many amino acids such as Glu, Tyr, Met, and Lys were found to be compatible to the cross-coupling reaction giving 74–95% yield. However, Cys and His were not tolerated for the ligation presumably due to chelation of palladium with thiol and imidazole. Three protecting groups of Cys, such as *t*-butylthio (*S*tBu), acetamidomethyl (Acm), and *t*-butyl (*t*Bu) were thus examined. Whereas a Cys(*S*tBu)-peptide was not successful in cross-coupling reaction, peptides possessing thioethers such as Cys(Acm) or Cys(*t*Bu) afforded the ligated peptide in 76–90% yield at 60°C. On the other hand, higher Pd loading (50 mol%) converted a His-containing peptide to the ligated peptide in high yield (82%) at 60°C (Figure 1b). We then carried out ligation reactions between long peptides (Figure 2a). Two 28-mer peptides were successfully ligated generating a 56-mer peptide in 83% yield. These results are notable as few methods were reported for efficient ligation between two long peptides.

The Suzuki-Miyaura ligation would be of great interest for multiple conjugations of peptides if it can be orthogonal to existing ligation methods. To investigate the feasibility of orthogonal ligations, we examined the compatibility of an azide, a reaction component of the 1,3-dipolar cycloaddition and the Staudinger ligation, to the Suzuki-Miyaura ligation reaction (Figure 2b). The azido-bearing peptide gave the ligated peptide in 90% yield (Figure 2b). In addition to peptide-peptide ligation, conjugation of fluorophores or affinity tags to peptides is also of high value in biomedical study. Fluorescein- and biotin-containing aryl iodides were efficiently conjugated to 20-mer peptide in 80% and 88% yield, respectively (Figure 2b).

In summary, we have optimized reaction conditions for Suzuki-Miyaura cross-coupling of peptides. Aqueous solutions containing SDS were found to be important for high-yielding ligation of long peptides. It also facilitated introduction of an affinity tag or a fluorescent probe to peptides. The reaction was found to be compatible with many functional groups, such as azide and S-protected thiol, and these render the Suzuki-Miyaura cross-coupling useful for multiple conjugations of peptides and proteins, together with conventional conjugation reactions.

Acknowledgments

This work was supported in part by the Welch Foundation (AT-1595), Juvenile Diabetes Research Foundation (37-2011-20), and Cancer Prevention and Research Institute of Texas (RP100718, RP120717-P4).

References

- Miyaura, N., et al. *Chem. Rev.* **95**, 2457–2483 (1995), <http://dx.doi.org/10.1021/cr00039a007>
- Alonso, F., et al. *Tetrahedron* **64**, 3047–3101 (2008), <http://dx.doi.org/10.1016/j.tet.2007.12.036>
- Doan, N., et al. *J. Comb. Chem.* **10**, 44–51 (2008), <http://dx.doi.org/10.1021/cc700128b>
- Ahn, J.-M., et al. *Chem. Commun.* 480–481 (2003), <http://dx.doi.org/10.1039/B210696E>
- Ojida, A., et al. *Tetrahedron Lett.* **46**, 3301–3305 (2005), <http://dx.doi.org/10.1016/j.tetlet.2005.03.094>
- Dumas, A., et al. *Angew. Chem. Int. Ed.* **52**, 3916–3921 (2013), <http://dx.doi.org/10.1002/anie.201208626>

Multiple Labeling of Peptides *via* Orthogonal Coupling Reactions and Its Applications

Bikash Manandhar, Tae-Kyung Lee, and Jung-Mo Ahn*

Dept. of Chemistry and Biochemistry, University of Texas at Dallas, Richardson, TX, 75080, USA

Introduction

Labeling peptides have been widely practiced in numerous applications in chemistry and biology. For example, fluorescent dyes make peptides useful probes for *in vitro* and *in vivo* imaging and suitable substrates for determining enzyme activity; biotinylation has vast applications including affinity-based protein purification; PEGylation enhances plasma half-life and protects against metabolic degradation; radiolabeling offers *in vitro* and *in vivo* molecular imaging agents and targeted radionuclide therapy; cell permeable peptides give access to intracellular targets. Thus, peptides bearing such multiple labels may serve as powerful research tools and become handy for diverse biomedical studies. For labeling peptides, a number of coupling methods have been reported, such as alkyne-azide click chemistry, thiol-maleimide coupling, Staudinger ligation, and oxime/hydrazone formation. Despite the versatility and broad use in traditional organic reactions, Suzuki-Miyaura coupling has been rarely practiced in peptide labeling. In addition, while each of these methods has been efficiently used alone in peptide conjugation, their combination for orthogonal coupling reactions was not well studied.

Results and Discussion

Previously, we examined and optimized the Suzuki-Miyaura cross-coupling for peptide ligation by surveying various catalysts, bases, temperature, solvents, and additives [1]. We also determined the effects of amino acid side chains on the ligation reactions of peptides. In order to demonstrate its orthogonality towards widely used thiol-maleimide chemistry and copper-catalyzed azide-alkyne cycloaddition (CuAAC), peptide **1** bearing three different functional groups (a phenyl boronic acid, a sulphydryl group, and an azide) was designed and synthesized. Since a thiol is not compatible to Suzuki reactions, it was kept protected with a *t*Bu group. We also prepared a cell penetrating poly-lysine peptide with iodobenzoate (**2**); an acetylene-conjugated biotin (**3**); and a maleimide-functionalized fluorescein (**4**) (Figure 1). Peptides **1** and **2** were synthesized in solid-phase by following standard Fmoc-*t*Bu protocol. The resulting peptides were cleaved from resin with TFA and purified by RP-HPLC.

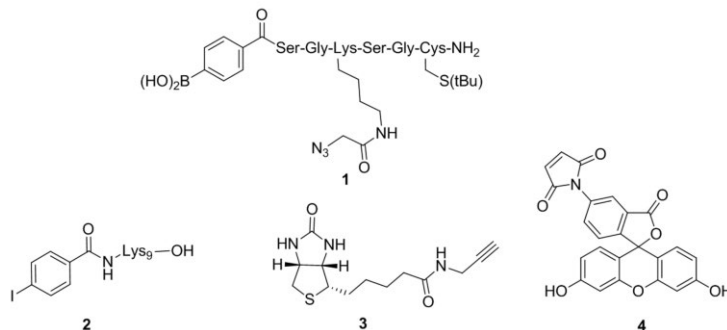
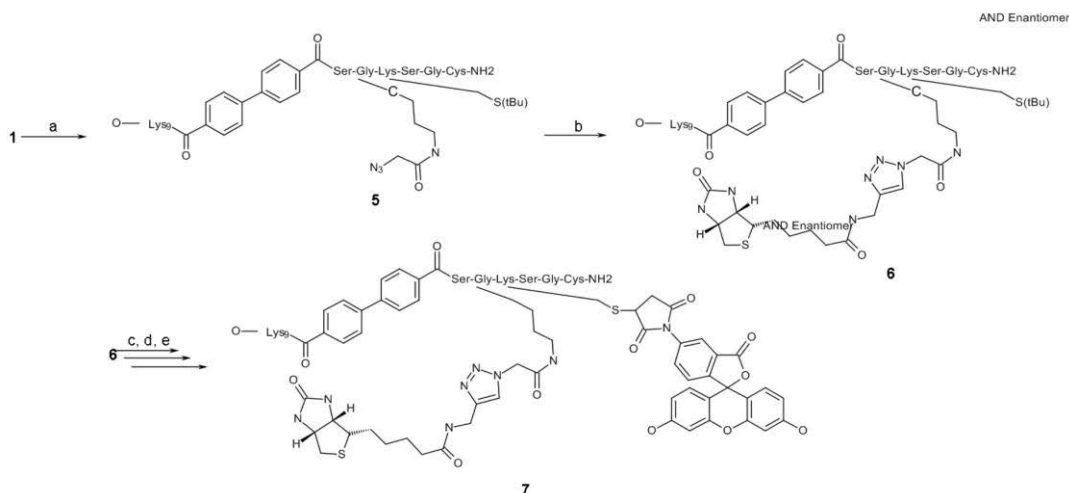


Fig. 1. Structures of reacting components used for multiple labeling.

Consecutive labeling of peptide **1** was carried out with poly-lysine **2**, biotin **3** and fluorescein **4** via Suzuki-Miyaura cross-coupling, CuAAC, and thiol-maleimide methods, respectively (Scheme 1). The conditions and reagents of these coupling reactions were found to be compatible and orthogonal to each other as indicated by a high purity of the products analyzed by HPLC. The multiply labeled peptide **7** was incubated with HEK293 cells for 12 hours in an attempt to demonstrate the utility of multiple labeling. Peptide **7** was carried into the cells by the conjugated cell penetrating poly-lysine peptide moiety, which was easily visualized with fluorescence microscope owing to the fluorescein moiety (Figure 2).



Scheme 1. Multiple labeling of peptides. (a) **2**, Pd(dppf)Cl₂, K₂CO₃, DMF, H₂O; (b) **3**, CuSO₄, NaAsc, DMF, tBuOH, H₂O; (c) DTNP, TFA; (d) TCEP, H₂O; (e) **4**, PBS.

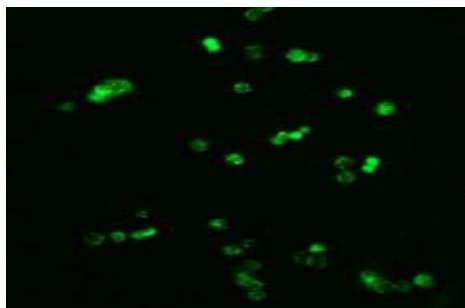


Fig. 2. Fluorescence microscope image of HEK293 cells after 12h incubation with peptide **7**.

In summary, we have developed an efficient synthetic strategy for multiple labeling of peptides *via* various orthogonal coupling reactions, such as Suzuki-Miyaura cross-coupling, thiol-maleimide reaction, and alkyne-azide cycloaddition. The potential of these orthogonal chemistries was demonstrated by a peptide with multiple labels of a cell penetrating peptide, a fluorescent dye, and a biotin.

Acknowledgments

This work was supported in part by the Welch Foundation (AT-1595), Juvenile Diabetes Research Foundation (37-2011-20), and Cancer Prevention and Research Institute of Texas (RP120717-P4).

References

1. Lee, T.-K. Manandhar, B. and Ahn, J.-M., in Lebl, M. (Ed.) *Peptides: Peptides Across the Pacific (Proceedings of the 23rd American Peptide Symposium)*, American Peptide Society, San Diego, 2013, p. 234, <http://dx.doi.org/10.17952/23APS.2013.234>

4,5-Disubstituted N-Aminoindazol-2-One Mimics of Peptide Turn Backbone and Side Chain Conformation

Julien Poupart, Duc Doan-Ngoc, and William D. Lubell

Department of chemistry, Université de Montréal, Montreal, Canada

Introduction: N-aminoindazol-2-one (Nai) residues

Nai residues have been shown by NMR spectroscopy and X-ray crystallography to adopt turn conformations, and have been incorporated into biologically active peptides to study structure-activity relationships (Figure 1) [1,2]. The synthesis of Nai residues has entailed alkylation of aza-glycyl dipeptides with propargyl bromide using tetraethyl ammonium hydroxide, followed by sodium hydride

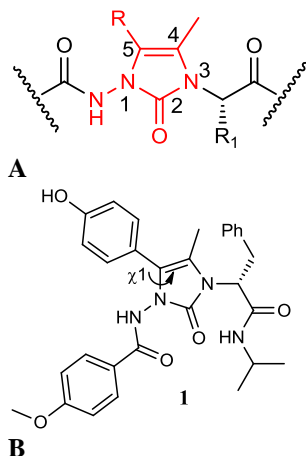
induced 5-*exo*-dig cyclisation and *exo*- to *endo*-alkene epimerization. By performing a Sonogashira reaction on the aza-propargylglycine residue prior to ring formation, various aromatic and heteroaromatic ring systems have been introduced at the 4-position of the aminoindazol-2-one residue. Although the use of strong base led to epimerization of aza-glycyl dipeptide C-terminal α -amino esters, the Nai dipeptide enantiomers were effectively separated by chiral supercritical fluid chromatography [3]. After liberation of the carboxylic acid, the resulting Nai dipeptide building blocks have been inserted into longer peptide structures by standard coupling methods [1,2].

The current method for Nai peptide construction offers effective means for introducing substituents at the 4-position to mimic different amino acid side chains. Moreover, the 4-position substituents have been observed by crystallographic analyses to influence the conformation of the C-terminal α -amino acid residue side chain in model Nai peptides [2]. Considering the natural orientation of amino acid side chains in chi-space [4], the Nai 5-position represents a promising location for the attachment of substituents for peptide mimicry [5]. Evidence that the backbone and side chain geometry of natural amino acids involved in β -turns may be mimicked by 5-aryl Nai residues was derived from molecular modelling using HyperChem 8TM, which predicted that model Nai peptide 1 adopted a type II' β -turn conformation in which the aromatic side chain χ^1 torsion angle was oriented in a gauche (–) conformation (Figure 1).

Aromatic residues are abundant at the central positions of turn conformations of naturally occurring bioactive peptides, such as somatostatin [6]. Constrained mimics of aryl amino acids that adopt turn conformations may thus offer interesting potential for studying structure-activity relationships [7]. Arylation of the Nai 5-position is thus being studied to provide rigidified aryl and heteroarylalanine residues for turn mimicry.

Results and Discussion

Palladium catalyzed arylation was performed in solution on a protected Nai analog to functionalize the 5-position. For example, employing Nai dipeptide 2 [1], the palladium-catalyzed arylation with 4-iodophenyl-4-methylbenzenesulfonate gave 5-aryl Nai dipeptide 3 in 86% yield (Figure 2). In the interest of studying the conformation of the 5-aryl Nai residue, efforts are now being pursued to incorporate Nai dipeptide 3 into model peptides as a constrained aza-tyrosine surrogate. Moreover, the scope of the palladium-catalyzed arylation will be explored to assess its tolerance to different functionalities on both the alkene and aryl iodine.



B
Fig. 1. 4,5-disubstituted Nai residue in a peptide (A) and model Nai peptide 1 (B).

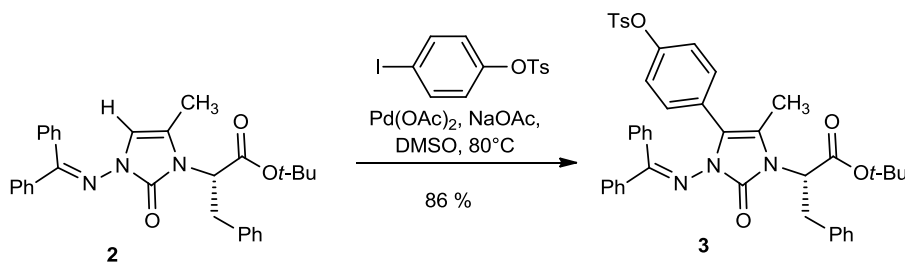


Fig. 2. Synthesis of 3.

(S)-tert-butyl 2-{3-[(diphenylmethylene)amino]-5-methyl-2-oxo-4-[4-(tosyloxy)phenyl]-2,3-dihydro-1H-imidazol-1-yl}-3-phenylpropanoate (3)

tert-Butyl (2*R*)-2-{3-[(diphenylmethylidene)amino]-5-methyl-2-oxo-2,3-dihydro-1*H*-imidazol-1-yl}-3-phenylpropanoate (1 eq., 67 mg, 0.14 mmol, prepared according to reference 8), 4-iodophenyl 4-methylbenzene-1-sulfonate (3 eq., 156 mg, 0.42 mmol, prepared according to reference 9), sodium acetate (3 eq., 34 mg, 0.42 mmol) and palladium acetate (10 mol%, 3 mg, 0.014 mmol) were dissolved in degassed DMSO (1 mL) in a pressure vessel. The vessel was purged with argon, heated to 80°C, and stirred overnight, when complete reaction was observed by TLC (disappearance of starting material, R_f 0.45, 30% EtOAc/Hexanes). The reaction mixture was partitioned between DCM (10 mL) and a mixture of brine (8 mL) and 5% citric acid (2 mL). The phases were separated and the organic layer was washed with brine (3x5 mL). The combined organic phases were dried over magnesium sulfate, filtered and evaporated to a residue that was purified by column chromatography on silica gel using 15–30% EtOAc in hexanes as eluent. Evaporation of the collected fractions gave 5-aryl *N*ai 3 as a yellow oil (87 mg, 86%): R_f 0.34 (30 % EtOAc / hexanes); ¹H NMR (400 MHz, CDCl₃) δ 1.49 (9H, s), 1.61 (3H, s), 2.40 (3H, s), 3.39–3.43 (2H, m), 4.64–4.68 (1H, m), 6.81–6.92 (5H, m), 7.00–7.02 (2H, m), 7.13 (2H, d, *J* = 8 Hz), 7.18–7.22 (5H, m), 7.34–7.39 (3H, m), 7.45–7.49 (2H, m), 7.54 (2H, d, *J* = 8 Hz), 7.63 (2H, d, *J* = 8 Hz). ¹³C NMR (75 MHz, CDCl₃) δ 174.6, 168.4, 148.3, 148.1, 145.4, 137.8, 137.1, 135.0, 132.2, 131.2, 130.1, 129.7, 129.6, 129.2, 128.7, 128.4, 128.0, 127.8, 126.6, 122.1, 117.8, 116.1, 82.4, 57.6, 35.4, 29.7, 28.0, 21.7, 9.5. HRMS Calcd. (C₄₃H₄₂N₃O₆S)⁺ = 728.2789, found = 728.2802 (M+H)⁺.

Acknowledgments

The authors would like to thank the Natural Sciences and Engineering Research Council of Canada (NSERC), the Canadian Institutes of Health Research (CIHR), the Ministère du développement économique de l'innovation et de l'exportation du Québec (#878-2012, Traitement de la dégénérescence maculaire), Amorchem and the NSERC Collaborative Research and Training Experience Program (CREATE) in Continuous Flow Science.

References

1. Proulx, C., Lubell, W.D. *Biopolymers, Pep. Sci.* **102**, 7–15 (2014), <http://dx.doi.org/10.1002/bip.22327>
2. Proulx, C., Lubell, W.D. *Org. Lett.* **14**, 4552–4555 (2012), <http://dx.doi.org/10.1021/ol302021n>
3. García-Ramos, Y., Proulx, C., Camy, C., Lubell, W.D., in G. Kokotos, V. Constantinou-Kokotou, J. Matsoukas (Editors), *Proceedings of the 32nd Europ. Peptide Symp.*, European Peptide Society, 2012, pp. 366–367.
4. Hruby, V.J., Li, G., Haskell-Luevano, C., Shenderovich, M. *Peptide Science* **43**, 219–266 (1997), [http://dx.doi.org/10.1002/\(SICI\)1097-0282\(1997\)43:3<219::AID-BIP3>3.0.CO;2-Y](http://dx.doi.org/10.1002/(SICI)1097-0282(1997)43:3<219::AID-BIP3>3.0.CO;2-Y)
5. Doan, N.D., Hopewell, R., Lubell, W.D. *Org. Lett.* **16**, 2232–2235 (2014), <http://dx.doi.org/10.1021/ol500739k>
6. Mattern, R.H., Tran, T.A., Goodman, M. *J. Pept. Sci.* **5**, 161–175 (1999), [http://dx.doi.org/10.1002/\(SICI\)1099-1387\(199904\)5:4<161::AID-PSCI177>3.0.CO;2-F](http://dx.doi.org/10.1002/(SICI)1099-1387(199904)5:4<161::AID-PSCI177>3.0.CO;2-F)
7. Makwana, K.M., Mahalakshmi, R. *Org. Biomol. Chem.* **12**, 2053–2061 (2014), <http://dx.doi.org/10.1039/C3OB42247J>

Trends to Acid-Labile Cys Protecting Groups: Thp as an Efficient and Non-Aromatic Cys Protecting Group for Fmoc Chemistry

Iván Ramos-Tomillero¹⁻³, Hortensia Rodríguez⁴, and Fernando Albericio¹⁻⁵

¹Institute for Research in Biomedicine; ²Department of Organic Chemistry, University of Barcelona;

³CIBER-BBN, 08028, Barcelona, Spain; ⁴School of Chemistry, Yachay Tech, Urcuqui, Ecuador;

⁵School of Chemistry University of KwaZulu Natal Durban, 4000, South Africa

Introduction

Since the discovery of solid-phase peptide synthesis (SPPS) by Merrifield [1], the peptide field has suffered a dramatic change in a wide set of points such as the development of new solid supports, the discovery of highly efficient coupling reagents and additives, as well as the fashionable design of linkers and protecting groups. Consequently, the solid phase peptides synthesis is considered the most efficient way to synthesize a broad number of complex molecules.

Into the complete process of the SPPS, a large number of problematic side reactions occur, in consequence during the past decades tremendous efforts have been done in order to avoid this drawbacks that jeopardize the efficiency of this methodology. Amino acid racemization is still an issue in SPPS because of the similarity between the desired product and the concomitant racemic product. In this sense, several factors such as the coupling reagents, the handles or the protecting groups, or even the basic conditions used during the peptide synthesis, could affect directly the integrity of the α -proton, which are able to modulate the amino acid racemization.

Cysteine

In nature, cysteine (Cys) is crucial due to its capacity to confer stability to peptides and proteins, but also constrain the specific conformation of these biomolecules through disulfide bonds [2,3]. In addition, its use has modernized the chemical synthesis of large polypeptides and proteins by Native Chemical Ligation [4]. Accordingly, Cys is considered one of the most problematic amino acid in SPPS, due to the high instability of its α -proton caused by the proximity of the thiol group, which promotes the racemization of its chiral center. Furthermore, β -elimination, oxidation and alkylation are other examples of potentials Cys side reactions. All these Cys collateral reactions are responsible of the complex peptide crude products obtained during the synthesis of Cys-rich peptides [5]. Nowadays, extensive possibilities to avoid these Cys promoted side reactions have been studied. In that sense, the development of new coupling reagents and additives for SPPS, assisted the by-products minimization [6]. Additionally, special efforts were focused into Cys side chain protection and as a result, a myriad of Cys protecting groups stable to a set of chemical conditions have been developed for their use in SPPS [7].

Protection schemes

The stability and lability of protecting groups play an important role into the strategy selection criteria for SPPS. While Boc chemistry requires base-labile protecting groups, the Fmoc/*t*Bu strategy involves the use of acid cleavable groups. The conferred stability is related by the kind of binding between the β -thiol group of Cys and the protecting group. As reported in the literature, thioether linkage is the most commonly used thiol protection form, due to the stability under several conditions. Thus, in recent years the development of the most successful protecting groups for Cys are based on this special linkage. In this regard, herein we will focus our attention in acid-labile Cys protecting groups in general, and in the recently developed non-aromatic acid-labile Cys protecting group, in particular.

Acid-labile Cys protecting groups

The conscious design of protecting groups had triggered a myriad of groups, which are stable in a broad range of acidic conditions (Figure 1). Therefore, the selective protecting group elimination is possible, depending on the acidic conditions used. As a result of years of studies in the field, there are several Cys protecting groups available; some of them are labile in low acid concentration such as

Mmt [8], Trt [9-11] or Thp [12,13]; others are more stable in low concentrations of trifluoroacetic acid (TFA) but cleavable using higher quantity of TFA - Diphenylmethyl (Dpm) [9,11,14], *t*Bu [15,16] or MBom [17] and moreover, there are groups which are completely stable to TFA and removable using harsh conditions such as HF, for example Bom [18], Meb or Mob [19-21] groups.

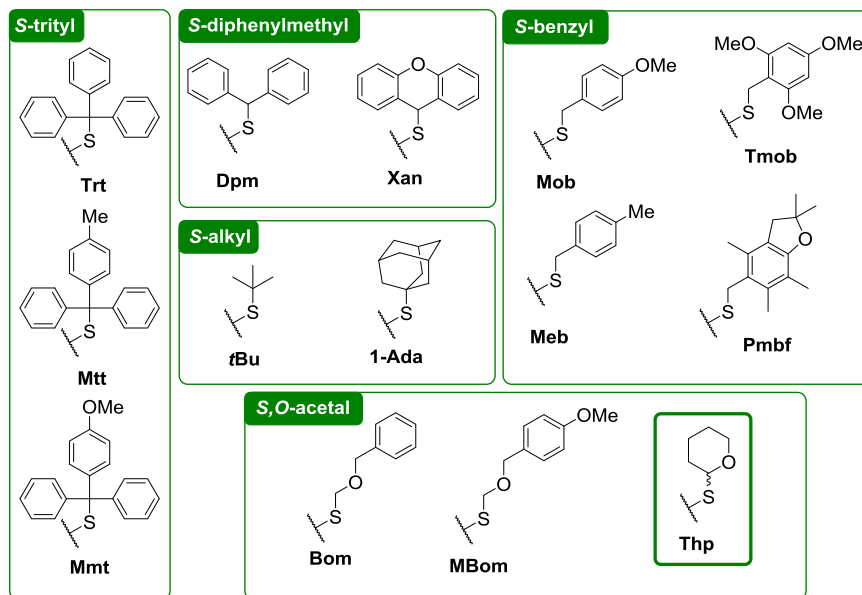


Fig. 1. Acid-labile Cys protecting groups.

Due to their chemical properties, most protecting groups and linkers used in SPPS [22] are based on benzyl, diphenylmethyl, and triphenylmethyl structures. The mechanisms of elimination are based on the protonation of the thiol group, and followed by the carbocation formation. Herein, the stability of the liberated carbocation in acidic conditions manages the protecting group lability. Consequently, the more acid labile the more stable carbocation [23]. Some factors contribute to their stability such as steric hindrances or field-inductive effects, but the most imperative effect correspond to the electronic delocalization, which increase the carbocation stability [24].

New generation of Cys protecting groups

Although trityl-, diphenylmethyl-, and benzyl-like scaffolds are the most used for the protection of Cys, in the recent years the studies with S,O-acetal protecting groups has presented extremely low racemization levels [25]. While benzyloxymethyl (Bom) is used for Boc chemistry, 4-methoxybenzyloxymethyl (MBom) and the recently published tetrahydropyranyl (Thp) are compatible with the Fmoc/*t*Bu approach. Regarding the molecular structures (Figure 1), most of the protecting groups available contain aromatics rings, except *t*Bu, 1-Ada and Thp. In that sense, in the production of protected hydrophobic peptides, the use of bulky protecting groups in SPPS, such as trityl-like scaffolds as well as *t*Bu, 1-Ada, affects their inter/intrachain interaction during peptide elongation and this fact jeopardize the purity of the final product.

Apart of its recent application in Fmoc chemistry [26], Thp is extensively used as hydroxyl protecting group [27-30] as well as a linker [31-34], due to its chemical properties and its stability in strong bases, and acylating and alkylating agents among others. Accordingly, Thp is an excellent candidate for use in SPPS, but it is known that the main drawback should be the formation of a new stereocenter that leads to diastereomeric mixtures. Nevertheless, as with other protecting groups or linkers, their use is temporary. Consequently, the formation of the stereocenter is not a limitation.

Tetrahydropyranyl (Thp) for Fmoc peptide chemistry

Seeking a protecting group which will be able to decrease the racemization to minimum levels, MBom and Thp could be the choice for Fmoc chemistry. While the MBom presents a straightforward preparation of the protected amino acid unit, Thp is easily introduced into the Cys thiol group by the using a catalytic amount of acid in presence on dihydropyran. Regarding the final protecting group elimination (Figure 2), in both cases an aldehyde is generated, formaldehyde and 5-hydroxypentanal for MBom and Thp, respectively.

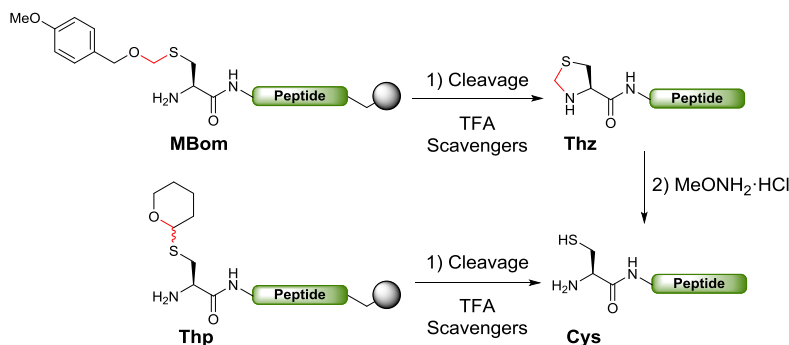


Fig. 2. *N*-terminal Cys protecting group elimination.

Accordingly, the formaldehyde formation supposes an important drawback because of the hydroxymethylation. An undesirable side reaction is the formation of the thiazolidine (Thz) ring in *N*-terminal Cys. In that sense, as it was demonstrated for Thp in their use for *N*-terminal peptides Cys containing peptides [26], the formation of 5-hydroxypentanal does not create a problem due to the fact that the hydroxyl group present in the molecule, suffer an intramolecular hydroxymethylation, trapping the reactive electrophilic carbon atom.

Table 1. Cys racemization studies for Ala-Cys-Leu tripeptide.

Resin	Cys PG	% Racemization ^a
Sieber Amide	Thp	0.7%
	Trt	3.3%
	Dpm	6.8%
Rink Amide	Thp	0.5%
	Trt	2.3%
2-Chlorotriyl chloride	Thp	0.2%
	Trt	0.7%

^aCalculated as (D-peptide peak area / L-peptide peak area) x 100

Conclusions

The methodological spectrum available for the synthesis of peptides in solid supports, has suffered during several years an impressive transformation. Always seeking to avoid the side reactions, which make the synthesis of this kind of special molecules difficult. In that sense, all the scientific contributions in the field make the SPPS an outstanding and rigorous way to obtain the myriad of interesting small molecules, peptides or proteins. Our recent contribution to the field, the Cys protecting group Thp, demonstrated that now with a lot of work done in the field, it is possible to

obtain extremely low racemization levels (<1%). Due to the scientific ambition, the field is tending to reach the synthetic perfection. The question is: will it be possible?

Acknowledgments

I. R-T. thanks the Generalitat de Catalunya for a predoctoral fellowship. This work was funded in part by the following: the CICYT (CTQ2012-30930), the Generalitat de Catalunya (2014 SGR 137), the Institute for Research in Biomedicine Barcelona (IRB Barcelona) (Spain).

References

1. Merrifield, R.B. *J. Am. Chem. Soc.* **85**, 2149-2154 (1963), <http://dx.doi.org/10.1021/ja00897a025>
2. Góngora-Benítez, M., et al. *Chem. Rev.* **114**, 901-926 (2013), <http://dx.doi.org/10.1021/cr400031z>
3. Postma, T.M., et al. *Eur. J. Org. Chem.* **2014**, 3519-3530 (2014), <http://dx.doi.org/10.1002/ejoc.201402149>
4. Dawson, P.E., et al. *Science* **266**, 5186, 776-779 (1994), <http://dx.doi.org/10.1126/science.7973629>
5. Stathopoulos, P., et al. *Amino Acids* **44**, 1357-1363 (2013), <http://dx.doi.org/10.1007/s00726-013-1471-7>
6. Han, S.-Y., Kim, Y.-A. *Tetrahedron* **60**, 2447-2467 (2004), <http://dx.doi.org/10.1016/j.tet.2004.01.020>
7. Isidro-Llobet, A., et al. *Chem. Rev.* **109**, 2455-2504 (2009), <http://dx.doi.org/10.1021/cr800323s>
8. Barlos, K., et al. *Int. J. Pept. Protein Res.* **47**, 148-153 (1996), <http://dx.doi.org/10.1111/j.1399-3011.1996.tb01338.x>
9. Zervas, L., Photaki, I. *J. Am. Chem. Soc.* **84**, 3887-3897 (1962), <http://dx.doi.org/10.1021/ja00879a019>
10. Hiskey, R.G., Adams, J.B.J. *J. Org. Chem.* **30**, 1340 (1965), <http://dx.doi.org/10.1021/jo01015a567>
11. Photaki, I., et al. *J. Chem. Soc. C Org.* **19**, 2683-2687 (1970), <http://dx.doi.org/10.1039/j39700002683>
12. Holland, G.F., et al. *J. Am. Chem. Soc.* **80**, 3765-3769 (1958), <http://dx.doi.org/10.1021/ja01547a075>
13. Ramos-Tomillero, I., et al. *Org. Lett.* **17**, 1680-1683 (2015), <http://dx.doi.org/10.1021/acs.orglett.5b00444>
14. Góngora-Benítez, M., et al. *Org. Lett.* **14**, 5472-475 (2012), <http://dx.doi.org/10.1021/ol302550p>
15. Chimiak, A. *Rocz. Chem.* **38**, 883-885 (1964).
16. Pastuszak, J.J., et al. *J. Org. Chem.* **46**, 1868-1873 (1981), <http://dx.doi.org/10.1021/jo00322a024>
17. Hibino, H., Nishiuchi, Y. *Org. Lett.* **14**, 1926-1929 (2012), <http://dx.doi.org/10.1021/ol300592w>
18. Otake, A., et al. *Chem. Pharm. Bull.* **37**, 526-528 (1989), <http://dx.doi.org/10.1248/cpb.37.526>
19. Akabori, S., et al. *Bull. Chem. Soc. Jpn.* **37**, 433-434 (1964), <http://dx.doi.org/10.1246/bcsj.37.433>
20. Erickson, B.W., et al. *J. Am. Chem. Soc.* **95**, 3750-3756 (1973), <http://dx.doi.org/10.1021/ja00792a046>
21. Live, D.H., et al. *J. Org. Chem.* **42**, 3556-3561 (1977), <http://dx.doi.org/10.1021/jo00442a025>
22. Guillier, F., et al. *Chem. Rev.* **100**, 2091-2157 (2000), <http://dx.doi.org/10.1021/cr980040+>
23. Ramos-Tomillero, I., et al. *Molecules* **18**, 5155-5162 (2013), <http://dx.doi.org/10.3390/molecules18055155>
24. Hoffmann, R., et al. *J. Phys. Chem.* **73**, 1789-1800 (1969), <http://dx.doi.org/10.1021/j100726a027>
25. Hibino, H., et al. *J. Pept. Sci.* **20**, 30-35 (2014), <http://dx.doi.org/10.1002/psc.2585>
26. Ramos-Tomillero, I., Rodríguez, H. & Albericio, F. Tetrahydropyranyl (Thp), a Non-Aromatic Acid-Labile Cys Protecting Group for SPPS. *Proceedings of 24th American Peptide Symposium*. 2015, Poster YI-404
27. Miyashita, M., et al. *J. Org. Chem.* **42**, 3772-3774 (1977), <http://dx.doi.org/10.1021/jo00443a038>
28. Bernady, K.F., et al. *J. Org. Chem.* **44**, 1438-1447 (1979), <http://dx.doi.org/10.1021/jo01323a017>
29. Liu, J., et al. *Tetrahedron Lett.* **43**, 4037-4039 (2002), [http://dx.doi.org/10.1016/S0040-4039\(02\)00740-2](http://dx.doi.org/10.1016/S0040-4039(02)00740-2)
30. Stephens, J.R., et al. *Eur. J. Org. Chem.* **2003**, 3827-3831 (2003), <http://dx.doi.org/10.1002/ejoc.200300295>
31. Thompson, L.A., et al. *Tetrahedron Lett.* **35**, 9333-9336 (1994), [http://dx.doi.org/10.1016/S0040-4039\(00\)78535-2](http://dx.doi.org/10.1016/S0040-4039(00)78535-2)
32. Smith, A.L., et al. *Tetrahedron Lett.* **39**, 8317-8320 (1998), [http://dx.doi.org/10.1016/S0040-4039\(98\)01824-3](http://dx.doi.org/10.1016/S0040-4039(98)01824-3)
33. Basso, A., Ernst, B. *Tetrahedron Lett.* **42**, 6687-6690 (2001), [http://dx.doi.org/10.1016/S0040-4039\(01\)01368-5](http://dx.doi.org/10.1016/S0040-4039(01)01368-5)
34. Torres-García, C., et al. *Int. J. Pept. Res. Ther.* **18**, 7-19 (2011), <http://dx.doi.org/10.1007/s10989-011-9274-8>
35. Lukszo, J., et al. *Lett. Pept. Sci.* **3**, 157-166 (1996), <http://dx.doi.org/10.1007/BF00132978>

Development of Chemistry-Based Protocol for Sequence-Dependent Thioesterification

Yusuke Tsuda, Akira Shigenaga, Kohei Tsuji, Masaya Denda, Kohei Sato,
Keisuke Kitakaze, Tsubasa Inokuma, Kohji Itoh, and Akira Otaka

Institute of Biomedical Sciences and Graduate School of Pharmaceutical Sciences, Tokushima University
1-78-1, Shomachi, Tokushima, 770-8505, Japan

Introduction

One of the useful methods for exploration of the function of proteins is utilization of the synthesized proteins which include artificial units such as fluorescence dye. For the synthesis of such proteins, a peptide thioester and an *N*-terminal cysteinyl peptide prepared by Solid Phase Peptide Synthesis (SPPS) are coupled to each other using Native Chemical Ligation (NCL) [1]. However, due to the limitation of the number of amino acid residues applicable to SPPS, multistep NCLs are required for chemical synthesis of large proteins. On the other hand, in semi-synthesis of proteins, only single NCL of protein thioester prepared from expressed protein with chemically synthesized *N*-terminal cysteinyl peptide enables to incorporate functional moieties to large proteins. However, there are only a few methods for preparation of protein thioesters applicable to naturally occurring sequences [2]. Therefore, new protocols for preparation of protein thioesters has been required.

Results and Discussion

We attempted to develop a chemistry-based novel protocol for sequence-dependent thioesterification of protein using sequential quadruple acyl transfer consisting of *N*-*O*, *O*-*O*, *O*-*N*, and *N*-*S* acyl transfer. We named this system SQAT system (Figure 1) [3]. At first, Ni(II)-mediated *N*-*O* acyl transfer at Ser residue in Ser-Xaa-His-Zaa sequence containing peptide resulted in the formation of *O*-acyl intermediate reported by Bal's group [4]. Secondly, this intermediate was converted to the corresponding methyl ester by *O*-*O* acyl transfer with methanol. Thirdly, by addition of hydrazine, resulting peptide methyl ester was transformed to acyl hydrazide (*O*-*N* acyl transfer). In the last conversion, peptide hydrazide was converted to thioester *via* peptidyl azide by *N*-*S* acyl transfer reported by Liu and co-workers [5].

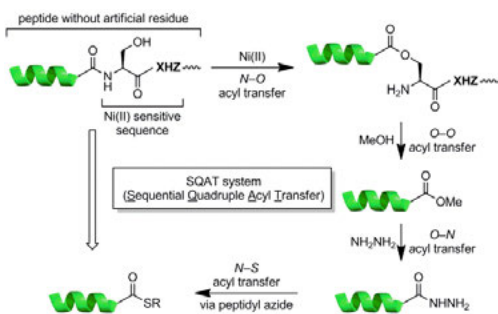


Fig. 1. Sequential quadruple acyl transfer (SQAT) system.

Table 1. Evaluation of Ni(II)-mediated methanolysis.

Ac-LYRAA-SRHWKFL-NH ₂		0.2 M HEPES, Ni(II) MeOH, pH, 37 °C, 12 h		Ac-LYRAA-OMe 2
1				Ac-LYRAA-OH 3
				H-SRHWKFL-NH ₂ 4
Entry	Ni(II) [mM]	MeOH [% (v/v)]	pH	Fraction converted ^a
1	10	10	8.2	0.44
2	10	30	8.2	0.70
3	10	50	8.2	0.72
4	1	30	8.2	0.69
5	20	30	8.2	0.68
6	10	30	7.8	0.61
7	10	30	8.6	0.53
8 ^b	10	30	8.2	0.43

[a] The fraction converted was determined by HPLC separation and integration of 2 as a fraction of the sum of the integration of unreacted 1 + hydrolysed 3 + 2. [b] In the presence of 6 M Gn-HCl.

We examined Ni(II)-mediated methanolysis using model peptide **1** (Table 1). Fraction converted was depended on the concentration of methanol (entries 1-3). Concentration of Ni(II) had no influence on the fraction converted (entries 2, 4 and 5). Appropriate pH of the reaction mixture was found to be 8.2 (entries 2, 6 and 7). Addition of guanidine hydrochloride as a denaturing agent decreased the fraction converted (entries 2 and 8). Then, Ni(II)-mediated methanolysis of peptide **1** followed by addition of

$\text{NH}_2\text{NH}_2 \cdot \text{H}_2\text{O}$ (final concentration: 5% (v/v) NH_2NH_2) into the reaction mixture yielded the corresponding peptide hydrazide (data not shown).

In order to examine the applicability of the SQAT system, we attempted the chemical synthesis of CNP 53 peptide by using this system. For the preparation of 36-residue thioester peptide, initially 43-residue SRHW-Ni(II)-sensitive sequence-incorporated peptide **5** was synthesized chemically. Ni(II)-mediated methanolysis of peptide **5** yielded the desired peptide methyl ester **6** as major product. Then addition of hydrazine into the reaction mixture gave 36-residue peptide hydrazide **7**. After conversion of peptide hydrazide **7** to peptide thioester via peptidyl azide according to Liu's protocol, NCL of the resulting thioester with *N*-terminal cysteinyl peptide **8** followed by folding of the resulting peptide yielded the desired CNP 53.

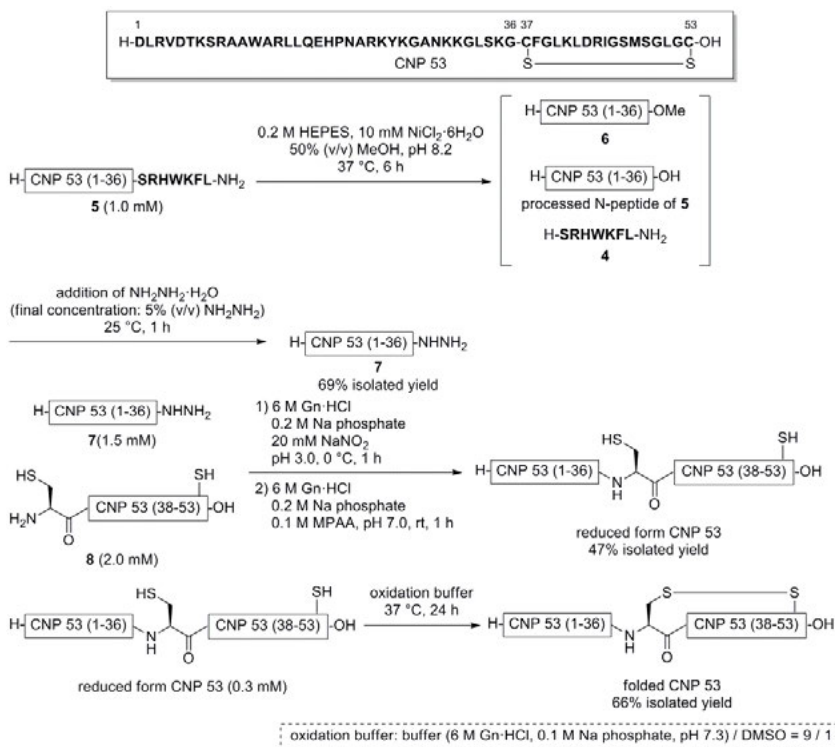


Fig. 2. Synthesis of CNP 53 using SQAT system.

Acknowledgments

This research was supported in part by a Grant-in-Aid for Scientific Research (KAKENHI) and research grants from the Takeda Science and the Uehara Memorial Foundations. Y.T. and M.D. thank Japan Society for the Promotion of Science for a fellowship.

References

1. Kent, S.B.H., et al. *Science* **266**, 776-779 (1994), <http://dx.doi.org/10.1126/science.7973629>
2. (a) Muir, T.W., et al. *Proc. Natl. Acad. Sci. USA* **95**, 6705-6710 (1998); (b) Pentelute, B.L., et al. *J. Am. Chem. Soc.* **134**, 10749-10752 (2012), <http://dx.doi.org/10.1021/ja302354v>
3. Tsuda, Y., Otaka, A., et al. *Chemistry Open in press* (2015), <http://dx.doi.org/10.1002/open.201500086>
4. Bal, W., et al. *J. Am. Chem. Soc.* **132**, 3355-3366 (2010), <http://dx.doi.org/10.1021/ja907567r>
5. Liu, L., et al. *Angew. Chem. Int. Ed.* **50**, 7645-7649 (2011), <http://dx.doi.org/10.1021/anie.201100996>

N-Substituted Arylsulfonamides as Alternative Building Blocks in Peptoid and Peptide Synthesis

Simon Vézina-Dawod, Steve Jobin, Antoine Derson, Claire Herby, and
 Eric Biron

Faculty of Pharmacy, Université Laval and Laboratory of Medicinal Chemistry, CHU de Québec Research
 Centre, CHUL, Québec (QC), G1V 4G2, Canada

Introduction

Peptoids (oligo *N*-substituted glycines) are peptidomimetic oligomers showing attractive structural and pharmacological properties for the development of therapeutic candidates and molecular tools [1,2]. Compared to peptides, peptoids are resistant to proteases and show improved cell permeability [3,4]. Moreover, their synthesis is straightforward and the great chemical diversity that can be accessed with peptoids has prompted their use in combinatorial libraries. The submonomer method introduced by Zuckermann, *et al.* is the most frequently used approach to prepare peptoids [5]. This method is performed on solid support and involves iterative acylation and amination reactions to build up peptoid residues and generate oligomers after multiple rounds. A major advantage of this method is the large number of commercially available primary amines that allows the incorporation of an important chemical diversity. However, despite the great diversity of available primary amines, we observed that the number of submonomers bearing protected hydroxyl side chains is very limited. The very few that are commercially available are expensive. Protection of hydroxyl groups is recommended to avoid *O*-acylation during the acylation but the preparation of *O*-protected submonomers usually requires multistep synthesis or harsh conditions and they are recovered in low yields or often obtained as inconvenient gummy oils. To overcome these drawbacks and introduce interesting reactive or polar functionalities into peptoids, our strategy was to use amino alcohols as starting material and perform a two-step synthesis involving *N*-protection with an arylsulfonyl group followed by *O*-protection with *tert*-butyl to prepare fully protected submonomers. Then, the *N*-substituted arylsulfonamides could be used directly for the nucleophilic displacement step on solid support in the submonomer approach or for the synthesis of protected *N*-substituted glycines for the monomer approach (Figure 1).

Results and Discussion

The 2-nitrobenzenesulfonyl group (2-Nos) was particularly interesting because it is compatible with *tert*-butylation reactions, has a high propensity to form solid product, allows efficient *N*-alkylation under mild conditions and could be easily and selectively removed during solid phase synthesis [6]. *N*-Protection of commercially available amino alcohols **1a-f** was performed with 2-Nos-Cl under standard conditions followed by *O*-*tert*-butylation of compounds **2a-f** with magnesium perchlorate and di-*tert*-butylcarbonate in refluxing dichloromethane (Figure 1) [7].

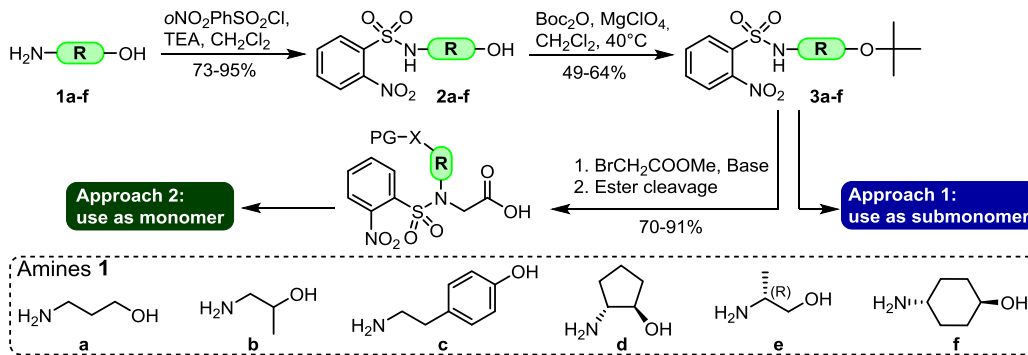


Fig. 1. Synthesis of *O*-protected *N*-substituted arylsulfonamides and their use in peptoid synthesis.

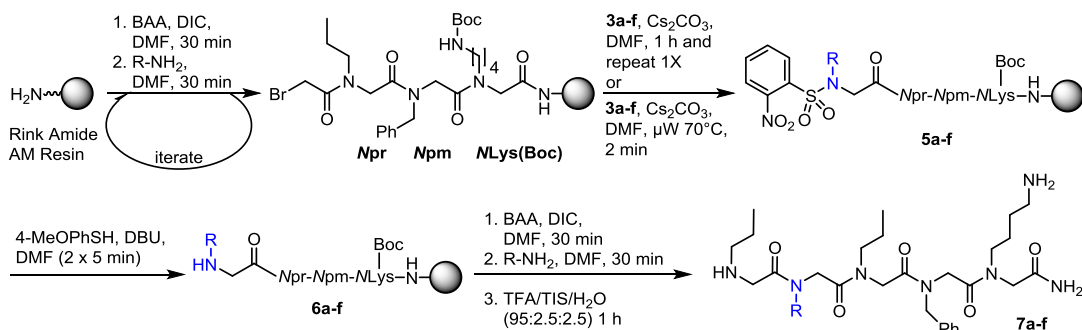


Fig. 2. Synthesis of peptoid oligomers **7a-f** with *N,O*-protected submonomers **3a-f**.

A first study was performed with the submonomer *N*-(2-methoxyethyl)-2-nitrobenzenesulfonamide on a supported bromoacetylated Phe to identify the optimal conditions for bromine displacement with the *N*-substituted arylsulfonamide derivatives [7]. Different reaction parameters were tested and after the nucleophilic displacement and cleavage from the Rink amide resin, the conversion rate was evaluated by HPLC. In our hands the reaction proceeded poorly in DMSO in the presence of K_2CO_3 with or without microwave (μW) irradiation and the use of 1,8-diazabicyclo[5.4.0]undec-7-ene (DBU) as base yielded a mixture of compounds. The use of DMF as solvent increased the conversion rate and an improvement was observed when the quantities of submonomer and K_2CO_3 were doubled. Under μW irradiation, a higher temperature did not improve the conversion rate but its combination with a longer reaction time increased the conversion to 81%. The best results have been obtained when K_2CO_3 was replaced by Cs_2CO_3 . By using Cs_2CO_3 as base, the conversion rates were significantly increased and allowed the reduction of submonomer equivalents necessary to reach completion when μW irradiation was applied. Next, the best room temperature and μW conditions were applied to the supported bromoacetylated Phe with the *N,O*-protected submonomers **3a-f**. The results showed that the reaction was complete with submonomers **3a-c** but did not reach completion with more hindered derivatives **3d-f**. To overcome this drawback and assure complete displacement, the quantity of submonomers was increased to 12 equiv and Cs_2CO_3 to 18 equiv. In this case, complete conversion was observed with compounds **3d-f** for μW conditions while at room temperature the step had to be repeated once to reach comparable conversion rates. To demonstrate the compatibility of building blocks **3a-f** with the submonomer method, peptoid heteropentamers based on the sequence *Npr-Nxxx-Npr-Npm-Nlys* were prepared on solid support (Figure 2). Following cleavage from the resin, the crude purities of oligomers **7a-f** were evaluated by HPLC and the isolated yields calculated after purification (Table 1). The results showed that *N*-substituted arylsulfonamide derivatives can be efficiently used in peptoid synthesis by the submonomer method.

Table 1. Crude purities and isolated yields for peptoid oligomers containing amino alcohols **1a-f**.

Peptoid		Room temp		Microwave		Monomer	
		Purity ^a	Yield ^b	Purity ^a	Yield ^b	Purity ^a	Yield ^b
		(%)	(%)	(%)	(%)	(%)	(%)
7a	<i>Npr-1a-Npr-Npm-Mlys</i>	91	58	90	67	92	59
7b	<i>Npr-1b-Npr-Npm-Mlys</i>	88	58	85	66	88	68
7c	<i>Npr-1c-Npr-Npm-Mlys</i>	97	76	96	76	89	71
7d	<i>Npr-1d-Npr-Npm-Mlys</i>	39	56	54	68	58	38
7e	<i>Npr-1e-Npr-Npm-NLys</i>	71	71	88	79		
7f	<i>Npr-1f-Npr-Npm-Mlys</i>	50	48	63	67		
7g	<i>Npr-1c-Npr-1c-Mlys</i>	76	55	93	67		

^aCrude purities were determined by integrating the peaks in the HPLC trace ($\lambda = 220$ nm); ^bIsolated yield after purification by HPLC and lyophilization. Based on initial loading of Rink Amide AM resin (0.56 mmol/g).

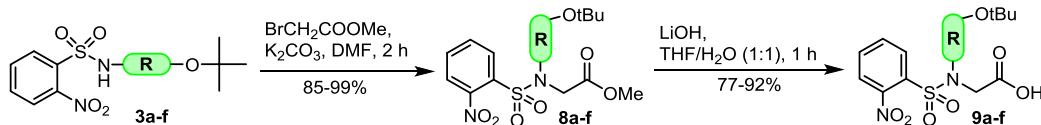


Fig. 3. Synthesis of *N*-arylsulfonyl-*N*-substituted glycines **9a-f**.

In a second study, the *N*-arylsulfonamide building blocks **3a-f** were used to prepare protected *N*-substituted glycine monomers **9a-f** (Figure 3). The monomer approach could be more appropriate for hindered α -disubstituted amino alcohols. The first study with submonomers **3a-f** showed that the bromine displacement on solid support was the limiting step. In the monomer approach [8], this step is performed in solution and could be more efficient since a greater quantity of alkylating derivatives can be used. This strategy offers, for more hindered residue, an important submonomer economy and the opportunity to increase oligomer purities and isolated yields. Different approaches were evaluated to prepare monomers **9a-f** and the most efficient was found to be *N*-alkylation with methyl bromoacetate and K_2CO_3 in DMF followed by selective ester cleavage with LiOH (Figure 3). After purification by flash chromatography, the *N*-2-Nos-*N*-substituted glycines **9a-f** were obtained in good yields (70-91% for 2 steps). To demonstrate their compatibility with peptoid synthesis, monomers **9a-d** (3 equiv) were coupled to the peptoid *N*pr-*N*pm-*M*Lys on solid support using HATU (3 equiv) as coupling reagent in presence of NMM (6 equiv) in DMF for 3 h to yield **5a-d**. Afterward, the 2-Nos was cleaved with a solution of *p*-methoxybenzenethiol and DBU and a last residue was added to peptoids **6a-f** by standard submonomer methodology as described above (Figure 2). After cleavage from the resin, the crude purities of oligomers **7a-d** were evaluated by HPLC (Table 1). The results showed that *N*-substituted arylsulfonamides are convenient building blocks to prepare *N*-substituted glycine monomers that can be efficiently used in the synthesis of peptoids or *N*-alkylated peptides on solid support.

Overall, these results demonstrate that *N*-substituted 2-nitrobenzenesulfonamides can be used in peptoid synthesis as submonomers or monomers. In the submonomer approach, μ W irradiation is recommended for α -substituted amines as previously observed. We have also shown that the more efficient conditions with Cs_2CO_3 are compatible with the submonomer method and could be used to introduce expensive or commercially unavailable side chain protected amines and relevant functional groups. Moreover, *N*-substituted arylsulfonamides are also useful building blocks to prepare side chain protected *N*-substituted glycines for the monomer approach. The conditions used in this work allow a substantial building block economy compared to standard conditions. Simple and affordable, the described procedures represent a complementary and interesting alternative approach to introduce relevant functionalized side chains into peptoids and peptide-peptoid hybrids, increasing the chemical diversity accessible with both submonomer and monomer approaches.

Acknowledgments

Simon Vézina-Dawod and Steve Jobin thank the Fond d'enseignement et de recherche de la Faculté de pharmacie de l'Université Laval (FER) for research scholarships. This work was supported by the National Sciences and Engineering Research Council of Canada (NSERC) (371503-2010).

References

1. Fowler, S.A., Blackwell, H.E. *Org. Biomol. Chem.* **7**, 1508-1524 (2009), <http://dx.doi.org/10.1039/B817980H>
2. Dohm, M.T., Kapoor, R., Barron, A.E. *Curr. Pharm. Des.* **17**, 2732-2747 (2011), <http://dx.doi.org/10.2174/138161211797416066>
3. Miller, S.M., Simon, R.J., Ng, S., Zuckermann, R.N., Kerr, J.M., Moos W.H. *Bioorg. Med. Chem. Lett.* **4**, 2657-2662 (1994), [http://dx.doi.org/10.1016/S0960-894X\(01\)80691-0](http://dx.doi.org/10.1016/S0960-894X(01)80691-0)
4. Kwon, Y.U., Kodadek, T. *Chem. Biol.* **14**, 671-677 (2007), <http://dx.doi.org/10.1016/j.chembiol.2007.05.006>
5. Zuckermann, R.N., et al. *J. Am. Chem. Soc.* **114**, 10646-10647 (1992), <http://dx.doi.org/10.1021/ja00052a076>
6. Fukuyama, T., Jow, C.K., Cheung, M. *Tetrahedron Lett.* **36**, 6373-6374 (1995), [http://dx.doi.org/10.1016/0040-4039\(95\)01316-A](http://dx.doi.org/10.1016/0040-4039(95)01316-A)
7. Vézina-Dawod, S., Derson, A., Biron, E. *Tetrahedron Lett.* **56**, 382-385 (2015), <http://dx.doi.org/10.1016/j.tetlet.2014.11.104>
8. Kruijtzter, J.A.W., et al. *Chem. Eur. J.* **4**, 1570-1580 (1998), [http://dx.doi.org/10.1002/\(SICI\)1521-3765\(19980807\)4:8<1570::AID-CHEM1570>3.0.CO;2-2](http://dx.doi.org/10.1002/(SICI)1521-3765(19980807)4:8<1570::AID-CHEM1570>3.0.CO;2-2)

Optimizing a Larger Scale Synthesis of Zyklophin, a Highly Selective Peptide Kappa Opioid Receptor Antagonist

Tatyana V. Yakovleva^{1,2} and Jane V. Aldrich^{1,2}

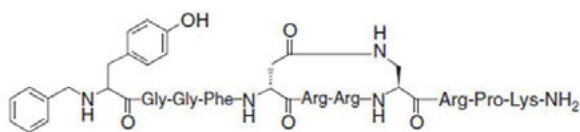
¹Department of Medicinal Chemistry, the University of Kansas, Lawrence, KS, 66045, USA;

²Department of Medicinal Chemistry, the University of Florida, Gainesville, FL, 32610, USA

Introduction

We are interested in developing metabolically stable peptidic ligands for kappa opioid receptors (KOR) as potential treatments for drug abuse and pain. In particular KOR antagonists have recently demonstrated potential therapeutic applications in the treatment of drug addiction, depression and anxiety [1]. Our research group has designed the KOR antagonist zyklophin ([N-benzylTyr¹,*cyclo*-(D-Asp⁵,Dap⁸)]dynorphin A-(1-11) amide, Figure 1) [2] based on the endogenous KOR peptide dynorphin A. Zyklophin is a selective KOR antagonist that exhibits activity in the CNS after peripheral administration [3]. Utilization of this important peptide *in vivo* requires the synthesis and purification of the peptide on a larger scale, but structural modifications (cyclization and *N*-terminal modification) make its larger scale synthesis and purification more challenging.

Here we describe the optimization of the solid phase synthesis of zyklophin, in particular the



Zyklophin

H₂-Tyr-Gly-Gly-Phe-Leu-Arg-Arg-Ile-Arg-Pro-Lys-OH

Dynorphin A (1-11)

Fig. 1. Structures of zyklophin and dynorphin A (1-11).

Results and Discussion

Zyklophin was synthesized by a combination of solid phase peptide synthesis (SPPS) of the (2-11) fragment followed by coupling of the *N*-terminal N-benzyl-Tyr-OH. SPPS of zyklophin (2-11) was performed at room temperature or by microwave irradiation using the Fmoc synthetic strategy on the low load (0.18 mmol/g) Fmoc-PAL-PEG-PS resin. The peptide was assembled through D-Asp⁵, then cyclized, followed by further extension of the peptide chain to give *cyclo*(D-Asp⁵,Dap⁸)]Dyn A (2-11)-NH₂.

The synthesis conditions were optimized for a 1 mmol scale synthesis of zyklophin (Table 1). The time for selective deprotection of the 2-phenylisopropyl (OPip) and *N*-methyltrityl (Mtt) protecting groups with 3% TFA was increased by 2-fold since it appeared that the deprotection, possibly of the OPip group, required longer time in the larger scale syntheses. Prolonging the selective deprotection of the side chains of Dap(Mtt) and D-Asp(OPip) allowed the cyclization step to go to completion at room temperature overnight, thereby improving the overall yield of pure zyklophin.

Table 1. Comparison of small and larger scale zyklophin syntheses.

	Small scale	Larger scale
Resin used	36-90 μ mol (0.2-0.5 g)	900 μ mol (5 g)
Yield crude peptide	49-124 mg	1175 mg
Crude peptide purity	68-72%	78-82%

selective deprotection [4,5] and cyclization of the side chains of D-Asp⁵ and Dap⁸ (2,3-diaminopropionic acid), and the use of microwave irradiation to facilitate the rapid cyclization of the side chains. To substantially increase the amount of peptide purified per chromatographic run we utilized a modified reversed phase HPLC purification method [6]. These modified procedures permitted preparation of the larger quantities of pure peptide (>200 mg) necessary for extensive studies *in vivo*.

To facilitate the synthesis microwave irradiation (Biotage Initiator+ Alstra) was also investigated. A 180 μ mol scale synthesis of zyklophin (2-11) was performed successfully using microwave irradiation on the PAL-PEG-PS resin, and the crude peptide was obtained in high purity (78-82%). Figure 2 shows that the cyclization

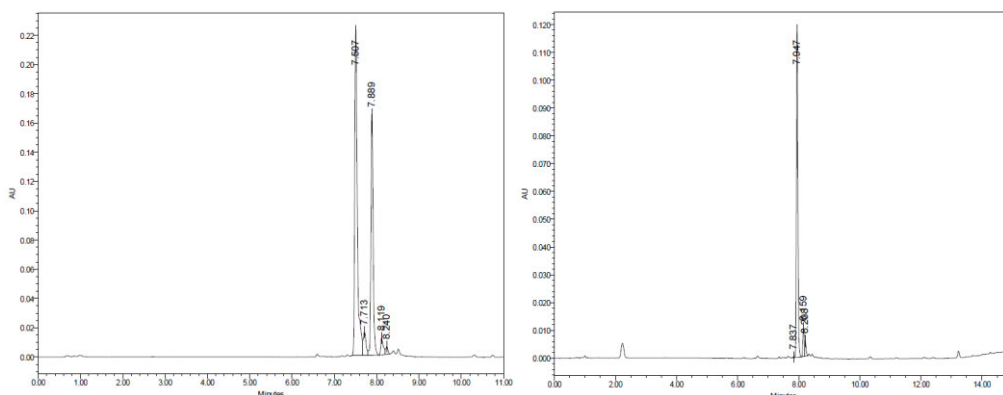


Fig. 2. Microwave-assisted cyclization of zykhlophin 5-11, a) Cyclization for 5 min at 75°C, 46% cyclization ($t_R = 7.51$ min, linear; $t_R = 7.89$ min, cyclic peptide; b) Cyclization 2x5 min at 75°C, >99% cyclization ($t_R = 7.94$ min).

reaction with PyClock, HOAt, and DIEA in DMF went to completion after 2 x 5 min microwave irradiation at 75°C, compared to overnight at r.t.

Purification was performed by reversed phase HPLC. A modified method [6] with a slow gradient and high TFA concentration was used that substantially increased the amount of purified peptide obtained per chromatogram run compared to the standard method, permitting preparation of the larger quantities of pure peptide needed for its extensive evaluation *in vivo*, and decreasing expenses related to larger columns and larger volumes of solvent consumption. This method allowed purification of 220 mg of zykhlophin in a single chromatographic run, compared to loading of 20-25 mg crude peptide per run using the standard method (Table 2), with similar overall purity (>97.5%).

N-Benzyl-Tyr-OH was prepared in solution by reductive amination [2] of Tyr-OrBu followed by TFA deprotection of the *t*-butyl ester. This amino acid was then coupled to zykhlophin (2-11) using PyClock, HOAt and DIEA in DMF. Dissolution of N-benzyl-Tyr-OH in DMF required warming to 80-85°C, then cooling to 25-30°C prior to adding the coupling reagents and addition of the mixture to zykhlophin (2-11) to prevent possible racemization. The zykhlophin derivative with N-benzyl-D-Tyr¹ was also synthesized and used as an HPLC standard to verify that racemization of the *N*-terminal residue did not occur during the final coupling.

Table 2. Comparison of small and larger scale zykhlophin purifications.

	Small scale/ Standard purification ^a	Larger scale/ Modified purification ^b
Amount purified/injection	20-25 mg	55-220 mg
Total crude peptide (# chromatograph runs)	150 mg (7)	676 mg (7)
Yield pure peptide/injection, (% recovery)	5 mg (28%)	12-42 mg (19-29%)
Total pure peptide	37 mg	139 mg
Amount of solvent used	9.8 L	3.9 L

^aVydac C18 column (22 x 250 mm, 300 Å pore size, 10 µm), equipped with a Vydac guard cartridge; 5-30% aq. MeCN/0.1% TFA over 50 min.; ^bZorbax SB-C18 column (9.4 x 250 mm, 300 Å pore size, 5 µm), equipped with a Zorbax guard cartridge; 5-30% aq. MeCN/0.2% TFA over 250 min.

The larger scale synthesis and purification of zyklophin were optimized by utilizing microwave irradiation and a modified HPLC purification protocol, respectively. Microwave irradiation facilitated the cyclization, decreasing the reaction time from overnight to 10 min with comparable yields and purity of the final peptide. Utilizing a modified HPLC protocol allowed purification of a 10-fold larger amount of zyklophin on a smaller diameter column compared to our standard method. These optimized synthesis and purification conditions should be applicable to a variety of cyclic peptides, facilitating their *in vivo* pharmacological evaluation where larger quantities are required.

Acknowledgments

Research supported by grant R01 DA023924 (National Institute on Drug Abuse).

References

1. Aldrich, J.V., McLaughlin, J.P. *AAPS J.* **11**, 312-322 (2009), <http://dx.doi.org/10.1208/s12248-009-9105-4>
2. Patkar, K., et al. *J. Med. Chem.* **48**, 4500-4503 (2005), <http://dx.doi.org/10.1021/jm050105i>
3. Aldrich, J.V., et al. *Proc. Natl. Acad. Sci. USA* **106**, 18396-18401 (2009), <http://dx.doi.org/10.1073/pnas.0910180106>
4. Li, D., Elbert, D.L. *J. Peptide Res.* **60**, 300-303 (2002), <http://dx.doi.org/10.1034/j.1399-3011.2002.21018.x>
5. Yue, C., et al. *Tetrahedron Lett.* **34**, 323-326 (1993), [http://dx.doi.org/10.1016/S0040-4039\(00\)60578-6](http://dx.doi.org/10.1016/S0040-4039(00)60578-6)
6. Chen, Y., et al. *J. Chromatogr. A* **1140**, 112-120 (2007), <http://dx.doi.org/10.1016/j.chroma.2006.11.052>

Application of the DoE Concept for Peptide API Process Development at Bachem

Daniel Samson¹, Wolfgang Seufert¹, Matteo Villain², and Alex Fässler¹

¹Bachem AG, Hauptstrasse 144, 4416 Bubendorf, Switzerland; ²Bachem Americas, Inc., 3132 Kashiwa Street, Torrance, CA, 90505, USA

Introduction

ICH guideline Q11 [1] describes approaches to developing process and drug substance understanding. In a traditional approach, set points and operating ranges for process parameters are defined, and the drug substance control strategy is typically based on demonstration of process reproducibility and testing to meet established acceptance criteria. In an enhanced approach, risk management and more extensive scientific knowledge are used to select process parameters and unit operations that impact critical quality attributes (CQAs) for evaluation in further studies to establish design space(s) and control strategies applicable over lifecycle of the drug substance [1].

Results and Discussion

The design of experiments (DoE) concept is applied at various stages of peptide API manufacturing processes at Bachem for design space definition. For unit operations with multiple process parameters the impact of each parameter on the relevant product and process quality attributes can be assessed utilizing DoE software [2]. Two case studies taken from the manufacturing process of different peptide APIs are presented to demonstrate the benefit of DoE for process development. Both, optimization of reaction conditions and process economy can be addressed by DoE.

Case study #1 comprises the optimization of TFA cleavage conditions for an Eptifibatide intermediate. The objective was to optimize the cleavage variables in order to maximize product purity and minimize the formation of cleavage related impurities.

Optimal TFA cleavage conditions (cleavage cocktail composition and cleavage duration) were predicted by DoE software with regard to maximized product purity and minimized contents of cleavage related impurities (Figure 1). Predicted results were confirmed at small and medium scale (from grams up to several 100 grams), as well as at large scale (multi kg manufacturing campaigns).

Table 1. Scope of DoE case study #1. TFA cleavage of Eptifibatide intermediate.

<i>DoE setup</i>		<i>Parameters</i>
Variables	EDT vol. %, TIS vol. %, H ₂ O vol. %, cleavage time at RT	
Response	Product purity [%], crude recovery [mg], peptide content [mg], PbF adduct [%], EDT adduct [%], tBu adduct [%], des-Acm Eptifibatide intermediate [%]	

Case study #2 had the objective to optimize the anti-solvent filtration rate of a precipitated Bivalirudin crude suspension without negative impact on product quality. Filtration optimization is a typical economic concern in large scale peptide manufacturing; it improves overall process duration and reduces production equipment allocation times. The impact of precipitation and filtration conditions (temperature during addition of anti-solvent to the peptide solution, temperature during aging of precipitated suspension, ratio of anti-solvent to peptide solution, and aging time) on product filtration rate and product quality attributes (product purity, peptide content, and crude recovery) was evaluated using DoE.

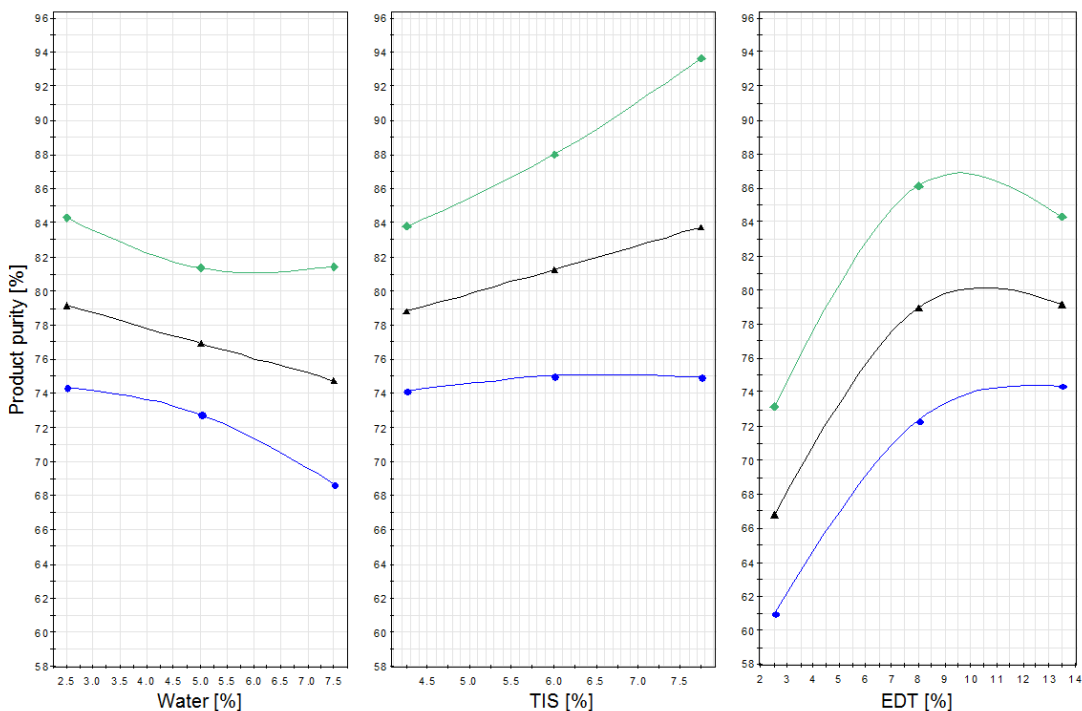


Fig. 1. Example of DoE results for case study #1. Impact of scavenger percentage on product purity (black line). Confidence interval of DoE results described by blue and green lines.

Table 2. Scope of DoE case study #2. Bivalirudin crude precipitation and filtration.

DoE setup	Parameters
Variables	Addition temperature, aging temperature, aging time, ratio anti-solvent to cleavage cocktail volume
Response	Filtration rate [$\mu\text{L/s}$], aspect of filtration [semi-qual.], product purity [%], peptide content [%], crude recovery [%]

Both the temperatures during anti-solvent addition and during aging were identified as variables with a significant impact on Bivalirudin crude filtration rate, with increased filtration rate at higher addition and aging temperatures; other variables, for example aging time, turned out to be insignificant (Figure 2).

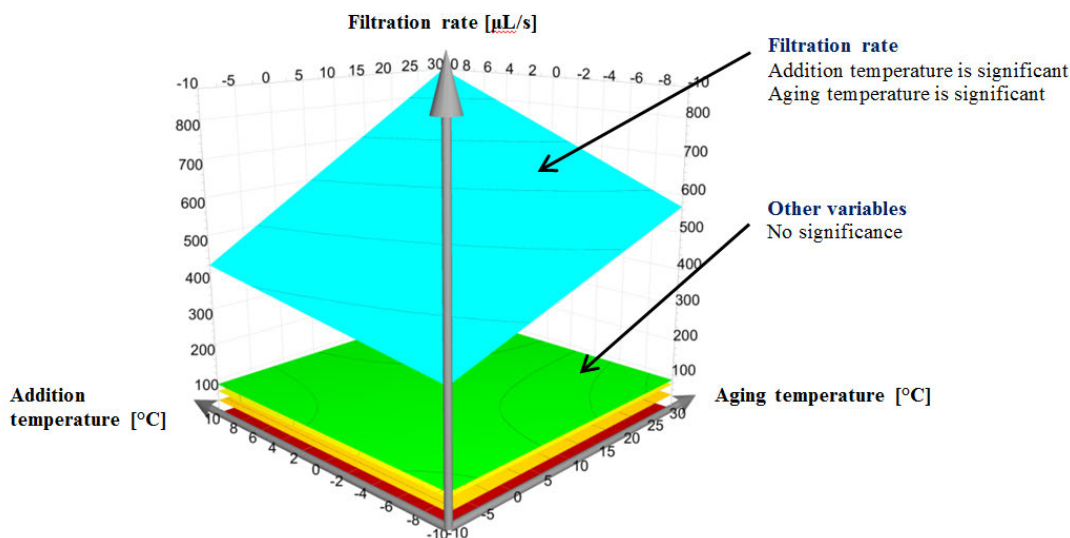


Fig. 2. DoE surface plot for case study #2. Impact of temperatures on filtration rate.

Summary

The concept of DoE is regularly used at Bachem for process development at different stages of peptide API manufacturing, particularly for the optimization of process steps with multiple variables. Different types of DoE are applied depending on the objective. The information obtained by application of the DoE concept has been proven essential for peptidic API manufacturing process characterization and qualification to satisfy regulatory expectations.

Acknowledgments

We thank Andreas Stadelmaier and Ralf Eisenhuth for their valuable contributions.

References

1. ICH guideline Q11 on development and manufacture of drug substances
2. DoE software MODDE 10.1 by UMETRICS

Author Index

Abraham, Parvin	45	Cabrera, H. Rodríguez	252
Acker, Andrea	195, 197	Cai, Minying	98, 189, 207, 236, 255
Adank, Danielle N.	162	Cain, James P.	112, 169, 259, 260
Agger, Else M.	262	Camperi, Silvia A.	131, 137
Ahn, Jung-Mo	154, 170, 268, 270	Capurro, Margareth L.	61, 64
Alabanza, Anginelle M.	12	Carpenter, Andrew	195, 197
Albericio, Fernando	137, 274	Caruso, M.	141
Aldrich, Jane V.	22, 125, 177, 283	Cascone, Osvaldo	131, 137
Alves, Flávio L.	61, 64	Cazares, M.	57
Andricopulo, Adriano D.	91	Chatenet, David	184
Apostol, C. R.	69	Chau, William	150, 165
Araújo, Daniele Ribeiro	88	Chauhan, Satendra	238
Ávila, Lucía	137	Chemtob, Sylvain	187
Babinska, Anna	174	Chen, Lin	266
Ball, Zachary T.	24	Chen, Qian	143, 147, 150, 158, 165
Banday, Abid H.	255	Chen, Rong	232
Barany, George	1, 266	Chen, Yao	232
Barany, Michael J.	266	Chingle, Ramesh	172
Barsotti, Robert	143, 147, 150, 158, 165	Cilli, Eduardo M.	91
Bartol, Kyle	150	Clement, Cristina C.	174
Becker, Christian F. W.	257	Colon, Cyf N. Ramos	71, 96
Bédard, François	47, 122	Cordeiro, Rodrigo M.	61
Bednarek, Radoslaw	174	Cosper, Nathaniel	112, 169, 259, 260
Beeton, Christine	238	Couture, Frédéric	249
Bello, Claudia	257	Craik, David	236
Benjamin, Israel	143, 165	Crescenzi, M. De	141
Bergwall, Peter	112, 169, 259, 260	Croston, Glenn	204
Bertolet, Matthew L.	158	Curtiss, Linda K.	30
Bertucci, Michael A.	51	D'Alessandro, Angelo	241
Bhakta, Sanjib	193	Davis, P.	69
Biron, Eric	47, 122, 127, 280	Day, Robert	119, 249
Bitsaktsis, Constantine	117	De Zotti, M.	141, 210
Black, Audrey S.	30	Decker, Megan E.	12
Blankesteijn, W. Matthijs	212	Denda, Masaya	278
Bolzani, Vanderlan S.	91	Derson, Antoine	280
Bonnet, David J.	30	Dias, Carolina C.	86
Bordeleau, Louis-Jean	127	Doan-Ngoc, Duc	272
Bottex, Amelie	150, 165	Doering, Skye R.	162
Bunnell, A.	57	Dooley, C.T.	57, 113
Cabral, H.	54	Dufour, Frédéric	249
		Dufour-Gallant, Julien	184
		Ebo, Chinyere	147, 165

Eckhardt, S. Gail	241	Hamamoto, Hiroshi	9
Ejchart, Andrzej	73	Hamidon, Johan K.	16
Erra-Balsells, Rosa	131	Hamin-Neto, Y. A. A.	54
Estrada, Rosendo	238	Hammami, Riadh	47
Ewul, Ebenezer L.V.	174	Hammer, Robert P.	264, 266
Fairlie, David P.	16	Hansen, Paul R.	262
Fässler, Alex	286	Hargrove, Diane M.	204
Fernández-Llamazares, Ana	212	Haskell-Luevano, Carrie	162, 200
Ferracane, Michael J.	22	Hatcher, Cathy J.	143, 165
Ferrie, John J.	12	Hemu, Xinya	27
Fliss, Ismail	47	Henley, Matthew J.	266
Formaggio, F.	141, 210	Herby, Claire	280
Fortin, Sophie	127	Herman, Davis S.	43
Fraczak, Oliwia	73, 77	Hermans, Kevin C. M.	212
Freeman, Katie	200	Heyl, Deborah	181
Freitas, Danieli Melo de	67	Hodges, Robert S.	36, 241, 245
Fuente-Moreno, M.	264	Hou, Xin	187
Galbreath, Tyler	158	Hozumi, Kentaro	215
Garavito, Jenny Najas Z.	91	Hruby, Victor J.	43, 71, 80, 96, 98, 189, 207, 223, 236, 255
Garg, Tripti	105	Hunter, Robert	195, 197
Garvey, Jennifer	181	Huq, Redwan	238
Gatto, E.	141	Imura, Tomohiro	30
Gentile, Kayla	12	Inokuma, Tsubasa	278
Gera, Lajos	36, 241, 245	Inoue, Masayuki	9
Ghadiri, M. Reza	30	Itoh, Kohji	278
Gioseffi, A.	57, 113	Iyer, Abishek	16
Giri, Aswini	43, 69	Jallow, Alhassan	174
Gisemba, Solomon A.	177	Jiang, Ziqing	36, 241, 245
Giudicessi, Silvana L.	131, 137	Jobin, Steve	280
Gobeil, Stéphane	127	Joodaki, Faramarz	109
Goldwaser, Ari L.	12	Kaji, Takuya	9
Gomaa, Ahmed	47	Karankevich, Katya	112, 169, 259, 260
Gong, Chunjie	179	Katagiri, Fumihiko	215
Gonzalez, Janet	174	Kato, Tamaki	139
Greenfield, Michael L.	109	Kessler, Horst	236
Grieco, Paolo	184, 207	Kikkawa, Yamato	215
Gruber, Christian W.	91	Kim, Joongsoo	170
Gruskos, Jessica J.	12	Kim, Young	156
Guarracino, Danielle A.	12	Kitakaze, Keisuke	278
Guo, Huiling	179	Knox, Susan	12
Haghighi, Saghar M.	98, 189	Konstantinidis, George	105
Hall, Sara M.	71, 80, 96	Kosson, Piotr	77

Kumar, Amit	154	Mant, Colin T.	36, 245
Kumar, K. Santhosh	45	March, Kareem	51
Kumar, Rakesh	170	Marletta, G.	210
Kuranaga, Takefumi	9	Maro, Salvatore Di	184
Kuzmin, Alexander	80	Martin, Lenore M.	105, 109
Kwiatkowska, Anna	119, 249	Martinez, Daniel	112, 169, 259, 260
LaCroix, Roxanne	105	Martínez-Ceron, María C.	131, 137
Lahtinen, Bailey	189	Maryanoff, Bruce E.	30
Lai, Josephine	71, 80, 96	Mazzuca, C.	210
Largent-Milnes, Tally	43	McLeod, Kaitlyn	98
Lasota, Anika	73, 77	Mebrahtu, Makda	195, 197
Lavigne, Justin	223	Merlino, F.	207
Lee, Tae-Kyung	268, 270	Merlino, Francesco	184
Lee, Yeon Sun	71, 80, 96	Messina, G. M. L.	210
Leman, Luke J.	30	Minni, Michael	158
Lensing, Cody J.	162	Minor, Maria	12
Lepek, Teresa	119	Miranda, Antonio	61, 64, 82, 84, 86
Levesque, Christine	249	Misicka, Aleksandra	73, 77
Lewandowska-Goch, Monika	119	Mohammadpour, Fatemeh	187
Lewandowski, Bartosz	234	Molnar, G.	69
Li, Ling	179	Monteiro, Admir	105
Li, Qianhui	179	Muchowska, Adriana	73, 77
Li, Y.	57, 113	Murai, Motoki	9
Liang, Xinxia	122	Naito, Atsushi	215
Lim, Junxian	16	Napoli, B. Di	210
Lipscombe, Christina	143, 147, 165	Newberry, Robert W.	20
Liyanage, Wathsala	134	Newman, Rebecca	181
Lo, Su-Tang	154	Neyer, Gebhard	204
Lohman, Rink-Jan	16	Nguyen, Dylan H.	12
Longo, E.	141	Nguyen, Giang K. T.	27
Lopes, Flavio A.	82	Nilsson, Bradley L.	33, 134, 228
Lovas, Sándor	217	Nogueira-Pedro, Amanda	86
Lubell, William D.	40, 94, 172, 184, 187, 202, 272	Nomizu, Motoyoshi	215
Ly, Kévin	249	Novellino, Ettore	184
Maciejczyk, Maciej	73	Nowakowski, Michal	73
Magalhães, Luma G.	91	Oddo, A.	264
Mahalakshmi, Radhakrishnan	220	Oliva, Maria Luiza V.	82
Makwana, Kamlesh	220	Oliveira, Jr., Vani X.	61, 64, 67, 88, 266
Madhusudan		Olma, Aleksandra	73, 77
Malkinson, John P.	193	Olson, Keith M.	223
Manandhar, Bikash	154, 268, 270	Otaka, Akira	278
		Palleschi, A.	141, 210

Paredes-Gamero, Edgar J.	84, 86	Salum, María L.	131
Park, Yeji	181	Samson, Daniel	286
Patel, Harsh	143, 147, 150, 165	Sanghvi, Sanjna S.	12
Patel, Samir	143	Santicioli, Paolo	184
Paulik, Mark	195, 197	Sato, Daisuke	139
Peckham, Joan	105	Sato, Kohei	278
Pedron, Cibele Nicolaski	88	Sawyer, Jonathon R.	98
Pennington, Michael W.	238	Scarselli, M.	141
Perrin, Marie	127	Schmidgall, Carly	143, 147
Pes, Lara	156	Schnell, Sathya M.	200
Philipp, Manfred	174	Schrader, Alex M.	266
Phillips, Mariana	117	Schteingart, Claudio D.	204
Pickering, D.S.	264	Scotti, Francesca	193
Pinheiro, Ana A. S.	64	Sekimizu, Kazuhisa	9
Pinto, Angelo C.	91	Senadheera, Sanjeewa N.	125
Pinto, Meri Emili F.	91	Seufert, Wolfgang	286
Popp, Brian V.	24	Sheykhzade, M.	264
Porreca, Frank	43, 69, 71, 80, 96, 223	Shigenaga, Akira	278
Poupart, Julien	94, 272	Silva, Adriana F.	61, 64
Prahl, Adam	119	Silva, Jones M.	82
Qian, Shuo	225	Silva, Leandro S.	64
Qin, Lingyun	232	Silvers, William	154
Qiu, Zhiyong	174	Singh, Anamika	200
Raines, Ronald T.	20	Singh, Ranee	16
Rajbhandary, Annada	228	Srivastava, Ved	195, 197
Ramos-Colon, Cyf	80	Steele, Preston	109
Ramos-Tomillero, Iván	274	Stoermer, Martin J.	16
Rana, Niki	191	Streicher, John	223
Rankin, David	69, 80	Stutzman, Devon	143, 165
Raymond, Danielle M.	33	Su, Fei Yang	232
Reid, Robert C.	16	Su, Zhengding	179
Remarcke, Ryan	150	Subirade, Muriel	47
Remesic, Michael	80	Suen, Jacky Y.	16
Restituyo-Rosario, E.	112, 169, 259, 260	Sun, Honghao	179
Rivière, Pierre J-M.	204	Sun, Xiankai	154
Robertson, Camille T.	12	Swiatkowska, Maria	174
Rodríguez, Hortensia	274	Swiger, Erin	195, 197
Roller, Shane	195, 197	Tajhya, Rajeev	238
Rowley, Jessica A.	16	Takeyama, Kazuki	215
Saavedra, Soledad L.	137	Tala, Srinivasa R.	200
Sabatino, David	117, 191	Tam, James P.	27
Salifu, Moro O.	174	Tariga, Hiroe	204

Tentler, John	241	Zhe, Wu	139
Timmerman, Peter	212	Zheng, Li	179
Timpo, Edem	174	Zhou, Jinjin	232
Tokuyama, Paula Y.	84	Zhou, Yang	98, 189, 255
Toniolo, C.	141		
Torres, Marcelo D. T.	61, 64		
Traore, Mariam	202		
Tsuda, Yusuke	278		
Tsuji, Kohei	278		
Tung, Ching-Hsuan	156		
Turcotte, Stéphane	40, 184		
Tymecka, Dagmara	77		
Vanderah, T. W.	43, 69, 80		
Venanzi, M.	141		
Vézina-Dawod, Simon	122, 127, 280		
Villain, Matteo	286		
Vispo, Nelson Santiago	252		
Vladaj, Yllka	181		
Vohidov, Farrukh	24		
Vu, Jonathan	143		
Walker, Sydney	150		
Wang, Desuo	101		
Watts, Charles R.	217		
Welch, Jade J.	33		
Wennemers, Helma	234		
Wiard, Robert	195, 197		
Wilhelm, Patrick	234		
Wisniewski, Kazimierz	204		
Woodworth, Joshua S.	262		
Wright, K.	141		
Wu, Steve	101		
Wu, Zhiqian	101		
Xu, Jianhao	179		
Yakovleva, Tatyana V.	283		
Yamada, Nobuko	215		
Yamada, Satomi	215		
Yamamoto, Takashi	43		
Yau, Mei-Kwan	16		
Young, Lindon H.	143, 147, 150, 158, 165		
Young, Victor G.	266		
Yousif, A.M.	184, 207		
Zhao, Yannan	30		

